$Np^{cr} rR_ 165,631,v_2$

NASA-CR-165631-VOL-2
19840020734

INTEGRATED APPLICATION
OF ACTIVE CONTROLS (IAAC)
TECHNOLOGY TO AN ADVANCED
SUBSONIC TRANSPORT PROJECT—

CURRENT AND ADVANCED
ACT CONTROL SYSTEM
DEFINITION STUDY—VOLUME II,
APPENDICES

FINAL REPORT

BOEING COMMERCIAL AIRPLANE COMPANY
P.O. BOX 3707, SEATTLE, WASHINGTON 98124

CONTRACTS NAS1-14742 AND NAS1-15325
October 1981

FOR EARLY DOMESTIC DISSEMINATION

Because of their possible commercial value, these data developed under Government contracts NAS1-14742 and NAS1-15325 are being disseminated within the United States in advance of general publication. These data may be duplicated and used by the recipient with the expressed limitations that the data will not be published nor will they be released to foreign parties without prior permission of The Boeing Company. Release of these data to other domestic parties by the recipient shall only be made subject to these limitations. The limitations contained in this legend will be considered void after October 1983. This legend shall be marked on any reproduction of these data in whole or in part.

NASA

National Aeronautics and
Space Administration

Langley Research Center
Hampton, Virginia 23665

NF02007

FOREWORD

This document constitutes the final report of the Current Technology ACT Control System Definition and the Advanced Technology ACT Control System Definition Tasks of the Integrated Application of Active Controls (IAAC) Technology to an Advanced Subsonic Transport Project. The report covers work performed from July 1978 through October 1980 under Contracts NAS1-14742 and NAS1-15325.

Volume I contains the principal results of the study, and supplementary technical data are contained in Volume II.

The NASA Technical Monitors for these contract tasks were R. V. Hood and D. B. Middleton of the Energy Efficient Transport Project Office at Langley Research Center.

The work was accomplished within the Preliminary Design and the Engineering Technology Departments of the Vice President-Engineering organization of the Boeing Commercial Airplane Company. Key contractor personnel who contributed were:

G. W. Hanks	Program Manager
H. A. Shomber	IAAC Project Manager
H. A. Dethman	Design Integration
L. B. Gratzer	Technology Integration
A. Maeshiro	Task Manager (Current Technology ACT Control System Definition)
D. Gangsaas	Task Manager (Advanced Technology ACT Control System Definition)
J. D. Blight	Flight Controls Technology
S. M. Buchan	Flight Controls Technology
C. B. Crumb	Flight Control Design
R. J. Dorwart	Product Assurance
C. C. Flora	Flight Controls Technology
U. Ly	Flight Controls Technology
K. A. B. Macdonald	Product Assurance
D. C. Norman	Flight Controls Technology

i

E. T. Reiquam   Systems Technology

J. Shen   Flight Controls Technology

R. D. Smith   Flight Control Design

T. D. Verrill   Flight Control Design

T. B. Cunningham   Honeywell Systems and Research Center

J. C. Larson   Honeywell Avionics Division

E. R. Rang   Honeywell Systems and Research Center

R. K. Mason   Hydraulic Research Textron

O. A. Walkes   Hydraulic Research Textron

During this study, principal measurements and calculations were made in U.S. customary units and were converted to Standard International units for this document.

Use of trade names or names of manufacturers in this report does not constitute an official endorsement of such products or manufacturers, either expressed or implied, by the National Aeronautics and Space Administration.

CONTENTS

CONTENTS (Continued)

CONTENTS (Continued)

v

CONTENTS (Continued)

CONTENTS (Continued)

CONTENTS (Continued)

CONTENTS (Continued)

CONTENTS (Concluded)

FIGURES

Page

FIGURES (Continued)

Page

Page

Page

FIGURES (Continued)

FIGURES (Continued)

FIGURES (Concluded)

This Page Intentionally Left Blank

TABLES

TABLES (Concluded)

This Page Intentionally Left Blank

SYMBOLS AND ABBREVIATIONS

GENERAL ABBREVIATIONS

ac	alternating current
app	appendix
$a_i, b_i,$	control law transfer function parameters
$c_i, d_i,$	control law transfer function parameters
p_i	control law transfer function parameters
A	ampere; piston area; system state matrix
AAL	angle-of-attack limiter
AB	address bus
ACES	airline cost-estimating system (program)
ACT	Active Controls Technology
A/D	analog to digital
AEC	Atomic Energy Commission
AFCS	automatic flight control system
Ah	ampere-hour
AIL	aileron
ALU	arithmetic logic unit
AP	autopilot
APB	auxiliary power breaker
APD	avalanche photodiodes
APFDC	autopilot flight director computer
APU	auxiliary power unit
AR	analog reversion
ARCS	Airborne Advanced Reconfigurable Computer System
ARINC	Aeronautical Radio Incorporated

ASYM	asymmetry detection electronics
ATDP	air-turbine-driven pump
ATE	automatic test equipment
A_a	airplane state matrix
A_u	actuator state matrix
A_w	wind state matrix
A_O	steady aerodynamic stiffness matrix
$\bar{A}_O$	steady aerodynamic stiffness matrix associated with control surface deflection
A_1, A_2	unsteady aerodynamic stiffness matrix
$\bar{A}_1, \bar{A}_2$	unsteady aerodynamic stiffness matrix associated with control surface deflection
bps	bits per second
brkr	breaker
b_i	unsteady aerodynamic lag coefficients
B	control input distribution matrix
B′	transformed control distribution matrix
BIT	built-in test
BTB	bus tie breaker
BPCU	bus power control unit
B_a	airplane control distribution matrix
B_i	bending moment at the ith station
B_u	actuator input distribution matrix
B_w	wind input distribution matrix
B_1	input to system matrix for full-state feedback system
B_2	command to input matrix for full-state feedback system
c	characteristic chord length
cg	center of gravity

cm	centimeter
$\bar{c}$	mean aerodynamic chord
c_i	Kussner scaling coefficients
C	Celsius; state to output distribution matrix
C′	transformed state to output distribution matrix
CARE	computer-aided reliability estimates
CARSRA	computer-aided redundant system reliability analysis
CAS	control augmentation system
CB	circuit breaker
CCDL	cross-channel data link
CCDT	cross-channel data transfer
CDC	Control Data Corporation.
CLB	climb
CLP	control law processor
CMOS/SOS	complementary metal-oxide semiconductor/silicone on sapphire
CONT	continuous
CPU	central processing unit
CQ	servovalve spool gain
CRT	cathode-ray tube
CRZ	cruise
CSEU	control system electronic unit
CSU	computer service unit
CV	control valve
CWS	control wheel steering
CY	calendar year
C_a	airplane output distribution matrix
C_d	plant process noise covariance matrix

$\bar{C}_d$	fictitious input noise covariance matrix
C_p	state to performance output distribution matrix
C_u	actuator output distribution matrix
C_v	measurement noise covariance matrix
C_w	state to wind output distribution matrix
C_0	quasi-steady aerodynamic stiffness matrix
$\bar{C}_0$	quasi-steady aerodynamic stiffness matrix associated with control surface deflection
C_1	quasi-steady aerodynamic damping matrix
$\bar{C}_1$	quasi-steady aerodynamic damping matrix associated with control surface deflection
$\mathcal{C}$	controllability matrix
d	plant disturbance vector; control law transfer function denominator
$\bar{d}$	fictitious input noise
dB	decibel
dc	direct current
deg	degree
d_i	Kussner lag coefficients
D	control to output distribution matrix; drag
D/A	digital to analog
DADC	digital air data computer
DAST	drone for aerodynamic and structural testing
DC	don't care
DITS	digital information transfer system
DMA	direct memory access
DN	down
DRO	design requirements and objectives

D_i	unsteady aerodynamic matrices to model lift growth effects associated with rigid and elastic modes
$\bar{D}_i$	unsteady aerodynamic matrices to model lift growth effects associated with control surfaces
D_w	direct transmission matrix from wind to output
e	base for Napierian logarithms; system state estimate error
E	process noise distribution matrix; exponent; wind to output distribution matrix
EASY	environmental control analysis system
EDP	engine-driven pump
EET	Energy Efficient Transport (Program)
EHV	electrohydraulic valve
ELEV	elevator
EM	electric motor
EMA	electromechanical actuator
EMI	electromagnetic interference
EMP	electric-motor-driven pump; electromagnetic pulse
E(p)	fit error function
EPC	external power contactor
f	longitudinal correlation function
fig.	figure
ft	feet
F	Fahrenheit; FMC; force; measurement noise distribution matrix
FAA	Federal Aviation Administration
FAR	Federal Aviation Regulations
FBW	fly by wire
FCC	flight control computer
FD	failure detection

FH	flight hour
FMC	flutter-mode control
FMEA	failure mode and effect analysis
FO	fiber optic
FTAP	fault tree analysis program
FTMP	fault-tolerant multiple processor
FTREE	fault tree computer program
g	acceleration due to gravity; structural damping coefficient for neutral stability; transverse correlation function
g-dump	normal acceleration autopilot disconnect
g_i	unsteady aerodynamic lag coefficients
gal	gallon
gen	generator
G	feed forward gain; feedback gain matrix
GCB	generator circuit breaker
GCU	generator control unit
GG	device type identifier
GLA	gust-load alleviation
GMPS	general-purpose multiplex system
GPIB	general-purpose interface bus
GPM	gallons per minute
GPS	global positioning system
G(s)	transfer function
G_i	constants associated with representation of unsteady aerodynamic forces
hr	hour
H	feedback gain; Hamiltonian
HDC	device type identifier

HDP	device type identifier
HMOS	high-performance metal-oxide semiconductor
HPU	hydraulic power unit
Hz	hertz
in	inch
ips	inches per second
I	identity matrix; input
IAAC	Integrated Application of Active Controls Technology to an Advanced Subsonic Transport Project
IAP	integrated actuator package
IAS	indicated airspeed
IB	input bus
IC	integrated circuit
IDG	integrated drive generator
IEEE	Institute of Electrical and Electronics Engineers
ILD	injection laser diodes
ILS	instrument landing system
INBD	inboard
INOP	inoperable
INS	inertial navigation system
I/O	input/output
IOC	input/output controller
IRS	inertial reference system
ISO	International Standards Organization
I^2L	integrated injection logic
I_A, I_B, I_C	input current
J	cost function

JPL	Jet Propulsion Laboratory
kg	kilogram
km	kilometer
kn	knot
kPa	kilopascal
kVA	kilovoltampere
kW	kilowatt
k_i	gain at the ith control input
K	counter value; gain; gain matrix; state estimate error covariance matrix; thousand
KA	amplifier gain; angle-of-attack gain
KAM	model amplifier gain
KC	servovalve monitor gain
KD	demodulator gain
KE	elevator gain
KF	flutter-mode control gain
KFB	feedback transducer gain
KG	gust-load alleviation gain
KL	feedback gain; lever ratio
KM	maneuver gain
KMA	maneuver-load control aileron gain
KME	maneuver-load control elevator gain
K ops	thousand operations per second
KQ	pitch-rate gain
KSV	servovalve gain
KSVM	model servovalve gain
KTD	transducer gain

KU	speed gain
K_f	filter gain
K_{ss}	steady-state solution to matrix Riccati equation
$K_{1/3}(\ )$	modified Bessel functions of the second kind of order 1/3
$K_{2/3}(\ )$	modified Bessel functions of the second kind of order 2/3
K_θ	pitch angle scaling constant
lb	pound
lbf	pound-force
lb/in	pounds per inch
lb/in^2	pounds per square inch
L	dynamic load vector; length; lift; transverse turbulence scale length
LAS	lateral/directional-augmented stability
LAT	lateral
LE	leading edge; left elevator
LED	light-emitting diode
LIA	left inboard aileron
LIF	left inboard flaperon
LOAI	left outboard aileron, inboard
LOAO	left outboard aileron, outboard
LOF	left outboard flaperon
LR	lower rudder
LRU	line replaceable unit
LSI	large-scale integration
LSIC	large-scale integrated circuit
LVDT	linear variable differential transformer
L_i	three-component vector of L consisting of shear, bending moment, and torsion of the ith station

L_u	longitudinal turbulence scale length
$L_{v,w}$	transverse turbulence scale lengths
ℓ	liter
$\mathcal{L}$	Laplace transform
m	meter
mA	milliampere
max	maximum
min	minute
mm	millimeter
ms	millisecond
μs	microsecond
M	feedforward gain matrix; Mach; mega; motor
MARG	marginal, one failure away from function loss
MCU	modular control unit (ARINC dimension specification)
MCV	main control valve
MEL	minimum equipment list
MG	main gear
MHD	magnetohydrodynamic
MLC	maneuver-load control
MMU	memory management unit
MOS	metal-oxide semiconductor
M/R	maximum range to its resolution
MTBF	mean time between failures
MUX	multiplexer
MVL	midvalue logic
MW	megawatt
MZFW+F	maximum zero fuel weight plus fuel (including full reserve tanks)

M_q	dimensional variation of pitching moment with pitching rate
M_u	dimensional variation of pitching moment with speed
M_α	dimensional variation of pitching moment with angle of attack
$M_{\dot{\alpha}}$	dimensional variation of pitching moment with angle-of-attack rate
M_{δ_E}	dimensional variation of pitching moment with elevator angle
nmi	nautical mile
ns	nanosecond
$n\lambda_{mp}$	Markov transition rate, stage n between states m and p
n_i	control law transfer function numerators
n_z	vertical acceleration
N	dummy vector; newton; ultimate normal load factor
NAV	navigation (mode)
NDP	numerical data processor
NG	nose gear
NMR	nuclear magnetic resonance
No.	number
N_1	speed of the No. 1 rotor
ops	operations per second
oz	ounce
o_B	body axis coordinates
o_I	inertial axis coordinates
O	output
OAI	outboard aileron (inboard section)
OB	output bus
OEM	original equipment manufacture
OMP	output monitor processor
OUTBD	outboard

$\mathcal{O}$	observability matrix
$p, \hat{p}$	Lagrange's multiplier
psi	pounds per square inch
pwr	power
P	inertial-to-body transformation matrix; probability; pump
Pa	pascal
PAS	pitch-augmented stability
PBW	power by wire
PCU	power control unit
PCM	power conditioning module
PF	pump and filter
PIN	p-layer intrinsic n-layer
PLIM	nonlinear actuator position limit
PM	permanent magnet
PROM	programmable read-only memory
P/S	parallel/serial
PSD	power spectral density
P_R	pressure, return
P_S	pressure, supply
P_1	hydraulic supply pressure, hydraulic system 1
P_2	hydraulic supply pressure, hydraulic system 2
q	dynamic pressure; perturbation value of pitch rate; rigid and flexible modal coordinates
$\dot{q}$	rigid and flexible mode rates
$\ddot{q}$	rigid and flexible mode accelerations
$\bar{q}_i$	unsteady aerodynamic states associated with q
Q	pitch rate

QA	device type identifier
QSAE	quasi-static aeroelastic
Q, Q_1, Q_2	cost weighting matrices for performance variables
r	yaw rate
rad	radian
ref	reference
rms	root mean square
r_i	ith gust input reference coordinate vector
R	cost weighting matrix for control inputs; receiver
RADC	Rome Air Development Center
RAM	random-access memory
RAT	ram air turbine
RE	right elevator
RIA	right outboard aileron
RIF	right inboard flaperon
RLIM	nonlinear rate limit
ROAD	right outboard aileron, outboard
ROAI	right outboard aileron, inboard
ROF	right outboard flaperon
ROI	return on investment
ROM	read-only memory
RPS	rotor position sensor
RT	remote terminal
RTS	real-time counter
R_i	unsteady aerodynamic force matrix associated with wind disturbance
R_{ij}	cross-correlation function between gust states i and j

$\bar{R}_{ij}$	Laplace transform of R_{ij}
R_x, R_y, R_z	rotations about x, y, z axes
R_O	steady aerodynamic force matrix associated with wind disturbance
R_1	hydraulic return pressure, system 1
R_2	hydraulic return pressure, system 2
$\mathcal{R}(\tau)$	cross-correlation matrix with time lag
s	Laplace variable; second (same as sec)
sec	second (same as s)
subsec	subsection
S	Kalman filter gain matrix; standby
SAS	stability augmentation system
S/C	short circuit
SDEU	servodrive electronics unit
S/H	sample and hold
SIFT	software-implemented fault tolerance
SKC	Singer-Kearfott Corporation
S/P	serial/parallel
SRI	Stanford Research Institute
SS	signal selection
SSFD	signal selection and failure detection
SVDED	dead band
SYNC	synchronization
S_i	shear force at the ith station
t	time limit; time setting; time variable
t_f	final time
t_i	ith column of the transformation matrix T
t_o	initial time

T	cycle time; sampling period; similarity transformation matrix; threshold; transistor
TD	Teledyne
TE	trailing edge
T/O	takeoff
T-R	transformer-rectifier
TRU	transformer-rectifier unit
TTL	transistor-transistor logic
TX/RCV	transmitter-receiver
T_i	torsion at the ith station
T_u	control effectiveness scaling matrix
T_x, T_y, T_z	translations along x, y, z directions
u	incremental value of forward-speed component; control input vector
$u*, \hat{u}*$	optimal control solutions
u_c	control input command
u_g	longitudinal turbulence (output of Dryden model)
u_n	white noise process for longitudinal turbulence (input to Dryden model)
UART	universal asynchronous receiver/transmitter
UPI	device type identifier
UR	upper rudder
USART	universal synchronous/asynchronous receiver/transmitter
UTIL-1,-2	utility bus
U,V,W	positive integer
v	measurement noise vector
v_i	ith system eigenvector
v_{ij}	cross-variance between the ith and jth output variables

$v_{jj/i}$	variance of jth output response to ith control input
V	steady-state airspeed; true airspeed; variable displacement; velocity; volt
VA	volt-ampere
V ac	volt alternating current
VC	actuator position command voltage; voltage, common; volts, command
V dc	volt direct current
VFB	volts, feedback
VHSIC	very-high-speed integrated circuits
VLSI	very-large-scale integrated
VLSIC	very-large-scale integrated circuit
V/N	volts per Newton
VOR	very-high-frequency omnidirectional radio range
VPB	volts, pitch, channel B
VPC	volts, pitch, channel C
V/V	verification and validation
VWRS	vibrating wire rate sensor
VYRO	pitch-rate sensor (trade name)
V_{bias_A}	bias voltage of channel A
V_{bias_B}	bias voltage of channel B
V_{bias_C}	bias voltage of channel C
V_A, V_B, V_C	voltage of channels A, B, C
V_1	forward velocity
w, wg	wind input vector
wps	words per second
w_c	white noise wind input
w_g	transverse turbulence (output of Dryden model)

1

$\bar{w}_g$	unsteady gust states
W	vertical-speed component; watt
WLA	wing-load alleviation
W_n	white noise process for transverse turbulence (input to Dryden model)
x	system state estimate vector; system state vector
$\hat{x}$	estimated state vector
x_a	airplane state vector
x_o	initial state vector
x_u	actuator state vector
x_w	wind state vector
x_B	state vector, body-fixed axis coordinates
x_I	state vector, moving-inertial axis coordinates
X	index
XAH	actuator displacement
XBIAS	null bias
XDED	feedback dead band
X_q	dimensional variation of X force with pitch rate
X_u	dimensional variation of X force with speed
X_{wz}	intermediate state variable for transverse turbulence in Dryden model
X_α	dimensional variation of X force with angle of attack
X_{δ_E}	dimensional variation of X force with elevator angle
X_{δ_i}	state vector for standard controllable form
$\underline{\bar{X}}$	state covariance matrix
$\underline{\bar{X}}'$	covariance matrix for $\dot{x}(t)$
$\underline{\bar{X}}_o$	initial state covariance matrix
y	output; output positions; output vector

$\dot{y}$	output rates
$\ddot{y}$	output accelerations
$\hat{y}$	estimated sensor output vector
y_i	component of y
$\underline{Y}$	output covariance matrix
$\underline{Y}'$	covariance matrix for $\dot{y}(t)$
z	system modal vector
$\dot{z}$	vertical velocity
z_i	unsteady aerodynamic states associated with $\dot{z}$
Z	Z transform variable; modal response covariance matrix
$\ddot{Z}_{cg}$	vertical acceleration at body station 922.7 (cg)
Z_q	dimensional variation of Z force with pitch rate
Z_u	dimensional variation of Z force with speed
Z_α	dimensional variation of Z force with angle of attack
$Z_{\dot{\alpha}}$	dimensional variation of Z force with angle-of-attack rate
Z_{δ_E}	dimensional variation of Z force with elevator angle

SUBSCRIPTS

Subscripts Related to Velocity V or Mach Number M

B	gust penetration
D	dive
e	equivalent airspeed
MO	maximum operating

General Subscripts

a	airplane model
A	aileron; amplifier
c	command inputs
cg	(at) center of gravity
com	command
COL	control column
D	demodulator
E	elevator
f	final time
FB	feedback
g	gust model state
i	initial time
m	implicit or explicit model
max	maximum of
MU	minimum unstick speed condition
n	white noise
OAI	outboard aileron (inboard section)
OAO	outboard aileron (outboard section)
R	reduced-order model
ss	steady-state value of
SCS	steady aero control surfaces
SM	steady aero model
SV	servovalve
SW	steady aero wind gusts
u	control actuator model

UCS	unsteady aero control surfaces
UM	unsteady aero model
UW	unsteady aero wind gusts
w	gust model

SUPERSCRIPTS

T	transpose of
-1	inverse of
$\wedge$	auxiliary variable; Kalman filter estimated quantity
$'$	auxiliary variable
$-$	auxiliary variable

OPERATORS

Det(-)	determinant of
E(-)	expected value of
exp(-)	exponential function
Im(-)	imaginary part of
Re(-)	real part of
sgn(-)	signum or sign function
$\delta(-)$	impulse function
.	derivative with respect to time or rate of change (superscript)
..	acceleration or second derivative with respect to time (superscript)

SYMBOLS

0	zero matrix
₵	centerline

α	angle of attack; prescribed degree of stability
α_{wc}	difference between airplane angle of attack with respect to the air and ideal model angle of attack
β	sideslip angle
Γ	disturbance distribution matrix, gamma function
Γ, Γ_a	gust distribution matrix
δ	control surface command; control surface vector
$\bar{\delta}$	steady aerodynamic states associated with δ
δ_A	commanded aileron angle
δ_{A_c}	outboard aileron command
δ_c	column angle; control column deflection
δ_{c_i}	ith control surface command
δ_E	commanded elevator angle
$\delta_{E'}$	intermediate state variable elevator actuator
δ_{E_c}	elevator deflection command
δ_i	ith control surface position
$\dot{\delta}_i$	ith control surface rate
$\ddot{\delta}_i$	ith control surface acceleration
δ_{kl}	Kronecker delta
Δ	change in quantity
ΔP	difference in pressure
ϵ	state estimate error vector
ζ	damping ratio
η	fraction of semispan (2 y/b)
θ	incremental pitch angle; input matrix in modal coordinates (discrete time); pitch attitude; pitch-rate sensor output; surface angular position
θ_i	phase at the ith control input

$\bar{\theta}_i$	unsteady aerodynamic states associated with $\dot{\theta}$
λ	failure rate
λ_i	ith system eigenvalue
Λ, Λ_a	diagonal or block diagonal state matrix
μ	micro
ξ	spatial separation vector
ξ_i	flexible mode displacements
σ	mean rms turbulence intensity
σ_d	discrete gust intensity
σ_i	real part of the complex eigenvalue λ_i
σ_u	longitudinal rms gust intensity
σ_{vw}	transverse rms gust intensity
τ	time lag; time constant
τ_f	time constant of filter
ϕ	roll attitude
Φ	mode shape matrix at ith station; output mode shape matrix; state transmission matrix in modal coordinate (discrete time)
Φ_L	load distribution matrix
ω	frequency, radians
ω_i	imaginary part of the complex eigenvalue λ_i

APPENDIX A: CRUCIAL FUNCTION CONFIGURATION FOR RELIABILITY

To meet the reliability requirements of the Essential Pitch-Augmented Stability (PAS) function in the Integrated System, it was necessary to select a level of redundancy, a configuration, and the components for this function. The reliability requirements for the other Active Controls Technology (ACT) functions, which are less severe, would also be met by this configuration.

RELIABILITY PREDICTION FOR THE ALTERNATIVE CONFIGURATIONS

The reliability prediction for the three initially selected system configurations was made with the computer-aided redundant system reliability analysis (CARSRA) computer program (see app B, subsec B.1.0), and software reliability and coverage were neglected.

The component failure rates used in this set of predictions were the preliminary estimates of the values to be expected; no allowances were made for airplane interconnect wiring or connector unreliability. The failure rates so obtained are not compatible with later calculations but are entirely adequate to show the relative merits of the several versions. Table A-1 shows the calculated failure rates for three configurations and five cases evaluated. The configurations and cases in Table A-1 are defined as follows:

Configuration 1   Quadruple redundancy; hardwired cross strapping of sensor outputs; only Q sensors (short-period PAS); no computer intercommunication; sensor voting within each computer

Configuration 2   Same as configuration 1, except that hardwired cross strapping is replaced with computer cross-channel communication

Configuration 3   Same as configuration 2, except that electronic voting (λ = 71.4 x 10^{-6} per flight hour failure rate) is inserted between computers and actuators

Table A-1. Quadruple-Channel System Configuration Comparison

Case	Description of case	Configuration 1	Configuration 2	Configuration 3
		Sensor Computer Actuator	Sensor Computer Actuator	Sensor Computer Actuator
A	4 IRS Q sensors, $\lambda = 263$ 4 computers, $\lambda = 250$ 4 mechanical, actuators λ (includes hydraulics) = 56.6	1.87×10^{-10}	5.92×10^{-10}	5.47×10^{-10}
B	Like A, except 3 mechanical actuators and a mathematical model, $\lambda = 0$	1.48×10^{-10}	5.53×10^{-10}	5.42×10^{-10}
C	Like B, except 3 IRS-based Q sensors, $\lambda = 263$, and 1 VYRO Q sensor, $\lambda = 73$	9.52×10^{-11}	3.51×10^{-10} selected configuration	3.4×10^{-10}
D	Like C, except all Q from VYRO sensors	7.56×10^{-11}	8.13×10^{-11}	7.12×10^{-11}
E	Like D, except a different computer, $\lambda = 167$	2.49×10^{-11}	2.75×10^{-11}	2.4×10^{-11}

Notes: 1. Figures indicate short-period PAS reliability as probability of failure per 1-hr flight given that software reliability and coverage are neglected.

2. Failure rates (λ) of components per 10^6 hr.

3. Table shows probability of function loss during a 1-hr flight assuming fault-free software and coverage = 1.0.

Case A   Four Q sensors based on inertial reference system (IRS); computers with failure rates, $\lambda = 250 \times 10^{-6}$ each per flight hour

Four mechanical secondary actuators (failure rate, $\lambda = 31.6 \times 10^{-6}$ each per flight hour)

Three hydraulic systems (failure rate, $\lambda = 25 \times 10^{-6}$ each per flight hour)

Case B   Same as case A, except three mechanical secondary actuators plus one mathematical model

Case C   Same as case B, except three IRS-based Q sensors and one dedicated Q sensor

Case D   Same as case C, except all dedicated Q sensors

Case E   Same as case D, but using a more reliable computer (failure rate, $\lambda = 167 \times 10^{-6}$ per flight hour)

As shown in Table A-1 (under stated analysis assumptions), all three configurations meet the reliability requirements. Configuration 2, case C in Table A-1, was selected for the Integrated System after considering system implementation complexity and reliability.

A similar study was conducted to investigate the feasibility of triply redundant channels. The results are shown in Table A-2. No version of the triply redundant PAS meets the requirements.

Table A-1 shows that when sensors and computers have high reliability, cross strapping between the sensors and computers has little effect. The same is observed for a system with a voter between the computers and the actuators. It is not expected that any foreseeable improvement in component reliability will permit the triply redundant crucial PAS system to meet the requirements.

Table A-2. Three-Channel Configuration Comparison

Requirements:		3 actuators + 1 mathematical model		2 actuators + 1 mathematical model	
At least 2 ———————→ At least 2 ———————→ At least 2 ———————→ {		Case A: 3 IRS Q sensors 3 computers 3 hardware actuators 1 mathematical model	Case B: 3 dedicated Q sensors 3 computers 3 hardware actuators 1 mathematical model	Case C: 3 IRS Q sensors 3 computers 2 hardware actuators 1 mathematical model	Case D: 3 VYRO sensors 3 computers 2 hardware actuators 1 mathematical model
Sensor Computer Secondary actuator Configuration 5	Mechanical voter	3.95×10^{-7}	1.88×10^{-7}	3.98×10^{-7}	1.91×10^{-7}
Sensor Computer Secondary actuator Configuration 6	Mechanical voter	7.89×10^{-7}	1.99×10^{-7}	8.34×10^{-7}	2.44×10^{-7}

Note: Figures indicate probability of function loss during a 1-hr flight neglecting software reliability and coverage.

**APPENDIX B: RELIABILITY
MODELING METHODS**

APPENDIX B: RELIABILITY MODELING METHODS

B.1.0 CARSRA PROGRAM

Reliabilities of the alternative Essential Pitch-Augmented Stability (PAS) configurations were determined with the aid of the computer-aided redundant system reliability analysis (CARSRA) computer program, which was developed during the NASA-Boeing Airborne Advanced Reconfigurable Computer System (ARCS) Program (ref B-1).

The CARSRA computer program was designed for and is particularly suited to systems with redundant stages, which it defines as "sets of identical redundant modules." CARSRA can accommodate complicated systems because it splits them into stages and uses stage Markov diagrams, instead of the Markov diagram of the entire system, to develop the logic. Because all components in a stage are identical by definition, there is no need to distinguish which module fails first, which second, and so forth. For systems with a set of redundant modules performing the same function but having different failure rates, the program adaptability is limited. The program also makes some approximations; e.g., it truncates calculations of dependency-stage failures at two module failures (extendable to three in the high-accuracy mode). This may not always provide enough accuracy.

An example of a CARSRA reliability calculation is the Active Controls Technology (ACT) function shown as a block diagram in Figure B-1. This is a redundant system with three velocity inputs from the digital air data computer (DADC), three control column force sensor inputs, three pitch-rate inputs from the inertial reference system (IRS), and one pitch-rate input from a dedicated pitch-rate sensor. There are three mechanical actuators and a mathematical model of an actuator simulated in each computer. At least two of each kind of component must be functional or the system is considered to have failed. All sensors and actuators are connected to and dependent upon the four computers. This dependency means that the loss of one computer results in loss of the sensors and actuator in that channel. Each actuator is also dependent upon its hydraulic power source, but in this problem a single failure rate was used for each actuator and its hydraulic system. If realistically different failure rates for the three hydraulic systems had been assumed, CARSRA could not have handled this prediction.
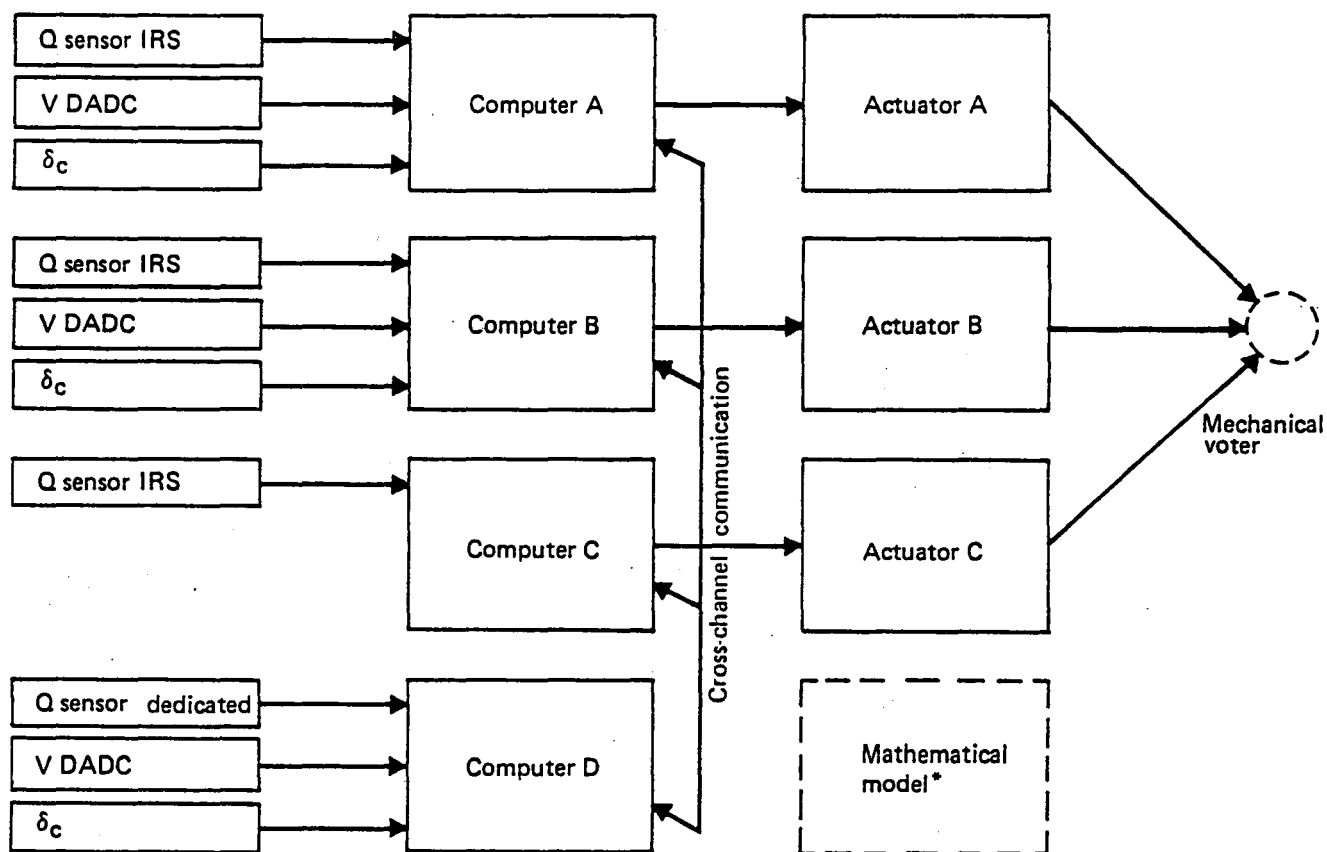
Figure B-1. Block Diagram for an ACT Function

The mathematical model of Figure B-1 is not actual hardware, but a computed simulation assumed to be perfectly reliable. For this prediction, the mechanical voter is also assumed to be perfectly reliable.

Figure B-2 numbers the components according to stage and channel. For example, the third-channel velocity sensor is number 223 (stage 22, channel 3). A dependency matrix composed of these numbers, as shown in Figure B-2, is entered into the computer.

Each computer, velocity sensor, or column force sensor set is identified as a stage. In the CARSRA model, however, a stage must consist of identical redundant components, so the Q sensors (one of which is different) cannot be considered to be one stage. CARSRA permits listing each Q sensor as a stage and declaring in another matrix which of these stages may be permitted to fail without system loss. In this instance, all combinations of

Q sensors taken two or fewer at a time (11 combinations) must be listed. The mathematical model and the real actuators also have different failure rates, but because the mathematical model was considered perfectly reliable, the requirement for at least two working components in the stage may be restated as "at least one working real actuator." Had it been necessary to apply the technique used on the Q sensors, this problem would have been beyond the capability of CARSRA.

The heart of the CARSRA process is the ability to use several simple stage Markov models instead of one system Markov model. In Figure B-3, the circled numbers represent states. The numbers at the bottom of each diagram indicate system failure state and hidden failure state. The transition rates, $_n\lambda_{mp}$, represent the transition (failure) rate between the state m and p for stage n. Table B-1 lists the values for these transitions. These values are the main data entries to CARSRA.
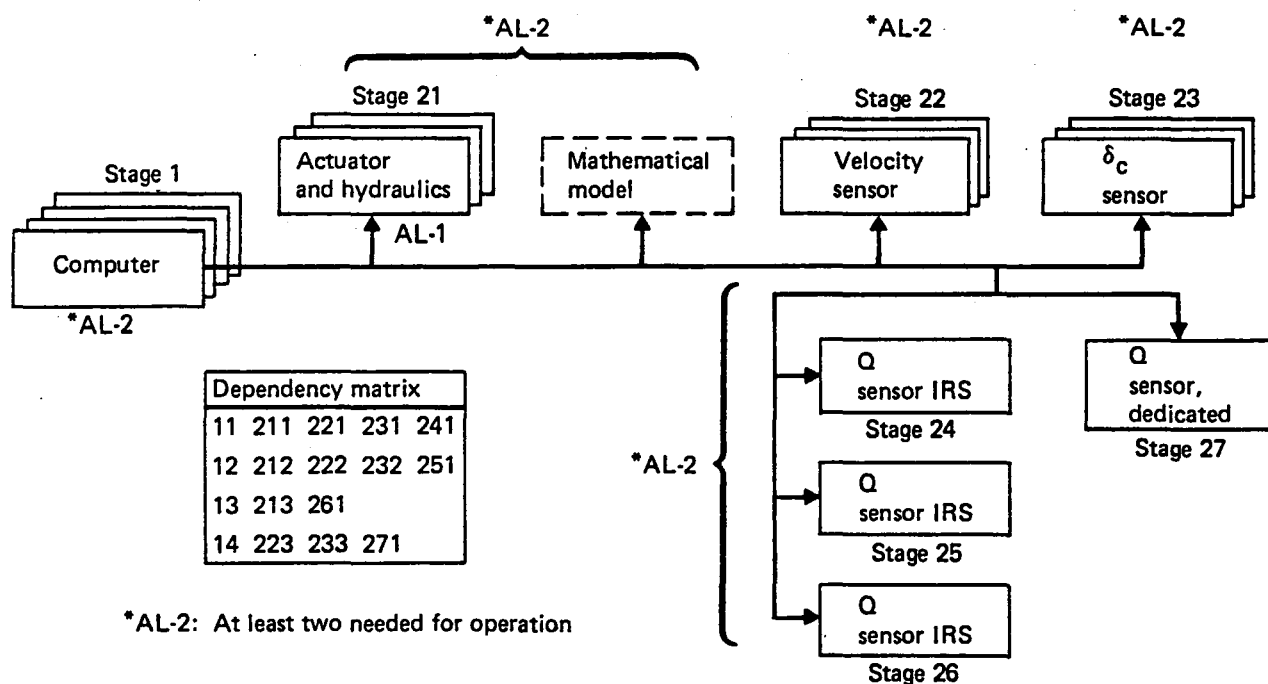
Figure B-2. Dependency Diagram and Matrix for Function in Figure B-1
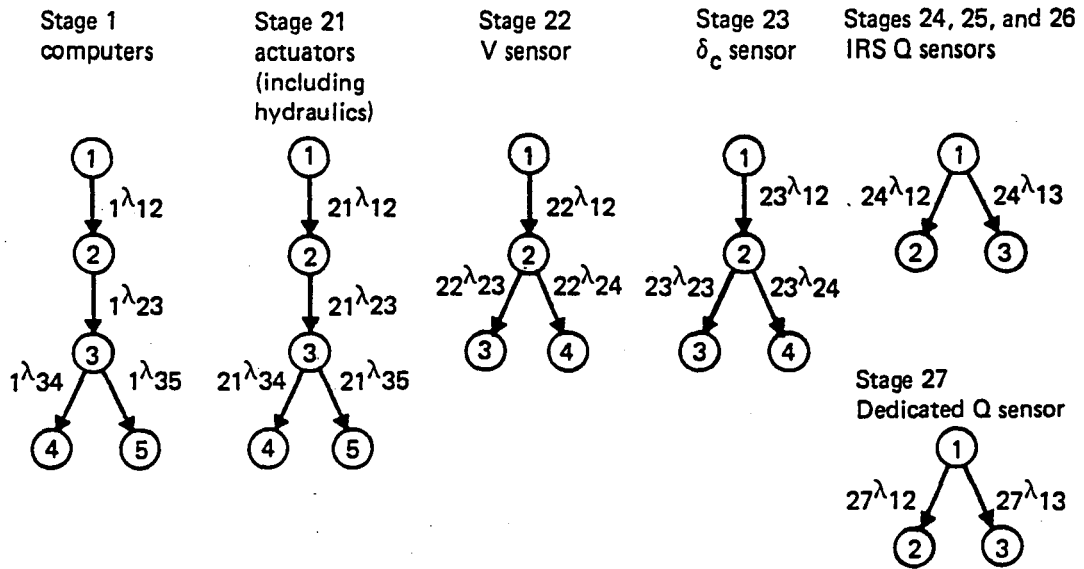
Figure B-3. Stage Markov Models

Table B-1. State Transition Rates

Stage		Failure rate per 10^6 hr	λ_{12}	λ_{23}	λ_{34}	λ_{35} or λ_{13} or λ_{24}
1	Computers	150.6	602.0	452.0	301.0	0
21	Actuator and hydraulics	38.6	201.6	134.4	67.2	0
22	V sensors	85.0	250.0	170.0	—	0
23	δ_c sensors	13.6	41.0	7.2	—	0
24,25,26	IRS Q sensors	418.0	418.0	—	—	0
27	Dedicated Q sensors	9.86	9.86	—	—	0

B.2.0 FTREE PROGRAM

B.2.1 REQUIREMENT FOR AN IMPROVED SOLUTION

The ACT systems are composed of so many parts with multiple interconnections and multiple-occurring events that manual calculation of system reliabilities is not practical. Early studies in Active Controls Technology (ref B-2) were accomplished with CARSRA. The limited capacity of CARSRA required a change to another program, FTREE (fault tree), developed at The Boeing Company. The advantages of this program will be apparent in the following example of its use.

B.2.2 FTREE REQUIREMENTS AND METHODS

Inputs to FTREE are derived from a reliability fault tree model for the system under consideration. The tree is built from standard logic symbols and the shorthand symbols shown and defined in Figure B-4. Fault trees for all ACT functions are drawn in the standard format (see fig. B-5). The input events are numbered in a consecutive series, each event having the same number wherever it appears. There may be no more than 1000 input events. Starting with a number greater than the last input event, the logic gates are then numbered in a consecutive series with the requirement that no gate may feed into a lower numbered gate. A logic gate may be multiple occurring if no other multiple-occurring event or logic gate is an input to it. Should such a combination occur, it is possible to assign a different number to the higher gate wherever it occurs. The maximum number of gates and input events combined may not exceed 2000. Normally, the number of multiple-occurring events is limited to 70. That number can be increased, but numbers above about 50 become expensive to run. The highest sequentially numbered logic gate, referred to as the top gate in any function, represents failure of that function. The computer program calculates the probability of failure for the output of each gate, including the top gate, which represents failure of the function.

A system fault tree can be composed of all the individual ACT function fault trees if the gates are numbered in one continuous sequence. This offers several advantages; e.g., evaluation of the probabilities of combinations of functions. Figure B-5 illustrates, in a condensed form, such a combination. The lowest gates are all the top gates of single ACT functions and actually represent an entire fault tree of that function with all its input

Gate name	Code	Symbol	Remarks
AND	A	(o)	All of two or more failures must occur to fail next higher event.

$P(I) = P1 * P2^* .... PN$

| OR | O | (+) | Any one or more of a number of failure events will cause next event to fail. |

$P(I) = 1 - \quad (1-P1)(1-P2) ... (1-PN)$

CONDITIONAL-SEQUENTIAL-AND

| | C | (C) | All of two or more failure events must occur in a specific sequence to fail next event. |

$P(I) = \dfrac{P1 * P2 .... PN}{N!}$

where N = number of input events

| STANDBY | S | (S) | To fail next event, five failure events must be considered as follows: |

$P(I) = P1^*P4+(P1^*P2+P1^*P3^*+P2^*P5+ P3^*P5)/2.0$

1. Active component fails during operation

2. Passive component fails during standby

3. Passive component fails during operation

4. Switching device fails to switch

5. Switching device inadvertently switches

(A zero probability of failure may be assigned to any of these input event probabilities. The logic statement in the data file must list the input events in the precise order stated here.)

| M of N | M | (M/N) | Failure of any "m" or more of "n" input failure events will fail the next event; e.g., m=2, n=3; thus, any two of the three inputs. "n" may not exceed 20. |

P(I) is calculated by a summing of the minterm probabilities

| EXCLUSIVE OR | | (DESCRIPTION) | In FTREE this condition is best modeled by using an "OR," an "AND," and an INVERT gate. |

$P(I) = P1 + P2 * P1$

| INVERT | V | (V) | The next event probability is one minus the failure event probability. |

$P(I) = 1-P1$

| INPUT | I | O | The failure probability fed into the model in the form of a failure rate and time or directly as a probability. |

$P(I) = P1$

Figure B-4. Fault Tree Logic Symbols
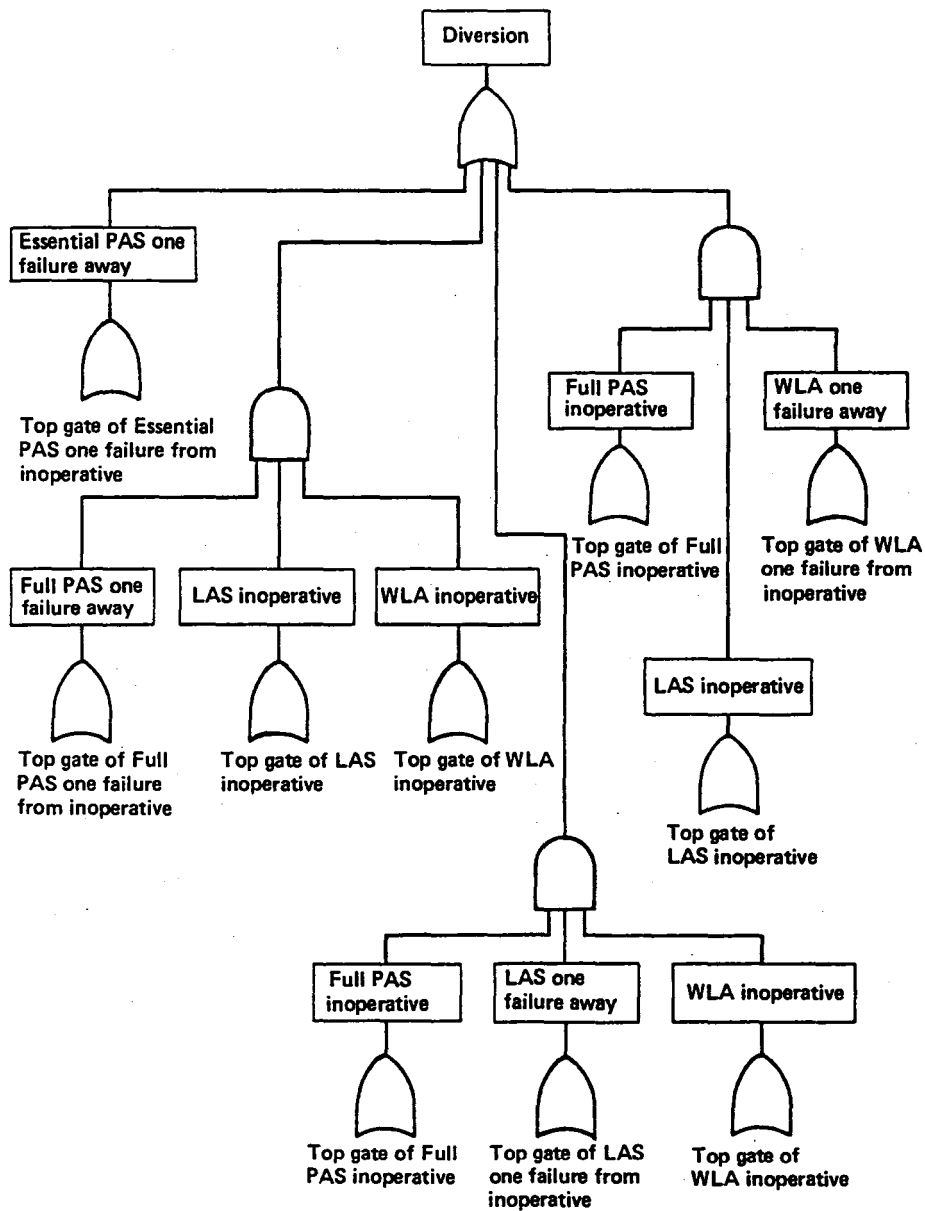
Figure B-5. Fault Tree for the Probability of Diversion Upon One Failure Away From Function Loss

events. In this way, the computer model can take account of multiple-occurring events throughout the tree.

Excerpts from a typical input file for the FTREE program, including all ACT functions, are shown in Figure B-6.

REVACT DATA ALL FUNCTIONS 8 20 80 ————— Name and date of file

1 2 ——————————————————————— Option 1, failure combinations taken two at a time

10 119 200 386 1.D-6 200 ———10 through 119 are input events, 200 through 386 are logic gates

0 ———— All failure rates times 10^{-6} per hr

1.0 ———— Specified multiple-occurring events; none

———— Time (flight duration)

```
10   2  1 ⎫
11   2  1 ⎪   Actuators, aileron, outboard inner segment; failure rate
12   2  1 ⎬   2 x 10⁻⁶/hr; exposure = 1 hr (two left and two right)
13   2  1 ⎭
14  35.9 1 ⎫
15  35.9 1 ⎪   Actuators, aileron, outboard outer segment; failure rate
16  35.9 1 ⎬   35.9 x 10⁻⁶/hr; exposure = 1 hr (two left and two right)
17  35.9 1 ⎭
18  29.6 1 ⎫
19  29.6 1 ⎪   Actuators, flaperon, inboard; failure rate 29.6 x 10⁻⁶/hr;
20  29.6 1 ⎬   exposure = 1 hr (two left and two right)
21  29.6 1 ⎭
22  29.6 1 ⎫
23  29.6 1 ⎪   Actuators, flaperon, outboard; failure rate 29.6 x 10⁻⁶/hr;
24  29.6 1 ⎬   exposure = 1 hr (two left and two right)
25  29.6 1 ⎭
26  38.6 1 ⎫
27  38.6 1 ⎬   Actuators, elevator, secondary; failure rate
28  38.6 1 ⎭   38.6 x 10⁻⁶/hr; exposure = 1 hr
29  37.4 1 ⎫   Actuators, rudder, secondary; failure rate 37.4 x 10⁻⁶/hr;
30  37.4 1 ⎭   exposure = 1 hr
31  50  1
32  50  1      Actuators, stick pusher; failure rate 50.0 x 10⁻⁶/hr; exposure = 1 hr
```

```
116 11  1
117 13.6 1 ⎫
118 13.6 1 ⎬   Last input events
119 13.6 1 ⎭
                              First gates
200 0 49 52 77 80 83 ⎫ Three DADC velocity functions made up of primary computer input set OR
201 0 50 53 78 81 84 ⎬ primary computer common parts OR sensor dynamic pressure OR DADC
202 0 51 54 79 82 85 ⎭ computer parts
203 2 200 201 202 ————— Velocity from three DADC—at least two must fail for signal to be lost
204 0 49 52 86 89 95 98 ⎫ Pitch angles computer input set OR computer common parts OR IRS pitch
205 0 50 53 87 90     ⎬ rate analog OR IRS yaw rate OR IRS remaining parts (computer) OR IRS
                      ⎭ common parts
```

```
384 A 381 382 383   Elevator actuation; three secondary actuation top gate "AND'ed" together
385 0 375 380 384   Essential PAS; Q sensors, computers, and elevator actuation "OR'ed" together
386 0 235 265 323   Top gate, Full PAS OR LAS OR FMC failed
EOF:
E>
```

Figure B-6. Typical Fault Tree Input File

Figure B-7 shows how the computer prints out successive approximations to the top gate reliability and prompts the user about options when the operation is accomplished in the interactive mode on a terminal. In the illustrated instance, because the problem was familiar, the operator elected to bypass option 1, which provides an inexpensive troubleshoot of the entry file, and went directly to option 3. This option, in addition to giving failure rates at all logic gates, causes the computer to print out sensitivities of the top gate to all multiple-occurring events. The computer calculates the failure probability of the top gate (the last gate in fig. B-6) truncated at combinations of failed components taken up to two at a time, as previously selected in line 2 of the control block, Figure B-6. It then informs the operator that the solution is still converging on the true answer, asks if combinations up to three at a time should be tried, and displays a number of computer service units (CSU) accumulated in the session. CSUs are a measure of the cost of running the program and enable the user to estimate the cost of running additional failure combinations. In this instance, another combination was authorized, but an opportunity to assess four combinations was turned down. The total output was then printed out at a remote terminal.

Figure B-8 shows excerpts from the remote terminal printout of the FTREE results, annotated to show the identity of the logic gates and input events. Each output event represents a logic gate in the combined fault tree of all ACT functions. The top gate, an OR gate, selects Full PAS, lateral/directional-augmented stability (LAS), and flutter-mode control (FMC) and combines them to show the probability that any one or more of the functions will become inoperable in a 1-hr flight. This represents the probability of having to institute a flight restriction while in flight.

A notable advantage of FTREE is that, in one computer run, not only the top gate reliability but many other reliabilities are displayed. For example, opposite gate 235 is the probability that Full PAS will fail. Within Full PAS, gate 203 is the probability that the airspeed output signals from three DADCs will be reduced to fewer than two signals. Gate 208 gives the probability that both the DADCs and their backup function (pitch angle from the IRS) will be reduced below the minimum two outputs. Gate 226 gives the probability that the Full PAS function will fail for loss of some sensor input. It is apparent that such information can be useful in design optimization.

```
C>FTREE

        FTREE(FAULT TREE) PROGRAM
                VERSION A.1



        ENTER INPUT FILENAME AND FILETYPE.

>REVACT DATA
EXECUTION BEGINS...


 IF YOU WANT TO CHANGE THE OPTION ENTER OPTION NUMBER(1,2 OR 3)
 (IF YOU WANT TO KEEP OPTION SPECIFIED IN THE INPUT FILE, HIT CR)


>3
 FAILURE    UNRELIABILITY        RELIABLITY        GATE       CSU


    1        1.094D-07    0.9999998905774120        386         87
    2        5.972D-07    0.9999994028494359        386        494

 THE DIFFERENCE BETWEEN  2 FAILURES AND  1 FAILURES IS GREATER THAN 1.D-13

  DO YOU WANT TO RUN ANOTHER FAILURE COMBINATION?


>YES
    3        5.978D-07    0.9999994022342390        386       7650

 THE DIFFERENCE BETWEEN  3 FAILURES AND  2 FAILURES IS GREATER THAN 1.D-13

  DO YOU WANT TO RUN ANOTHER FAILURE COMBINATION?


>NO

        DO YOU WANT THE ANALYSIS OUTPUT TO :

            1. THE TERMINAL - TYPE 'PRINT'
            2. A FILE       - TYPE 'FILE'
            3. BOTH         - TYPE 'BOTH'


>2

        PLEASE ENTER FILENAME FILETYPE FOR YOUR OUTPUT FILE.

>DDD DATA

    DO YOU WANT TO MAKE ANOTHER RUN?
        ('YES' OR 'NO')

>NO
R;

C>SPOOL PRINTER TO RIO DIST REMOTE Q 3 CONT
```

Figure B-7. Interactive Terminal Printout

OPTION 3, SUMMARY OF THE SYSTEM PROBABILITIES.
         VERSION NO. 1.A

FLIGHT HOURS (FH): 1= 1.000D+00

INPUT EVENT	UNRELIABILITY	RELIABILITY	GATE TYPE	HOURLY RATE			FH	
OUTPUT EVENT	UNRELIABILITY	RELIABILITY	GATE TYPE	GATE INPUT				
200	1.736D-04	0.9998264150677376	C	49 52 77 83			80	Airspeed from DADC
201	1.736D-04	0.9998264150677376	C	50 53 78 84			81	
202	1.736D-04	0.9998264150677376	C	51 54 79 85			82	
203	9.038D-08	0.9999999090961535+7	2	200 201 202				
204	2.827D-04	0.9997172599787033	C	49 52 86 89 95 98				
205	2.827D-04	0.9997172599787033	C	50 53 87 90 96 99				Pitch angle from IRS
206	2.827D-04	0.9997172599787033	C	51 54 88 91 97 100				
207	2.398D-07	0.9999997602196518	2	204 205 206				
208	2.574D-08	0.9999999742626313	A	203 207				Both above sensors
209	1.439D-04	0.9998560703599861	C	49 52 86 98				
210	1.439D-04	0.9998560703599861	C	50 53 87 99				Pitch angular rate
211	1.439D-04	0.9998560703599861	C	51 54 88 100				from IRS
212	6.214D-08	0.9999999378598136	2	209 210 211				
213	1.062D-04	0.9998937856412365	C	49 52 101				
214	1.062D-04	0.9998937856412365	C	50 53 102				Column force
215	1.062D-04	0.9998937856412365	C	51 54 103				
216	3.384D-08	0.9999999661577705	2	213 214 215				
217	1.554D-04	0.9998446120740853	C	49 52 77			80	
218	1.554D-04	0.9998446120740853	C	50 53 78			81	Dynamic pressure, q,
219	1.554D-04	0.9998446120740853	C	51 54 79			82	from DADC
220	7.243D-08	0.9999999275713665	2	217 218 219				
221	1.036D-04	0.9998964053663846	C	49 52 114				
222	1.036D-04	0.9998964053663946	C	50 53 115				Flap position
223	1.036D-04	0.9998964053663846	C	51 54 116				(backup for q)
224	5.219D-08	0.9999999478567212	2	221 222 223				
225	2.572D-08	0.9999999742789577	A	220 224				q with backup
226	7.028D-08	0.9999999297245910	C	208 212 216	225			All sensors
227	1.332D-04	0.9998668088708349	C	43 49 52				
228	1.332D-04	0.9998668088708349	C	44 50 53				Computation
229	1.332D-04	0.9998668088708389	C	45 51 54				
230	5.321D-05	0.9999959467851602	2	227 228 229				
231	2.086D-04	0.9997914217556323	C	26 35 39	57			
232	1.356D-04	0.9998644091933742	C	27 36 40	58			
233	1.356D-04	0.9998644091933792	C	28 37 41	59			Elevator actuators
234	7.494D-06	0.9999925250603042	2	231 232 233				
235	1.727D-07	0.9999998272932571	C	226 230 234				Full PAS, top gate
236	1.554D-04	0.9998446120740859	C	49 52 77			80	
237	1.554D-04	0.9998446120740859	C	50 53 78			81	
238	1.554D-04	0.9998446120740859	C	51 54 79			82	
239	7.243D-08	0.9999999275713665	2	236 237 238				

Figure B-8. Fault Tree Computer Printout

240	1.0360-04	0.9998964053663846	C	49	52	114	
241	1.0360-04	0.9998964053663846	C	50	53	115	
242	1.0360-04	.9998964053663846	C	51	54	116	
243	3.2190-08	.9999995678067212	2	240	241	242	
244	2.5720-08	0.9999997427895 77	A	239	243		
245	1.0620-04	0.9998937856412365	C	49	52	101	
246	1.0620-04	.9998937856412365	C	50	53	102	
247	1.0620-04	.9998937856412365	C	51	54	103	
248	3.3840-08	0.9999996615/9705	2	245	246	247	
249	3.1440-04	0.9996855994344449	C	49	52	86	89
				92	95	98	
250	3.1440-04	.9996855994344449	C	50	53	87	90
				93	96	99	
251	3.1440-04	0.9996855994344449	C	51	54	88	91
				94	97	100	
252	2.9650-07	.9999970351924 51	2	249	250	251	
253	1.0360-04	.9998964053663846	C	49	52	114	
254	1.0360-04	0.9998964053663846	0	50	53	115	
255	1.0360-04	0.9998964053663846	C	51	54	116	
256	3.2190-08	0.9999995678067212	2	253	254	255	
257	3.1110-07	.9999996889307135	C	244	248	252	256
258	1.3320-04	.9998668088708389	C	43	49	52	
259	1.3320-04	0.9998668088708349	C	44	50	53	
260	1.3320-04	0.9998668088708384	C	45	51	54	
261	5.3210-08	0.9999994678516 02	2	258	259	260	
262	2.0240-04	0.9997976204816349	C	29	43	46	49
				52	59		
263	2.0240-04	.9997976204816349	C	30	44	47	50
				53	58		
264	4.0960-08	0.9999995904 25666	A	262	263		
265	3.6180-07	0.9999996382384330	C	257	261	264	← LAS top gate
266	1.4390-04	0.9998560703589861	C	49	52	86	98
267	1.4390-04	0.9998560703589861	C	50	53	87	99
268	1.4390-04	.9998560703589861	C	51	54	88	100
269	6.2140-08	0.9999999378588136	2	266	267	268	
270	1.8160-04	0.9998184164883776	C	49	52	74	80
271	1.8160-04	0.9998184164883776	C	50	53	75	81
272	1.8160-04	.9998184164883776	C	51	54	76	82
273	9.8910-08	0.9999990109430 69	2	270	271	272	
274	1.5540-04	0.9998446120740839	C	49	52	77	80
275	1.5540-04	.9998446120740839	C	50	53	78	81
276	1.5540-04	.9998446120740839	C	51	54	79	82
277	7.2430-08	0.9999999275713663	2	274	275	276	
278	1.0620-04	0.9998938056391013	C	49	52	117	
279	1.0620-04	0.9998938056391013	C	50	53	118	
280	1.0620-04	.9998938056391013	C	51	54	119	
281	3.3830-08	0.9999999661707024	2	278	279	280	
282	1.0360-04	.9998964053663846	C	49	52	114	
283	1.0360-04	0.9998964053663846	0	50	53	115	
284	1.0360-04	0.9998964053663846	C	51	54	116	
285	3.2190-08	0.9999999678067212	2	282	283	284	
286	1.8550-07	.9999998145028384	C	269	273	277	281
				285			
287	1.3320-04	0.9998668088708389	C	43	49	52	
288	1.3320-04	.9998668088708399	C	44	50	53	
289	1.3320-04	.9998668088708399	C	45	51	54	
290	5.3210-08	0.9999999467851602	2	287	288	289	
291	1.6630-04	0.9998337138272048	C	43	46	49	52
				110			
292	1.5100-04	.9998490114000524	C	44	47	50	53
293	1.5100-04	.9998490114000524	C	45	48	51	54

Figure B-8. Fault Tree Computer Printout (Continued)

294	2.286D-08	0.9999999772024733	A	292	293		
295	1.532D-05	0.9999846773198666	C	111	294		
296	2.316D-04	0.9997684040250833	C	31	291	295	
297	1.510D-04	0.9998490114000524	C	43	46	49	52
298	1.510D-04	0.9998490114000524	C	44	47	50	53
299	2.286D-08	0.9999999772024733	A	297	298		
300	1.532D-05	0.9999846773198666	C	113	299		
301	1.663D-04	0.9998337138272046	C	45	48	51	54
				112			
302	2.316D-04	0.9997684040250833	C	32	300	301	
303	9.921D-08	0.9999999007853862	A	296	302		
304	2.593D-07	0.9999997410323336	C	286	290	303	◄── AAL top gate
305	1.554D-04	0.9998446120740859	C	49	52	77	80
306	1.554D-04	0.9998446120740859	C	50	53	78	81
307	1.554D-04	0.9998446120740859	C	51	54	79	82
308	7.243D-08	0.9999994275713663	2	305	306	307	
309	2.013D-04	0.9997987202595665	C	49	52	62	65
310	2.013D-04	0.9997987202595665	C	50	53	63	66
311	2.013D-04	0.9997987202595665	C	51	54	64	67
312	1.215D-07	0.9999998784757415	2	309	310	311	
313	1.332D-04	0.9998668088708389	C	43	49	52	
314	1.332D-04	0.9998668088708389	C	44	50	53	
315	1.332D-04	0.9998668088708389	C	45	51	54	
316	5.321D-08	0.9999999467851602	2	313	314	315	
317	1.670D-04	0.9998330139438620	C	10	43	46	49
				52	58		
318	1.670D-04	0.9998330139438620	C	11	44	47	50
				53	59		
319	2.768D-08	0.9999999721156959	A	317	318		
320	2.400D-04	0.9997600287378890	C	12	43	46	49
				52	57		
321	1.670D-04	0.9998330139438620	C	13	44	47	50
				53	59		
322	4.070D-08	0.9999999599242256	A	320	321		
323	2.210D-07	0.9999997739909922	C	308	312	316	319 ◄── FMC top gate
				322			
324	2.013D-04	0.9997987202595665	C	49	52	68	71
325	2.013D-04	0.9997987202595665	C	50	53	69	72
326	2.013D-04	0.9997987202595665	C	51	54	70	73
327	1.215D-07	0.9999998784757415	2	324	325	326	
328	1.554D-04	0.9998446120740859	C	49	52	77	80
329	1.554D-04	0.9998446120740859	C	50	53	78	81
330	1.554D-04	0.9998446120740859	C	51	54	79	82
331	7.243D-08	0.9999999327571363	2	328	329	330	
332	1.062D-04	0.9998937856412365	C	49	52	101	
333	1.062D-04	0.9998937856412365	C	50	53	102	
334	1.062D-04	0.9998937856412365	C	51	54	103	
335	5.384D-08	0.9999999661579705	2	332	333	334	
336	1.553D-04	0.9998447420538921	C	49	52	92	98
337	1.553D-04	0.9998447420538921	C	50	53	93	99
338	1.553D-04	0.9998447420538921	C	51	54	94	100
339	7.231D-08	0.9999999276924806	2	336	337	338	
340	2.229D-07	0.9999997708144412	C	327	331	335	339
341	1.332D-04	0.9998668088708389	C	43	49	52	
342	1.332D-04	0.9998668088708389	C	44	50	53	
343	1.332D-04	0.9998668088708389	C	45	51	54	
344	5.321D-08	0.9999999467851602	2	341	342	343	
345	2.086D-04	0.9997914217556308	0	26	35	39	57
346	1.356D-04	0.9998644091933742	C	27	36	40	58
347	1.356D-04	0.9998644091933742	C	28	37	41	59

Figure B-8. Fault Tree Computer Printout (Continued)

349	7.4940-08	0.9999993250603042	2	345	346	347	
349	2.6760-04	0.9997324358019700	C	22	43	46	45
				52	57		
350	1.9460-04	0.9998054189334846	C	23	44	47	50
				53	58		
351	5.2060-08	0.9999999479371223	A	349	350		
352	2.6760-04	0.9997324358018730	C	24	43	46	49
				52	57		
353	1.9460-04	0.9998054189334836	C	25	44	47	50
				53	58		
354	5.2060-08	0.9999999479371223	A	352	353		
355	2.0090-04	0.9997991201791905	C	14	43	46	49
				52	58		
356	2.0090-04	0.9997991201791905	C	15	44	47	50
				53	59		
357	4.0350-08	0.9999959596473337	A	355	356		
358	2.7390-04	0.9997261375073641	C	16	43	46	49
				52	57		
359	2.0090-04	0.9997991201791905	C	17	44	47	50
				53	59		
360	5.5010-08	0.9999999449866009	A	358	359		
361	2.6760-04	0.9997324358018730	C	18	44	47	50
				53	57		
362	1.9460-04	0.9998054189334846	C	19	45	48	51
				54	58		
363	5.2060-08	0.9999999479371223	A	361	362		
364	2.6760-04	0.9997324358018730	C	20	44	47	50
				53	57		
365	1.9460-04	0.9998054189334836	C	21	45	48	51
				54	58		
366	5.2060-08	0.9999999479371223	A	364	365		
367	1.6700-04	0.9998330139438620	C	10	43	46	49
				52	58		
368	1.6700-04	0.9998330139438620	C	11	44	47	50
				53	59		
369	2.7880-08	0.9999999721156939	A	367	368		
370	2.4000-04	0.9997600287978803	C	12	43	46	49
				52	57		
371	1.6700-04	0.9998330139438620	C	13	44	47	50
				53	59		
372	4.0070-08	0.9999999599282056	A	370	371		
373	2.3470-07	0.9999997653289723	C	348	351	354	357
				360	363	366	369
				372			
374	4.4960-07	0.9999995504411301	C	340	344	373	← WLA top gate
375	4.1210-15	0.9999999999999959	2	104	105	106	107
376	8.3000-05	0.9999170034444775	C	35	39		
377	8.3000-05	0.9999170034444775	C	36	40		
378	8.3000-05	0.9999170034444775	C	37	41		
379	8.3000-05	0.9999170034444046	C	38	42		
380	2.2860-12	0.9999999999977141	2	376	377	378	379
381	2.0860-04	0.9997914217556308	C	26	35	39	57
382	1.3560-04	0.9998644091933792	C	27	36	40	58
383	1.3560-04	0.9998644091933792	C	28	37	41	59
384	3.8290-12	0.9999999999961712	A	381	382	383	
385	5.5480-12	0.9999999999944521	C	375	380	384	← Essential PAS top gate
386	5.9780-07	0.9999994022542340	C	235	265	323	← Full PAS or LAS or FMC

Figure B-8. Fault Tree Computer Printout (Continued)

B-14

SENSITIVITIES OF MULTIPLE OCCURING EVENTS TO TOP EVENT 386

EVENT NO.	UNRELIABILITY	DELTA PROBABILITY	TOP PROB	RANK
10	2..000-06	0.00000000033367239	5.9740-07	53
11	2...00L-06	0.000000000033363467	5.9740-07	52
12	2.0000-06	0.00000000033367210	5.9740-07	54
13	2..000-06	0.00000000047961018	5.9730-07	51
26	3.4600-05	0.00000001046380662	5.8730-07	34
27	3.4600-05	0.00000001329046218	5.8450-07	26
28	3.8600-05	0.00000001329046326	5.8450-07	25
35	1.410C-05	0.00000000033322222421	5.9390-07	44
36	1.4100-05	0.00000000485109353	5.9290-07	42
37	1.4100-05	0.00000000485109392	5.9290-07	41
39	6.8900-05	0.00000001867790844	5.7910-07	19
40	6.8900-05	0.00000002370564202	5.7410-07	17
41	6.8900-05	0.00000002570564395	5.7410-07	11
43	4..600-05	0.00000001143433002	5.8340-07	21
44	4.0600-05	0.00000001737336720	5.7990-07	20
45	4.0600-05	0.00000001030473589	5.8700-07	33
46	1.7800-05	0.00000000331975870	5.9380-07	43
47	1.7800-05	0.00000000546761594	5.9230-07	40
48	1.7800-05	-0.00000000000001080	5.9780-07	55
49	6.6600-05	0.00000007914353902	5.1860-07	2
50	6.6600-05	0.00000008492925362	5.1250-07	1
51	6.6600-05	0.00000007334342472	5.2440-07	6
52	2.6000-05	0.00000003066614000	5.6690-07	9
53	2.6000-05	0.00000003331548223	5.6460-07	8
54	2.6000-05	0.00000002863193567	5.6910-07	10
57	8.7000-05	0.00000003687976317	5.6090-07	7
58	1.4000-05	0.00000000953061806	5.8820-07	36
59	1.4000-05	0.00000000961859896	5.8810-07	35
77	4.4600-05	0.00000001384931475	5.8390-07	23
78	4.4600-05	0.00000001384967734	5.8390-07	22
79	4.4600-05	0.00000001304895922	5.8390-07	24
80	1.8200-05	0.00000000565144074	5.9210-07	38
81	1.8200-05	0.00000000565154706	5.9210-07	37
82	1.8200-05	0.00000000565129403	5.9210-07	39
86	2.0340-05	0.00000001277977648	5.8500-07	29
87	2.0340-05	0.00000001277994001	5.8530-07	27
88	2.0340-05	0.00000001277961252	5.8500-07	31
89	2.0340-05	0.00000001277977648	5.8500-07	30
90	2.0340-05	0.00000001277994001	5.8500-07	28
91	2.0340-05	0.00000001277961252	5.8500-07	32
92	3.1670-05	0.00000001989861463	5.7790-07	14
93	3.1670-05	0.00000001989885926	5.7790-07	13
94	3.1670-05	0.00000001989835934	5.7790-07	15
95	1.1850-04	0.00000007445811596	5.2330-07	4
96	1.1850-04	0.00000007445906884	5.2330-07	3
97	1.1850-04	0.00000007445716065	5.2330-07	5
98	3.1000-05	0.00000001947765961	5.7830-07	17
99	3.1000-05	0.00000001947783885	5.7830-07	16
100	3.1000-05	0.00000001947738372	5.7830-07	18
101	1.3620-05	0.00000000289021214	5.9490-07	46
102	1.3620-05	0.00000000289032164	5.9490-07	45
103	1.3620-05	0.00000000289010235	5.9490-07	47
114	1.1000-05	0.00000000227661510	5.9550-07	49
115	1.1000-05	0.00000000227670354	5.9550-07	48
116	1.1000-05	0.00000000227652643	5.9550-07	50

3 FAILURE COMBINATIONS.

Figure B-8. Fault Tree Computer Printout (Concluded)

Another FTREE advantage is that a minor change in the makeup of the last gate of the file will permit investigation of other combinations of events.

The last page of Figure B-8 shows sensitivity of the top gate to multiple-occurring events. The number given is the change in unreliability that would occur at the top gate if the component under consideration were made perfectly reliable. Events (components) are ranked in decreasing order of influence.

B.2.3 MINTERM PROVISION

FTREE provides outputs of all minterms that represent failures of the function (top gate). This information is helpful when determining what input signals are needed to provide fault advisories to the flight crew. Unfortunately, the entire set of failure-producing minterms are calculated and printed. For example, if loss of computer A and actuator B could disable LAS, then all minterms that include computer A and actuator B will be provided.

The fault tree analysis program (FTAP) is a new program initiated at Stanford University. FTAP provides the same information in a more convenient form, which is cut sets. Cut sets are all those combinations of components that can produce a failure probability as great as a preset threshold. In the preceding example, the A computer failure and B actuator failure will make up an entry if the probability of their joint occurrence is as great as a value the operator has preset. Figure B-9 is a portion of a printout of such an FTAP computer run. FTAP also can combine many more problems into one computer run, thereby saving cost.

For future studies, we are coordinating with the Raytheon Corporation to incorporate the FTREE program as the input end to the computer-aided reliability estimates (CARE III) program. This should expand the reliability calculation capability to include latent failures, leakage, coverage, intermittence, and recovery from transient failures.

B.2.4 PREDICTION OF SELECTED SYSTEM FLIGHT SCHEDULE RELIABILITY

Construction of the fault trees defines the logic that the FTREE program uses in prediction. A brief examination of the fault trees will help to explain how the Selected System flight schedule reliability predictions of Volume I, Subsection 9.2.2, were made.

SUMMARY OF THE SYSTEM PROBABILITIES.
VERSION NO. 1.4

FLIGHT HOURS (FH):   1= 1.000E+00

INPUT EVENT	UNRELIABILITY	RELIABILITY	GATE TYPE	HOURLY RATE		FH
OUTPUT EVENT	UNRELIABILITY	RELIABILITY	GATE TYPE	GATE INPUT		
375			3	104	105	106	107
376			C	35	39		
377			C	36	40		
378			C	37	41		
379			C	38	42		
380			3	376	377	378	379
381			C	26	35	39	57
382			C	27	36	40	58
383			C	28	37	41	59
384			A	381	382	383	
385	5.555D-12	0.99999999999944453	C	375	380	384	

MINIMAL CUT SETS
RANKED HIGH TO LOW

PROBABILITY	CUT SET		
4.13.D-13	40	41	57
3.270D-13	40	41	42
3.270D-13	39	41	42
3.270D-13	39	42	42
3.270D-13	39	40	41
2.314D-13	28	40	57
2.314D-13	27	41	57
1.832D-13	28	39	40
1.832D-13	27	39	41
1.832D-13	26	40	41
1.28..	7	2.	57
1.360D-14	36	39	59
1.360D-14	35	41	58
1.360D-14	35	42	59
1.350D-14	39	58	59

SENSITIVITY ANALYSIS OF EVENTS
FOR TOP GATE

RANK	EVENT	PROBABILITY
1	40	6.890D-05
1	41	6.890D-05
3	39	6.890D-05
	57	8.700D-05
15		6. 05
15	106	.010..
15	107	1.010D-05

Figure B-9. Fault Tree Analysis Program and Cut Sets

Figure B-10 is the crucial PAS fault tree. The OR gate at the top of the tree feeds the undesirable event "Essential PAS Inoperative." If any of the three inputs to this gate is positive (indicating a fault), the output indicates a fault; namely, that Essential PAS is inoperative. The sensor fault gate is an M of N gate described in Figure B-10, meaning that if any three of the four inputs (or all four) are positive, the output is positive. The FTREE program tries all the possible combinations. Each input to this gate is simply the event that one dedicated Q sensor is inoperative. The computer fault gate is similar, except that the four inputs to the M of N are now the outputs of OR gates. The event that a computer is inoperable is combined with the possible event that the computer program is faulty, because either of these could suffice to make the computer function faulty. The actuator fault gate is similar in that the actuator is combined in an OR gate with the supporting hydraulic system and with the appropriate computer. The actuator depends upon the hydraulic system for power and upon its own channel's computer to provide it with control signals; i.e., the actuator is dependent on its own computer. Any one of the three could, by failing, make that channel's actuation inoperative. The Essential PAS fault tree is unique among the set in that the sensors do not show such a dependency upon their associated computers to accept their signals; i.e., in this instance only, the sensors are each cross strapped into all computers.

The Full PAS fault tree (fig. B-11) is very similar in structure. The sensors are dependent upon the computers to accept their signals. The partitioning of computer failure rates (vol. I, subsec 9.2.1.1) permits including only those parts of the computer that are required to be operable to receive the sensor inputs. Under q sensing fault, the DADC also has been partitioned into the q parts and those common parts (power supplies, cooling, structure) that are required to provide a q (dynamic pressure) output. A failure is not charged for other parts. The additional function, gain scheduling, is backed up by an alternate, flap position, so that both must have produced a fault input to the gain scheduling fault AND gate to get a fault output. These backup functions appear in several ACT functions and result in the backed-up function being virtually infallible. The phugoid stabilizer sensing fault is another such backed-up function. The computers are conspicuous by being included in every sensor and actuator branch of the tree. The dependency of sensors and actuators for communication to the rest of the system makes the computers and their reliability extraordinarily important. In this tree, the computers, subfunctions of the DADC, and the IRS are all multiple-occurring events.
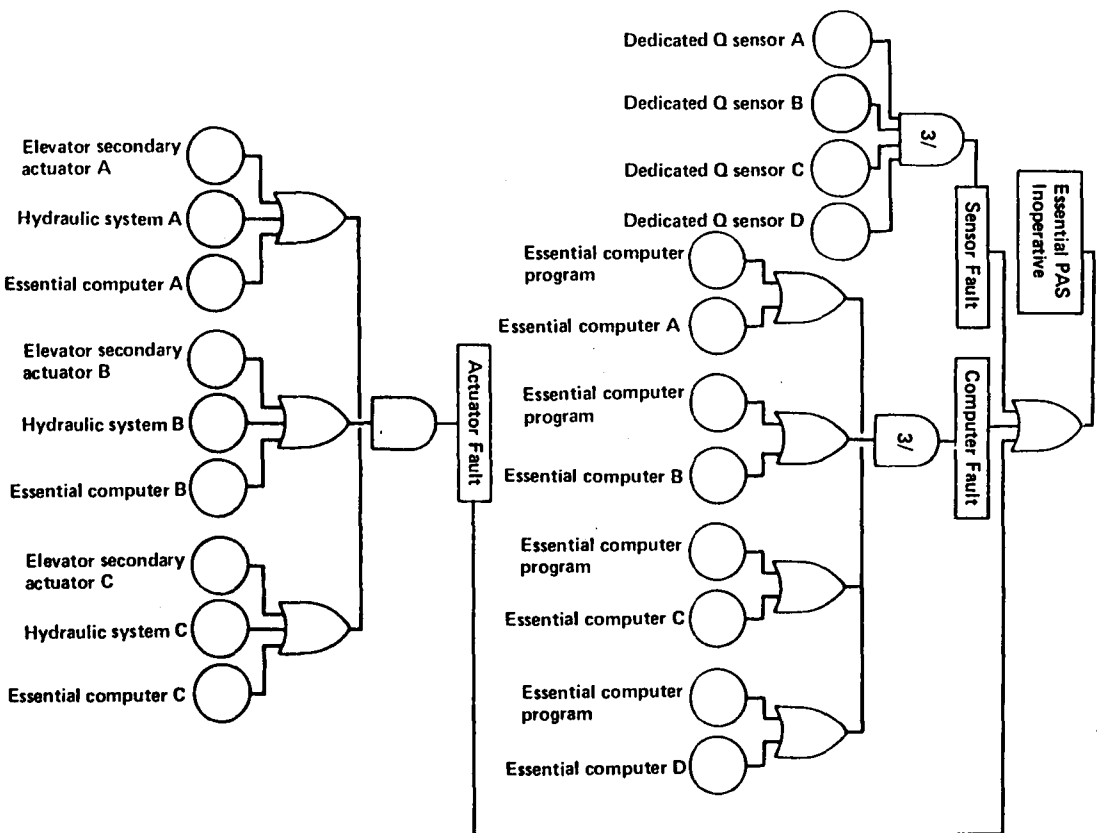
Figure B-10. Crucial Pitch-Augmented Stability Fault Tree

Figure B-11. Full Pitch-Augmented Stability Fault Tree
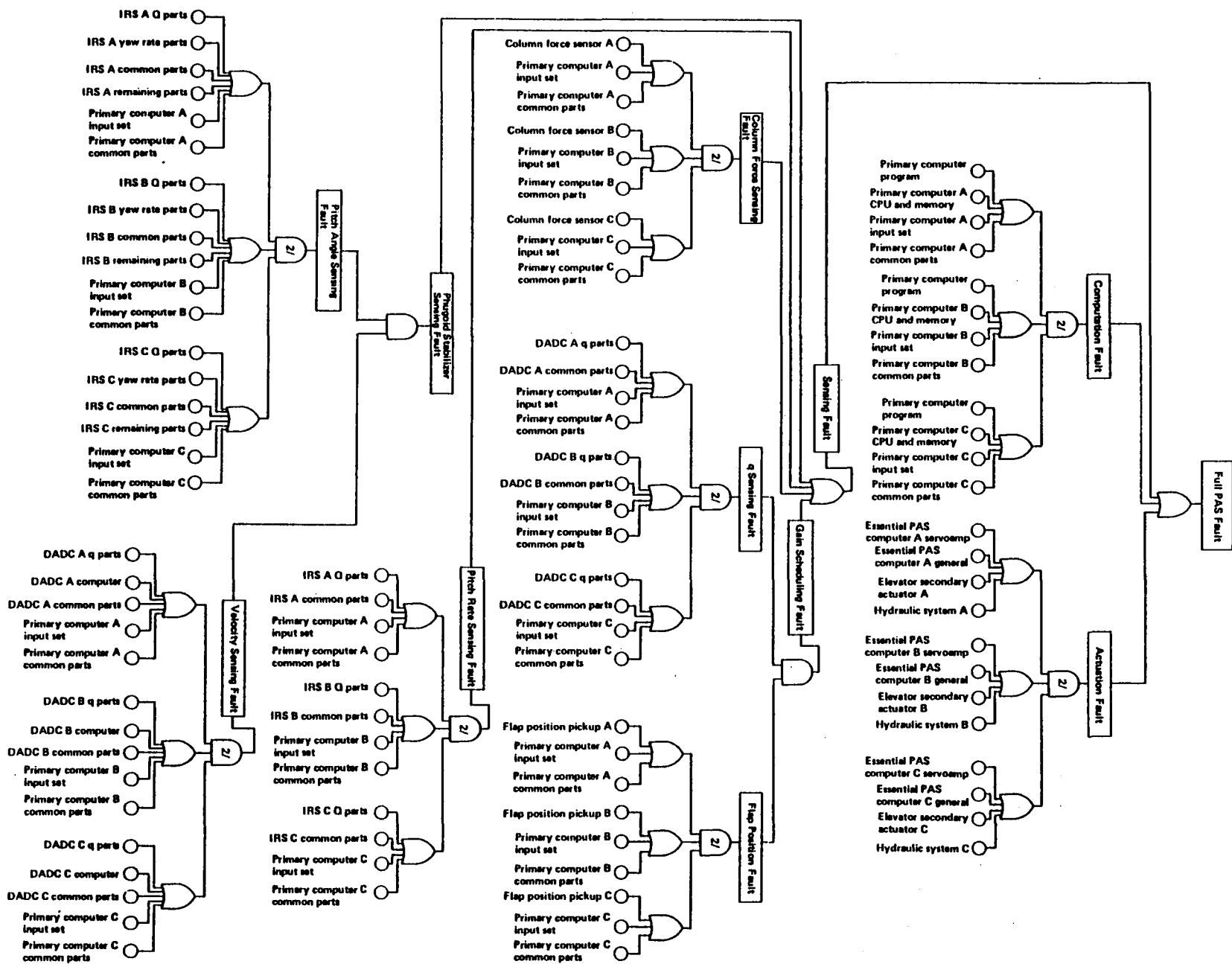
The LAS and angle-of-attack limiter (AAL) (stick pusher and stick shaker) fault trees (figs. B-12 through B-14) follow the same pattern. The stick pusher actuation is complicated by the need to ensure against inadvertent actuation. Each actuator is precluded from operating unless both solenoid valves open, so both valves and two power sources are combined in an OR gate; thus failure of any one could produce actuator failure, but both actuators would have to fail to produce AAL actuation failure.

Figure B-15 predicts the probability of inadvertent stick pusher actuation. In this case, failure in the sensors is not passive but produces a false signal that calls for actuation when it is not required. Failure in the actuation consists of actuation in the absence of a computer input signal calling for actuation. The computer fault consists of the computer producing an output, in the absence of the appropriate sensor inputs, that the program and the rest of the computer fail to detect and deactivate. Commercial aircraft experience provided almost no data from which to calculate rates for such failure modes, so conservative estimates were made. This fault tree, having an entirely different set of failure mode input events, cannot be combined with the rest of the ACT function fault trees to find the probability of joint failures.

The wing-load alleviation (WLA) fault tree (fig. B-16) is the most complex because of the large number of surfaces controlled, but the same principles apply. The multiple actuators are each dependent upon one of these hydraulic systems, which makes the hydraulic systems multiple-occurring events. The FMC fault tree is shown in Figure B-17.

The fault trees described detail the failure modes that can lead to an ACT function becoming inoperative. In some instances it is necessary to know the probability of encountering the condition in which one more component failure would cause a function failure, because this may call for flight envelope restriction. Such a probability can be calculated with a similar fault tree that simply redefines what constitutes failure. The adaptation of the Full PAS fault tree for one failure away (fig. B-18) is an example. The only change necessary was to replace the gates that required two of three redundant inputs to fail with gates that require one of three (i.e., one less than what would cause the function to become inoperable). A one of three gate is simply an OR gate.

The probability of being required to divert during a 1-hr flight is the probability of being one failure away from the loss of Essential PAS or one failure away from loss of all of the

Figure B-12.   Lateral/Directional-Augmented Stability Fault Tree

B-22
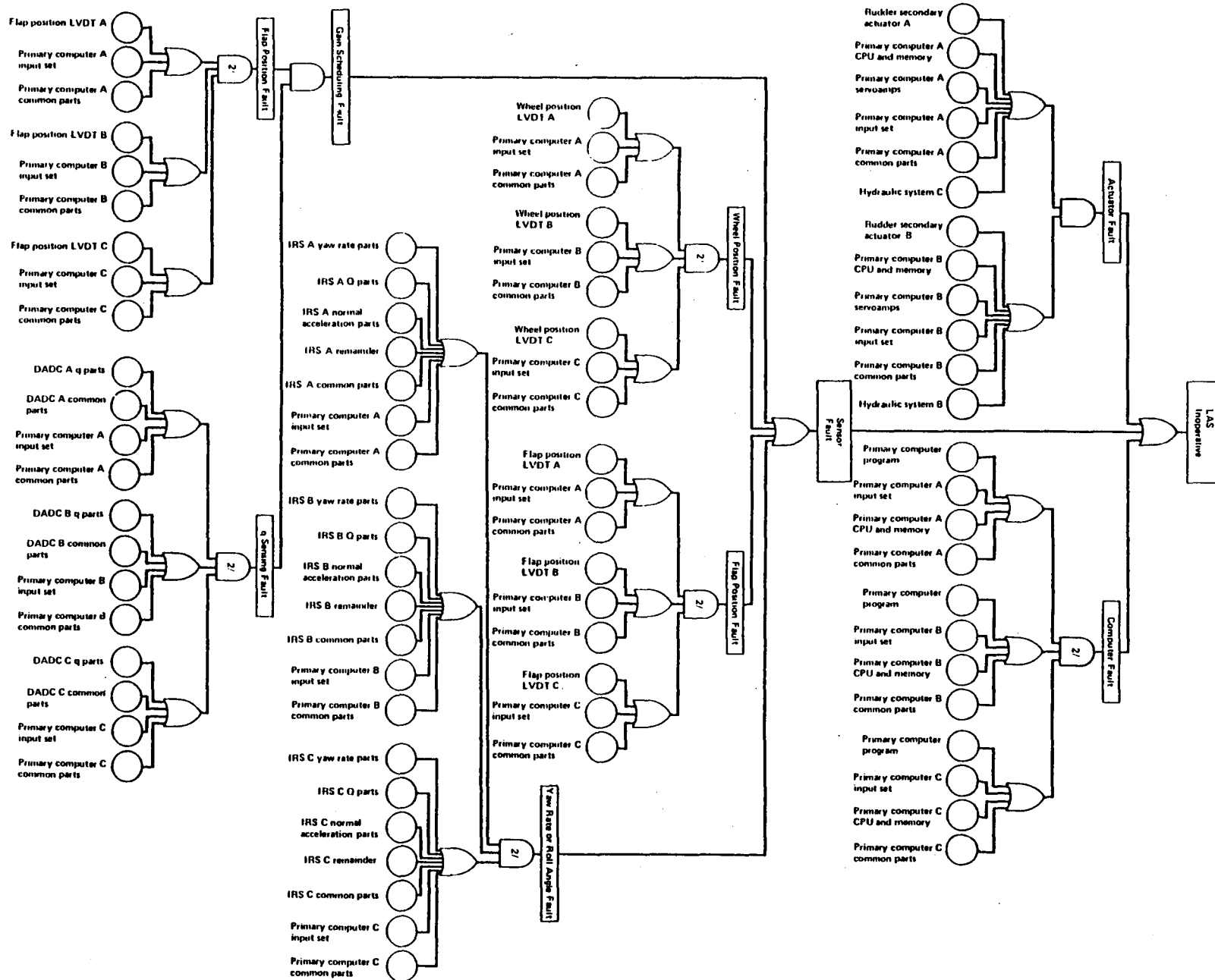
set (Full PAS and LAS and WLA). Figure B-5 shows the fault tree for this condition. Four gates feed into the top OR gate. Any of them can produce a condition where the pilot should divert. The first, being one failure away from loss of Essential PAS, is simple enough. We need three other inputs, each representing two functions failed and one function one failure from becoming inoperable for the set of Full PAS and LAS and WLA.
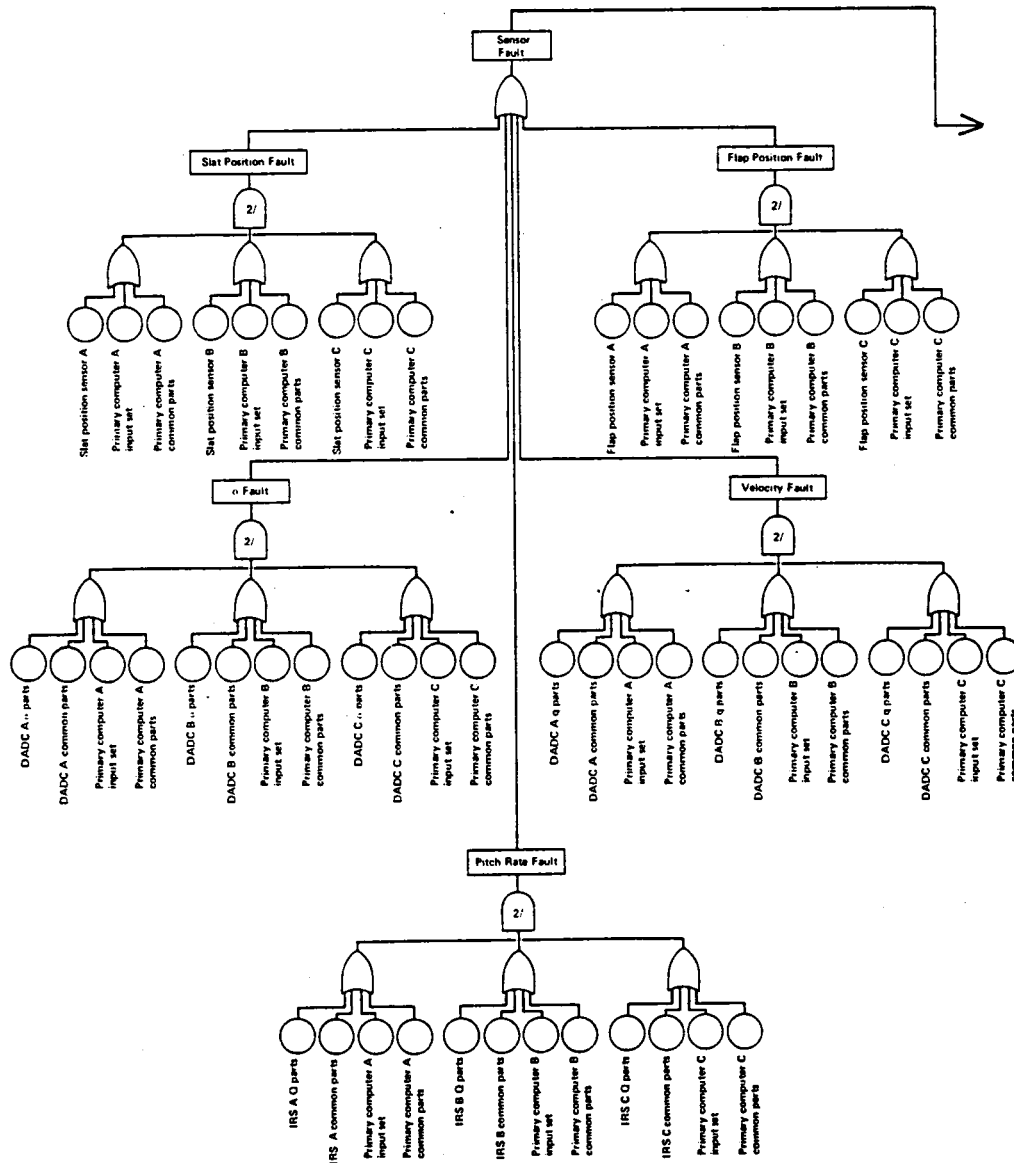
Figure B-13. Angle-of-Attack Limiter (Stick Pusher) Fault Tree

Figure B-13. Angle-of-Attack Limiter (Stick Pusher) Fault Tree (Continued)

B-24

Figure B-14. Angle-of-Attack Limiter (Stick Shaker) Fault Tree

B-25
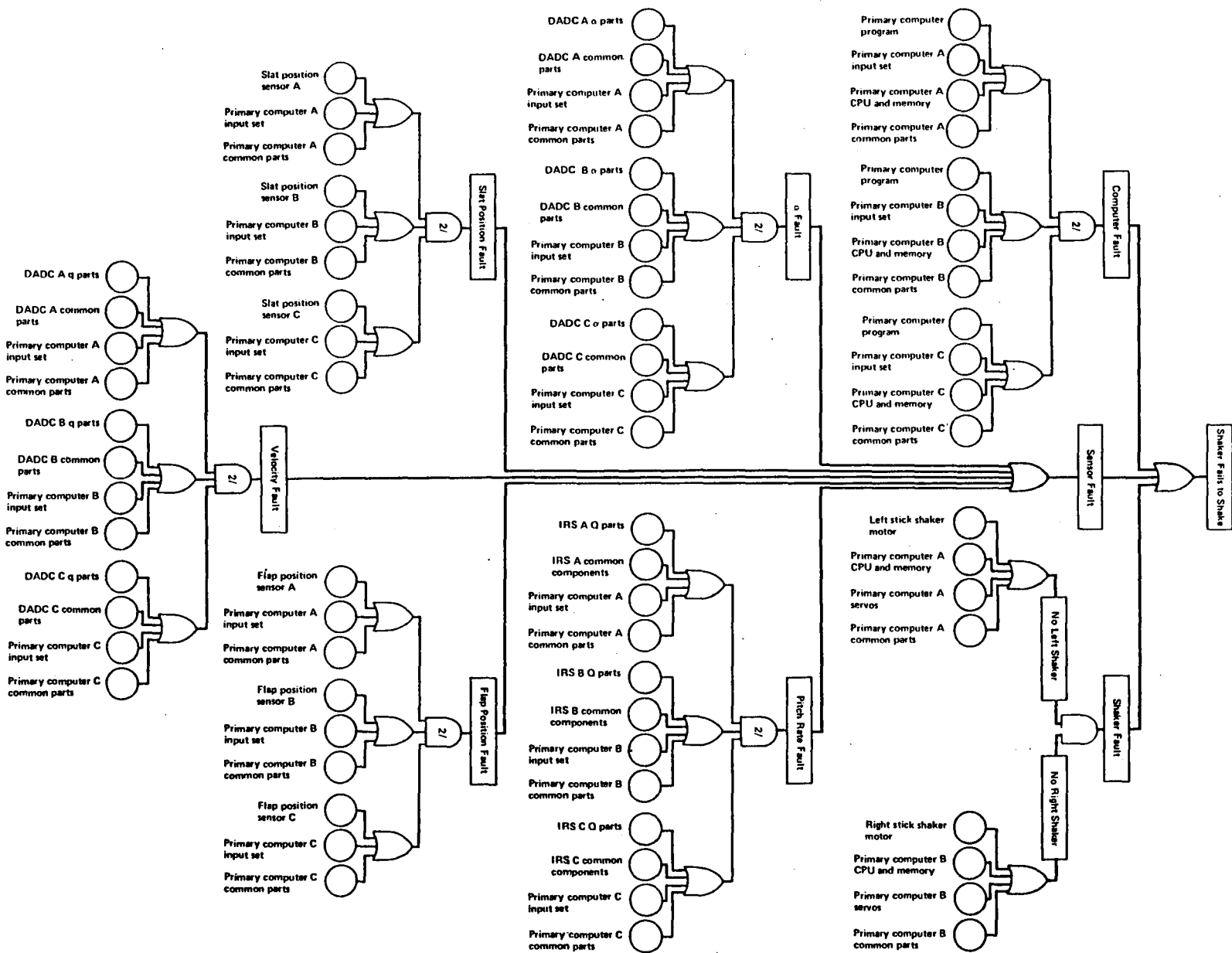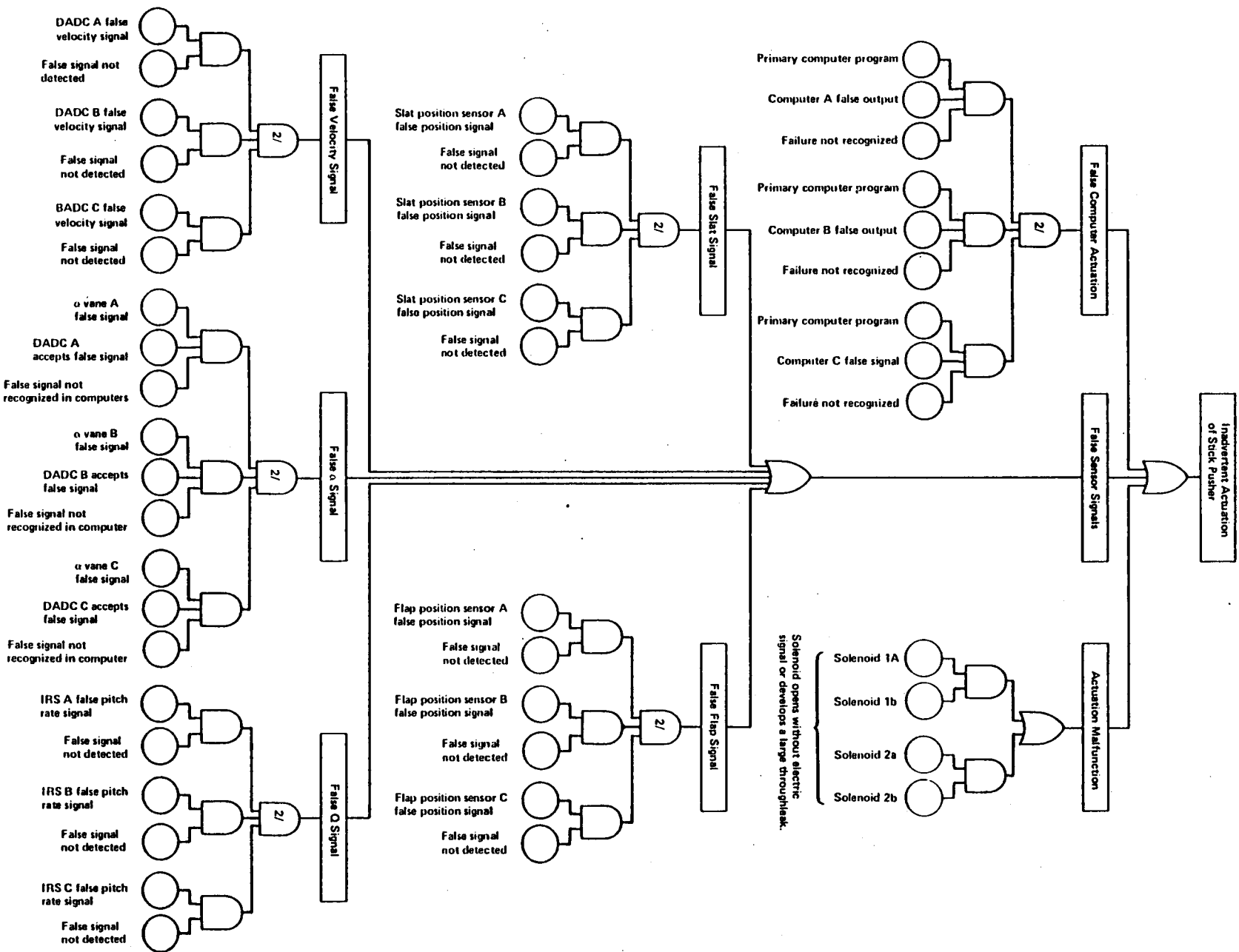
Figure B-15. Stick Pusher Inadvertent Action Fault Tree

B-26

Figure B-16. Wing-Load Alleviation Fault Tree

Figure B-16. Wing-Load Alleviation Fault Tree (Continued)
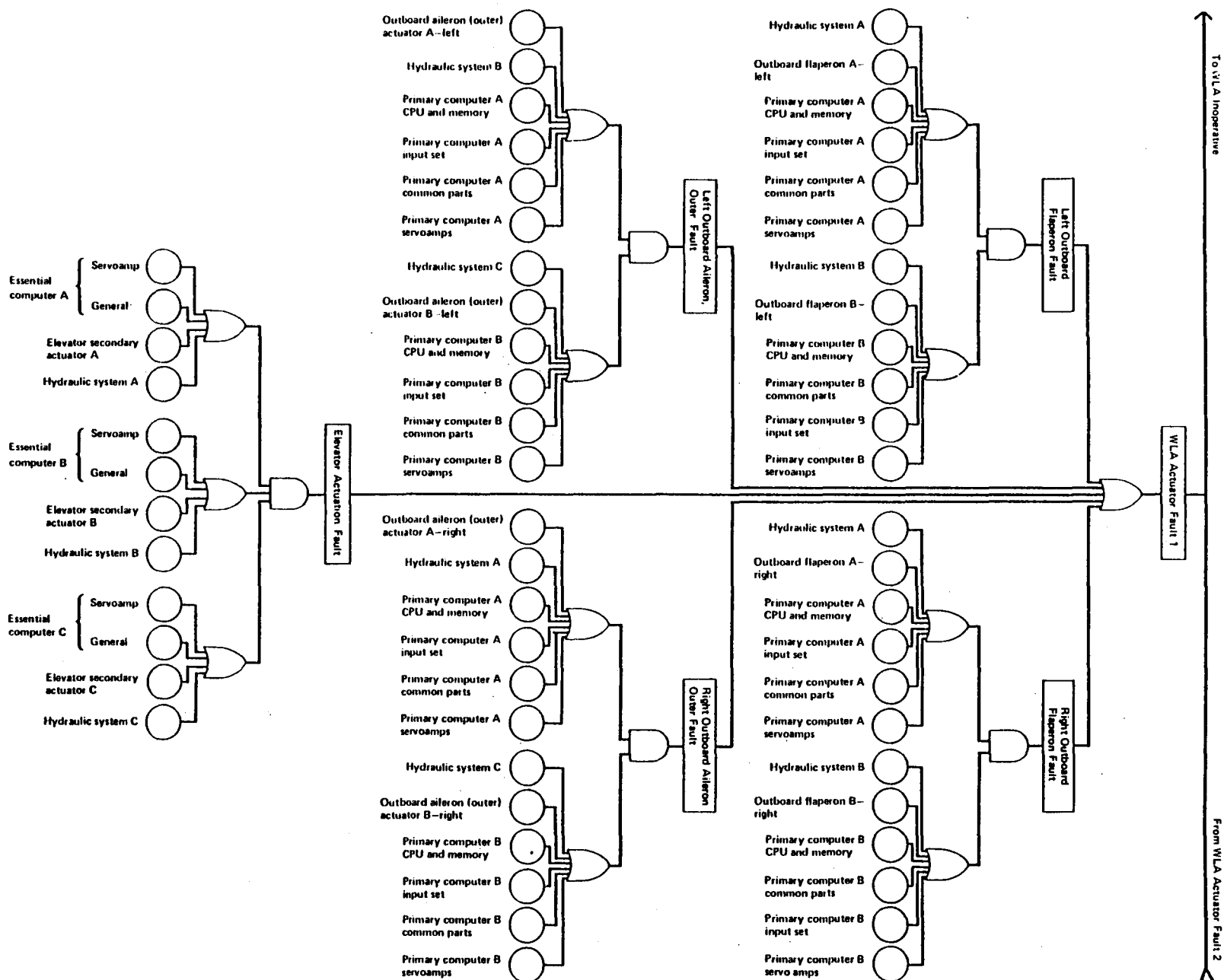
Figure B-16. Wing-Load Alleviation Fault Tree (Concluded)
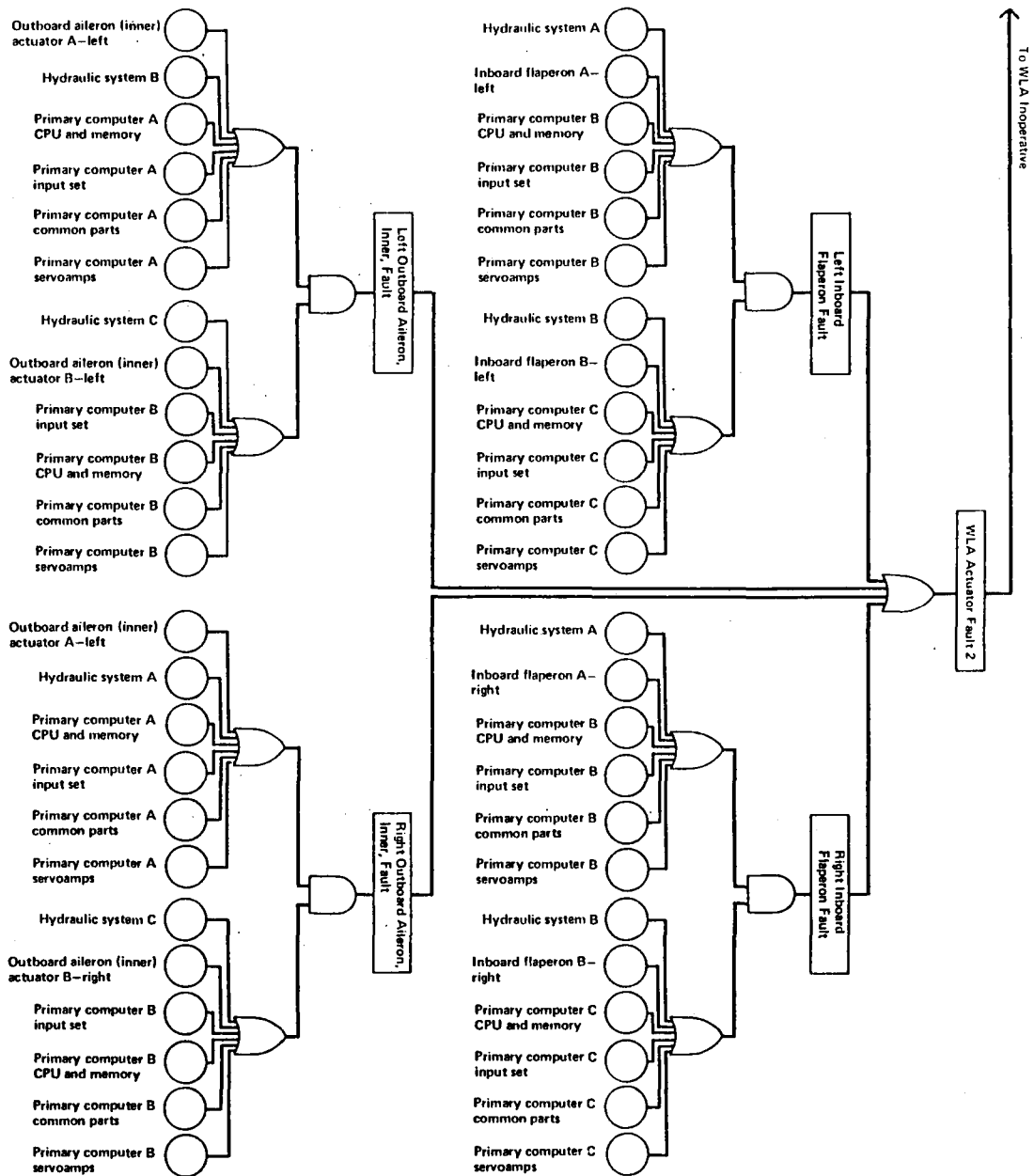
Figure B-17. Flutter-Mode Control Fault Tree
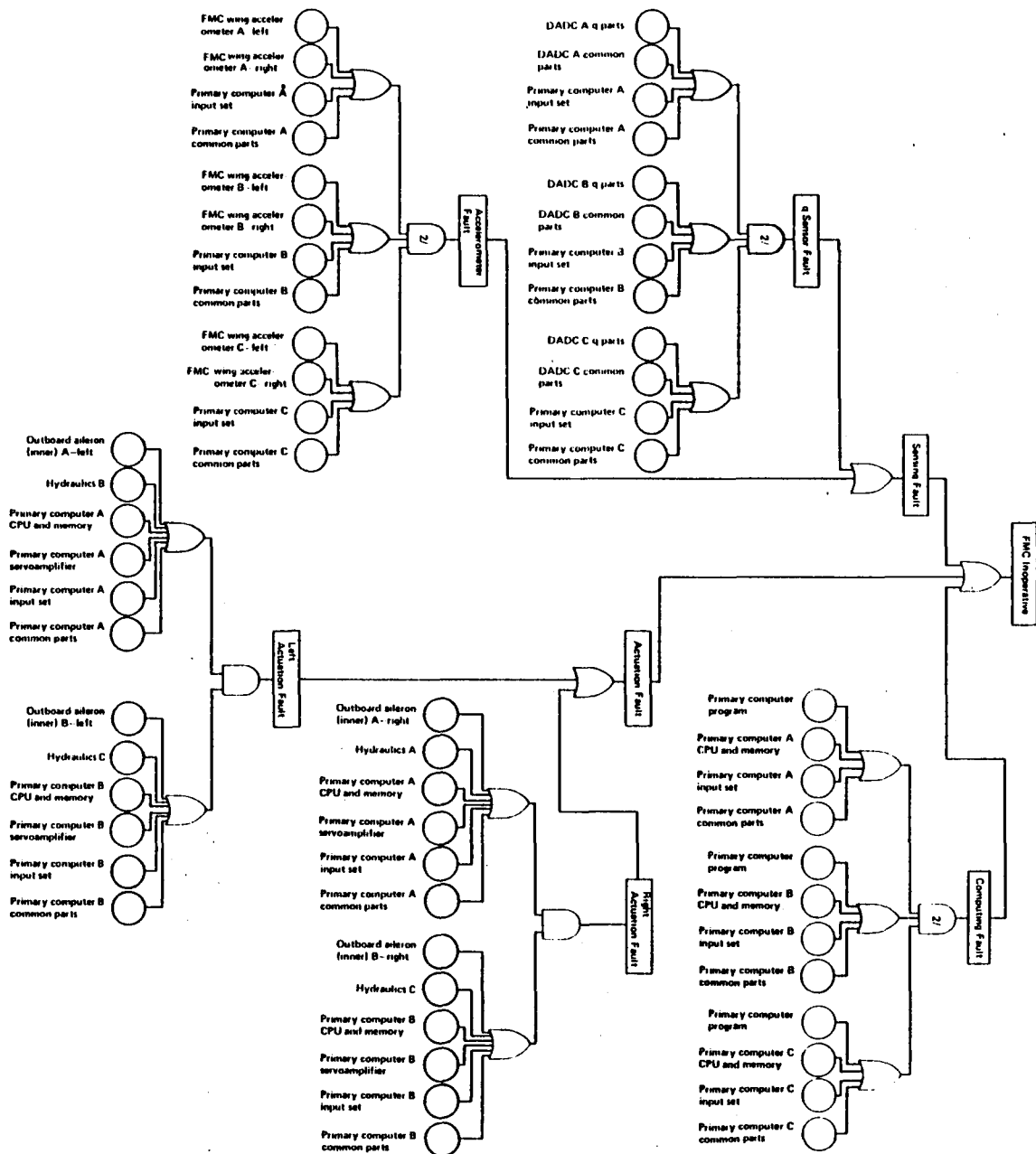
Figure B-18. Adaptation of Full Pitch-Augmented Stability Fault Tree for One Failure Away

B-31
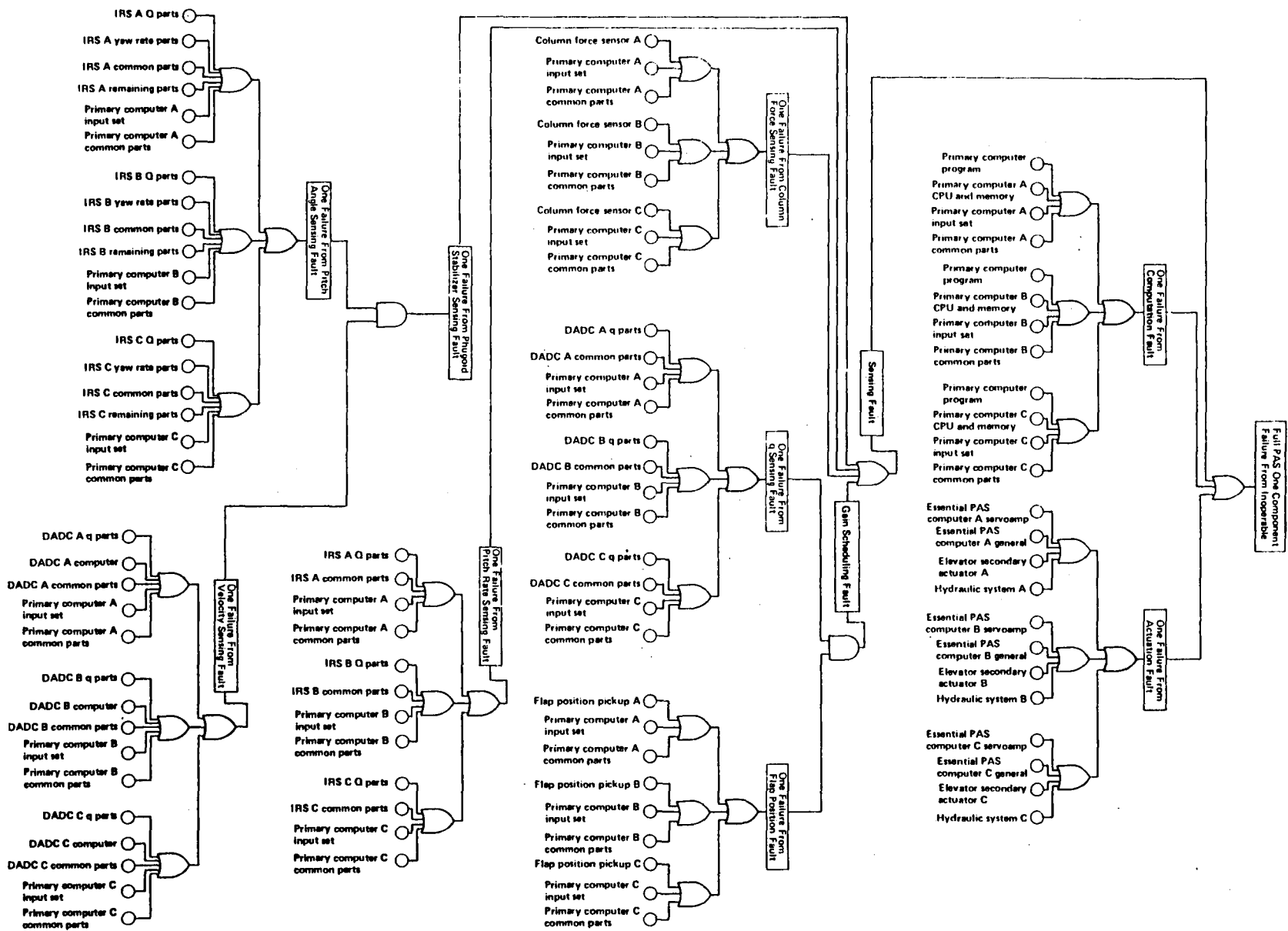
REFERENCES

B-1   Bjurman, B. E., G. M. Jenkins, C. J. Maereliez, K. L. McClellan, and J. E. Templeman. Airborne Advanced Reconfigurable Computer System. NASA CR-145024, 1976.

B-2   Integrated Application of Active Controls (IAAC) Technology to an Advanced Subsonic Transport Project—Initial ACT Configuration Design Study. NASA CR-159249, Boeing Commercial Airplane Company, July 1980.

APPENDIX C: PITCH AXIS
FLY-BY-WIRE ACTUATOR

APPENDIX C: PITCH AXIS FLY-BY-WIRE ACTUATOR

Volume I, Subsection 6.5, describes a pitch axis fly-by-wire (FBW) control actuator and compares it with a conventional actuator system in terms of weight, cost, and reliability.

The pitch axis FBW actuator installation drawing (fig. C-1), in conjunction with Figure 16 (vol. I), provides schematics of the elevator FBW control system.

C.1.0 DESCRIPTION OF THE SERVOACTUATOR DESIGN

The actuator is sized to provide the elevator full force and rate capability. The pitch axis FBW servoactuator is shown in Figure C-2. The actuator is driven by a jet pipe servovalve. A linear variable differential transformer (LVDT) is attached to the spool of the servovalve for redundancy management. A differential pressure transducer is installed between each servovalve and actuator to equalize the output forces of the three servoactuators. A bypass valve is employed to control the operational mode of the servoactuator. If a control loop failure occurs, the normally closed dual-coil solenoid valve will allow the bypass spring to drive the bypass valve to a position that disconnects the servoactuator from the hydraulic supply and reduces its output force to a minimum. As long as the control loop is free of failure, the solenoid valve will position the bypass valve to allow the servoactuator to operate normally.

C.2.0 NONLINEAR DYNAMIC SIMULATION

A nonlinear dynamic mathematical model computer program was written for the servoactuator and its failure detection scheme to ensure that the servoactuator system would respond as required.

A computer run was made using this mathematical model. A 50% step input command was applied. Results of this computer run show that the servoactuator response is overdamped and the control loop is stable.

Section A-A (Rotated)
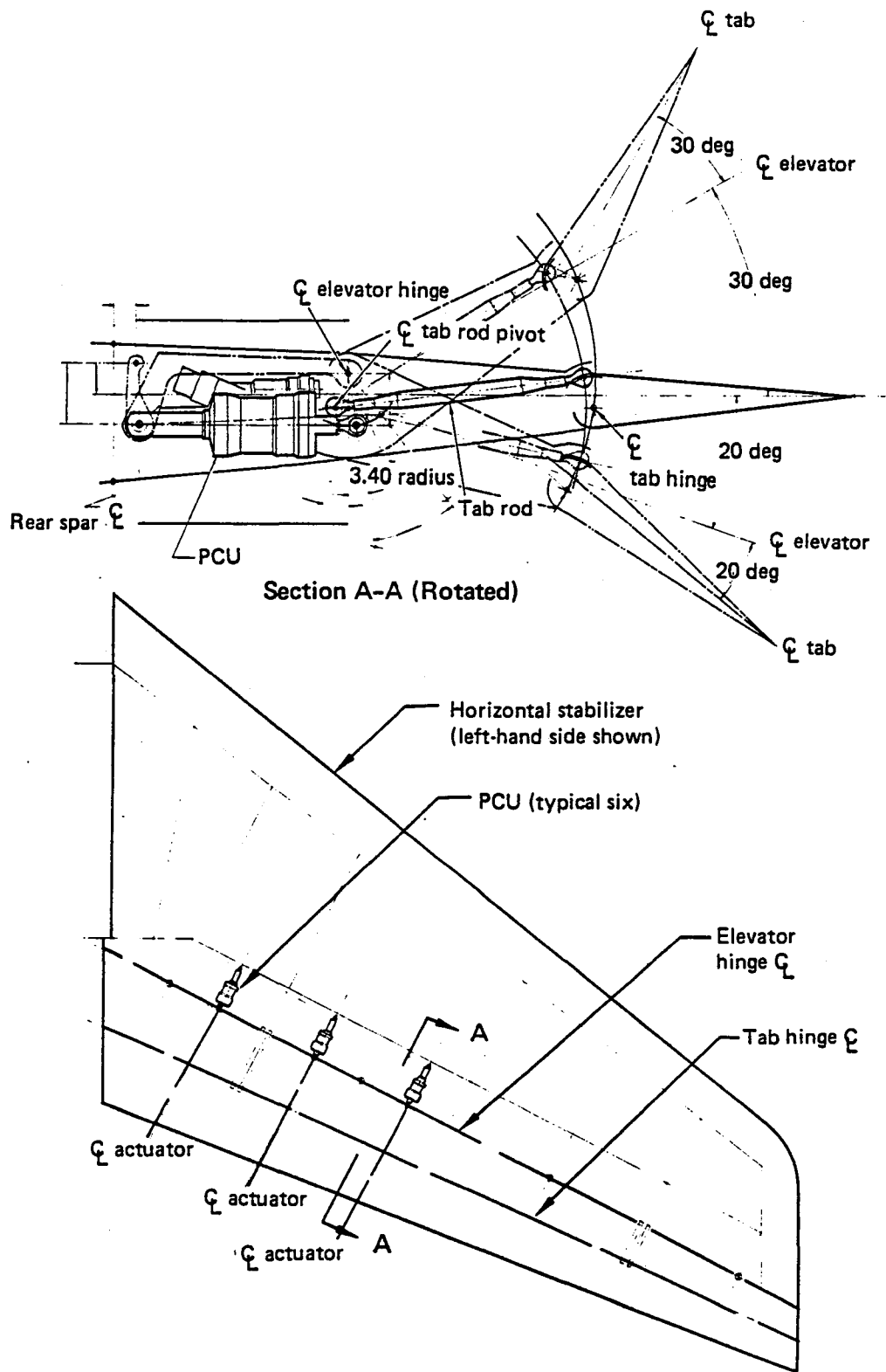
Figure C-1. Pitch Axis Fly-by-Wire Installation Drawing

Rod end seals

Bypass valve

Tailstock seals

Piston seal

Piston

B

B

ΔP transducer

Ram LVDT

Servovalve

Servovalve spool

LVDT

Partial Section B–B
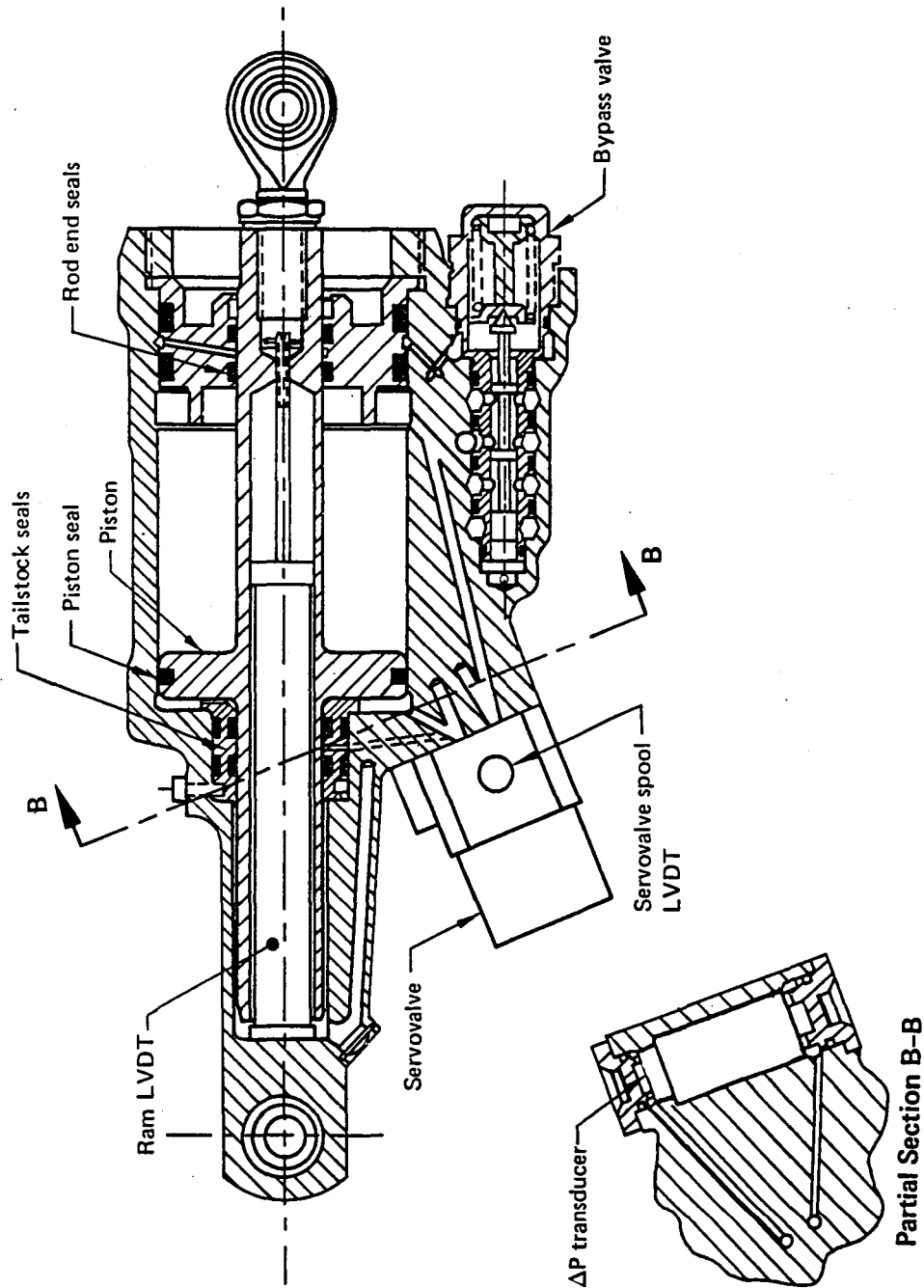
Figure C-2. Servoactuator Drawing

C-3

C.3.0 REDUNDANCY CONCEPT

C.3.1 SERVOVALVE MONITOR CONCEPT

The redundancy concept used for the pitch axis FBW servoactuator is shown schematically in Figure C-3. This figure shows that the response of the servodriver amplifier and servovalve is compared to the response of a model of the servodriver amplifier and servovalve driven by an identical command signal. The LVDT is the only component in the control loop whose performance is not monitored by this redundancy method. Hence a center tap (self-monitoring) LVDT is used. When the difference between the displacement of the second-stage spool and its electronic model exceeds a preset threshold level, a failure detect signal is attained. Also, a first-order filter with a time constant τ_c is incorporated to reduce the dynamic mismatch between the electronic servovalve model and the actual servovalve during transient conditions.

To investigate the effects of a control loop component failure, the nonlinear dynamic mathematical model computer program discussed previously was used to conduct a failure transient analysis. The failure analysis run was made by applying a zero command to the servoactuator control loop and inducing a hardover servovalve failure. Results of the computer run show that following a failure, the actuator will travel less than 10% of full stroke before it is placed in the failed mode. Worst case static and dynamic mismatches between the servovalve and the electronic model were used.

C.3.2 SERVOACTUATOR EQUALIZATION

One problem associated with connecting multiple actuators to a common load is getting them to share the load equally instead of engaging in force fight due to tolerances in the control loop. To minimize force fight, a scheme of one active and two online channels is used as shown in Figure C-4. In this scheme, one active channel or actuator is position responsive and establishes elevator position. The two online actuators are also position responsive and are force output limited. This force limiting is accomplished by using differential pressure feedback from the two online actuators.

If the elevator is subjected to oscillatory loads, it is desirable to have the two online servoactuators share these loads with the active actuator. The online actuators are soft

at low frequencies but can respond to their share of the oscillatory loads at high frequencies.

If one of the active actuator channels fails, then one of the online actuators becomes active by automatically turning off the ΔP feedback to that actuator. If the second active actuator channel fails, then the remaining online actuator becomes active.

Various channel mismatch conditions were investigated in the pitch axis FBW system. The types of mismatching considered were (1) servovalve null bias mismatches and (2) servovalve pressure gain mismatching. The latter was obtained by mismatching the amount of overlap or underlap length on each servovalve.

Legend:

KA	amplifier gain	s	Laplace operator
KAM	model amplifier gain	SVDED	dead band
KC	servovalve monitor gain	τ_c	time constant
KD	demodulator gain	VC	actuator position command voltage
KFB	LVDT feedback gain		
KL	feedback gain	XBIAS	null bias
KSV	servovalve gain	XDED	feedback dead band
KSVM	model servovalve gain		
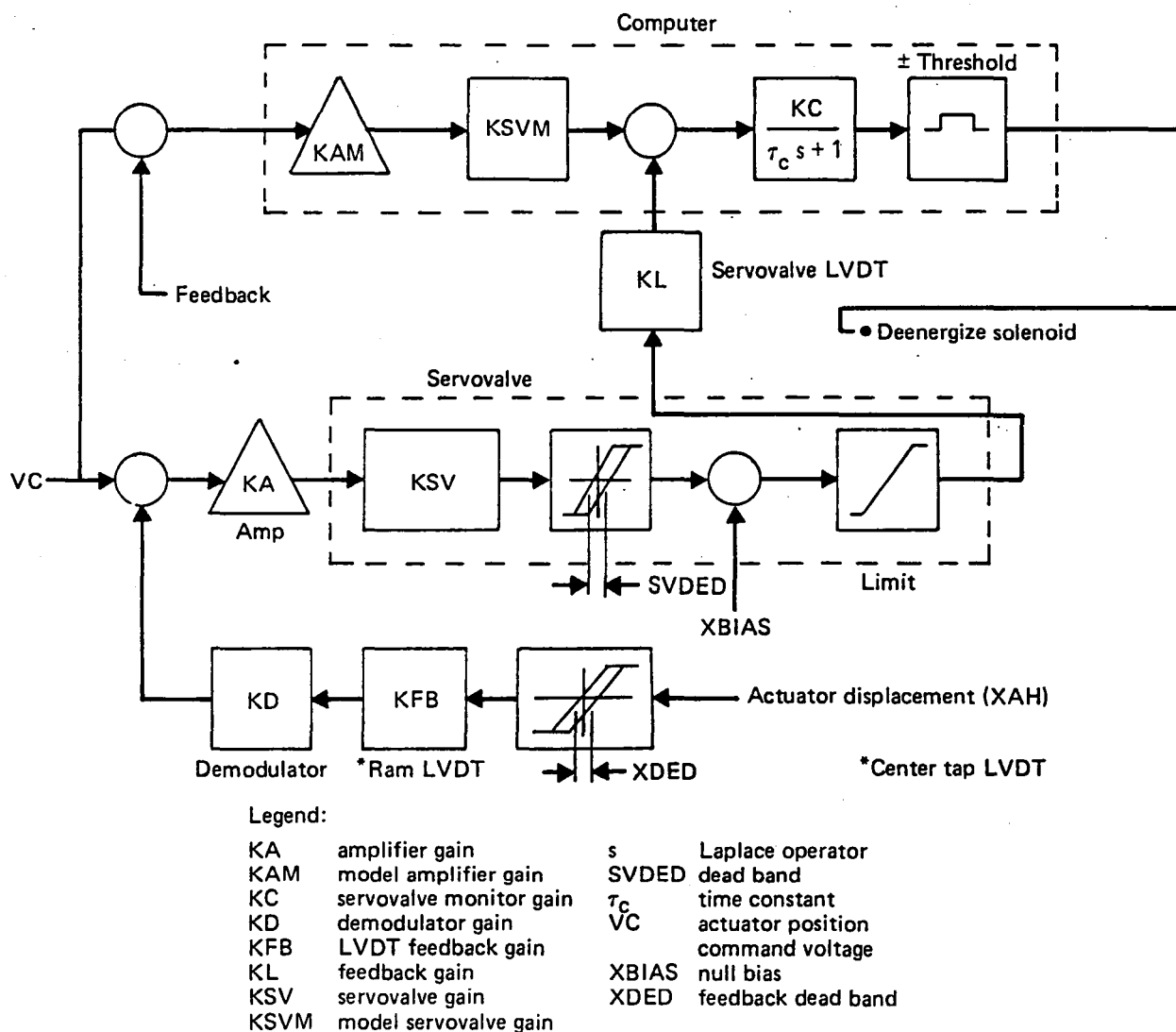
Figure C-3. Failure Detection Schematic for Pitch Axis Fly by Wire
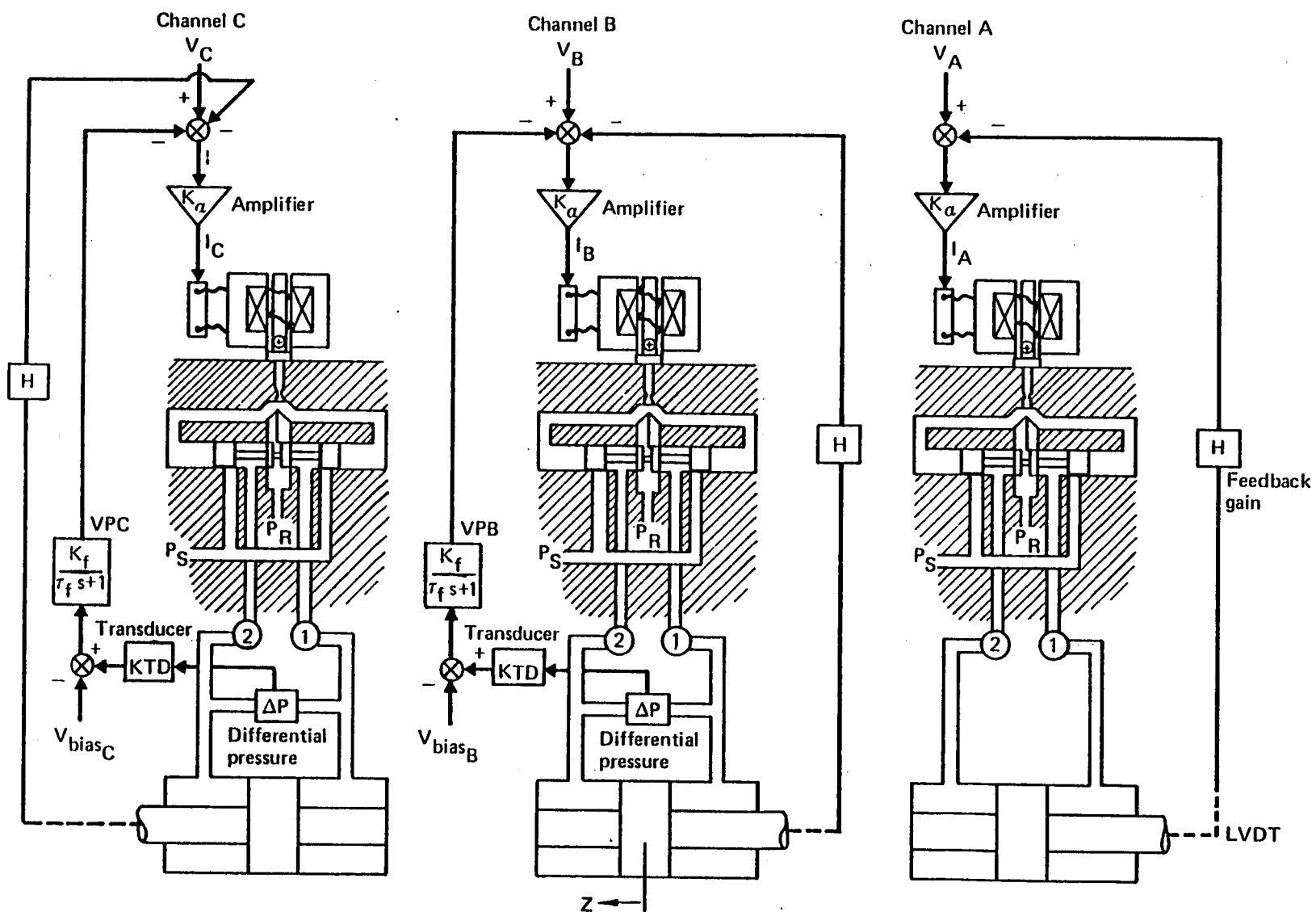
Figure C-4. Pitch Axis Fly-by-Wire Equalization

Frequency response was investigated to determine whether mismatching could cause force fighting between channels that might attenuate the dynamic response. The frequency response was not significantly different under any of the conditions investigated.

Step commands for various mismatch conditions were input into the system in an attempt to trigger nuisance failures. At no time did the detection parameters come close to the threshold level.

C.4.0 PITCH AXIS FBW ACTUATOR INSTALLATION

The pitch axis FBW actuator installation is shown in Figure C-1. The pitch axis FBW actuator is within its prescribed envelope.

C.5.0 RELIABILITY ANALYSIS

Analysis of the pitch axis FBW servoactuator yields an estimated mean time between failures of 25 253 hr, as shown in Figure C-5. Table 30 of Reference C-1 lists the failure rates used.

ΔP transducer 15×10^{-6}	Servovalve $*10 \times 10^{-6}$	Solenoid and bypass $*6.0 \times 10^{-6}$	Actuator $*1.6 \times 10^{-6}$	LVDT $*7.0 \times 10^{-6}$
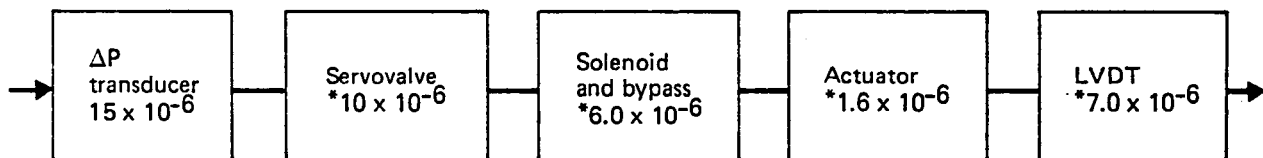
● Mean time between failures: 25 253 hr

*Failure rates (λ) based on Table 30 of Reference C-1

Figure C-5. Pitch Axis Fly-by-Wire System Reliability Model

REFERENCES

C-1 <u>Integrated Application of Active Controls (IAAC) Technology to an Advanced Subsonic Transport Project—Initial ACT Configuration Design Study.</u> NASA CR-159249, Boeing Commercial Airplane Company, July 1980.

APPENDIX D: FLAPERON ACTUATION SYSTEM DESIGN TRADE STUDY

APPENDIX D: FLAPERON ACTUATION SYSTEM DESIGN TRADE STUDY

The purpose of the flaperon study was to develop three viable actuation design concepts to operate a wing trailing-edge flaperon and assess the relative merits of each concept. These actuation concepts were studied:

● Hydromechanical actuation system
● Electromechanical actuation system
● Integrated actuator package

The only constraint imposed during the study was that the actuation systems be designed with state-of-the-art hardware technology that has proved its maturity in commercial and military applications. This constraint ensured that assessment of system performance and reliability would be based on available technical data.

The following design ground rules were assumed for all three concepts:

● The flaperon actuation system is flight critical.

● A minimum of two systems is required for redundancy management.

● Failure transients shall be held to a minimum, and hardover failures are not allowed.

● Because it is not practical to provide mass balance in the flaperon structure for surface flutter suppression, means must be provided to prevent surface flutter in the event of total power loss to the flaperon actuation system. Flaperon surface locking is the means provided.

● Preflight test must be performed.

D.1.0 HYDROMECHANICAL ACTUATION SYSTEM

The hydromechanical actuation system, based on performance, weight, cost, reliability, and state of the art, was selected as the ACT system technology base flaperon actuation system. This system is discussed in Volume I, Subsection 8.1.3.3, Flaperon Actuation System.

D.2.0 ELECTROMECHANICAL ACTUATION SYSTEM

An industry survey was conducted to determine usage of electromechanical actuation systems on commercial and military aircraft. The results of the survey showed that no electromechanical actuation systems were employed on primary control surfaces. It was found that the most advanced electromechanical actuation system is the prototype unit built by Delco for NASA. A design constraint was imposed that only state-of-the-art hardware be used. Hence, this constraint eliminated the electromechanical actuation system as a viable flaperon actuation system option.

D.3.0 INTEGRATED ACTUATOR PACKAGE

The integrated actuator package (IAP) is a system that takes aircraft electric power in lieu of hydraulic power. The IAP will apply the specified hinge moment and rate to the surface by hydraulic power that is generated within the IAP. The package contains the motor-pump reservoir and valving necessary to generate and control the hydraulic power, the servoactuator, and the heat-dispensing mechanism.

D.3.1 IAP SYSTEM DESCRIPTION

Three IAP concepts were investigated during this study: (1) servopump, (2) pump-motor-reservoir with an accumulator, and (3) pump-motor-reservoir without an accumulator. These three concepts were examined to determine their suitability for the flaperon requirements. This investigation is summarized in the following paragraphs.

Servopump—The Air Force has done considerable development work on servopumps. An example is the Sperry Vickers servopump on the Air-Force-funded 680J using the F-4 aircraft (ref D-1). This research program was concluded in 1973. Neither this program nor any Air Force projects has resulted in a production servopump. Because one of the ground rules for this study was state of the art, it was concluded that none of the Air Force servopumps qualifies.

D-2

The British Aircraft Corporation commercial aircraft VC-10 does use servopumps manufactured by Boulton-Paul. The characteristics of this servopump are as follows:

- Rate   25.2 deg/s
- Hinge moment   468 887 N·m (91 500 in-lbf)
- Weight   37.14 kg (81.9 lb)

The rate was not sufficient (80 deg/s required), and Boulton-Paul was not interested in a redesign.

Pump-Motor-Reservoir With an Accumulator—The pump-motor-reservoir with an accumulator adds stored energy to the system by an accumulator, allowing a possible reduction in the size of the pump-motor. Use of an accumulator requires detailed knowledge of the duty cycle, and this duty cycle was not available until late in the study. The objective of this phase of the study was a trade between the IAP concept and the other concepts as noted in Volume I, Subsection 8.1.3.3. The addition of an accumulator would not influence the conclusion of this trade; therefore, study on this concept was terminated.

Pump-Motor-Reservoir Without an Accumulator—The pump-motor-reservoir without an accumulator is the concept included in this study.

The system schematic is shown in Figure D-1. The electric power is supplied to the motor, which drives a variable-displacement pump. The flow from the pump is routed to the servovalve through a filter. The pump outlet pressure is also routed to the bootstrap reservoir to maintain the 690-kPa (100-lbf/in^2) return pressure. The return flow comes from the electrohydraulic valve through the return filter and flows through the electric motor for cooling. From the motor the flow connects with the case drain flow and goes to the reservoir and/or to the pump inlet. The system also contains a bypass valve around the supply pressure filter and various differential pressure, pressure, and thermal switches. The thermal switch signals the blower motor to turn on or off and informs the aircraft computer of an overtemperature condition. The pressure switches inform the aircraft computer of a failure. The differential pressure switch and fluid-level indicator switch are used during routine maintenance to indicate a dirty filter and fluid level.

Figure D-1. *Flaperon Integrated Actuator Package Schematic (Large Droop Cutoff Pump)*
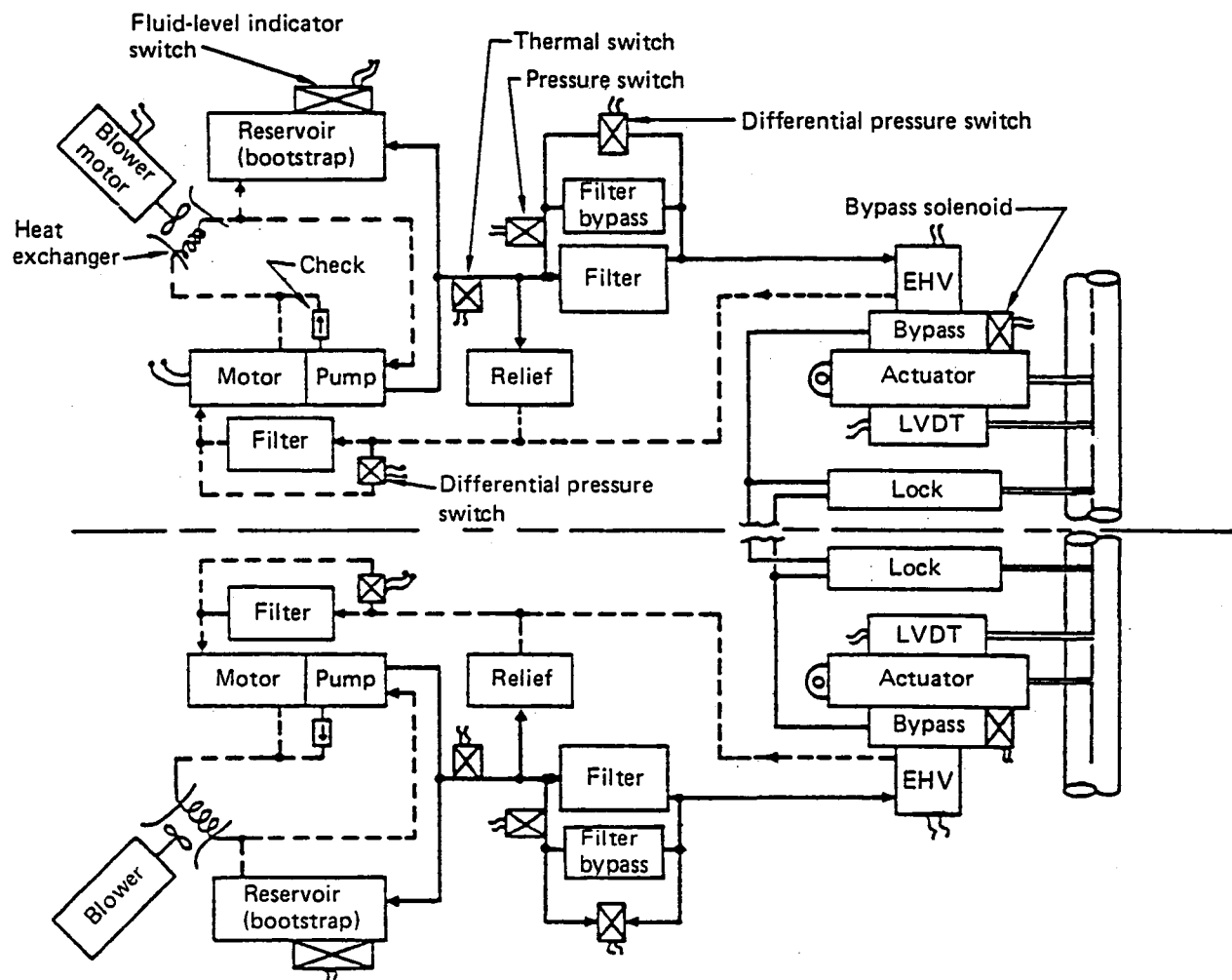
Abbreviations:

EHV   electrohydraulic valve
LVDT   linear variable differential transformer

D.3.2 REDUNDANCY CONCEPTS

The redundancy concept for the servoactuator in the IAP is exactly the same as the concept for the hydromechanical actuator system. Two force-sharing actuators and two models are used, as shown in Volume I, Figure 52.

The hydraulic power unit (HPU) is completely redundant. Each servoactuator has its own HPU. The HPU has several monitor points for failure detection: the thermal indicator and the pressure switch. These two signals are monitored by the computer, and if the temperature or pressure is excessive, the IAP will be shut down. The ΔP across the filter and the reservoir level are monitored and used as a ground maintenance reference.

D.3.3 DESCRIPTION OF HARDWARE

Figure D-2 shows the general arrangement of the components. The pump reservoir package is supplied by Abex Corporation.
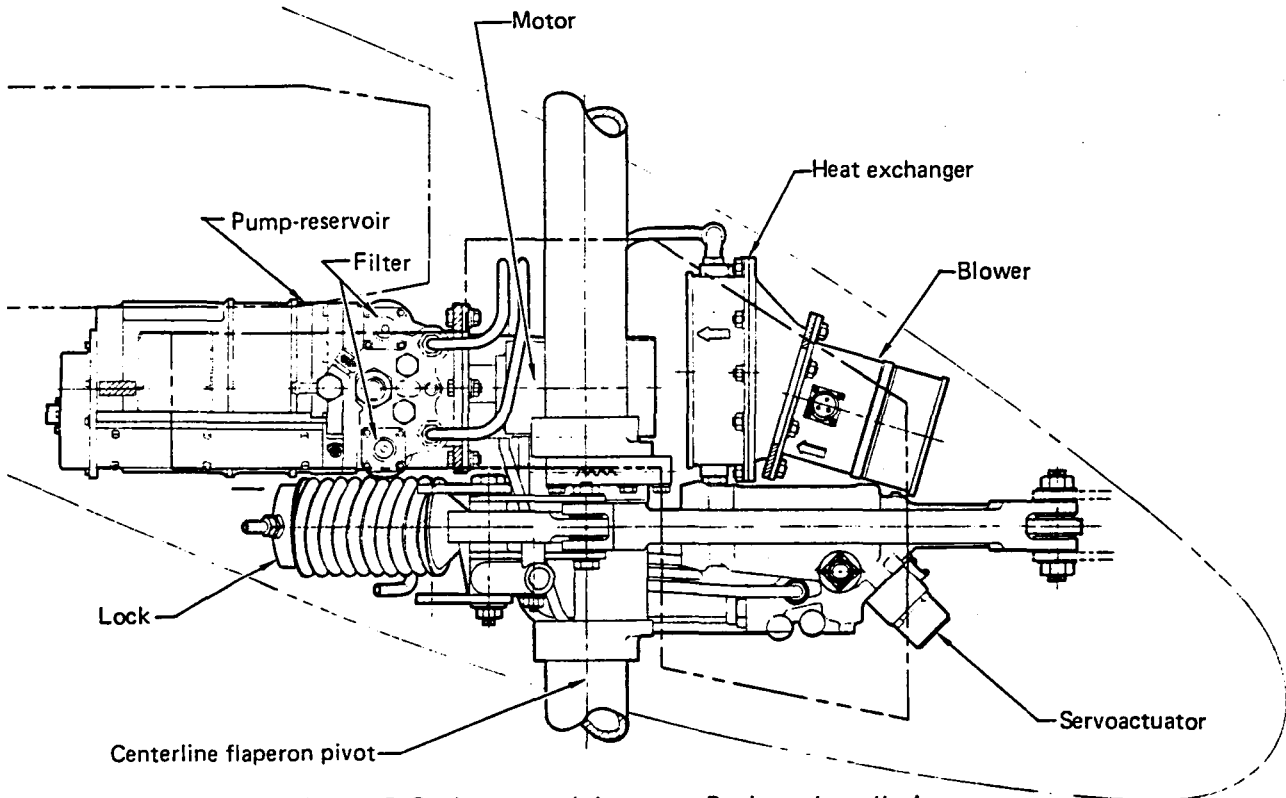
Figure D-2. Integrated Actuator Package Installation

The motor is a wet design with Skydrol fluid flowing through for cooling. This is a 440-Hz, 112V, three-phase motor.

The heat exchange is a two-pass, cross-flow, oil-to-air heat exchanger. The air for the heat exchange is provided by a blower driven by a 440-Hz, 112V, three-phase motor.

D.3.4 WEIGHT ANALYSIS

The necessary brackets and mounts and local structural enhancements will await detailed design of the flap-flaperon and supporting structure. Most of this weight omission (i.e., the weight of parts required to react the actuator loads) is the same for both the IAP and hydromechanical systems. The extra weight for this IAP (i.e., mounting brackets for the various IAP components) would be less than 2.3 kg (5 lb). Weights are as follows:

Servoactuator	4.34 kg	(9.56 lb)
Lock	2.70 kg	(5.95 lb)
HPU	10.48 kg	(23.10 lb)
Blower	1.31 kg	(2.88 lb)
Heat exchanger	2.27 kg	(5.00 lb)
Fluid	1.30 kg	(2.86 lb)
Motor	4.76 kg	(10.50 lb)
Total	27.16 kg	(59.85 lb) + brackets

D.3.5 RELIABILITY ANALYSIS

The reliability block diagram for the IAP is shown in Figure D-3. The predicted mean time between failures (MTBF) is 15 186 hr, which appears reasonable because VC-10 IAPs have demonstrated an MTBF of over 16 000 flight hours.

| Blower motor and fan *0.79 x 10^{-6} | Heat exchanger 0.01 x 10^{-6} | Pump motor 4.30 x 10^{-6} | Pump 14.00 x 10^{-6} | Check valve (three) 0.02 x 10^{-6} |

| Reservoir 16.0 x 10^{-6} | Fluid-level switch 2.00 x 10^{-6} | Thermal switch 0.40 x 10^{-6} | Relief valve 0.16 x 10^{-6} | Filter 0.20 x 10^{-6} |

| Filter bypass 0.56 x 10^{-6} | Differential pressure switch 0.07 x 10^{-6} | Pressure switch 0.07 x 10^{-6} | Filter 0.20 x 10^{-6} | Differential pressure switch 0.07 x 10^{-6} |

| Lock 1.60 x 10^{-6} | Servo-valve 10 x 10^{-6} | Solenoid-bypass valve 6.00 x 10^{-6} | Actuator 1.60 x 10^{-6} | Linear variable differential transformer 7.00 x 10^{-6} |

*Failure rate, λ

● Mean time between failures is 15 186 hr

Figure D-3. Integrated Actuator Package Reliability Model (Worst Case)

D.4.0 TRADE STUDY ASSESSMENT

Following completion of the designs of the hydromechanical actuation and IAP systems, a trade study was conducted to determine the optimum actuation system for the flaperon. Assessment of each system was based on performance, weight, and reliability.

Because the same servoactuator was used on both systems, it can be concluded that the performance of the two servoactuators is identical. Table D-1 shows the weight and reliability comparison. It can be concluded from Table D-1 that the hydromechanical system is the optimum actuation system for the flaperon.

Table D-1. Trade Study Assessment

	Hydromechanical system		IAP system	
Weight	Actuator	4.34 kg (9.56 lb)	Actuator	4.34 kg (9.56 lb)
	Lock	2.70 kg (5.95 lb)	Lock	2.70 kg (5.95 lb)
			HPU	10.48 kg (23.10 lb)
			Motor	4.76 kg (10.50 lb)
			Blower	1.31 kg (2.88 lb)
			Heat exchanger	2.27 kg (5.00 lb)
			Fluid	1.30 kg (2.86 lb)
		7.04 kg (15.51 lb)		27.16 kg (59.85 lb)
Reliability	Mean time between failures	33 168 hr	Mean time between failures	15 186 hr

REFERENCES

D-1 Hooker, D. S. Survivable Flight Control System Final Report. AFFDL-TR-73-105, McDonnell Douglas Corporation, McDonnell Douglas Aircraft Division, December 1973.

APPENDIX E: TECHNICAL
APPROACH FOR ADVANCED
TECHNOLOGY CONTROL LAW
SYNTHESIS AND ANALYSIS

APPENDIX E: TECHNICAL APPROACH FOR ADVANCED TECHNOLOGY CONTROL LAW SYNTHESIS AND ANALYSIS

This appendix describes in some detail the technical approach used for advanced technology control law synthesis and analysis. The objective has been to develop synthesis and analysis methods suitable for the design of gust-load alleviation (GLA), flutter-mode control (FMC), and rigid-body stability command and augmentation control laws and to demonstrate the potential benefits of thereby evaluating the closed-loop performance at specific flight conditions.

The complexity of the control task and the dynamic characteristics of a typical flexible transport airplane dictate the solution of a coupled multiloop control problem. The classical approach of synthesizing one loop at a time is not well suited to deal efficiently with coupled multiloop systems. Modern control theory offers the capability of synthesizing multiloop systems directly, thus taking advantage of favorable interactions between the control loops.

Figure E-1 indicates the design process flow. The main elements are model generation, linear analysis, optimal controller design, and simulation. The design is accomplished using a set of experimental computer programs on the Control Data Corporation (CDC) 6600 system. These programs, which were developed by Boeing prior to this contract, are particularly suited for the analysis and synthesis of multivariable controllers for Active Controls Technology (ACT) airplanes. They are based on time-domain modern control theory; key elements are state-space representation of dynamic systems, modal analysis, and optimal control and observer (Kalman filter) designs. In addition, portions of the environmental control analysis system (EASY 5) and QR programs are used (refs E-1 and E-2).

E.1.0 DYNAMIC MODELS

Control law synthesis and analysis require models of the flexible airplane, the measurements and loads, the actuation system, and the wind disturbances. These models are connected to perform open-loop analysis, control law synthesis, and, when combined with a control law, closed-loop performance evaluation.
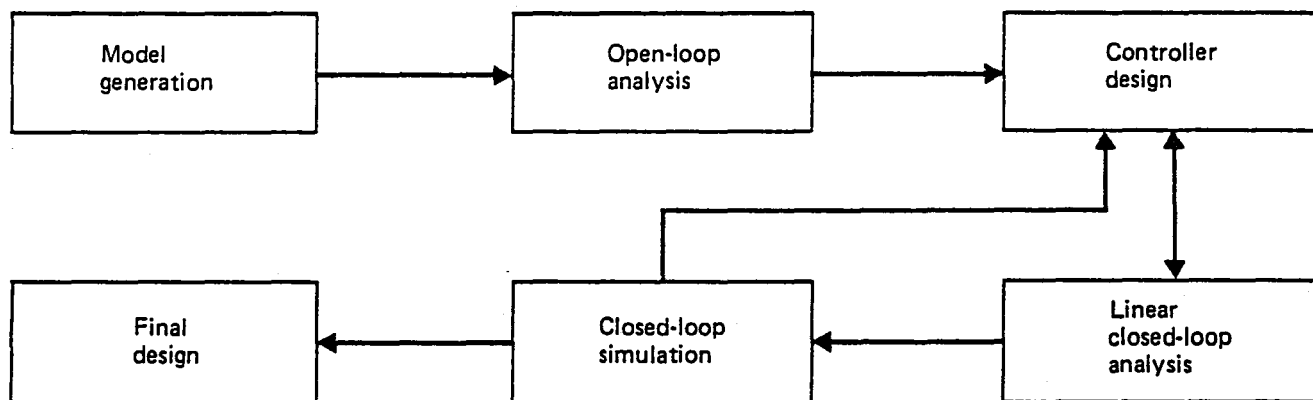
Figure E-1. Program Structure

E.1.1 FLEXIBLE AIRPLANE MODELS

Two configurations were analyzed during this study. The first was based on the drone for aerodynamic and structural testing (DAST 2) model. The second was based on the Initial ACT model. The unsteady aerodynamic representation differed in these two analyses, although in both cases the equations of motion for the flexible airplane were represented in the Laplace domain.

Figure E-2 shows the two forms of the flexible airplane equations of motion that were used. In both cases, the airplane at each flight condition is represented by a set of constant coefficient linear second-order differential equations modified by the addition of first-order lag terms that represent the effects of unsteady aerodynamics. Figures E-3 and E-4 are block diagram descriptions of the DAST 2 and Initial ACT Airplanes, respectively. There are blocks representing the steady and unsteady aerodynamic forces, the structural model, and the measurement model. These block diagrams are graphical descriptions of how the models are assembled using the EASY 5 model generation routine. After the input-to-output relations of each block and the block interconnections are specified by the user, a precompiler program generates Fortran subroutines that are combined to represent the complete model in program form. The individual blocks may represent nonlinear relationships. These models are used to perform static trim calculations, conduct simulations, and generate linear state models at specified operating points. These particular formulations produce well-structured state vectors consisting of q, rigid and elastic model coordinates; $\dot{q}$, the corresponding rates; $\bar{w}_g$, unsteady aero-

dynamic states due to wind; and, in the case of the DAST 2 model, $\bar{q}$ and $\bar{\delta}$, unsteady aerodynamic states associated with q and the control surface vector, δ, respectively. With this choice of states, it is seen that the unsteady aerodynamic forces are well defined and second and higher order derivatives of the vectors q, δ, and gust velocity vector w_g do not occur as states.

DAST 2

$$\left([\text{mass}]\ s^2 + [\text{damping}]\ s + [\text{stiffness}]\right)\ \left\{q(s)\right\}$$

$$+\left(\rho V\left[C_1\right]s + \rho V^2\left[C_0\right] + \rho V^2\sum_{i=1}^{4}\frac{s}{s+Vb_i}\left[D_i\right]\right)\left\{q(s)\right\}$$

$$+\left(\rho V\left[\bar{C}_1\right]s + \rho V^2\left[\bar{C}_0\right] + \rho V^2\sum_{i=1}^{4}\frac{s}{s+Vb_i}\left[\bar{D}_i\right]\right)\left\{\delta(s)\right\}$$

$$+\left(\rho V\left[R_0\right] + \rho V\sum_{i=1}^{4}\frac{s}{s+Vg_i}\left[R_i\right]\right)\ \left\{w_g(s)\right\} = \left\{0\right\}$$

Initial ACT Airplane

$$\left([S_2]\ s^2 + [S_1]\ s + [S_0]\right)\left\{q(s)\right\} + \left([\bar{S}_2]\ s^2 + [\bar{S}_1]\ s + [\bar{S}_0]\right)\left\{\delta(s)\right\}$$

$$\left([R_0] + \sum_{i=1}^{3}\frac{c_i s}{s+d_i}\left[R_0\right]\right)\left\{w_g(s)\right\} = \left\{0\right\}$$

where
$$[S_0] = [\text{stiffness}] + \frac{\rho V}{2}\ [A_0]$$
$$[S_1] = [\text{damping}] + \frac{\rho V}{2}\ [A_1]$$
$$[S_2] = [\text{mass}] + \frac{\rho}{2}[A_2]$$
$$[\bar{S}_0] = \frac{\rho V^2}{2}\ [\bar{A}_0]$$
$$[\bar{S}_1] = \frac{\rho V}{2}\ [\bar{A}_1]$$
$$[\bar{S}_2] = [\text{control surface inertia}] + \frac{\rho}{2}\ [\bar{A}_2]$$

$A_0, \bar{A}_0$ are quasi-steady airforces matrices

$A_1, \bar{A}_1, A_2, \bar{A}_2$ are unsteady airforces matrices

q   Rigid- and flexible-body deflections

δ Control surface deflections

w_g Gust velocities

Figure E-2. Equations of Motion

E-3
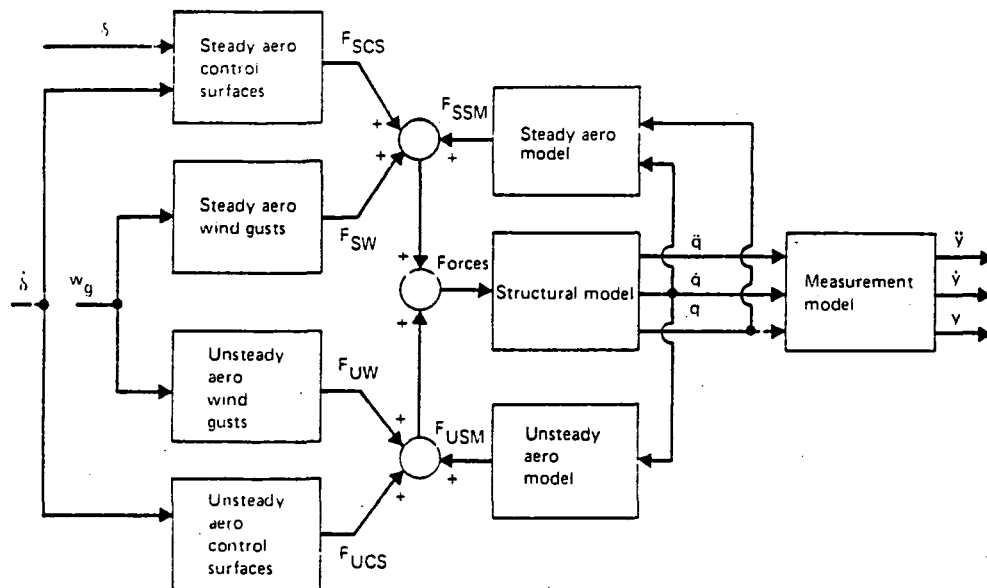
States:

q   Rigid- and flexible-mode deflections
$\dot{q}$ Corresponding rates
$\overline{q}$ Unsteady aerodynamic states associated with q
$\overline{\delta}$ Steady aerodynamic states associated with δ
$\overline{w}_g$ Unsteady gust states

*Figure E-3.   Model of Drone for Aerodynamic
and Structural Testing 2 Airplane*
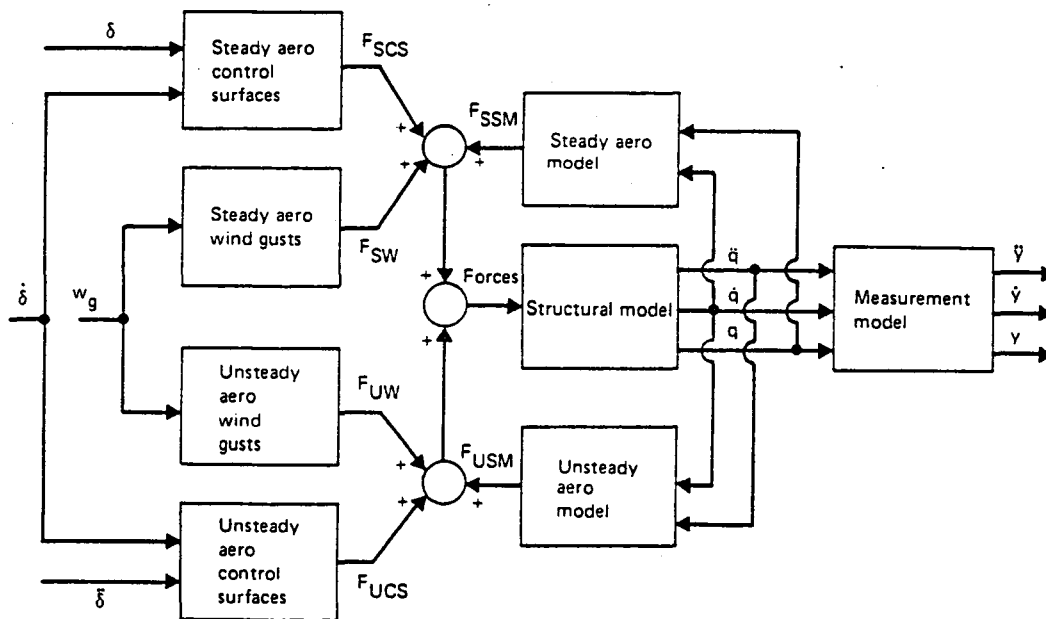
States:

q   Rigid- and flexible-mode deflections
$\dot{q}$ Corresponding rates
$\overline{w}_g$ Unsteady gust states

Figure E-4.   Model of Initial ACT Airplane

E-4

Transfer function:

$$F(s) = \rho V^2 \sum_{i=1}^{4} \frac{D_i s}{s + Vb_i} q(s)$$

q = coordinates for elastic and rigid modes

$\bar{q}_i$ = unsteady aerodynamic states, i = 1,2,3,4

f = forces due to unsteady aerodynamics

● Second-order and higher order derivatives of the vector q will not occur as states.
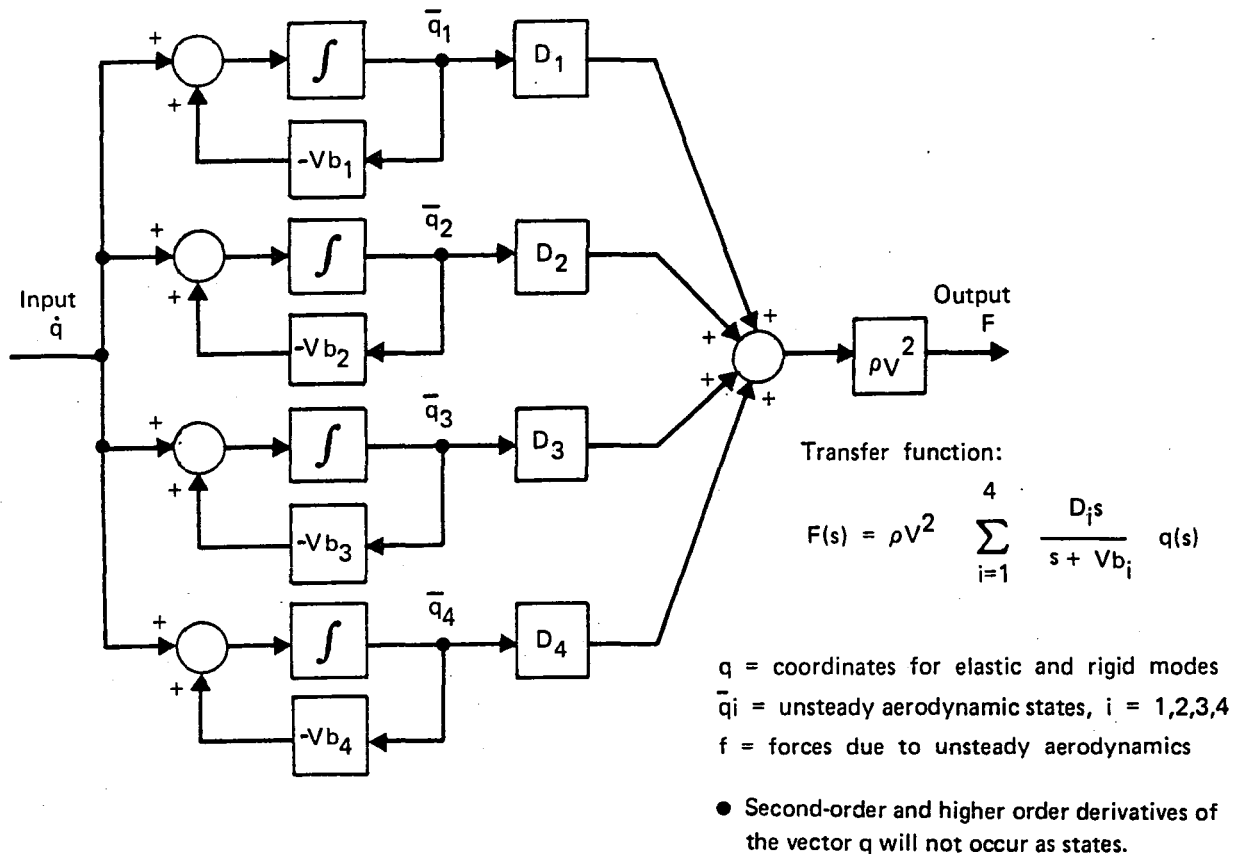
Figure E-5. Modeling of Unsteady Aerodynamics—Drone for Aerodynamic and Structural Testing 2

Some detailed comments are pertinent with respect to modeling unsteady aerodynamic forces. For the DAST 2 model, the unsteady aerodynamic forces are represented by the summation of the outputs from four first-order lags as shown in Figure E-5. This is the result of an approximate transformation from a frequency- to time-domain representation of these forces. The output from each integrator is a state. For each element of the input vector, $\dot{q}$, there are four unsteady aerodynamic states. The same holds for the control surface vector, δ, and the gust disturbance vector, w_g. Thus, in this case the unsteady aerodynamic representation increases the dynamic order of the model significantly.

For the Initial ACT Airplane, the approximate transformation from frequency- to time-domain representations of the aerodynamic forces, except for gust inputs, is accomplished with a least-square fit of a second-order polynomial in the Laplace variable s. This leaves the steady and unsteady aerodynamic forces as functions of displacements and the

corresponding first- and second-order time derivatives. This formulation does not increase the dynamic order of the system. The unsteady effects associated with gust inputs are approximated with Kussner lift growth functions. These are handled by introducing unsteady aerodynamic states much the same way as for the DAST 2 model. The state model of the flexible airplane takes the form

$$\dot{x}_a = A_a x_a + B_a u + \Gamma_a w_g \tag{E-1}$$

where x_a, u, and w_g are the state, control surface, and gust velocity vectors, respectively. Figure E-6 shows with more detail the linear state models for the DAST 2 and Initial ACT Airplanes. In the case of the DAST 2 model, the state vector was transformed from moving-inertial to body-fixed axes. This transformation is shown in Figure E-7, and the inertial-to-body axis transformation matrix, P, is shown in Figure E-8.

$$\dot{x}_a = A_a x_a + B_a u + \Gamma_a w_g$$

DAST 2

$$x_a = \begin{bmatrix} q \\ \dot{q} \\ \overline{\dot{q}} \\ \overline{\delta} \\ \overline{w}_g \end{bmatrix} \quad \text{and} \quad u = \begin{bmatrix} \delta \\ \dot{\delta} \end{bmatrix}$$

Initial ACT Airplane

$$x_a = \begin{bmatrix} q \\ \dot{q} \\ \overline{w}_g \end{bmatrix} \quad \text{and} \quad u = \begin{bmatrix} \delta \\ \dot{\delta} \\ \ddot{\delta} \end{bmatrix}$$

Figure E-6. State Models—Flexible Airplane

$$\dot{x}_I = A_a x_I + B_a u + \Gamma_a w_g \qquad \text{Airplane dynamics}$$

$$y = C_a x_I + D_a u + E_a w_g \qquad \text{Output equations}$$

Let

$$x_I = P x_B \qquad \text{Airplane dynamics}$$

$$\dot{x}_B = P^{-1} A_a P x_B + P^{-1} B_a u + P^{-1} \Gamma_a w_g$$

$$y = C_a P x_B + D_a u + E_a w_g \qquad \text{Output equations}$$

where

x_I = state vector moving-inertial axis coordinates

x_B = state vector body-fixed axis coordinates

P = inertial-to-body axis transformation matrix

Figure E-7. Axis Transformation—Drone for Aerodynamic and Structural Testing 2 (Symmetric Equations of Motion)

Figure E-8. Inertial-to-Body Axis Transformation Matrix—Drone for Aerodynamic and Structural Testing 2

$\dot{z}$ = vertical velocity

θ = pitch angle

$\bar{z}_1, \bar{z}_2, \bar{z}_3, \bar{z}_4$ = unsteady aerodynamic states associated with $\dot{z}$

$\bar{\theta}_1, \bar{\theta}_2, \bar{\theta}_3, \bar{\theta}_4$ = unsteady aerodynamic states associated with $\dot{\theta}$

V = true velocity

G_1, G_2, G_3, G_4 = constants associated with representations of unsteady aerodynamic forces

$G_i = V b_i$

I = identity matrix

E.1.2 QUASI-STATIC AEROELASTIC AIRPLANE MODELS

The quasi-static aeroelastic (QSAE) models were used for the design of the pitch-augmented stability (PAS) system. The QSAE model for each flight condition is a state model consisting of four first-order differential equations. The state equations are shown in terms of the dimensional derivatives in equation (E-2).

$$
\begin{bmatrix} \dot{u} \\[2ex] \dot{\alpha} \\[2ex] \dot{q} \\[2ex] \dot{\theta} \end{bmatrix}
=
\begin{bmatrix}
X_u & X_\alpha & X_q & g \\[2ex]
\dfrac{Z_u}{V-Z_{\dot\alpha}} & \dfrac{Z_\alpha}{V-Z_{\dot\alpha}} & \dfrac{(Z_q+V)}{V-Z_{\dot\alpha}} & 0 \\[2ex]
M_u + \dfrac{M_{\dot\alpha}Z_u}{V-Z_{\dot\alpha}} & M_\alpha + \dfrac{M_{\dot\alpha}Z_\alpha}{V-Z_{\dot\alpha}} & M_q + \dfrac{M_{\dot\alpha}(Z_q-V)}{V-Z_{\dot\alpha}} & 0 \\[2ex]
0 & 0 & 1 & 0
\end{bmatrix}
\begin{bmatrix} u \\[2ex] \alpha \\[2ex] q \\[2ex] \theta \end{bmatrix}
+
\begin{bmatrix}
X_{\delta_E} \\[2ex]
\dfrac{Z_{\delta_E}}{V-Z_{\dot\alpha}} \\[2ex]
\dfrac{M_{\dot\alpha}Z_{\delta_E}}{V-Z_{\dot\alpha}} + M_{\delta_E} \\[2ex]
0
\end{bmatrix}
\delta_E
$$

$$
+
\begin{bmatrix}
X_u & \dfrac{X_\alpha}{V} \\[2ex]
\dfrac{Z_u}{V-Z_{\dot\alpha}} & \dfrac{Z_\alpha/V}{V-Z_{\dot\alpha}} \\[2ex]
M_u + \dfrac{M_{\dot\alpha}Z_u}{V-Z_{\dot\alpha}} & \dfrac{M_\alpha}{V} + \dfrac{M_{\dot\alpha}/V}{V-Z_{\dot\alpha}} \\[2ex]
0 & 0
\end{bmatrix}
\begin{bmatrix} u_g \\[2ex] w_g \end{bmatrix}
$$

$$\text{(E-2)}$$

where the state vector, x_a, in stability coordinates has elements

$\quad u \quad = \quad$ incremental forward velocity (m/s)

$\quad \alpha \quad = \quad$ incremental angle of attack (rad)

$\quad q \quad = \quad$ incremental pitch rate (rad/s)

$\quad \theta \quad = \quad$ incremental pitch angle (rad)

and the control input is

$\quad \delta_E \quad = \quad$ incremental elevator deflection (rad)

The individual dimensional derivatives in the state model are

X_u = dimensional variation of X force with speed

X_α = dimensional variation of X force with angle of attack

X_q = dimensional variation of X force with pitch rate

g = acceleration of gravity

Z_u = dimensional variation of Z force with speed

Z_α = dimensional variation of Z force with angle of attack

$Z_{\dot{\alpha}}$ = dimensional variation of Z force with angle-of-attack rate

Z_q = dimensional variation of Z force with pitch rate

V = steady-state airspeed

M_u = dimensional variation of pitching moment with speed

M_α = dimensional variation of pitching moment with angle of attack

$M_{\dot{\alpha}}$ = dimensional variation of pitching moment with angle-of-attack rate

M_q = dimensional variation of pitching moment with pitch rate

X_{δ_E} = dimensional variation of X force with elevator angle

Z_{δ_E} = dimensional variation of Z force with elevator angle

M_{δ_E} = dimensional variation of pitching moment with elevator angle

E.1.3 OUTPUT MODELS

The needed output models are the displacements, velocities, accelerations, and loads at various airplane stations. The first three items are related to the modal coordinates, q, and the mode shape matrix, Φ , as follows:

$$
\begin{aligned}
\text{Positions} \quad & y = \Phi q \\
\text{Velocities} \quad & \dot{y} = \Phi \dot{q} \\
\text{Accelerations} \quad & \ddot{y} = \Phi \ddot{q}
\end{aligned}
\tag{E-3}
$$

The vector y is defined as

$$y = \begin{bmatrix} y_1 \\ y_2 \\ \cdot \\ \cdot \\ \cdot \\ y_m \end{bmatrix} \qquad\qquad \text{(E-4)}$$

where m is the number of sensor locations, and y_i (i = 1 to m) is a six-component translation and rotation vector at the ith station expressed as

$$y_i = \begin{bmatrix} Tx_i \\ Ty_i \\ Tz_i \\ Rx_i \\ Ry_i \\ Rz_i \end{bmatrix} \qquad\qquad \text{(E-5)}$$

For the DAST 2 model, the equations of motion and the mode shape matrix are in moving-inertial coordinates. The corresponding linear state models that included the output equations are transformed to body-fixed axes. For the Initial ACT Airplane, the equations of motion are expressed in body-fixed axes while the mode shape matrix is referenced to moving-inertial axes. Also, the x and z measurement axes are reversed with respect to the standard convention (x forward and z downward). The proper measurement equations are obtained by two coordinate transformations as shown in Figure E-9.

The loads are expressed as a function of the mode deflections, q, and load distribution matrix, Φ_L, as follows:

$$L = \Phi_L q \qquad\qquad \text{(E-6)}$$

where the vector L is defined as

$$L = \begin{bmatrix} L_1 \\ L_2 \\ \cdot \\ \cdot \\ \cdot \\ L_p \end{bmatrix} \qquad\qquad \text{(E-7)}$$

$$
\begin{bmatrix} q_I \\ \dot{q}_I \\ \ddot{q}_I \end{bmatrix} = T \begin{bmatrix} q_B \\ \dot{q}_B \\ \ddot{q}_B \end{bmatrix}
$$

Then for the measurements at the ith station

$$
\begin{bmatrix} y_i \\ \dot{y}_i \\ \ddot{y}_i \end{bmatrix} = \begin{bmatrix} s & 0 & 0 \\ 0 & s & 0 \\ 0 & 0 & s \end{bmatrix} \begin{bmatrix} \Phi_i & 0 & 0 \\ 0 & \Phi_i & 0 \\ 0 & 0 & \Phi_i \end{bmatrix} T \begin{bmatrix} q_B \\ \dot{q}_B \\ \ddot{q}_B \end{bmatrix}
$$

where

Φ_i = mode shape matrix at ith station

q_I = fixed inertial axis coordinates

q_B = moving-body axis coordinate

$$
q_I = \begin{bmatrix} x_I \\ z_I \\ \theta \\ \xi_1 \\ \xi_2 \\ \cdot \\ \cdot \end{bmatrix}, \quad q_B = \begin{bmatrix} x_B \\ z_B \\ \theta \\ \xi_1 \\ \xi_2 \\ \cdot \\ \cdot \end{bmatrix}
$$

● x_I, x_B, z_I, z_B are x and z axis rigid-body displacements in inertial and body axes, respectively

● $\theta, \xi_1, \xi_2 \ldots$ are pitch angle and flexible mode displacements, respectively

and

$$
S = \begin{bmatrix} -1 & 0 & 0 & 0 & 0 & 0 \\ 0 & 1 & 0 & 0 & 0 & 0 \\ 0 & 0 & -1 & 0 & 0 & 0 \\ 0 & 0 & 0 & -1 & 0 & 0 \\ 0 & 0 & 0 & 0 & 1 & 0 \\ 0 & 0 & 0 & 0 & 0 & -1 \end{bmatrix}, \quad T = \begin{bmatrix} T_1 & 0 & 0 \\ T_2 & T_1 & 0 \\ 0 & T_2 & T_1 \end{bmatrix}, \quad T_1 = \left[\begin{array}{ccc:c} -1 & 0 & 0 & 0 \\ 0 & -1 & 0 & \\ 0 & 0 & K_\theta & \\ \hdashline & 0 & & 1 \end{array} \right], \quad T_2 = \left[\begin{array}{ccc:c} 0 & 0 & 0 & 0 \\ 0 & 0 & V & \\ 0 & 0 & 0 & \\ \hdashline & 0 & & 0 \end{array} \right]
$$

I = identity matrix (size $n_{q2} \times n_{q2}$ where n_{q2} is number of flexible modes)

0 = zero matrix

V = true airspeed

K_θ = pitch angle scaling constant

Figure E-9. Axis Transformation—Initial ACT Airplane (Symmetric Equations of Motion)

where p is the number of load stations, and L_i (i = 1 to p) is a three-component vector consisting of the bending, torsion, and shear at the ith station, expressed as

$$L_i = \begin{bmatrix} B_i \\ T_i \\ S_i \end{bmatrix} \tag{E-8}$$

The displacement, velocity, and acceleration measurements and loads are all expressed in the general form of the state model output equation

$$y = C_a x_a + D_a u + E_a w_g \tag{E-9}$$

where y is a vector of measurements and loads, x_a is the state vector, u is the control surface vector, and w_g is the gust velocity vector.

E.1.4 ACTUATOR MODELS

Only linear actuator models have been considered during the control law synthesis portion of this study. They are supplied as transfer functions that are transformed to state models in the standard controllable form. Figure E-10 shows that the state vector consists of the surface position and its first and higher order derivatives. The surface deflection and the corresponding first and second time derivatives are selected as outputs because they are required as inputs to the flexible airplane model described in Subsection E.2.1. The general form of the model of the complete actuation system is

$$\dot{x}_u = A_u x_u + B_u u_c \tag{E-10}$$

$$u = C_u x_u \tag{E-11}$$

where x_u is the state vector for all the actuators, u is the control surface vector, and u_c is the control command vector. The nonlinear actuator model will be discussed in Subsection E.6.2.

Transfer function form
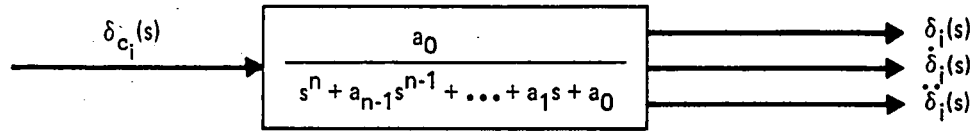
δ_{c_i} = ith control surface command (scalar)

δ_i = ith control surface position

State model formulation

- Standard controllable form

$$\dot{x}_{\delta_i}(t) = \begin{bmatrix} 0 & 1 & 0 & \cdot & \cdot & \cdot & 0 \\ 0 & 0 & 1 & & & & 0 \\ \cdot & \cdot & & \cdot & & & \cdot \\ \cdot & \cdot & & & \cdot & & \\ 0 & 0 & 0 & \cdot & & \cdot & 1 \\ -a_0 & -a_1 & -a_2 & \cdot & \cdot & \cdot & -a_{n-1} \end{bmatrix} x_{\delta_i}(t) + \begin{bmatrix} 0 \\ 0 \\ \cdot \\ \cdot \\ 0 \\ a_0 \end{bmatrix} \delta_{c_i}(t)$$

$$\begin{bmatrix} \delta_i(t) \\ \dot{\delta}_i(t) \\ \ddot{\delta}_i(t) \end{bmatrix} = \begin{bmatrix} 1 & 0 & 0 & 0 & \cdot & \cdot & 0 \\ 0 & 1 & 0 & 0 & \cdot & \cdot & \cdot \\ 0 & 0 & 1 & 0 & 0 & 0 & 0 \end{bmatrix} x_{\delta_i}(t)$$

$$x_{\delta_i}(t) = \begin{bmatrix} \delta_i(t) \\ \dot{\delta}_i(t) \\ \ddot{\delta}_i(t) \\ \cdot \\ \cdot \\ \cdot \end{bmatrix}$$

- m actuators are combined to one actuation system model

$$\dot{x}_u = A_u x_u + B_u u_c$$

$$u = C_u x_u$$

where

$$x_u = \begin{bmatrix} x_{\delta_1} \\ x_{\delta_2} \\ \cdot \\ \cdot \\ x_{\delta_m} \end{bmatrix}, \text{ and } u_c = \begin{bmatrix} \delta_{c_1} \\ \delta_{c_2} \\ \cdot \\ \cdot \\ \delta_{c_m} \end{bmatrix}$$

Figure E-10. Actuator Dynamic Model

E-13

E.1.5 WIND MODEL

Because of its simplicity and its ease in state model realization, the Dryden model was selected to represent gust disturbances. Gust penetration effects were neglected for the same reason. Figure E-11 shows the model in transfer function form and standard observable state model form for both the longitudinal and transverse gust velocities. The input is white noise, and the output is correlated gust velocities that have the Dryden power density spectrum. The general form of the gust disturbance model is

$$\dot{x}_w = A_w x_w + B_w w_c \qquad\qquad (E-12)$$

$$w_g = C_w x_w \qquad\qquad (E-13)$$

where x_w is the wind state vector, w_c is the white noise input scalar, and w_g is the gust velocity vector.

● Longitudinal gust velocity u:

$$w_c(s) \rightarrow \boxed{\dfrac{\sigma_u \sqrt{2}}{\sqrt{\gamma_u}} \cdot \dfrac{1}{(\gamma_u^{-1} s + 1)}} \rightarrow u(s)$$

$$\begin{cases} \dot{x}_w(t) = \begin{bmatrix} -\gamma_u \end{bmatrix} x_w(t) + \sigma_u \begin{bmatrix} \sqrt{2\gamma_u} \end{bmatrix} w_c(t) \\[2mm] u(t) = \begin{bmatrix} 1 \end{bmatrix} x_w(t) \end{cases}$$

● Transverse gust velocities v, w:

$$w_c(s) \rightarrow \boxed{\dfrac{\sigma_{v,w}}{\sqrt{\gamma_{v,w}}} \cdot \dfrac{(\sqrt{3}\,\gamma_{v,w}^{-1} s + 1)}{(\gamma_{v,w}^{-1} s + 1)^2}} \rightarrow v(s), w(s)$$

$$\begin{cases} \dot{x}_w(t) = \begin{bmatrix} 0 & -\gamma_{v,w}^2 \\ 1 & -2\gamma_{v,w} \end{bmatrix} x_w(t) + \\[3mm] \sigma_{v,w} \begin{bmatrix} \dfrac{\gamma_{v,w}\sqrt{\gamma_{v,w}}}{\sqrt{3\gamma_{v,w}}} \end{bmatrix} w_c(t) \\[3mm] v(t), w(t) = \begin{bmatrix} 0 & 1 \end{bmatrix} x_w(t) \end{cases}$$
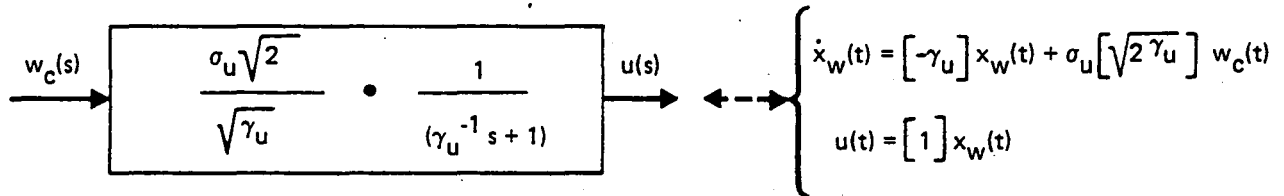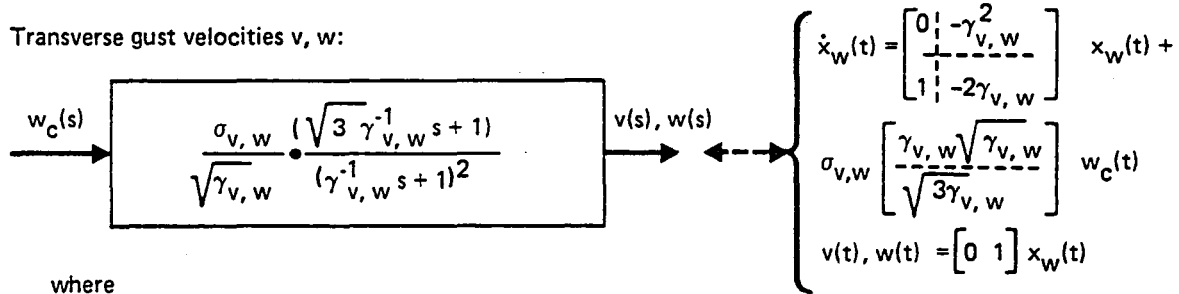
where

$$\gamma_u = \dfrac{V}{L_u} \quad , \quad \gamma_{v,w} = \dfrac{V}{L_{v,w}}$$

w_c = white noise of unity intensity

V = true airspeed

L_u = longitudinal turbulence scale length

$L_{v,w}$ = transverse turbulence scale lengths

σ_u = longitudinal rms gust intensity

$\sigma_{v,w}$ = transverse rms gust intensities

s = Laplace variable

Figure E-11. Dryden Turbulence Models

E.2.0 EIGENVALUE AND EIGENVECTOR COMPUTATION AND BLOCK DIAGONAL TRANSFORMATION

E.3.0 RESPONSE CALCULATION

E.2.0 EIGENVALUE AND EIGENVECTOR COMPUTATION
AND BLOCK DIAGONAL TRANSFORMATION

The stability and response characteristics of a linear aeroelastic system represented by a state model are completely described by the associated eigenvalues, eigenvectors, and the input and output distribution matrices. Consider a state model of the general form

$$\dot{x} = Ax + Bu + \Gamma w \qquad (E-14)$$

where

    x is an $n \times 1$ state vector

    u is an $m \times 1$ control vector

    w is a $p \times 1$ disturbance vector

    A is an $n \times n$ state matrix

    B is an $n \times m$ control distribution matrix

    Γ is an $n \times p$ disturbance distribution matrix

The eigenvalues of the system are the n values of $\lambda = (\lambda_1, \lambda_2, \dots \lambda_n)$ that satisfy the equation

$$\det (\lambda I - A) = 0 \qquad (E-15)$$

where I is an $n \times n$ identity matrix and $\det(\lambda I - A)$ means the determinant of the argument.

The eigenvectors v_i ($i = 1, 2, \dots n$) of the system are defined by the relation

$$Av_i = \lambda_i v_i \qquad i = 1, 2, \dots n \qquad (E-16)$$

If λ_i is a complex eigenvalue, then the corresponding eigenvector v_i is also complex. Because the state matrix A is real, it can be shown that complex eigenvalues and eigenvectors always occur in conjugate pairs. The complete eigensystem consists of n eigenvalues $\lambda_i (i = 1, 2, \dots n)$ and the corresponding n eigenvectors $v_i (i = 1, 2, \dots n)$.

Consider a similarity transformation T of the form

$$T = \begin{bmatrix} v_1 v_2 \cdots v_n \end{bmatrix} \tag{E-17}$$

whose columns are the eigenvectors of the matrix A. Let

$$x = Tz = \sum_{i=1}^{n} z_i v_i \tag{E-18}$$

where z_i (scalar) is a transformed coordinate of x in the direction of the eigenvector v_i. The matrix T of the similarity transformation is complex and so are the matrices of the transformed state model

$$\dot{z} = \Lambda z + (T^{-1}B)u + (T^{-1}\Gamma)w \tag{E-19}$$

where Λ is a diagonal matrix whose diagonal elements are the eigenvalues

$$\lambda_i \; (i = 1, 2, \ldots n)$$

i.e.,

$$\Lambda = T^{-1}AT = \begin{bmatrix} \lambda_1 & & & 0 \\ & \lambda_2 & & \\ & & \ddots & \\ 0 & & & \lambda_n \end{bmatrix} \tag{E-20}$$

An alternate form of the transformed system that avoids use of complex matrices can be obtained using a new similarity transformation matrix, T, whose columns now consist of the following vectors

$$T = \begin{bmatrix} t_1 t_2 \cdots t_i \, t_{i+1} \cdots t_n \end{bmatrix} \tag{E-21}$$

where the elements of the vectors t_i (i = 1, 2, ... n) are all real and defined as follows. For any real eigenvalue λ_i, the vector t_i is equal to the eigenvector v_i, while for any complex eigenvalue λ_i and its conjugate λ_{i+1} $(=\bar{\lambda}_i)$, the vectors t_i and t_{i+1} are given by

$$t_i = Re(v_i) + Im(v_i)$$

and

$$t_{i+1} = Re(v_i) - Im(v_i)$$

where Re(-) and Im(-) denote, respectively, the real and complex part of the argument. The matrix A is transformed by this similarity transformation into a block diagonal form

$$\Lambda = T^{-1}AT = \begin{bmatrix} \Lambda_1 & & & \\ & \ddots & & \\ & & \Lambda_i & \\ & & & \ddots \\ & & & & \Lambda_r \end{bmatrix} \qquad n/2 \leqslant r < n \tag{E-22}$$

Λ_i is block diagonal with 1 x 1 blocks for real eigenvalues and 2 x 2 blocks for complex conjugate pairs of eigenvalues; i.e.,

$$\Lambda_i = \begin{bmatrix} \sigma_i \end{bmatrix}_{1 \times 1} \text{ for real } \lambda_i = \sigma_i \tag{E-23}$$

and

$$\Lambda_i = \begin{bmatrix} \sigma_i & -\omega_i \\ \omega_i & \sigma_i \end{bmatrix}_{2 \times 2} \tag{E-24}$$

for the complex conjugate pairs

$$\lambda_i = \sigma_i + j\omega_i \text{ and } \lambda_{i+1} = \sigma_i - j\omega_i$$

The complete state model in block diagonal form is expressed in terms of the modal coordinate, z, as

$$\dot{z} = (T^{-1}AT)z + (T^{-1}B)u + (T^{-1}\Gamma)w \tag{E-25}$$

$$y = (CT)z + Du + Ew \tag{E-26}$$

E.3.0 RESPONSE CALCULATION

Traditionally, the frequency-domain power-spectral-density technique has been widely used to compute steady-state gust responses. This technique requires determination of a complex frequency response matrix relating gust-velocity inputs to output response variables and computation and integration of a large number of power and cross spectra. For a flexible airplane with a large number of lightly damped modes that are subjected to distributed random gust inputs, these calculations are costly and require careful modeling for accuracy. Using an option in the QR program (ref E-2), this technique has been used to compute the output power spectral density for a limited number of gust loads. The purpose of expressing the loads as a function of frequency is to establish the required bandwidth of gust control laws and understand the significant frequency content of the loads. For the majority of the response calculations, root-mean-square (rms) responses generate the most interest. In the present study, these responses are obtained by computing correlation matrices for the steady-state responses due to random gust inputs.

Time history simulation of the airplane dynamic response is a necessary part of evaluating system performance. Time history response calculation is accomplished using a state transition matrix approach. By incorporating the block diagonal form of the system matrix, this technique is more efficient and accurate than existing methods for simulation of linear systems. Load responses, control surface activities, and the time histories of other performance variables can be calculated in response to various inputs such as pilot commands and random and discrete wind gusts.

E.3.1 COVARIANCE ANALYSIS FOR ROOT-MEAN-SQUARE RESPONSE

A new approach is used to compute the steady-state response correlation matrices of a dynamic system subjected to random inputs. This method avoids computational difficulties and inaccuracies associated with lightly damped modes, approximate gust penetration effects, and the finite frequency range for integration. The calculations are performed using time-domain state-space representation of the airplane model. A transformed covariance matrix is obtained by computing convolution integrals. The values of the integrals can be evaluated in closed form for white and Dryden spectra, among others. Gust penetration effects as the airplane traverses the field of atmospheric turbulence are modeled by pure time delays, avoiding the use of Pade approximations.

Atmospheric turbulence in general is represented by a set of three-dimensional random velocity components. The gust velocities encountered at point r (measured with respect to the aircraft frame) are given by w_g (r + Vt, t), where V is the true airspeed vector. The various gust velocity input vectors at different stations are combined to form the single gust vector

$$w_g(t) = \begin{bmatrix} w_g(r_1 + Vt,t) \\ w_g(r_2 + Vt,t) \\ \cdot \\ \cdot \\ \cdot \\ w_g(r_m + Vt,t) \end{bmatrix}$$

(E-27)

where m is the total number of points at which gust forcing functions are applied. Only deviations from the mean wind velocity components are considered in the gust input; i.e., $E\left[w_g(t)\right] = 0$, where $E\left[\cdot\right]$ is the expected value operator of the ensemble average. Then, by definition, the time-lag cross-correlation functions between velocity components of $w_g(t)$ measured at the various points may be written as

$$\mathcal{R}(\tau) = E\left[W_g(t+\tau)W_g^T(t)\right] = \begin{bmatrix} R(r_{11} + V\tau.\tau) \cdots R(r_{1m} + V\tau,\tau) \\ \cdot \quad\quad\quad \cdot \\ \cdot \quad\quad\quad \cdot \\ \cdot \quad\quad\quad \cdot \\ R(r_{m1} + V\tau,\tau) \cdots R(r_{mm} + V\tau,\tau) \end{bmatrix}$$

(E-28)

The ijth element, $R(r_{ij} + V\tau, \tau)$, is a 3 x 3 correlation matrix given by

$$R(r_{ij}+V\tau,\tau) = E\left[w_g(r_i+V(t+\tau),t+\tau)w_g^T(r_j+Vt,t)\right]$$

(E-29)

and $r_{ij} = r_i - r_j$ for i,j = 1,m.

It can be shown that if the true airspeed, V, is large enough, then $R(r_{ij} + V\tau, \tau)$ is effectively independent of its explicit time argument, τ, so that

$$R(r_{ij}+V\tau,\tau) = R(r_{ij}+V\tau,0)$$

(E-30)

This equation expresses what is commonly termed Taylor's hypothesis and is valid under typical flight conditions. In isotropic turbulence, the klth element of the 3 x 3 correlation matrix $R(r_{ij} + V\tau, 0)$ can be expressed in terms of two correlation functions, $f(\tau)$ and $g(\tau)$, as

$$R_{kl}\ (r_{ij} + V\tau, 0) = \sigma^2 \left([f(\xi) - g(\xi)]\frac{\xi_k \xi_l}{\xi^2} + g(\xi)\delta_{kl}\right)$$ (E-31)

where

$$\xi = r_{ij} + V\tau$$ (E-32)

$$|\xi| = \sqrt{\xi_1^2 + \xi_2^2 + \xi_3^2}$$ (E-33)

σ^2 is the mean square turbulence intensity

ξ_i (i = 1,3) is the ith cartesian component of ξ

δ_{kl} is the Kronecker delta:

$$\delta_{kl} = \begin{cases} 1, k = 1 \\ 0. k \neq 1 \end{cases}$$ (E-34)

and $f(\xi)$ and $g(\xi)$ are the longitudinal and transverse correlation functions, respectively. The von Karman, Dryden, band-limited white noise, and white noise turbulence models have correlation functions of the forms shown in Figure E-12.

Consider a state model of the following form

$$\dot{x}(t) = Ax(t) + \Gamma w_g(t)$$ (E-35)

The initial conditions are $x(o) = x_o$, where $E\left[x_o\right] = 0$ and $E\left[x_o w_g^T(t)\right] = 0$. This means that the initial conditions, x_o, have zero mean values and are not correlated with the wind disturbance inputs $w_g(t)$ for all time t. The system output variables are written as

$$y(t) = Cx(t)$$ (E-36)

It can be shown that the state covariance matrix $\underline{X}(t) = E\left[x(t)x^T(t)\right]$ satisfies the Lyapunov matrix differential equation

$$\dot{\underline{X}}(t) = A\underline{X}(t) + \underline{X}(t)A^T + \int_{-\infty}^{T} \exp\left[A(t-u)\right] \Gamma \mathcal{R}(t-u)\Gamma^T du$$

$$+ \int_{-\infty}^{t} \Gamma \mathcal{R}^T(t-\tau)\Gamma^T \exp\left[A^T(t-u)\right] du$$

(E-37)

with initial conditions $\underline{X}(o) = E\left[x_0 x_0^T\right] = \underline{X}_o$.

	Von Karman	Dryden	Band-limited white noise	White noise
Longitudinal correlation function	$f(\xi) = \dfrac{2^{2/3}}{\Gamma(1/3)}(\beta\xi)^{1/3} K_{1/3}(\beta\xi)$	$f(\xi) = e^{-\alpha\xi}$	$f(\xi) = \dfrac{2\sin\omega_c\xi}{\pi\alpha\xi}$	$f(\xi) = \dfrac{2}{\alpha}\,\delta(\xi)$
Transverse correlation function	$g(\xi) = \dfrac{2^{2/3}}{\Gamma(1/3)}(\beta\xi)^{1/3}$ $\left[K_{1/3}(\beta\xi) - 1/2\beta\xi K_{2/3}(\beta\xi)\right]$	$g(\xi) = e^{-\alpha\xi}(1 - 1/2\alpha\xi)$	$g(\xi) = \dfrac{\sin\omega_c\xi}{\pi\alpha\xi}$	$g(\xi) = \dfrac{1}{\alpha}\,\delta(\xi)$

$\xi \geqslant o$

$\beta = 1/aL \qquad a = \dfrac{\Gamma(1/3)}{\Gamma(1/2)\,\Gamma(5/6)} \cong 1.339$

$\alpha = 1/L$

L = turbulence scale length

$K_{1/3}(\ )$ and $K_{2/3}(\ )$ are modified Bessel functions of the second kind

Figure E-12. Von Karman, Dryden, Band-Limited White Noise, and White Noise Correlation Functions

Assuming that A is a stable matrix, the equation has a steady-state solution $\underline{X}(\infty) = \lim\limits_{t\to\infty}$ $\underline{X}$ (t), which satisfies the algebraic matrix equation

$$A\,\underline{X}\,(\infty) + \underline{X}\,(\infty)\,A^T = -\int_0^\infty \exp[Au]\,\Gamma\,\mathfrak{R}(u)\Gamma^T du - \int_0^\infty \Gamma\mathfrak{R}^T(u)\Gamma^T \exp\left[A^Tu\right]\,du \qquad (E\text{-}38)$$

The solution of $\underline{X}(\infty)$ from equation (E-38) can be obtained efficiently using a modified version of the Bartel's and Stewart's algorithm, with the exception that the orthogonal similarity transformation of the matrix A to real Schur form has been replaced by a transformation to block diagonal form. The latter allows the indefinite integral on the right-hand side of equation (E-38) to be evaluated in closed form for the Dryden and white noise turbulence models. Numerical integration may still be required for other types of turbulence models such as von Karman and band-limited white noise. An efficient algorithm was developed to compute the incomplete Laplace transform of von Karman turbulence. It is described in Subsection E.3.2.

In terms of the block diagonal transformation, T, which is described in Section E.2.0, the system state transition matrix exp (Au) is

$$\exp[Au] = T\exp[\Lambda u]\,T^{-1} \qquad (E\text{-}39)$$

where

$$\exp[\Lambda u] = \begin{bmatrix} \exp[\Lambda_1 u] & & & \\ & \exp[\Lambda_2 u] & & 0 \\ & & \ddots & \\ & 0 & & \ddots \\ & & & \exp[\Lambda_r u] \end{bmatrix}$$

or

$$\exp[\Lambda_i u] = \begin{cases} \exp(\sigma_i u) & ,\lambda_i = \sigma_i \\[2ex] \begin{bmatrix} \exp(\sigma_i u)\cos\omega_i u & -\exp(\sigma_i u)\sin\omega_i u \\[2ex] \exp(\sigma_i u)\sin\omega_i u & \exp(\sigma_i u(\cos\omega_i u \end{bmatrix} & ,\lambda_i = \overline{\lambda}_{i+1} = \sigma_i + j\omega_i \end{cases} \qquad (E\text{-}40)$$

Using equation (E-39), the indefinite integral in equation (E-38) simplifies to

$$\int_0^\infty \exp[Au]\ \Gamma\mathcal{R}(u)\Gamma^T\ du = T\ \int_0^\infty \exp[\Lambda u]\ T^{-1}\ \Gamma\mathcal{R}(u)\Gamma^T\ du$$

$$= T\ \sum_{i=1}^{P}\ \sum_{j=1}^{P}\ \overline{\mathcal{R}}_{ij}T^{-1}\Gamma\ \Delta_{ij}\Gamma^T \tag{E-41}$$

where Δ_{ij} is a p x p matrix whose klth element is equal to $\delta_{ki}\,\delta_{1j}$, and

$$\overline{\mathcal{R}}_{ij} = \int_0^\infty \exp\left\{\Lambda u\right\}\ \mathcal{R}_{ij}(u)\ du \tag{E-42}$$

Note that p = 3m for a three-dimensional turbulence. The correlation function $\mathcal{R}_{ij}(u)$ is as defined in equation (E-28). It can be shown that the integration involved in equation (E-41) reduces to the evaluation of the Laplace transforms of the respective correlation functions, $\mathcal{R}_{ij}(u)$, which in turn depends only upon two scalar functions $f(\xi)$ and $g(\xi)$. The Laplace variable s of the transforms is evaluated at the system eigenvalues . $\lambda_i(i = 1,n)$. In this case, the Laplace transform is defined as

$$\mathcal{L}\left[\mathcal{R}_{ij}\right] = \int_0^\infty \mathcal{R}_{ij}(u)\ \exp(su)\ du \tag{E-43}$$

where the region of convergence lies in the left half of the complex s-plane; i.e., Re(s) < 0, which is identical to the domain of system stability. Thus, this approach eliminates the need for numerical integration when analytic expressions for the transforms of the longitudinal and transverse correlation functions, $f(\xi)$ and $g(\xi)$, respectively, are available. Gust-penetration effects are included by introducing a time shift in the argument ξ of the correlation function as shown in equation (E-32). The argument ξ is further simplified by assuming that

$$|\xi_2|\ ,\ |\xi_3|\ \ll\ |\xi_1|$$

This approximation implies that the spanwise correlations between gust stations are perfect and only gust penetration in the longitudinal direction is considered. The argument of the correlation function takes on the simplified form

$$\xi = |(X_i - X_j) + V_1 \tau|$$ (E-44)

The Laplace transforms of $f(\xi)$ and $g(\xi)$ for the Dryden and white noise turbulence models are shown in Figure E-13. Subsection E.3.2 describes the procedures whereby gust penetration effects can be included for the case of the von Karman turbulence model.

Using block diagonal transformation $\Lambda = T^{-1} A T$ and equation (E-41), the algebraic matrix equation (E-38) becomes

$$\Lambda Z + Z \Lambda^T = - \sum_{i=1}^{p} \sum_{j=1}^{p} \bar{\mathcal{R}}_{ij} T^{-1} \Gamma \Delta_{ij} (T^{-1} \Gamma)^T$$
$$- \left(\sum_{i=1}^{p} \sum_{j=1}^{p} \bar{\mathcal{R}}_{ij} T^{-1} \Gamma \Delta_{ij} (T^{-1} \Gamma)^T \right)^T$$ (E-45)

where $Z = T^{-1} \bar{X}(\infty) T^{-T}$. The system of linear equations in Z_{ij} arising from the matrix equation (E-45) is partitioned and solved using the Crout reduction. Solutions for the steady-state covariance matrix $\bar{X}(\infty)$ are given by

$$\bar{X}(\infty) = T Z T^T$$ (E-46)

Similarly, the steady-state covariance matrix for the system response rate $\dot{x}(t)$, defined as $\bar{X}'(\infty) = \lim_{t \to \infty} E[\dot{x}(t)\dot{x}^T(t)]$. is computed directly from an equivalent matrix Z'. It is given by

$$\bar{X}'(\infty) = T Z' T^T$$ (E-47)

where the matrix Z' satisfies the equation

$$\dot{Z} = \Lambda Z \Lambda^T + T^{-1} \Gamma \mathcal{R}(0)(T^{-1} \Gamma)^T + \Lambda \sum_{i=1}^{p} \sum_{j=1}^{p} \bar{\mathcal{R}}_{ij} T^{-1} \Gamma \Delta_{ij} (T^{-1} \Gamma)^T$$
$$+ \left(\Lambda \sum_{i=1}^{p} \sum_{j=1}^{p} \bar{\mathcal{R}}_{ij} T^{-1} \Gamma \Delta_{ij} (T^{-1} \Gamma) \right)^T$$ (E-48)

	Dryden	White noise
Longitudinal correlation function	$$\mathcal{L}\{f(\xi)\} = \begin{cases} \dfrac{e^{-\gamma\Delta}}{-s+\gamma} & ,\Delta \geq 0 \\[2ex] \dfrac{e^{-\gamma\Delta}-e^{s\Delta}}{-s-\gamma} + \dfrac{e^{s\Delta}}{-s+\gamma} & ,\Delta < 0 \end{cases}$$	$$\mathcal{L}\{f(\xi)\} = \begin{cases} 0 & ,\Delta > 0 \\[1ex] 1/\gamma & ,\Delta = 0 \\[1ex] \dfrac{2}{\gamma}e^{s\Delta} & ,\Delta < 0 \end{cases}$$
Transverse correlation function	$$\mathcal{L}\{g(\xi)\} = \begin{cases} \dfrac{(1-\frac{1}{2}\gamma\Delta)e^{-\gamma\Delta}}{-s+\gamma} - \dfrac{\frac{1}{2}\gamma e^{-\gamma\Delta}}{(-s+\gamma)^2} & ,\Delta \geq 0 \\[2ex] \dfrac{(1-\frac{1}{2}\gamma\Delta)e^{-\gamma\Delta}}{-s-\gamma} + \dfrac{\frac{1}{2}\gamma e^{-\gamma\Delta}}{(-s-\gamma)^2} & ,\Delta < 0 \\[2ex] + \dfrac{-3\gamma s^2 + \gamma^3}{(s^2-\gamma^2)^2}e^{s\Delta} \end{cases}$$	$$\mathcal{L}\{g(\xi)\} = \begin{cases} 0 & ,\Delta > 0 \\[1ex] 1/2\gamma & ,\Delta = 0 \\[1ex] \dfrac{1}{\gamma}e^{s\Delta} & ,\Delta < 0 \end{cases}$$

$$\Delta = \frac{X_i - X_j}{V}, \quad \gamma = \frac{V}{L}, \quad \mathcal{L}\{f(\xi)\} = \int_0^\infty f(\xi)e^{st}\, dt, \quad \mathcal{L}\{g(\xi)\} = \int_0^\infty g(\xi)e^{st}\, dt, \quad \xi = V(t + \Delta)$$

V = true airspeed, L = turbulence scale length

s = Laplace variable

Figure E-13. Laplace Transforms of the Longitudinal and Transverse Correlation Functions for the Dryden and White Noise Turbulence Models

The solution of the matrix $\underline{X}'(\infty)$ provides a means to compute the steady-state covariance for variables such as velocities and accelerations. Finally, the covariance matrices for the performance variables described in equation (E-36) and their rates are calculated from

$$\underline{Y}(\infty) = \lim_{t \to \infty} E[y(t)y^T(t)] = C\underline{X}(\infty)C^T \tag{E-49}$$

and

$$\underline{Y}'(\infty) = \lim_{t \to \infty} E[\dot{y}(t)\dot{y}^T(t)] = C\underline{X}'(\infty)C^T \tag{E-50}$$

respectively.

E-25

E.3.2 INTEGRAL REPRESENTATION OF INCOMPLETE LAPLACE TRANSFORM OF VON KARMAN TURBULENCE CORRELATIONS

Computation of gust covariance described in Subsection E.3.1 requires knowledge of the incomplete Laplace transform of the gust correlation function $\rho(t)$. For the Dryden turbulence model, integration can be performed in closed form as shown in Figure E-13. The computational procedure becomes complicated for the more realistic von Karman turbulence model. The correlation function of such a turbulence model involves evaluation of modified Bessel functions of the second kind. Numerical integration of these functions is cumbersome. An alternative method will be presented that requires only numerical integration of products of elementary and exponential functions.

The von Karman power-spectral-density functions are of the form

$$\Phi_1(\omega) = \frac{1}{2\pi} \frac{A^2}{(1 + B^2\omega^2)^{\theta}} \qquad \text{(E-51)}$$

for the longitudinal gust components and

$$\Phi_2(\omega) = \frac{1}{2\pi} \frac{C^2(1 + D^2\omega^2)}{(1 + B^2\omega^2)^{\theta+1}} \qquad \text{(E-52)}$$

for the transverse gust components where

$$A^2 = 2\sigma^2 \frac{L}{V}$$

$$B = a\frac{L}{V}$$

$$C^2 = \sigma^2 \frac{L}{V}$$

$$D = \sqrt{\frac{8}{3}} \, a \, \frac{L}{V}$$

$$\theta = \frac{5}{6}$$

$$a = 1.339$$

L = turbulence scale length

σ = turbulence rms intensity

It can be easily shown that equations (E-51) and (E-52) are in fact the output power spectral densities of the following linear filters, when driven by white noise input,

$$h_1(s) = \frac{A}{(1 + Bs)^\theta} \tag{E-53}$$

and

$$h_2(s) = \frac{C(1 + Ds)}{(1 + Bs)^{\theta+1}} \tag{E-54}$$

respectively.

The impulse response function of the linear filter $h_1(s)$ is given by the following integral representation:

$$h_1(t) = \frac{A}{B} \Gamma(\theta)^{-1}\Gamma(1-\theta) \int_{u=0}^{\infty} e^{-(u+1)t/B} u^{-\theta}du \tag{E-55}$$

From equation (E-55), the linear filter, equation (E-53), can be seen as being a combination, in parallel, of a continuum of first-order lag filters with poles located at $-(u + 1)/B$ and corresponding residues $\frac{A}{B}\Gamma(\theta)^{-1}\Gamma(1-\theta)^{-1}u^{-\theta}du$ for $0 < u < \infty$.

From equation (E-55), the von Karman correlation function for the longitudinal gust component can be represented (ref E-3)

$$\rho_1(t) = \int_{s=0}^{\infty} h_1(s) h_1(s+t) \, ds \quad (t > 0)$$

$$= \left(\frac{A}{B}\right)^2 \Gamma(\theta)^{-2}\Gamma(1-\theta)^{-2} \iiint e^{-(u+1)s/B} u^{-\theta} e^{-(y+1)(s+t)/B} y^{-\theta} dudyds \tag{E-56}$$

$$= \frac{A^2}{B} \Gamma(\theta)^{-2}\Gamma(1-\theta)^{-2} \iint e^{-(y+1)t/B} (u+y+2)^{-1} u^{-\theta} y^{-\theta} dudy$$

The incomplete Laplace transform of the correlation function $\rho_1(t)$ is given by

$$r_1(\Delta,\lambda) = \int_0^{\Delta} e^{-\lambda t}\rho(t) \, dt$$

$$= \frac{A^2}{B} \Gamma(\theta)^{-2}\Gamma(1-\theta)^{-2} \iint (1-e^{-\left[(y+1)/B+\lambda\right]\Delta}) \left[(y+1)/B+\lambda\right]^{-1}(u+y+2)^{-1} \tag{E-57}$$
$$\cdot u^{-\theta} y^{-\theta} dudy$$

To simplify this expression, the following equality was used:

$$\int_{u=0}^{\infty} u^{-\theta}(u+a)^{-1} du = \pi a^{-\theta}/\sin\pi\theta \qquad (E-58)$$

Integrating out the variable u in equation (E-57) using equation (E-58) to get

$$r_1(\Delta,\lambda) = K \int_{y=0}^{\infty} y^{-\theta}(y+2)^{-\theta}((y+1)/B+\lambda)^{-1}(1-e^{-\left[(y+1)/B+\lambda\right]}\Delta) dy \qquad (E-59)$$

where

$$K = \frac{A^2}{B} \Gamma(\theta)^{-2}\Gamma(1-\theta)^{-2}\pi/\sin\pi\theta = 2\pi\Gamma(5/6)^{-2}\Gamma(1/6)^{-2} \frac{A^2}{B}$$

The integrand in the right-hand side of equation (E-59) involves only elementary and exponential functions; therefore, the numerical integration can be easily performed. Due to a discontinuity at y = 0 of the function $y^{-\theta}$ in the integrand, the ordinary Simpson's rule is modified to avoid numerical inaccuracies near the origin. The procedure is described in the following paragraphs.

The integral in equation (E-59) can be rewritten as

$$I(\lambda,\Delta,\theta) = K \int_{y=0}^{\infty} y^{-\theta} f(y) dy \qquad (E-60)$$

where

$$f(y) = (y+2)^{-\theta}((y+1)/B+\lambda)^{-1}(1-e^{-\left[(y+1)/B+\lambda\right]}\Delta) \qquad (E-61)$$

Let $y_0 = 0$, y_1, ..., y_{2n} be a chosen grid for the numerical integration of equation (E-60). On the interval y_i, y_{i+2} where i = 0, 2, 4, ... , the function of f(y) can be approximated by a second-degree polynomial

$$p(y) = f(y_i)(y-y_{i+1})(y-y_{i+2})/(y_i-y_{i+1})(y_i-y_{i+2})$$
$$+ f(y_{i+1})(y-y_i)(y-y_{i+2})/(y_{i+1}-y_i)(y_{i+1}-y_{i+2}) \qquad (E-62)$$
$$+ f(y_{i+2})(y-y_i)(y-y_{i+1})/(y_{i+2}-y_i)(y_{i+2}-y_{i+1})$$

E-28

The contribution to the integral in equation (E-60) on the interval $\left[y_i, y_{i+2} \right]$ is therefore

$$
\begin{aligned}
I_i \; = \; & f(y_i)S(y_i,y_{i+2},y_{i+1},y_{i+2})/(y_i{-}y_{i+1})(y_i{-}y_{i+2}) \\[2mm]
& + \; f(y_{i+2})S(y_i,y_{i+2},y_i,y_{i+2})/(y_{i+1}{-}y_i)(y_{i+1}{-}y_{i+2}) \\[2mm]
& + \; f(y_{i+2})S(y_i,y_{i+2},y_i,y_{i+1})/(y_{i+2}{-}y_i)(y_{i+2}{-}y_{i+1})
\end{aligned}
\tag{E-63}
$$

where

$$
\begin{aligned}
S(a,b,c,d) \; = & \int_a^b (y{-}c)(y{-}d)y^{-\theta}dy \\[2mm]
= & \; (b^{3-\theta}{-}a^{3-\theta})/(3{-}\theta) - (c{+}d)(b^{2-\theta}{-}a^{2-\theta})/(2{-}\theta) \\[2mm]
& + \; cd(b^{1-\theta}{-}a^{1-\theta})/(1{-}\theta)
\end{aligned}
$$

The incomplete Laplace transform in equation (E-57) becomes

$$
r_1(\Delta,\lambda) \; = \; I(\Delta,\lambda,\theta) \; \cong \; K \sum_{i=0}^{N} I_i
\tag{E-64}
$$

Using this approach, fast convergence of the integration is achieved. For typical time delay constants encountered in gust penetration, turbulence scale length, airspeed, and range of rigid and flexible airplane dynamic modes, the number of integration points $N = 100$ was sufficient for the accuracy required to compute gust response covariance matrices. The coefficients of $f(y)$ in I_i of equation (E-63) need only to be evaluated once for the grid $y_0, \ldots, y_{2n}$, after which the incomplete Laplace transform defined in equation (E-57) can be simply computed for various values of Δ and λ.

The linear filter $h_2(s)$ shown in equation (E-54) can be rewritten in the following form:

$$
h_2(s) \; = \; \frac{C}{(1+Bs)^{\theta}} \left[\frac{D}{B} + \frac{(1-D/B)}{1+Bs} \right]
\tag{E-65}
$$

E-29

Its impulse response function $h_2(t)$ is equal to

$$h_2(t) = \frac{CD}{AB} h_1(t) + \frac{C}{AB} (1-D/B) h_1(t)*e^{-t/B} \tag{E-66}$$

where $h_1(t)$ is the longitudinal impulse response function introduced in equation (E-55) and * signifies the convolution. It follows from this that

$$h_2(t) = \frac{CD}{AB} h_1(t) + \frac{C}{AB} (1-D/B) h_T(t) \tag{E-67}$$

where

$$h_T(t) = \frac{A}{B} \Gamma(\theta)^{-1}\Gamma(1-\theta)^{-1} \int_{u=0}^{\infty} (e^{-(u+1)t/B}*e^{-t/B}) u^{-\theta}du$$

$$\tag{E-68}$$

$$h_T(t) = A \Gamma(\theta)^{-1}\Gamma(1-\theta)^{-1} \int_{u=0}^{\infty} (e^{-t/B} - e^{-(u+1)t/B}) u^{-(\theta+1)} du$$

Starting from equation (E-67) and proceeding in the same manner as shown previously, the following is the integral representation for the incomplete Laplace transform of the transverse correlation function $\rho_2(t)$ defined by

$$\rho_2(t) = \int_{s=0}^{\infty} h_2(s) h_2(s+t)ds \tag{E-69}$$

is obtained. It is given by

$$r_2(\Delta,\lambda) = \int_0^{\Delta} e^{-\lambda t}\rho_2(t)dt$$

$$= \left(\frac{CD}{AB}\right)^2 J_{11} + \left(\frac{CD}{AB}\right)^2 (1/D - 1/B)(J_{1T}+J_{T1}) \tag{E-70}$$

$$+ \left(\frac{CD}{AB}\right)^2 (1/D - 1/B)^2 J_{TT}$$

E-30

where

$$J_{11} = r_1(\Delta, \lambda) = \text{incomplete Laplace of the longitudinal correlation function}$$

$$J_{1T} = BK \int_{y=0}^{\infty} y^{-(\theta+1)} \left[\frac{1-e^{-(\lambda+1/B)\Delta}}{2^{\theta}(\lambda+1/B)} - \frac{1-e^{-(\lambda+(y+1)/B)\Delta}}{(y+2)^{\theta}(\lambda+(y+1)/B)} \right] dy \qquad \text{(E-71)}$$

$$J_{T1} = BK \int_{y=0}^{\infty} y^{-\theta}(y+2)^{-(\theta+1)} \frac{(1-e^{-(\lambda+(y+1)/B)\Delta})}{\lambda+(y+1)/B} \, dy \qquad \text{(E-72)}$$

and

$$J_{TT} = BK \int_{y=0}^{\infty} y^{-(\theta+1)} \left[\frac{1-e^{-(\lambda+1/B)\Delta}}{2^{\theta+1}(\lambda+1/B)} - \frac{1-e^{-(\lambda+(y+1)/B)\Delta}}{(y+2)^{\theta+1}(\lambda+(y+1)/B)} \right] dy \qquad \text{(E-73)}$$

Equations (E-71), (E-72), and (E-73) can be numerically integrated using the same algorithm described previously. It should again be emphasized that the computation involves only simple summations of elementary and exponential functions.

The approximate gust penetration effects described in Section E.3.0 can be easily accommodated using the preceding incomplete Laplace transforms. For a delay time constant Δ, the Laplace transforms of the correlation functions with this delay shift are computed from

$$R(\Delta,s) = \int_{0}^{\infty} e^{-st} \rho_i(t+\Delta) \, dt \qquad (i=1,2)$$

$$= \begin{cases} e^{s\Delta} \left(\int_{0}^{\infty} e^{-su} \rho_i(u) du + \int_{0}^{\Delta} e^{su} \rho_i(u) du \right) & , \quad \Delta < 0 \\[3mm] e^{s\Delta} \left(\int_{0}^{\infty} e^{-su} \rho_i(u) du - \int_{0}^{\Delta} e^{-su} \rho_i(u) du \right) & , \quad \Delta \geqslant 0 \end{cases} \qquad \text{(E-74)}$$

$$= \begin{cases} e^{s\Delta} \left[r_i(\infty,s) + r_i(-\Delta,-s) \right] & ; \quad \Delta < 0 \\[3mm] e^{s\Delta} \left[r_i(\infty,s) - r_i(\Delta,s) \right] & , \quad \Delta \geqslant 0 \end{cases}$$

where $r_i(\cdot,\cdot)$ are the incomplete Laplace transforms of von Karman correlation functions given in equations (E-59) and (E-70) for the longitudinal and transverse gust components, respectively.

E.3.3 LINEAR SIMULATION ALGORITHM

The linear dynamic model can be expressed in state-variable form as

$$\dot{x}(t) = Ax(t) + Bu(t) \tag{E-75}$$

where the state vector x(t) may consist of the rigid and flexible airplane modes, actuator states, and controller states and u(t) is the input vector consisting of pilot commands to the control surface and gust input. The output response variables are contained in the vector y(t) and given by

$$y(t) = Cx(t) + Du(t) \tag{E-76}$$

Equations (E-75) and (E-76) are rewritten using the block diagonal similarity transformation

$$x = Tz \tag{E-77}$$

to get

$$\dot{z}(t) = \Lambda z(t) + B'u(t) \tag{E-78}$$

and

$$y(t) = C'z(t) + Du(t) \tag{E-79}$$

where $\Lambda = T^{-1}AT$, $B' = T^{-1}B$, $C' = CT$, T is the block diagonalization transformation matrix, and Λ is the block diagonal system matrix (see sec E.2.0).

The transition of the system modal responses z(t) from time t to $t + \Delta t$ is given by

$$z(t+\Delta t) = e^{\Lambda\,\Delta t}z(t) + \int_{t}^{t+\Delta t} e^{\Lambda(t+\Delta t-\tau)}Bu(\tau)d\tau \tag{E-80}$$

E-32

where $e^{\Lambda \Delta t}$ is the modal state transition matrix. It is also given in block diagonal form by

$$e^{\Lambda \Delta t} = \begin{bmatrix} e^{\Lambda 1 \, \Delta t} & & & 0 \\ & e^{\Lambda 2 \, \Delta t} & & \\ & & \cdot & \\ & & e^{\Lambda i \, \Delta t} & \\ 0 & & & \cdot \end{bmatrix} \qquad \text{(E-81)}$$

where

$$e^{\Lambda_i \Delta t} = e^{\sigma_i \Delta t} \quad \text{for real eigenvalue} \quad \lambda_i = \sigma_i$$

and

$$e^{\Lambda_i \Delta t} = \begin{bmatrix} e^{\sigma_i \Delta t} \cos \omega_i \Delta t & -e^{\sigma_i \Delta t} \sin \omega_i \Delta t \\ e^{\sigma_i \Delta t} \sin \omega_i \Delta t & e^{\sigma_i \Delta t} \cos \omega_i \Delta t \end{bmatrix} \qquad \text{(E-82)}$$

for complex conjugate pair of eigenvalues $\lambda_i = \overline{\lambda}_{i+1} = \sigma_i + j \omega_i$. If again a constant input in the time interval between t and t + Δt is assumed, equation (E-80) becomes

$$z(t+\Delta t) = e^{\Lambda \, \Delta t} z(t) + \int_{t}^{t+\Delta t} e^{\Lambda(t+\Delta t - \tau)} B d\tau \, u^* \qquad \text{(E-83)}$$

or

$$z(t+\Delta t) = \phi z(t) + \overline{\theta} \, u^* \qquad \text{(E-84)}$$

where u* being some value of the input function in the interval $\left[t, \, t + \Delta t \right]$. Evaluation of the integral of the transition matrix can also be performed in closed-form based on the system eigenvalues λ_i (i = 1, n). It is given by

$$\int_{t}^{t+\Delta t} e^{\Lambda(t+\Delta t - \tau)} \, d\tau = \begin{bmatrix} I_1 & & 0 \\ & I_2 & \\ & & \cdot \\ 0 & & \cdot \end{bmatrix} \qquad \text{(E-85)}$$

E-33

where

$$I_i = \left[\sigma \frac{1}{i} \ (e^{\sigma_i \Delta t} - 1) \right] \text{ for real eigenvalue } \lambda_i = \sigma_i$$

and

$$I_i = \begin{bmatrix} \alpha_i & -\beta_i \\ \beta_i & \alpha_i \end{bmatrix} \tag{E-86}$$

for complex conjugate pair of eigenvalue $\lambda_i = \overline{\lambda}_{i+1} = \sigma_i + j\omega_i$. The parameters α_i and β_i are determined by the following expressions:

$$
\begin{aligned}
\alpha_i &= -\frac{\sigma_i(1-e^{\sigma_i \Delta t} \cos \omega_i \Delta t) + \omega_i \, e^{\sigma_i \Delta t} \sin \omega_i \Delta t}{\sigma_i^2 + \omega_i^2} \\[2em]
\beta_i &= \frac{\omega_i(1-e^{\sigma_i \Delta t} \cos \omega_i \Delta t) + \sigma_i \, e^{\sigma_i \Delta t} \sin \omega_i \Delta t}{\sigma_i^2 + \omega_i^2}
\end{aligned}
\tag{E-87}
$$

If the responses of the original states are required, they can be readily included as part of the output vector $y(t)$ through the use of the block diagonal transformation T; see equation (E-77). With the formulation stated in equation (E-81), the transition of the system modal responses $z(t)$ from time t to $t + \Delta t$ involves only multiplication of a sparse matrix.

For an nth-order system, the total number of operations at each integration step is at most $2n$ multiplications and additions plus n multiplications and additions for each input. This compares with n^2 and n, respectively, for a system that is not block diagonalized. For high-order systems with small time increments, the cost saving is substantial.

E.4.0   MODEL REDUCTION

E.5.0   OPEN-LOOP ANALYSIS

E.4.0 MODEL REDUCTION

The open-loop dynamic model must be simplified prior to the design of a practical controller for a flexible airplane. Likewise, any high-order Kalman filter that has been synthesized based on either a full-order or reduced-order open-loop model must, in most cases, be simplified before it is implemented in the flight computers. In both cases, the purpose is to reduce the order to a level consistent with computational capabilities while preserving the significant dynamic characteristics relative to the control objectives. Many techniques are available, but none will consistently produce accurate and meaningful results without a good understanding of the inherent physical relations behind the control task. Three methods and their use will be described here.

E.4.1 DELETION OF NONESSENTIAL STATES

Figure E-14 illustrates this method. The dynamic model is reduced in size by deleting rows and columns from the state model matrices. If the full model is of order n, and m states are deleted, the reduced model is of order n - m. This method is suitable for deleting nonessential states such as the x and z rigid-body displacement states from the longitudinal equations of motion. In this case, perturbations in x and z do not produce forces and moments, and the corresponding columns in the matrix A are filled with zeros. This method can also be used when the deleted states are not strongly coupled with the retained states. In the case of the phugoid mode, the forward velocity and pitch angle states can be deleted with insignificant impact on the remaining short-period and structural modes.

E.4.2 MODAL RESIDUALIZATION

This method for model reduction is suitable for systems with fast dynamics that are not significant with respect to the control task, or with uncontrollable or unobservable modes. This is typical for flexible airplanes that may have a large number of stable high-frequency modes and a number of weakly controllable or weakly observable modes. The dynamic contribution of the high-frequency modes is generally not modeled very accurately, and they need not be controlled to meet closed-loop design objectives, except that the control loop gain at high frequency must be sufficiently low so as not to destabilize any high-frequency mode. However, modal residualization retains the steady-state effect of higher frequency modes.

● Full-order state model:

$$
\begin{bmatrix} \dot{x}_1 \\ \dot{x}_2 \\ \vdots \\ \dot{x}_k \\ \vdots \\ \dot{x}_n \end{bmatrix}
=
\begin{bmatrix}
A_{11} & A_{12} & \cdots & A_{1k} & \cdots & A_{1n} \\
A_{21} & A_{22} & \cdots & A_{2k} & \cdots & A_{2n} \\
\vdots & & & \vdots & & \vdots \\
A_{k1} & A_{k2} & \cdots & A_{kk} & \cdots & A_{kn} \\
\vdots & & & \vdots & & \vdots \\
A_{n1} & A_{n2} & \cdots & A_{nk} & \cdots & A_{nn}
\end{bmatrix}
\begin{bmatrix} x_1 \\ x_2 \\ \vdots \\ x_k \\ \vdots \\ x_n \end{bmatrix}
+
\begin{bmatrix} B_1 \\ B_2 \\ \vdots \\ B_k \\ \vdots \\ B_n \end{bmatrix} u
+
\begin{bmatrix} \Gamma_1 \\ \Gamma_2 \\ \vdots \\ \Gamma_k \\ \vdots \\ \Gamma_n \end{bmatrix} w_g
$$

$$
y = \begin{bmatrix} C_1 & C_2 & \cdots & C_k & \cdots & C_n \end{bmatrix}
\begin{bmatrix} x_1 \\ x_2 \\ \vdots \\ x_k \\ \vdots \\ x_n \end{bmatrix} + Du + Ew_g
$$

● Delete rows and columns of matrix A

● Delete rows of matrix B

● Delete columns of matrix C

Figure E-14. Deletion of Nonessential States

The flexible airplane is represented by a set of linear time-invariant system equations of the form

$$\dot{x}_a = A_a x_a + B_a u + \Gamma_a w_g \qquad (E\text{-}88)$$

$$y = C_a x_a + D_a u + E_a w_g \qquad (E\text{-}89)$$

Assuming that the matrix A_a has a set of n independent eigenvectors, the equations are transformed to block diagonal form as described in Section E.2.0. The transformed system is described by the equations

$$x = Tz \qquad (E\text{-}90)$$

$$\dot{z} = T^{-1} A_a T z + T^{-1} B_a u + T^{-1} \Gamma_a w_g \qquad (E\text{-}91)$$

$$y = C_a T z + D_a u + E_a w_g \qquad (E\text{-}92)$$

The transformation matrix, T, is a square real matrix derived from the column eigenvectors of A_a. $\Lambda_a = (T^{-1} A_a T)$ is a block diagonal matrix whose elements are the eigenvalues (modes) of the system matrix A_a, and z is the modal coordinates. The state model is partitioned into two sets of modes, z_1 and z_2, as shown in Figure E-15. Having ordered the modes so that the upper partition contains low-frequency modes and all unstable modes, and the lower partition contains high-frequency stable modes, it is assumed that $z_2 \approx 0$. The practical interpretation of this assumption is that the modes z_2 respond much faster than the modes z_1 and that only the dynamics of z_1 are important with respect to the control task. If z_2 consists of i modes, the original nth-order system has been reduced to an (n - i)th-order system. The eigenvalues of the system are simply those of the retained modes, and the controllability and observability of these are unchanged from the original full-order model. The steady-state effects from the deleted modes z_2 are included in the outputs y through additional input terms.

E.4.3 LEAST-SQUARE ERROR MINIMIZATION

The design of an optimal controller combines the Kalman estimator design with the optimal gain matrix and generally has the same order as the dynamic model under investigation. The procedure of reduction using the modal residualization technique described in Subsection E.4.2 allows the designer to neglect fast stable dynamic modes and modes that are weakly controllable or weakly observable. The latter case corresponds

● Full-order model (in block diagonal form):

$$\dot{z} = \begin{bmatrix} \dot{z}_1 \\ \dot{z}_2 \end{bmatrix} = \begin{bmatrix} \Lambda_1 & 0 \\ 0 & \Lambda_2 \end{bmatrix} \begin{bmatrix} z_1 \\ z_2 \end{bmatrix} + \begin{bmatrix} B'_1 \\ B'_2 \end{bmatrix} \mu + \begin{bmatrix} \Gamma'_1 \\ \Gamma'_2 \end{bmatrix} w_g$$

$$y = \begin{bmatrix} C'_1 & C'_2 \end{bmatrix} \begin{bmatrix} z_1 \\ z_2 \end{bmatrix} + D_a u + E_a w_g$$

● Assumption:

$$\dot{z}_2 \simeq 0$$

● Reduced-order model:

$$\dot{z}_1 = \Lambda_1 z_1 + B'_1 u + \Gamma'_1 w_g$$

$$z_2 = -\Lambda_2^{-1} B'_2 u - \Lambda_2^{-1} \Gamma'_2 w_g$$

$$y = C'_1 z_1 + (D_a - C'_2 \Lambda_2^{-1} B'_2) u + (E_a - C'_2 \Lambda_2^{-1} \Gamma'_2) w_g$$

Figure E-15. Modal Residualization

to near pole-zero cancellations in the controller transfer functions. Even with these modes reduced, the resulting filter may still be too complex to be implemented on a flight computer. This subsection presents a procedure whereby a lower order filter can be derived from a high-order controller while preserving the same frequency response characteristics essential to the control tasks and lying within the bandwidth of the controlled system. The technique is based on the curve-fitting of filter single-loop frequency response against a specified model filter over a finite range of frequencies.

For example, suppose it is desired to approximate the ijth control loop transfer function $G(s)$ using a lower order filter $\hat{G}(s,p)$ that retains the dominant characteristics of the frequency response $G(j\omega)$ at a specified range of frequencies. To achieve this, a fit error function E is defined to be the integral of the error square between the actual and the modeled filter

$$E(p) = \frac{1}{2\pi} \int_{-\omega_{min}}^{\omega_{max}} |G(j\omega) - \hat{G}(j\omega, p)|^2 \, d\omega \tag{E-93}$$

over a range of frequencies between ω_{min} and ω_{max}. If $\omega_{min} = 0$ and $\omega_{max} = \infty$, this error function is also the integral of the deviation square in the impulse responses of the filters $G(s)$ and $\hat{G}(s,p)$, according to the Parseval's identity.

The set of transfer function parameters p is determined from the minimization of the error cost function E defined in equation (E-93). An efficient and simple algorithm has been developed by Boeing to solve for values of the parameter vector p. It is based mostly on the procedure described in Reference E-4. Briefly, the method consists of a modified conjugate gradient search to minimize the error function using proper scaling on the model parameters. Further constraints on the parameter signs are also imposed to ensure consistent filter phase and gain characteristics and to maintain filter stability requirements.

The aforementioned procedures can be applied to integrate design filters at various flight conditions. This is achieved by curve-fitting design frequency responses at different design points with a common filter whose parameters are determined such that the frequency responses closely match the results of individual filters developed for each flight condition.

E.5.0 OPEN-LOOP ANALYSIS

For the open-loop analysis, state models of the airplane, actuation systems, and wind disturbances are needed as shown in Figure E-16. All models are full order except for deletion of nonessential states. These three models are combined appropriately to perform the various analysis tasks.

E.5.1 STABILITY

Stability of the airplane rigid and flexible modes is determined by computing the eigenvalues of the dynamic models as described in Section E.2.0. This is done for several flight conditions and airplane mass distributions.

● Airplane dynamic model
and measurement model:
$$\begin{cases} \dot{x}_a = A_a x_a + B_a u + \Gamma_a w_g \\ y = H_a x_a + D_a u + E_a w_g \end{cases}$$

● Actuation system model:
$$\begin{cases} \dot{x}_u = A_u x_u + B_u u_c \\ u = C_u x_u \end{cases}$$

● Wind disturbance model:
$$\begin{cases} \dot{x}_w = A_w x_w + B_w w_c \\ w_g = C_w x_w \end{cases}$$

● Combined state model for analysis:
$$\begin{cases} \dot{x} = Ax + Bu_c + \Gamma w_c \\ y = Cx \end{cases}$$

where

$$x = \begin{pmatrix} x_a \\ x_u \\ x_w \end{pmatrix} \qquad A = \begin{bmatrix} A_a & B_a C_u & \Gamma_a C_w \\ 0 & A_u & 0 \\ 0 & 0 & A_w \end{bmatrix}$$

$$B = \begin{pmatrix} 0 \\ B_u \\ 0 \end{pmatrix}, \qquad \Gamma = \begin{bmatrix} 0 \\ 0 \\ B_w \end{bmatrix} \qquad C = \begin{bmatrix} H_a & D_a C_u & E_a C_w \end{bmatrix}$$

Figure E-16. Formulation of State Model for Open-Loop Analysis

E.5.2 OPEN-LOOP ROOT-MEAN-SQUARE GUST RESPONSES

For flight conditions where the open-loop airplane is stable, the steady-state gust response correlation matrices for the state; modal state; measurements; performance parameters such as bending moments, torsional moments, acceleration, etc.; and the output power spectral density of selected performance parameters are computed. The computational techniques are described in Section E.3.0. Because the load equations are based on a truncated set of modal coordinates, the load levels are only approximate. However, because all modes are included that are significant with respect to the control task, these approximate loads were considered adequate to evaluate the relative merits of various control laws.

For the various correlation matrices, the diagonal elements represent the variance of the gust response and the offdiagonal elements represent the cross-variance of the gust response. The significant frequency content of selected loads was determined by computing the load output power-spectral-density functions.

E.5.3 OPEN-LOOP LINEAR SIMULATIONS

The linear simulation algorithm described in Subsection E.3.2 was used to simulate the open-loop airplane. The open-loop equations are

$$\begin{bmatrix} \dot{x}_a \\ \\ \dot{x}_u \end{bmatrix} = \begin{bmatrix} A_a & | & B_a C_u \\ -- & | & --- \\ 0 & | & A_u \end{bmatrix} \begin{bmatrix} x_a \\ \\ x_u \end{bmatrix} + \begin{bmatrix} 0 \\ \\ B_u \end{bmatrix} \delta_c + \begin{bmatrix} \Gamma_a C_w \\ \\ 0 \end{bmatrix} x_w \qquad \text{(E-94)}$$

$$y = \begin{bmatrix} C_a & C_u \end{bmatrix} \begin{bmatrix} x_a \\ \\ x_u \end{bmatrix} + D_w x_w \qquad \text{(E-95)}$$

where x_a is the airplane state vector, defined in equation (E-2), and x_u is the state vector of the actuator, described in Volume I, Subsection 13.1.2. The matrices A_a and B_a are defined in Volume I, Subsection 13.1.1, and C_u is defined in Volume I, Subsection 13.1.2. Γ_a is defined in Volume I, Subsection 13.1.5, and C_w is defined in Volume I, Subsection 13.1.3. The y vector is the output vector consisting of the states and the scalar n_z, the normal acceleration, expressed as a linear combination of the state

E-40

variables, and the wind vector x_w, defined in Volume I, Subsection 13.1.3. D_w is the direct-transmission matrix relating the output to the wind disturbance. 0 denotes a zero matrix.

The differential equations and output equations (E-94) are converted to a set of difference equations in the form

$$z[(k+1)\Delta t] = \phi z[k(\Delta t)] + \theta u^*$$

(E-96)

$$y[k(\Delta t)] = C z[k(\Delta t)] + D u^*$$

where $z[k(\Delta t)]$ is a set of modal coordinates and ϕ is a sparse matrix as discussed in Subsection E.3.7.

Also,

$$u^* = \begin{bmatrix} \delta_c^* \\ x_w^* \end{bmatrix}$$

(E-97)

where δ_c is the commanded elevator angle and x_w is the wind state vector.

E.5.4 CONTROLLABILITY

The initial open-loop airplane model contains a selection of several possible control surfaces that may be suitable for the control task. One or more of these must be selected for the final design. Two criteria are used in this selection process: mode controllability and performance parameter controllability.

Consider an nth-order state model of the airplane and the actuation system

$$\dot{x} = Ax + Bu$$

(E-98)

$$y = Cx$$

(E-99)

All modes of this open-loop system are controllable by the control vector, u, if and only if the following controllability matrix

$$\mathcal{C} = [B, AB, \ldots A^{n-1}B] \qquad \text{(E-100)}$$

has rank n. In practice, satisfying this criterion is neither a necessary condition nor a sufficient condition with regard to adequacy of the control u to perform the control task. However, the relative controllability of a given mode by the various elements of the control vector u can be obtained by transforming equation (E-98) into block diagonal form (see sec E.2.0) and by appropriate scaling of the control vector. In practice, the elements of u are bounded in magnitude; therefore,

$$|u_i| \leq u_{i_{max}} \quad (i = 1, 2 \ldots m)$$

where $u_{i_{max}}$ is the maximum absolute value of the control u_i. Then the transformation is defined

$$u = T_u u_s \qquad \text{(E-101)}$$

where

$$T_u = \begin{bmatrix} u_{1_{max}} & & & 0 \\ & \ddots & & \\ & & u_{i_{max}} & \\ & & & \ddots \\ 0 & & & u_{m_{max}} \end{bmatrix}$$

and

$$|u_{s_i}| \leq 1 \quad (i = 1, 2 \ldots m)$$

u_s is a scaled control vector with elements bounded by ± 1.

Transforming equation (E-98) into block diagonal form and substituting equation (E-101) gives

$$\dot{z} = T^{-1}ATz + T^{-1}BT_u u_s \qquad \text{(E-102)}$$

Inspection of the columns of the transformed control matrix

$$B' = T^{-1}BT_u \qquad \text{(E-103)}$$

will show the coupling of each control into the various modes. To assess the relative effectiveness of the controls in controlling a particular mode, we only have to examine the corresponding row (or two rows, if the mode is oscillatory) of the matrix B'. The column with the largest absolute value will identify the most effective control.

The concern is not only the control of specific modes but also the control of certain performance parameters such as bending moments, torsional moments, accelerations, etc., at various airplane stations. These are represented by the state model output equation (E-99). The relative controllability of these can be assessed by computing the steady-state output response correlation matrices given an appropriately scaled white noise input at the individual control actuators.

Consider the state model with a single input u_i

$$\dot{x} = Ax + B_i u_i \qquad \text{(E-104)}$$

$$y = Cx \qquad \text{(E-105)}$$

where u_i is a scalar input corresponding to the ith control and is stationary white Gaussian noise with the properties

$$E[u_i] = 0 \qquad \text{(E-106)}$$

$$E[u_i(t)u_i(\tau)] = u_{i_{max}}^2 \, \delta(t-\tau) \qquad \text{(E-107)}$$

where $u_{i_{max}} > 0$ is the intensity of the input noise, $E[\,-\,]$ is the expected value operator, and $\delta(t-\tau)$ is the impulse function. Using the method described in Section E.3.0, the steady-state response correlation matrix is computed for the output vector y.

E-43

This is repeated for all the control inputs u_i (i = 1 to m). For a given performance parameter, y_j, there will be a set of m variances

$$v_{jj} \Big|_i = E\left[y_j y_j\right]_i \quad i = 1 \text{ to } m \tag{E-108}$$

where m is the number of controls. The most effective control, u_i, with respect to the performance parameter y_j is identified by the largest variance $v_{jj}\big|_i$.

Both mode controllability and performance parameter controllability criteria described previously only assess relative controllability and do not guarantee that the selected controls are adequate to perform the control task. However, evaluating the closed-loop control surface responses of a full-state feedback design will determine whether or not a given choice of controls is adequate to perform the control task.

E.5.5 OBSERVABILITY

The initial open-loop model contains measurement equations for sensors placed at a large number of possible locations. One or more of these will be selected for the final design. Two criteria are used for this selection: mode observability and performance parameter observability.

Consider an nth-order state model of an airplane that is excited by random gust velocities, w_g, and expressed as

$$\dot{x} = Ax + \Gamma w_g \tag{E-109}$$

$$y = Cx + E w_g \tag{E-110}$$

All the modes of this system are observable from the output vector, y, if and only if the following observability matrix

$$\mathcal{O} = \begin{bmatrix} C \\ CA \\ CA^{n-1} \end{bmatrix} T \tag{E-111}$$

has rank n. In practice, satisfying this criterion is neither a necessary condition nor a sufficient condition with regard to the adequacy of the measurements relative to the control task. However, the relative observability of the rigid and flexible modes from measurements at the various airplane stations can be obtained by transforming equation (E-109) into block diagonal form (see sec E.2.0). Consider a set of like measurements, y; e.g., all linear accelerations or all angular accelerations, at the possible sensor locations and expressed in terms of the block diagonal coordinate, z, as

$$y = CTz + Ew_g \qquad \text{(E-112)}$$

Inspection of the columns of the transformed measurement matrix

$$C' = CT \qquad \text{(E-113)}$$

shows the relative observability of the system modes from measurements at the various locations. The row containing the largest absolute value identifies the most suitable location for that particular type of sensor.

We are concerned not only with observation of specific modes but also with observation of certain performance parameters such as bending moments, torsional moments, accelerations, etc., that are excited by the random gust inputs, but which cannot be measured directly. Again, consider the state model represented by equations (E-109) and (E-110). In this case, the output vector, y, consists of various performance parameters that are not directly measurable, as well as a set of measurements at all possible sensor locations. Using the method described in Section E.3.0, the steady-state gust response correlation matrix is computed for the complete output vector y. For a given performance parameter, y_j, there is a set of p normalized cross-variances

$$v_{ji} = \frac{E\,[y_j y_i]}{\sqrt{E\,[y_j y_j]}} \qquad i = 1 \text{ to } p \qquad \text{(E-114)}$$

where p is the number of sensor locations. The most suitable sensor location is identified by the largest absolute value of the normalized cross-variance v_{ji}. For a given performance parameter, y_j, and input gust intensity, w_g, the relative magnitudes of the cross-variances depend on the correlation between the given performance variable y_j and the measurement y_i and the magnitude of the measurement variance v_{ii}. Thus, using the magnitude of the normalized cross-variance as a basis for sensor selection ensures the best combination of sensor-to-performance criteria correlation and sensor output signal-to-noise ratio.

This Page Intentionally Left Blank

E.6.0 CONTROL LAW SYNTHESIS

E.6.0 CONTROL LAW SYNTHESIS

Control law synthesis consists of formulation of a state model for synthesis, modified linear quadratic regulator design, modified Kalman state estimator design, and controller simplification.

E.6.1 FORMULATION OF STATE MODEL FOR SYNTHESIS

Figure E-17 shows the state model for synthesis. It comprises the airplane dynamic model, actuation system model, and the wind disturbance model. The airplane dynamic model is in block diagonal form and may be a full- or reduced-order model. This study has primarily been concerned with the full-order model except for deletion of nonessential states. The actuation system model contains the state models of all control surface actuators that will be used for the particular control task. The linear regulator provides optimum closed-loop response with respect to release from initial conditions and with respect to random input disturbances that have a flat power spectrum over the range of

● Airplane dynamic model (block diagonal form):

$$\begin{cases} \dot{z}_R = \Lambda_R z_R + B_R u + \Gamma_R w_g \\ y = C_R z_R + D_R u + E_R w_g \end{cases}$$

● Actuation system model:

$$\begin{cases} \dot{x}_u = A_u x_u + B_u u_c \\ u = C_u x_u \end{cases}$$

● Wind disturbance model:

$$\begin{cases} \dot{x}_w = A_w x_w + B_w w_c \\ w_g = C_w x_w \end{cases}$$

● Combined state model for synthesis:

$$\begin{cases} \dot{x} = Ax + Bu_c + \Gamma w_c \\ y = Cx \end{cases} \qquad C = \begin{bmatrix} C_R & D_R C_u & E_R C_W \end{bmatrix}$$

where

$$x = \begin{bmatrix} z_R \\ x_u \\ x_w \end{bmatrix}, A = \begin{bmatrix} \Lambda_R & B_R C_u & \Gamma_R C_w \\ 0 & A_u & 0 \\ 0 & 0 & A_w \end{bmatrix}, B = \begin{bmatrix} 0 \\ B_u \\ 0 \end{bmatrix}, \Gamma = \begin{bmatrix} 0 \\ 0 \\ B_w \end{bmatrix}$$

Figure E-17. Formulation of State Model for Synthesis

frequencies characteristic of the airplane. The power spectrum of turbulence is not flat over the range of rigid and structural mode frequencies of a transport airplane. Thus, it is necessary to augment the synthesis model with a model of the atmosphere that has white noise as an input and gust velocities with the desired power spectrums as an output. This implies that for a control law to alleviate loads due to gusts, it is necessary to feed back the gust states. These states are observable from acceleration sensors.

E.6.2 LINEAR REGULATOR DESIGN

Application of optimal control theory furnishes direct synthesis of the structure and gains of an aircraft control system. Optimal control is based on minimizing a cost functional, subjected to the constraints of the equations of motion. The most important prerequisite for the design is specification of the performance criterion. In some problems, the construction of the cost functional is obvious (e.g., minimum time, minimum fuel, etc.), but in most cases it is not. The quadratic cost function, which is an integral of quadratically weighted state or output perturbations and the control commands, has been used in the design of airplane controllers. It has won acceptance because, for linear systems, the solution is easily computed, the control is linear, and the method is readily applicable to multivariable systems.

To meet the closed-loop requirements of an active control transport, three methods for directly incorporating specific design criteria in the optimal control law synthesis have been adopted. The first method is the usual quadratic cost penalty on specific performance criteria such as deflection, velocity, acceleration, or load. The second method is implicit model-following, which is used to structure the cost function so that the dynamic response of the closed-loop system approaches that of the model. This is a suitable method for incorporating handling qualities criteria or other transient and steady-state response specifications. The third method is specification of a minimum degree of stability. This will ensure that all closed-loop eigenvalues will be placed to the left of a line parallel to the imaginary axis.

In the following, equations for a continous optimal system based on an implicit model with control terms are derived using the variational approach. The solution yields feedforward and feedback gains. These results are extended to the case where the cost function is structured using the implicit model technique for some states, while a conventional

quadratic cost formulation is used for the remaining states. Finally, a method is delineated for specifying a prescribed degree of stability for the closed-loop system via the cost function.

The airplane and controls are represented by an n-dimensional time-invariant vector differential equation

$$\dot{x} = Ax + Bu \qquad (E-115)$$

The desired performance is described by an n-dimensional time-invariant model

$$\dot{x}_m = A_m x_m + B_m u_m \qquad (E-116)$$

The problem is to find the p-dimensional control

$$u = Gx + Mu_m \qquad (E-117)$$

so as to minimize the cost function

$$J = \tfrac{1}{2} \int_0^\infty [(\dot{x}-\dot{x}_m)^T Q(\dot{x}-\dot{x}_m) + u^T Ru] \, dt \qquad (E-118)$$

where matrices Q(n x n) and R(p x p) are constant, symmetric, and positive semidefinite and positive definite, respectively. Substituting equations (E-115) and (E-116) into equation (E-118) and letting x_m = x, the cost function becomes

$$J = \tfrac{1}{2} \int_0^\infty [x^T(A-A_m)^T Q(A-A_m) x + 2x^T (A-A_m)^T Q(Bu-B_m u_m)$$
$$+ (Bu-B_m u_m)^T Q(Bu-B_m u_m) + u^T Ru] \, dt \qquad (E-119)$$

The Hamiltonian is formed

$$H = \tfrac{1}{2}[x^T(A-A_m)^T Q(A-A_m)x + 2x^T(A-A_m)^T QBu$$
$$- 2x^T (A-A_m)^T QB_m u_m + u^T B^T QBu$$
$$- 2u^T B^T QB_m u_m + u_m^T B_m^T QB_m u_m + u^T Ru] + p^T(Ax+Bu) \qquad (E-120)$$

E-49

where p is an n-dimensional vector of Lagrange multipliers (or costate vector).

On the optimal trajectory

$$\frac{\partial H}{\partial u} = 0 \qquad \text{control equation} \tag{E-121}$$

$$\dot{x} = \left(\frac{\partial H}{\partial p}\right)^T \qquad \text{state equation} \tag{E-122}$$

$$\dot{p} = -\left(\frac{\partial H}{\partial x}\right)^T \qquad \text{costate equation} \tag{E-123}$$

Using equations (E-120) and (E-121)

$$u = -(B^TQB+R)^{-1}B^TQ(A-A_m)x - (B^TQB+R)^{-1}B^Tp + (B^TQB+R)^{-1}B^TQB_mu_m \tag{E-124}$$

from equations (E-120), (E-122), and (E-124)

$$\dot{x} = (A-B(B^TQB+R)^{-1}B^TQ(A-A_m))x - B(B^TQB+R)^{-1}B^Tp + B(B^TQB+R)^{-1}B^TQB_mu_m$$

from equations (E-120), (E-123), and (E-124)

$$\dot{p} = (A-A_m)^T(QB(B^TQB+R)^{-1}B^TQ-Q)(A-A_m)x+((A-A_m)^TQB(B^TQB+R)^{-1}B^T-A^T)p$$
$$+ (A-A_m)^TQ(I-B(B^TQB+R)^{-1}B^TQ)B_mu_m$$

The state and costate equations become

$$\begin{bmatrix} \dot{x} \\ \dot{p} \end{bmatrix} = \begin{bmatrix} \bar{A} & -\bar{S} \\ -\bar{Q} & -\bar{A}^T \end{bmatrix} \begin{bmatrix} x \\ p \end{bmatrix} + \begin{bmatrix} \bar{B} \\ \bar{C} \end{bmatrix} u_m \tag{E-125}$$

with boundary conditions

$$x_{t_o} = x_o \tag{E-126}$$

$$p_{t_f} = 0 \tag{E-127}$$

where t_o is the initial time and t_f is the final time.

Also

$$\bar{A} = A - B (B^TQB+R)^{-1}B^TQ (A-A_m)$$

$$\bar{S} = B (B^TQB+R)^{-1}B^T$$

$$\bar{Q} = (A-A_m)^T(Q-QB(B^TQB+R)^{-1}B^TQ)(A-A_m)$$

$$\bar{B} = B(B^TQB+R)^{-1}B^TQB_m$$

$$\bar{C} = (A-A_m)^T(Q-QB(B^TQB+R)^{-1}B^TQ)B_m$$

The solution for p is of the form

$$p = Kx + N \tag{E-128}$$

Differentiating equation (E-128)

$$\dot{p} = \dot{K}x + K\dot{x} + \dot{N} \tag{E-129}$$

Substituting from equations (E-125) and (E-128) into equation (E-129)

$$\dot{p} = (\dot{K} + K\bar{A} - K\bar{S}K)x - K\bar{S}N + \dot{N} + K\bar{B}u_m \tag{E-130}$$

and from equations (E-125) and (E-128)

$$\dot{p} = -(\bar{Q} + \bar{A}^TK)x - \bar{A}^TN + \bar{C}u_m \tag{E-131}$$

Subtracting equation (E-131) from (E-130)

$$(\dot{K} + K\bar{A} - K\bar{S}K + \bar{A}^TK + \bar{Q})x + \dot{N} + (\bar{A}^T - K\bar{S})N + (K\bar{B} - \bar{C})u_m = 0 \tag{E-132}$$

Equation (E-132) must be satisfied for any arbitrary x and u_m. Thus, these two relations must be satisfied

$$\dot{K} + K\bar{A} - K\bar{S}K + \bar{A}^TK + \bar{Q} = 0 \tag{E-133}$$

$$\dot{N} + (\bar{A}^T - K\bar{S})N + (K\bar{B} - \bar{C})u_m = 0 \tag{E-134}$$

E-51

with boundary conditions from equations (E-127) and (E-128)

$$K_{t_f} = 0$$
$$N_{t_f} = 0$$

Equations (E-133) and (E-134) and the associated boundary conditions represent a linear tracking problem. The matrix Riccati equation (E-133) can be solved independently of equation (E-134), and the solution is used to compute the optimal feedback. This feedback is the same as that of the equivalent linear regulator problem. For an infinite time controller, only the steady-state solution is of interest. There are several methods for obtaining the solution to the matrix Riccati equation; however, the modified eigenvector technique used in the EASY 5 program appears to be the most efficient method.

Having obtained the solution to equation (E-133), equation (E-134) can be solved. Let K_{ss} be the steady-state solution to the matrix Riccati equation; then from equations (E-125), (E-128), and (E-134)

$$\begin{bmatrix} \dot{x} \\ \dot{N} \end{bmatrix} = \begin{bmatrix} (\bar{A} - \bar{S}K_{ss}) & -\bar{S} \\ 0 & -(\bar{A} - \bar{S}K_{ss})^T \end{bmatrix} \begin{bmatrix} x \\ N \end{bmatrix} + \begin{bmatrix} \bar{B} \\ (\bar{C} - K_{ss}\bar{B}) \end{bmatrix} u_m \qquad (E\text{-}135)$$

where

$$x_{t_0} = x_0$$
$$N_{t_f} = 0$$

The matrix $(\bar{A} - \bar{S}K_{ss})$ is the closed-loop system matrix. If all the unstable modes of the unaugmented plant are controllable, the closed-loop system eigenvalues all have negative real parts. The matrix $(\bar{S}K_{ss} - \bar{A})^T$ associated with the feedforward term N has an eigenvalue system that is the mirror image of that of the closed-loop system; i.e., all real parts are positive. It should be noted that both K_{ss} and $\bar{S}$ are symmetric matrices. The solution for N is obtained by integrating backward in time, starting with the boundary condition at time t_f (final time). Thus, to obtain the feedforward control at some point in time, it is necessary to know the control u_m for all time. To develop a practical solution,

it is necessary to assume that u_m is constant. The practical interpretation of this assumption is that the changes in u_m occur slowly with respect to the closed-loop system dynamics; i.e., $\dot{N}$ will be small. This agrees with the way steady-state control responses (e.g., elevator per g, steady-state roll rate, etc.) are specified in handling qualities criteria.

If u_m is assumed constant, then for an infinite-time controller, the steady-state value for N is

$$N_{ss} = (\bar{A}^T - K_{ss}\bar{S})^{-1}(\bar{C} - K_{ss}\bar{B})u_m \tag{E-136}$$

which reduces equation (E-135) to

$$\dot{x} = (\bar{A} - \bar{S}K_{ss})x + \left[\bar{B} - \bar{S}(\bar{A}^T - K_{ss}\bar{S})^{-1}(\bar{C} - K_{ss}\bar{B})\right]u_m \tag{E-137}$$

or

$$\dot{x} = (A + BG)x + BMu_m \tag{E-138}$$

Figure E-18 is a schematic of the closed-loop system described by equations (E-137) or (E-138). The feedback and feedforward gain matrices G and M are expressed as follows

$$G = -(B^TQB+R)^{-1}B^TQ(A-A_m) - (B^TQB+R)^{-1}B^TK_{ss} \tag{E-139}$$

$$M = (B^TQB+R)^{-1}B^TQB_m + (B^TQB+R)^{-1}B^T(\bar{A}^T-K_{ss}\bar{S})^{-1}(K_{ss}\bar{B}-\bar{C}) \tag{E-140}$$

Equations (E-124), (E-139), and (E-140) show that both the feedback and feedforward gains are made up of two parts. The first is synthesized directly from the cross product of state and control in the cost function, prior to the solution of the state and costate equations (E-125). The second part results from the solution of the matrix Riccati equation (E-133) and the forward control equation (E-134), respectively.

The optimal feedback matrix G is independent of the model control matrix B_m and is also identical to that of the equivalent linear regulator problem (i.e., with $B_m = 0$). The
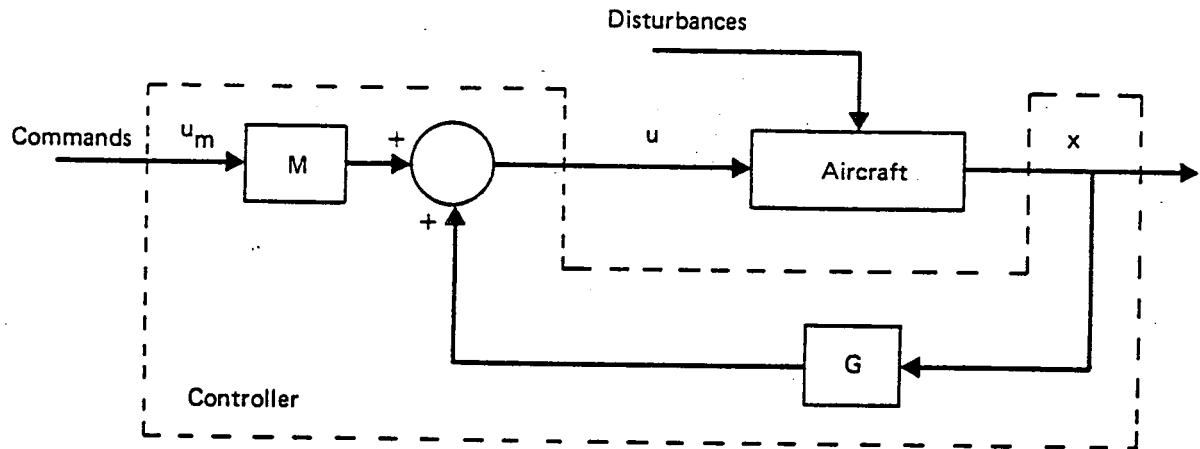
Figure E-18. Implicit Model-Following

optimal feedforward matrix M depends on the model, the unaugmented system, and the feedback matrix G.

For a solution to exist to the optimal control problem, a necessary condition is that the matrix $(B^T QB + R)$ is nonsingular. This is ensured by the constraints placed on the matrices Q and R. However, if Q is nonsingular and B has full rank, $B^T QB$ is nonsingular and R can be equal to zero. Furthermore, if B is square matrix, then perfect model-following is achieved. If $R = 0$ and $(B^T QB)^{-1} = B^{-1}Q^{-1}(B^T)^{-1}$ exists, then

$$\bar{A} = A - (A - A_m) = A_m$$
$$\bar{S} = Q^{-1}$$
$$\bar{Q} = 0$$
$$\bar{B} = B_m$$
$$\bar{C} = 0$$

Equation (E-125) is modified to

$$\begin{bmatrix} \dot{x} \\ \dot{p} \end{bmatrix} = \begin{bmatrix} A_m & -Q^{-1} \\ 0 & -A^T_m \end{bmatrix} \begin{bmatrix} x \\ p \end{bmatrix} + \begin{bmatrix} B_m \\ 0 \end{bmatrix} u_m \qquad (E-141)$$

Because $p_{t_f} = 0$, then $p = 0$; and from equation (E-128), $K = 0$ and $N = 0$ for all time.

The closed-loop system becomes

$$\dot{x} = A_m x + B_m u_m \tag{E-142}$$

To achieve this, the feedback and feedforward matrices are respectively

$$G = -B^{-1} (A-A_m) \tag{E-143}$$

and

$$M = B^{-1} B_m \tag{E-144}$$

These results could also be derived simply by inspection of equations (E-115), (E-116), and (E-117).

It may not be desirable to use the implicit model-following technique to structure the cost function for all states. Typically, for a flexible aircraft, implicit model-following could be used for the rigid-body modes and a conventional quadratic cost formulation used for the flexible structural modes. This problem is solved simply by extending the results derived in the preceding section.

Again, the flexible aircraft and associated controls are represented by the time-invariant vector differential equation

$$\dot{x} = Ax + Bu \tag{E-145}$$

The desired rigid mode performance is described by a time-invariant model

$$\dot{x}_m = A_m x_m + B_m u_m \tag{E-146}$$

A and A_m are $n \times n$ constant matrices.

B is an $n \times p$ constant matrix.

B_m is an n x j constant matrix.

Suppose implicit model-following is used for i states using j controls. Partition the matrices as follows:

$$A = \begin{bmatrix} A_{11} & \vdots & A_{12} \\ i \times i & \vdots & i \times (n-i) \\ \cdots\cdots\cdots & + & \cdots\cdots\cdots \\ A_{21} & \vdots & A_{22} \\ (n-i)\times i & \vdots & (n-i)\times(n-i) \end{bmatrix} \quad \text{where } x = \begin{bmatrix} x_1 \\ x_2 \\ \cdot \\ x_i \\ \cdot \\ x_m \end{bmatrix}$$

and

$$B = \begin{bmatrix} B_{11} & \vdots & B_{12} \\ i \times j & \vdots & i \times (p-j) \\ \cdots\cdots\cdots & + & \cdots\cdots\cdots \\ B_{21} & \vdots & B_{22} \\ (n-i)\times j & \vdots & (n-i)\times(p-j) \end{bmatrix} \quad \text{where } u = \begin{bmatrix} u_1 \\ u_2 \\ \cdot \\ u_j \\ \cdot \\ u_p \end{bmatrix}$$

Let

$$A_m = \begin{bmatrix} A_{m_{11}} & \vdots & A_{m_{12}} \\ i \times i & \vdots & i \times (n-i) \\ \cdots\cdots\cdots & + & \cdots\cdots\cdots \\ A_{m_{21}} & \vdots & A_{m_{22}} \\ (n-i)\times i & \vdots & (n-i)\times(n-i) \end{bmatrix} \quad \text{and } x_m = \begin{bmatrix} x_{m_1} \\ x_{m_2} \\ \cdot \\ x_{m_i} \\ \cdot \\ x_{m_n} \end{bmatrix}$$

and

$$B_m = \begin{bmatrix} B_{m_{11}} \\ i \times j \\ \cdots\cdots \\ 0 \\ (n-i)\times j \end{bmatrix} \quad \text{and } u_m = \begin{bmatrix} u_{m_1} \\ u_{m_2} \\ \cdot \\ \cdot \\ u_{m_p} \end{bmatrix}$$

Define

$$A_{m_{12}} = A_{12}$$

$$A_{m_{21}} = A_{21} \qquad\qquad \text{(E-147)}$$

$$A_{m_{22}} = A_{22}$$

then from equation (E-147)

$$A - A_m = \begin{bmatrix} A_{11} - A_{m_{11}} & \vdots & \\ i \times i & \vdots & 0 \\ \hline 0 & \vdots & 0 \end{bmatrix}$$

The problem is to find the p-dimensional control

$$u = Gx + Mu_m \qquad\qquad \text{(E-148)}$$

so as to minimize the cost function

$$J = \tfrac{1}{2} \int_0^\infty [(\dot{x} - \dot{x}_m)^T Q_1 (\dot{x} - \dot{x}_m) + x^T Q_2 x + u^T Ru] \ dt \qquad \text{(E-149)}$$

The first term represents the cost function for the rigid-body states, the second term represents additional quadratic cost, and the third term represents the cost function for the total control vector. The cost weight matrix, Q_2, is obtained from the cost weight matrix, Q'_2, on a set of output parameters, y, by letting

$$y = Cx$$

and

$$x^T Q_2 x = x^T C^T Q'_2 C x$$

then

$$Q_2 = C^T Q'_2 C$$

Substituting equations (E-145) and (E-146) into equation (E-149) and letting $x_m = x$, the cost function becomes

$$J = \tfrac{1}{2} \int_0^\infty [x^T (A-A_m)^T Q_1 (A-A_m)x + 2x^T (A-A_m)^T Q_1 (Bu-B_m u_m)$$
$$+ (Bu-B_m u_m)^T Q_1 (Bu-B_m u_m) + x^T Q_2 x + u^T Ru] \, dt \qquad \text{(E-150)}$$

Q_1 (n x n) and Q_2 (n x n) are positive, semidefinite, and symmetric; and R is positive, definite, and symmetric.

The Hamiltonian is formed

$$H = \tfrac{1}{2} \left\{ x^T [(A-A_m)^T Q_1 (A-A_m) + Q_2] x \right.$$
$$+ u^T (B^T Q_1 B + R) u + 2x^T (A-A_m)^T Q_1 Bu$$
$$- 2x^T (A-A_m)^T Q_1 B_m u_m - 2u^T B^T Q_1 B_m u_m \qquad \text{(E-151)}$$
$$\left. + u_m^T B_m^T Q_1 B_m u_m \right\} + p^T (Ax + Bu)$$

where p is an n-dimensional vector of Lagrange multipliers (or costate vector).

On the optimal trajectory

$$\frac{\partial H}{\partial u} = 0 \qquad \text{control equation} \qquad \text{(E-121)}$$

$$\dot{x} = \left(\frac{\partial H}{\partial p}\right)^T \qquad \text{state equation} \qquad \text{(E-122)}$$

$$\dot{p} = -\left(\frac{\partial H}{\partial x}\right)^T \qquad \text{costate equation} \qquad \text{(E-123)}$$

From equations (E-151) and (E-121)

$$u = -(B^TQ_1B+R)^{-1}B^TQ_1(A-A_m)x + (B^TQ_1B+R)^{-1}B^TQ_1B_mu_m$$

$$-(B^TQ_1B+R)^{-1}B^Tp$$

(E-152)

From equations (E-151), (E-122), and (E-152)

$$\dot{x} = [A-B(B^TQ_1B+R)^{-1}B^TQ_1(A-A_m)]\,x - B(B^TQ_1B+R)^{-1}B^Tp$$

$$+ B(B^TQ_1B+R)^{-1}B^TQ_1B_mu_m$$

From equations (E-151), (E-123), and (E-152)

$$\dot{p} = -[Q_2+(A-A_m)^T(Q_1-Q_1B(B^TQ_1B+R)^{-1}B^TQ_1)(A-A_m)]\,x$$

$$- (A^T- (A-A_m)^TQ_1B(B^TQ_1B+R)^{-1}B^T]\,p$$

$$- (A-A_m)^T[Q_1B(B^TQ_1B+R)^{-1}B^TQ_1-Q_1]\,B_mu_m$$

The state and costate equations become

$$\begin{bmatrix} \dot{x} \\ \dot{p} \end{bmatrix} = \begin{bmatrix} \bar{A}_1 & -\bar{S}_1 \\ -\bar{Q}_1 & -\bar{A}^T_1 \end{bmatrix} \begin{bmatrix} x \\ p \end{bmatrix} + \begin{bmatrix} \bar{B}_1 \\ \bar{C}_1 \end{bmatrix} u_m$$

(E-153)

with boundary conditions

$$x_{t_o} = x_o$$

$$p_{t_f} = 0$$

where t_o is initial time and t_f is final time.

Also

$$\bar{A}_1 = A-B(B^TQ_1B+R)^{-1}B^TQ_1(A-A_m)$$

$$\bar{S}_1 = B(B^TQ_1B+R)^{-1}B^T$$

$$\bar{Q}_1 = Q_2+(A-A_m)^T(Q_1-Q_1B(B^TQ_1B+R)^{-1}B^TQ_1)(A-A_m)$$

$$\bar{B}_1 = B(B^TQ_1B+R)^{-1}B^TQ_1B_m$$

$$\bar{C}_1 = (A-A_m)^T[Q_1-Q_1B(B^TQ_1B+R)^{-1}B^TQ_1]B_m$$

Equation (E-153) is of the same form as equation (E-125). Thus, the method of solution derived previously can be applied with appropriate substitutions for $\bar{A}$, $\bar{S}$, $\bar{Q}$, $\bar{B}$, and $\bar{C}$.

The feedback and feedforward gain matrices G and M are expressed respectively as

$$G = -(B^T Q_1 B + R)^{-1} B^T Q_1 (A - A_m) - (B^T Q_1 B + R)^{-1} B^T K'_{ss} \qquad \text{(E-154)}$$

$$M = (B^T Q_1 B + R)^{-1} B^T Q_1 B_m + (B^T Q_1 B + R)^{-1} B^T (\bar{A}_1{}^T K'_{ss} \bar{S}_1)^{-1} (K'_{ss} \bar{B}_1 - \bar{C}_1) \qquad \text{(E-155)}$$

where K'_{ss} is the steady-state solution to the matrix Riccati equation

$$\dot{K}' + K' \bar{A}_1 - K' \bar{S}_1 K' + \bar{A}_1{}^T K' + \bar{Q}_1 = 0$$

It can be shown by substitution of the partitioned matrices A, A_m, B, B_m, Q_1, Q_2, and R into equations (E-154) and (E-155) that the term $(B^T Q_1 B)$ adds cost penalty to the controls, and if

$$G = G' + G''$$

where

$$G' = -(B^T Q_1 B + R)^{-1} B^T Q_1 (A - A_m)$$

$$G'' = -(B^T Q_1 B + R)^{-1} B^T K'_{ss}$$

then

$$G = \begin{bmatrix} G'_{11} & 0 \\ j \times i & j \times (n-i) \\ \hline G'_{21} & 0 \\ (p-j) \times i & (p-j) \times (n-i) \end{bmatrix} + \begin{bmatrix} G''_{11} & G''_{12} \\ j \times i & j \times (n-i) \\ \hline G''_{21} & G''_{22} \\ (p-j) \times i & (p-j) \times (n-i) \end{bmatrix}$$

The first term in equation (E-154) provides feedback from the first i states (i.e., only the rigid-body states). Thus, this term is associated with the implicit model-following.

The feedforward matrix M has the following structure

$$M = \begin{bmatrix} M_{11} \\ \underline{j \times j} \\ M_{21} \\ (p-j) \times j \end{bmatrix}$$

Thus, only the j controls associated with the implicit model-following are fed forward.

The following describes a method for specifying a prescribed degree of stability for the closed-loop system via the cost function. It can be shown that for time-invariant systems, with performance indices of the form

$$J = \tfrac{1}{2} \int_0^\infty e^{2\alpha t} (x^T Q x + u^T R u) \, dt$$

where α is a positive scalar, Q is constant positive semidefinite, and R is constant positive definite matrices, the optimal synthesis leads to a linear and constant control law. Also, the closed-loop system is not merely asymptotically stable, but any nonzero initial states will decay faster than $e^{-\alpha t}$. This is equivalent to having eigenvalues with real parts less than $-\alpha$.

Multiplying the integrand of equation (E-150) by $e^{2\alpha t}$ gives

$$J = \tfrac{1}{2} \int_0^\infty e^{2\alpha t} \left[x^T (A-A_m)^T Q_1 (A-A_m) x + 2x^T (A-A_m)^T Q_1 (Bu-B_m u_m) \right.$$
$$\left. + (Bu-B_m u_m)^T Q_1 (Bu-B_m u_m) + x^T Q_2 x + u^T R u \right] dt \tag{E-156}$$

Transformations are introduced that convert this problem to one equivalent to the type solved previously. Accordingly, we define

$$\hat{x} = e^{\alpha t} x \tag{E-157a}$$

$$\hat{u} = e^{\alpha t} u \tag{E-157b}$$

$$\hat{x}_m = e^{\alpha t} x_m \tag{E-158a}$$

$$\hat{u}_m = e^{\alpha t} u_m \tag{E-158b}$$

Then

$$\dot{\hat{x}} = \frac{d}{dt}(e^{\alpha t}x) = \alpha e^{\alpha t}x + e^{\alpha t}\dot{x} \qquad \text{(E-159)}$$

Substituting equation (E-145) into equation (E-160)

$$\dot{\hat{x}} = (A + \alpha I)\hat{x} + B\hat{u} \qquad \text{(E-160)}$$

where I is the identity matrix, and the initial condition is

$$\hat{x}_{t_o} = e^{\alpha t_o}x_{t_o} \text{ where } x_{t_o} = x_o$$

and similarly

$$\dot{\hat{x}}_m = (A_m + \alpha I)\hat{x}_m + B_m\hat{u}_m \qquad \text{(E-161)}$$

Equation (E-156) can be rewritten as follows:

$$J = \frac{1}{2}\int_o^\infty \left[\hat{x}^T (A-A_m)^T Q_1 (A-A_m)\hat{x} + 2\hat{x}^T (A-A_m)^T Q_1 (B\hat{u}-B_m\hat{u}_m) \right.$$

$$\left. + (B\hat{u}-B_m\hat{u}_m)^T Q_1 (B\hat{u}-B_m\hat{u}_m) + \hat{x}^T Q_2\hat{x} + \hat{u}^T R\hat{u} \right] dt \qquad \text{(E-162)}$$

Suppose u* is optimal control for the problem described by equations (E-145) and (E-156), and x is the value of the state, given the initial value $x_{t_o} = x_o$. Then the optimal control for the problem described by equations (E-151) and (E-162) is $\hat{u}* = e^{\alpha t}u*$, and the state is given by $\hat{x} = e^{\alpha t}x$, provided $\hat{x}_{t_o} = e^{\alpha t_o}x_{t_o}$. The minimum performance index is the same for each problem [equation (E-156) is equivalent to equation (E-162)].

If the optimal control for the second problem is

$$\hat{u}* = K(\hat{x}, t) \qquad \text{(E-163)}$$

then the optimal control for the first problem is

$$u* = e^{-\alpha t}\hat{u}* = e^{-\alpha t}K(e^{\alpha t}x, t) \qquad \text{(E-164)}$$

Thus, the optimal control can be derived for the problem described by equations (E-145) and (E-156) from the optimal control for the problem described by equations (E-161) and (E-162).

From equation (E-153), making the appropriate substitutions,

$$\begin{bmatrix} \dot{\hat{x}} \\ \dot{\hat{p}} \end{bmatrix} = \begin{bmatrix} \hat{A}_1 & -\hat{S}_1 \\ -\hat{Q}_1 & -\hat{A}_1^T \end{bmatrix} \begin{bmatrix} \hat{x} \\ \hat{p} \end{bmatrix} + \begin{bmatrix} \hat{B}_1 \\ \hat{C}_1 \end{bmatrix} \hat{u}_m \qquad \text{(E-165)}$$

with boundary conditions

$$\hat{x}_{t_0} = e^{\alpha t_0} x_0$$
$$\hat{p}_{t_f} = 0$$

$\hat{p}$ is a vector of Lagrange multipliers (or costate vector).

Also

$$\hat{A}_1 = A + \alpha I - B(B^T Q_1 B + R)^{-1} B^T Q_1 (A - A_m)$$
$$\hat{S}_1 = B(B^T Q_1 B + R)^{-1} B^T$$
$$\hat{Q}_1 = Q_2 + (A - A_m)^T (Q_1 - Q_1 B(B^T Q_1 B + R)^{-1} B^T Q_1)(A - A_m)$$
$$\hat{B}_1 = B(B^T Q_1 B + R)^{-1} B^T Q_1 B_m$$
$$\hat{C}_1 = (A - A_m)^T [Q_1 - Q_1 B(B^T Q_1 B + R)^{-1} B^T Q_1] B_m$$

By inspection of the terms in equations (E-153) and (E-165), it can be seen that

$$\hat{A}_1 = \bar{A}_1 + \alpha I$$
$$\hat{S}_1 = \bar{S}_1$$
$$\hat{Q}_1 = \bar{Q}_1$$
$$\hat{B}_1 = \bar{B}_1$$
$$\hat{C}_1 = \bar{C}_1$$

E-63

The solution to the optimal control problem described by equation (E-165) is

$$\hat{u}^* = \hat{\hat{G}}x + \hat{\hat{M}}u_m \qquad (E-166)$$

Substituting equation (E-166) into equation (E-164), the optimal control can be obtained for the problem described by equations (E-145) and (E-156)

$$u^* = e^{-\alpha t}\hat{G}e^{\alpha t}x + e^{-\alpha t}\hat{M}e^{\alpha t}u_m$$

which reduces to

$$u^* = \hat{G}x + \hat{M}u_m$$

where

$$\hat{G} = -(B^TQ_1B+R)^{-1}B^TQ_1(A-A_m) - (B^TQ_1B+R)^{-1}B^T\hat{K}'_{ss} \qquad (E-167)$$

and

$$\hat{M} = (B^TQ_1B+R)^{-1}B^TQ_1B_m + (B^TQ_1B+R)^{-1}B^T$$

$$\cdot (\hat{A}_1{}^T-K'_{ss}\hat{S}_1)^{-1}(K'_{ss}\hat{B}_1-\hat{C}_1) \qquad (E-168)$$

$\hat{K}'_{ss}$ is the steady-state solution to the matrix Riccati equation

$$\dot{\hat{K}}' + \hat{K}'(\bar{A}_1 + \alpha I) - \hat{K}'\bar{S}_1\hat{K}' + (\bar{A}_1^T + \alpha I)\hat{K}' + \hat{Q}_1 = 0 \qquad (E-169)$$

To demonstrate the degree of stability achieved, rearrange equation (E-157) to

$$x = e^{-\alpha t}\hat{x} \qquad (E-170)$$

Because the optimal design guarantees that the closed-loop system is asymptotically stable, $\hat{x}$ approaches zero as time approaches infinity. Consequently, x approaches zero faster than $e^{-\alpha t}$.

In summary, if

$$J = \frac{1}{2} \int_{t_o}^{\infty} L(x, u)\, dt \qquad (E\text{-}171)$$

is a quadratic cost function, then the solution to the optimal control problem

$$J = \frac{1}{2} \int_{t_o}^{\infty} e^{2\alpha t}\, L(x,u)\, dt \qquad (E\text{-}172)$$

$$\dot{x} = Ax + Bu \qquad (E\text{-}173)$$

is equivalent to the solution to the optimal control problem.

$$J = \frac{1}{2} \int_{0}^{\infty} L(x.u)\, dt \qquad (E\text{-}174)$$

$$\dot{x} = (A + \alpha I)x + Bu$$

where $(A + \alpha I)$ has eigenvalues located at a distance α to the right of the eigenvalues of A with the imaginary parts remaining the same.

Apart from implicit model-following, another approach for incorporating command response criteria into the linear regulator design is explicit model-following. This method was found to be very useful in the synthesis of control laws that produced good pitch-rate and normal load factor responses. The method consists of placing an ideal model of the airplane to be controlled in the forward path of the control loop as shown in Figure E-19. The gain matrices G and G_m are synthesized based on the quadratic cost function

$$J = \frac{1}{2} \int_{0}^{\infty} [(y\text{-}y_m)^T Q(y\text{-}y_m) + (u_c{}^T Q u_c)]\, dt \qquad (E\text{-}175)$$

where

$$y_m = C_m x_m \qquad (E\text{-}176)$$

is the ideal model response to the input u_m and

$$y = C_s x \qquad (E\text{-}177)$$

E-65

$$\delta_{E_c} = G_a x_a + G_u x_u + G_m x_m$$

➡ = scalar signal

⟹ = vector signal
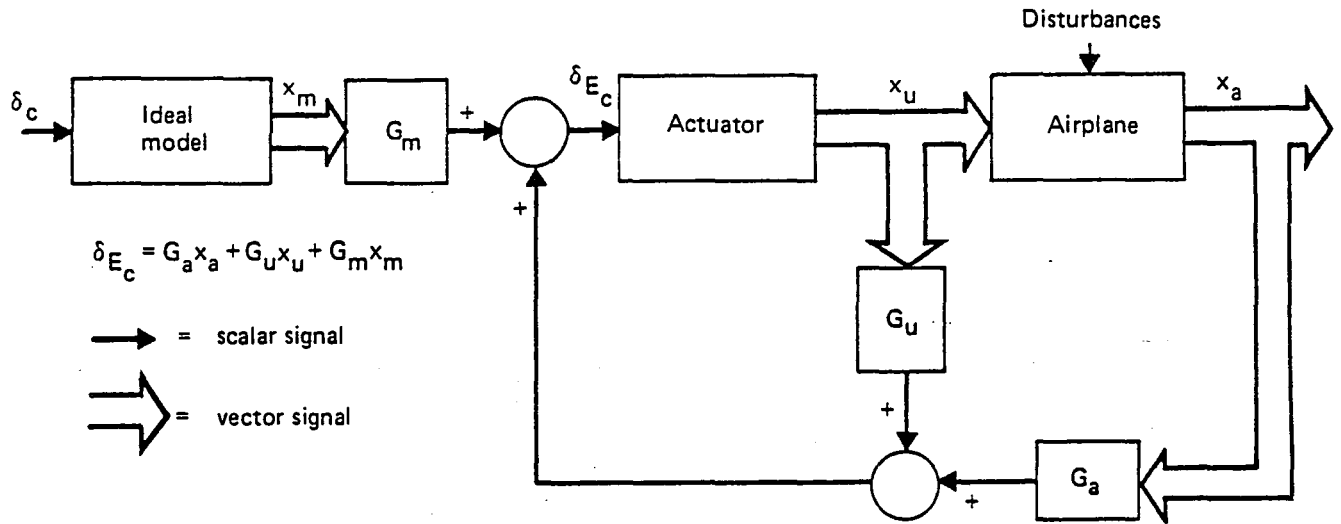
Figure E-19. System Using Explicit Model-Following

is the actual airplane response. The ideal model is described by the state model

$$\dot{x}_m(t) = A_m x_m(t) + B_m u_m(t) \qquad \text{(E-178)}$$

The control law synthesis is performed using the augmented open-loop state model

$$
\begin{bmatrix} \dot{x}(t) \\ \cdots \\ \dot{x}_m(t) \end{bmatrix} =
\begin{bmatrix} A_s & \vdots & 0 \\ \cdots & - & \cdots \\ 0 & \vdots & A_m \end{bmatrix}
\begin{bmatrix} x(t) \\ \cdots \\ x_m(t) \end{bmatrix} +
\begin{bmatrix} B_s \\ 0 \end{bmatrix} u_c(t) \qquad \text{(E-179)}
$$

$$
y \cdot y_m = \begin{bmatrix} C_s & \vdots & -C_m \end{bmatrix}
\begin{bmatrix} x(t) \\ x_m(t) \end{bmatrix} \qquad \text{(E-180)}
$$

The control $u_c(t)$ simply becomes

$$u_c(t) = G x(t) + G_m x_m(t) \qquad \text{(E-181)}$$

E-66

The state vectors $x(t)$ and $x_m(t)$ need not be of the same dimension. In particular for the synthesis of the pitch augmentation control laws, the vector $x_m(t)$ consisted of

$$x_m(t) = \begin{bmatrix} u_m \\ \alpha_m \\ q_m \\ \theta_m \end{bmatrix} \qquad \text{(E-182)}$$

where u_m is incremental forward velocity, α_m is incremental angle of attack, q_m is pitch rate, and θ_m is incremental pitch angle. The vector $x(t)$ comprised, in addition to states corresponding to the above, both actuator states and wind states.

E.6.3 MODIFIED KALMAN FILTER DESIGN

After the control problem has been solved using the modified linear quadratic regulator design outlined previously, a state estimator must be constructed. Stochastic optimal control theory has been applied widely to linear time-invariant systems having quadratic cost criteria and additive white Gaussian noise. However, the usefulness of the theory has been limited by the sensitivity of the closed-loop performance to parameter variations. Modeling of a process is never exact, and because design of a system is based on an approximate model, the design must be insensitive to modeling uncertainties, in particular with respect to the stability of the system. Optimal control with full-state feedback offers good stability margins, but when a Kalman filter is inserted into the loop to estimate state variables, the stability margins shrink, sometimes drastically. To alleviate this problem, a method has been implemented that increases the robustness of the closed-loop system with respect to parameter variations at the expense of filter performance when parameters are at their nominal values. The following outlines the problem and a method for designing robust control systems incorporating Kalman filters.

Not only is the system with full-state feedback optimal with respect to the cost function, but the system also has the property of being robust with respect to parameter variations in the control channels, as shown in Figure E-20. The closed-loop system is robust with respect to parameter variations in each of the control channels in the sense that if

$$\tfrac{1}{2} \leqslant k_i < \infty \qquad i = 1, \ldots, m$$

or if $\quad -60 \deg \leqslant \theta_i \leqslant 60 \deg \qquad i = 1, \ldots, m$
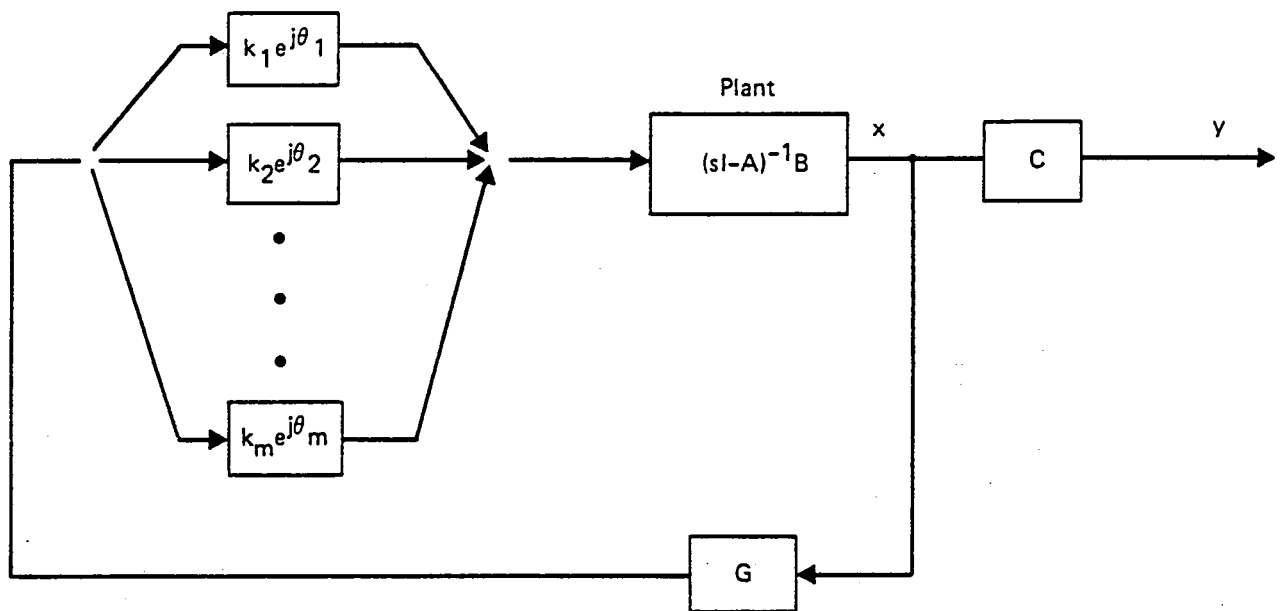
Figure E-20. Parameter Variations in the Control Loops

the system will remain stable; i.e., the system has gain margin of at least -6 dB to + ∞ simultaneously in all control channels and has phase margin of at least ±60 deg simultaneously in all control channels (ref E-5).

While these results are quite strong, they are based on the restrictive assumption that all of the state variables are available and thus can be multiplied by the optimal gain matrix to produce an optimal control. In most practical situations, the full-state vector is not available for feedback and instead a Kalman filter is inserted in the control loop to estimate the values of the states based on the available measurements.

A control loop incorporating a steady-state Kalman filter is shown in Figure E-21. The filter accepts as inputs the sensor outputs, y, and produces an optimal estimate, $\hat{x}$, of the state vector, x. This estimate, $\hat{x}$, is then multiplied by the optimal gain matrix, G, to produce the optimal control.
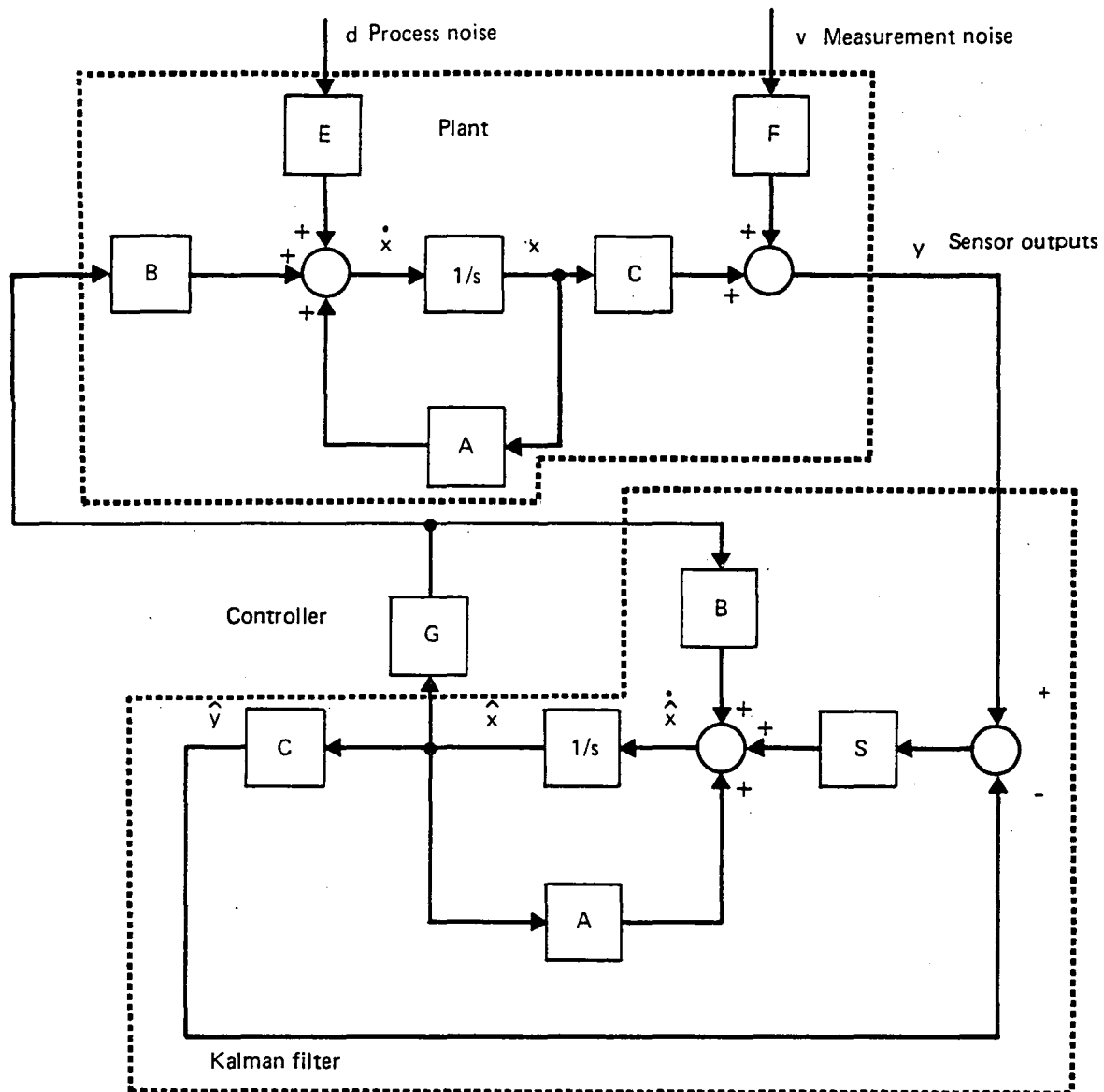
Figure E-21. Control System With Kalman Filter

The Kalman filter is essentially a mathematical replica of the plant, except that the sensor outputs, y, are compared with the estimated outputs, $\hat{y}$, to produce an error signal that drives the filter. The equations of the filter are

$$\dot{\hat{x}} = A\hat{x} + Bu + S(y - \hat{y})$$
$$\hat{y} = C\hat{x}$$

(E-183)

The Kalman filter gain matrix, S, is calculated as follows. The plant is assumed to be disturbed by random noise, d. This is referred to as "process noise" and is modeled as stationary white Gaussian noise. It may be used to represent such disturbances as wind gusts and may also be used as a measure of modeling uncertainty. The noise has the properties

$$
\begin{aligned}
E[d] &= 0 \\
E\left[d(t)\, d^T(\tau)\right] &= C_d\, \delta(t - \tau)
\end{aligned}
\tag{E-184}
$$

where $C_d = C^T_d \geqslant 0$ is the intensity matrix of the noise, and $E[-]$ is the expected value operator. There is noise also associated with the sensors. This "measurement noise," v, is also assumed to be stationary white Gaussian noise with the parameters

$$
\begin{aligned}
E[v] &= 0 \\
E\left[v(t)\, v^T(\tau)\right] &= C_v\, \delta(t - \tau)
\end{aligned}
\tag{E-185}
$$

where $C_v = C_v^T > 0$ is the intensity matrix of the noise. The process noise and measurement noise are passed through distribution matrices Γ and F, respectively, so that the intensity matrices seen at the plant are $\Gamma C_d\, \Gamma^T$ and $FC_v F^T$.

For the purpose of computing the filter gain matrix, the plant is assumed to have the form

$$
\begin{aligned}
\dot{x} &= Ax + Bu + \Gamma d \\
y &= Cx + Fv
\end{aligned}
\tag{E-186}
$$

The filter gain matrix is then given by

$$
S = KC^T(FC_v F^T)^{-1}
\tag{E-187}
$$

where K satisfies the algebraic Riccati equation

$$
AK + KA^T - KC^T(FC_v F^T)^{-1}\, CK + \Gamma C_d \Gamma^T = 0
\tag{E-188}
$$

It is assumed that F has maximum possible rank so that FC_vF^T is nonsingular. The pair (A, Γ) is assumed to be controllable, and the pair (A,C) is assumed to be observable to guarantee that there is a unique, symmetric, positive definite solution, K, for the Riccati equation (E-188).

While the control system employing the Kalman filter is optimal with respect to the cost function and the noise intensities d and v, the closed-loop system does not have the robustness properties associated with the full-state feedback controller. In fact, in some cases, the stability margins can become vanishingly small (ref E-6). This can be explained by the fact that if the loop is broken at point X in Figure E-21, the transfer function around the loop is not the same as it is for full-state feedback unless it happens that

$$S[I + C(sI - A)^{-1}S]^{-1} = B[C(sI - A)^{-1}B]^{-1} \qquad \text{(E-189)}$$

So unless this identity holds, perturbations appearing at point X will have a different effect when the filter is in the loop than in the case of full-state feedback (ref E-7).

However, equation (E-189) can be satisfied if $S = qBW$ and $q \to \infty$ and W is a nonsingular matrix. It can be shown that if $\Gamma C_d \Gamma^T$ is replaced by $\Gamma C_d \Gamma^T + q^2 BVB^T$ in equation (E-188) where $V = V^T > 0$ is arbitrary, and if the open-loop system has no right half-plane transmission zeros, then

$$S \to qBV^{\frac{1}{2}}(R^{\frac{1}{2}})^{-1}$$

as $q \to \infty$, where $V^{\frac{1}{2}}$ is some square root of V, and $R^{\frac{1}{2}}$ is some square root of R. S then approaches qBW as $q \to \infty$ where $W = V^{\frac{1}{2}}(R^{\frac{1}{2}})^{-1}$. Then in the limit, equation (E-189) is satisfied and the system employing the Kalman filter has the robustness properties of the full-state feedback system as $q \to \infty$.

If we let $\bar{C}_d \overset{\Delta}{=} q^2V$, then $\Gamma C_d \Gamma^T$ will have been replaced by $\Gamma C_d \Gamma^T + B\bar{C}_dB^T$ in the Riccati equation. $\bar{C}_d$ can be thought of as being the intensity matrix of a zero-mean stationary white Gaussian noise vector, $\bar{d}$, appearing at the input to the plant as shown in Figure E-22. The plant equations then become
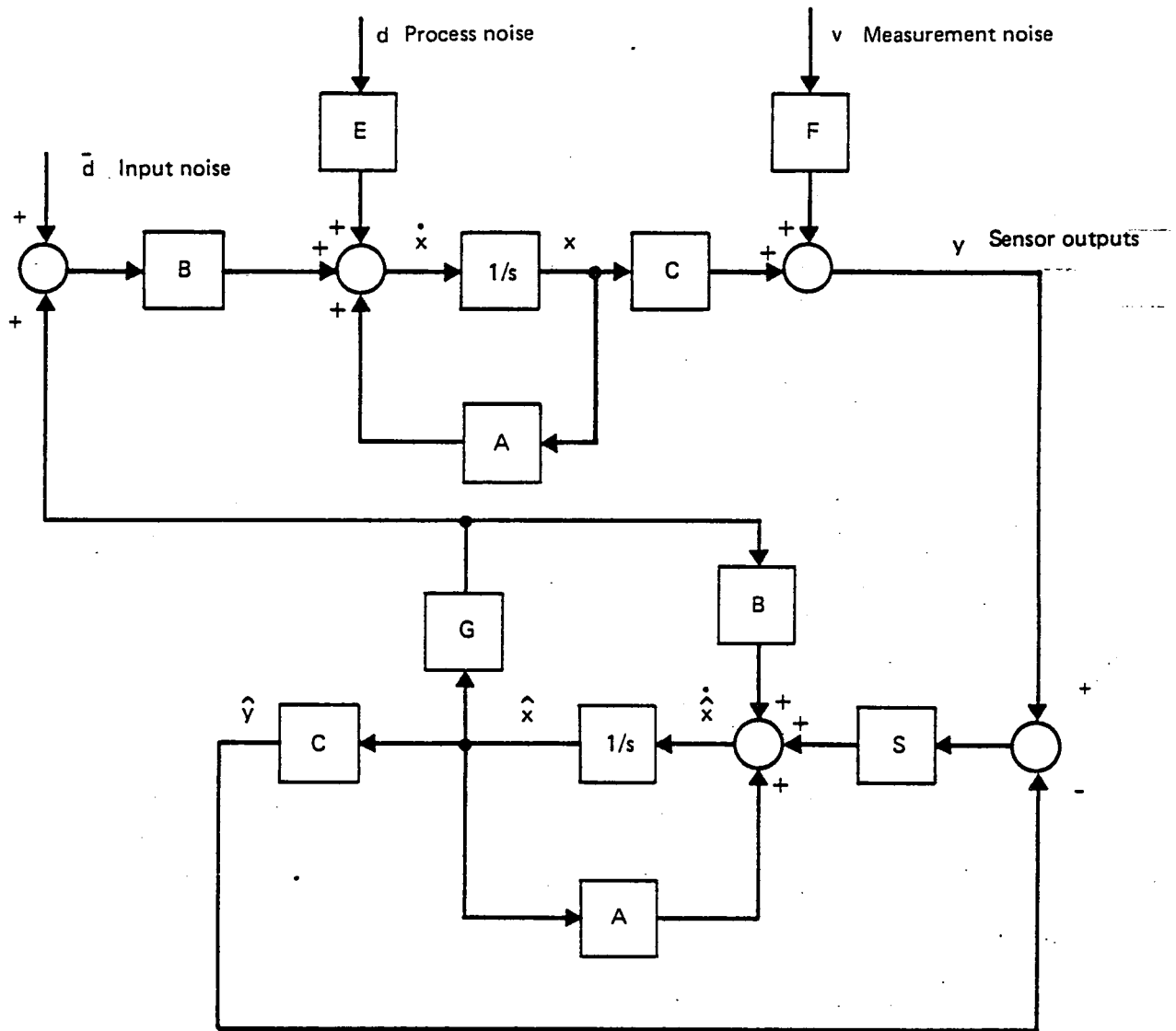
Figure E-22. Addition of Input Noise to Model

$$\dot{x} = Ax + Bu + \Gamma d + B\bar{d}$$

$$y = Cx + Fv \qquad\qquad\qquad\qquad \text{(E-190)}$$

The process noise has been augmented by a fictitious input noise, $\bar{d}$, with distribution matrix, B. The Riccati equation then becomes

$$AK + KA^T - KC^T(FC_vF^T)^{-1}CK + \Gamma C_d\Gamma^T + B\bar{C}_dB^T = 0 \qquad \text{(E-191)}$$

As the magnitude of the diagonal elements of $\bar{C}_d$ is increased (i.e., as the fictitious input noise becomes stronger), the robustness properties of the controller approach those of the system with full-state feedback. Adding fictitious noise at the input to the system tells the mathematics that uncertainties should be expected at that point, and the calculation of the filter takes this uncertainty into account by increasing robustness with respect to uncertainties at that point. But increasing the intensity of either the input noise or the process noise has the effect of telling the mathematics, via the Riccati equation (E-191), that the model is not accurate or that the disturbances to the model are great enough that the system should place more emphasis on the actual sensor measurements than on model accuracy.

Larger values of C_d or $\bar{C}_d$ in equation (E-191) have the effect of making the elements of K larger in the solution of equation (E-191). The result is that the elements of the filter gain matrix, S, become large in equation (E-187), increasing the gain and bandwidth of the filter and allowing more sensor noise to pass through the filter. Because K has the property (ref E-8)

$$K = \lim_{t \to \infty} E \left([x(t) - \hat{x}(t)] [x(t) - \hat{x}(t)]^T \right)$$

it follows that as K is increased, the accuracy of the filter is reduced. The design problem therefore involves a tradeoff between filtering accuracy (when the parameters are at their assumed nominal values) and robustness of the closed-loop system with respect to parameter variations shown in Figure E-20.

E.6.4 CONTROLLER SIMPLIFICATION

The Kalman filter will have the same dynamic order as that of the open-loop model used for the synthesis. For a flexible airplane model that contains a large number of structural modes, the high order of the filter imposes an excessive and unnecessary computational burden on flight computers. A preliminary approach to the design of a low-order suboptimal filter has been established during this study. It will be outlined here.

The first task is to establish the minimum bandwidth of the controller. The actuation bandwidth is set by the highest frequency at which we wish to control. In the case of

FMC, it is set by the highest frequency flutter mode, and, in the case of GLA, it is set by the highest frequency mode that contributes significantly to the gust loads. The latter is easily determined from cumulative power density plots of the appropriate performance parameters such as bending moments, torsional moments, accelerations, etc., at various airplane stations. A third factor that must be considered is the increasing uncertainty in the dynamic model with increasing frequency. The controller bandwidth must be limited such that at higher frequencies, the closed-loop system has sufficiently large stability margins. The modal residualization technique described in Subsection E.4.2 can be used to eliminate filter modes that are outside the required actuation bandwidth. Because the Kalman filter only has first-order rolloff characteristics at high frequencies, it may be necessary to insert an additional filter in the control loop to ensure the necessary attenuation at high frequencies.

The reduced filter may still be too complex for practical implementation on flight computers. Further reduction may still be possible without any significant loss in closed-loop performance. Again, the modal residualization technique can be used to eliminate filter modes that are within the actuation bandwidth but that are associated with weakly unobservable or weakly controllable airplane modes or with airplane modes that are not observable from the cost function.

In the previous discussion, it was assumed that the Kalman filter was synthesized using a full-order airplane model and that the lower order suboptimal filter was obtained by the reduction of this full-order filter. However, another approach would be to reduce the open-loop model using the modal residualization technique, leaving only the modes considered essential to the control task. A suboptimal filter (with respect to the full-order model) would then be synthesized using the lower order airplane open-loop model. This approach was not considered during this study.

Still another approach would be to use the full-order Kalman filter to define the required control-loop frequency responses over the actuation bandwidth and to design lower order filters with approximately the same frequency response characteristics. This involves least-square fitting of single-loop filter frequency responses against low-order filters of predetermined form; the procedure is described in Subsection E.4.4.

E.7.0 CLOSED-LOOP ANALYSIS

E.7.0 CLOSED-LOOP ANALYSIS

Closed-loop analysis consists of evaluating the performance of full- and partial-state feedback designs and full-order and reduced-order Kalman filter designs in terms of gust response and stability margins. As indicated in Figure E-1, this analysis is an important part of an iterative design procedure. The design can be divided into two parts: the control task and the state estimation task. The control problem is solved by synthesizing and analyzing the closed-loop performance of full- or partial-state feedback designs. After the proper cost function and associate state feedback gain matrix have been determined, the Kalman filter is synthesized, inserted in the control loop, and the closed-loop performance evaluated. The performance of various reduced-order filters is evaluated until one is found that gives close to optimum closed-loop performance with adequate stability margins and without imposing excessive computational burden on flight computers.

E.7.1 FORMULATION OF CLOSED-LOOP STATE MODELS

The full-state feedback closed-loop model is described by

$$\dot{x} = (A + BG)x + \Gamma w_g \tag{E-192}$$

$$y = C_p x \tag{E-193}$$

where x is the state vector consisting of the rigid and flexible mode displacements and rates, control surface states, and unsteady gust states; w_g is gust input vector; and y is the output vector consisting of all closed-loop performance parameters. A is the open-loop state matrix, B is the control distribution matrix, G is optimal state feedback gain matrix, Γ is the input gust distribution matrix, and C_p is the performance parameter distribution matrix.

The vector y does not contain any acceleration measurements because there are no direct gust inputs in equation (E-193). However, during the gust response calculations described in Section E.3.0, the covariance matrix of y as well as $\dot{y}$ is obtained. This ensures that if y contains velocity measurements, the corresponding acceleration responses will also be computed. A closed-loop state model with reduced-state feedback is simply obtained by setting the appropriate columns in the gain matrix G to zero.

The closed-loop model with a full-order Kalman filter is

$$
\begin{bmatrix} \dot{x} \\ \dot{\hat{x}} \end{bmatrix} = \begin{bmatrix} A & BG \\ SC & (A+BG-SC) \end{bmatrix} \begin{bmatrix} x \\ \hat{x} \end{bmatrix} + \begin{bmatrix} \Gamma \\ SE \end{bmatrix} w_g \qquad (E-194)
$$

In addition to the parameters defined previously, there are $\hat{x}$, the estimated state vector; C, the measurement distribution matrix; E, the measurement gust input distribution matrix; and S, the optimal Kalman filter input matrix.

With a reduced-order filter, the closed-loop equations are modified to

$$
\begin{bmatrix} \dot{x} \\ \dot{\hat{z}} \end{bmatrix} = \begin{bmatrix} A+BF_RC & BG_R \\ S_RC & \Lambda_R \end{bmatrix} \begin{bmatrix} x \\ \hat{z} \end{bmatrix} + \begin{bmatrix} \Gamma+BF_RE \\ S_RE \end{bmatrix} w_g \qquad (E-195)
$$

where, in addition to the terms defined previously, $\hat{z}_R$ is the filter state vector, Λ_R is the filter state matrix in block diagonal form, S_R is the filter input matrix, G_R is the filter output matrix, and F_R is the filter static gain matrix. Figure E-23 is a schematic of the reduced-order filter. Equation (E-193) represents the closed-loop performance parameters.

y = measurement vector
$\hat{x}$ = full-state estimates
u = control vector
$\hat{z}$ = reduced-order filter states

- Reduces order of filter
- Includes significant dynamics
- Preserves measurement-to-control static relationships
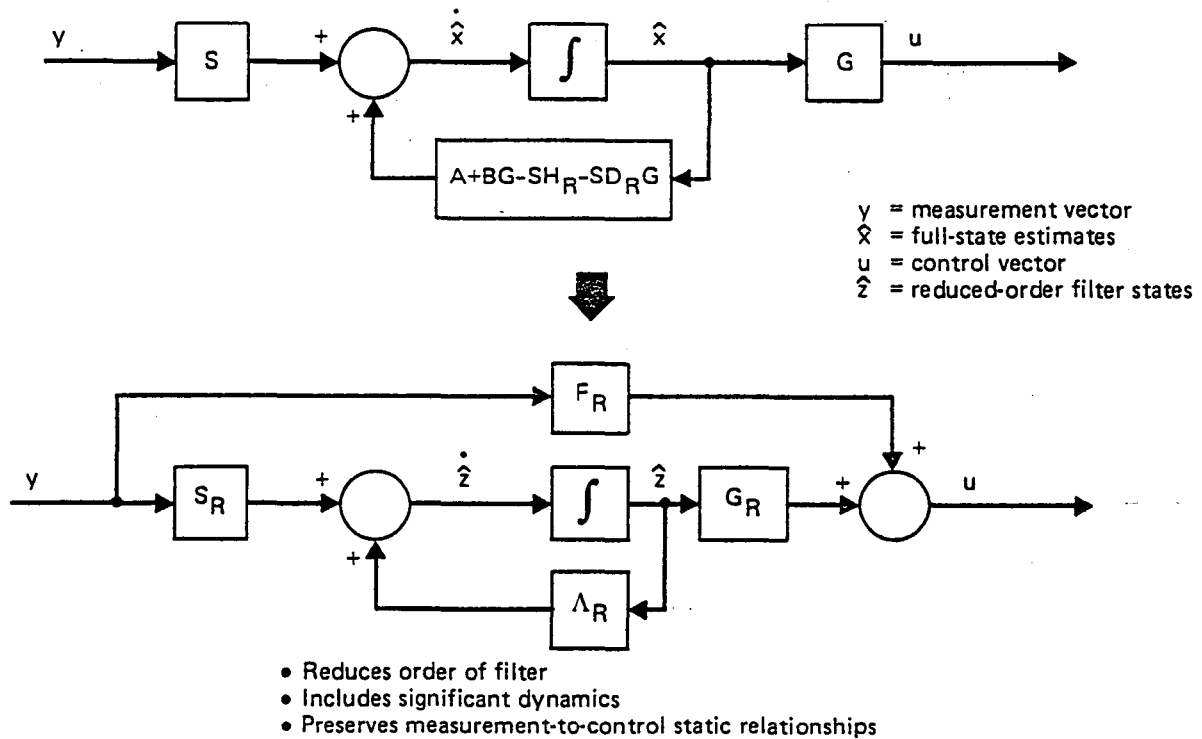
Figure E-23. Filter Simplification

E.7.2 CLOSED-LOOP STABILITY

Closed-loop stability analysis consists of computing eigenvalues, gain and phase margins in all control loops (see fig. E-20), and the range of values of key parameters such as dynamic pressure, for which the closed-loop system remains stable. The various closed-loop control laws are evaluated based on location of closed-loop poles and the margins of stability as a function of frequency.

The equations of the closed-loop systems with a full-order Kalman filter are from equation (E-194) without the input terms

$$\dot{x} = Ax + BG\hat{x} \qquad \text{(nth-order plant)}$$

$$\dot{\hat{x}} = (A + BG - SC)\hat{x} + SCx \qquad \text{(nth-order filter)}$$

or

$$\begin{bmatrix} \dot{x} \\ \dot{\hat{x}} \end{bmatrix} = \begin{bmatrix} A & BG \\ SC & A+BG-SC \end{bmatrix} \begin{bmatrix} x \\ \hat{x} \end{bmatrix} \qquad (E\text{-}196)$$

The eigenvalues of A are the poles of the open-loop plant without the controller connected, and the eigenvalues of (A + BG - SC) are the poles of the open-loop Kalman filter with its output disconnected from the plant. It is not clear, however, from equation (E-196) what the poles of the closed-loop control system are.

Introducing the transformation

$$\begin{bmatrix} x \\ e \end{bmatrix} = \begin{bmatrix} I & 0 \\ I & -I \end{bmatrix} \begin{bmatrix} x \\ \hat{x} \end{bmatrix} \qquad (E\text{-}197)$$

i.e., $e = x - \hat{x}$, the equations become

$$\begin{bmatrix} \dot{x} \\ \dot{e} \end{bmatrix} = \begin{bmatrix} A + BG & -BG \\ 0 & A - SC \end{bmatrix} \begin{bmatrix} x \\ e \end{bmatrix} \qquad (E\text{-}198)$$

From equation (E-197), it is clear that the poles of the closed-loop system, which are the eigenvalues of the 2n x 2n system matrix in equation (E-197), are simply the eigenvalues of (A + BG) and the eigenvalues of (A - SC). This follows from the fact that matrices

$$\begin{bmatrix} A & -BG \\ SC & A + BG - SC \end{bmatrix}$$

and

$$\begin{bmatrix} A + BG & -BG \\ 0 & A - SC \end{bmatrix}$$

have the same eigenvalues because they are related by the similarity transformation equation (E-197), and from the fact that

$$\det \begin{bmatrix} A + BG - \lambda I & -BG \\ 0 & A - SC - \lambda I \end{bmatrix} \tag{E-199}$$

$$= \det(A + BG - \lambda I) \det(A - SC - \lambda I)$$

The full-state feedback system $\left[$ equation (E-192)$\right]$ is optimal with respect to the cost function, stable if all unstable open-loop modes are controllable, and robust with respect to parameter variations in the control loops. In terms of the parameters defined in Figure E-20, the full-state feedback system has at least the following stability margins in each of the m control loops

$$1/2 \leq k_i \leq \infty \qquad i = 1, \ldots, m$$

and

$$\left| \theta_i \right| \leq 60 \text{ deg} \qquad i = 1, \ldots, m$$

Optimal control with full-state feedback offers good stability margins. The closed-loop system with the full-order Kalman filter $\left[$ equation (E-198)$\right]$ is always stable provided that all unstable open-loop modes are controllable and observable. However, when the Kalman filter is inserted into the control loop to estimate the states, the good stability margins of the full-state feedback design may shrink, sometimes drastically. For the closed-loop system with reduced-order filter $\left[$ equation (E-195)$\right]$, there is no guarantee that the system is stable even at the nominal gain and phase.

E.7.3 CLOSED-LOOP ROOT-MEAN-SQUARE GUST RESPONSE

The steady-state gust response correlation matrices for the states; modal states; measurements; performance parameters such as bending moments, torsional moments, accelerations, etc.; and the output power spectral density of selected performance parameters are computed. The computational techniques are described in Section E.3.0. Because the loads equations are based on a truncated set of modal coordinates, the load levels are only approximate. However, because all modes that are significant with respect to the control task are included, and the same truncated model has been used to compute the gust loads of the open-loop airplane, these approximate load calculations are considered adequate for evaluating the relative merits of various control laws.

The closed-loop gust response is evaluated in terms of the relative reduction in the related performance parameters and the root-mean-square (rms) deflections and rates of the control surfaces. Because the control surface positions and rates are states, the corresponding rms gust responses are obtained from the gust response correlation matrix for the state vector.

E.7.4 CLOSED-LOOP LINEAR SIMULATIONS

A closed-loop system can be defined either as a full-state feedback system or as a system employing a state estimator (Kalman filter). For a full-state feedback system, the equations can be written

$$\dot{x} = Ax + B_1 u \qquad \text{(E-200)}$$

$$u = Gx + G_2 u_c$$
$$y = Cx + D_w x_w \qquad \text{(E-201)}$$

or

$$\dot{x} + (A+B_1 G)x + B_1 B_2 u_c \qquad \text{(E-202)}$$

$$y = Cx + D_w x_w \qquad \text{(E-203)}$$

where u is the control applied to the airplane and u_c is an external input. The external input for this problem is δ_c, the column angle. A block diagram of the system is shown in Figure E-24. The system is simulated as a set of difference equations in modal coordinates

$$z\,[(k+1)\,\Delta t] = \phi z\,[k(\Delta t)] + \theta u^*$$
$$y\,[k(\Delta t)] = Cz\,[k(\Delta t)] + Du^* \tag{E-204}$$

that were discussed in Subsections E.3.3 and E.5.3.

For a system employing a Kalman filter to estimate the states, the system equations take the form

$$\dot{x} = Ax + B_1 u + Ed \tag{E-205}$$

$$u = G\hat{x} + B_2 u_c \tag{E-206}$$

$$\dot{\hat{x}} = A\hat{x} + B_1 u + S\,(y-\hat{y}) \tag{E-207}$$

$$y = Cx + Fv \tag{E-208}$$

$$\hat{y} = C\hat{x} \tag{E-209}$$
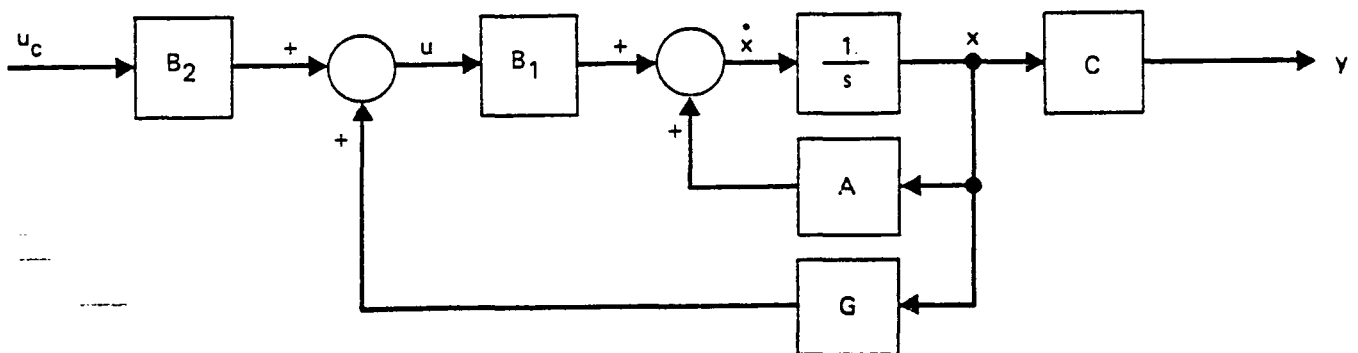
Figure E-24. Full-State Feedback System

where

d	=	process noise
v	=	measurement noise
$\hat{x}$	=	estimator state vector
y	=	sensor output vector
$\hat{y}$	=	estimated sensor output vector
G	=	full-state feedback gain matrix
S	=	Kalman filter gain matrix
E	=	process noise distribution matrix
F	=	measurement noise distribution matrix

The structure of the system is shown in Figure E-25.
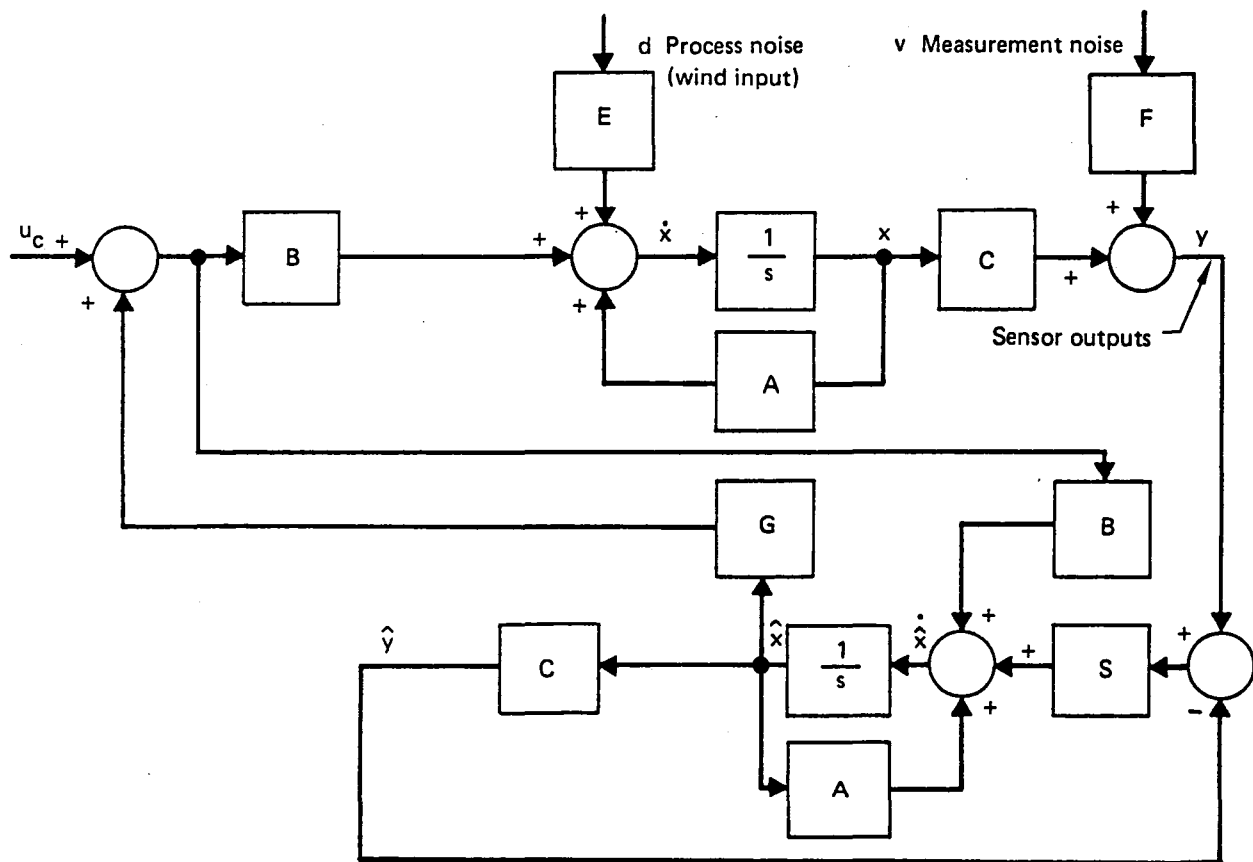
Figure E-25. Feedback System With Kalman Filter

The system can be represented by the dynamic equations

$$
\begin{bmatrix} \dot{x} \\ \dot{\hat{x}} \end{bmatrix} =
\left[\begin{array}{c|c} A & B_1 G \\ \hline SC & A+B_1 G-SC \end{array} \right]
\begin{bmatrix} x \\ \hat{x} \end{bmatrix}
$$

$$
+ \left[\begin{array}{c} B_1 B_2 \\ \hline B_1 B_2 \end{array} \right] u_c +
\left[\begin{array}{c|c} E & 0 \\ \hline 0 & SF \end{array} \right]
\begin{bmatrix} d \\ v \end{bmatrix}
\qquad (E\text{-}210)
$$

These equations are then converted to difference equations for simulation with the noise inputs, d and v, set equal to zero.

E.7.5 EVALUATION OF STATE FEEDBACK DESIGNS

The closed-loop analysis of the state feedback design is part of the iterative design cycle to solve the control task. Full-state feedback designs are evaluated until the proper cost function and control surfaces have been selected. The evaluations are based on gust-load reductions, control surface activities, and closed-loop pole locations.

Because the control law includes feedback of control surface states, the optimal linear regulator can be used to determine whether or not the control surface actuators have sufficient bandwidth. If there is a significant change in the actuator closed-loop poles from their nominal open-loop values, it will be necessary to increase the actuation bandwidth.

The trade between closed-loop performance and actuation bandwidth can be determined by considering the cumulative power-spectral-density plots of the open-loop and full-state closed-loop gust responses of the various performance parameters. The effects of eliminating modes from the feedback can be determined by evaluating the closed-loop performance with the appropriate columns in the optimal gain matrix set equal to zero.

E.7.6 EVALUATION OF KALMAN FILTER DESIGNS

Closed-loop analysis of the Kalman filter designs is part of the iterative design cycle to solve the state estimation problem. Full-order Kalman filters are evaluated until the closed-loop performance and stability margins meet or exceed the design requirements. The key design parameters that are evaluated are types, numbers, and locations of sensors and the trade between gust response and stability margins. This same iterative analysis is used to evaluate reduced-order filters.

REFERENCES

E-1   Burrough, J. D. Environmental Control System Transient Analysis, Vol. 3. Technical Report AFFDL-TR-77-102, July 1977.

E-2   Prakash, C. Shah. Linear System Analysis Program L224 (QR), Vol. I; Engineering and Usage. NASA CR-15346, October 1979.

E-3   Papoulis, A. Probability, Random Variables and Stochastic Processes. McGraw-Hill, New York, 1965.

E-4   Seidel, R. C. Transfer Function Parameter Estimation From Frequency Response Data—a Fortran Program. NASA TMX-3286, September 1975.

E-5   Safanov, M., and M. Athans. "Gain and Phase Margin for Multiloop LQR Regulators." IEEE Trans. on Automatic Control, Vol. AC-22, No. 2, pp. 173-179, April 1977.

E-6   Doyle, J. "Guaranteed Margins for LQG Regulators." IEEE Trans. on Automatic Control, August 1978.

E-7   Doyle, J., and G. Stein. "Robustness with Observers." Presented at the 1978 IEEE Conference on Decision and Control, January 10-12, 1979.

E-8   Kwakernaak, H., and R. Sivan. Linear Optimal Control Systems. Wiley-Interscience, 1972.

APPENDIX F: FMC AND GLA ANALYSIS RESULTS

F.1.0 MODE SHAPE MATRICES

Tables F-1 and F-2 show the dynamic loads and sensor mode shape matrices for the two mass conditions ($0.46\bar{c}$ and $0.22c$ center-of-gravity positions, respectively).

Table F-1. Dynamic Loads and Sensor Mode Shape Matrices for 0.8F Mass ($0.46\bar{c}$) Condition

		Sensors		Dynamic loads					
				Inboard at $\eta = 0.25$			Outboard at $\eta = 0.75$		
		Pitch-rate gyro, rad/s	Wing-tip acceler-ometer, m/s^2 (in/s^2)	Shear, N (lb)	Bending, N·m (lb-in)	Torsion, N·m (lb-in)	Shear, N (lb)	Bending, N·m (lb-in)	Torsion, N·m (lb-in)
Modes	q_2	0	-2.54×10^{-2} (-1.0)	0	0	0	0	0	0
	q_3	-8.30×10^{-4}	-6.98×10^{-3} (-0.275)	0	0	0	0	0	0
	q_5	-1.32×10^{-4}	0	0	0	0	0	0	0
	q_6	1.60×10^{-4}	0	0	0	0	0	0	0
	q_{12}	0	-2.54×10^{-2} (-1.0)	2.74×10^3 (6.17×10^2)	3.27×10^4 (2.89×10^5)	-3.84×10^2 (-3.40×10^3)	1.22×10^3 (2.75×10^2)	4.60×10^3 (4.07×10^4)	5.06×10^2 (4.48×10^3)
	q_{13}	0	-2.54×10^{-2} (-1.0)	-4.63×10^4 (-1.04×10^4)	-1.22×10^5 (-1.08×10^6)	-4.27×10^4 (-3.78×10^5)	4.67×10^3 (1.05×10^3)	2.61×10^4 (2.31×10^5)	1.45×10^3 (1.28×10^4)
	q_{14}	0	-1.49×10^{-2} (-0.587)	0	0	0	0	0	0
	q_{15}	0	-2.22×10^{-2} (-0.875)	1.04×10^5 (2.34×10^4)	-1.80×10^5 (-1.59×10^6)	5.50×10^5 (4.87×10^6)	3.15×10^3 (7.09×10^2)	3.20×10^4 (2.83×10^5)	1.31×10^4 (1.16×10^5)
	q_{16}	0	-2.54×10^{-2} (-1.0)	1.54×10^4 (3.47×10^3)	-1.27×10^4 (-1.12×10^5)	-7.21×10^4 (-6.38×10^5)	-2.21×10^3 (-4.97×10^2)	4.35×10^4 (3.85×10^5)	-6.61×10^3 (-5.85×10^4)
	q_{17}	0	-9.04×10^{-3} (-0.356)	0	0	0	0	0	0
	q_{18}	0	1.66×10^{-2} (0.654)	1.18×10^4 (2.66×10^3)	-4.88×10^5 (-4.32×10^6)	-1.15×10^5 (-1.02×10^6)	1.48×10^4 (3.32×10^3)	-5.21×10^4 (-4.61×10^5)	-2.21×10^4 (-1.96×10^5)
	q_{19}	0	-2.54×10^{-2} (-1.0)	1.10×10^4 (2.48×10^3)	5.99×10^4 (5.30×10^5)	3.06×10^4 (2.71×10^5)	-5.92×10^3 (-1.33×10^3)	1.72×10^3 (1.52×10^4)	-5.76×10^4 (-5.10×10^5)

Note: The wing-load equations were calculated
by a "modal displacement" technique
that relates wing load to the wing
out-of-plane structural deflections
through the wing modes. Two wing
modes that are predominately in-
plane bending are omitted.

Table F-2. Dynamic Loads and Sensor Mode Shape Matrices for MZFW+F Mass ($0.22\bar{c}$) Condition

		Sensors		Dynamic loads					
				Inboard at $\eta = 0.25$			Outboard at $\eta = 0.75$		
		Pitch-rate gyro, rad/s	Wing-tip accelerometer, m/s² (in/s²)	Shear, N (lb)	Bending, N·m (lb-in)	Torsion, N·m (lb-in)	Shear, N (lb)	Bending, N·m (lb-in)	Torsion, N·m (lb-in)
Modes	q_2	0	-2.54×10^{-2} (-1.0)	0	0	0	0	0	0
	q_3	-7.93×10^{-4}	-7.82×10^{-3} (-0.308)	0	0	0	0	0	0
	q_5	-1.22×10^{-4}	0	0	0	0	0	0	0
	q_6	1.56×10^{-4}	0	0	0	0	0	0	0
	q_{12}	0	-2.54×10^{-2} (-1.0)	2.37×10^3 (5.32×10^2)	3.12×10^4 (2.76×10^5)	-2.69×10^2 (-2.38×10^3)	1.63×10^3 (3.67×10^2)	4.77×10^3 (4.22×10^4)	-1.08×10^2 (-9.55×10^2)
	q_{13}	0	2.39×10^{-3} (0.094)	0	0	0	0	0	0
	q_{14}	0	-2.54×10^{-2} (-1.0)	-4.76×10^4 (-1.07×10^4)	-9.72×10^4 (-8.60×10^5)	-8.12×10^4 (-7.19×10^5)	-1.15×10^3 (-2.59×10^2)	2.42×10^4 (2.14×10^5)	1.53×10^3 (1.35×10^4)
	q_{15}	0	-2.44×10^{-2} (-0.962)	5.07×10^4 (1.14×10^4)	-1.67×10^5 (-1.48×10^6)	3.37×10^5 (2.98×10^6)	-3.70×10^3 (-8.32×10^2)	3.36×10^4 (2.97×10^5)	7.23×10^3 (6.40×10^4)
	q_{16}	0	-2.54×10^{-2} (-1.0)	1.55×10^4 (3.48×10^3)	-7.45×10^3 (-6.59×10^4)	-1.20×10^5 (-1.06×10^6)	-1.11×10^4 (-2.49×10^3)	4.15×10^4 (3.67×10^5)	2.80×10^3 (2.48×10^4)
	q_{17}	0	-9.25×10^{-3} (-0.364)	0	0	0	0	0	0
	q_{18}	0	1.387×10^{-2} (0.546)	-1.34×10^3 (-3.02×10^2)	-4.36×10^5 (-3.86×10^6)	-1.47×10^5 (-1.30×10^6)	-1.10×10^4 (-2.47×10^3)	-4.81×10^4 (-4.26×10^5)	-5.15×10^4 (-4.56×10^5)
	q_{19}	0	-2.54×10^{-2} (-1.0)	1.34×10^4 (3.02×10^3)	7.54×10^4 (6.67×10^5)	5.04×10^4 (4.46×10^5)	1.90×10^3 (4.28×10^2)	3.57×10^3 (3.16×10^4)	-5.31×10^4 (-4.70×10^5)

Note: The wing-load equations were calculated by a "modal displacement" technique that relates wing load to the wing out-of-plane structural deflections through the wing modes. Two wing modes that are predominately in-plane bending are omitted.

F.2.0 CONTROLLABILITY ANALYSIS

F.2.0 CONTROLLABILITY ANALYSIS

Table F-3 shows the relative flutter-mode controllability of the various elevator and aileron control surfaces. Tables F-4 through F-7 show the relative root-mean-square (rms) load open-loop responses for the various flight conditions due to white noise inputs to the actuators.

Table F-3. Relative Flutter-Mode Controllability

Flight condition	Elevator			Inboard aileron	Outboard aileron		
	Inboard	Outboard	Inboard and outboard		Inboard	Outboard	Inboard and outboard
5	0.15	0.06	0.20	0.42	0.39	1.00	0.99
6	0.20	0.09	0.28	0.36	0.44	0.97	1.00
7	0.13	0.03	0.13	1.00	0.50	0.75	0.86
8	0.19	0.03	0.17	0.91	0.53	0.91	1.00

● Assumed control authority:
  ● Elevator = ±3 deg
  ● Aileron = ±15 deg

● Normalized for each flight condition
  ● 1 indicates the control surface most effective
    for FMC
  ● 0 indicates a control surface makes no
    contribution to FMC

Table F-4. *Relative Root-Mean-Square Load Responses at Flight Condition 1*

	Elevator			Inboard aileron	Outboard aileron		
	Inboard	Outboard	Inboard and outboard		Inboard	Outboard	Inboard and outboard
Inboard at $\eta = 0.25$:							
Shear	0.587	0.430	1.000	0.773	0.468	0.698	0.651
Bending moment	0.617	0.386	1.000	0.418	0.315	0.686	0.871
Torsion	0.230	0.182	0.405	1.000	0.254	0.781	0.560
Outboard at $\eta = 0.75$							
Shear	0.396	0.251	0.645	0.369	0.350	0.793	1.000
Bending moment	0.267	0.225	0.477	0.461	0.417	0.857	1.000
Torsion	0.622	0.380	1.000	0.951	0.424	0.855	0.785

● Assumed control authority (white noise at each actuator input):
- ● Elevator = ± 3 deg
- ● Aileron = ± 15 deg

● Nomalized for each flight condition
- ● 1 indicates the control surface most effective for load reduction
- ● 0 indicates a control surface makes no contribution to load reduction

F-4

Table F-5. Relative Root-Mean-Square Load Responses at Flight Condition 2

	Elevator			Inboard aileron	Outboard aileron		
	Inboard	Outboard	Inboard and outboard		Inboard	Outboard	Inboard and outboard
Inboard at $\eta = 0.25$:							
Shear	0.501	0.391	0.873	1.000	0.439	0.634	0.459
Bending moment	0.503	0.315	0.813	0.657	0.391	0.803	1.000
Torsion	0.299	0.281	0.573	1.000	0.288	0.739	0.505
Outboard at $\eta = 0.75$							
Shear	0.401	0.260	0.652	0.364	0.418	0.795	1.000
Bending moment	0.164	0.165	0.316	0.583	0.386	0.845	1.000
Torsion	0.216	0.146	0.350	0.925	0.452	1.000	0.950

● Assumed control authority (white noise at each actuator input):
  ● Elevator = ± 3 deg
  ● Aileron = ± 15 deg
● Normalized for each flight condition
  ● 1 indicates the control surface most effective for load reduction
  ● 0 indicates a control surface makes no contribution to load reduction

Table F-6. Relative Root-Mean-Square Load Responses at Flight Condition 3

	Elevator			Inboard aileron	Outboard aileron		
	Inboard	Outboard	Inboard and outboard		Inboard	Outboard	Inboard and outboard
Inboard at $\eta = 0.25$ Shear	0.666	0.354	1.000	0.774	0.397	0.734	0.710
Bending moment	0.687	0.316	1.000	0.421	0.295	0.482	0.650
Torsion	0.246	0.144	0.382	1.000	0.250	0.742	0.653
Outboard at $\eta = 0.75$ Shear	0.534	0.251	0.780	0.437	0.403	0.789	1.000
Bending moment	0.317	0.206	0.503	0.531	0.437	0.905	1.000
Torsion	0.597	0.274	0.868	0.846	0.442	0.978	1.000

● Assumed control authority (white noise at each actuator input):
  ● Elevator = ± 3 deg
  ● Aileron = ± 15 deg
● Normalized for each load
  ● 1 indicates the control surface most effective for load reduction
  ● 0 indicates a control surface makes no contribution to load reduction

Table F-7. Relative Root-Mean-Square Load Responses at Flight Condition 4

	Elevator			Inboard aileron	Outboard aileron		
	Inboard	Outboard	Inboard and outboard		Inboard	Outboard	Inboard and outboard
Inboard at $\eta = 0.25$: Shear	0.490	0.291	0.760	1.000	0.384	0.670	0.576
Bending moment	0.683	0.322	1.000	0.921	0.428	0.658	0.769
Torsion	0.275	0.199	0.465	1.000	0.265	0.710	0.654
Outboard at $\eta = 0.75$: Shear	0.671	0.342	0.994	0.624	0.522	0.769	1.000
Bending moment	0.192	0.156	0.329	0.741	0.450	0.908	1.000
Torsion	0.181	0.111	0.274	0.781	0.435	0.967	1.000

- Assumed control authority (white noise at each actuator input):
  - Elevator = ±3 deg
  - Aileron = ±15 deg
- Normalized for each load
  - 1 indicates the control surface most effective for load reduction
  - 0 indicates a control surface makes no contribution to load reduction

This Page Intentionally Left Blank

F.3.0 OBSERVABILITY ANALYSIS

F.3.0 OBSERVABILITY ANALYSIS

Figure F-1 shows the various candidate locations for placing accelerometers on the wing. Figures F-2 through F-5 show the relative sensor-to-flutter-mode coupling at the various flight conditions. Figures F-6 through F-9 show the cross-variances between accelerometer responses and wing bending moment responses for the open-loop airplane at the various flight conditions. Figures F-10 through F-13 show the cross-variances between accelerometer responses and wing bending moment responses for the closed-loop airplane (full-state feedback) at the various flight conditions.

Sensor
1
2
3
4
5
6
7
8
9
10
11
12
13
14
15
16
17
18
19
20
21
22
23
24
25
26
27
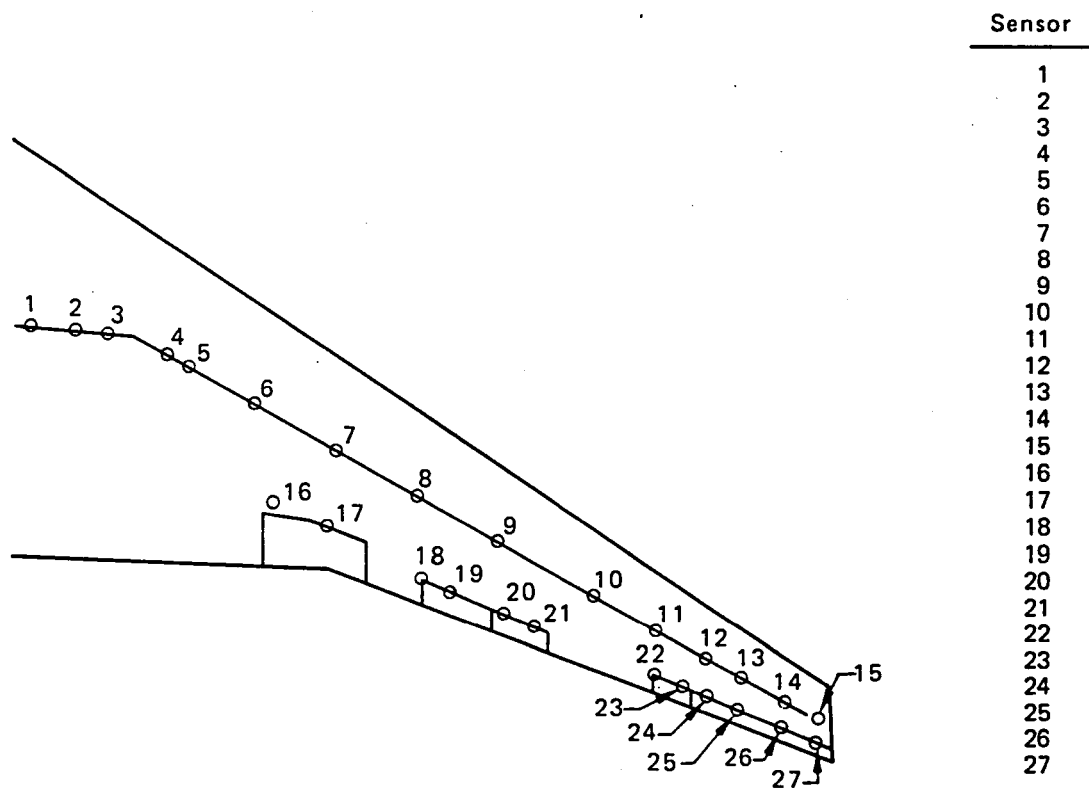
Figure F-1. Candidate Wing Accelerometer Locations
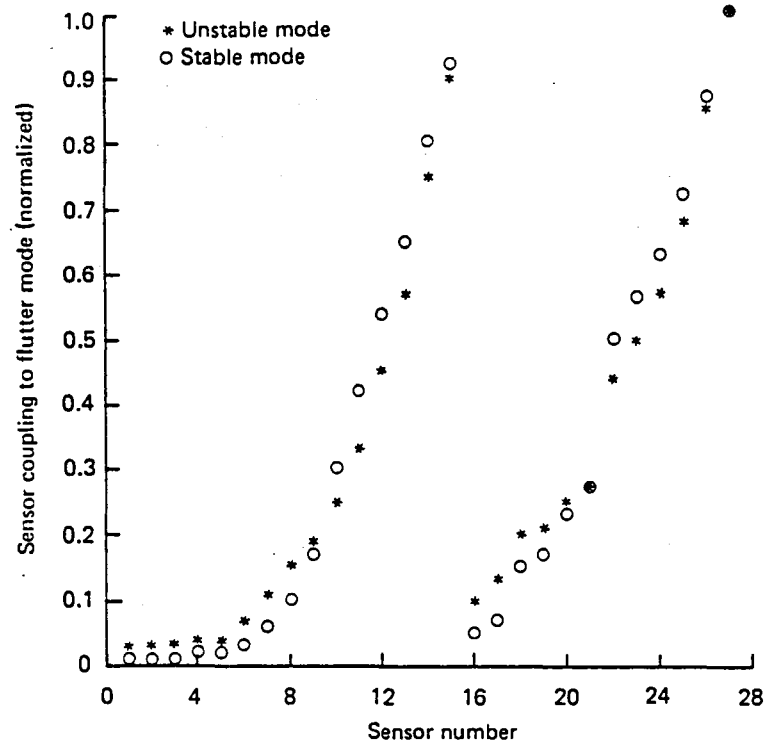
Figure F-2. Sensor Coupling to Flutter Modes, Flight Condition 5, Open Loop
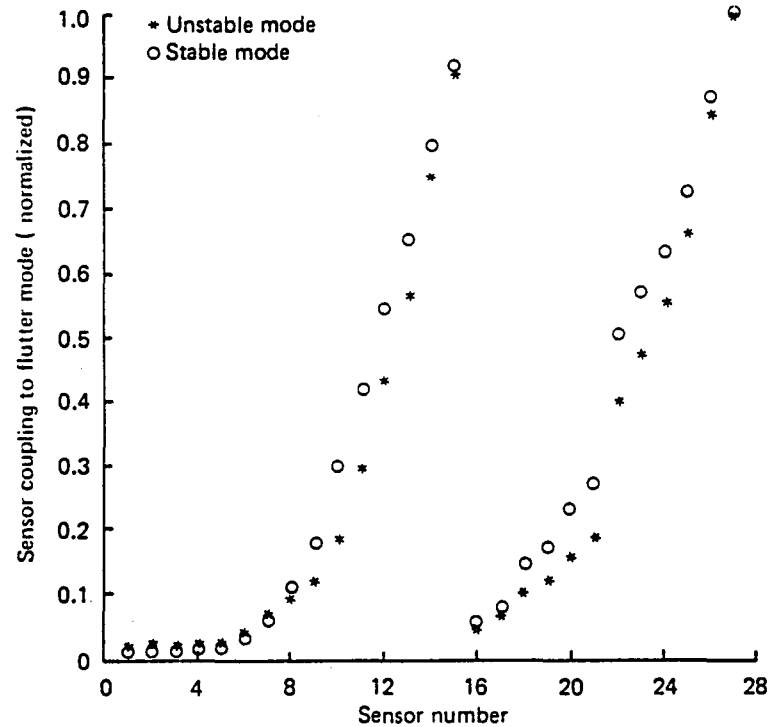
Figure F-3. Sensor Coupling to Flutter Modes, Flight Condition 6, Open Loop
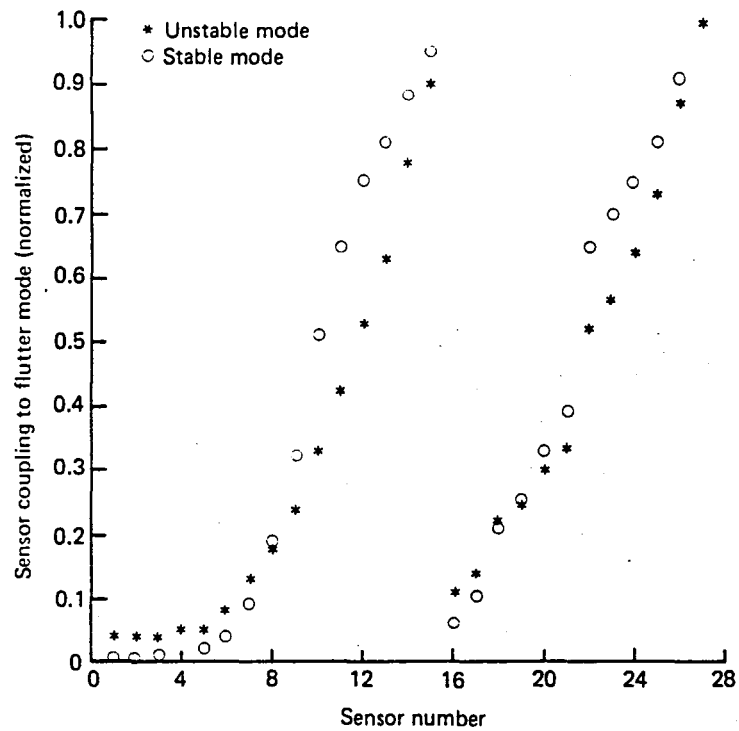
Figure F-4. Sensor Coupling to Flutter Modes, Flight Condition 7, Open Loop
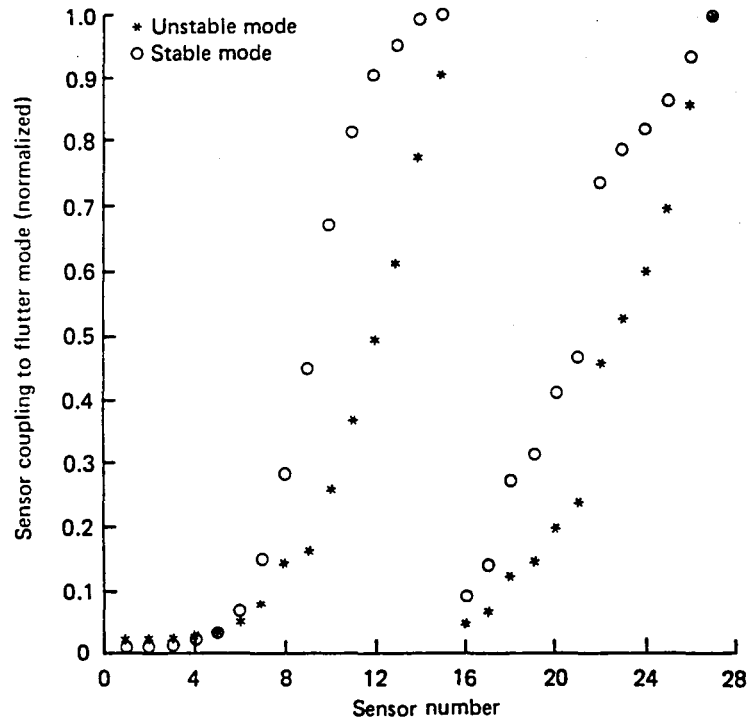
Figure F-5. Sensor Coupling to Flutter Modes, Flight Condition 8, Open Loop
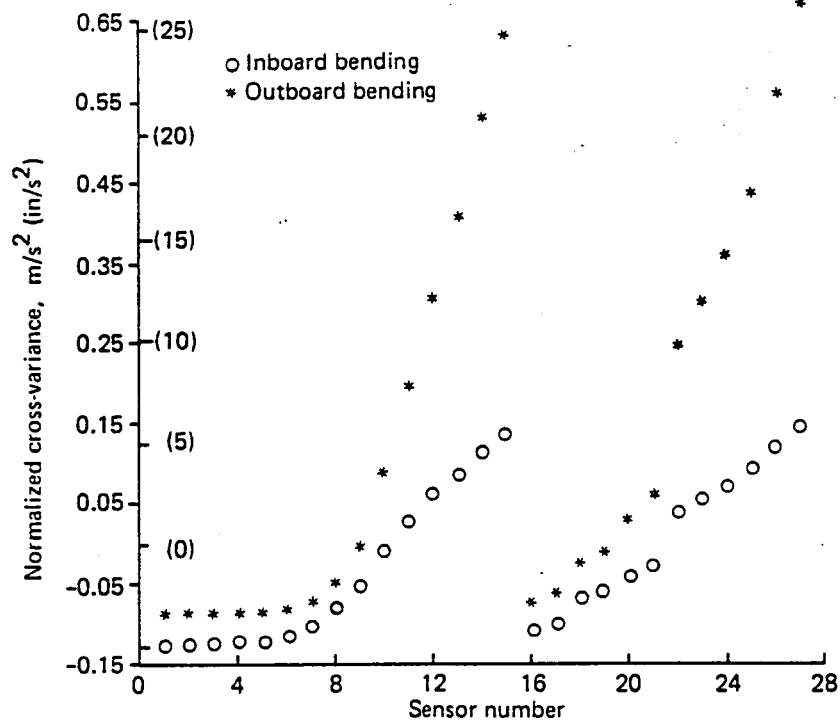
Figure F-6. *Cross-Variance Between Accelerometer Response and Wing Bending Responses, Flight Condition 1, Open Loop*
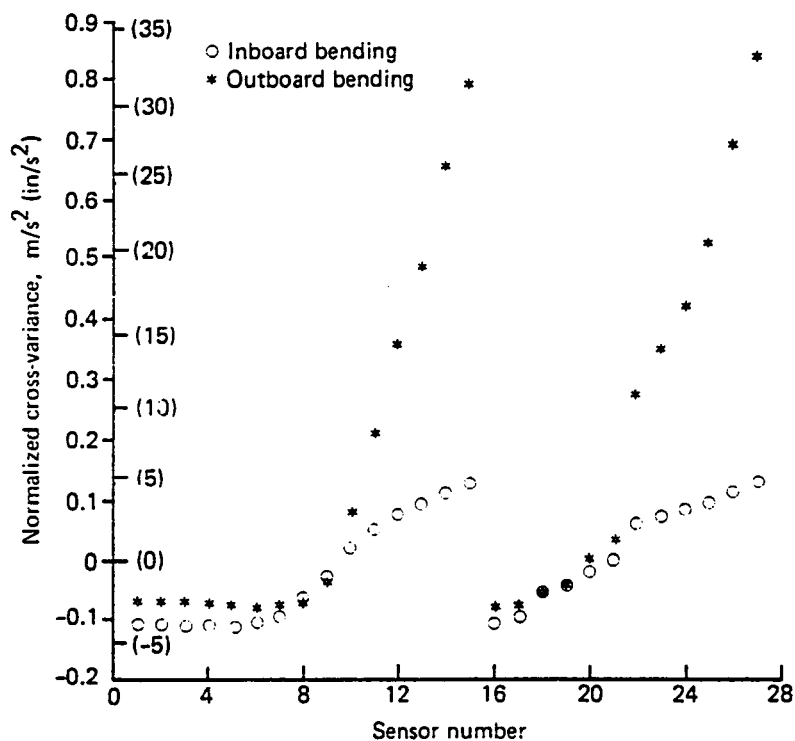
Figure F-7. *Cross-Variance Between Accelerometer Response and Wing Bending Responses, Flight Condition 2, Open Loop*
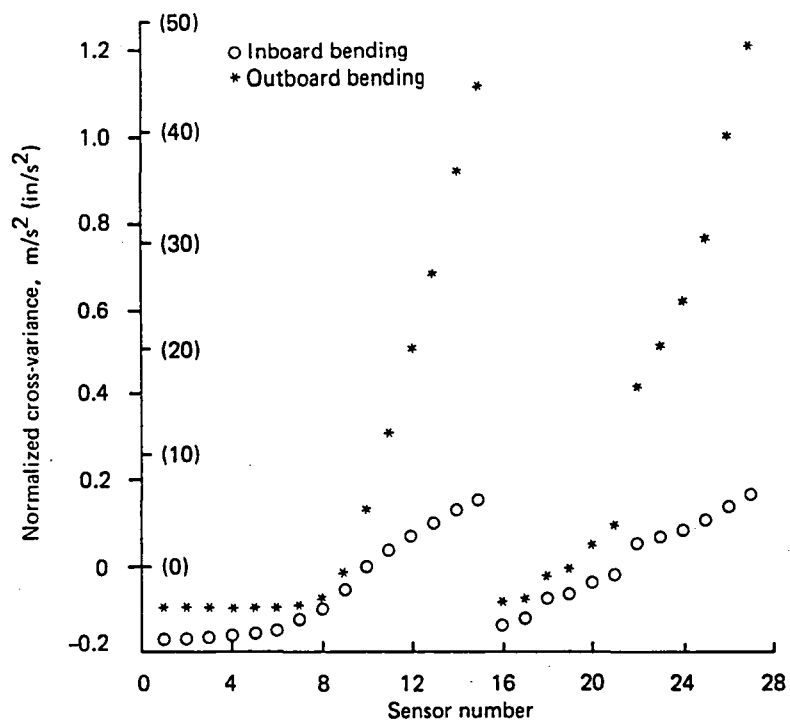
Figure F-8. Cross-Variance Between Accelerometer Response and Wing Bending Responses, Flight Condition 3, Open Loop
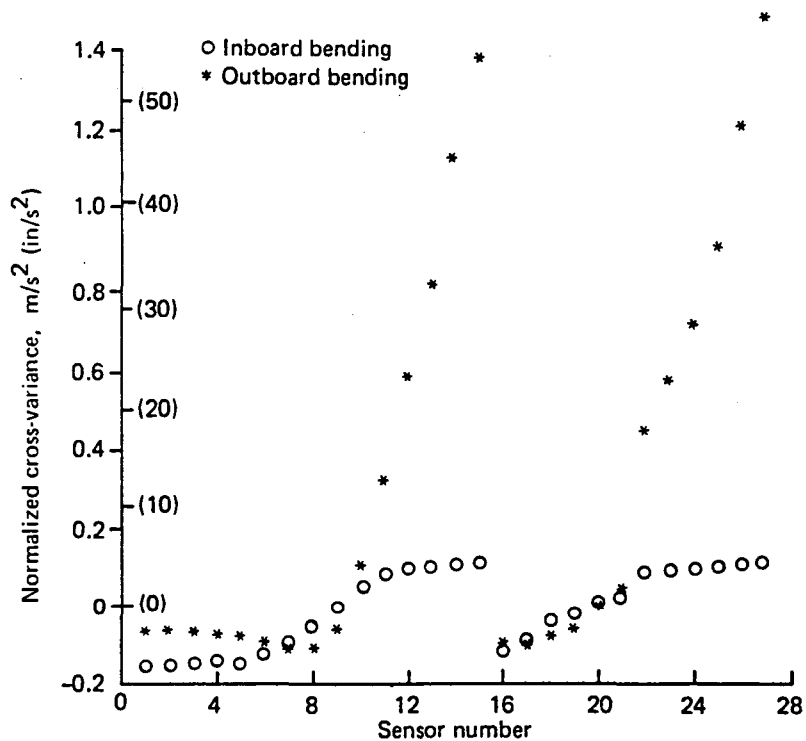
Figure F-9. Cross-Variance Between Accelerometer Response and Wing Bending Responses, Flight Condition 4, Open Loop
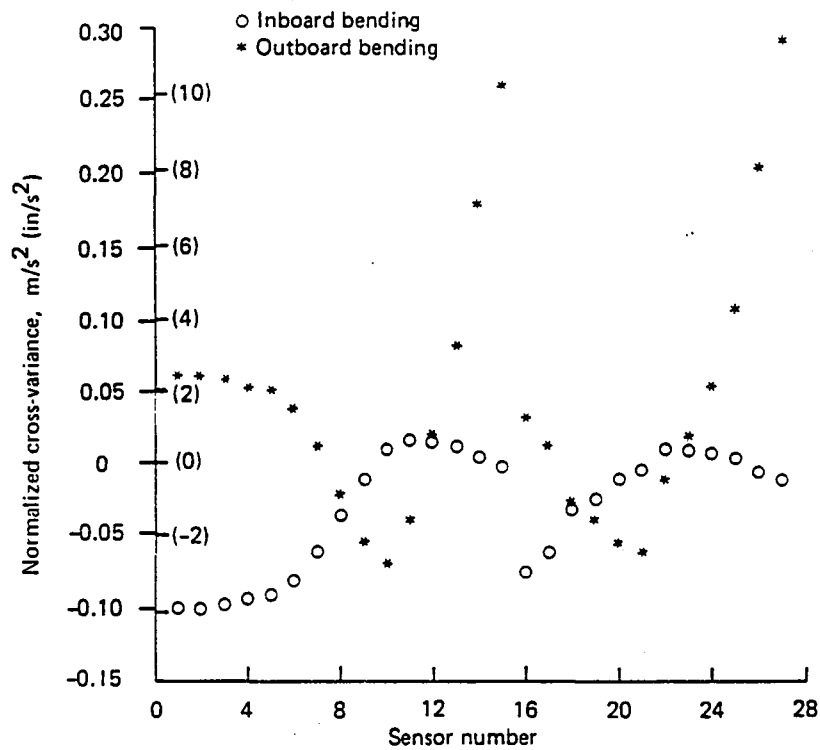
Figure F-10. Cross-Variance Between Accelerometer Response and Wing
Bending Responses, Flight Condition 1, Design A
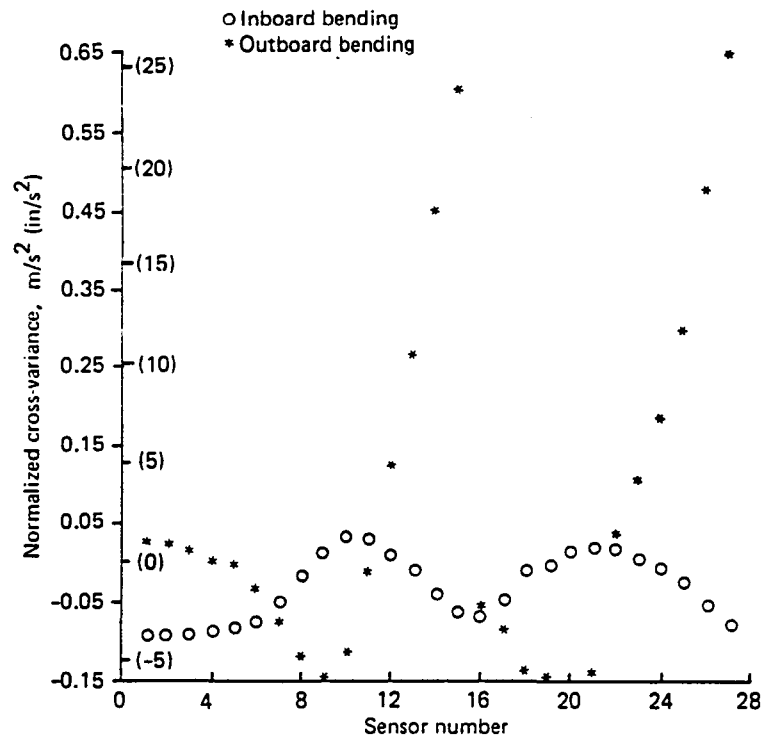
Figure F-11. Cross-Variance Between Accelerometer Response and Wing
Bending Responses, Flight Condition 2, Design A
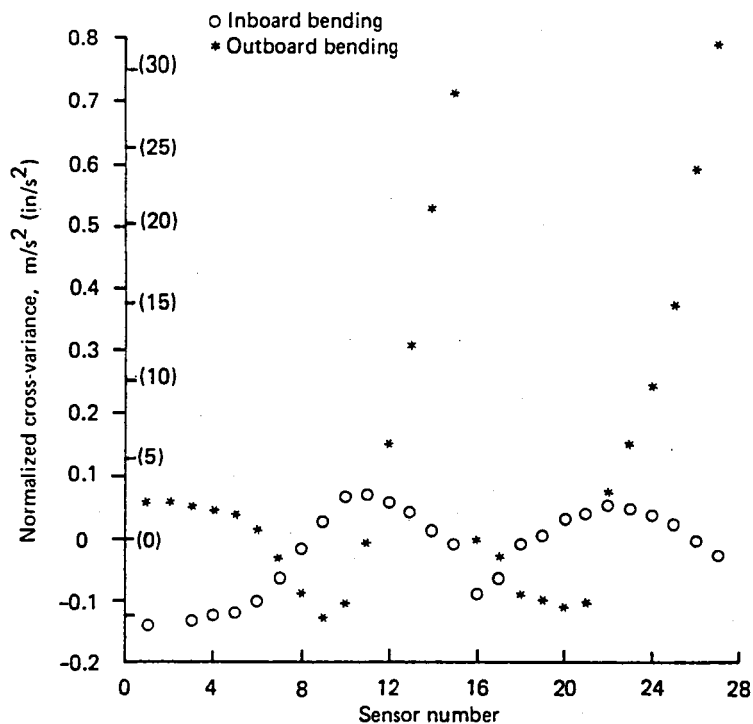
Figure F-12. Cross-Variance Between Accelerometer Response and Wing Bending Responses, Flight Condition 3, Design A
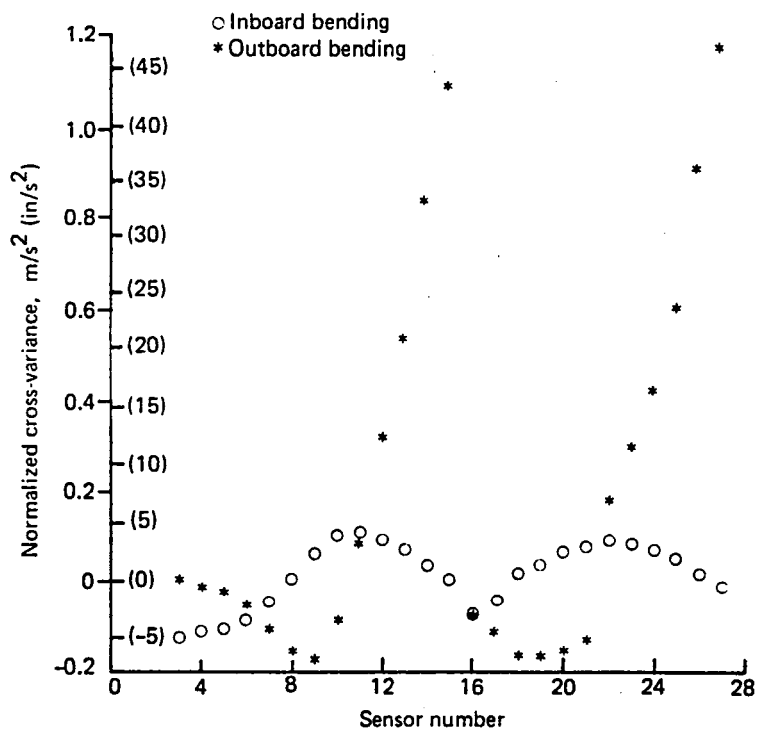
Figure F-13. Cross-Variance Between Accelerometer Response and Wing Bending Responses, Flight Condition 4, Design A

This Page Intentionally Left Blank

F.4.0 CONTROL LAW PERFORMANCE ANALYSIS

F.4.0 CONTROL LAW PERFORMANCE ANALYSIS

Numerical results of the open- and closed-loop characteristics and performance of the airplane at the gust and flutter flight conditions are presented in this section.

F.4.1 GLA PERFORMANCE

F.4.1.1 POWER-SPECTRAL-DENSITY PLOTS

Figures F-14 through F-29 present power-spectral-density (PSD) plots of gust-induced wing bending and torsion for the open- and closed-loop airplanes. Figures F-30 through F-45 show PSD plots of the corresponding elevator and aileron deflections and rates.
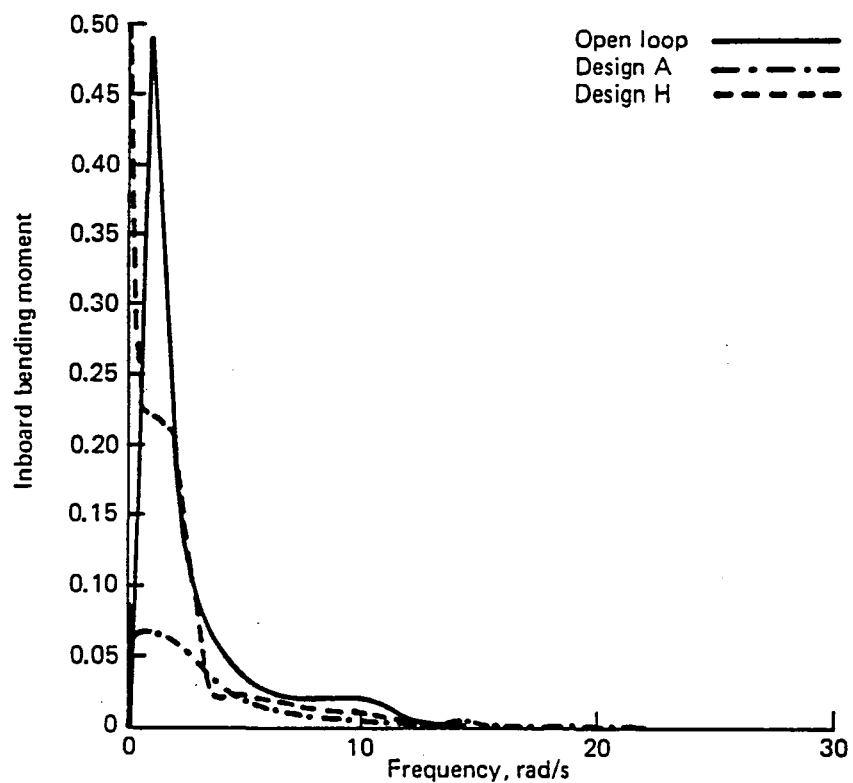
*Figure F-14. Normalized Power-Spectral-Density Plot,
Flight Condition 1 (Inboard Bending Moment)*
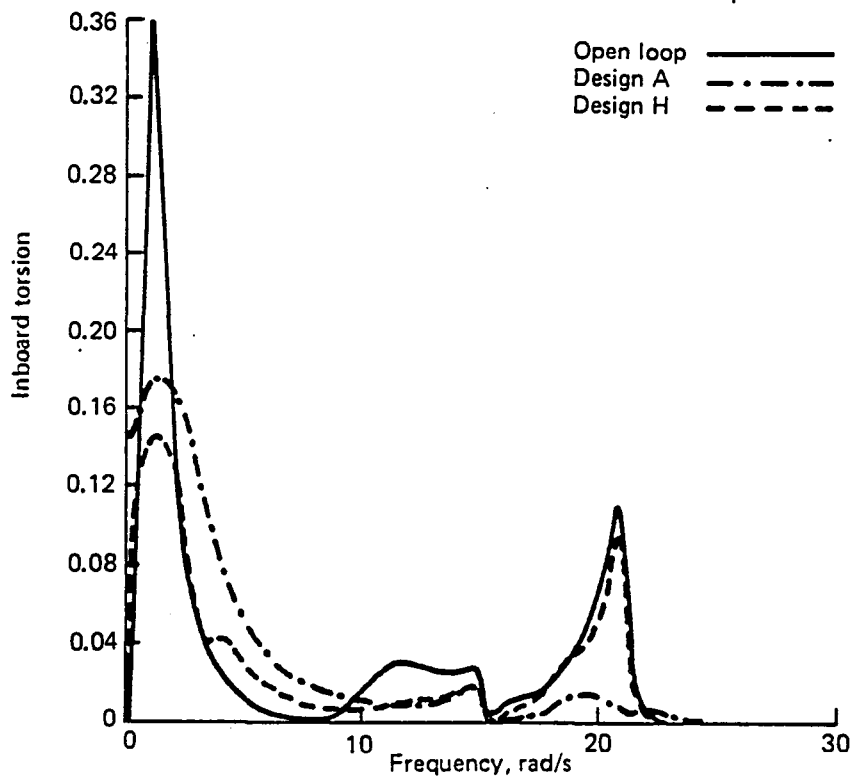
*Figure F-15. Normalized Power-Spectral-Density Plot,
Flight Condition 1 (Inboard Torsion)*

F-18
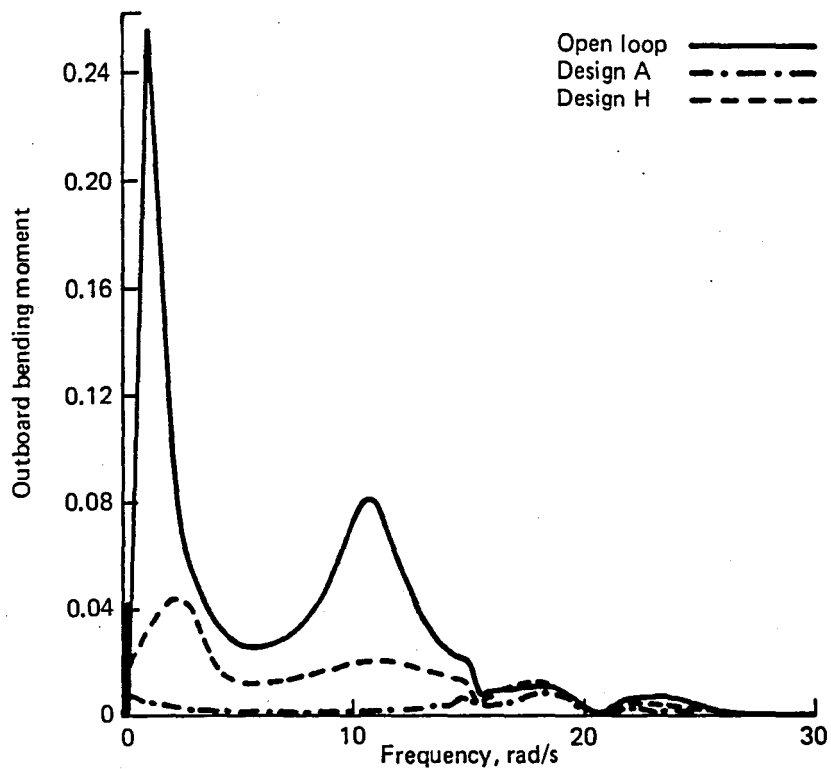
Figure F-16. *Normalized Power-Spectral-Density Plot,*
Flight Condition 1 (Outboard Bending Moment)
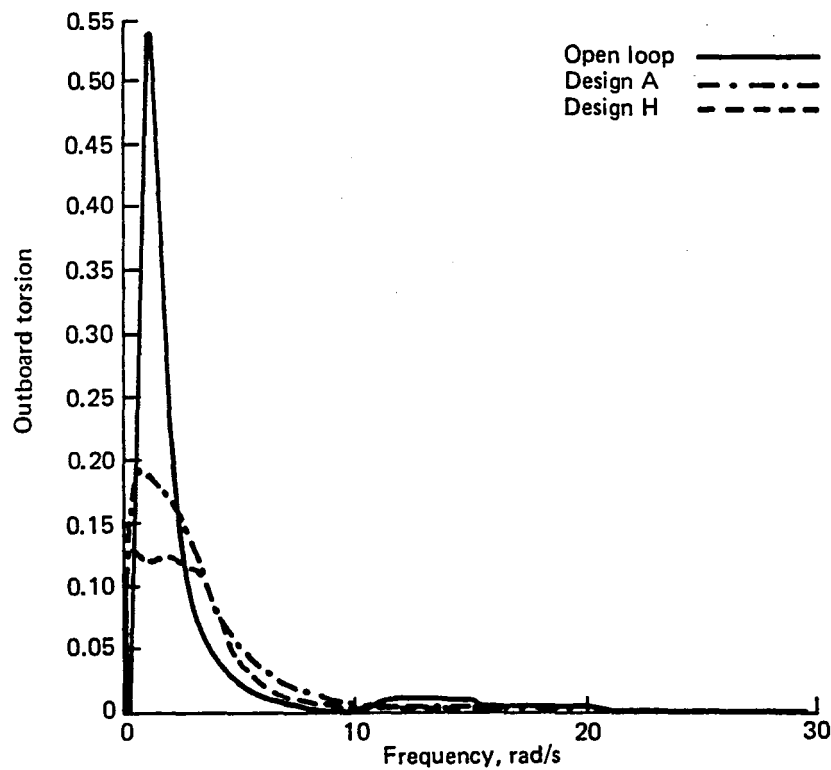
Figure F-17. *Normalized Power-Spectral-Density Plot,*
Flight Condition 1 (Outboard Torsion)

F-19
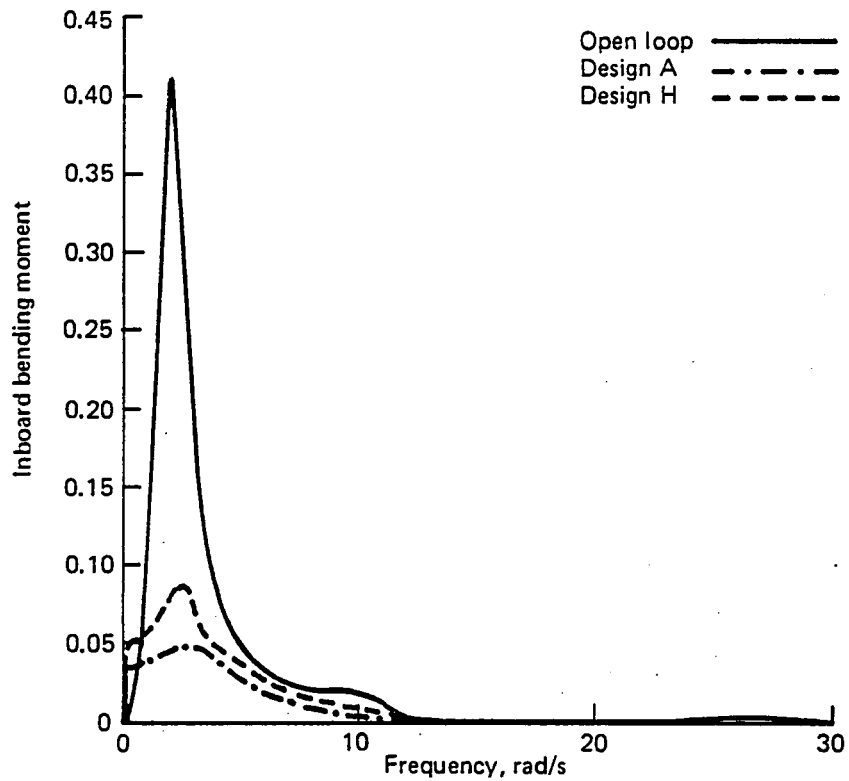
Figure F-18. Normalized Power-Spectral-Density Plot,
Flight Condition 2 (Inboard Bending Moment)
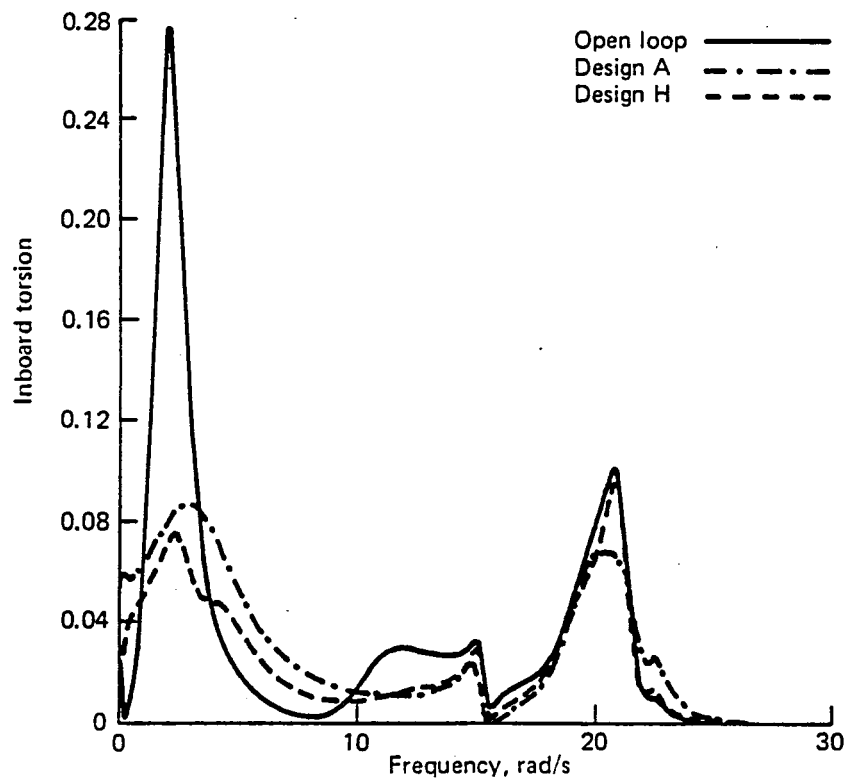
Figure F-19. Normalized Power-Spectral-Density Plot,
Flight Condition 2 (Inboard Torsion)
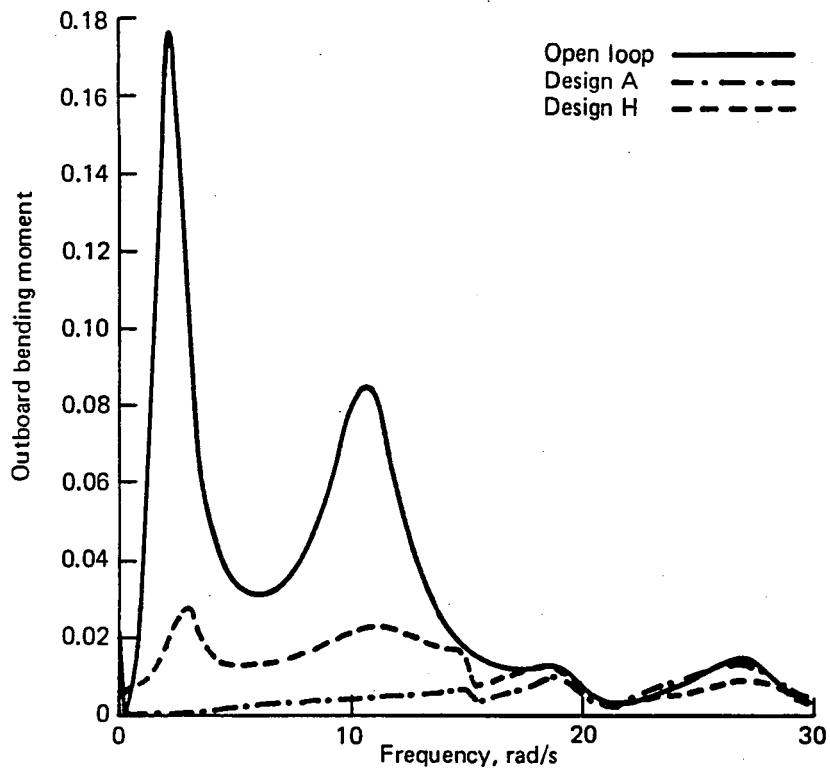
Figure F-20. Normalized Power-Spectral-Density Plot,
Flight Condition 2 (Outboard Bending Moment)
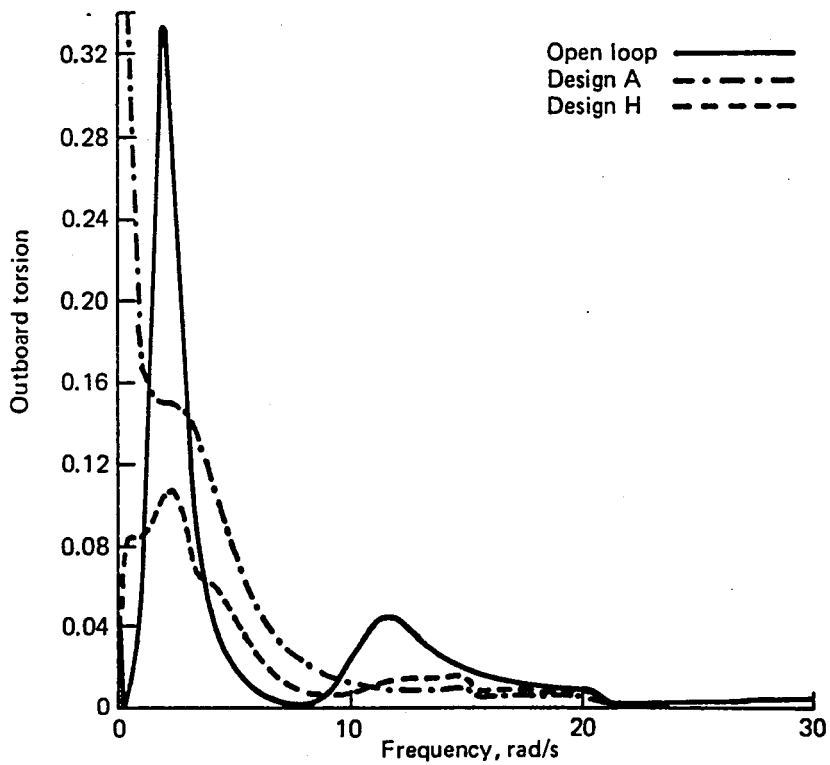
Figure F-21. Normalized Power-Spectral-Density Plot,
Flight Condition 2 (Outboard Torsion)

F-21
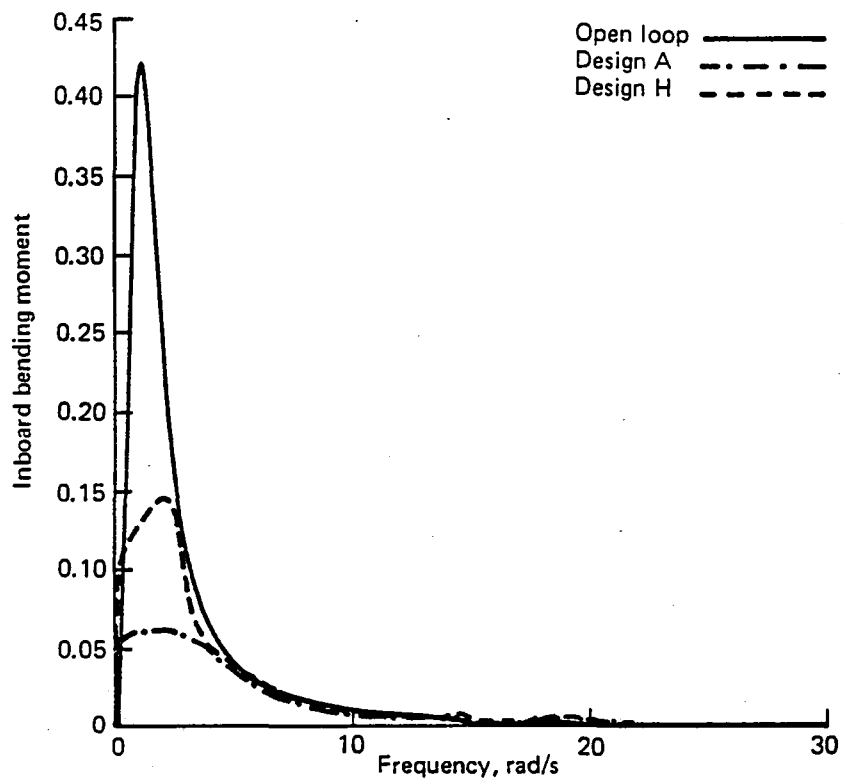
Figure F-22. Normalized Power-Spectral-Density Plot,
Flight Condition 3 (Inboard Bending Moment)
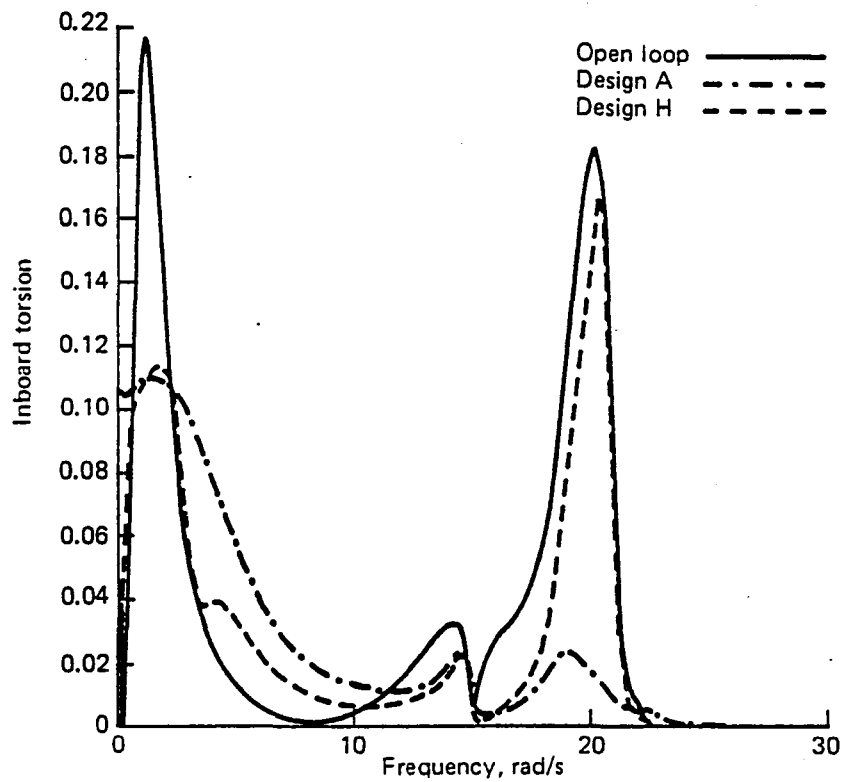
Figure F-23. Normalized Power-Spectral-Density Plot,
Flight Condition 3 (Inboard Torsion)
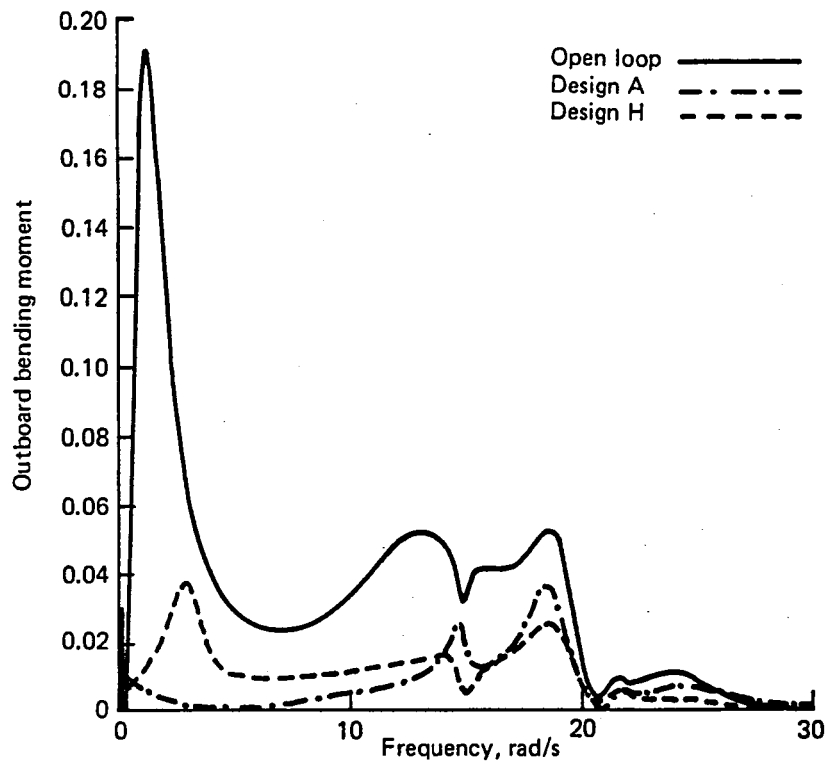
Figure F-24. Normalized Power-Spectral-Density Plot,
Flight Condition 3 (Outboard Bending Moment)
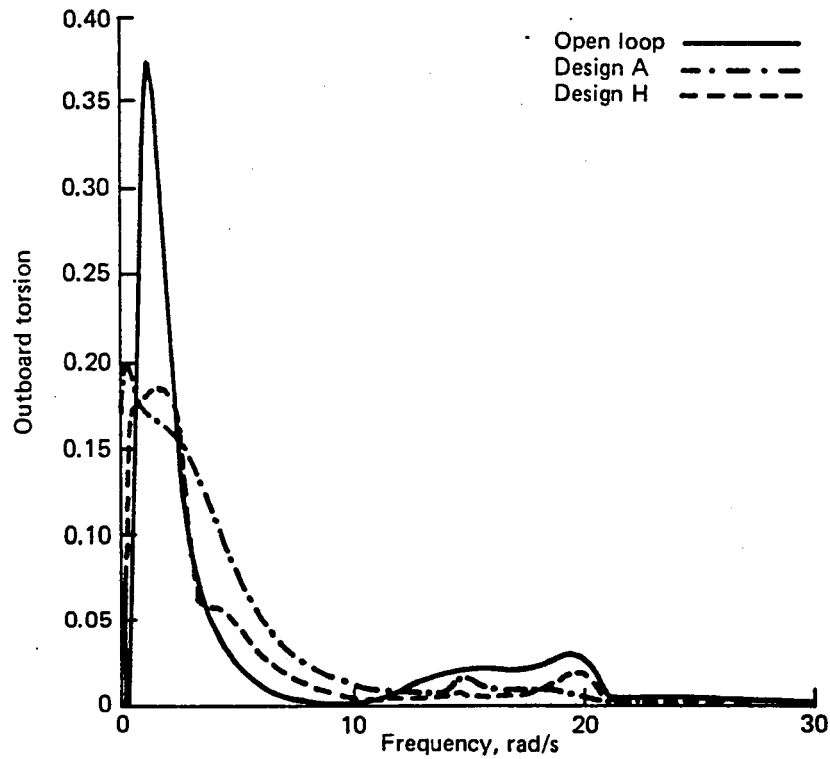
Figure F-25. Normalized Power-Spectral-Density Plot,
Flight Condition 3 (Outboard Torsion)
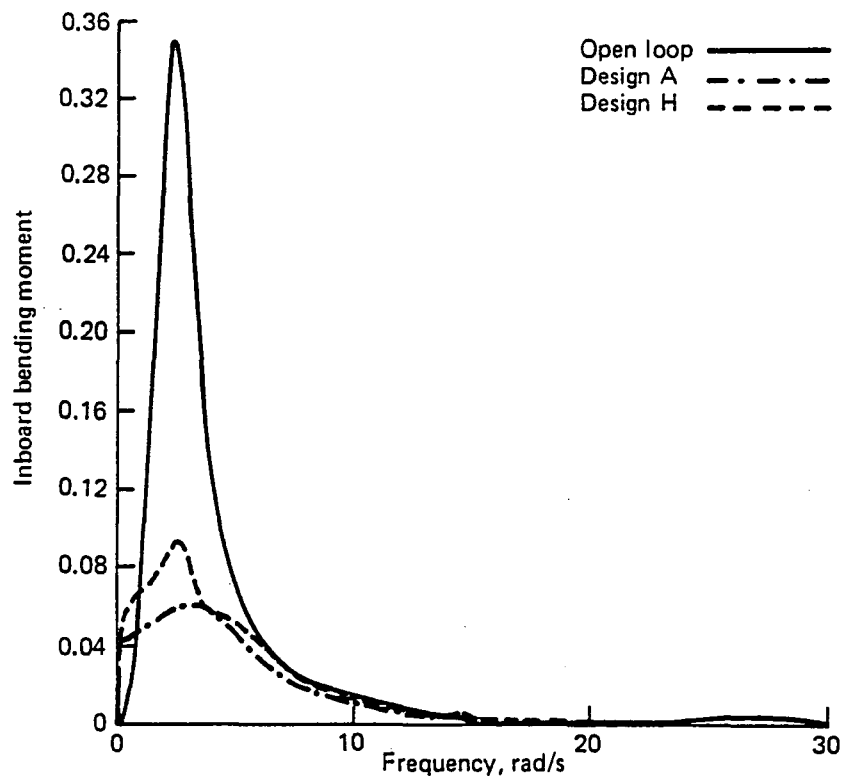
Figure F-26. Normalized Power-Spectral-Density Plot,
Flight Condition 4 (Inboard Bending Moment)
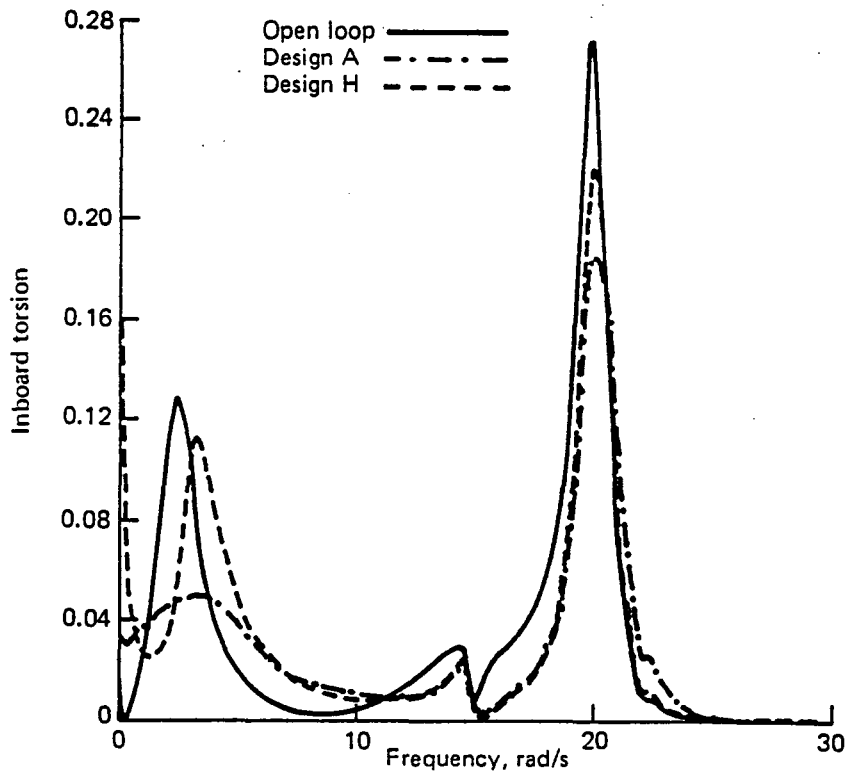
Figure F-27. Normalized Power-Spectral-Density Plot,
Flight Condition 4 (Inboard Torsion)
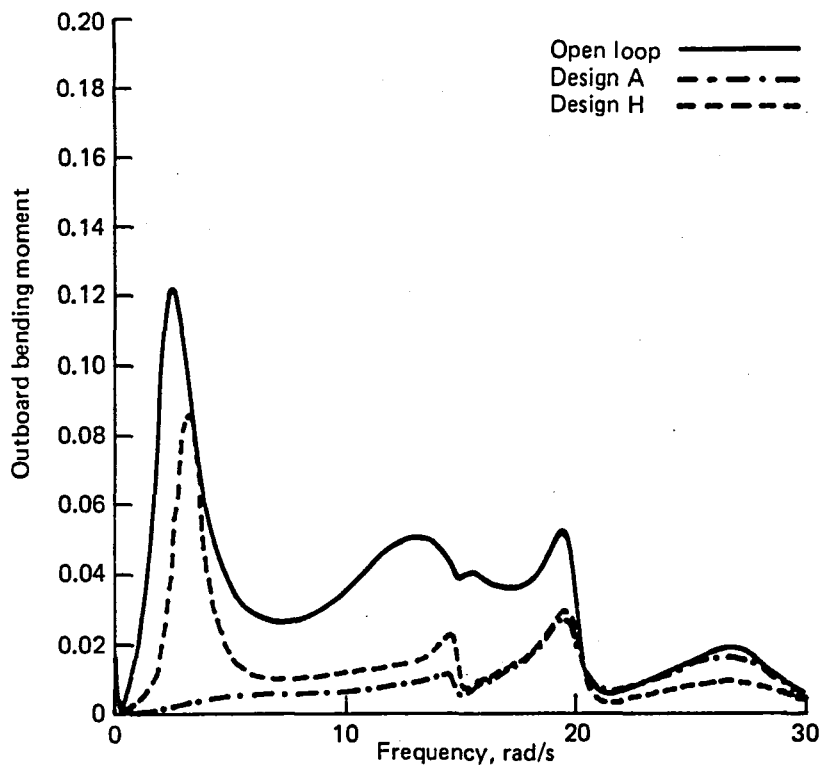
Figure F-28. Normalized Power-Spectral-Density Plot,
Flight Condition 4 (Outboard Bending Moment)
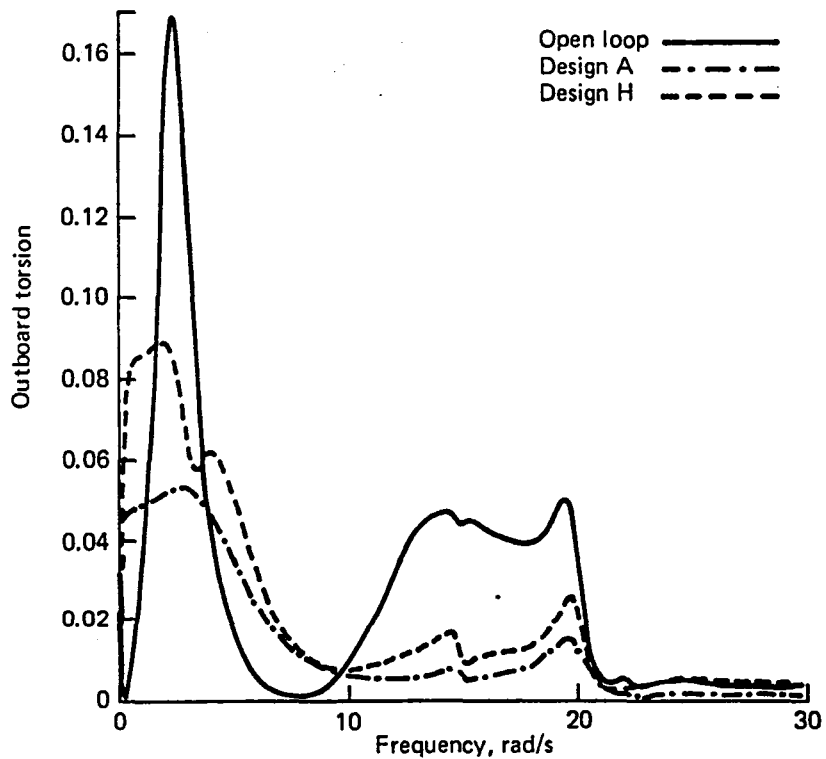
Figure F-29. Normalized Power-Spectral-Density Plot,
Flight Condition 4 (Outboard Torsion)
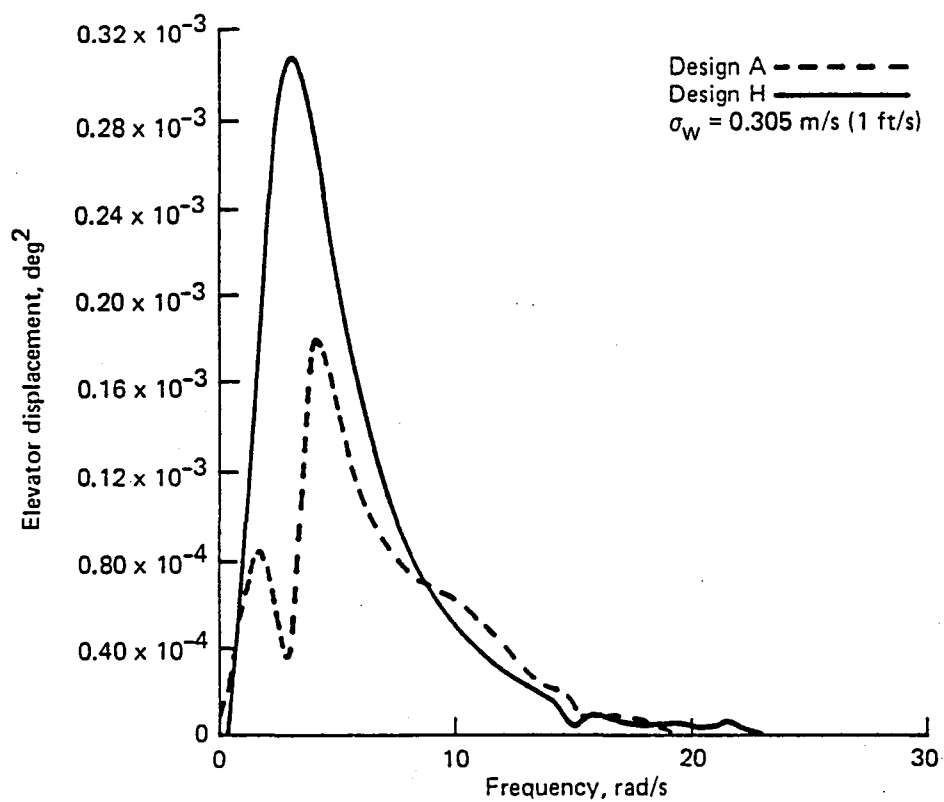
*Figure F-30. Power-Spectral-Density Plot, Flight Condition 1
(Elevator Displacement)*
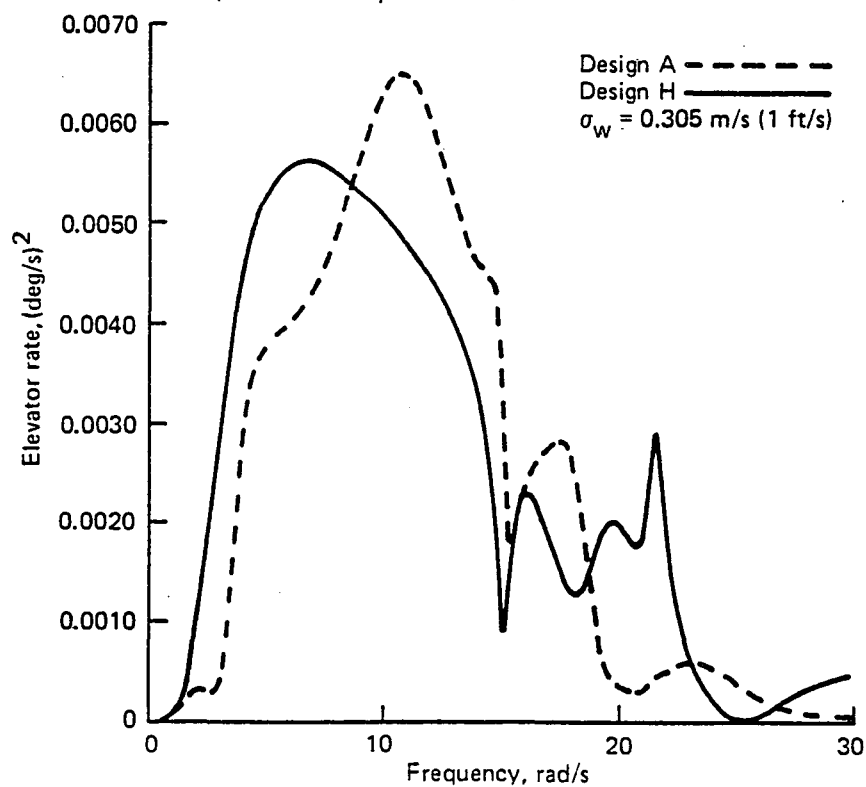
*Figure F-31. Power-Spectral-Density Plot, Flight Condition 1
(Elevator Rate)*
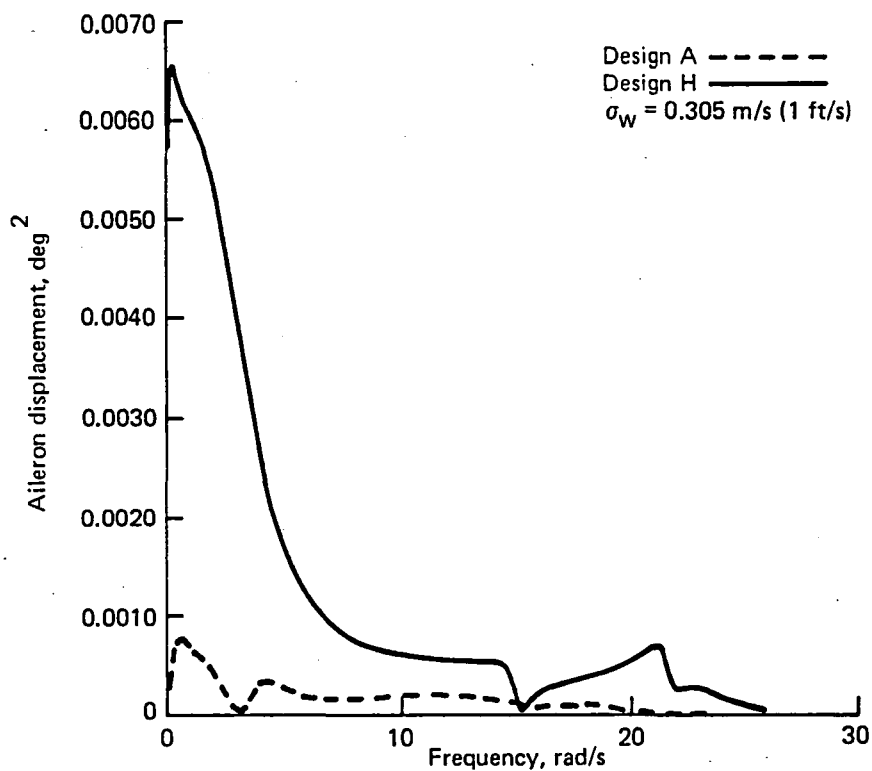
Figure F-32. Power-Spectral-Density Plot, Flight Condition 1
(Aileron Displacement)
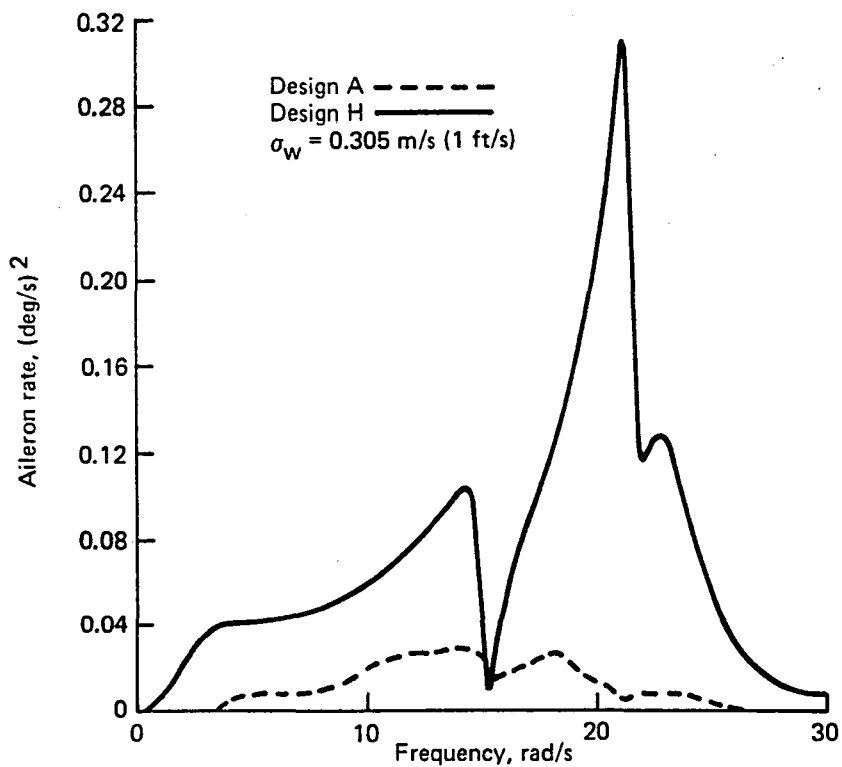
Figure F-33. Power-Spectral-Density Plot, Flight Condition 1
(Aileron Rate)
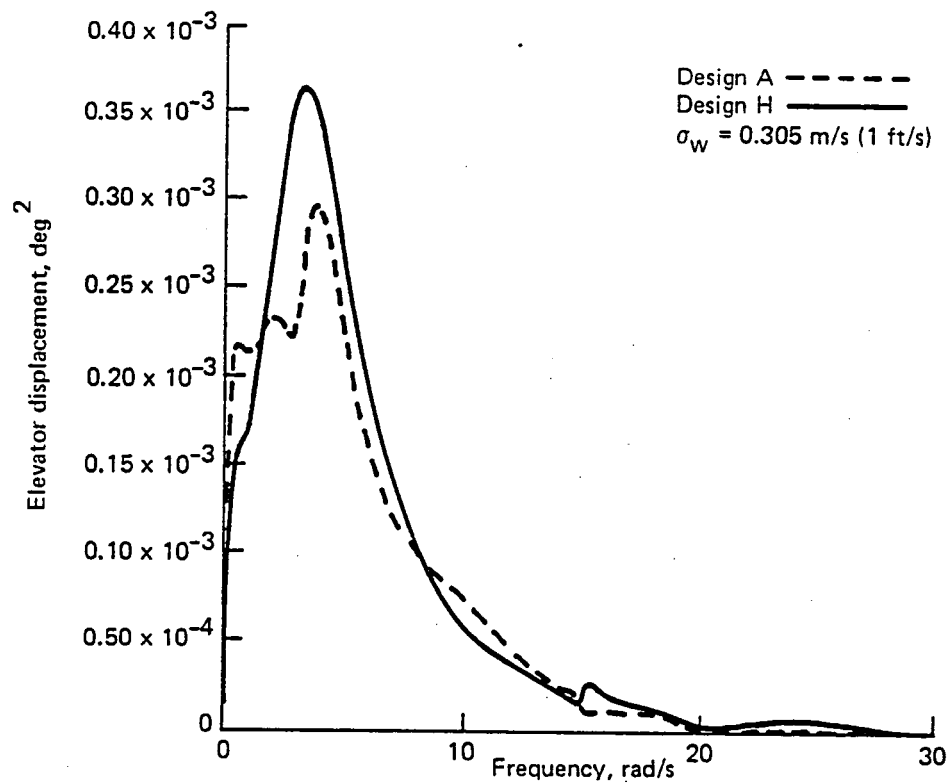
Figure F-34. Power-Spectral-Density Plot, Flight Condition 2 (Elevator Displacement)
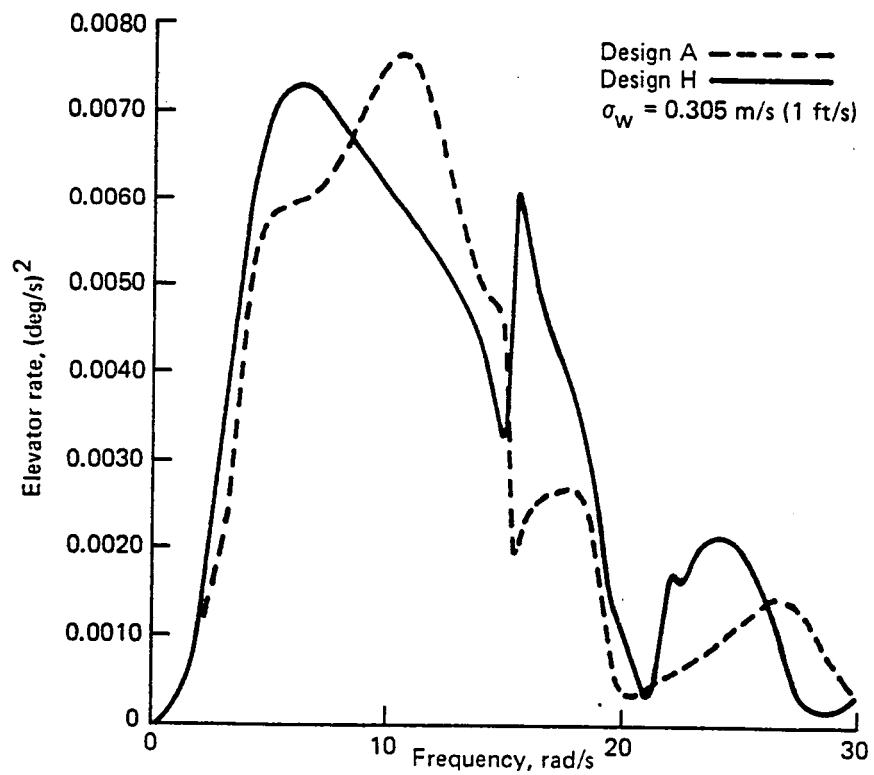
Figure F-35. Power-Spectral-Density Plot, Flight Condition 2 (Elevator Rate)
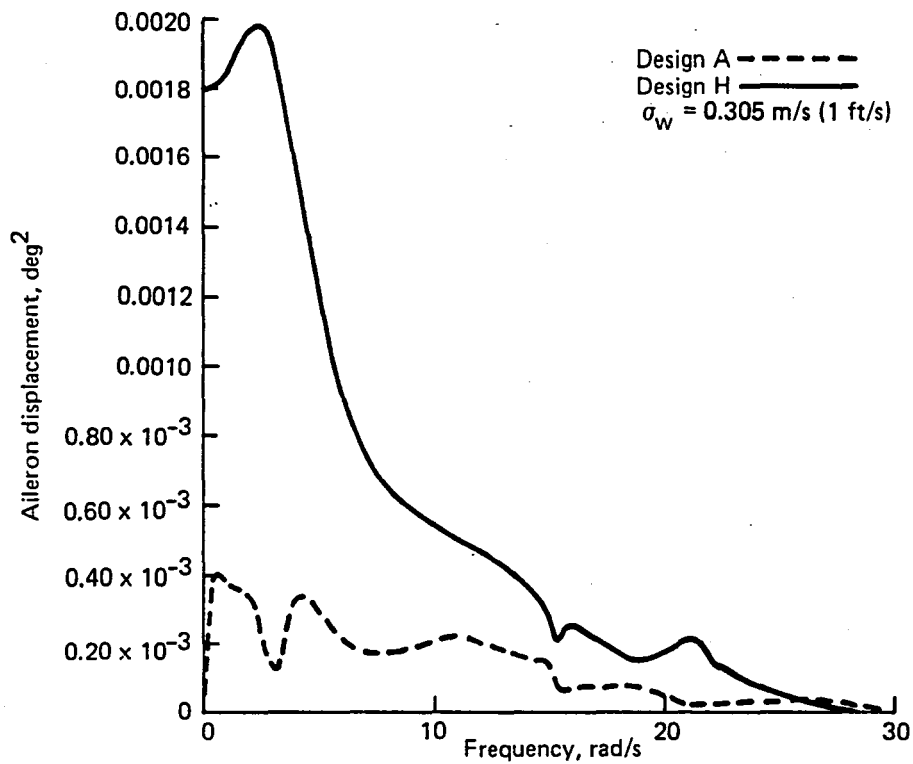
Figure F-36. Power-Spectral-Density Plot, Flight Condition 2
(Aileron Displacement)
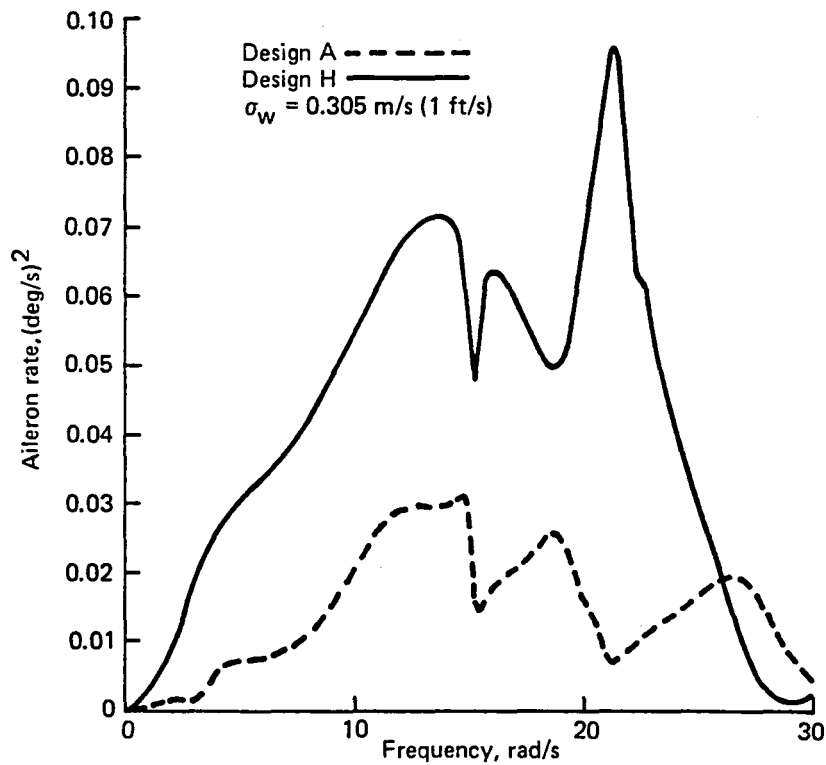
Figure F-37. Power-Spectral-Density Plot, Flight Condition 2
(Aileron Rate)
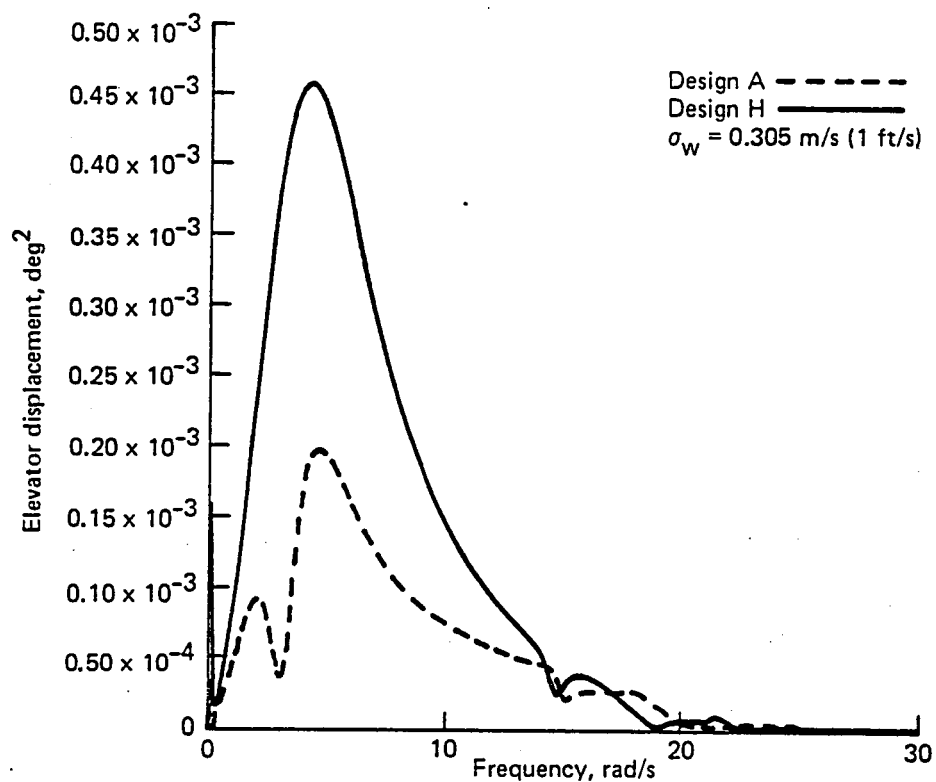
Figure F-38. Power-Spectral-Density Plot, Flight Condition 3
(Elevator Displacement)
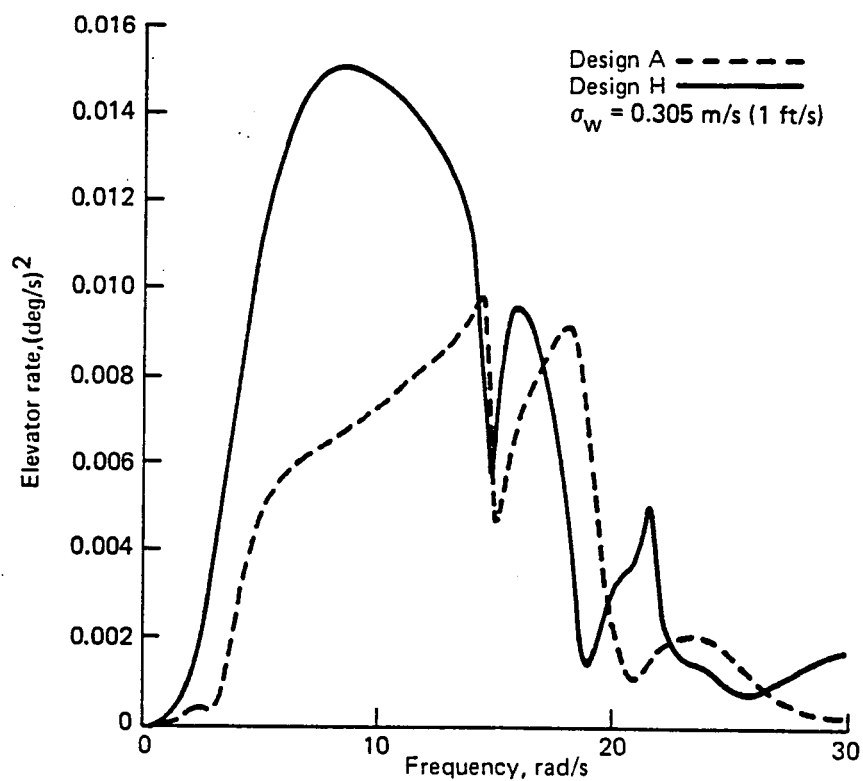
Figure F-39. Power-Spectral-Density Plot, Flight Condition 3
(Elevator Rate)
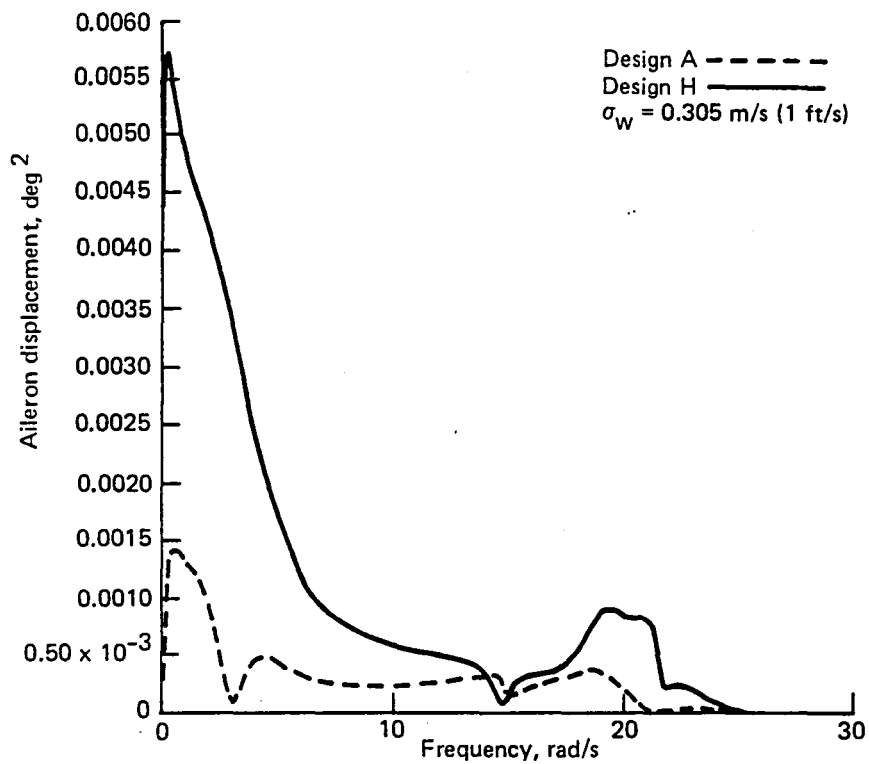
Figure F-40. Power-Spectral-Density Plot, Flight Condition 3
(Aileron Displacement)
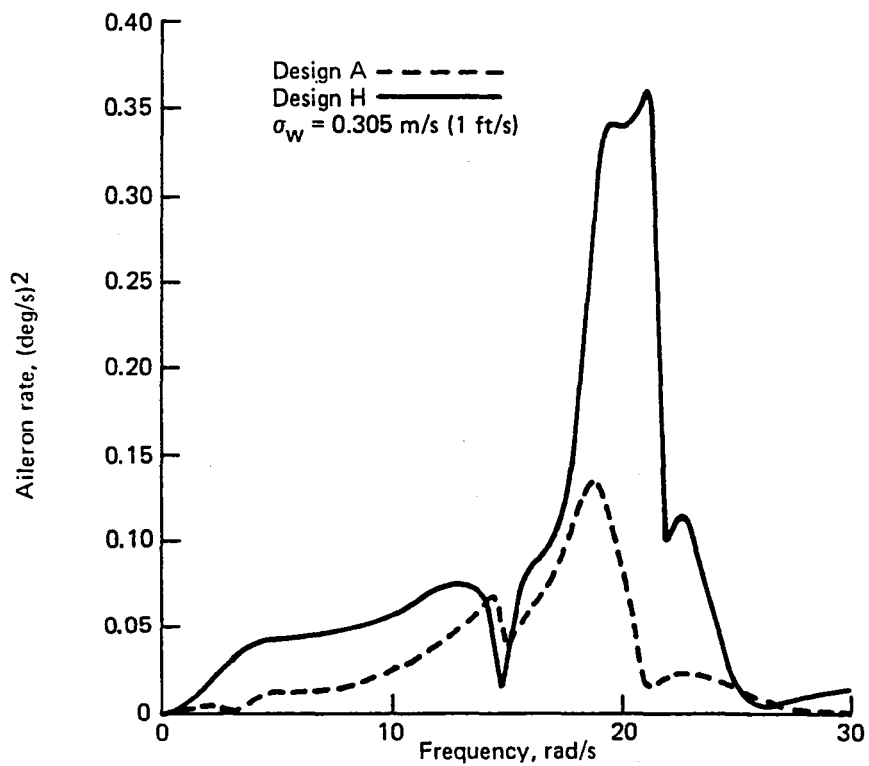
Figure F-41. Power-Spectral-Density Plot, Flight Condition 3
(Aileron Rate)
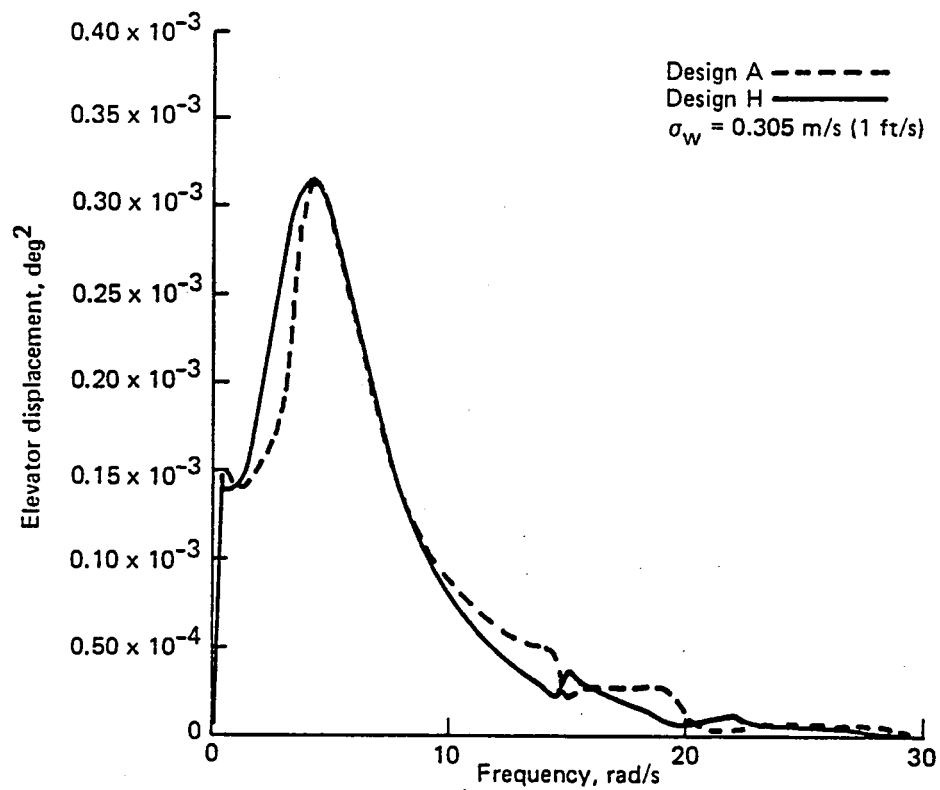
*Figure F-42. Power-Spectral-Density Plot, Flight Condition 4
(Elevator Displacement)*
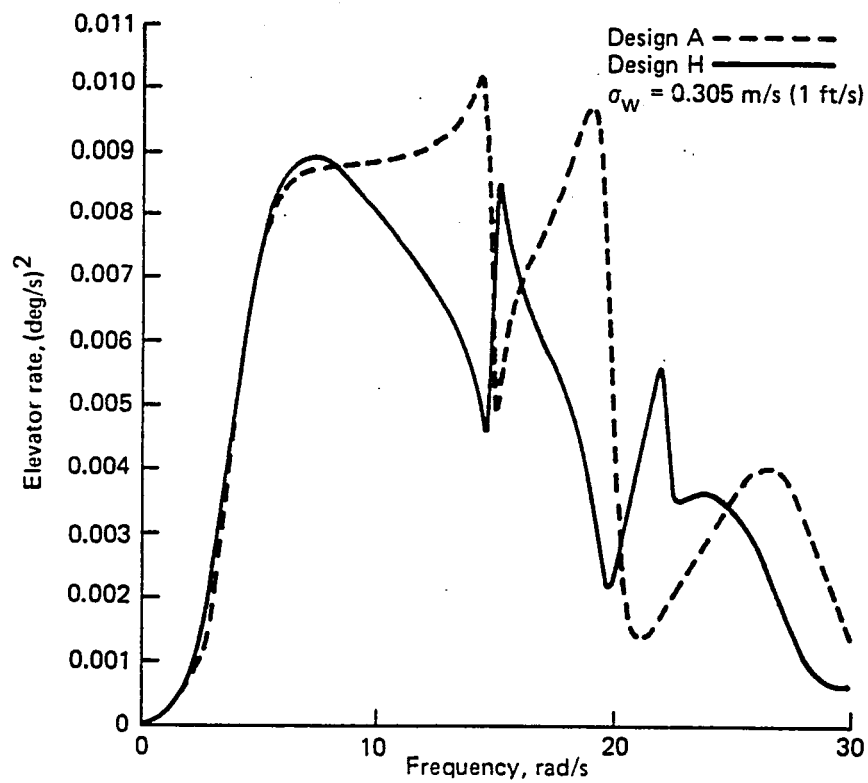
*Figure F-43. Power-Spectral-Density Plot, Flight Condition 4
(Elevator Rate)*
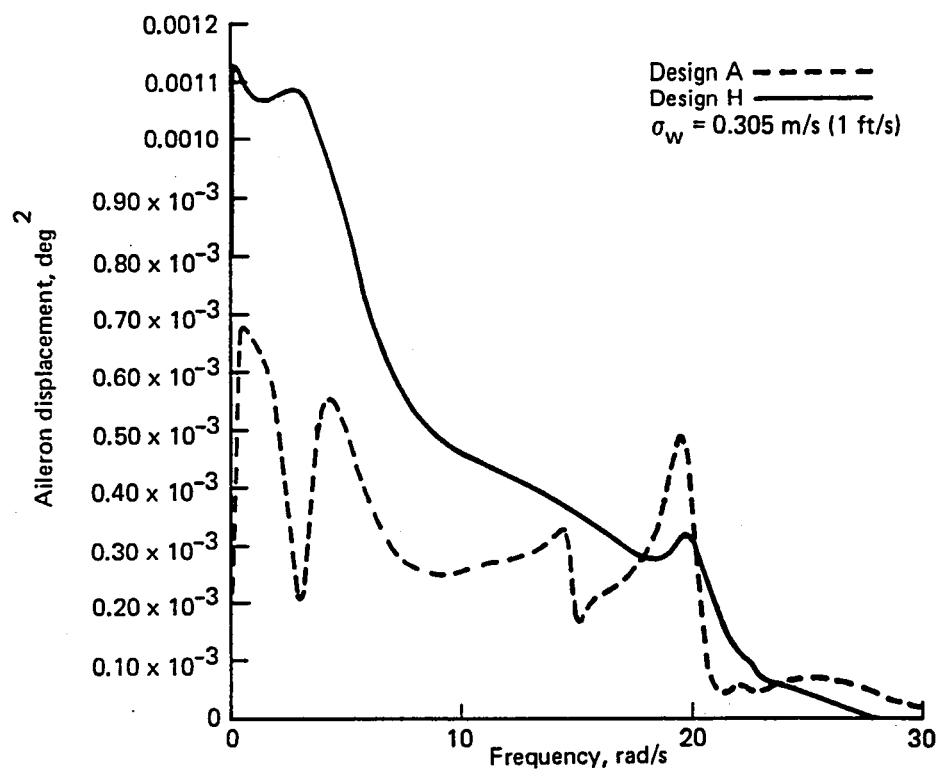
Figure F-44. Power-Spectral-Density Plot, Flight Condition 4
(Aileron Displacement)
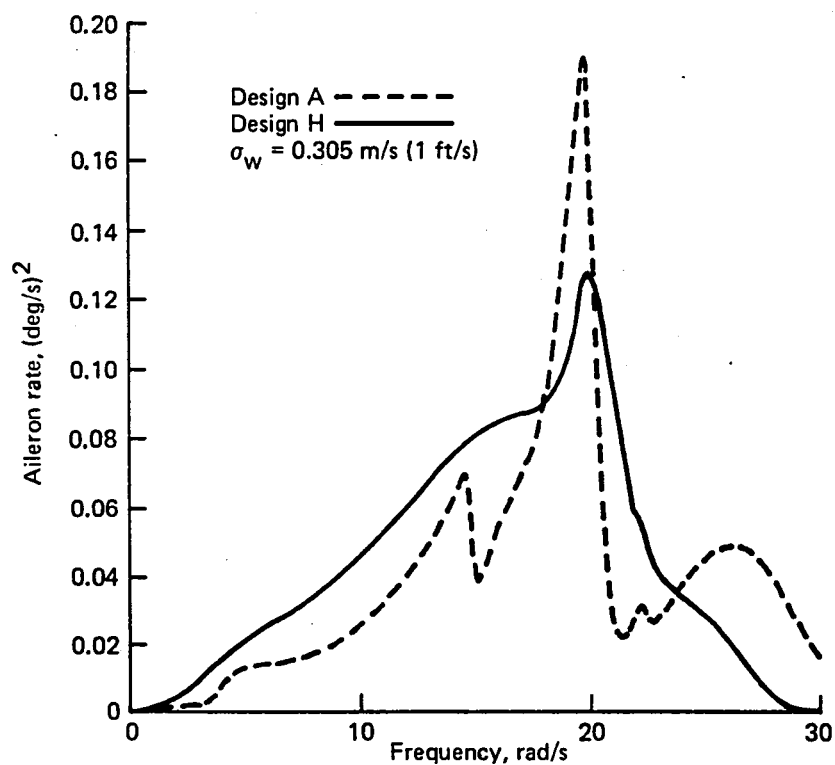
Figure F-45. Power-Spectral-Density Plot, Flight Condition 4
(Aileron Rate)

F.4.1.2 POLE LOCATIONS

Tables F-8 through F-11 show the open- and closed-loop (full-state feedback) poles. Tables F-12 through F-15 show the closed-loop poles for the full- and reduced-order filters.

Table F-8. Open- and Closed-Loop Dynamic Model Poles, Flight Condition 1

	Number	Open loop				Closed loop (design A)			
		Real, rad/s	Imaginary, rad/s	Magnitude, rad/s	Damping ratio	Real, rad/s	Imaginary, rad/s	Magnitude, rad/s	Damping ratio
Flexible airplane	1, 2	-3.27×10^{-2}	±0.125	0.130	0.252	-4.56×10^{-2}	$±1.20 \times 10^{-2}$	4.72×10^{-2}	0.970
	3, 4	-0.648	±0.887	1.10	0.590	-2.43	± 2.07	3.19	0.762
	5, 6	-1.95	±10.8	10.9	0.179	-8.20	±15.0	17.1	0.480
	7, 8	-0.281	±15.2	15.2	0.018	-0.462	±15.1	15.1	0.030
	9, 10	-1.20	±19.0	19.0	0.063	-1.58	±18.7	18.8	0.084
	11, 12	-0.533	±21.0	21.0	0.025	-2.58	±21.5	21.6	0.119
	13, 14	-0.387	±21.9	21.9	0.018	-0.426	±21.6	21.6	0.020
	15, 16	-1.97	±24.1	24.2	0.081	-3.38	±24.0	24.2	0.140
	17, 18	-1.96	±34.7	34.8	0.056	-3.00	±35.3	35.4	0.085
	19, 20	-1.08	±36.5	36.6	0.030	-0.980	±36.3	36.3	0.027
	21, 22	-2.47	±47.2	47.3	0.052	-2.70	±47.3	47.4	0.057
	23, 24	-1.33	±55.5	55.5	0.024	-1.30	±55.5	55.5	0.023
	25, 26	-1.96	±55.5	55.6	0.035	-2.02	±55.6	55.6	0.036
	27, 28	-3.82	±60.5	60.6	0.063	-4.22	±60.4	60.4	0.070
	29, 30	-7.76	±75.6	76.0	0.100	-7.77	±75.6	76.0	0.102
	31, 32	-1.99	±83.1	83.1	0.024	-2.03	±83.1	83.1	0.024
	33, 34	-5.28	±93.3	93.4	0.056	-5.46	±93.4	93.6	0.058
	35, 36	-6.54	±114.0	114.2	0.057	-6.54	±114.0	114.2	0.057
	37, 38	-7.20	±138.0	138.2	0.052	-7.20	±138.0	138.2	0.052
	39, 40	-8.31	±153.0	153.2	0.054	-8.30	±153.0	153.2	0.054
	41, 42	-10.5	±302.0	302.2	0.035	-10.5	±302.0	302.2	0.035
Elevator	43	-1000.0	0	1000.0	1.0	-1000.0	0	1000.0	1.0
	44	-40.0	0	40.0	1.0	-40.0	0	40.0	1.0
	45	-20.0	0	20.0	1.0	-20.0	0	20.0	1.0
Aileron	46	-1000.0	0	1000.0	1.0	-1000.0	0	1000.0	1.0
	47	-40.0	0	40.0	1.0	-40.0	0	40.0	1.0
	48	-20.0	0	20.0	1.0	-22.2	0	22.2	1.0
Kussner	49	-4.91	0	4.91	1.0	-4.90	0	4.90	1.0
	50	-30.8	0	30.8	1.0	-30.8	0	30.8	1.0
	51	-205.0	0	205.0	1.0	-205.0	0	205.0	1.0
Gust	52	-0.478	0	0.478	1.0	-0.478	0	0.478	1.0
	53	-0.478	0	0.478	1.0	-0.478	0	0.478	1.0

Table F-9. Open- and Closed-Loop Dynamic Model Poles, Flight Condition 2

		Open loop				Closed loop (design A)			
	Number	Real rad/s	Imaginary, rad/s	Magnitude, rad/s	Damping ratio	Real, rad/s	Imaginary, rad/s	Magnitude, rad/s	Damping ratio
Flexible airplane	1, 2	-2.96×10^{-2}	$\pm 8.08 \times 10^{-2}$	8.61×10^{-2}	0.344	-4.36×10^{-2}	$\pm 2.53 \times 10^{-2}$	5.04×10^{-2}	0.865
	3, 4	-0.755	±1.98	2.12	0.356	-2.06	±3.00	3.64	0.566
	5, 6	-2.03	±10.8	11.0	0.186	-7.05	±14.0	15.6	0.452
	7, 8	-0.276	±15.3	15.3	0.018	-0.302	±15.3	15.3	0.020
	9, 10	-1.14	±19.6	19.6	0.058	-1.19	±19.3	19.3	0.062
	11, 12	-0.724	±21.1	21.1	0.034	-1.35	±21.4	21.4	0.063
	13, 14	-0.399	±22.4	22.4	0.018	-0.430	±22.3	22.3	0.019
	15, 16	-1.98	±27.2	27.3	0.073	-2.39	±27.3	27.4	0.087
	17, 18	-2.18	±35.8	35.9	0.061	-2.31	±36.0	36.1	0.064
	19, 20	-1.28	±36.4	36.4	0.035	-1.26	±36.3	36.3	0.035
	21, 22	-2.21	±50.0	50.1	0.044	-2.24	±50.0	50.1	0.045
	23, 24	-2.52	±56.5	56.6	0.045	-2.52	±56.5	56.6	0.045
	25, 26	-2.08	±63.8	63.8	0.033	-1.94	±63.8	63.8	0.030
	27, 28	-3.79	±65.0	65.1	0.058	-4.74	±65.2	65.4	0.072
	29, 30	-4.63	±74.9	75.0	0.062	-4.72	±74.8	74.9	0.063
	31, 32	-2.58	±89.2	89.3	0.029	-2.61	±89.2	89.2	0.029
	33, 34	-4.91	±95.0	95.1	0.052	-5.01	±95.0	95.1	0.053
	35, 36	-6.27	±117.0	117.2	0.054	-6.27	±117.0	117.2	0.054
	37, 38	-6.80	±142.0	142.2	0.048	-6.80	±142.0	142.2	0.048
	39, 40	-8.93	±170.0	170.2	0.052	-8.93	±170.0	170.2	0.052
	41, 42	-11.7	±306.0	306.2	0.038	-11.7	±306.0	306.2	0.038
Elevator	43	-1000.0	0	1000.0	1.0	-1000.0	0	1000.0	1.0
	44	-40.0	0	40.0	1.0	-40.0	0	40.0	1.0
	45	-20.0	0	20.0	1.0	-20.0	0	20.0	1.0
Aileron	46	-1000.0	0	1000.0	1.0	-1000.0	0	1000.0	1.0
	47	-40.0	0	40.0	1.0	-41.2	0	41.2	1.0
	48	-20.0	0	20.0	1.0	-20.3	0	20.3	1.0
Kussner	49	-4.91	0	4.91	1.0	-4.91	0	4.91	1.0
	50	-30.8	0	30.8	1.0	-30.8	0	30.8	1.0
	51	-205.0	0	205.0	1.0	-205.0	0	205.0	1.0
Gust	52	-0.478	0	0.478	1.0	-0.478	0	0.478	1.0
	53	-0.478	0	0.478	1.0	-0.478	0	0.478	1.0

Table F-10. Open- and Closed-Loop Dynamic Model Poles, Flight Condition 3

	Number	Open loop				Closed loop (design A)			
		Real, rad/s	Imaginary, rad/s	Magnitude, rad/s	Damping ratio	Real, rad/s	Imaginary, rad/s	Magnitude, rad/s	Damping ratio
Flexible airplane	1, 2	-2.30×10^{-2}	±0.138	0.140	0.160	-3.61×10^{-2}	$±2.43 \times 10^{-2}$	4.35×10^{-2}	0.830
	3, 4	-0.908	±0.934	1.30	0.697	-3.44	±2.91	4.50	0.764
	5, 6	-3.42	±12.9	13.4	0.256	-8.58	±13.8	16.2	0.530
	7, 8	-0.319	±14.9	14.9	0.021	-0.432	±14.8	14.8	0.029
	9, 10	-1.12	±19.3	19.3	0.058	-1.10	±18.8	18.8	0.058
	11, 12	-0.748	±20.7	20.7	0.036	-2.81	±22.3	22.5	0.125
	13, 14	-0.396	±21.8	21.8	0.018	-0.406	±21.6	21.6	0.019
	15, 16	-2.27	±24.5	24.6	0.092	-3.08	±24.6	24.8	0.124
	17, 18	-1.12	±36.0	36.0	0.031	-1.01	±36.1	36.1	0.028
	19, 20	-3.14	±36.6	36.7	0.086	-3.65	±36.8	37.0	0.099
	21, 22	-3.43	±48.0	48.1	0.071	-3.48	±48.0	48.1	0.072
	23, 24	-1.29	±55.4	55.5	0.023	-1.27	±55.4	55.4	0.023
	25, 26	-3.31	±56.2	56.3	0.059	-3.30	±56.2	56.3	0.059
	27, 28	-4.47	±57.1	57.2	0.077	-4.75	±57.0	57.2	0.083
	29, 30	-6.65	±72.2	72.5	0.092	-6.65	±72.2	72.5	0.092
	31, 32	-2.19	±83.1	83.1	0.026	-2.23	±83.1	83.1	0.027
	33, 34	-5.46	±92.0	92.2	0.059	-5.64	±92.0	92.2	0.061
	35, 36	-8.20	±111.0	112.3	0.073	-8.20	±111.0	112.3	0.073
	37, 38	-6.98	±137.0	137.2	0.051	-6.98	±137.0	137.2	0.051
	39, 40	-10.0	±150.0	151.3	0.066	-10.0	±150.0	151.3	0.066
	41, 42	-10.6	±301.0	301.2	0.035	-10.6	±301.0	301.2	0.035
Elevator	43	-1000.0	0	1000.0	1.0	-1000.0	0	1000.0	1.0
	44	-40.0	0	40.0	1.0	-40.0	0	40.0	1.0
	45	-20.0	0	20.0	1.0	-20.0	0	20.0	1.0
Aileron	46	-1000.0	0	1000.0	1.0	-1000.0	0	1000.0	1.0
	47	-40.0	0	40.0	1.0	-40.3	0	40.3	1.0
	48	-20.0	0	20.0	1.0	-19.5	0	19.5	1.0
Kussner	49	-5.10	0	5.10	1.0	-5.10	0	5.10	1.0
	50	-32.0	0	32.0	1.0	-32.0	0	32.0	1.0
	51	-213.0	0	213.0	1.0	-213.0	0	213.0	1.0
Gust	52	-0.497	0	0.497	1.0	-0.497	0	0.497	1.0
	53	-0.497	0	0.497	1.0	-0.497	0	0.497	1.0

Table F-11. Open- and Closed-Loop Dynamic Model Poles, Flight Condition 4

	Number	Open Loop Real, rad/s	Imaginary, rad/s	Magnitude, rad/s	Damping ratio	Closed Loop Real, rad/s	Imaginary, rad/s	(Design A) Magnitude, rad/s	Damping ratio
Flexible airplane	1, 2	-2.41×10^{-2}	$\pm 8.59 \times 10^{-2}$	8.92×10^{-2}	0.027	-3.80×10^{-2}	$\pm 3.16 \times 10^{-2}$	4.94×10^{-2}	0.769
	3, 4	-1.03	±2.28	2.50	0.412	-3.11	±3.53	4.70	0.662
	5, 6	-3.62	±12.9	13.4	0.270	-7.99	±16.1	18.0	0.444
	7, 8	-0.306	±14.9	14.9	0.021	-0.305	±14.9	14.9	0.020
	9, 10	-0.766	±19.9	19.9	0.038	-0.945	±19.8	19.8	0.048
	11, 12	-1.48	±21.0	21.1	0.070	-1.40	±21.2	21.2	0.066
	13, 14	-0.408	±22.3	22.3	0.018	-0.414	±22.3	22.3	0.018
	15, 16	-2.57	±27.3	27.4	0.094	-2.84	±27.4	27.5	0.103
	17, 18	-0.996	±36.2	36.2	0.028	-0.986	±36.2	36.2	0.027
	19, 20	-3.96	±37.4	37.6	0.105	-4.01	±37.5	37.7	0.106
	21, 22	-3.06	±50.2	50.3	0.061	-3.10	±50.2	50.3	0.062
	23, 24	-2.91	±56.5	56.6	0.051	-2.91	±56.5	56.6	0.051
	25, 26	-5.03	±60.5	60.7	0.083	-5.56	±60.7	61.0	0.091
	27, 28	-2.17	±64.0	64.1	0.034	-2.21	±64.0	64.0	0.034
	29, 30	-4.60	±72.0	72.2	0.064	-4.61	±72.0	72.1	0.064
	31, 32	-2.94	±89.0	89.0	0.033	-2.97	±89.0	89.0	0.033
	33, 34	-5.25	±94.0	94.1	0.056	-5.30	±94.0	94.2	0.056
	35, 36	-8.54	±114.0	114.3	0.075	-8.54	±114.0	114.3	0.075
	37, 38	-7.50	±141.0	141.2	0.053	-7.50	±141.0	141.2	0.053
	39, 40	-9.56	±166.0	166.3	0.057	-9.56	±166.0	166.3	0.057
	41, 42	-11.7	±306.0	306.2	0.038	-11.7	±306.0	306.2	0.038
Elevator	43	-1000.0	0	1000.0	1.0	-1000.0	0	1000.0	1.0
	44	-40.0	0	40.0	1.0	-40.0	0	40.0	1.0
	45	-20.0	0	20.0	1.0	-20.0	0	20.0	1.0
Aileron	46	-1000.0	0	1000.0	1.0	-1000.0	0	1000.0	1.0
	47	-40.0	0	40.0	1.0	-41.3	0	41.3	1.0
	48	-20.0	0	20.0	1.0	-20.1	0	20.1	1.0
Kussner	49	-5.10	0	5.10	1.0	-5.10	0	5.10	1.0
	50	-32.0	0	32.0	1.0	-32.0	0	32.0	1.0
	51	-213.0	0	213.0	1.0	-213.0	0	213.0	1.0
Gust	52	-0.497	0	0.497	1.0	-0.497	0	0.497	1.0
	53	-0.497	0	0.497	1.0	-0.497	0	0.497	1.0

Table F-12. Closed-Loop Controller Poles, Flight Condition 1

Design B

Number	Real, rad/s	Imaginary, rad/s	Magnitude, rad/s	Damping ratio
1, 2	-7.59×10^{-2}	±0.129	0.150	0.506
3, 4	–0.815	±3.08	3.19	0.256
5, 6	–0.266	±15.3	15.3	0.017
7, 8	–1.53	±19.4	19.5	0.079
9, 10	–0.398	±21.1	21.1	0.019
11, 12	–0.385	±21.9	21.9	0.018
13, 14	–2.06	±28.0	28.1	0.073
15, 16	–30.4	± 6.18	31.0	0.980
17, 18	–1.88	±34.4	34.4	0.054
19, 20	–1.27	±37.1	37.1	0.034
21, 22	–3.37	±49.6	49.7	0.068
23, 24	–1.30	±55.5	55.5	0.023
25, 26	–2.31	±56.3	56.3	0.041
27, 28	–26.9	±65.4	70.7	0.380
29, 30	–7.74	±75.9	76.3	0.101
31, 32	–1.63	±82.9	82.9	0.020
33, 34	–6.36	±91.2	91.4	0.070
35, 36	–6.49	±114.0	114.2	0.057
37, 38	–7.20	±138.0	138.2	0.052
39, 40	–8.31	±153.0	153.2	0.054
41, 42	–10.5	±302.0	302.2	0.035

Number	Real, rad/s	Imaginary, rad/s	Magnitude, rad/s	Damping ratio
43	–1000.0	0	1000.0	1.0
44	–40.0	0	40.0	1.0
45	–20.0	0	20.0	1.0
46	–1000.0	0	1000.0	1.0
47	–40.0	0	40.0	1.0
48	–20.0	0	20.0	1.0
49	–1.04	0	1.04	1.0
50	–6.31	0	6.31	1.0
51	–203.0	0	203.0	1.0
52	–0.105	0	0.105	1.0
53	–0.257	0	0.257	1.0

Design H

Number	Real, rad/s	Imaginary, rad/s	Magnitude, rad/s	Damping ratio
1, 2	-3.76×10^{-2}	$\pm 3.96 \times 10^{-2}$	5.46×10^{-2}	0.688
3	–0.144	0	0.144	1.0
4	–0.280	0	0.280	1.0
5, 6	–0.895	±3.40	3.52	0.254
7, 8	–6.12	±1.47	6.29	0.972

F-38

Table F-13. Closed-Loop Controller Poles, Flight Condition 2

Design B

Number	Real, rad/s	Imaginary, rad/s	Magnitude, rad/s	Damping ratio
1, 2	-4.81×10^{-2}	$\pm 6.86 \times 10^{-2}$	8.38×10^{-2}	0.574
3, 4	-1.16	± 3.74	3.92	0.296
5, 6	-0.268	± 15.3	15.3	0.018
7, 8	-1.33	± 19.9	19.9	0.067
9, 10	-0.579	± 21.2	21.2	0.027
11, 12	-0.398	± 22.4	22.4	0.018
13, 14	-30.5	± 5.86	31.1	0.981
15, 16	-1.11	± 34.7	34.7	0.032
17, 18	-3.53	± 34.5	34.7	0.102
19, 20	-2.62	± 38.6	38.7	0.068
21, 22	-2.81	± 50.3	50.4	0.056
23, 24	-2.60	± 57.0	57.1	0.046
25, 26	-1.62	± 64.4	64.4	0.025
27, 28	-28.1	± 65.1	70.9	0.396
29, 30	-4.55	± 74.0	74.1	0.061
31, 32	-3.97	± 92.5	92.6	0.043
33, 34	-4.91	± 93.6	93.7	0.052
35, 36	-6.23	± 117.0	117.2	0.053
37, 38	-6.80	± 142.0	142.2	0.048
39, 40	-8.94	± 170.0	170.2	0.052
41, 42	-11.7	± 306.0	306.2	0.038

Number	Real, rad/s	Imaginary, rad/s	Magnitude, rad/s	Damping ratio
43	-1000.0	0	1000.0	1.0
44	-40.0	0	40.0	1.0
45	-20.0	0	20.0	1.0
46	-1000.0	0	1000.0	1.0
47	-40.0	0	40.0	1.0
48	-20.0	0	20.0	1.0
49	-2.39	0	2.39	1.0
50	-6.31	0	6.31	1.0
51	-203.0	0	203.0	1.0
52	-0.154	0	0.154	1.0
53	-0.252	0	0.252	1.0

Design H

Number	Real, rad/s	Imaginary, rad/s	Magnitude, rad/s	Damping ratio
1, 2	-3.43×10^{-2}	$\pm 4.76 \times 10^{-2}$	5.88×10^{-2}	0.584
3	-0.177	0	0.177	1.0
4	-0.266	0	0.266	1.0
5, 6	-0.896	± 3.11	3.24	0.277
7, 8	-6.15	± 1.44	6.32	0.974

Table F-14. Closed-Loop Controller Poles, Flight Condition 3

Design B

Number	Real, rad/s	Imaginary, rad/s	Magnitude, rad/s	Damping ratio
1, 2	-5.30×10^{-2}	±0.156	0.165	0.322
3, 4	-0.650	±3.16	3.23	0.201
5, 6	-0.284	±14.9	14.9	0.019
7, 8	-1.65	±20.0	20.1	0.082
9, 10	-0.452	±20.9	20.9	0.021
11, 12	-0.399	±21.8	21.8	0.018
13, 14	-1.99	±28.7	28.8	0.069
15, 16	-1.70	±35.8	35.8	0.047
17, 18	-35.9	±7.14	36.6	0.981
19, 20	-2.72	±37.4	37.5	0.072
21, 22	-4.17	±49.9	50.1	0.083
23, 24	-1.22	±55.6	55.6	0.022
25, 26	-3.49	±56.6	56.7	0.062
27, 28	-6.76	±72.6	72.9	0.093
29, 30	-44.1	±68.8	81.7	0.540
31, 32	-1.43	±83.1	83.1	0.017
33, 34	-5.84	±89.3	89.5	0.065
35, 36	-8.09	±111.0	111.3	0.073
37, 38	-6.98	±137.0	137.2	0.051
39, 40	-10.0	±150.0	150.3	0.067
41, 42	-10.6	±301.0	301.2	0.035

Number	Real, rad/s	Imaginary, rad/s	Magnitude, rad/s	Damping ratio
43	-1000.0	0	1000.0	1.0
44	-40.0	0	40.0	1.0
45	-20.0	0	20.0	1.0
46	-1000.0	0	1000.0	1.0
47	-40.0	0	40.0	1.0
48	-20.0	0	20.0	1.0
49	-1.13	0	1.13	1.0
50	-6.50	0	6.50	1.0
51	-208.0	0	208.0	1.0
52	-9.62×10^{-2}	0	9.62×10^{-2}	1.0
53	-0.273	0	0.273	1.0

Design H

Number	Real, rad/s	Imaginary, rad/s	Magnitude, rad/s	Damping ratio
1, 2	-3.77×10^{-2}	$±2.10 \times 10^{-2}$	4.32×10^{-2}	0.874
3	-0.156	0	0.156	1.0
4	-0.265	0	0.265	1.0
5, 6	-0.900	±3.08	3.21	0.280
7, 8	-6.34	±1.27	6.46	0.980

Table F-15. Closed-Loop Controller Poles, Flight Condition 4

Design B

Number	Real, rad/s	Imaginary, rad/s	Magnitude, rad/s	Damping ratio
1, 2	-4.71×10^{-2}	$\pm 7.50 \times 10^{-2}$	8.86×10^{-2}	0.532
3, 4	-1.14	±3.77	3.94	0.289
5, 6	-0.286	±14.9	14.9	0.019
7, 8	-1.55	±20.7	20.8	0.075
9, 10	-0.780	±21.0	21.0	0.037
11, 12	-0.415	±22.4	22.4	0.018
13, 14	-1.07	±34.4	34.4	0.031
15, 16	-3.90	±36.3	36.5	0.106
17, 18	-35.9	±6.83	36.5	0.982
19, 20	-2.72	±39.2	39.3	0.069
21, 22	-3.77	±50.5	50.6	0.074
23, 24	-3.03	±57.1	57.2	0.053
25, 26	-2.02	±64.1	64.1	0.031
27, 28	-4.39	±71.6	71.7	0.061
29, 30	-44.8	±65.9	79.7	0.562
31, 32	-6.42	±92.4	92.6	0.069
33, 34	-2.85	±93.4	93.4	0.030
35, 36	-8.42	±114.0	114.3	0.074
37, 38	-7.49	±141.0	141.2	0.053
39, 40	-9.58	±166.0	166.3	0.058
41, 42	-11.7	±306.0	306.2	0.038

Number	Real, rad/s	Imaginary, rad/s	Magnitude, rad/s	Damping ratio
43	-1000.0	0	1000.0	1.0
44	-40.0	0	40.0	1.0
45	-20.0	0	20.0	1.0
46	-1000.0	0	1000.0	1.0
47	-40.0	0	40.0	1.0
48	-20.0	0	20.0	1.0
49	-2.39	0	2.39	1.0
50	-6.50	0	6.50	1.0
51	-209.0	0	209.0	1.0
52	-0.156	0	0.156	1.0
53	-0.262	0	0.262	1.0

Design H

Number	Real, rad/s	Imaginary, rad/s	Magnitude, rad/s	Damping ratio
1, 2	-3.20×10^{-2}	$\pm 4.71 \times 10^{-2}$	5.69×10^{-2}	0.561
3	-0.187	0	0.187	1.0
4	-0.255	0	0.255	1.0
5, 6	-0.781	±3.06	3.16	0.248
7, 8	-6.41	±1.22	6.52	0.982

F-41

F.4.1.3 STABILITY MARGINS

Figures F-46 through F-81 show Bode plots for the aileron and elevator control loops with various filters and at the gust-load flight conditions.
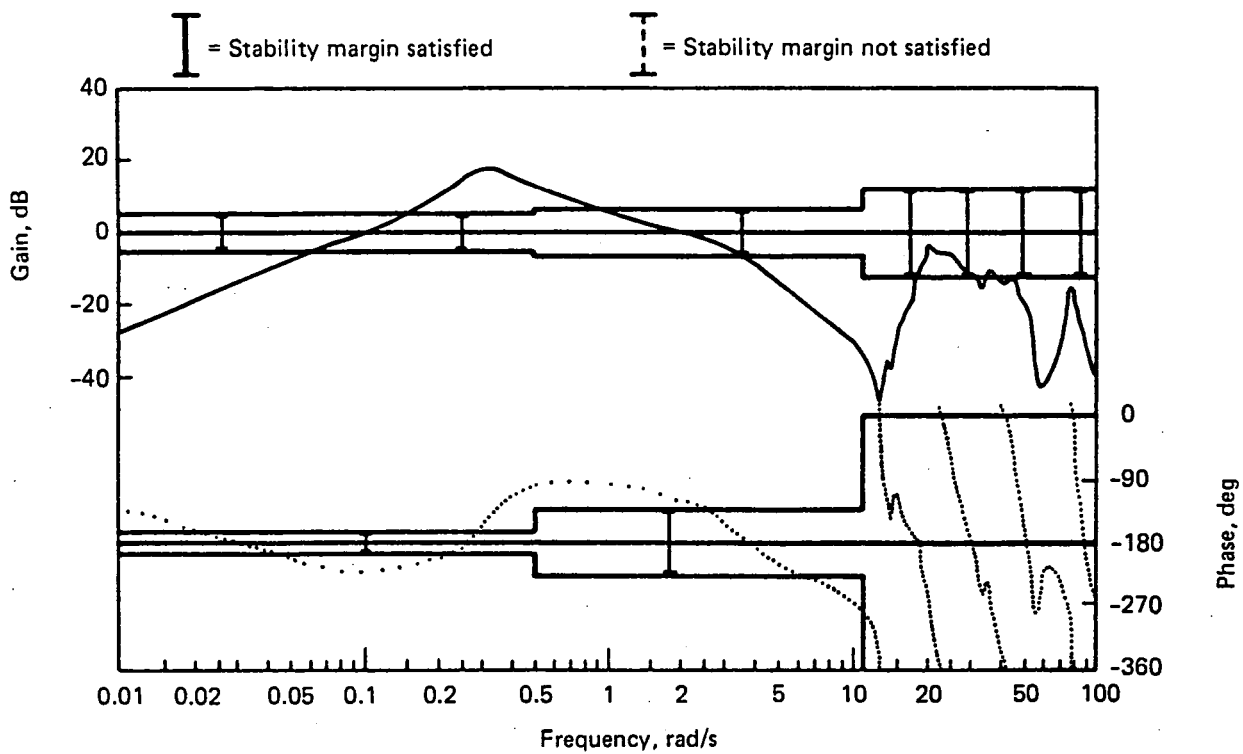
Figure F-46. Phase and Gain Margin, Elevator Loop, Filter Type B, Flight Condition 1
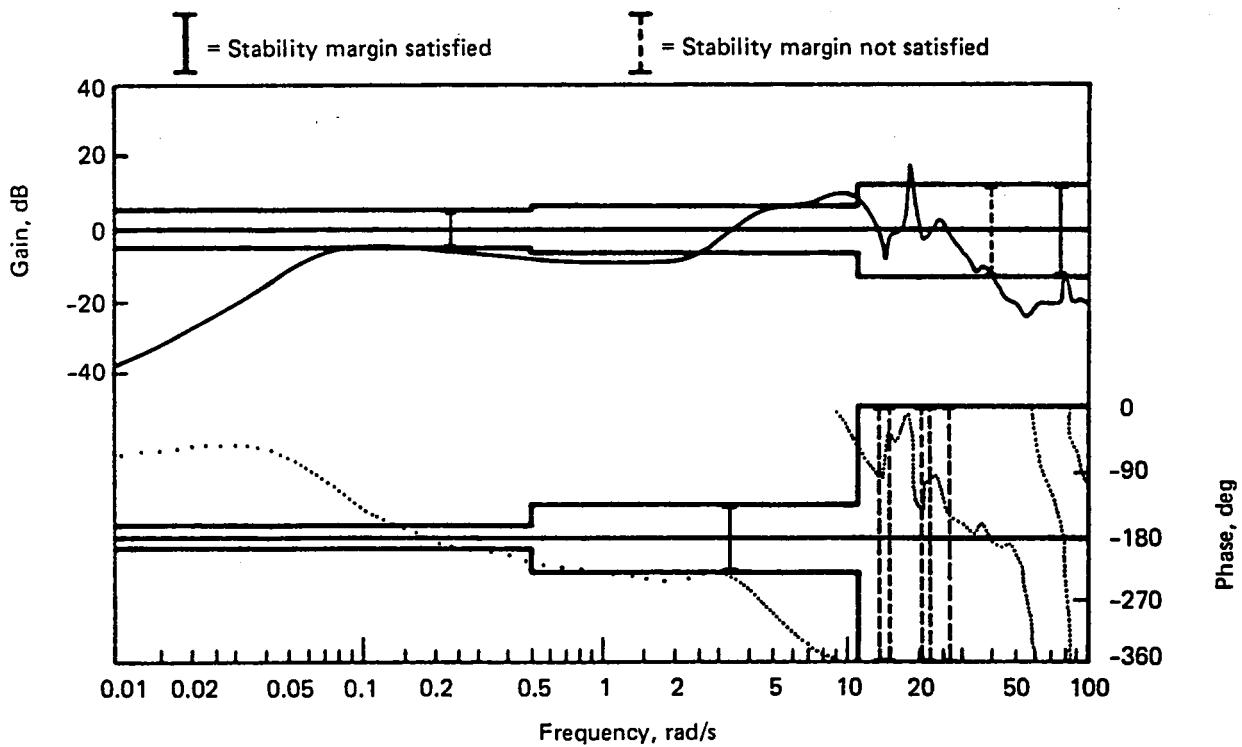
Figure F-47. Phase and Gain Margin, Aileron Loop, Filter Type B, Flight Condition 1
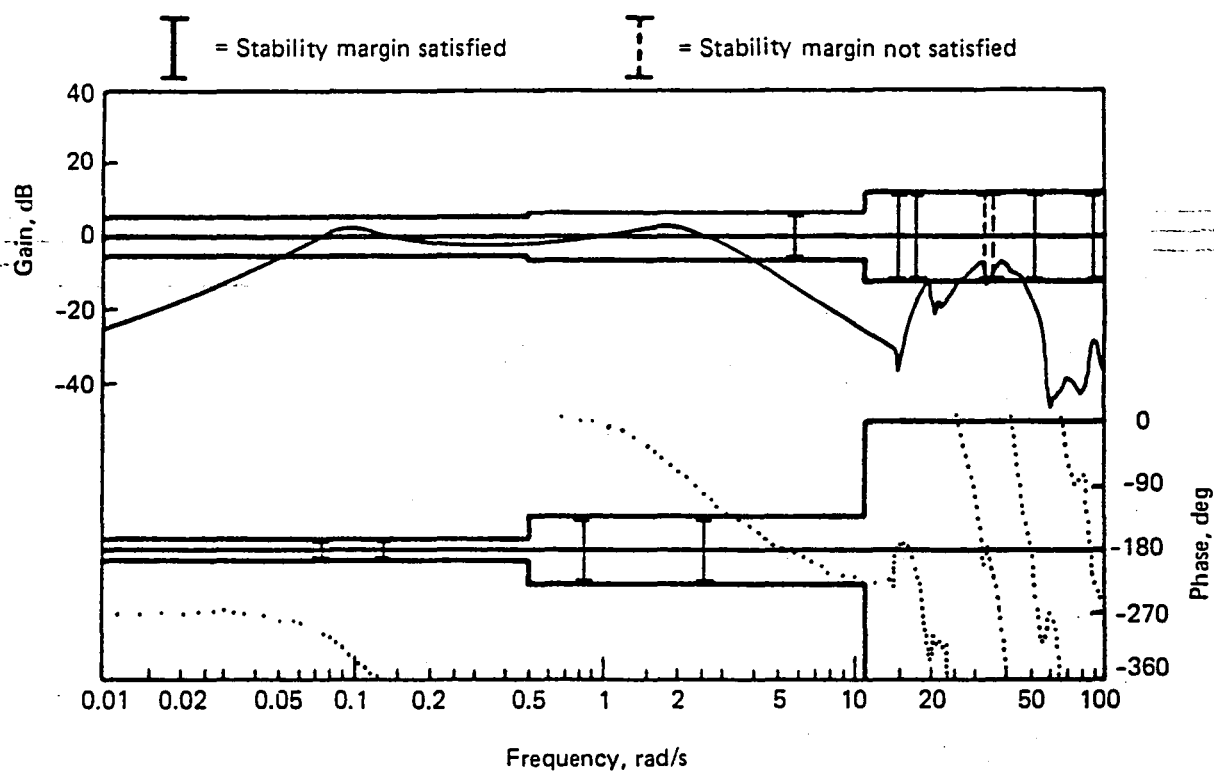
Figure F-48. Phase and Gain Margin, Elevator Loop, Filter Type B, Flight Condition 2
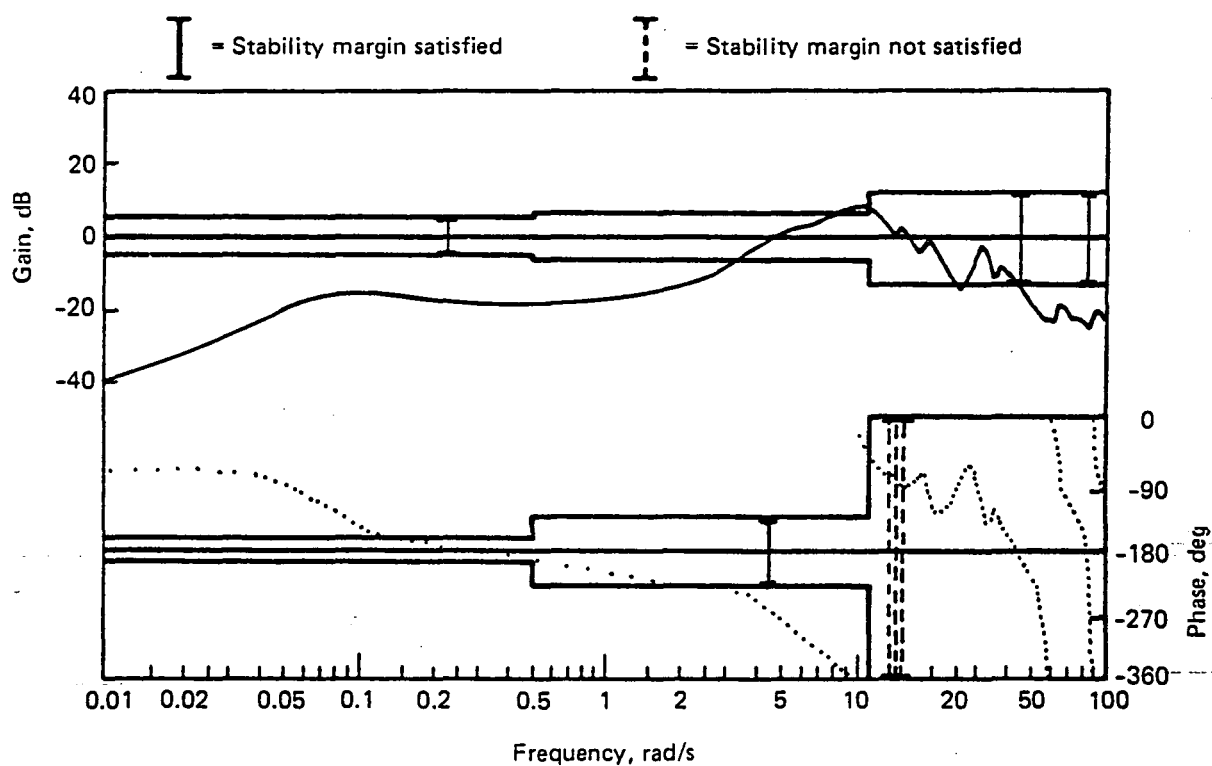
Figure F-49. Phase and Gain Margin, Aileron Loop, Filter Type B, Flight Condition 2
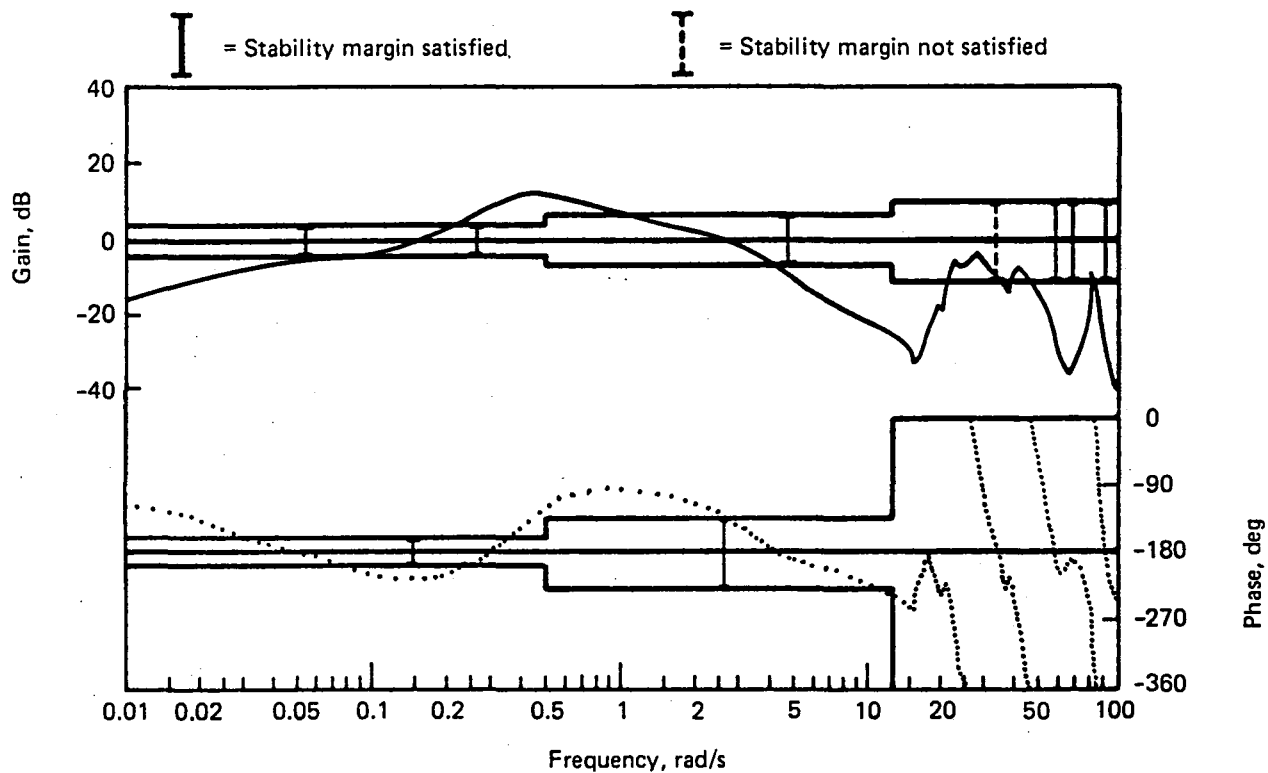
Figure F-50. Phase and Gain Margin, Elevator Loop, Filter Type B, Flight Condition 3
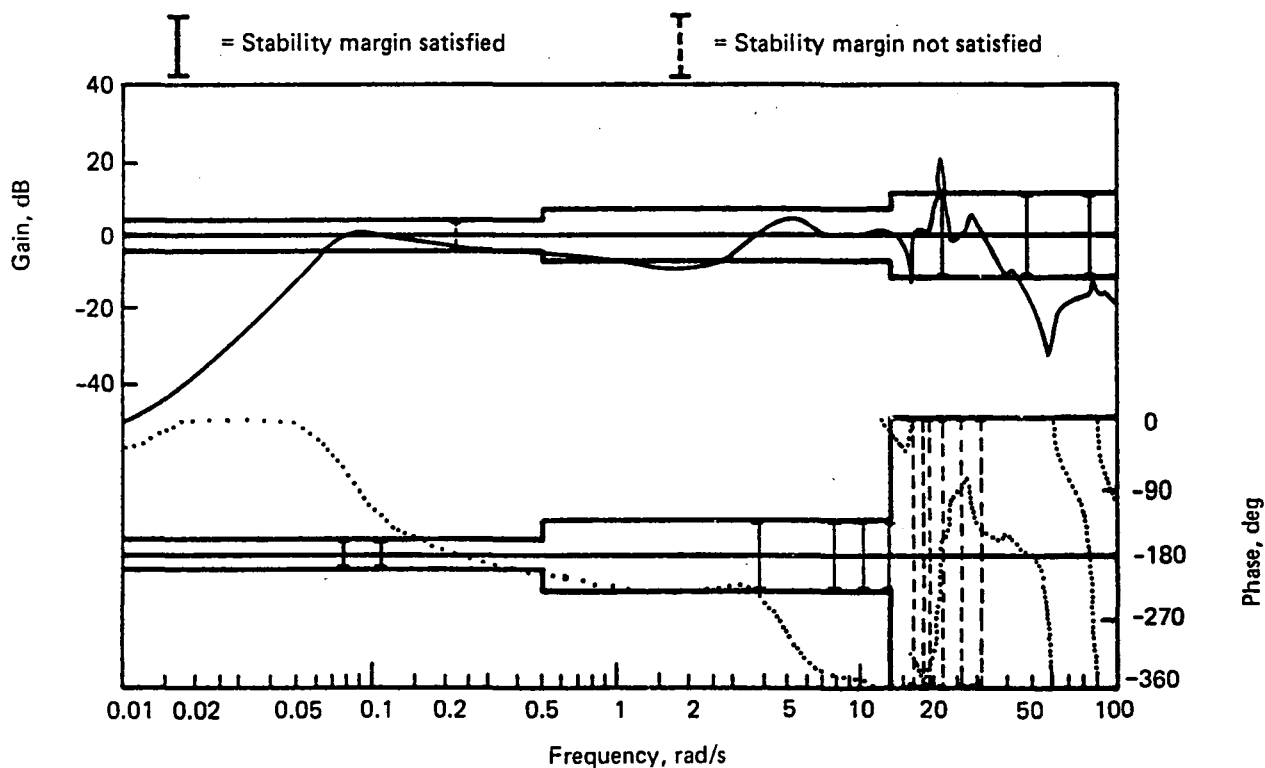
Figure F-51. Phase and Gain Margin, Aileron Loop, Filter Type B, Flight Condition 3
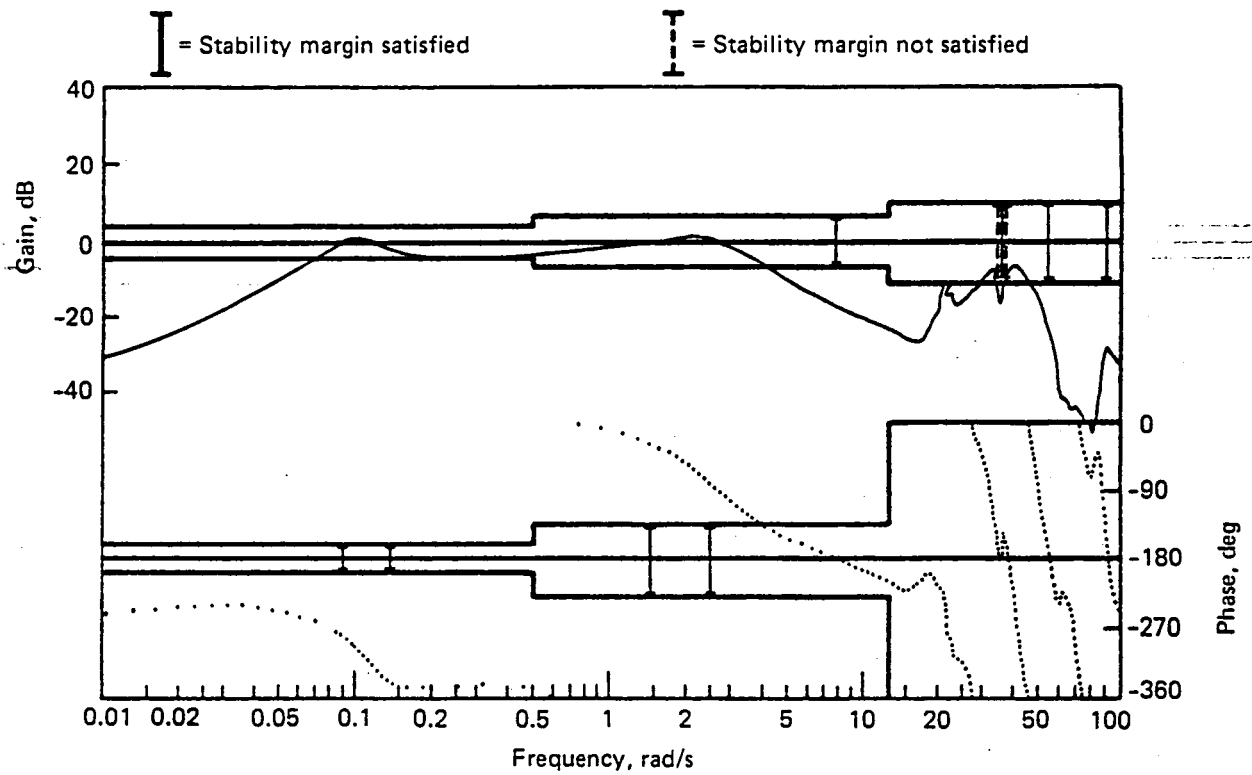
Figure F-52. Phase and Gain Margin, Elevator Loop, Filter Type B, Flight Condition 4
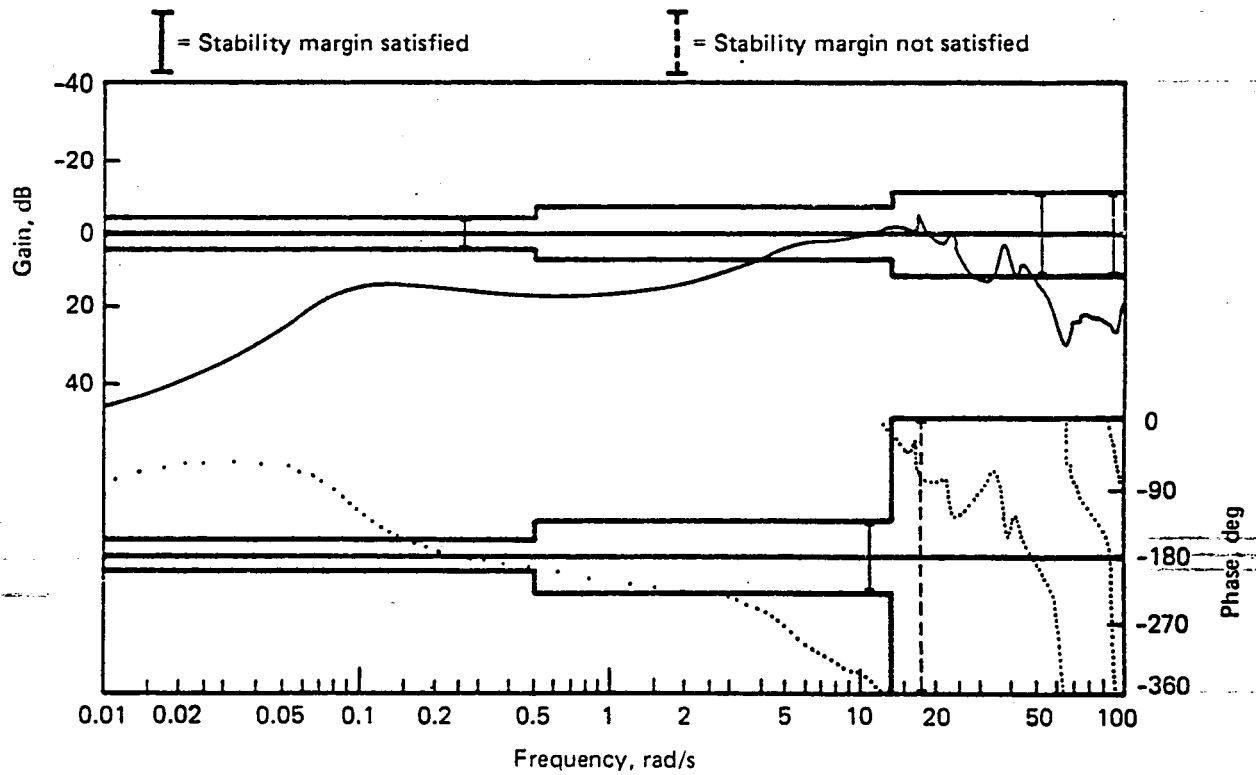
Figure F-53. Phase and Gain Margin, Aileron Loop, Filter Type B, Flight Condition 4
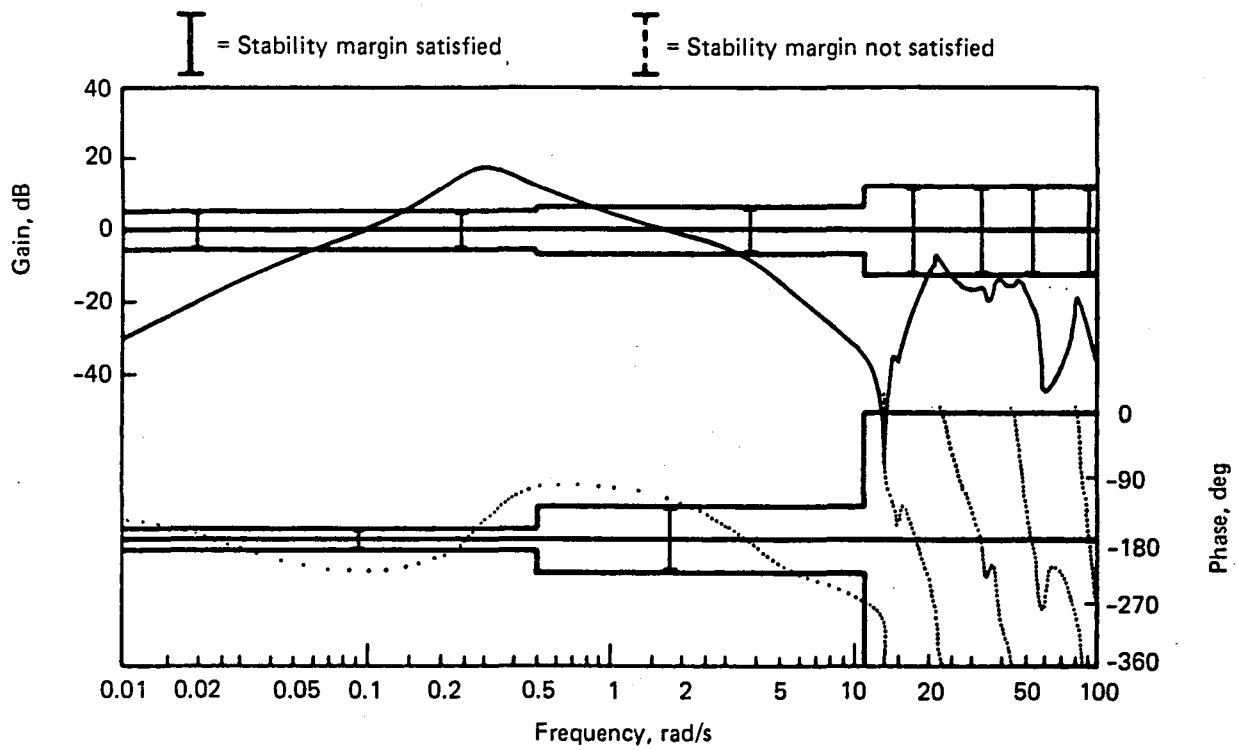
Figure F-54. Phase and Gain Margin, Elevator Loop, Filter Type C, Flight Condition 1
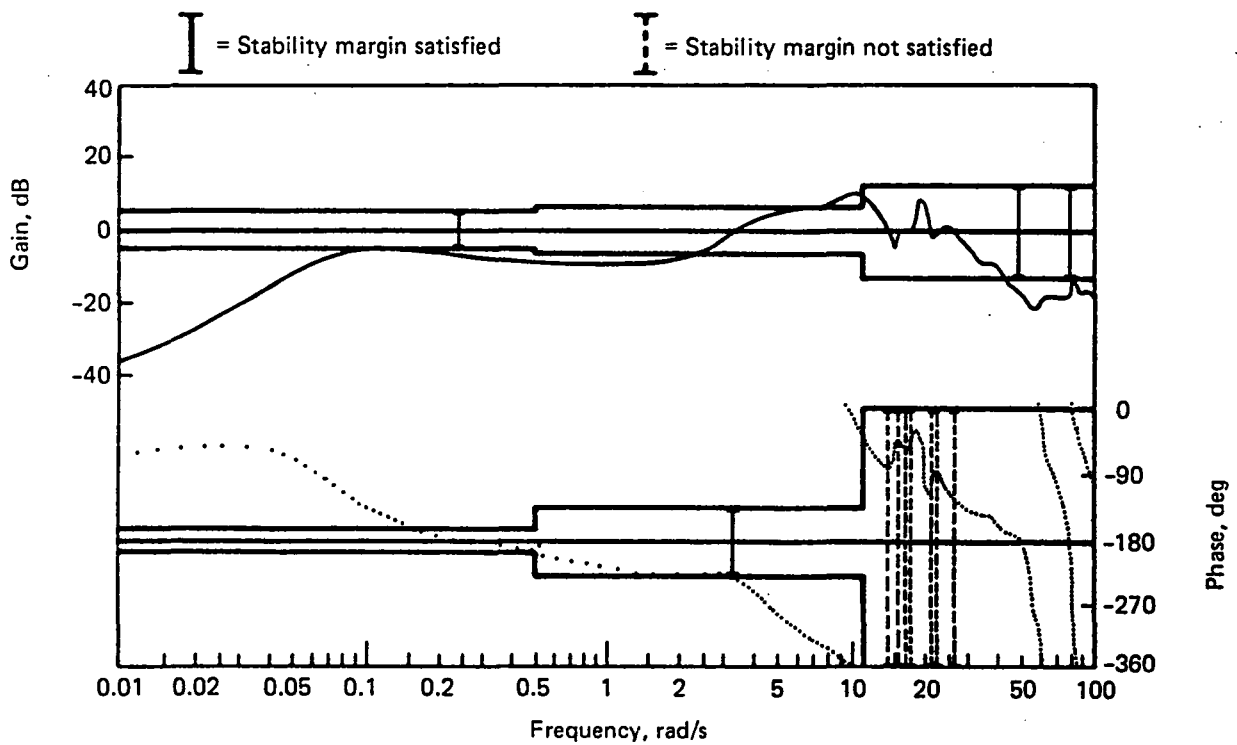
Figure F-55. Phase and Gain Margin, Aileron Loop, Filter Type C, Flight Condition 1
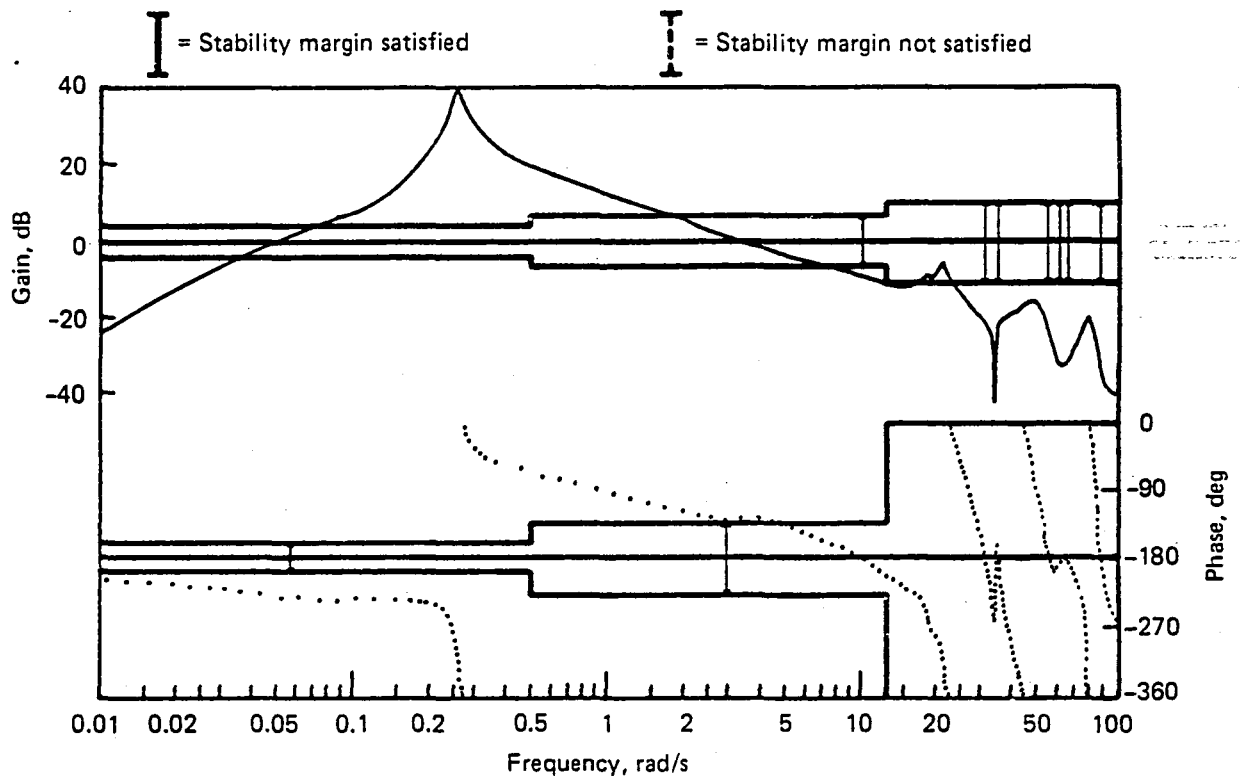
Figure F-56. Phase and Gain Margin, Elevator Loop, Filter Type C, Flight Condition 3
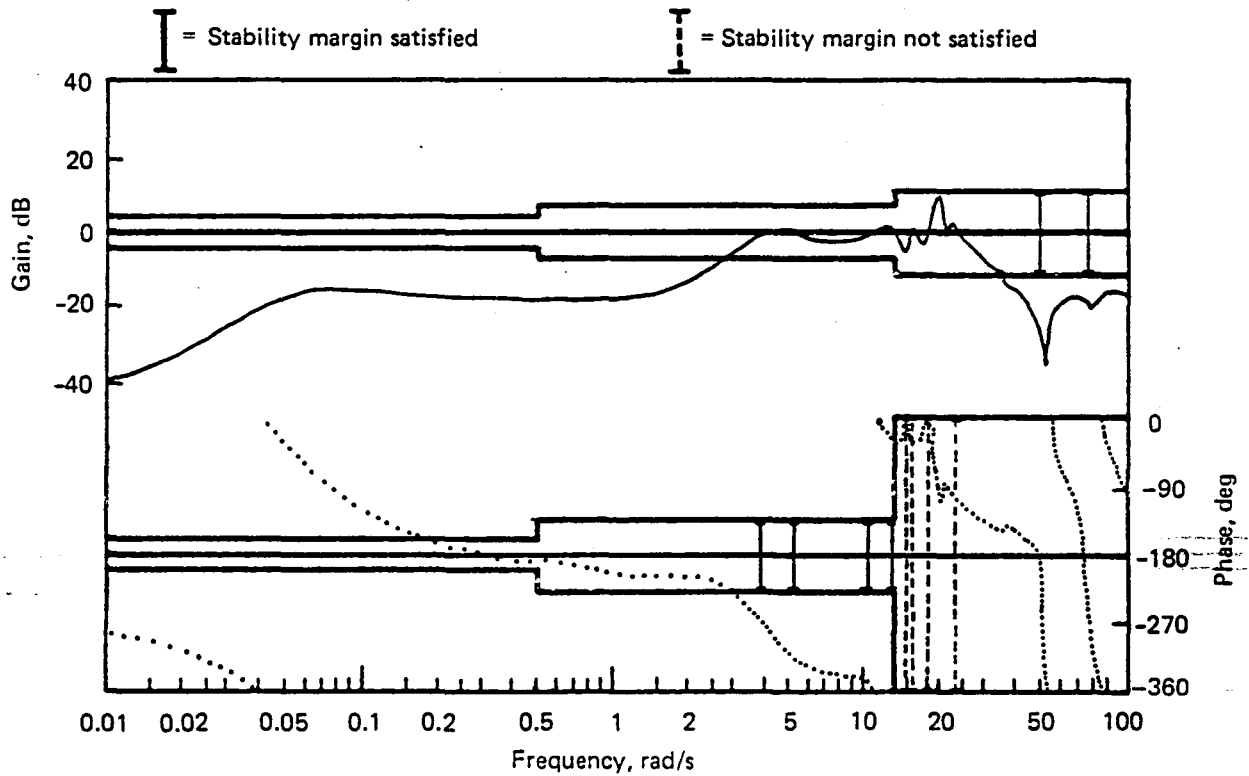
Figure F-57. Phase and Gain Margin, Aileron Loop, Filter Type C, Flight Condition 3
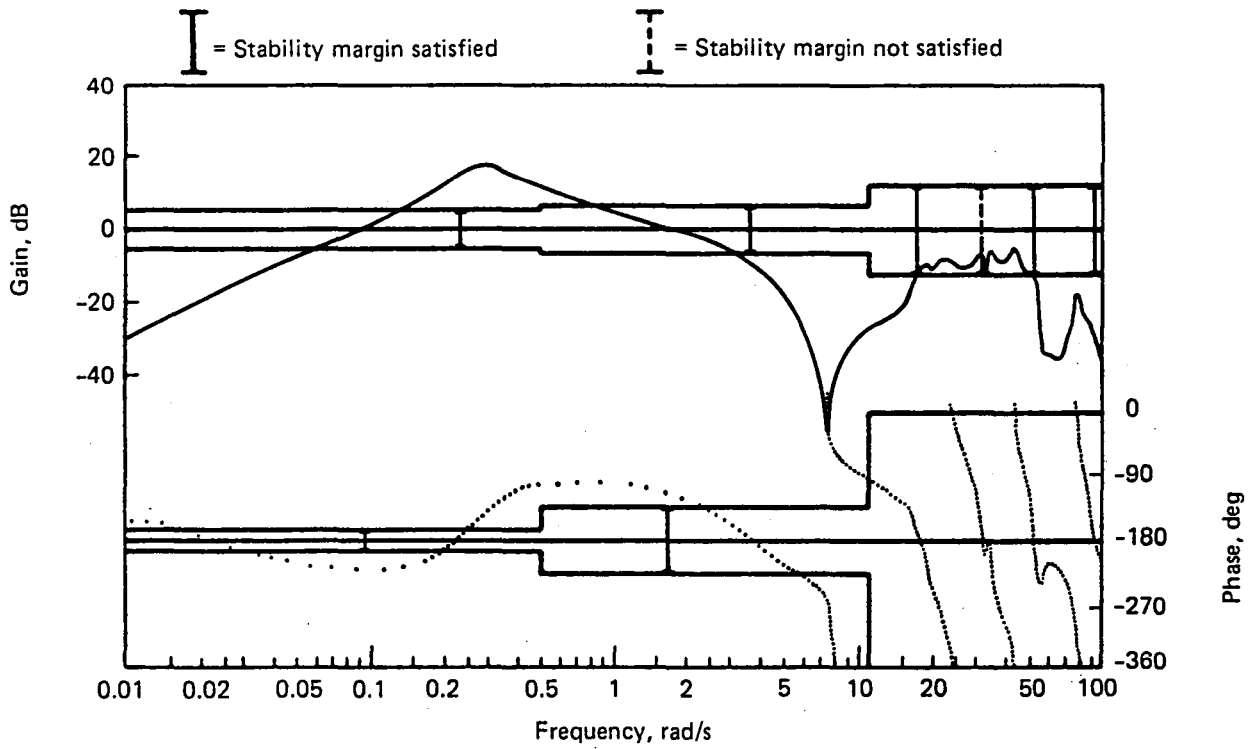
Figure F-58. Phase and Gain Margin, Elevator Loop, Filter Type D, Flight Condition 1
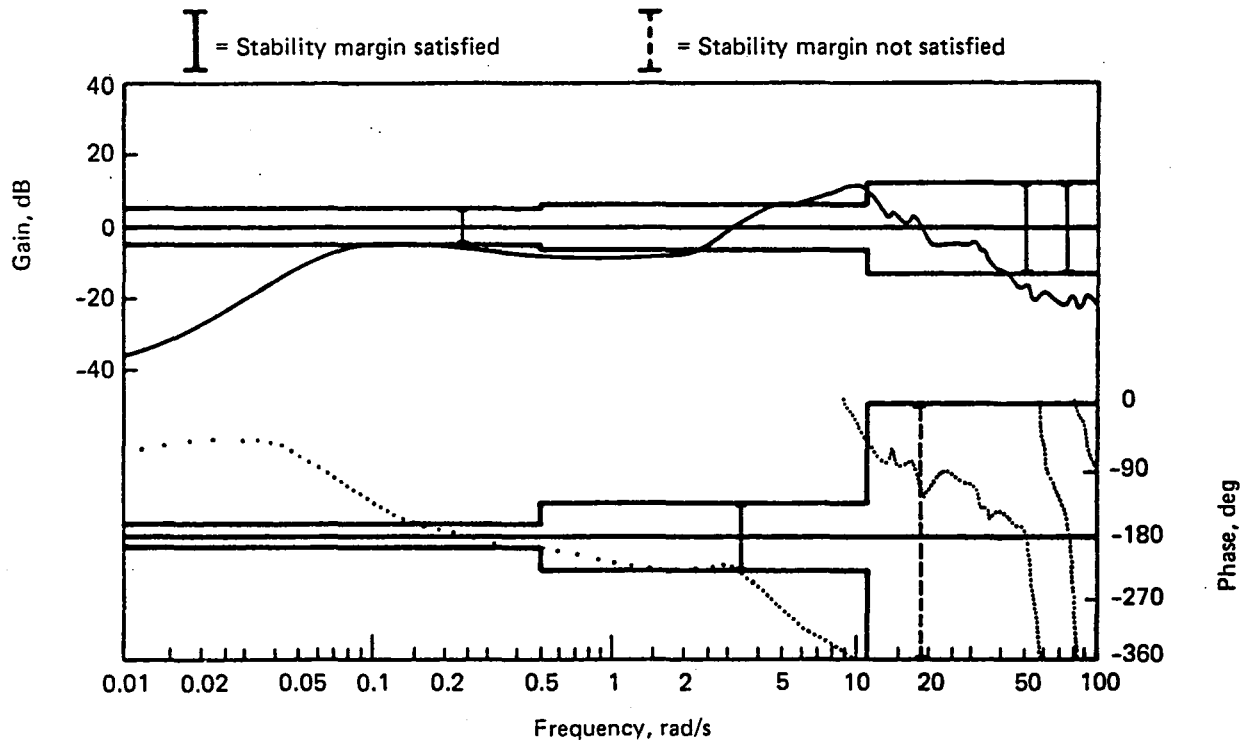
Figure F-59. Phase and Gain Margin, Aileron Loop, Filter Type D, Flight Condition 1

F-49
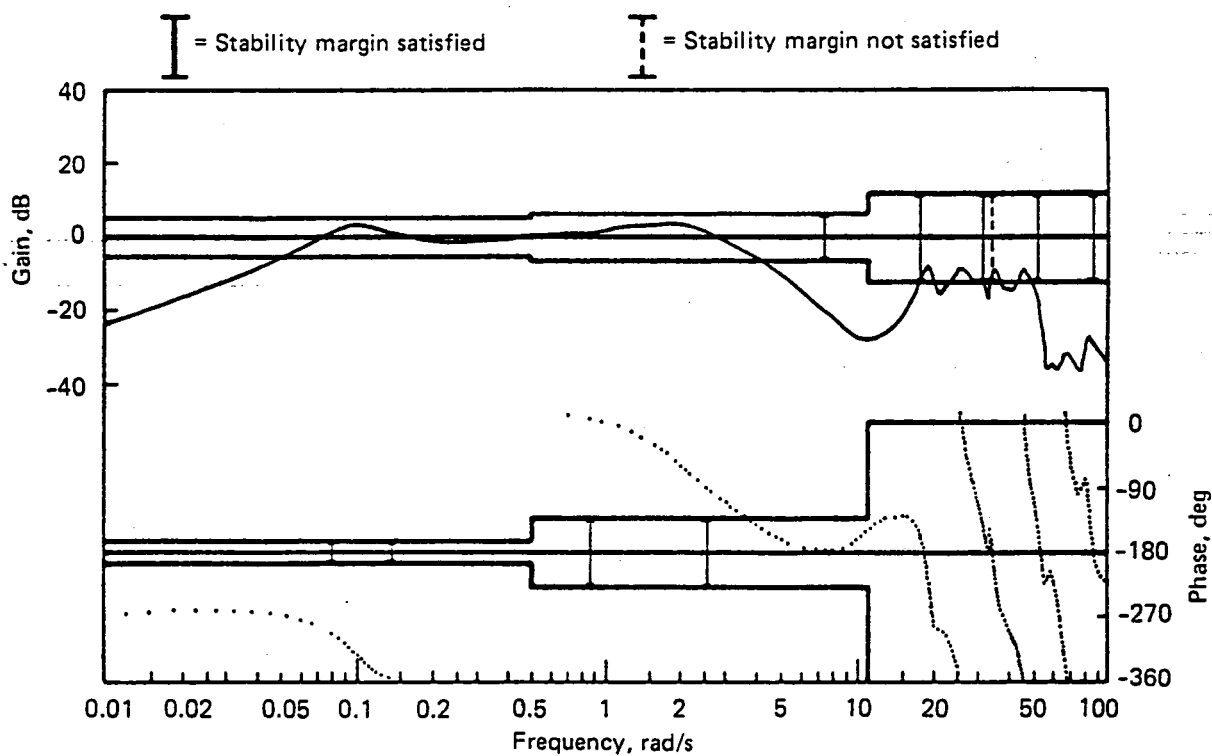
Figure F-60. Phase and Gain Margin, Elevator Loop, Filter Type D, Flight Condition 2
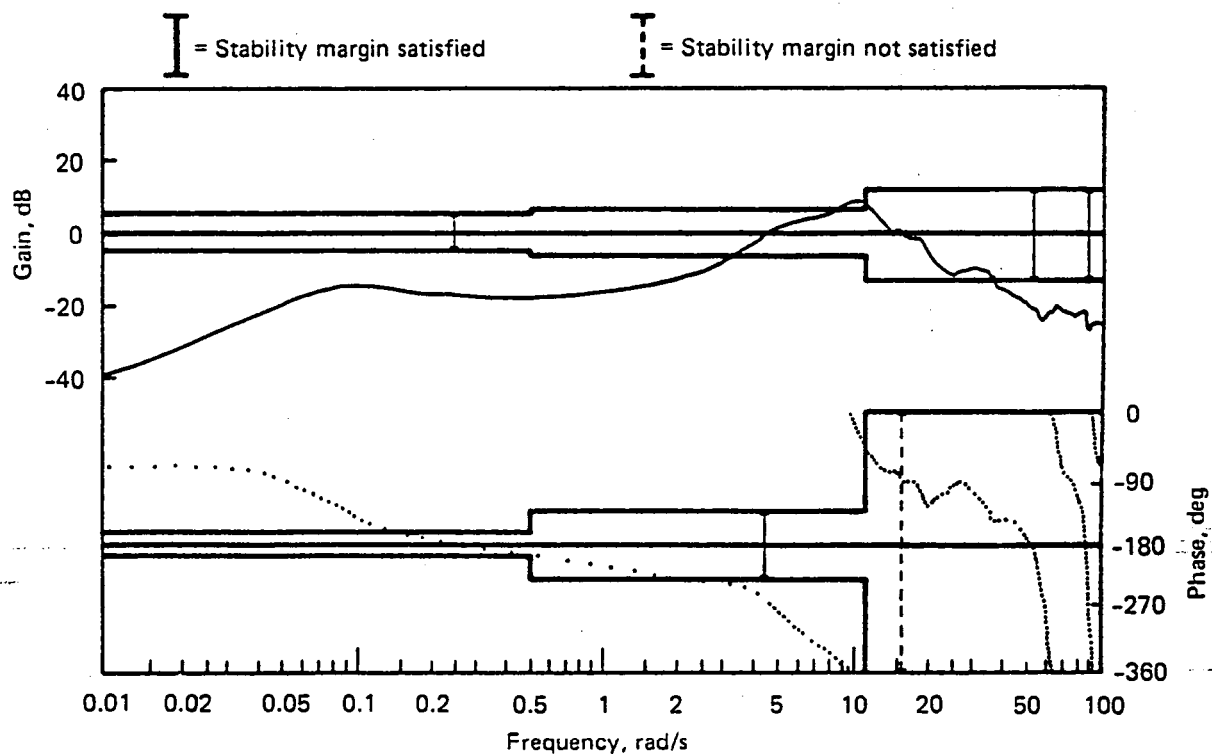
Figure F-61. Phase and Gain Margin, Aileron Loop, Filter Type D, Flight Condition 2
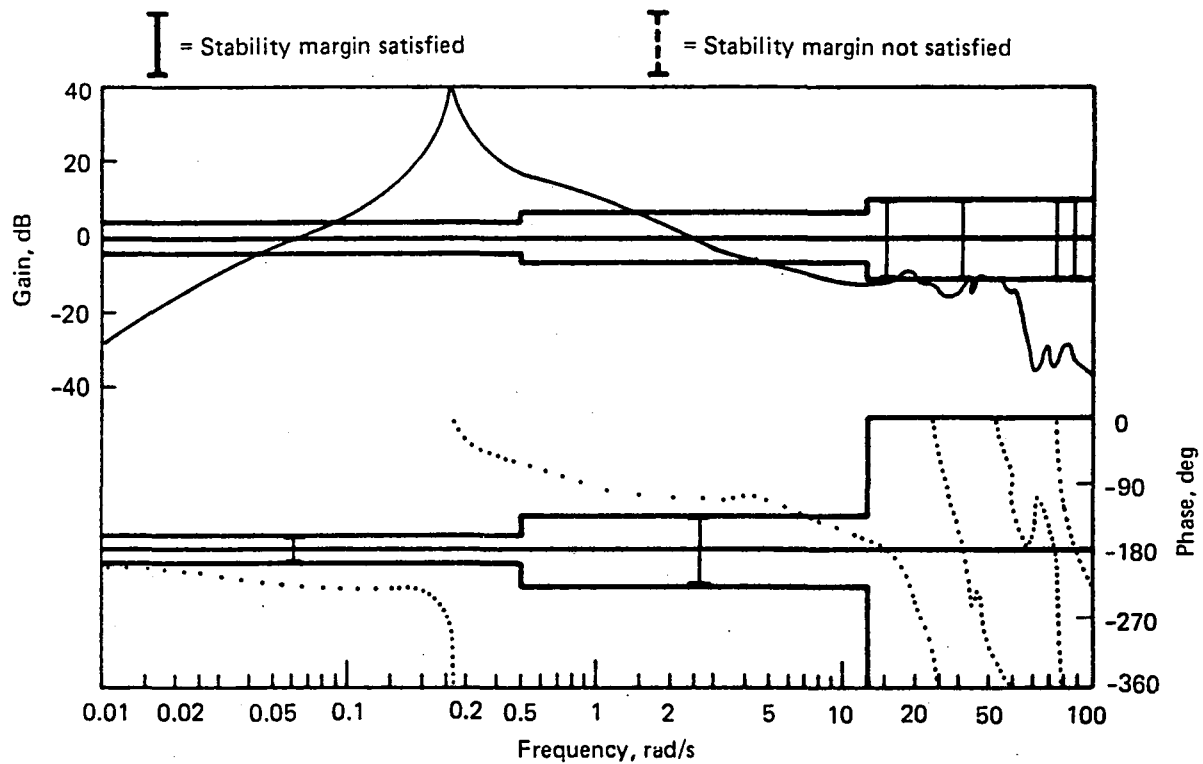
Figure F-62. Phase and Gain Margin, Elevator Loop, Filter Type D, Flight Condition 3
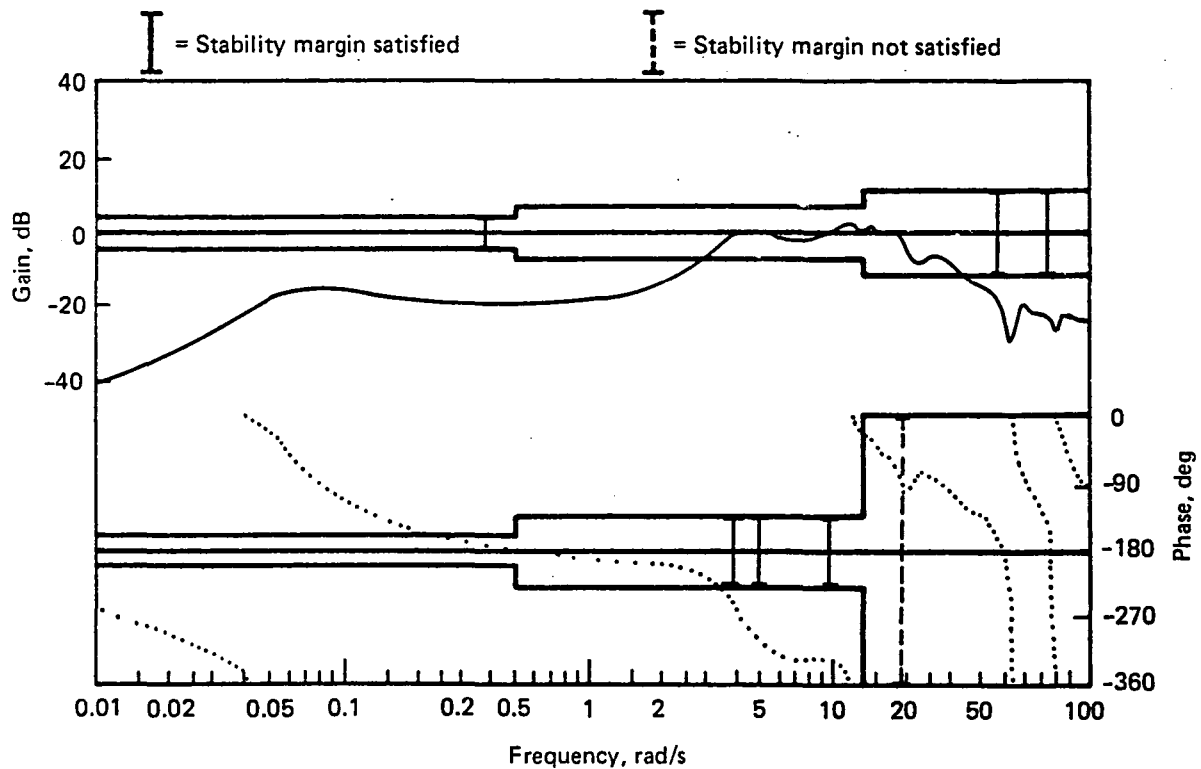
Figure F-63. Phase and Gain Margin, Aileron Loop, Filter Type D, Flight Condition 3

F-51
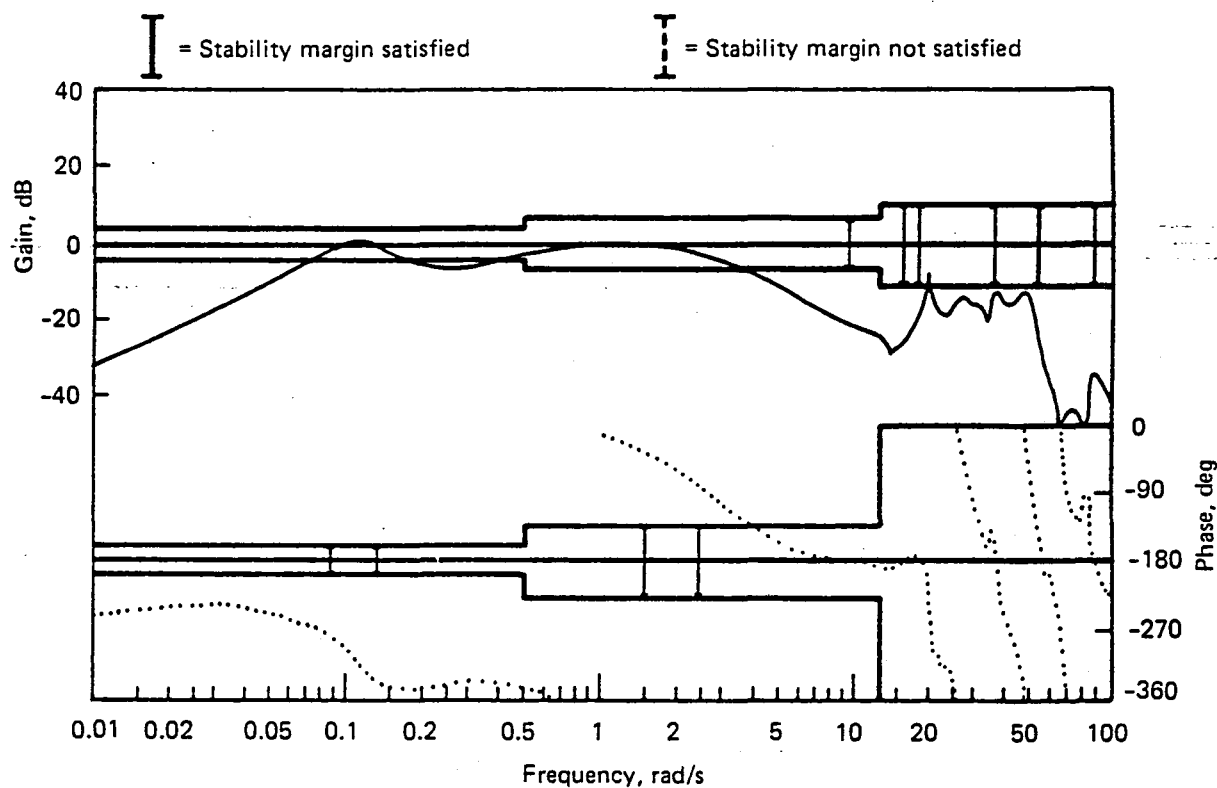
Figure F-64. Phase and Gain Margin, Elevator Loop, Filter Type D, Flight Condition 4
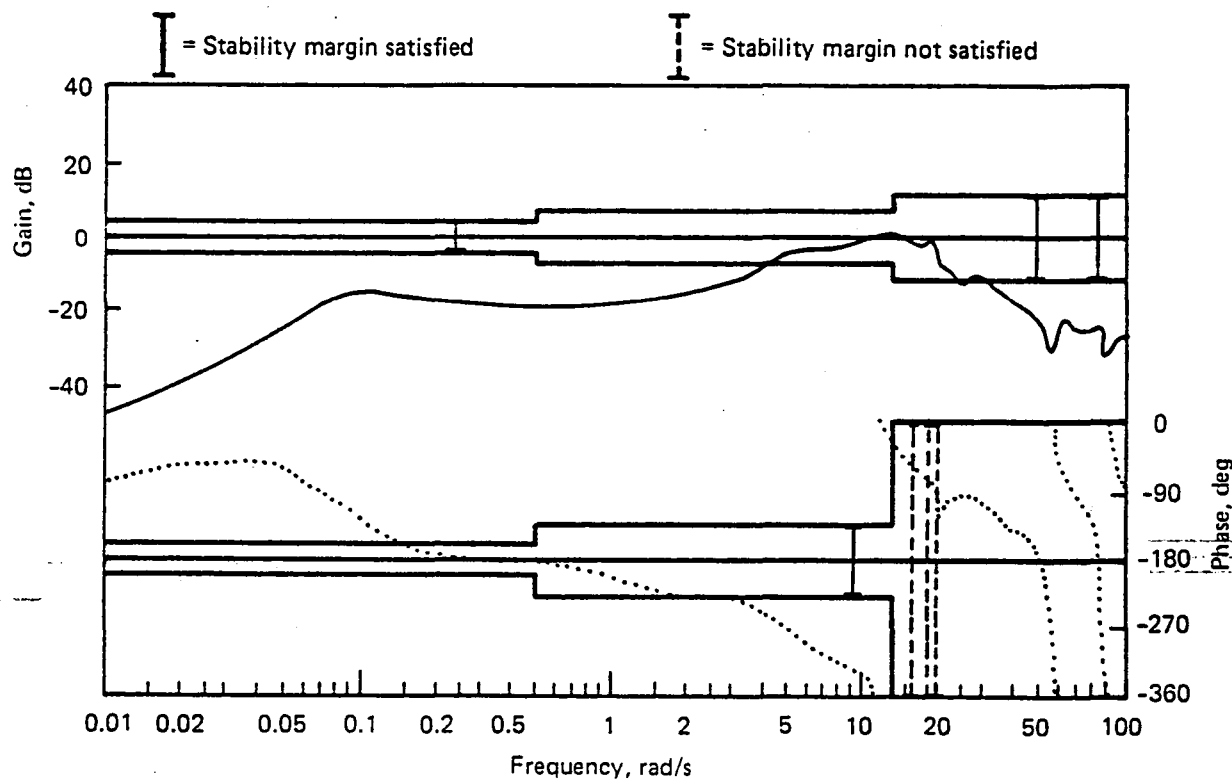
Figure F-65. Phase and Gain Margin, Aileron Loop, Filter Type D, Flight Condition 4

F-52
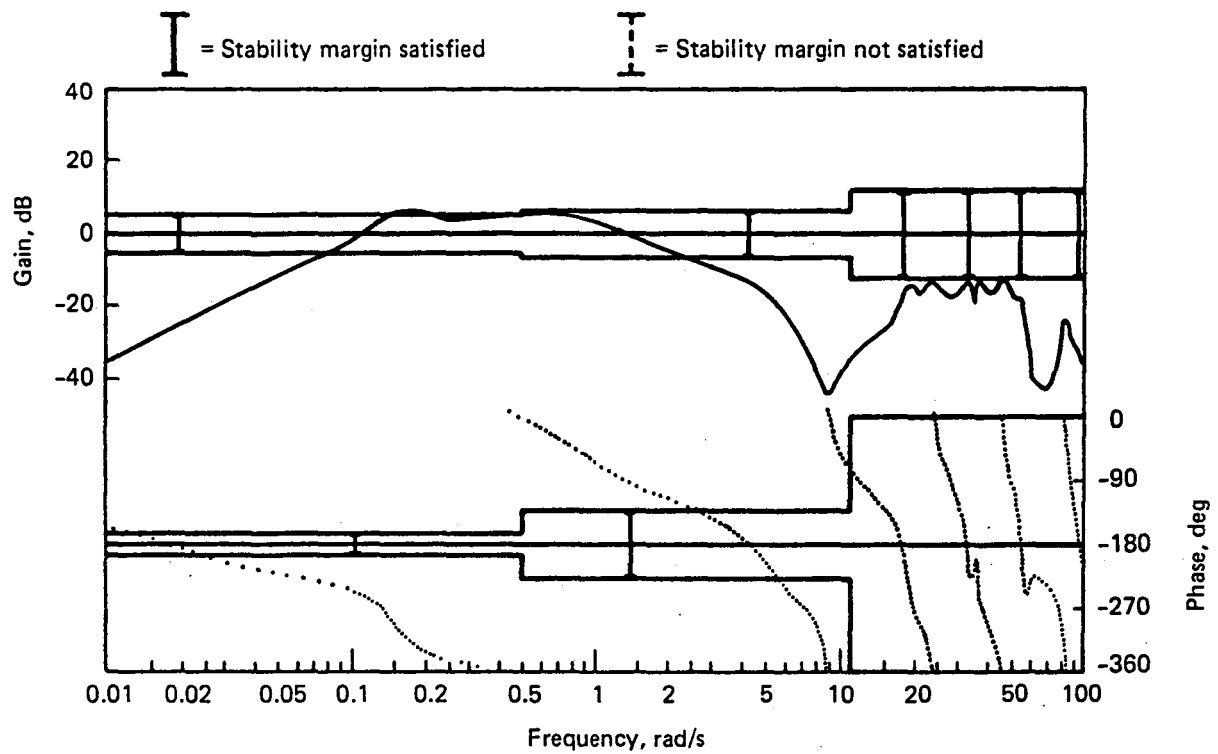
Figure F-66. Phase and Gain Margin, Elevator Loop, Filter Type E, Flight Condition 1
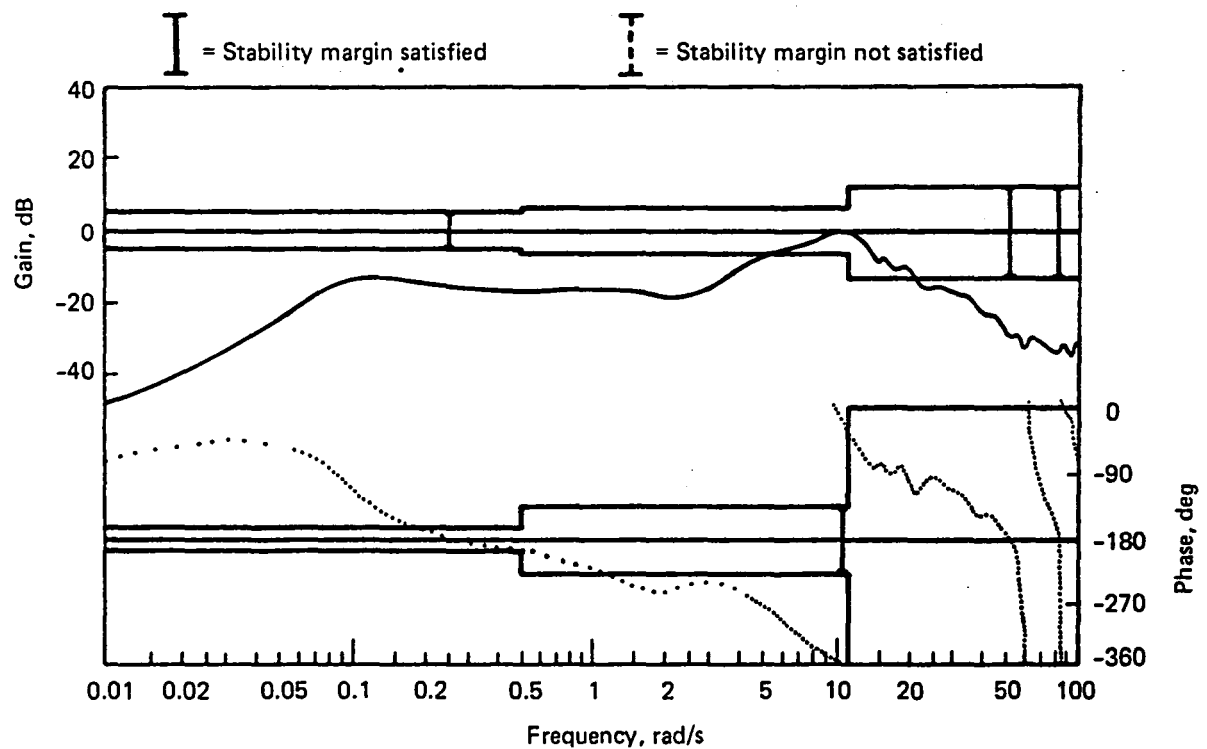
Figure F-67. Phase and Gain Margin, Aileron Loop, Filter Type E, Flight Condition 1
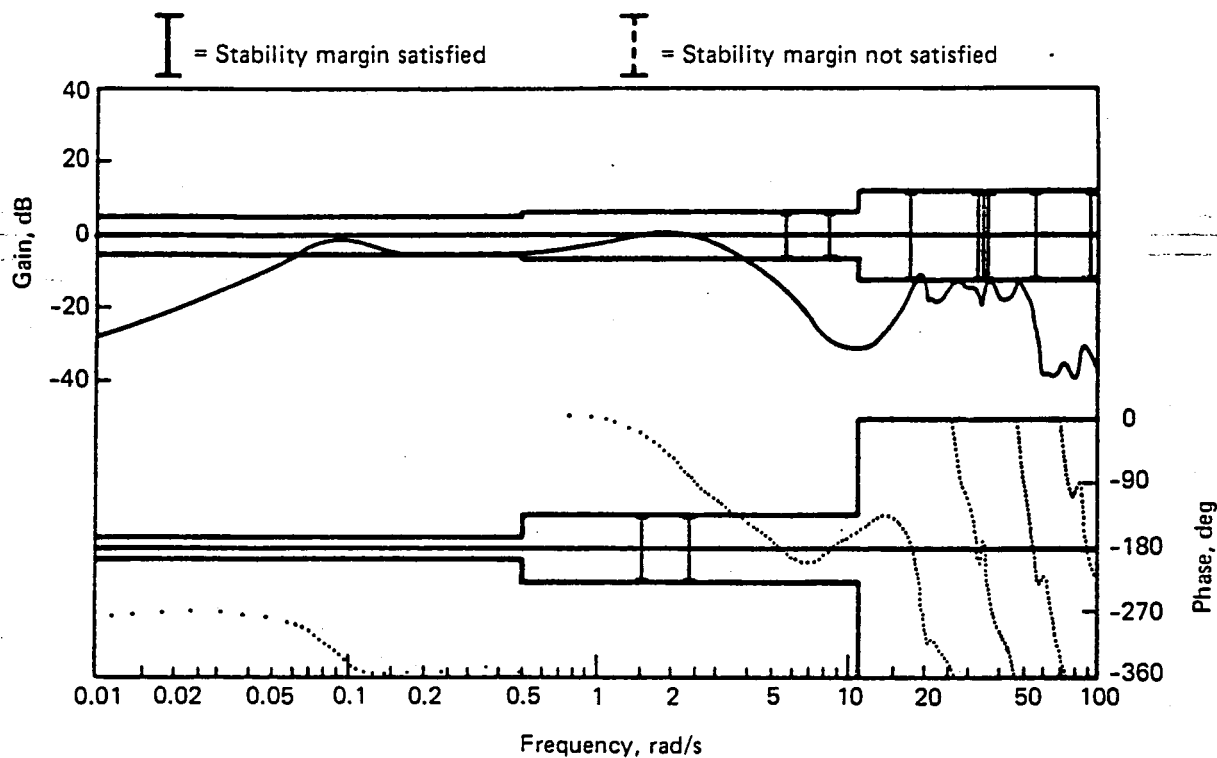
Figure F-68. Phase and Gain Margin, Elevator Loop, Filter Type E, Flight Condition 2
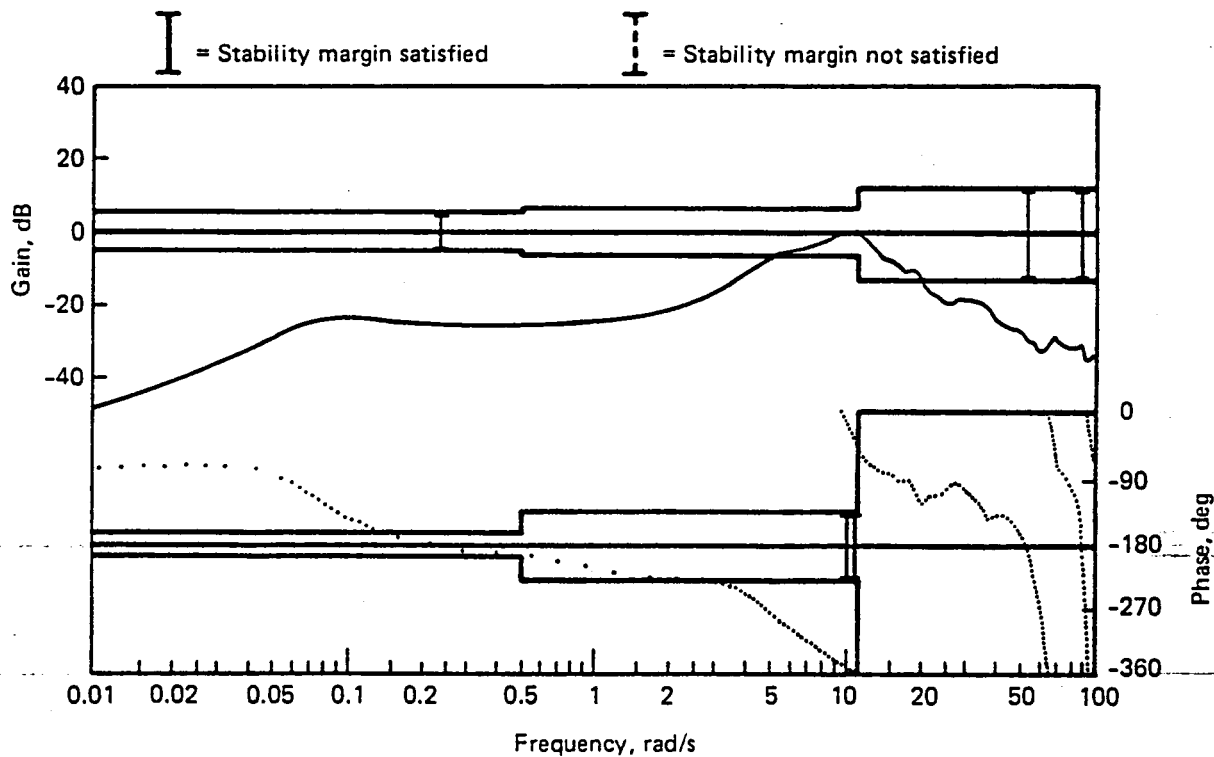
Figure F-69. Phase and Gain Margin, Aileron Loop, Filter Type E, Flight Condition 2
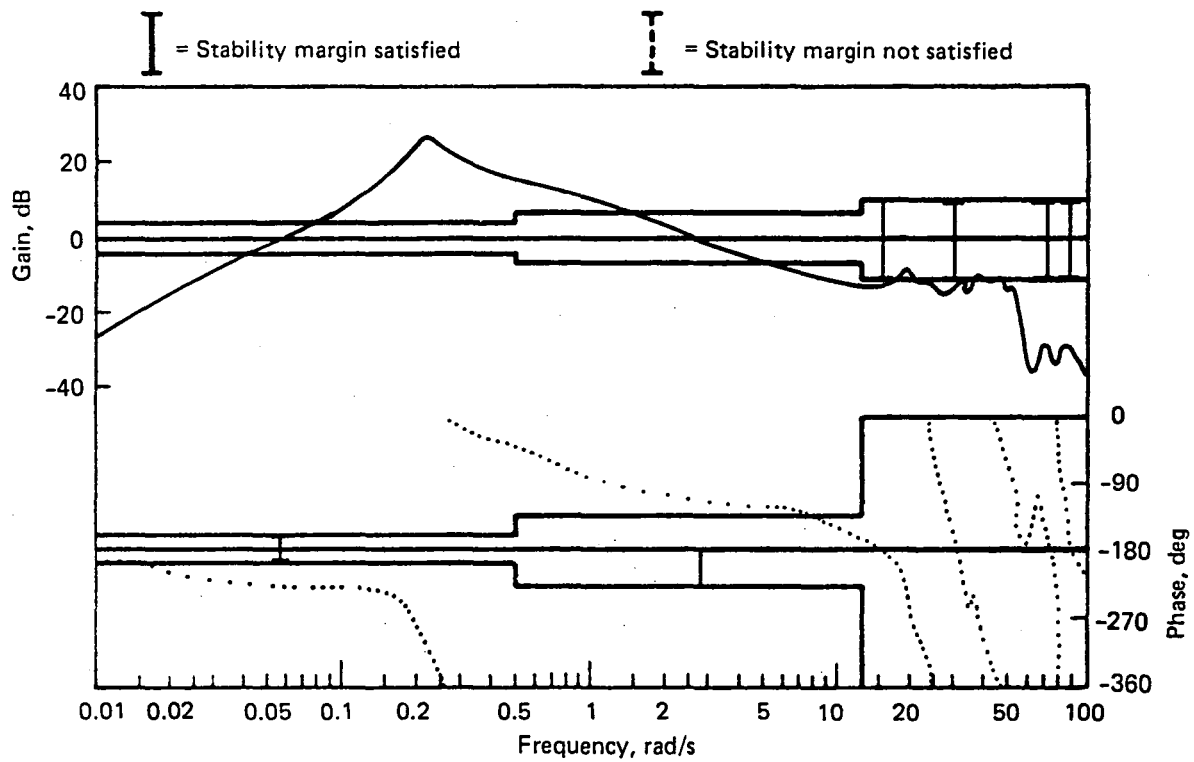
Figure F-70. Phase and Gain Margin, Elevator Loop, Filter Type E, Flight Condition 3
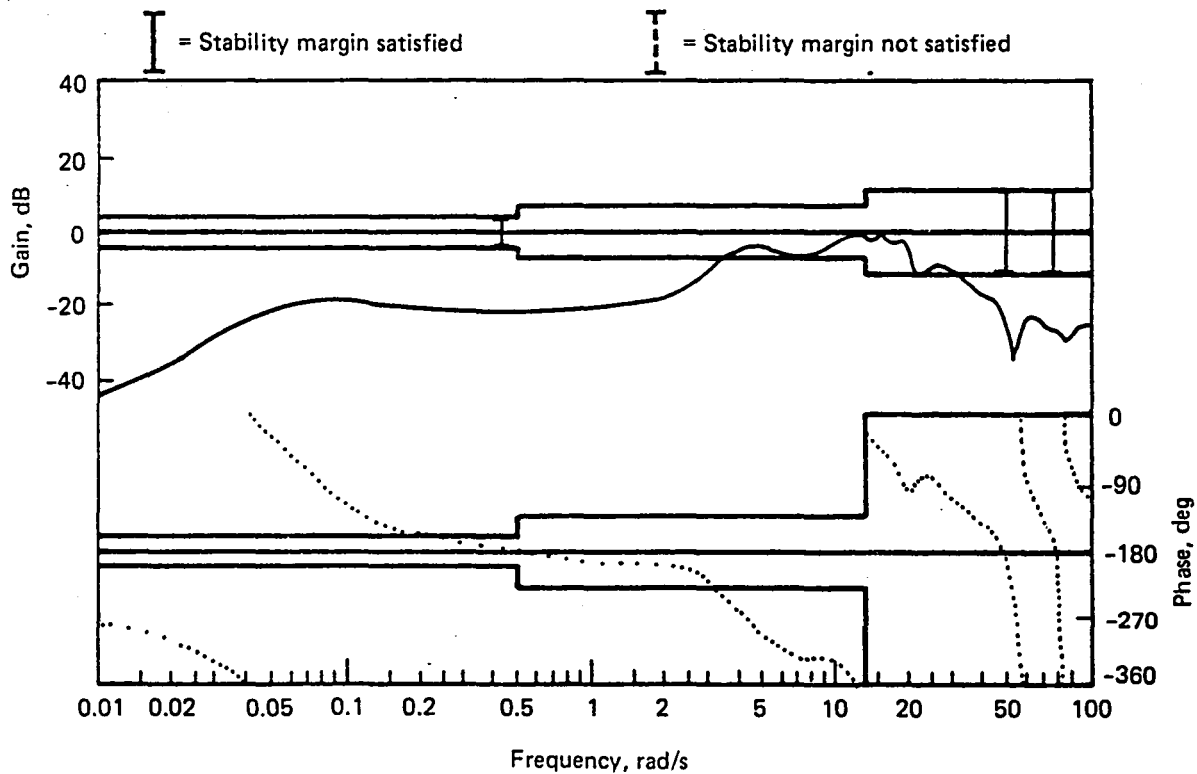
Figure F-71. Phase and Gain Margin, Aileron Loop, Filter Type E, Flight Condition 3
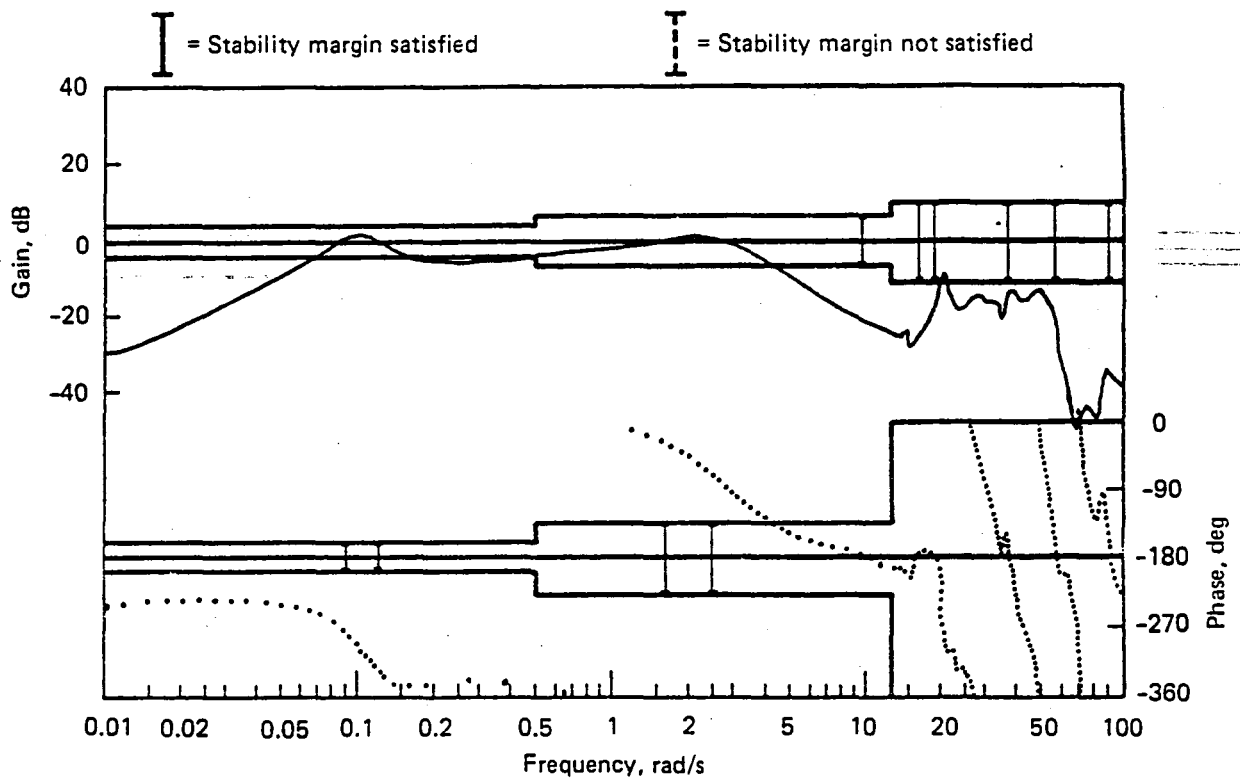
Figure F-72. Phase and Gain Margin, Elevator Loop, Filter Type E, Flight Condition 4
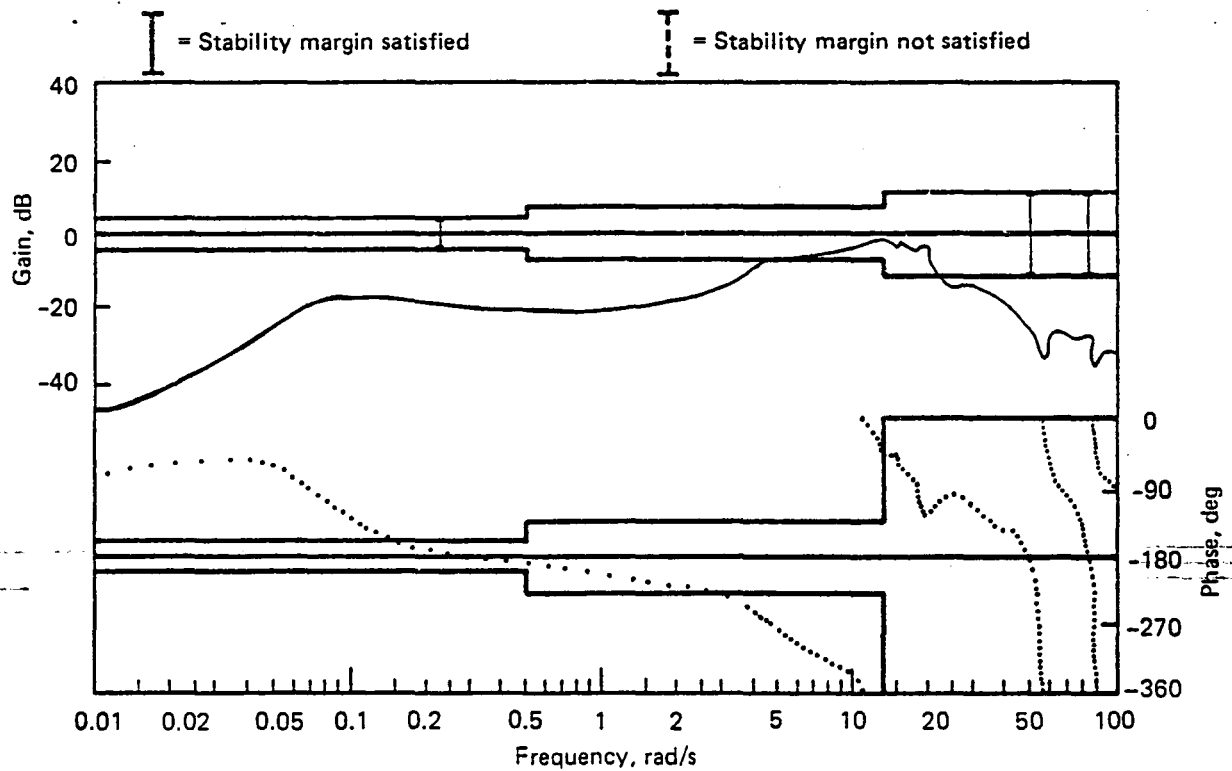
Figure F-73. Phase and Gain Margin, Aileron Loop, Filter Type E, Flight Condition 4
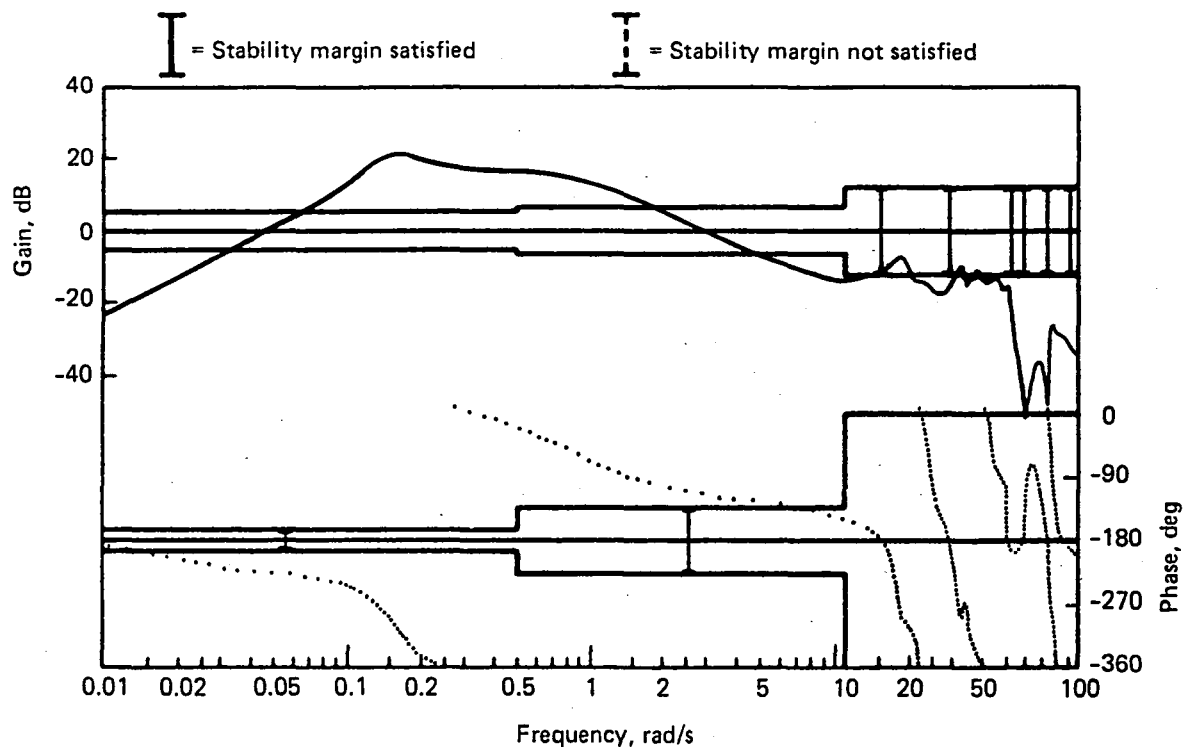
Figure F-74. Phase and Gain Margin, Elevator Loop, Filter Types F and H, Flight Condition 1
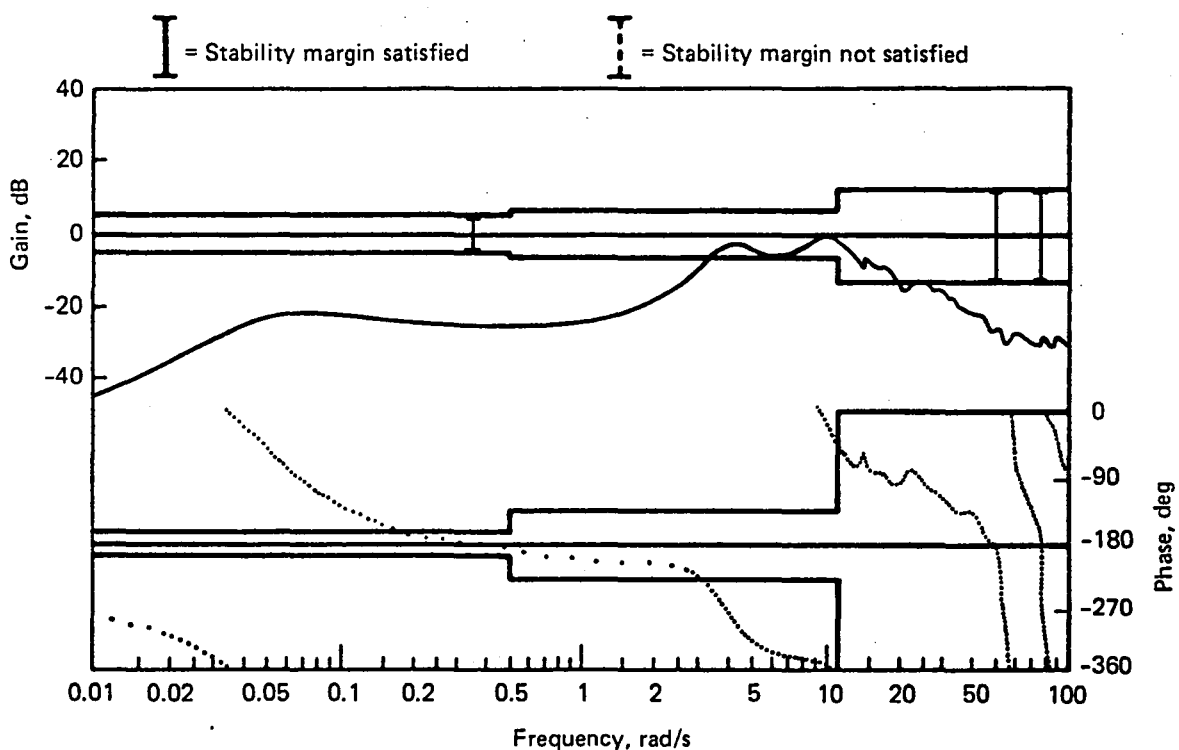
Figure F-75. Phase and Gain Margin, Aileron Loop, Filter Types F and H, Flight Condition 1

F-57
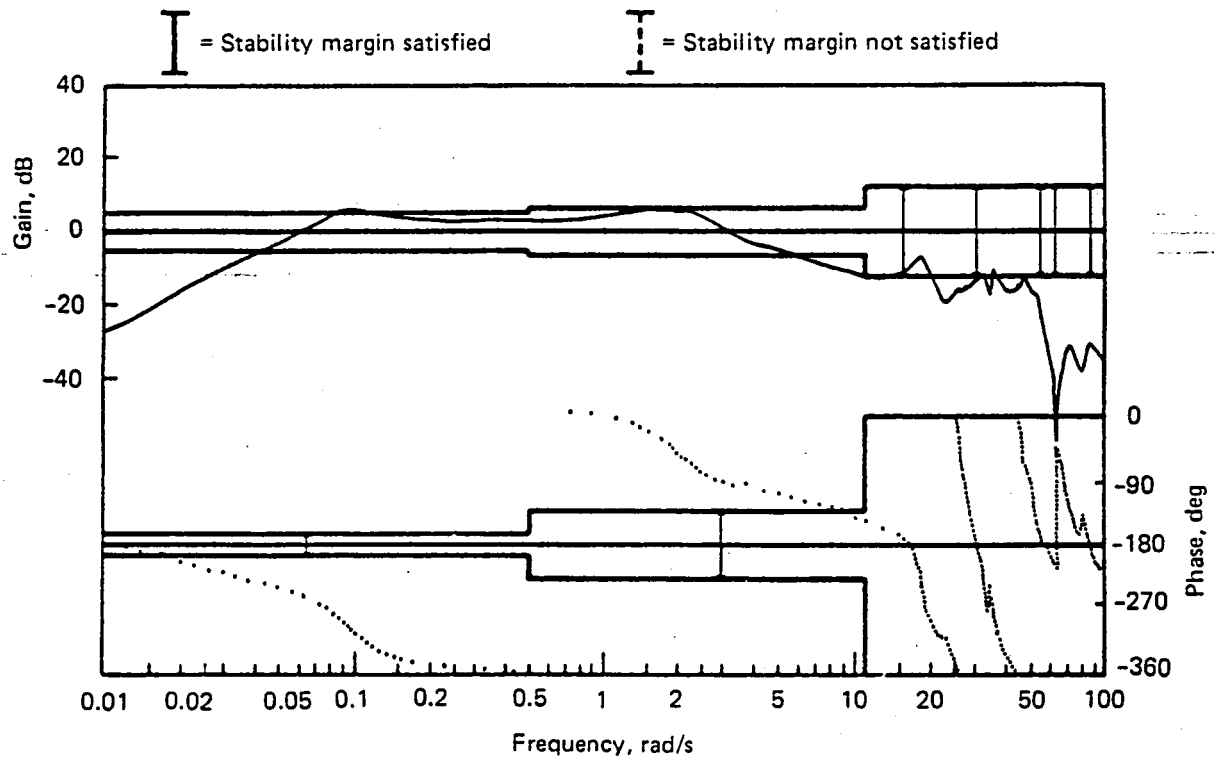
Figure F-76. Phase and Gain Margin, Elevator Loop, Filter Types F and H, Flight Condition 2
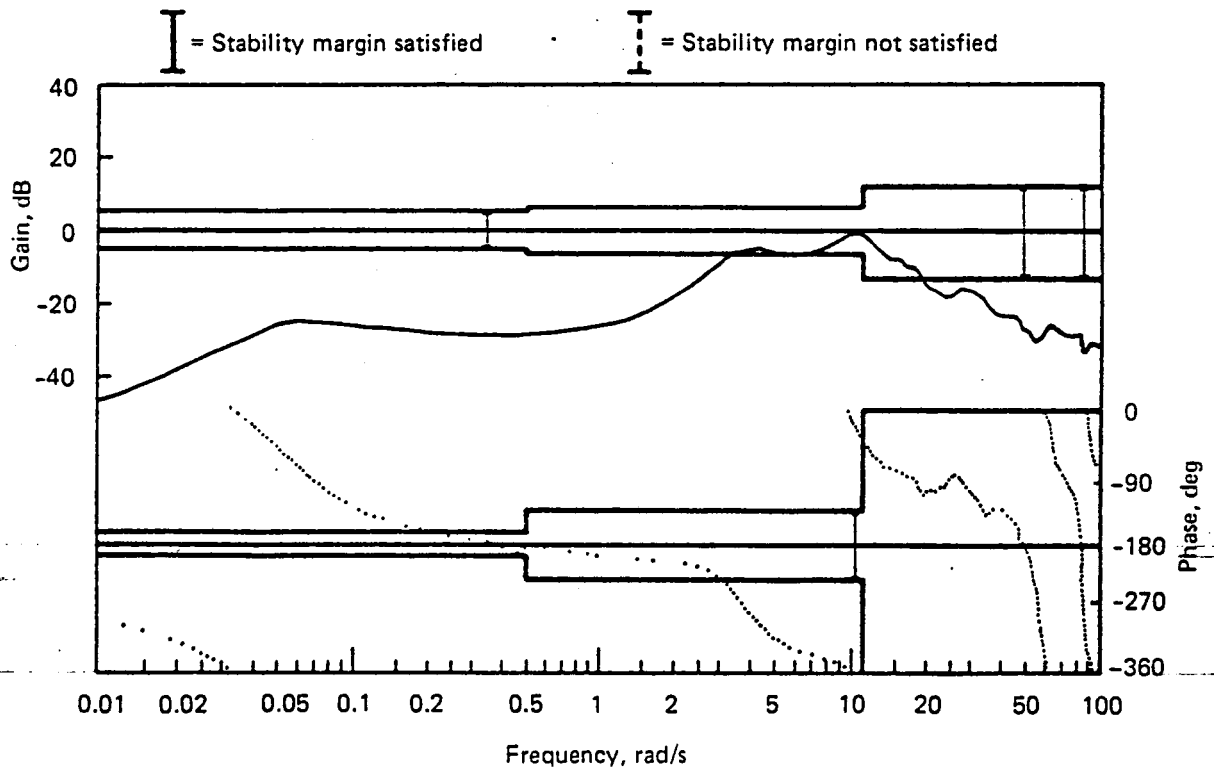
Figure F-77. Phase and Gain Margin, Aileron Loop, Filter Types F and H, Flight Condition 2
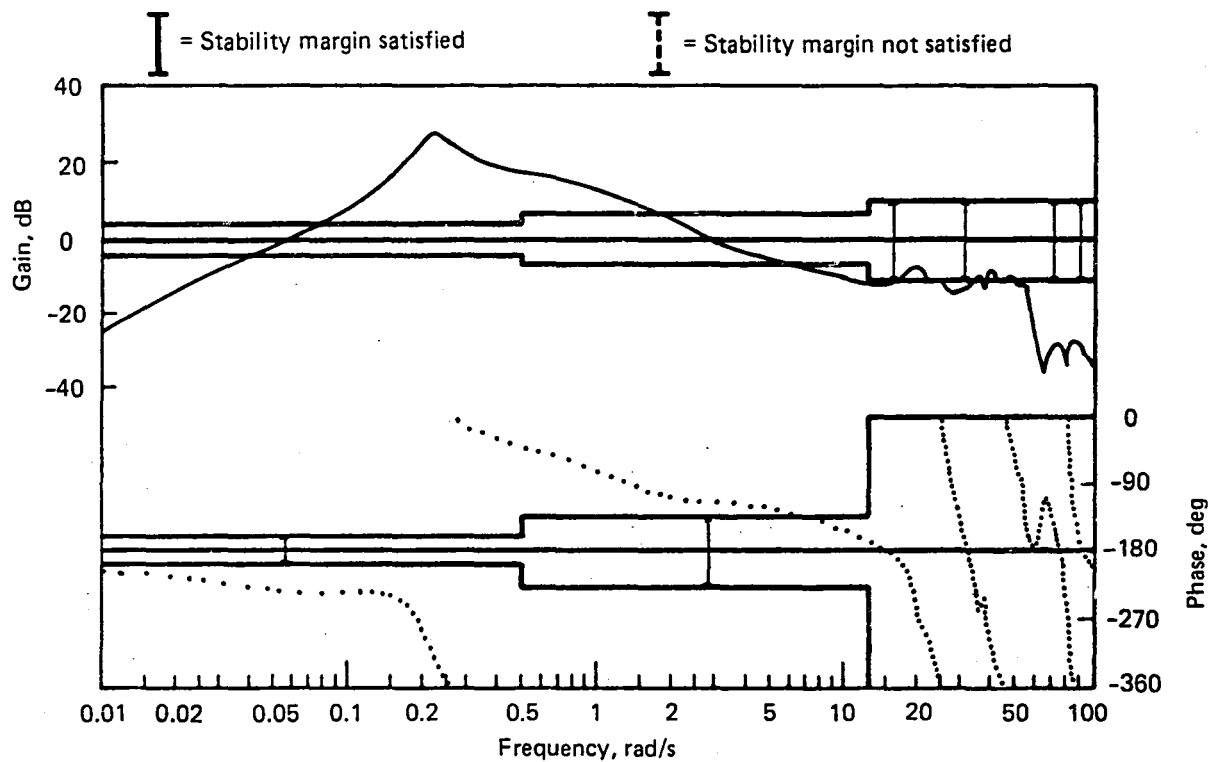
Figure F-78. Phase and Gain Margin, Elevator Loop, Filter Types F and H, Flight Condition 3
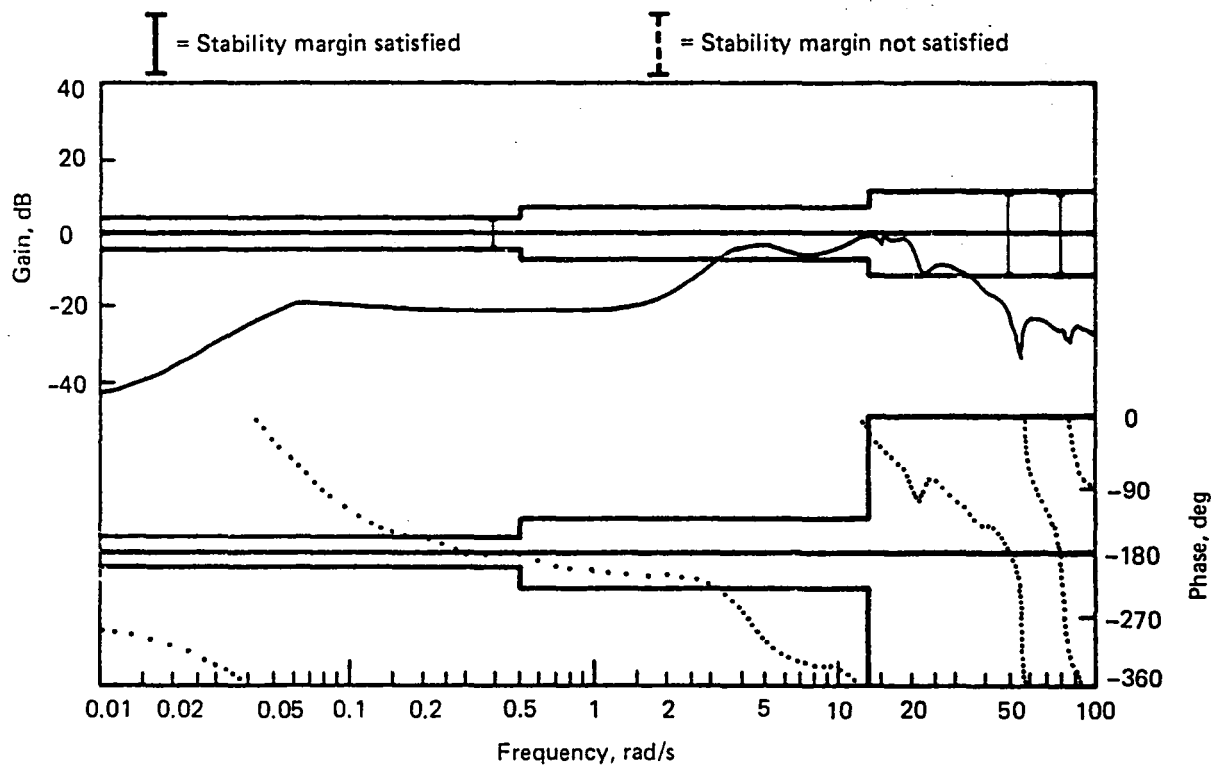
Figure F-79. Phase and Gain Margin, Aileron Loop, Filter Types F and H, Flight Condition 3

F-59
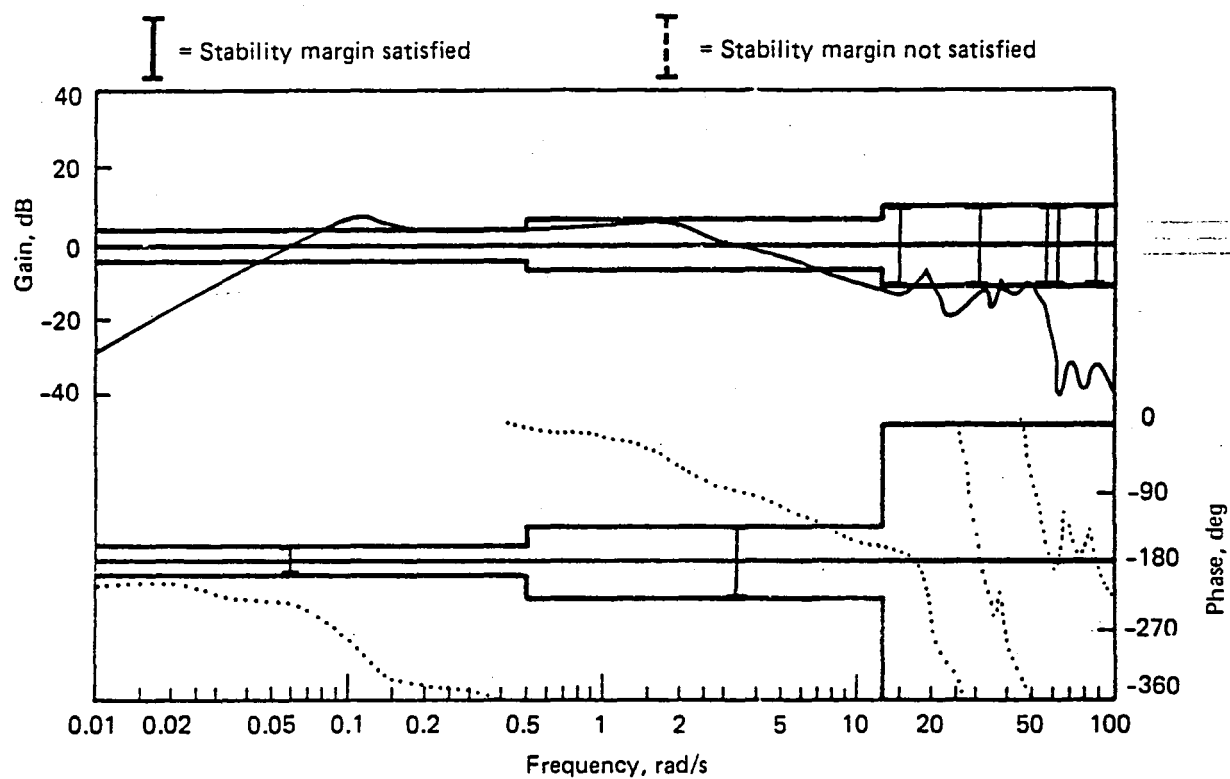
Figure F-80. *Phase and Gain Margin, Elevator Loop, Filter Types F and H, Flight Condition 4*
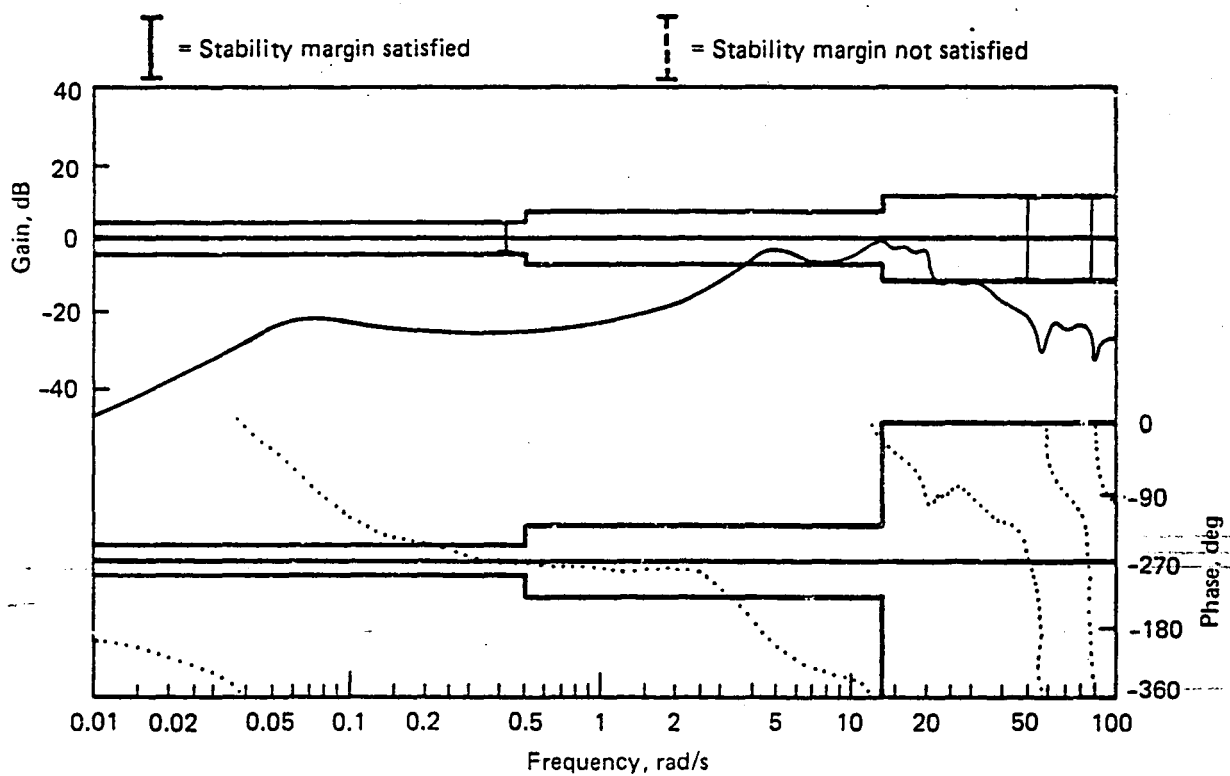
Figure F-81. *Phase and Gain Margin, Aileron Loop, Filter Types F and H, Flight Condition 4*

F-60

F.4.2 FMC PERFORMANCE

F.4.2.1 POLE LOCATIONS

Tables F-16 through F-19 show the open- and closed-loop (full-state feedback) pole locations. Tables F-20 through F-23 show the closed-loop pole locations for full- and reduced-order filters.

Table F-16. Open- and Closed-Loop Dynamic Model Poles, Flight Condition 5

		Open loop				Closed loop (design A)			
	Number	Real, rad/s	Imaginary, rad/s	Magnitude, rad/s	Damping radio	Real, rad/s	Imaginary, rad/s	Magnitude, rad/s	Damping ratio
Flexible airplane	1, 2	-1.77×10^{-2}	±0.159	0.160	0.111	-3.02×10^{-2}	$\pm 5.00 \times 10^{-2}$	5.84×10^{-2}	0.517
	3, 4	-1.19	±0.845	1.46	0.816	-3.10	±3.17	4.43	0.699
	5, 6	-0.321	±14.3	14.3	0.022	-0.387	±14.4	14.4	0.027
	7, 8	-7.48	±16.4	18.0	0.416	-10.1	±16.3	19.2	0.528
	9, 10	3.51×10^{-2}	±19.8	19.8	-0.002	-1.55	±19.1	19.2	0.080
	11, 12	-1.64	±20.4	20.5	0.080	-2.15	±22.0	22.1	0.097
	13, 14	-0.383	±21.8	21.8	0.018	-0.422	±21.6	21.6	0.020
	15, 16	-2.00	±24.5	24.6	0.081	-2.56	±24.7	24.8	0.103
	17, 18	-0.916	±36.0	36.0	0.025	-0.910	±36.0	36.0	0.025
	19, 20	-5.10	±38.5	38.8	0.131	-5.20	±38.6	38.9	0.133
	21, 22	-6.26	±48.5	48.9	0.128	-6.30	±48.4	48.8	0.129
	23, 24	-3.71	±51.3	51.4	0.074	-3.80	±51.3	51.4	0.074
	25, 26	-1.27	±55.6	55.6	0.023	-1.27	±55.6	55.6	0.023
	27, 28	-5.49	±56.6	56.9	0.096	-5.51	±56.6	56.9	0.097
	29, 30	-5.52	±69.2	69.4	0.080	-5.53	±69.2	69.4	0.080
	31, 32	-2.54	±82.6	82.7	0.031	-2.55	±82.6	82.6	0.031
	33, 34	-5.79	±90.6	90.8	0.064	-5.87	±90.7	90.9	0.064
	35, 36	-11.0	±107.0	107.6	0.102	-11.0	±107.0	107.6	0.102
	37, 38	-7.04	±136.0	136.2	0.052	-7.04	±136.0	136.2	0.052
	39, 40	-11.7	±146.0	146.5	0.080	-11.7	±146.0	146.5	0.080
	41, 42	-10.8	±300.0	301.2	0.036	-10.8	±300.0	301.2	0.036
Elevator	43	-1000.0	0	1000.0	1.0	-1000.0	0	1000.0	1.0
	44	-40.0	0	40.0	1.0	-40.0	0	40.0	1.0
	45	-20.0	0	20.0	1.0	-20.0	0	20.0	1.0
Aileron	46	-1000.0	0	1000.0	1.0	-1000.0	0	1000.0	1.0
	47	-40.0	0	40.0	1.0	-40.3	0	40.3	1.0
	48	-20.0	0	20.0	1.0	-19.3	0	19.3	1.0
Kussner	49	-5.3	0	5.3	1.0	-5.3	0	5.3	1.0
	50	-33.3	0	33.3	1.0	-33.3	0	33.3	1.0
	51	-221.0	0	221.0	1.0	-221.0	0	221.0	1.0
Gust	52	-0.517	0	0.517	1.0	-0.517	1.69×10^{-4}	0.517	1.0
	53	-0.517	0	0.517	1.0	-0.517	-1.69×10^{-4}	0.517	1.0

Table F-17. Open- and Closed-Loop Dynamic Model Poles, Flight Condition 6

	Number	Open loop				Closed loop (design A)			
		Real, rad/s	Imaginary, rad/s	Magnitude, rad/s	Damping ratio	Real, rad/s	Imaginary, rad/s	Magnitude, rad/s	Damping ratio
Flexible airplane	1,2	-2.32×10^{-2}	$\pm 9.25 \times 10^{-2}$	9.54×10^{-2}	0.243	-2.96×10^{-2}	$\pm 4.65 \times 10^{-2}$	5.51×10^{-2}	0.537
	3, 4	-1.34	± 2.55	2.88	0.466	-3.10	± 4.17	5.20	0.597
	5, 6	-0.317	± 14.3	14.3	0.022	-0.349	± 14.3	14.3	0.024
	7, 8	-8.18	± 16.6	18.5	0.442	-12.8	± 21.2	30.0	0.516
	9, 10	0.102	± 19.8	19.8	-0.005	-1.48	± 19.8	19.8	0.074
	11, 12	-2.31	± 21.5	21.6	0.107	-2.44	± 22.2	22.3	0.109
	13, 14	-0.389	± 22.3	22.3	0.017	-0.410	± 22.2	22.2	0.018
	15, 16	-2.79	± 26.7	26.9	0.104	-3.08	± 27.1	27.3	0.113
	17, 18	-0.988	± 36.2	36.2	0.027	-0.944	± 36.2	36.2	0.027
	19, 20	-6.20	± 40.0	40.5	0.153	-6.31	± 40.0	40.5	0.156
	21, 22	-5.20	± 50.6	50.9	0.102	-5.66	± 50.8	51.1	0.111
	23, 24	-5.10	± 53.4	53.6	0.095	-5.45	± 53.2	53.5	0.102
	25, 26	-3.33	± 56.4	56.5	0.059	-3.33	± 56.4	56.5	0.059
	27, 28	-2.80	± 63.8	63.9	0.044	-2.84	± 63.8	63.9	0.044
	29, 30	-4.44	± 69.4	69.5	0.064	-4.41	± 69.4	69.5	0.063
	31, 32	-3.42	± 88.7	88.7	0.039	-3.44	± 88.7	88.8	0.039
	33, 34	-5.67	± 93.0	93.1	0.061	-5.77	± 93.0	93.2	0.062
	35, 36	-11.7	± 109.0	109.6	0.107	-11.7	± 109.0	109.6	0.107
	37, 38	-8.22	± 139.0	139.2	0.059	-8.22	± 139.0	139.2	0.059
	39, 40	-10.3	± 163.0	163.3	0.063	-10.3	± 163.0	163.3	0.063
	41, 42	-11.8	± 305.0	305.2	0.039	-11.8	± 305.0	305.2	0.039
Elevator	43	-1000.0	0	1000.0	1.0	-1000.0	0	1000.0	1.0
	44	-40.0	0	40.0	1.0	-40.0	0	40.0	1.0
	45	-20.0	0	20.0	1.0	-20.0	$+6.50 \times 10^{-2}$	20.0	1.0
Aileron	46	-1000.0	0	1000.0	1.0	-1000.0	0	1000.0	1.0
	47	-40.0	0	40.0	1.0	-42.6	0	42.6	1.0
	48	-20.0	0	20.0	1.0	-20.0	-6.50×10^{-2}	20.0	1.0
Kussner	49	-5.30	0	5.30	1.0	-5.30	0	5.30	1.0
	50	-33.3	0	33.3	1.0	-33.3	0	33.3	1.0
	51	-221.0	0	221.0	1.0	-221.0	0	221.0	1.0
Gust	52	-0.517	0	0.517	1.0	-0.517	$+1.69 \times 10^{-4}$	0.517	1.0
	53	-0.517	0	0.517	1.0	-0.517	-1.69×10^{-4}	0.517	1.0

Table F-18. Open- and Closed-Loop Dynamic Model Poles, Flight Condition 7

	Number	Open loop				Closed loop (design A)			
		Real, rad/s	Imaginary, rad/s	Magnitude, rad/s	Damping ratio	Real, rad/s	Imaginary, rad/s	Magnitude, rad/s	Damping ratio
Flexible airplane	1, 2	-8.18×10^{-3}	±0.219	0.219	0.037	-5.78×10^{-2}	±0.119	0.132	0.438
	3, 4	−1.46	±0.192	1.47	0.993	−1.83	±1.56	2.40	0.760
	5, 6	−0.342	±13.4	13.4	0.026	−0.372	±13.5	13.5	0.028
	7, 8	0.286	±20.5	20.5	−0.014	−1.18	±21.2	21.2	0.055
	9, 10	−2.15	±20.8	20.9	0.103	−1.89	±19.7	19.8	0.095
	11, 12	−0.380	±21.8	21.8	0.017	−0.429	±21.7	21.7	0.020
	13, 14	−0.358	±25.7	25.7	0.014	−3.14	±25.4	25.6	0.122
	15, 16	−20.5	±16.7	26.5	0.775	−25.9	±29.1	39.0	0.665
	17, 18	−1.08	±36.4	36.4	0.030	−1.02	±36.1	36.1	0.028
	19, 20	−3.40	±37.1	37.2	0.091	−3.52	±39.1	39.2	0.089
	21, 22	−2.64	±44.1	44.2	0.060	−3.08	±44.0	44.1	0.070
	23, 24	−5.70	±51.8	52.1	0.110	−5.65	±51.9	52.2	0.108
	25, 26	−1.04	±55.3	55.3	0.019	−1.04	±55.3	55.3	0.019
	27, 28	−14.9	±59.3	61.1	0.244	−14.9	±59.3	61.1	0.244
	29, 30	−3.66	±65.0	65.1	0.056	−3.68	±65.0	65.1	0.056
	31, 32	−3.20	±82.5	82.5	0.039	−3.23	±82.5	82.5	0.039
	33, 34	−5.90	±89.0	89.2	0.066	−6.06	±89.0	89.2	0.068
	35, 36	−14.7	±97.4	98.5	0.149	−14.7	±97.4	98.5	0.149
	37, 38	−7.49	±135.0	135.2	0.055	−7.49	±135.0	135.2	0.055
	39, 40	−12.2	±140.0	140.5	0.086	−12.2	±140.0	140.5	0.086
	41, 42	−11.0	±300.0	300.2	0.037	−11.0	±300.0	300.2	0.037
Elevator	43	−1000.0	0	1000.0	1.0	−1000.0	0	1000.0	1.0
	44	−40.0	0	40.0	1.0	−40.0	0	40.0	1.0
	45	−20.0	0	20.0	1.0	−20.0	0	20.0	1.0
Aileron	46	−1000.0	0	1000.0	1.0	−1000.0	0	1000.0	1.0
	47	−40.0	0	40.0	1.0	−48.1	0	48.1	1.0
	48	−20.0	0	20.0	1.0	−22.8	0	22.8	1.0
Kussner	49	−5.51	0	5.51	1.0	−5.51	0	5.51	1.0
	50	−34.6	0	34.6	1.0	−34.6	0	34.6	1.0
	51	−230.0	0	230.0	1.0	−230.0	0	230.0	1.0
Gust	52	−0.537	0	0.537	1.0	−0.537	0	0.537	1.0
	53	−0.537	0	0.537	1.0	−0.537	0	0.537	1.0

Table F-19. Open- and Closed-Loop Dynamic Model Poles, Flight Condition 8

	Number	Open loop				Closed loop (design A)			
		Real, rad/s	Imaginary, rad/s	Magnitude, rad/s	Damping ratio	Real, rad/s	Imaginary, rad/s	Magnitude, rad/s	Damping ratio
Flexible airplane	1, 2	-2.94×10^{-2}	±0.108	0.112	0.263	-3.09×10^{-2}	±0.104	0.109	0.284
	3 4	-1.63	±2.90	3.33	0.490	-1.62	±2.91	3.33	0.486
	5, 6	-0.341	±13.4	13.4	0.025	-0.348	±13.4	13.4	0.026
	7, 8	0.227	±20.3	20.3	-0.011	-0.442	±20.2	20.2	0.022
	9, 10	-2.72	±22.1	22.3	0.122	-2.53	±22.2	22.4	0.113
	11, 12	-0.373	±22.3	22.3	0.017	-0.394	±22.3	22.3	0.018
	13, 14	-23.6	±13.7	27.3	0.864	-25.8	±25.3	36.1	0.714
	15, 16	-0.498	±27.8	27.8	0.017	-3.11	±28.1	28.3	0.110
	17, 18	-1.24	±36.0	36.1	0.034	-1.13	±36.0	36.0	0.031
	19, 20	-1.80	±41.7	41.8	0.043	-2.25	±41.9	42.0	0.053
	21, 22	-3.71	±45.1	45.2	0.082	-4.06	±45.4	45.6	0.089
	23, 24	-13.5	±53.4	55.1	0.244	-13.4	±53.4	55.0	0.244
	25, 26	-2.29	±56.4	56.4	0.041	-2.33	±56.4	56.4	0.041
	27, 28	-6.02	±63.1	63.4	0.095	-6.01	±63.1	63.4	0.095
	29, 30	-3.34	±67.0	67.1	0.050	-3.38	±67.0	67.1	0.050
	31, 32	-4.07	±88.2	88.3	0.046	-4.07	±88.2	88.3	0.046
	33, 34	-6.12	±91.7	91.9	0.067	-6.15	±91.6	91.8	0.067
	35, 36	-15.0	±99.0	100.1	0.150	-15.0	±99.0	100.1	0.150
	37, 38	-9.06	±137.0	137.3	0.066	-9.06	±137.0	137.3	0.066
	39, 40	-10.8	±159.0	159.4	0.068	-10.8	±159.0	159.4	0.068
	41, 42	-12.0	±304.0	304.2	0.040	-12.0	±304.0	304.2	0.040
Elevator	43	-1000.0	0	1000.0	1.0	-1000.0	0	1000.0	1.0
	44	-40.0	0	40.0	1.0	-40.0	0	40.0	1.0
	45	-20.0	0	20.0	1.0	-20.0	0	20.0	1.0
Aileron	46	-1000.0	0	1000.0	1.0	-1000.0	0	1000.0	1.0
	47	-40.0	0	40.0	1.0	-47.7	0	47.7	1.0
	48	-20.0	0	20.0	1.0	-22.3	0	22.3	1.0
Kussner	49	-5.51	0	5.51	1.0	-5.51	0	5.51	1.0
	50	-34.6	0	34.6	1.0	-34.6	0	34.6	1.0
	51	-230.0	0	230.0	1.0	-230.0	0	230.0	1.0
Gust	52	-0.537	0	0.537	1.0	-0.537	0	0.537	1.0
	53	-0.537	0	0.537	1.0	-0.537	0	0.537	1.0

Table F-20. Closed-Loop Controller Poles, Flight Condition 5

Design B

Number	Real, rad/s	Imaginary, rad/s	Magnitude, rad/s	Damping ratio
1, 2	-2.53×10^{-2}	± 0.176	0.178	0.142
3, 4	-0.526	± 3.21	3.25	0.162
5, 6	-0.309	± 14.4	14.4	0.022
7, 8	-1.83	± 20.5	20.6	0.089
9, 10	-0.454	± 20.8	20.8	0.022
11, 12	-0.404	± 21.8	21.8	0.018
13, 14	-2.02	± 28.8	28.9	0.070
15, 16	-1.14	± 36.0	36.0	0.032
17, 18	-5.23	± 39.7	40.0	0.131
19, 20	-41.6	± 6.44	42.1	0.988
21, 22	-5.32	± 50.0	50.3	0.106
23, 24	-1.14	± 55.6	55.6	0.021
25, 26	-5.96	± 57.1	57.4	0.104
27, 28	-5.94	± 69.9	70.2	0.085
29, 30	-1.24	± 82.8	82.8	0.015
31, 32	-5.46	± 88.5	88.8	0.062
33, 34	-67.4	± 71.0	97.9	0.689
35, 36	-10.8	± 107.0	107.5	0.100
37, 38	-7.03	± 136.0	136.2	0.052
39, 40	-11.7	± 146.0	146.5	0.080
41, 42	-10.8	± 300.0	300.2	0.036

Number	Real, rad/s	Imaginary, rad/s	Magnitude, rad/s	Damping ratio
43	-1000.0	0	1000.0	1.0
44	-40.0	0	40.0	1.0
45	-20.0	0	20.0	1.0
46	-1000.0	0	1000.0	1.0
47	-40.0	0	40.0	1.0
48	-20.0	0	20.0	1.0
49	-1.37	0	1.37	1.0
50	-6.72	0	6.72	1.0
51	-208.0	0	208.0	1.0
52	-8.88×10^{-2}	0	8.88×10^{-2}	1.0
53	-0.290	0	0.290	1.0

Design H

Number	Real, rad/s	Imaginary, rad/s	Magnitude, rad/s	Damping ratio
1, 2	-2.76×10^{-2}	$\pm 9.73 \times 10^{-3}$	2.93×10^{-2}	0.943
3, 4	-0.236	$\pm 5.17 \times 10^{-2}$	0.242	0.977
5, 6	-1.07	± 4.08	4.22	0.254
7, 8	-2.16	± 19.2	19.3	0.111

Table F-21. Closed-Loop Controller Poles, Flight Condition 6

Design B

Number	Real, rad/s	Imaginary, rad/s	Magnitude, rad/s	Damping ratio
1, 2	-5.07×10^{-2}	$\pm 8.38 \times 10^{-2}$	9.79×10^{-2}	0.518
3, 4	-1.13	± 3.79	3.95	0.285
5, 6	-0.311	± 14.4	14.4	0.022
7, 8	-0.614	± 20.7	20.7	0.030
9, 10	-2.13	± 21.6	21.7	0.098
11, 12	-0.418	± 22.3	22.3	0.019
13, 14	-1.42	± 34.0	34.0	0.042
15, 16	-2.50	± 37.2	37.3	0.067
17, 18	-6.24	± 40.7	41.2	0.151
19, 20	-41.8	± 6.05	42.2	0.990
21, 22	-5.19	± 51.0	51.3	0.101
23, 24	-3.59	± 57.1	57.2	0.063
25, 26	-2.58	± 63.9	64.0	0.040
27, 28	-4.29	± 69.5	69.6	0.061
29, 30	-6.82	± 91.8	92.0	0.074
31, 32	-2.58	± 93.9	93.9	0.027
33, 34	-66.8	± 66.7	94.4	0.708
35, 36	-11.4	± 110.0	110.6	0.104
37, 38	-8.20	± 139.0	139.2	0.059
39, 40	-10.4	± 163.0	163.3	0.064
41, 42	-11.8	± 304.0	304.2	0.039

Number	Real, rad/s	Imaginary, rad/s	Magnitude, rad/s	Damping ratio
43	-1000.0	0	1000.0	1.0
44	-40.0	0	40.0	1.0
45	-20.0	0	20.0	1.0
46	-1000.0	0	1000.0	1.0
47	-40.0	0	40.0	1.0
48	-20.0	0	20.0	1.0
49	-2.44	0	2.44	1.0
50	-6.72	0	6.72	1.0
51	-210.0	0	210.0	1.0
52	-0.152	0	0.152	1.0
53	-0.274	0	0.274	1.0

Design H

Number	Real, rad/s	Imaginary, rad/s	Magnitude, rad/s	Damping ratio
1, 2	-2.79×10^{-2}	$\pm 9.42 \times 10^{-3}$	2.94×10^{-2}	0.947
3, 4	-0.235	$\pm 5.19 \times 10^{-2}$	0.241	0.976
5, 6	-1.07	± 4.13	4.27	0.251
7, 8	-2.38	± 20.2	20.3	0.117

Table F-22. Closed-Loop Controller Poles, Flight Condition 7

Design B

Number	Real, rad/s	Imaginary, rad/s	Magnitude, rad/s	Damping ratio
1, 2	-1.45×10^{-2}	± 0.207	0.208	0.070
3, 4	-0.474	± 3.36	3.39	0.140
5, 6	-0.345	± 13.5	13.5	0.026
7, 8	-0.410	± 20.6	20.6	0.020
9, 10	-2.06	± 20.9	21.0	0.098
11, 12	-0.404	± 21.8	21.8	0.018
13, 14	-2.18	± 28.6	28.7	0.076
15, 16	-1.00	± 36.0	36.0	0.028
17, 18	-6.58	± 44.8	45.3	0.145
19, 20	-47.9	± 3.56	48.0	0.997
21, 22	-6.30	± 50.5	50.9	0.123
23, 24	-1.03	± 55.3	55.3	0.018
25, 26	-15.1	± 59.7	61.5	0.245
27, 28	-4.30	± 66.1	66.2	0.065
29, 30	-1.57	± 83.2	83.2	0.019
31, 32	-5.06	± 88.2	88.3	0.057
33, 34	-14.3	± 97.6	98.6	0.145
35, 36	-109.0	± 67.4	128.2	0.852
37, 38	-7.47	± 135.0	135.2	0.057
39, 40	-12.2	± 140.0	140.5	0.087
41, 42	-11.0	± 300.0	300.2	0.037

Number	Real, rad/s	Imaginary, rad/s	Magnitude, rad/s	Damping ratio
43	-1000.0	0	1000.0	1.0
44	-40.0	0	40.0	1.0
45	-20.0	0	20.0	1.0
46	-1000.0	0	1000.0	1.0
47	-40.0	0	40.0	1.0
48	-20.0	0	20.0	1.0
49	-1.56	0	1.56	1.0
50	-6.97	0	6.97	1.0
51	-185.0	0	185.0	1.0
52	-8.38×10^{-2}	0	8.38×10^{-2}	1.0
53	-0.305	0	0.305	1.0

Design H

Number	Real, rad/s	Imaginary, rad/s	Magnitude, rad/s	Damping ratio
1, 2	-2.77×10^{-2}	$\pm 9.77 \times 10^{-3}$	2.94×10^{-2}	0.943
3, 4	-0.237	$\pm 5.17 \times 10^{-2}$	0.243	0.977
5, 6	-1.11	± 4.03	4.18	0.266
7, 8	-2.13	± 18.4	18.5	0.115

Table F-23. Closed-Loop Controller Poles, Flight Condition 8

Design B

Number	Real, rad/s	Imaginary, rad/s	Magnitude, rad/s	Damping ratio
1, 2	-6.69×10^{-2}	± 0.101	0.121	0.552
3, 4	-1.15	± 3.93	4.09	0.280
5, 6	-0.347	± 13.5	13.5	0.026
7, 8	-0.528	± 20.5	20.5	0.025
9, 10	-0.408	± 22.3	22.3	0.018
11, 12	-2.62	± 22.2	22.4	0.117
13, 14	-2.37	± 33.4	33.5	0.071
15, 16	-1.91	± 36.3	36.4	0.053
17, 18	-6.77	± 48.0	48.5	0.140
19, 20	-48.7	± 1.56	48.7	0.999
21, 22	-12.0	± 52.4	53.8	0.223
23, 24	-3.66	± 57.0	57.1	0.064
25, 26	-6.58	± 62.4	62.7	0.105
27, 28	-3.28	± 67.6	67.7	0.048
29, 30	-6.66	± 91.1	91.3	0.073
31, 32	-3.00	± 94.9	94.9	0.032
33, 34	-14.4	± 99.1	100.1	0.144
35, 36	-105.0	± 61.6	121.7	0.862
37, 38	-9.04	± 137.0	137.3	0.066
39, 40	-10.8	± 159.0	159.4	0.068
41, 42	-12.0	± 304.0	304.2	0.040

Number	Real, rad/s	Imaginary, rad/s	Magnitude, rad/s	Damping ratio
43	-1000.0	0	1000.0	1.0
44	-40.0	0	40.0	1.0
45	-20.0	0	20.0	1.0
46	-1000.0	0	1000.0	1.0
47	-40.0	0	40.0	1.0
48	-20.0	0	20.0	1.0
49	-2.52	0	2.52	1.0
50	-6.97	0	6.97	1.0
51	-191.0	0	191.0	1.0
52	-0.140	0	0.140	1.0
53	-0.286	0	0.286	1.0

Design H

Number	Real, rad/s	Imaginary, rad/s	Magnitude, rad/s	Damping ratio
1, 2	-2.77×10^{-5}	$\pm 9.78 \times 10^{-3}$	0.943	0.943
3, 4	-0.239	$\pm 5.33 \times 10^{-2}$	0.245	0.976
5, 6	-1.11	± 4.01	4.16	0.266
7, 8	-1.68	± 19.0	19.1	0.088

F.4.2.2 STABILITY MARGINS

Figures F-82 through F-115 are Bode plots for the aileron and elevator control loops with various filters and at the flutter flight conditions.
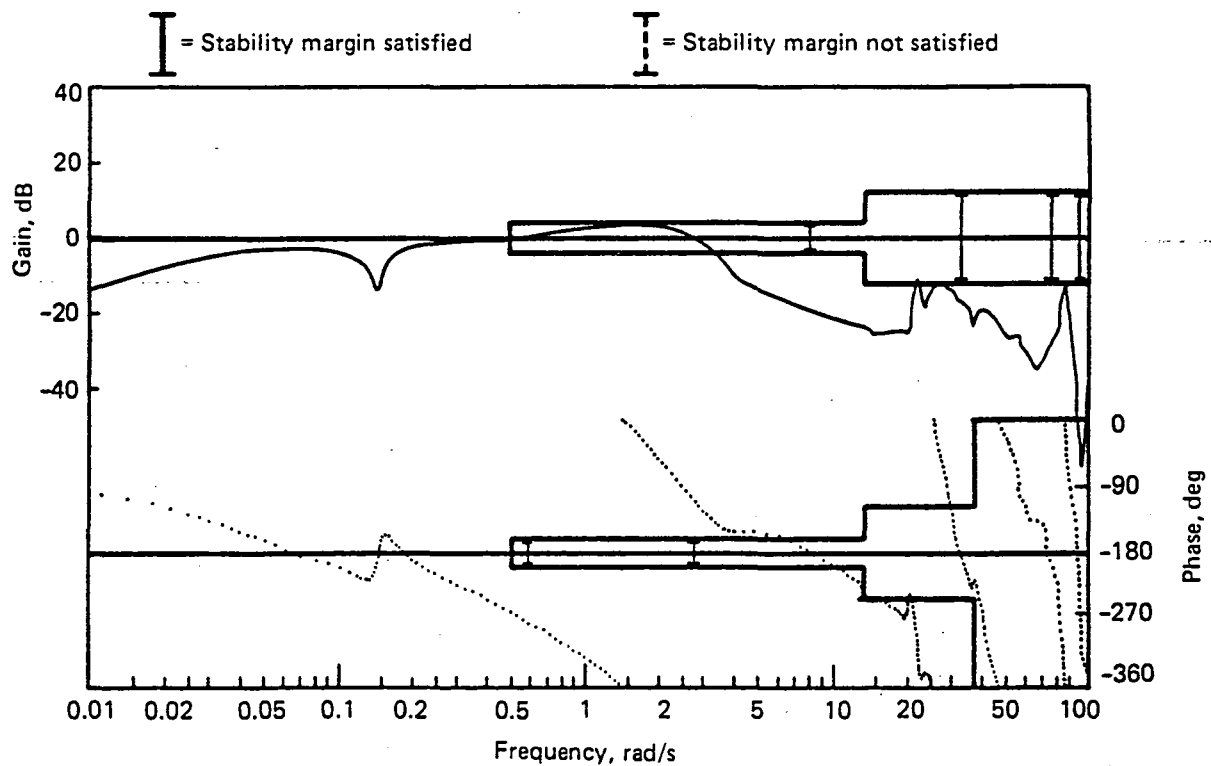
Figure F-82. Phase and Gain Margin, Elevator Loop, Filter Type B, Flight Condition 5
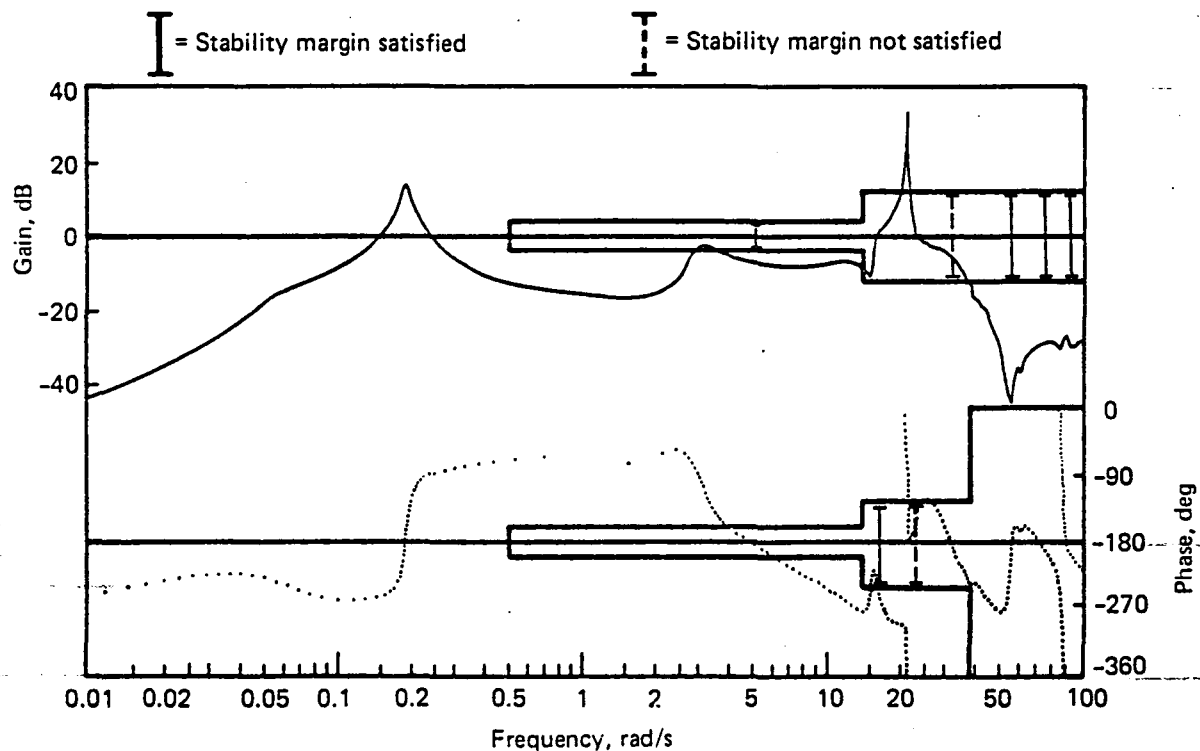
Figure F-83. Phase and Gain Margin, Aileron Loop, Filter Type B, Flight Condition 5
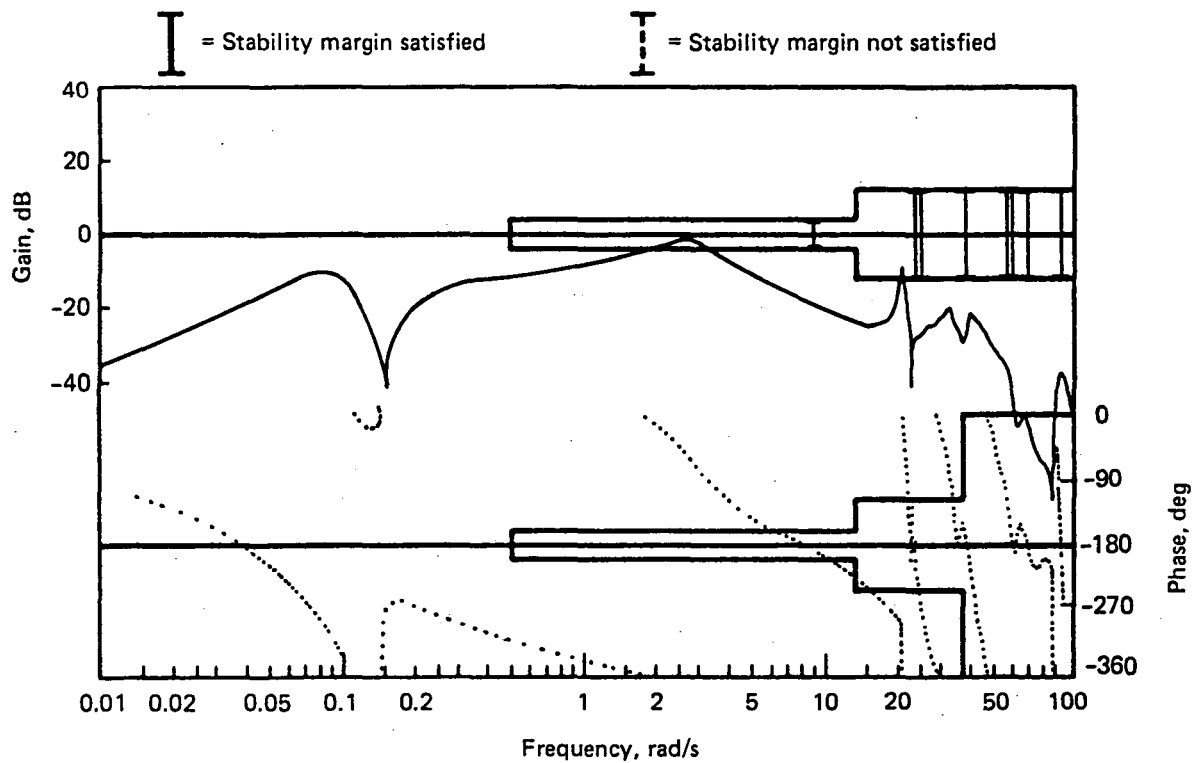
Figure F-84. Phase and Gain Margin, Elevator Loop, Filter Type B, Flight Condition 6
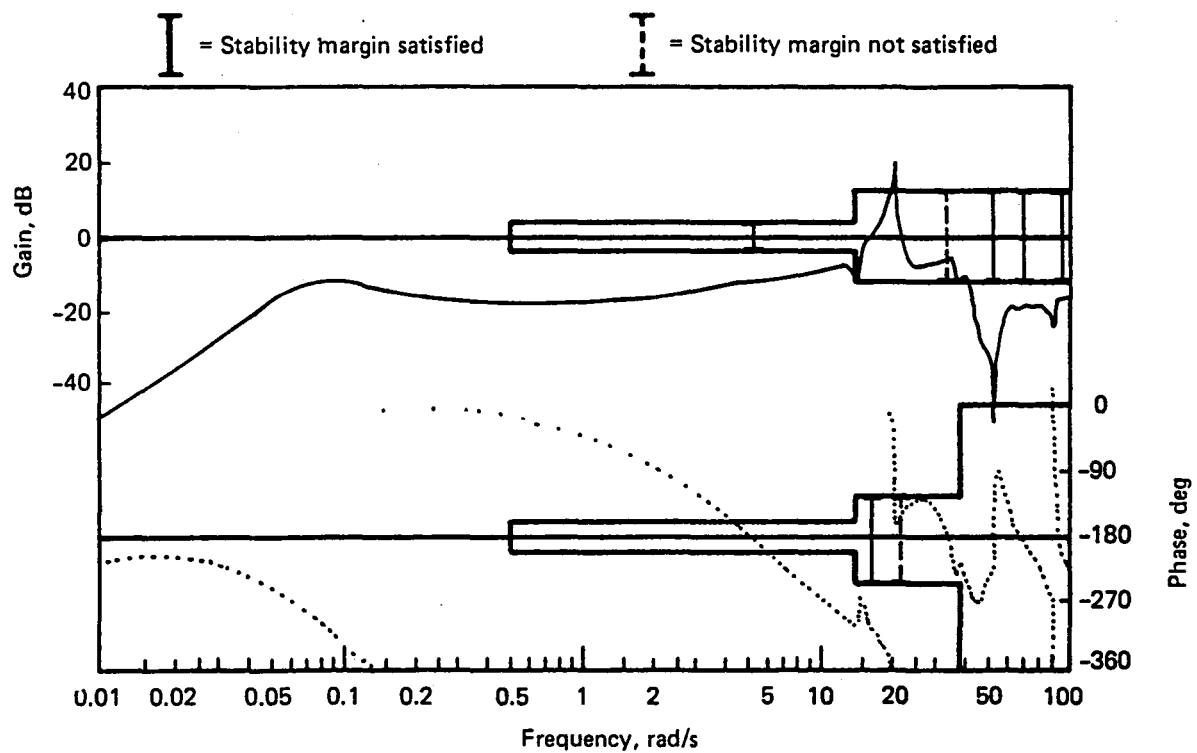
Figure F-85. Phase and Gain Margin, Aileron Loop, Filter Type B, Flight Condition 6
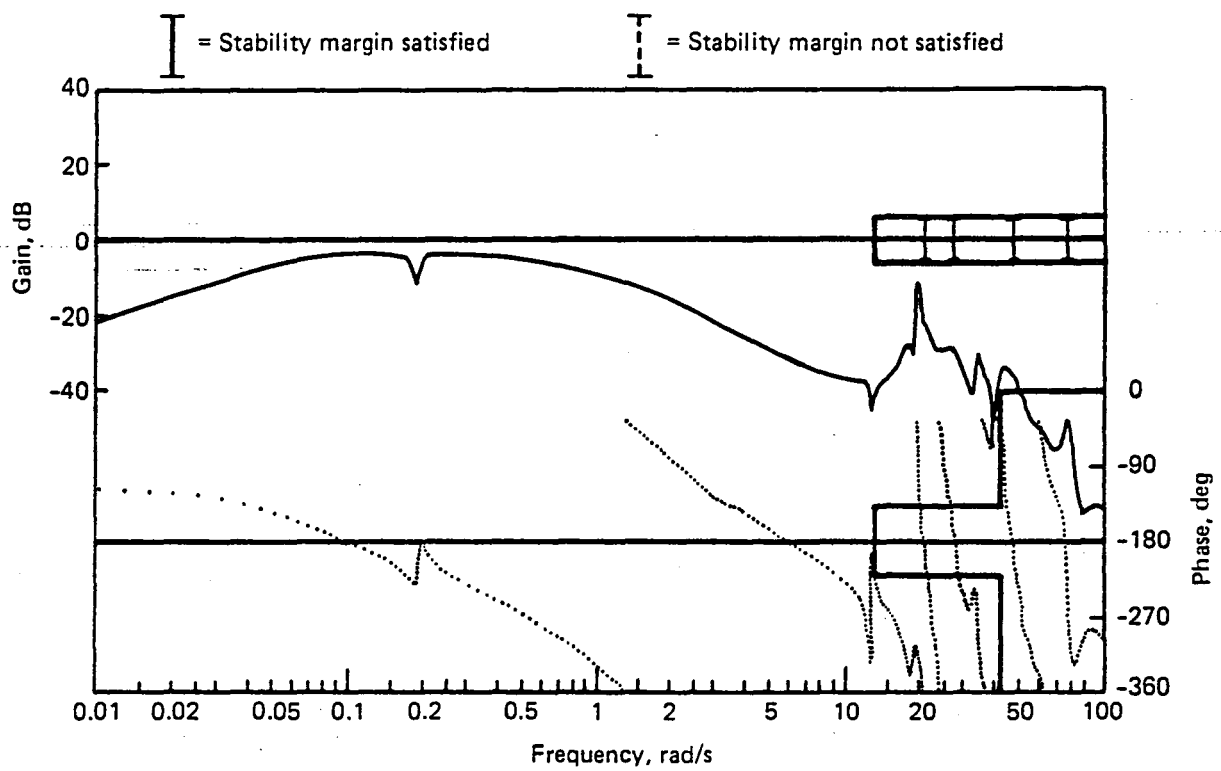
Figure F-86. Phase and Gain Margin, Elevator Loop, Filter Type B, Flight Condition 7
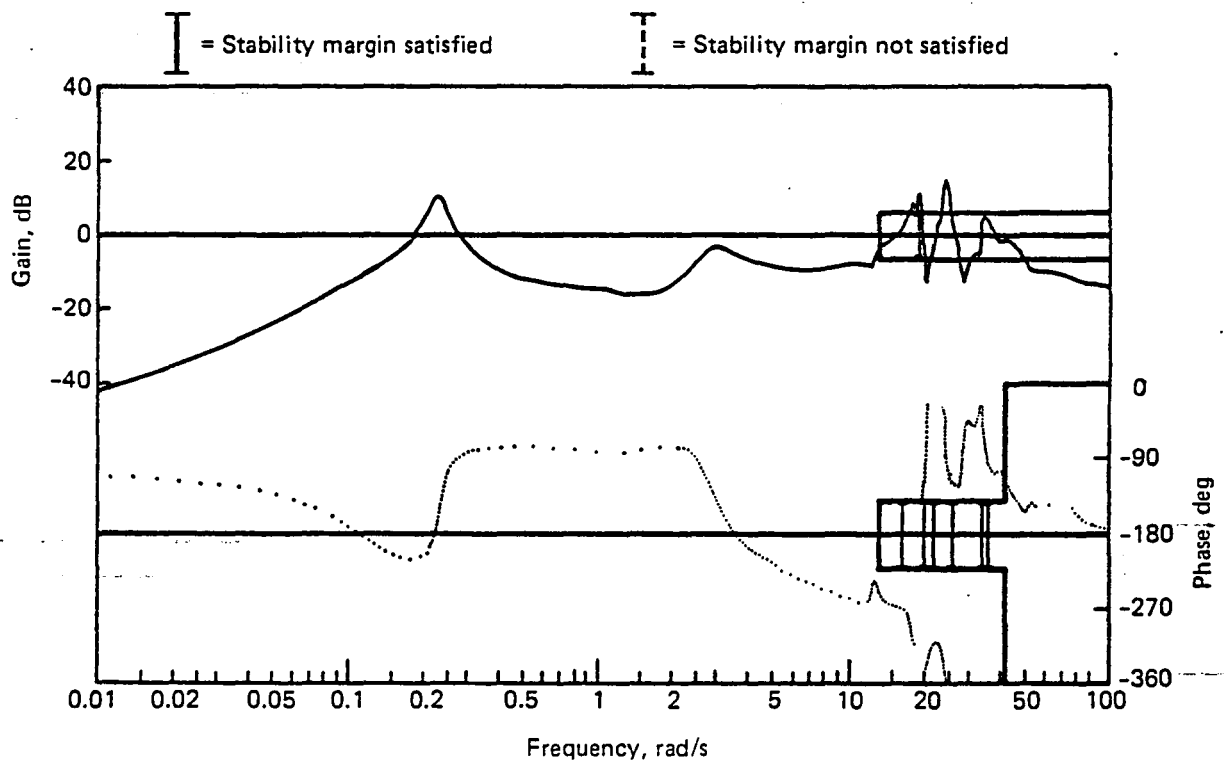
Figure F-87. Phase and Gain Margin, Aileron Loop, Filter Type B, Flight Condition 7
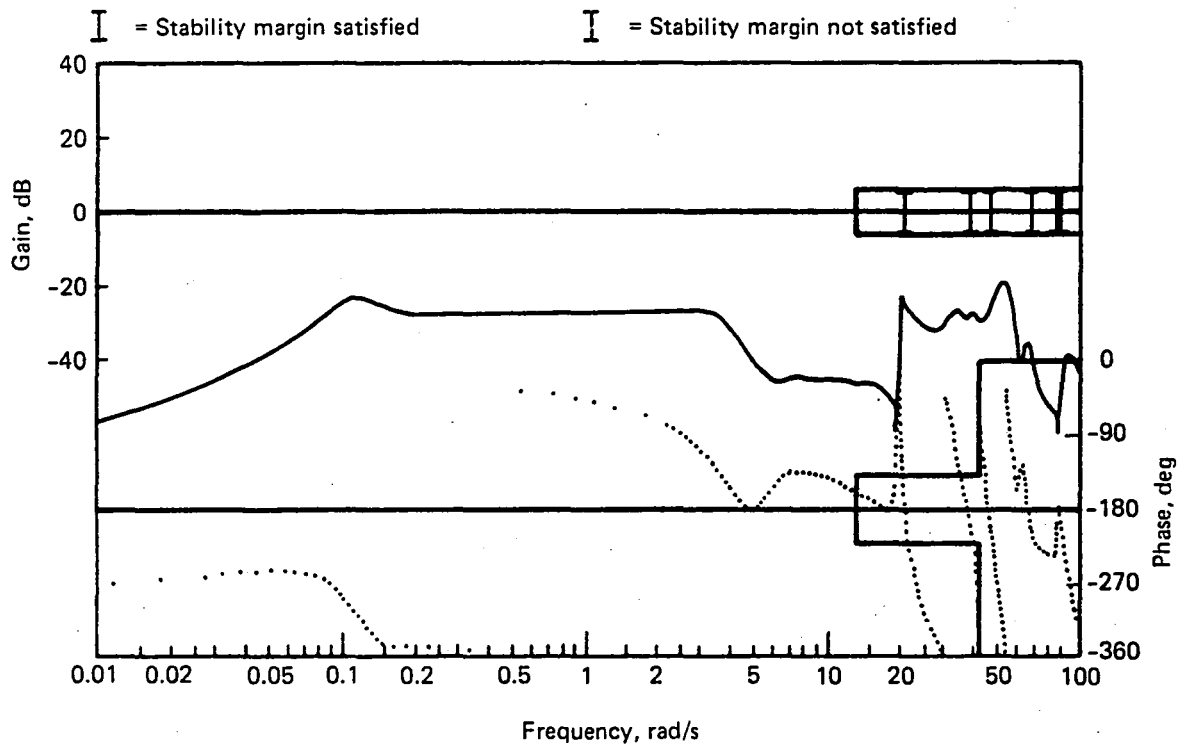
Figure F-88. Phase and Gain Margin, Elevator Loop, Filter Type B, Flight Condition 8
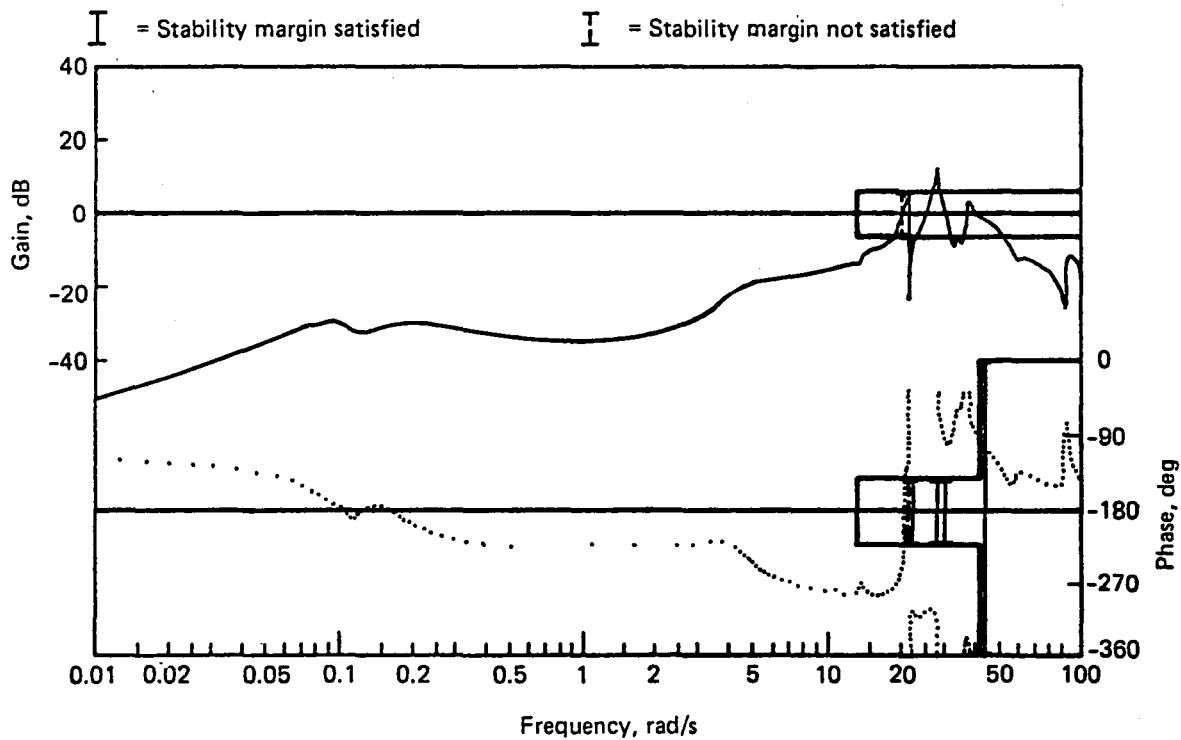
Figure F-89. Phase and Gain Margin, Aileron Loop, Filter Type B, Flight Condition 8
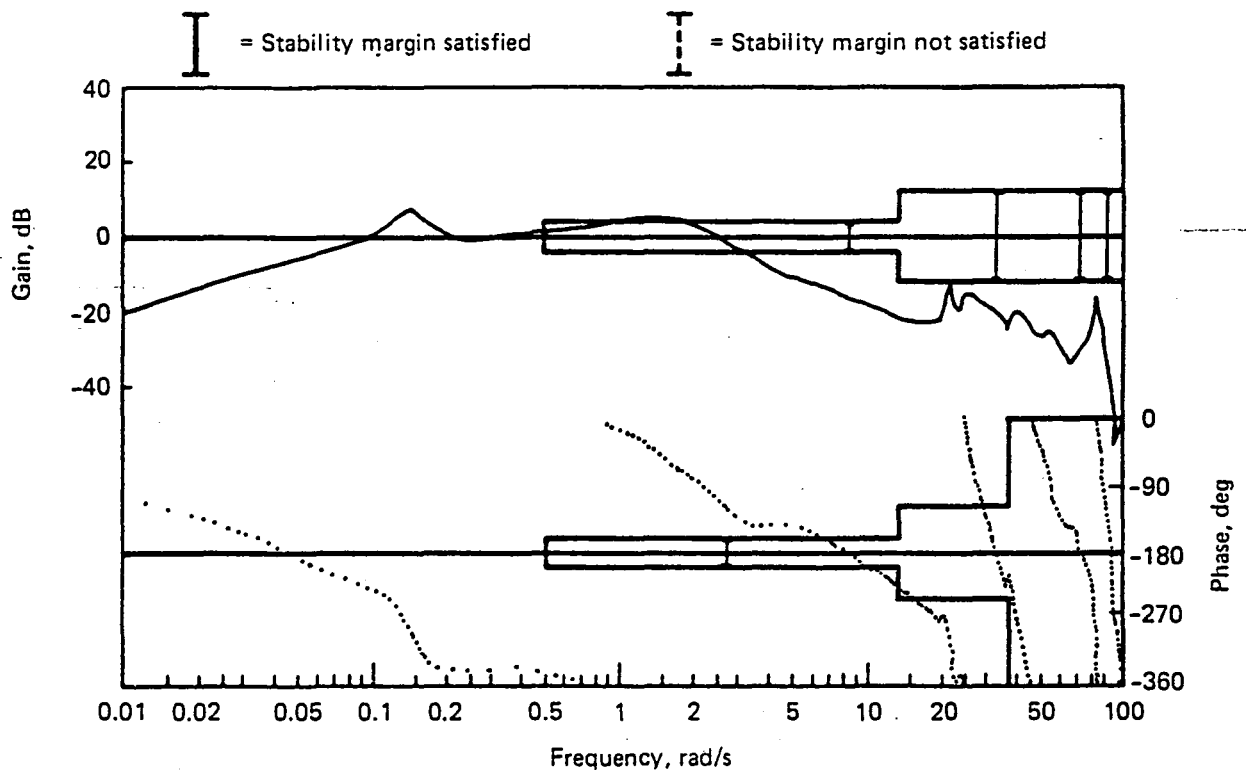
Figure F-90. Phase and Gain Margin, Elevator Loop, Filter Type C, Flight Condition 5
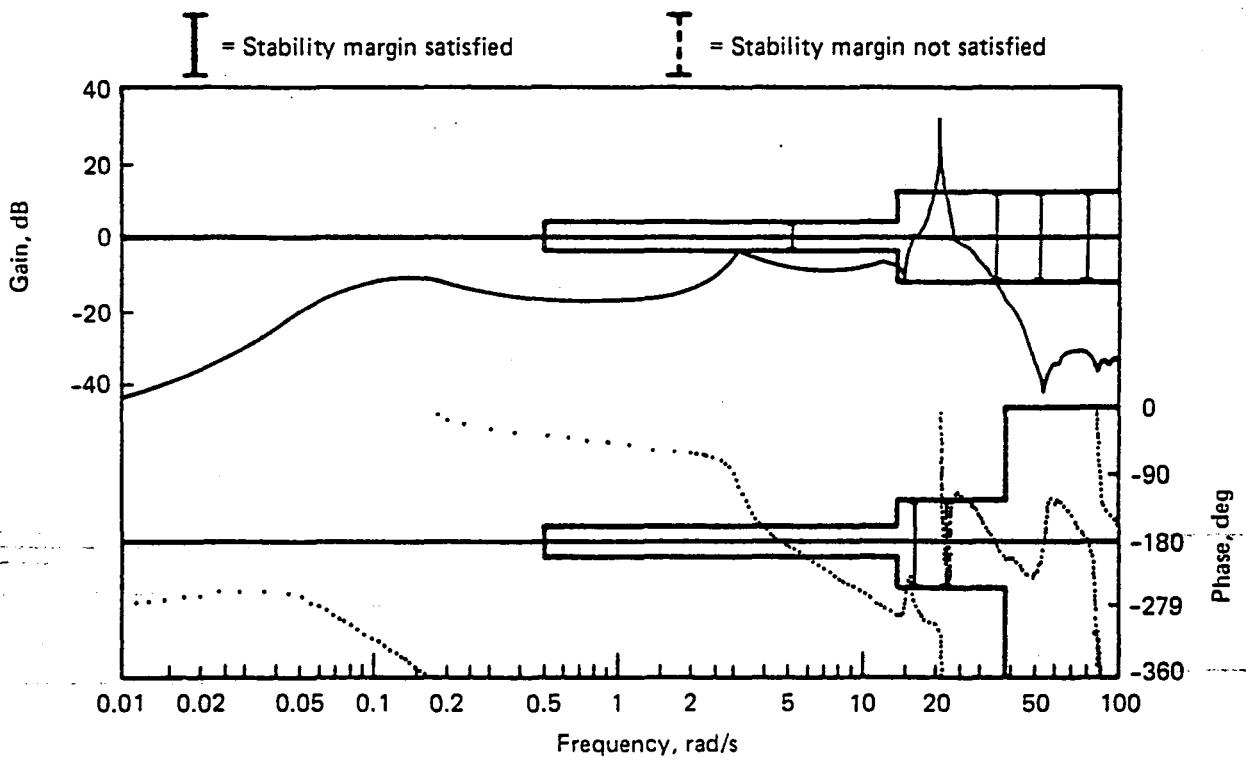
Figure F-91. Phase and Gain Margin, Aileron Loop, Filter Type C, Flight Condition 5
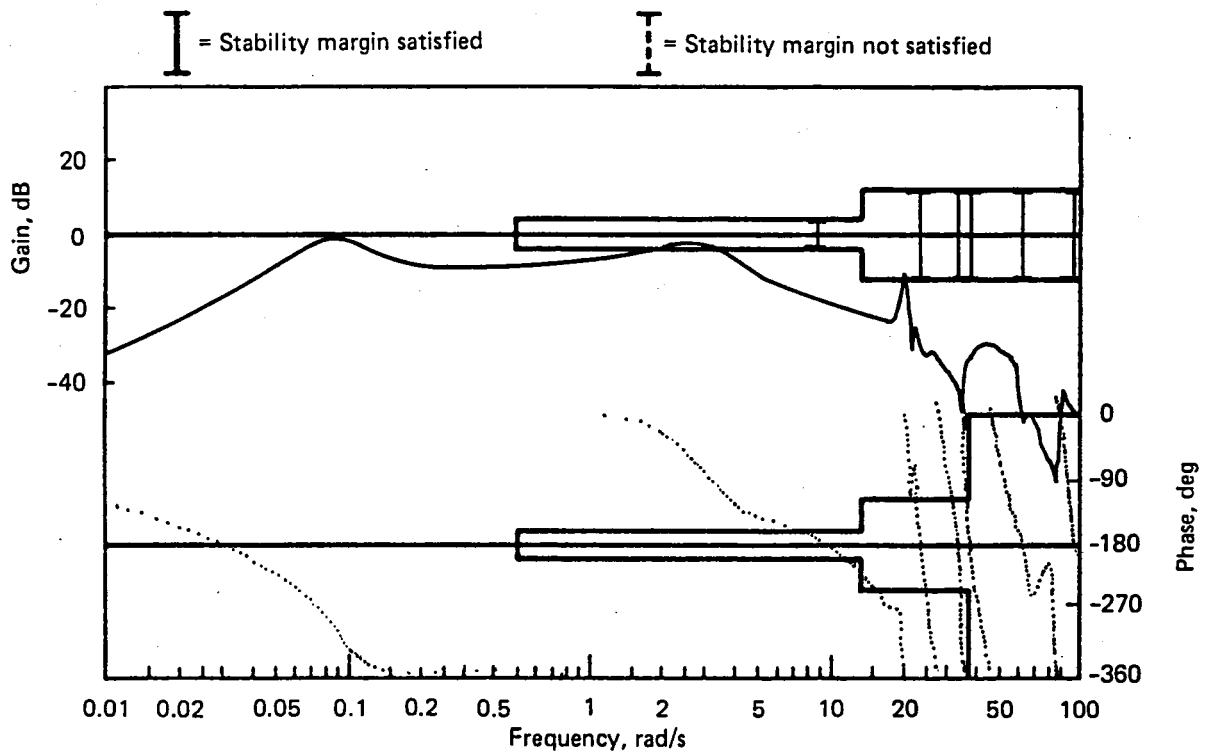
Figure F-92. Phase and Gain Margin, Elevator Loop, Filter Type C, Flight Condition 6
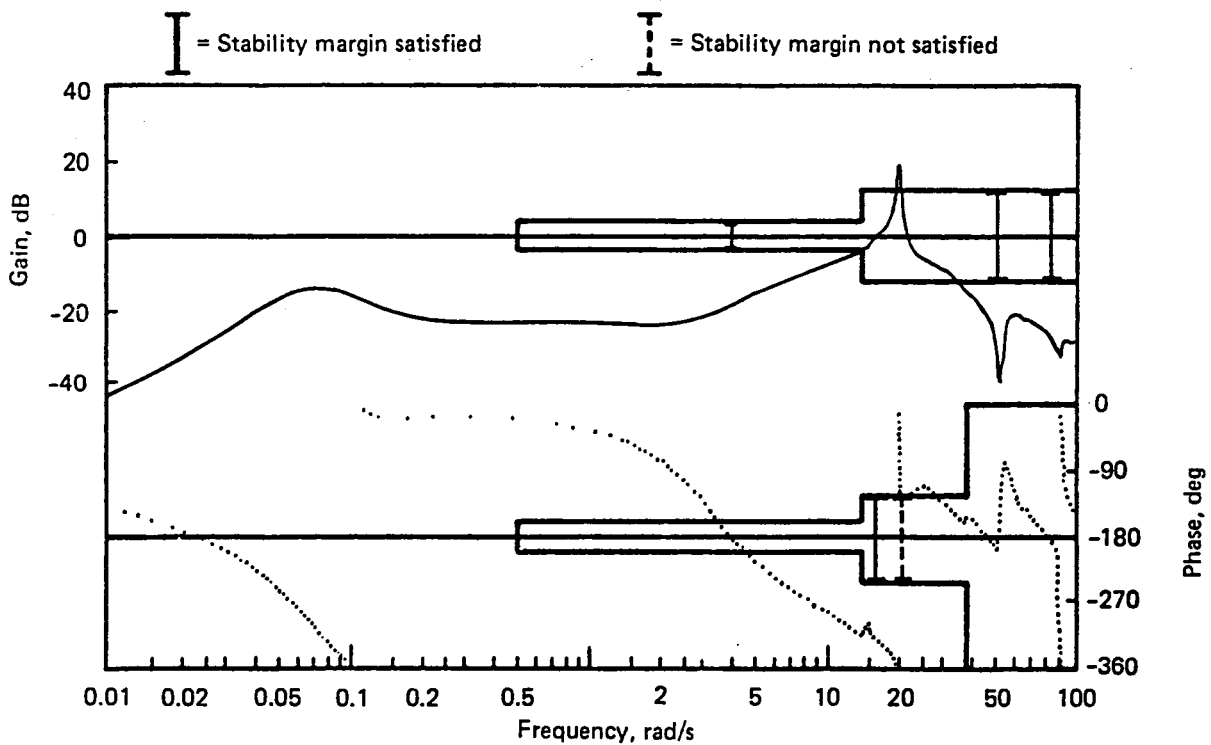
Figure F-93. Phase and Gain Margin, Aileron Loop, Filter Type C, Flight Condition 6

F-75
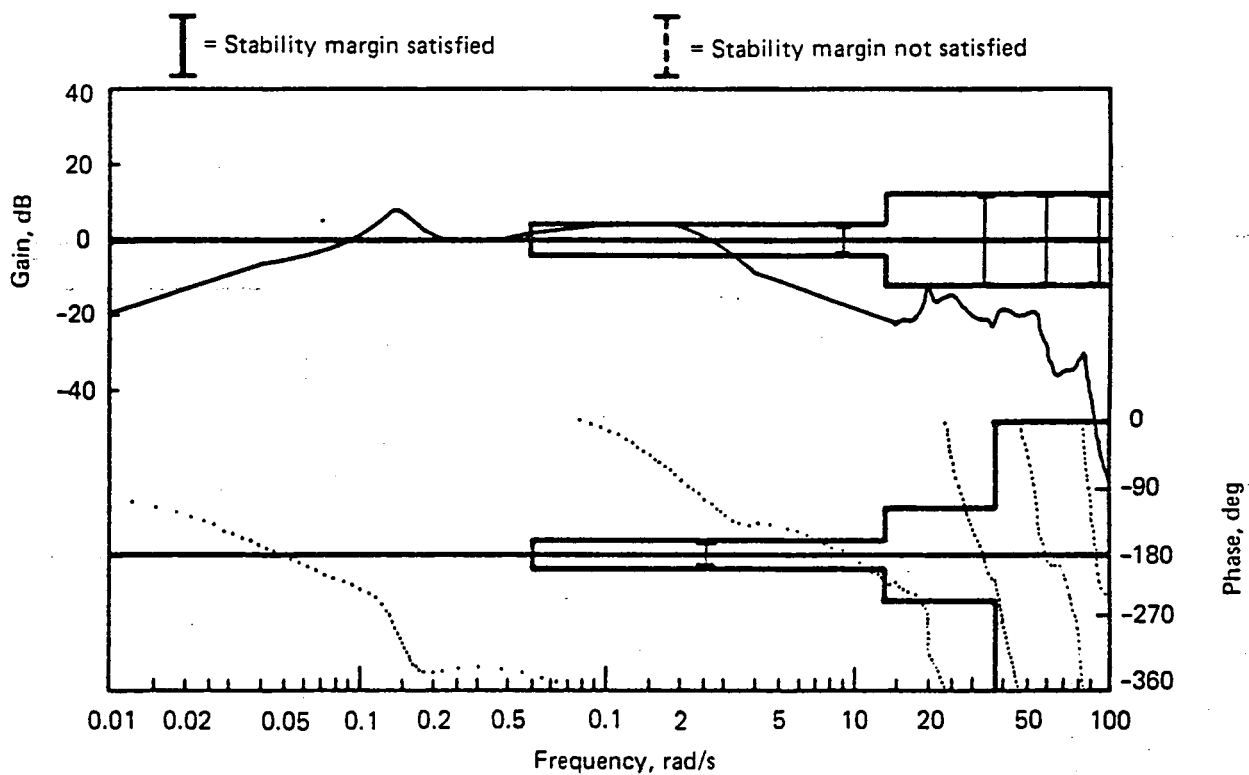
Figure F-94. Phase and Gain Margin, Elevator Loop, Filter Type D, Flight Condition 5
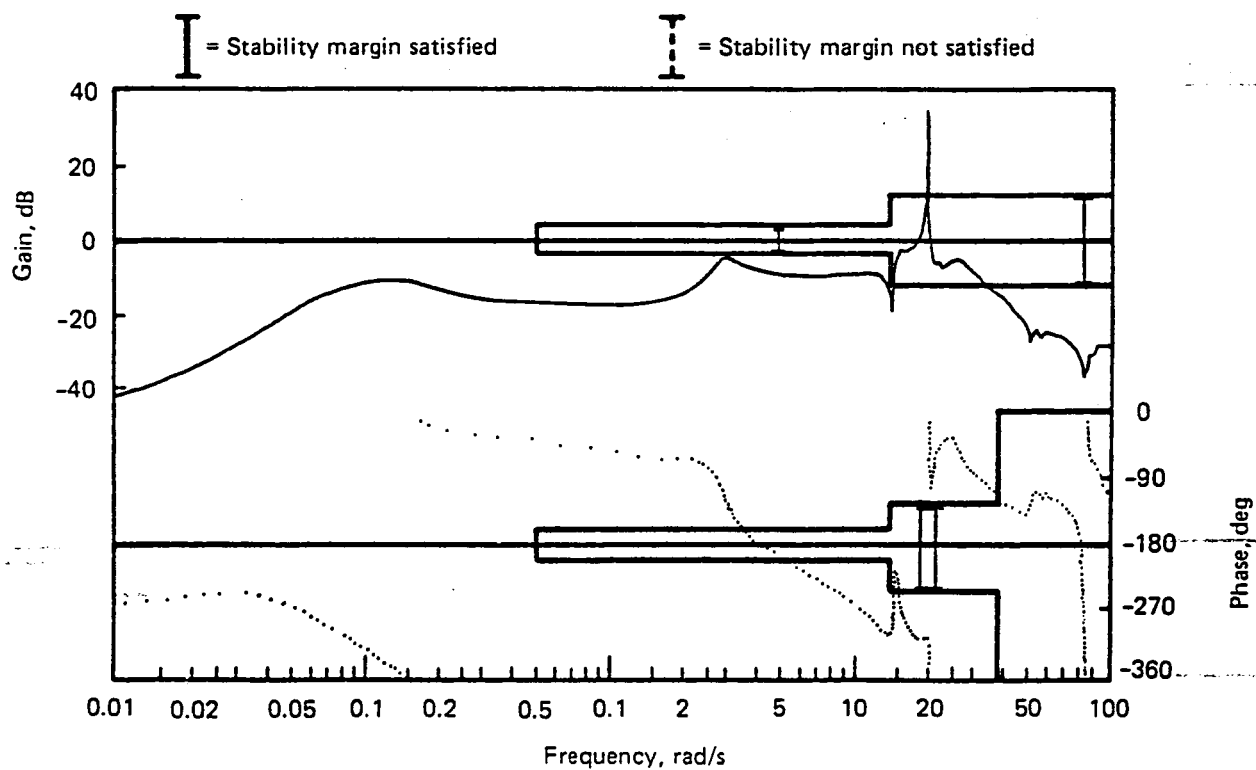
Figure F-95. Phase and Gain Margin, Aileron Loop, Filter Type D, Flight Condition 5
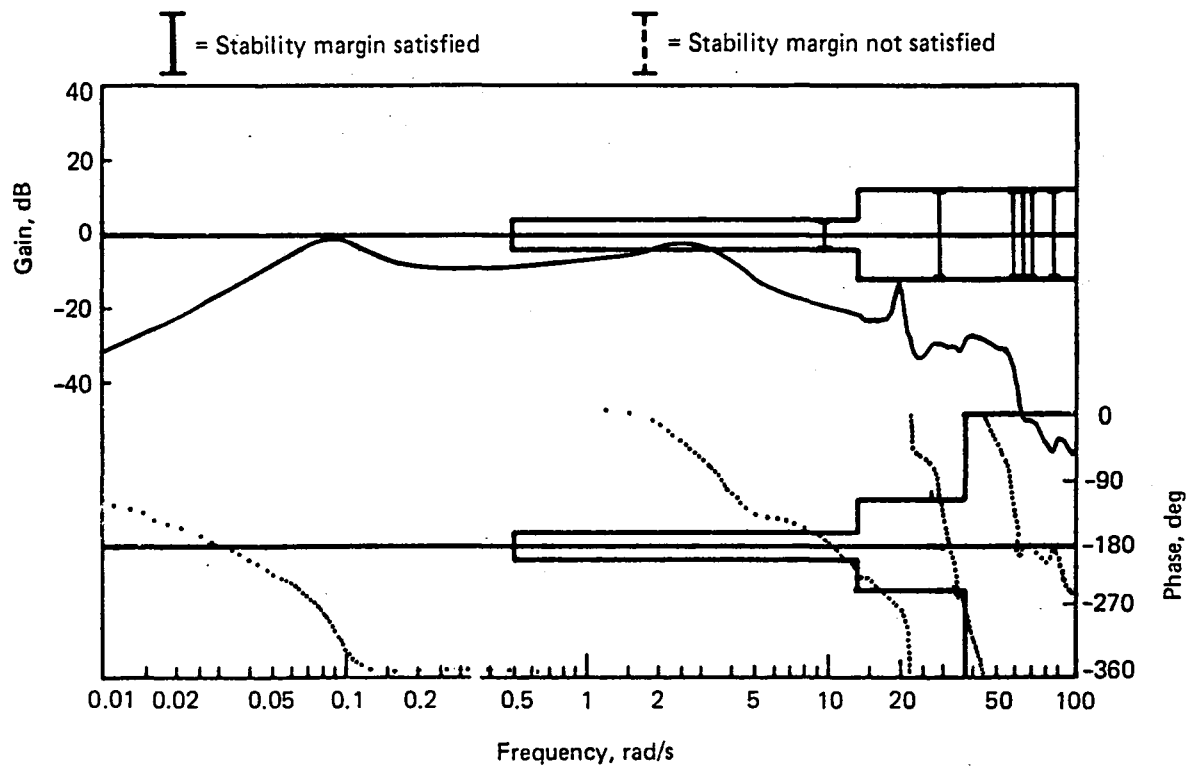
Figure F-96. Phase and Gain Margin, Elevator Loop, Filter Types D and G, Flight Condition 6
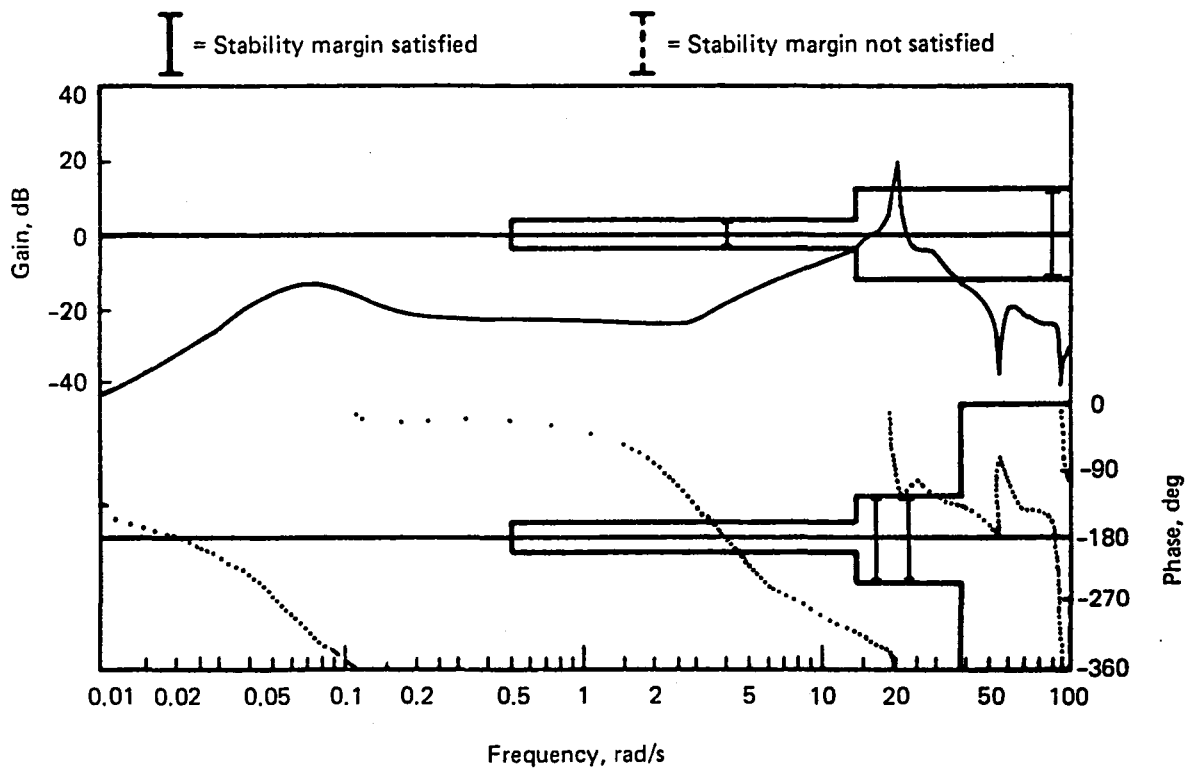
Figure F-97. Phase and Gain Margin, Aileron Loop, Filter Types D and G, Flight Condition 6
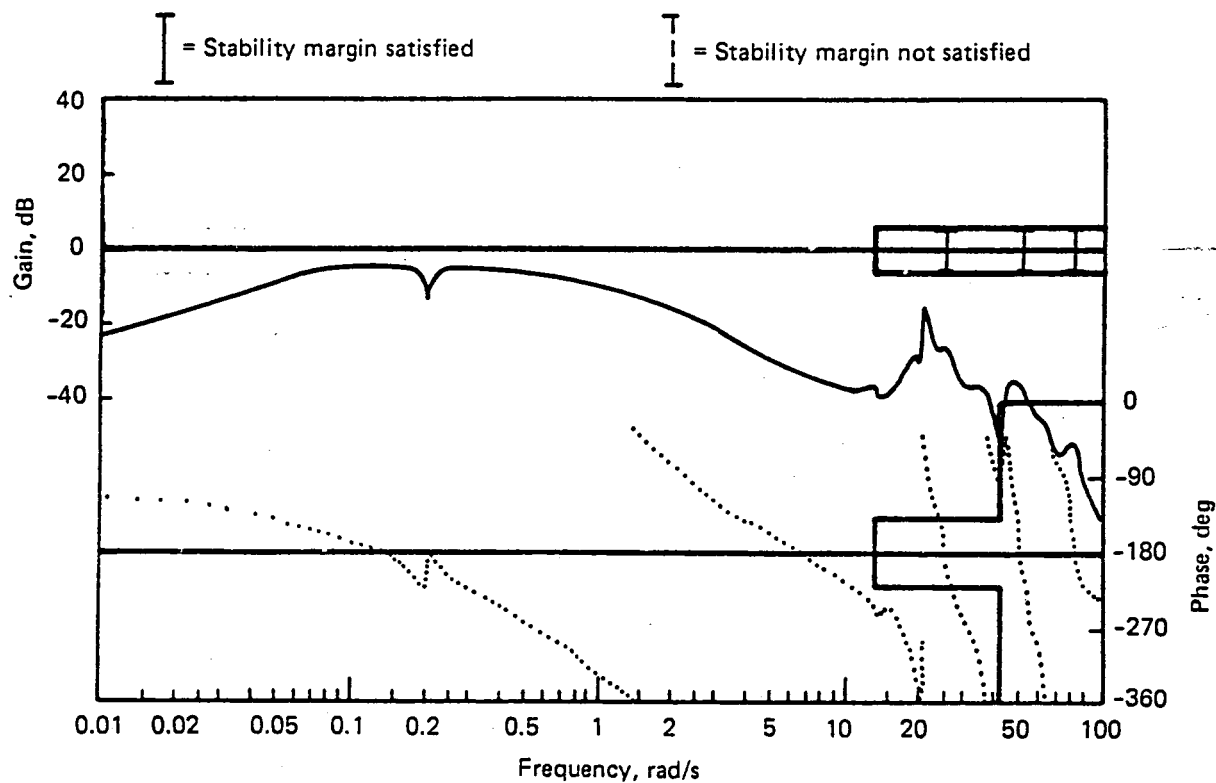
Figure F-98. Phase and Gain Margin, Elevator Loop, Filter Type D, Flight Condition 7
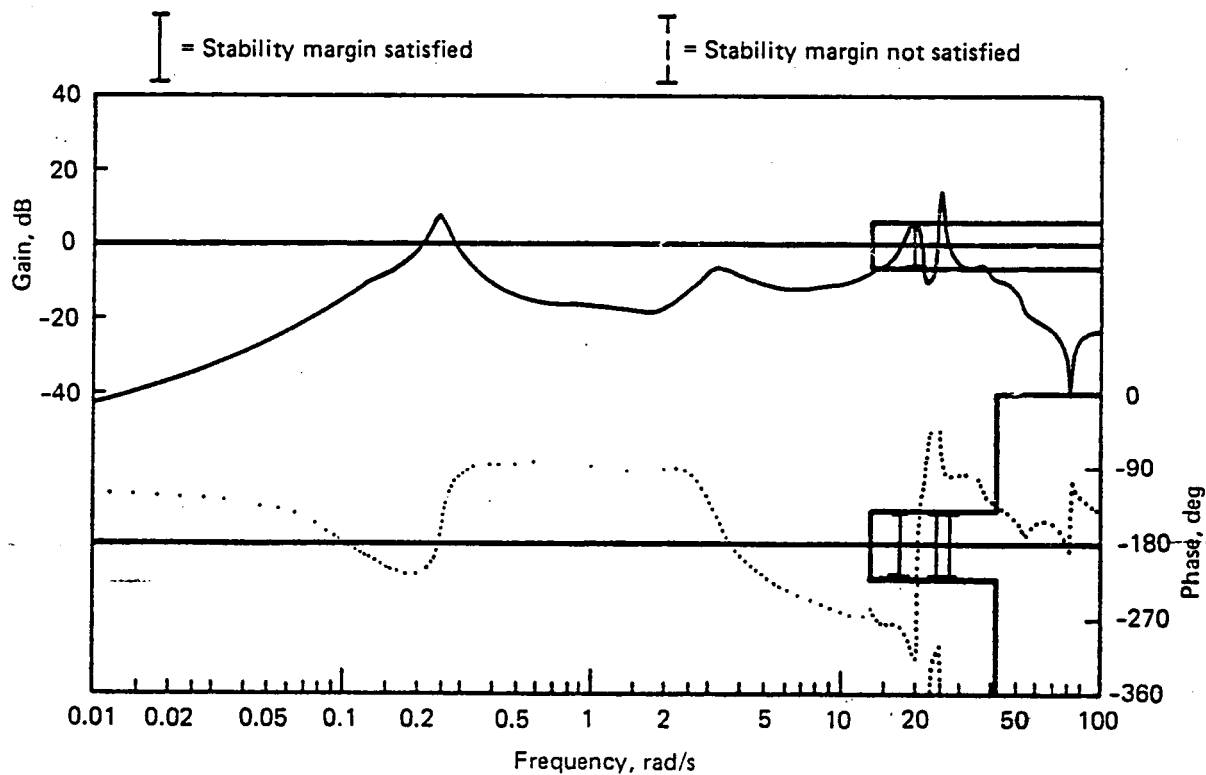
Figure F-99. Phase and Gain Margin, Aileron Loop, Filter Type D, Flight Condition 7

F-78
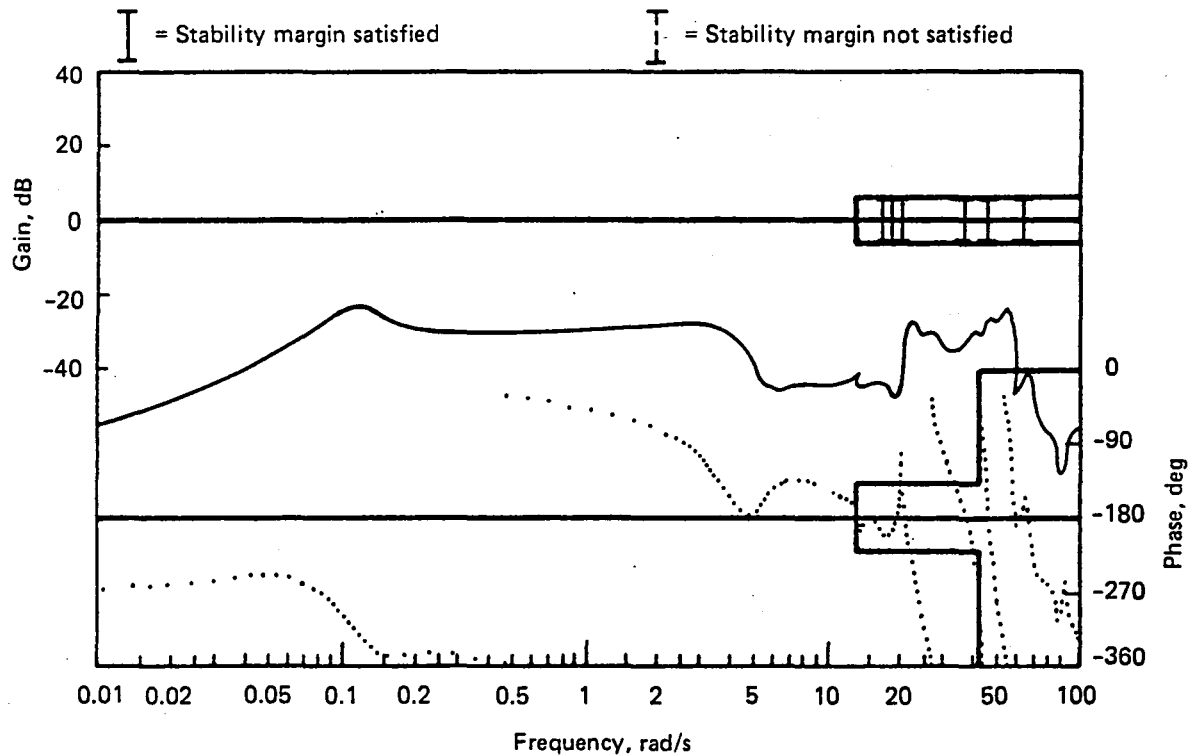
Figure F-100. Phase and Gain Margin, Elevator Loop, Filter Type D, Flight Condition 8
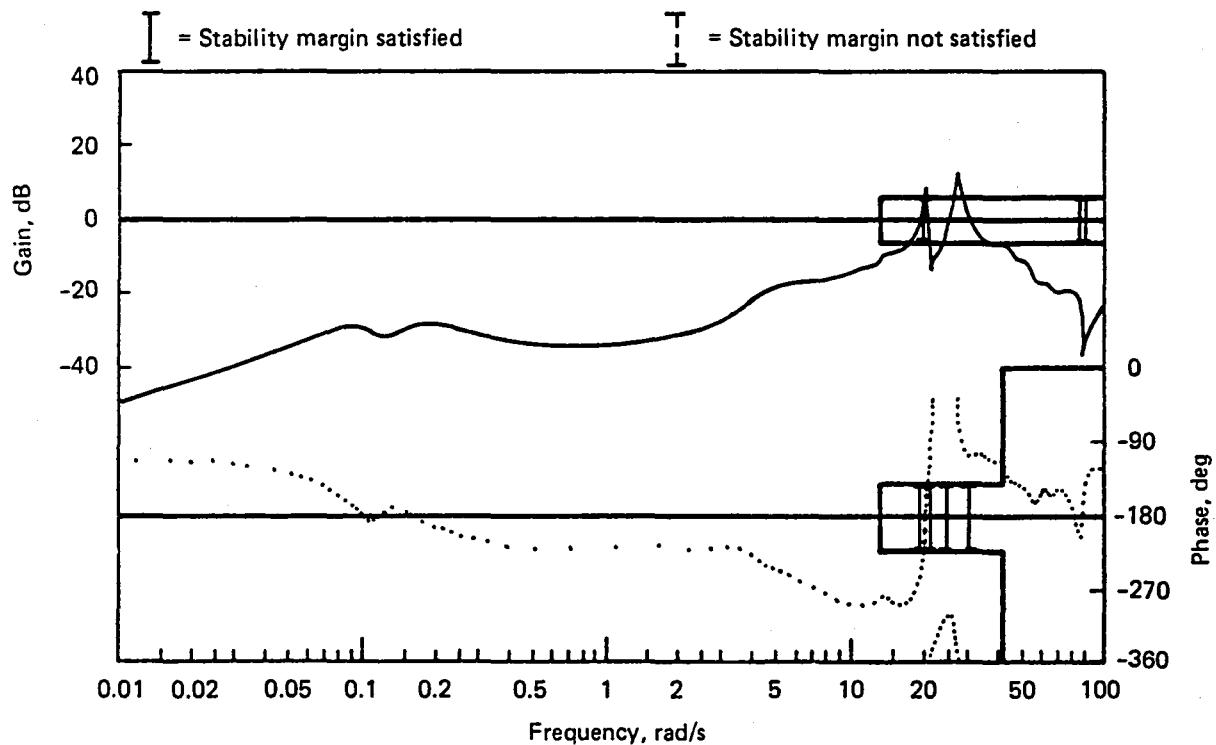
Figure F-101. Phase and Gain Margin, Aileron Loop, Filter Type D, Flight Condition 8
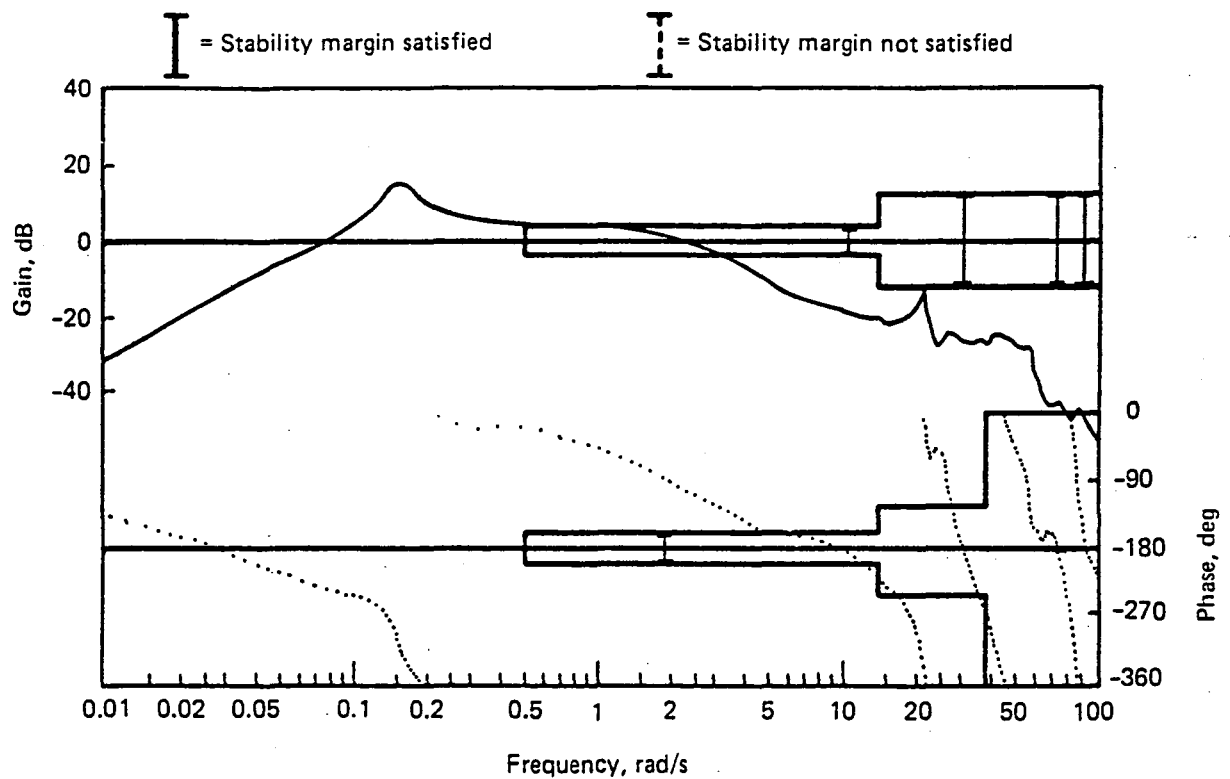
Figure F-102. Phase and Gain Margin, Elevator Loop, Filter Type G, Flight Condition 5
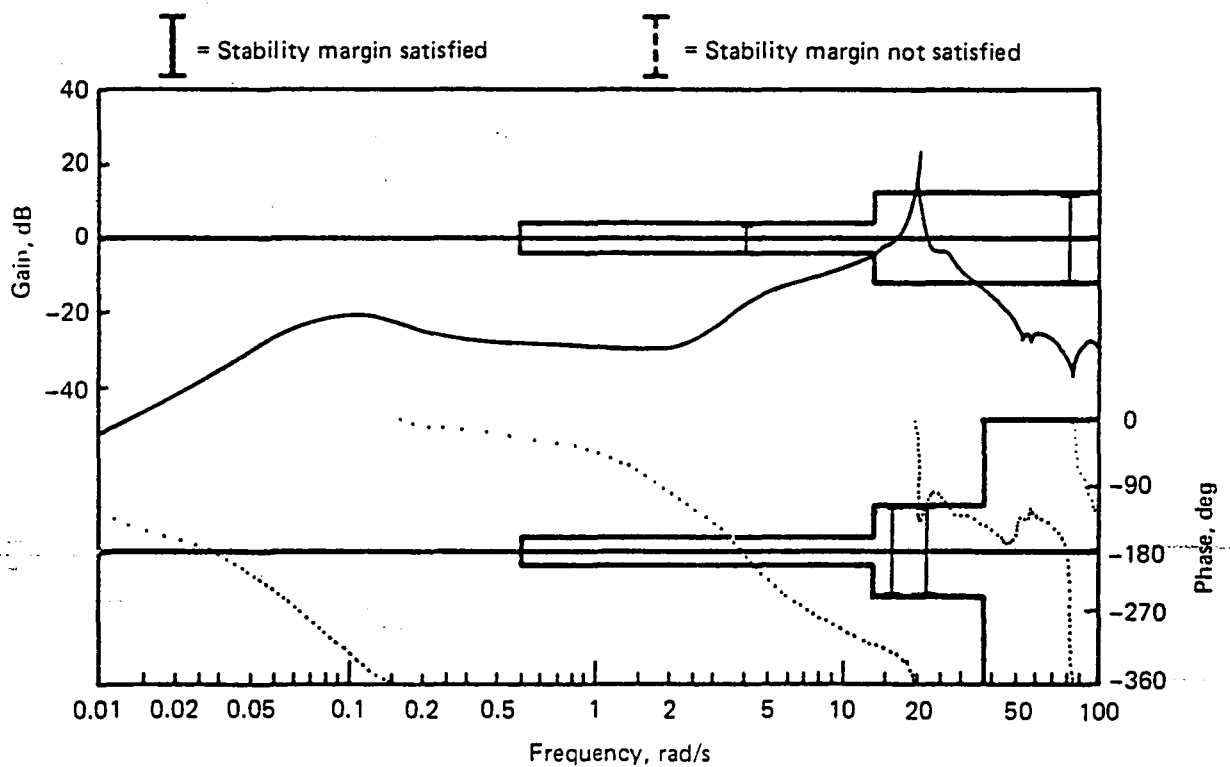
Figure F-103. Phase and Gain Margin, Aileron Loop, Filter Type G, Flight Condition 5
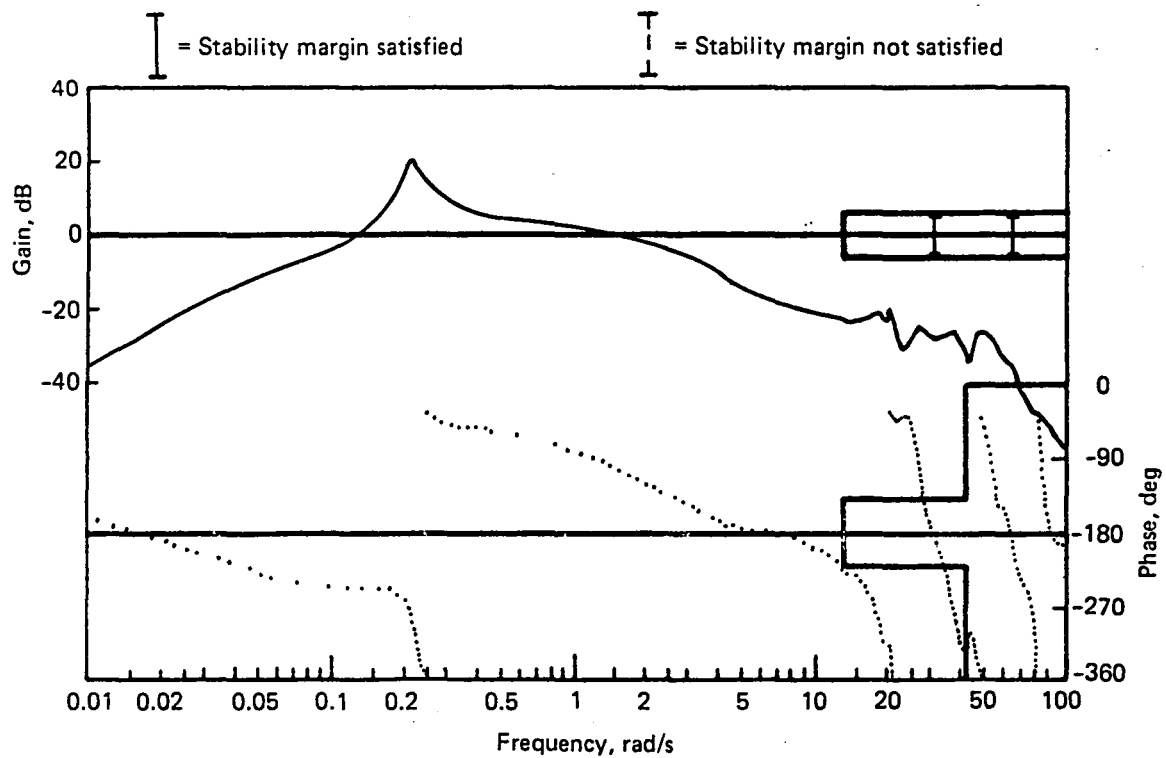
Figure F-104. Phase and Gain Margin, Elevator Loop, Filter Type G, Flight Condition 7
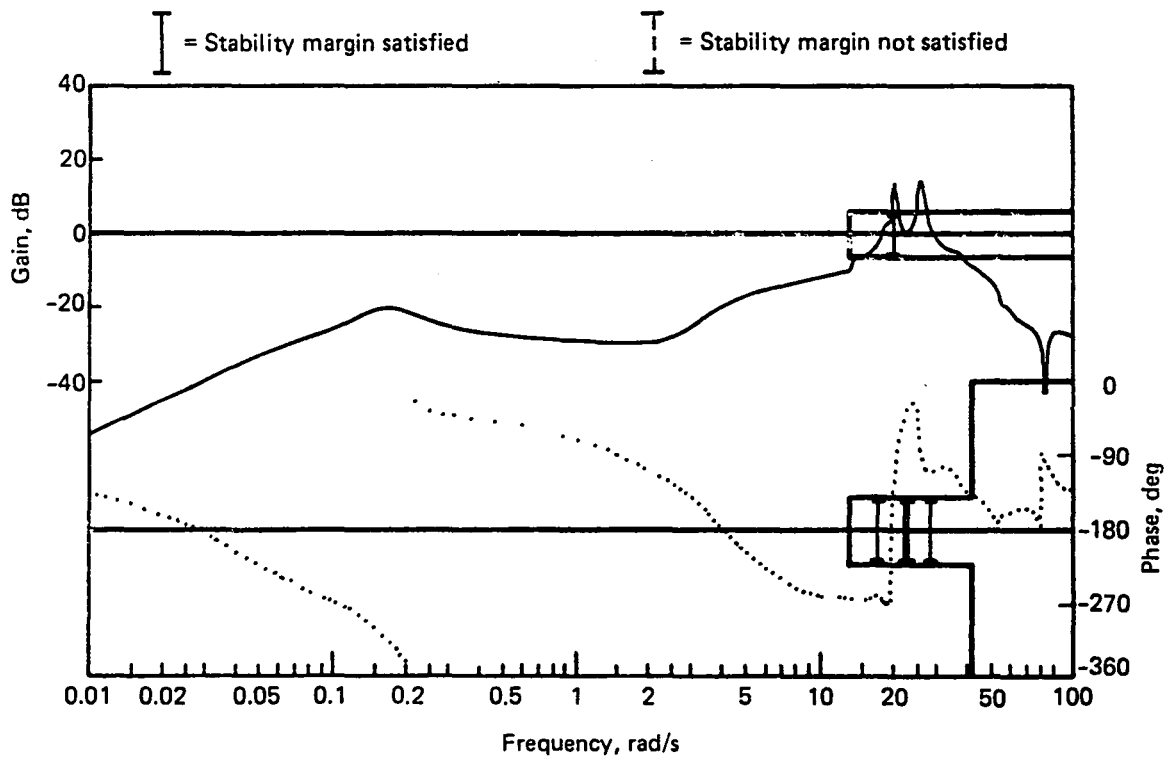
Figure F-105. Phase and Gain Margin, Aileron Loop, Filter Type G, Flight Condition 7
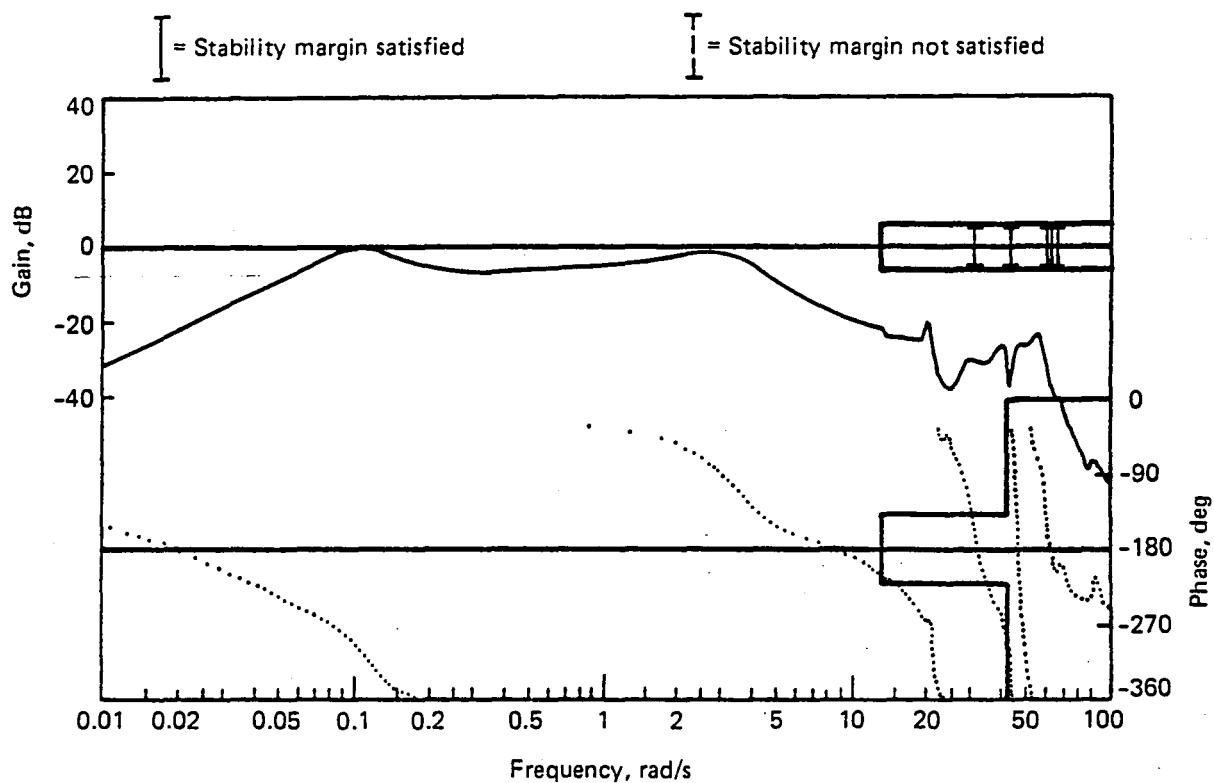
Figure F-106. Phase and Gain Margin, Elevator Loop, Filter Type G, Flight Condition 8
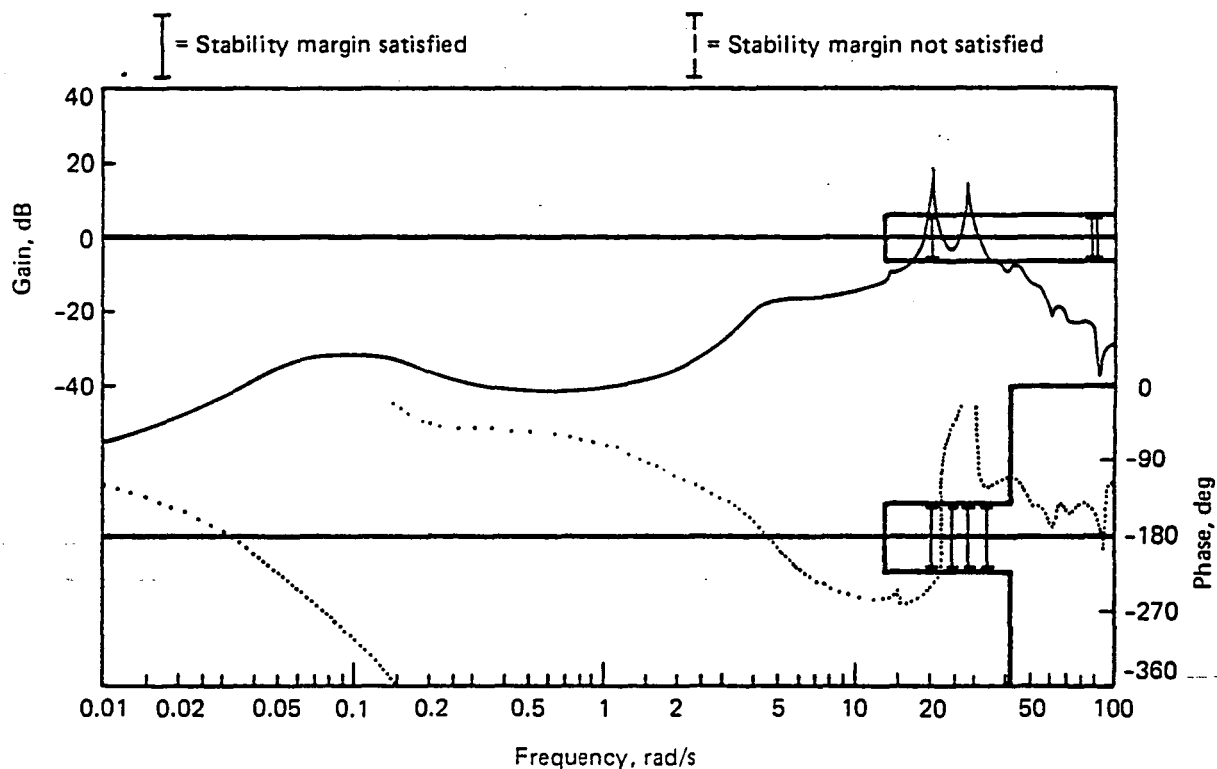
Figure F-107. Phase and Gain Margin, Aileron Loop, Filter Type G, Flight Condition 8
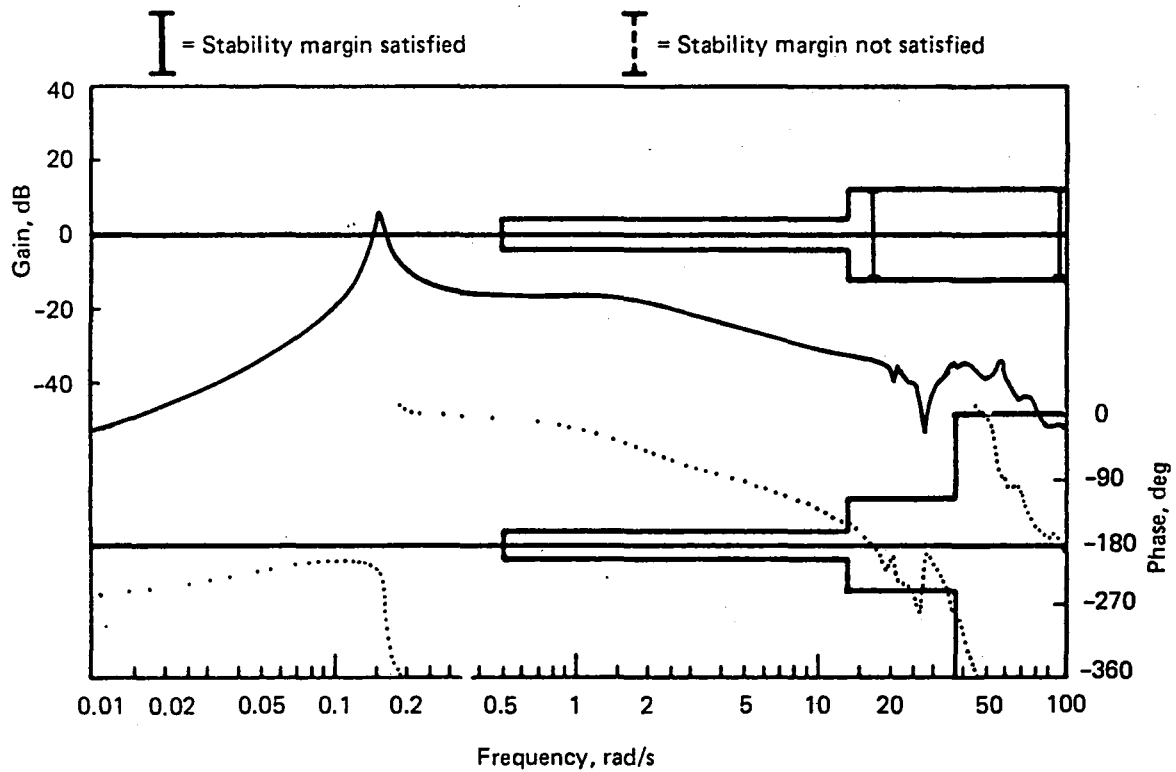
Figure F-108. Phase and Gain Margin, Elevator Loop, Filter Type H, Flight Condition 5
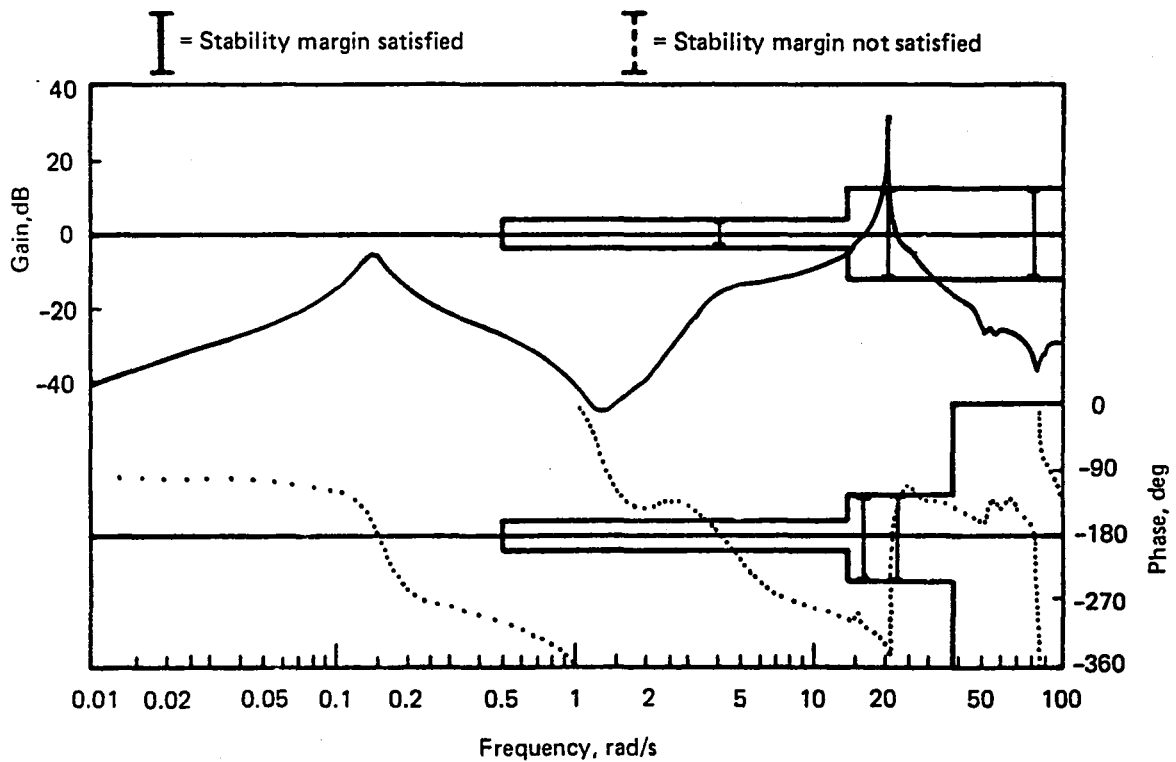
Figure F-109. Phase and Gain Margin, Aileron Loop, Filter Type H, Flight Condition 5
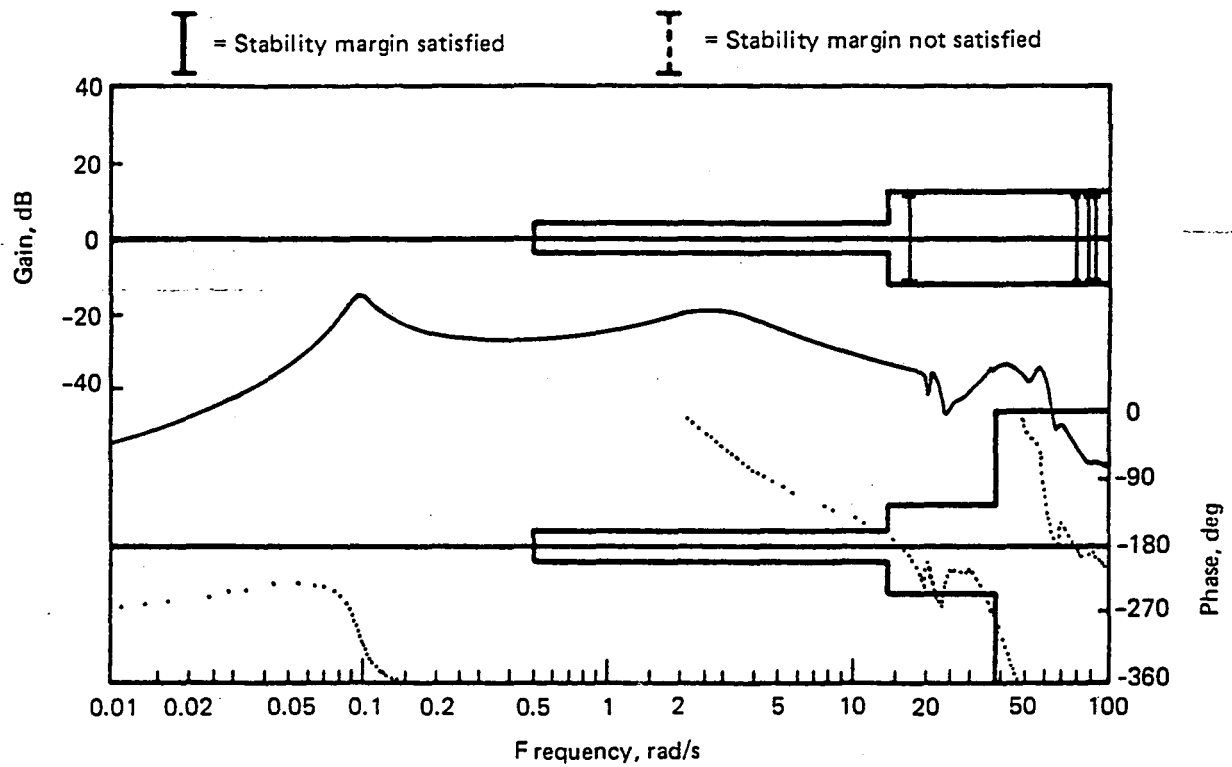
Figure F-110. Phase and Gain Margin, Elevator Loop, Filter Type H, Flight Condition 6
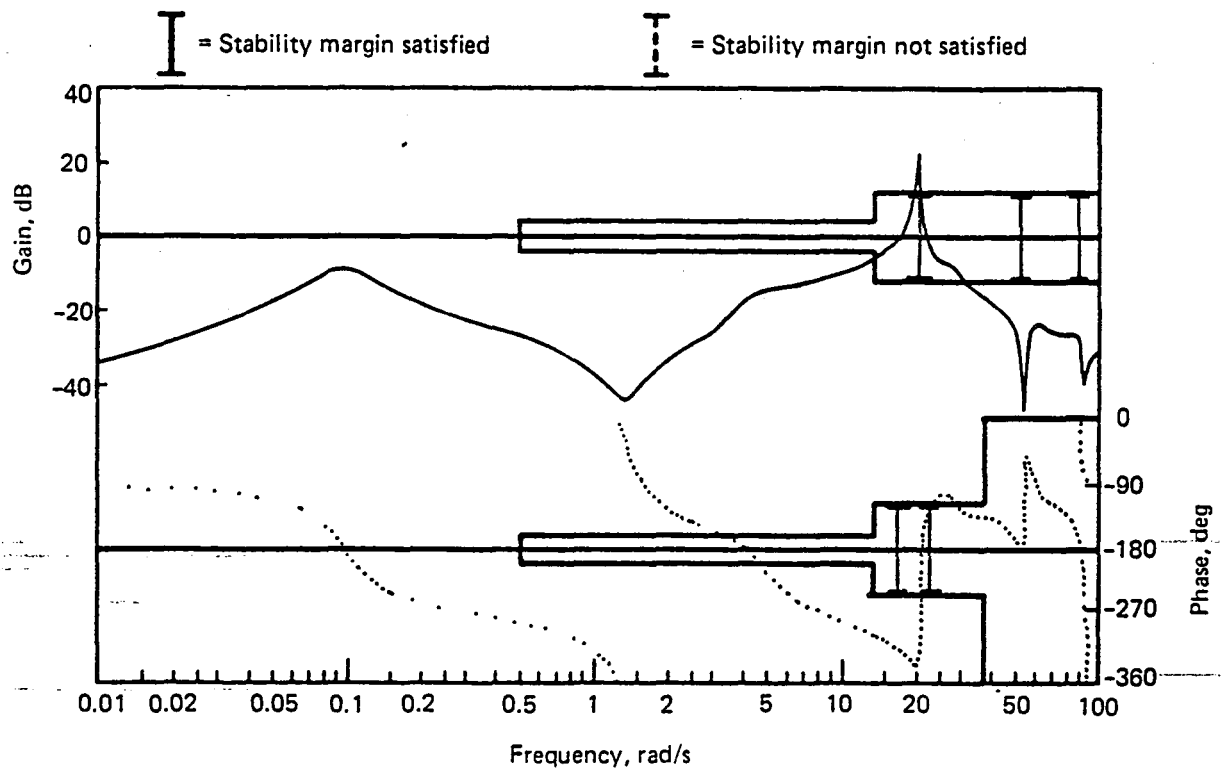
Figure F-111. Phase and Gain Margin, Aileron Loop, Filter Type H, Flight Condition 6
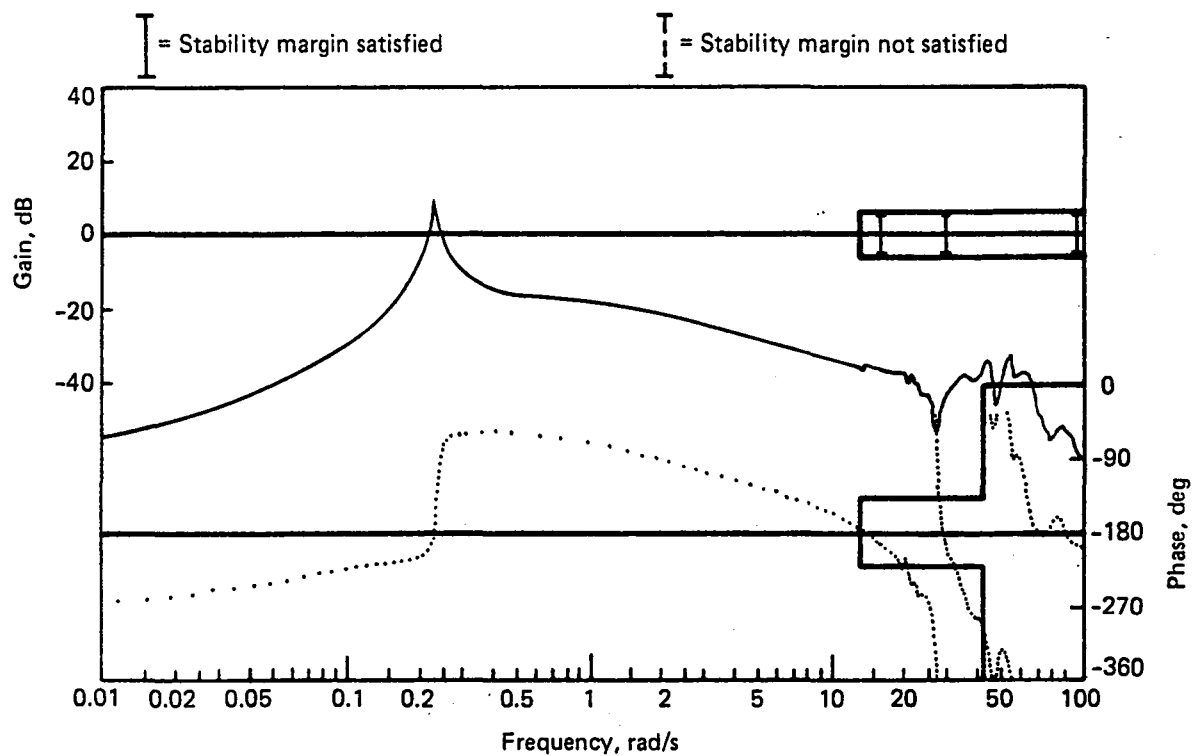
Figure F-112. Phase and Gain Margin, Elevator Loop, Filter Type H, Flight Condition 7
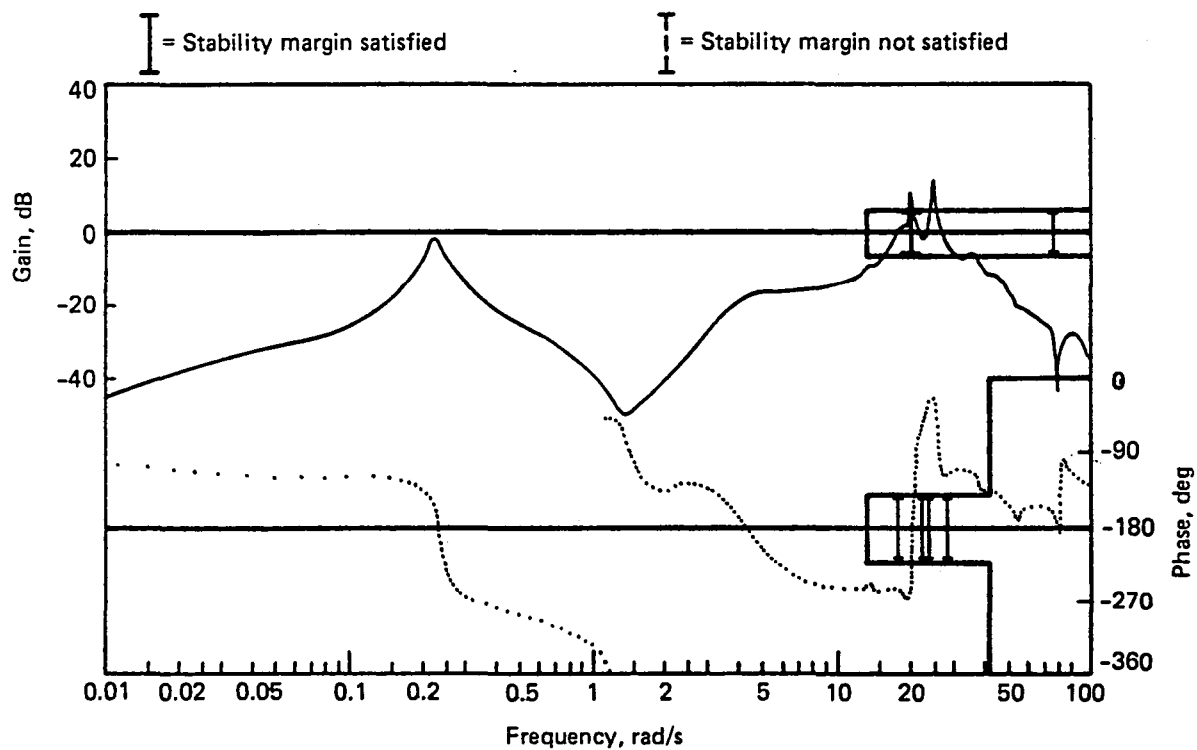
Figure F-113. Phase and Gain Margin, Aileron Loop, Filter Type H, Flight Condition 7
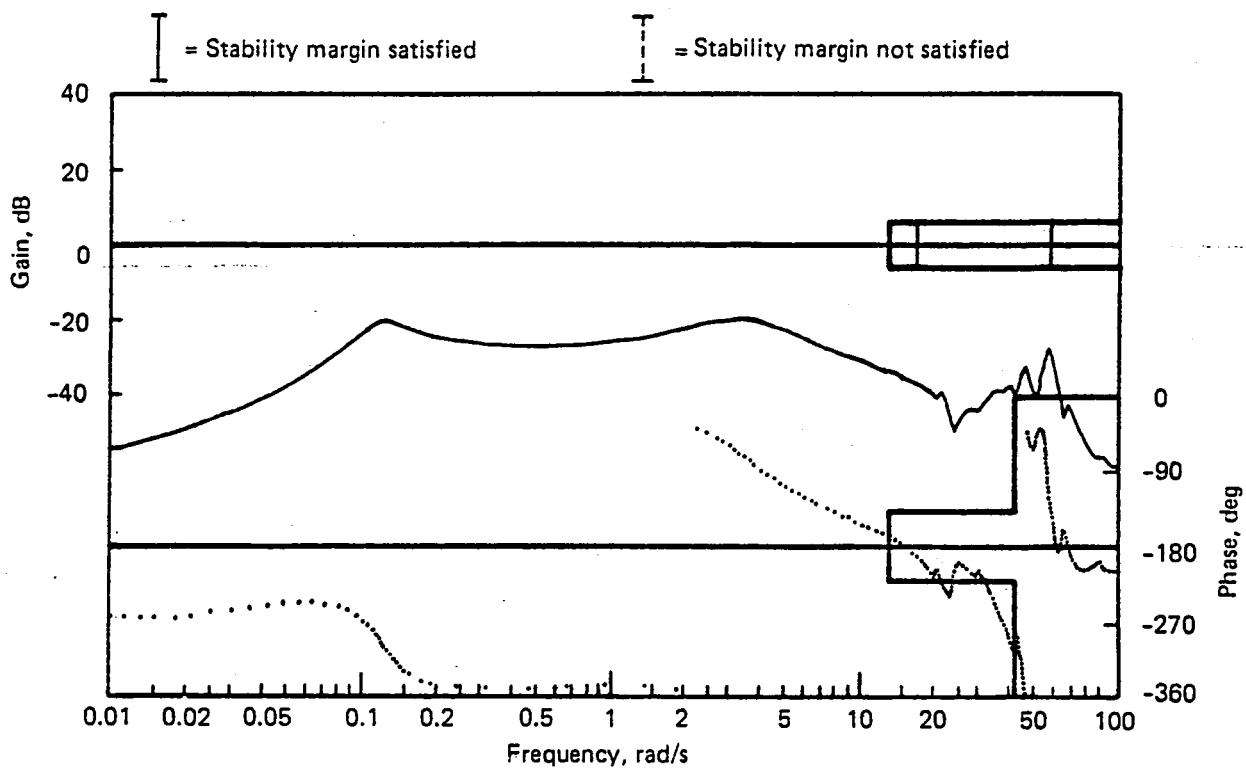
Figure F-114. Phase and Gain Margin, Elevator Loop, Filter Type H, Flight Condition 8
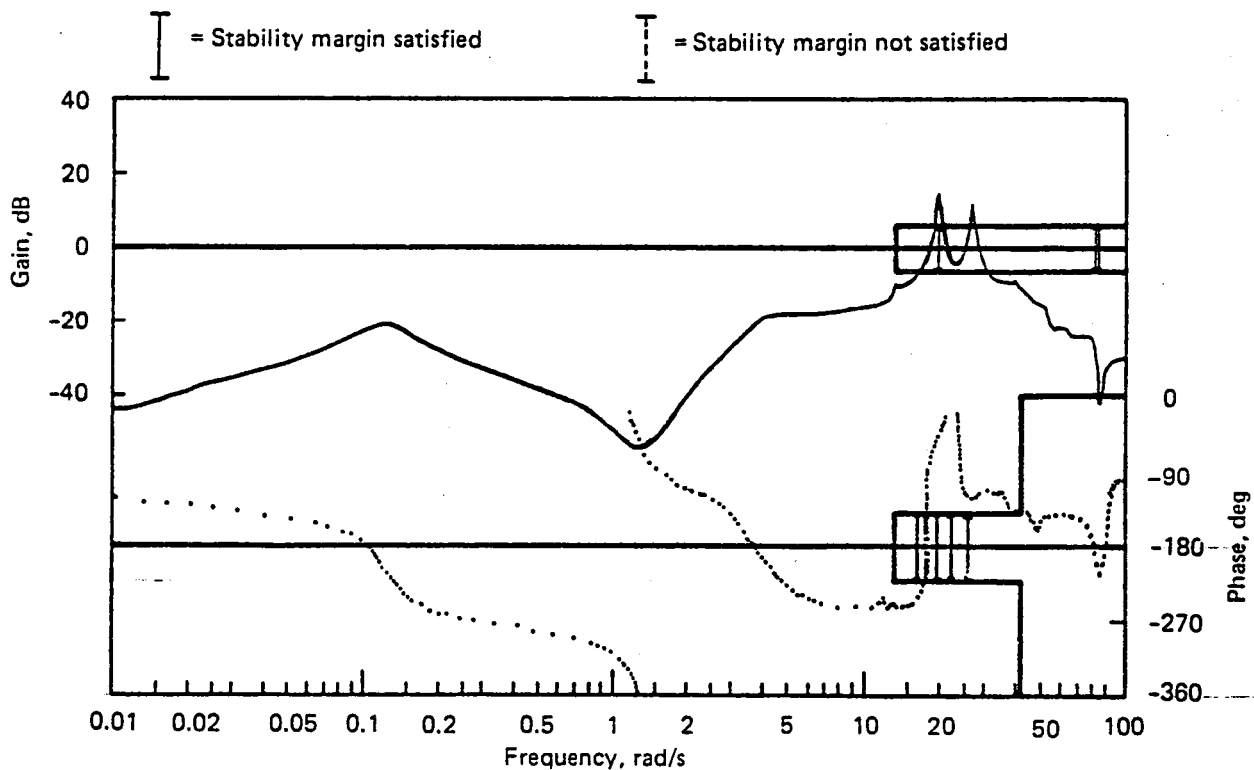
Figure F-115. Phase and Gain Margin, Aileron Loop, Filter Type H, Flight Condition 8

F.4.2.3 POWER-SPECTRAL-DENSITY PLOTS

Figures F-116 through F-131 are PSD plots of elevator and aileron deflections and rates at the various flutter flight conditions.
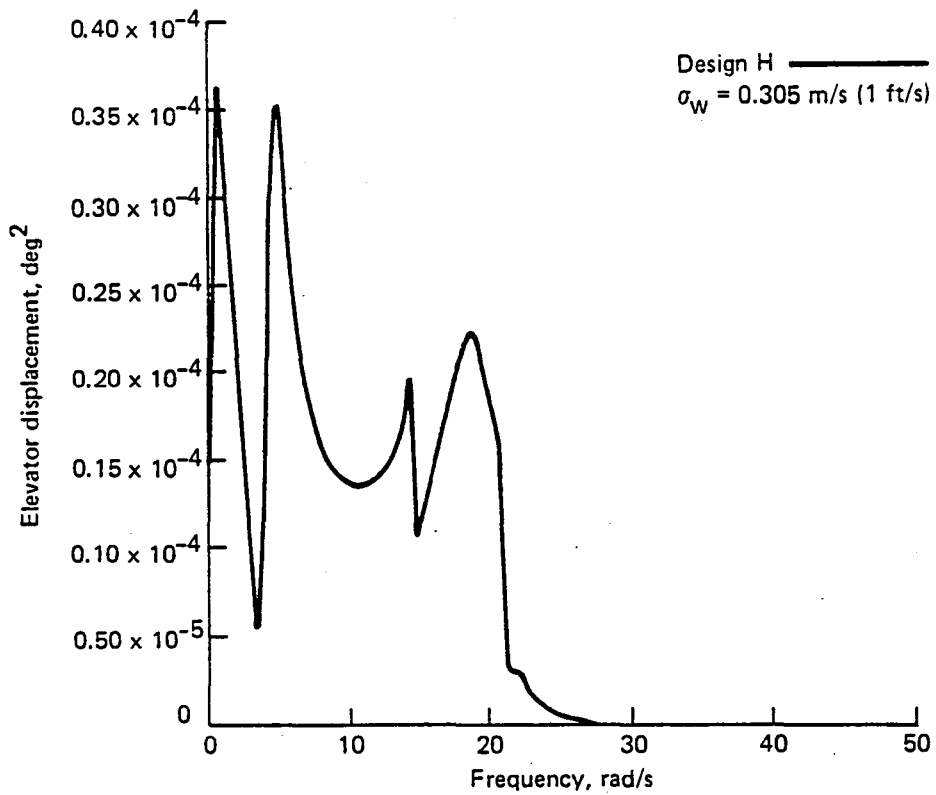
Figure F-116. Power-Spectral-Density Plot, Flight Condition 5
(Elevator Displacement)
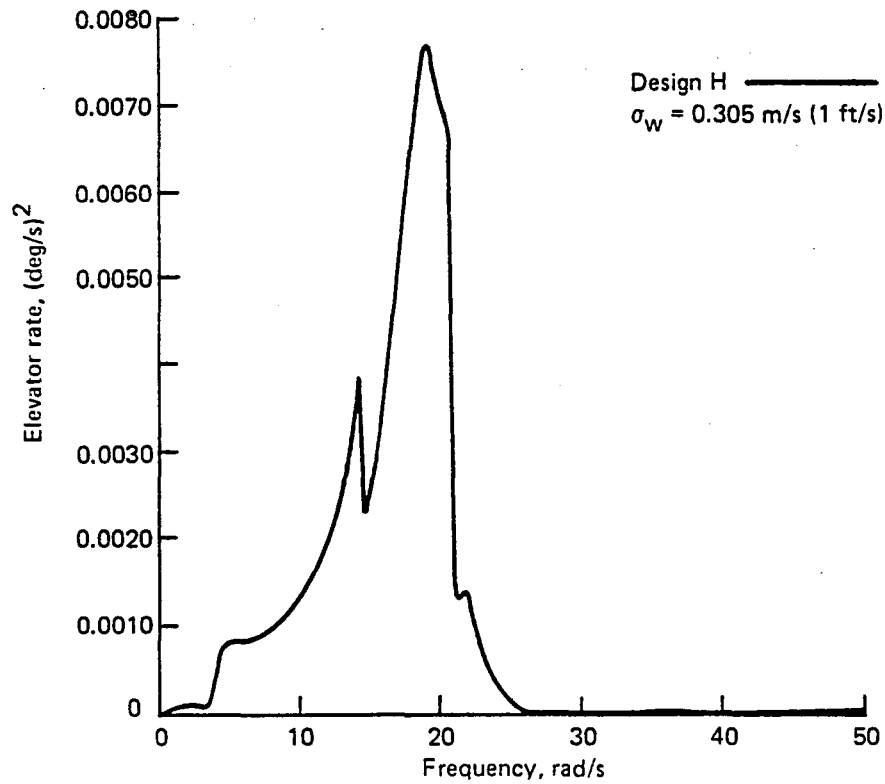
Figure F-117. Power-Spectral-Density Plot, Flight Condition 5
(Elevator Rate)
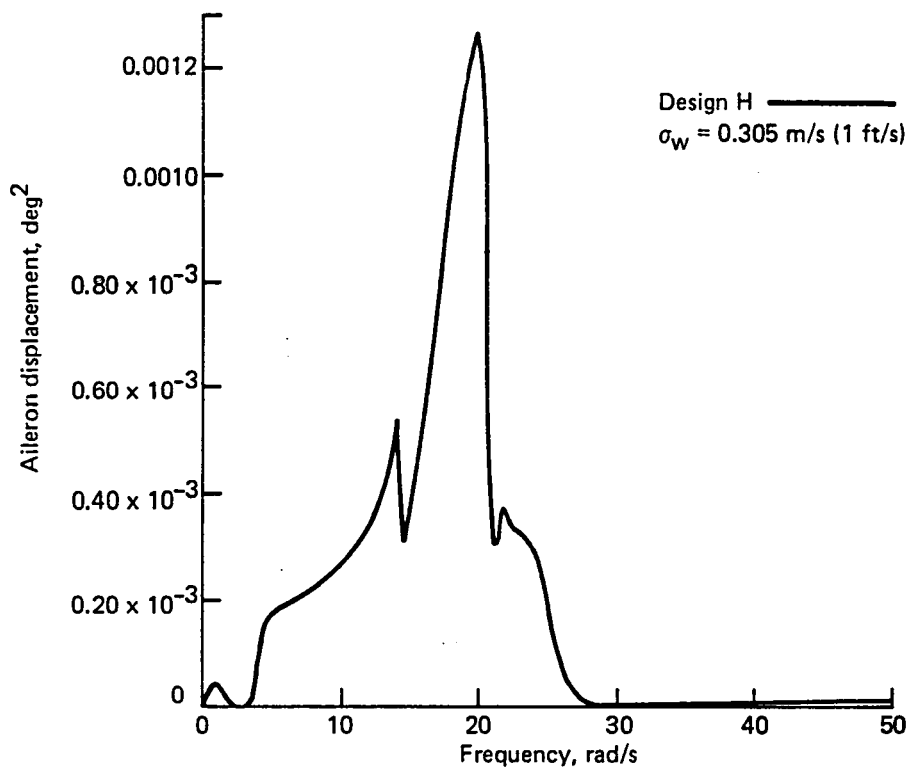
*Figure F-118. Power-Spectral-Density Plot, Flight Condition 5
(Aileron Displacement)*
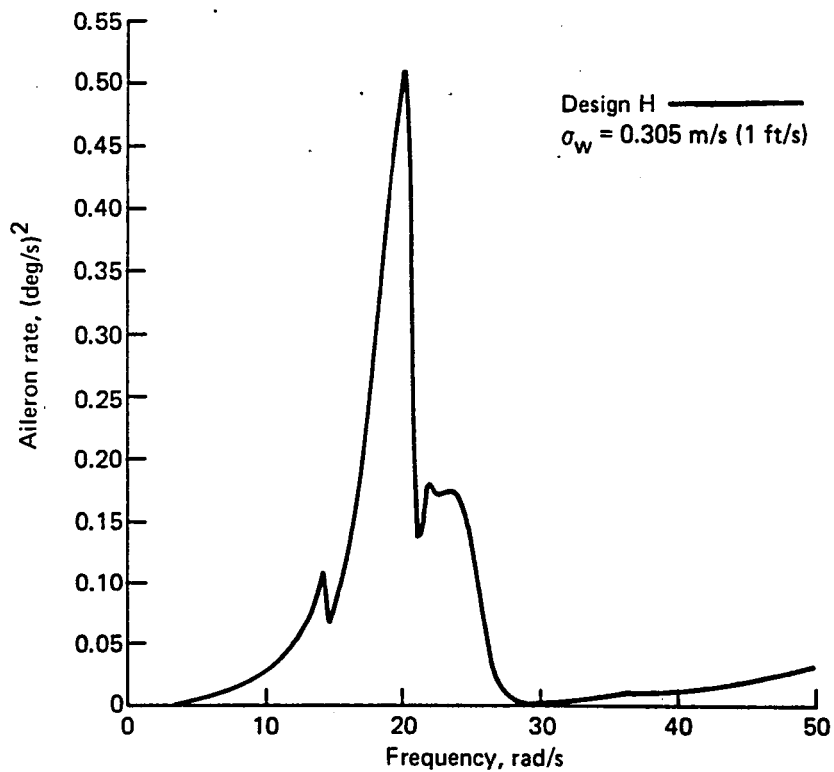
*Figure F-119. Power-Spectral-Density Plot, Flight Condition 5
(Aileron Rate)*
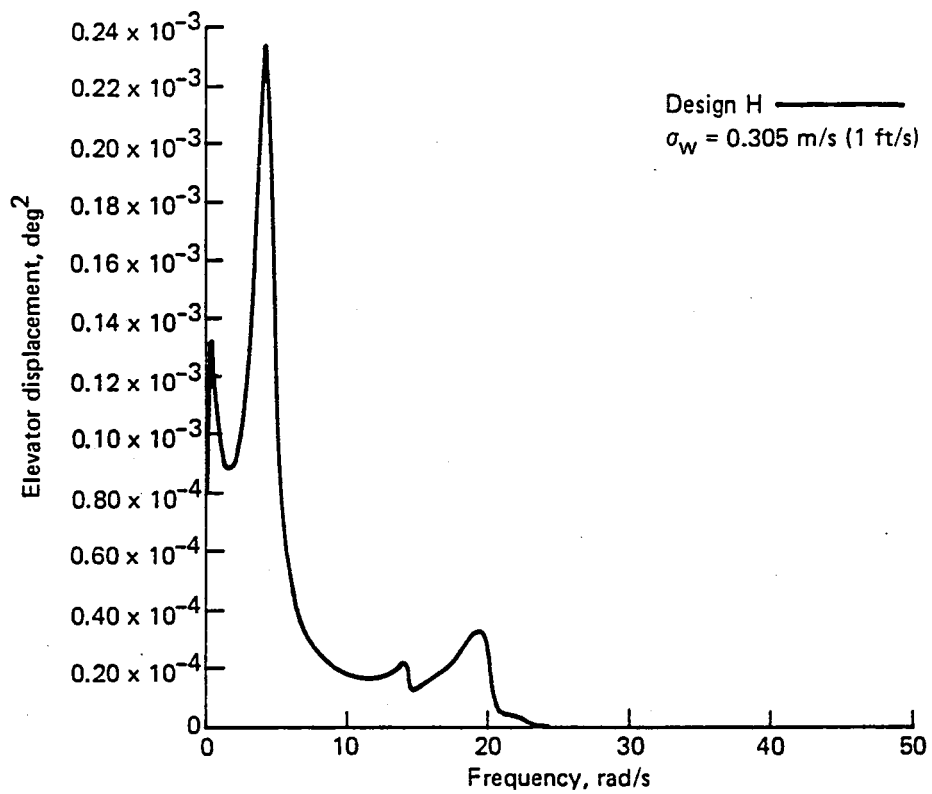
Figure F-120. Power-Spectral-Density Plot, Flight Condition 6
(Elevator Displacement)
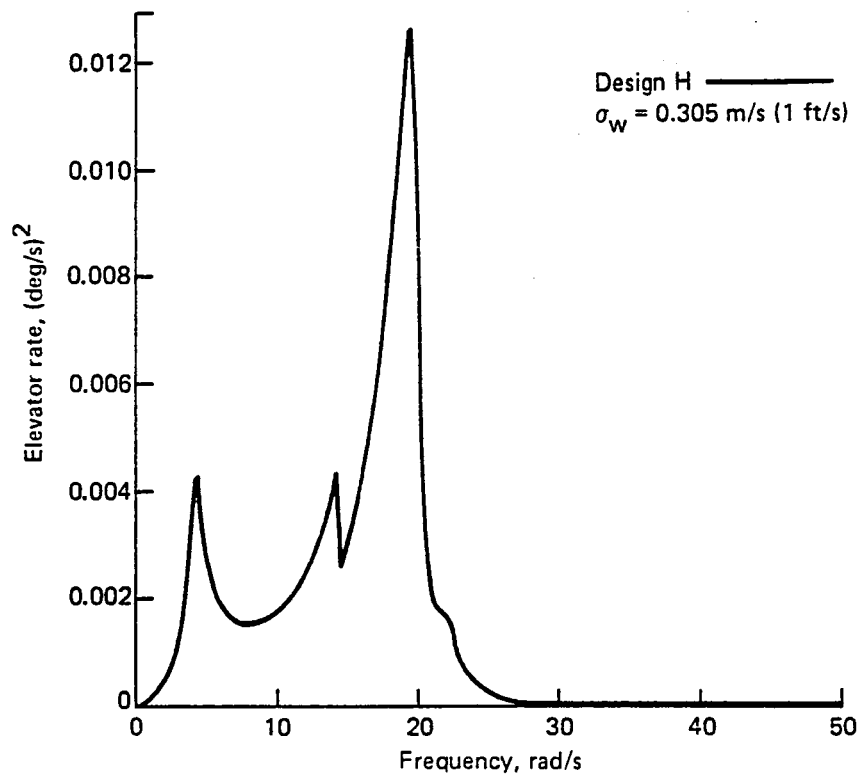
Figure F-121. Power-Spectral-Density Plot, Flight Condition 6
(Elevator Rate)
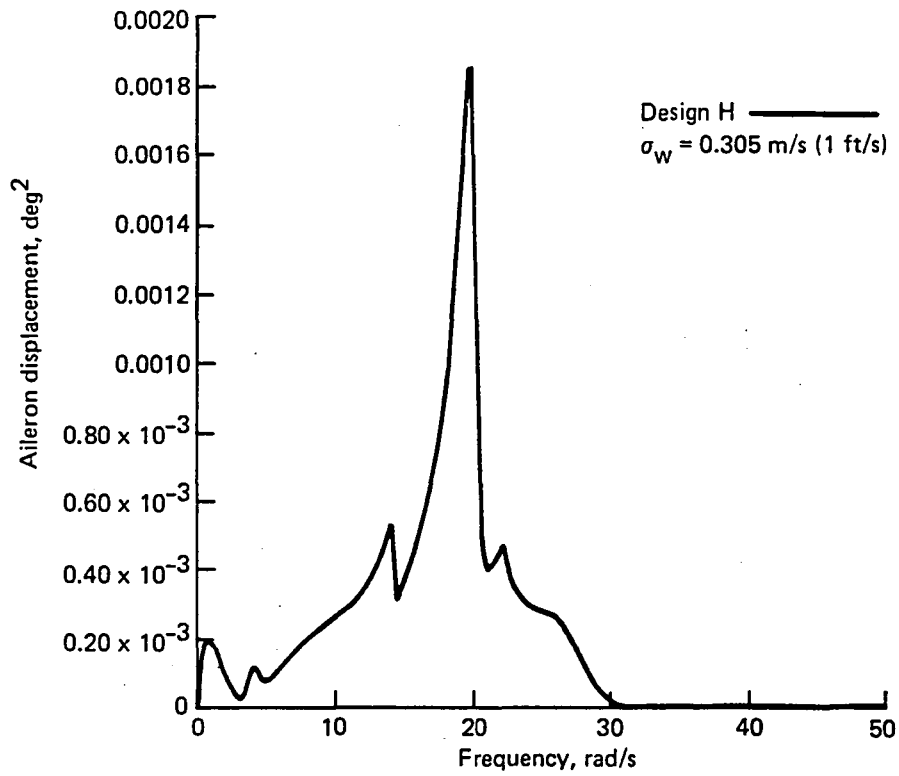
*Figure F-122. Power-Spectral-Density Plot, Flight Condition 6
(Aileron Displacement)*
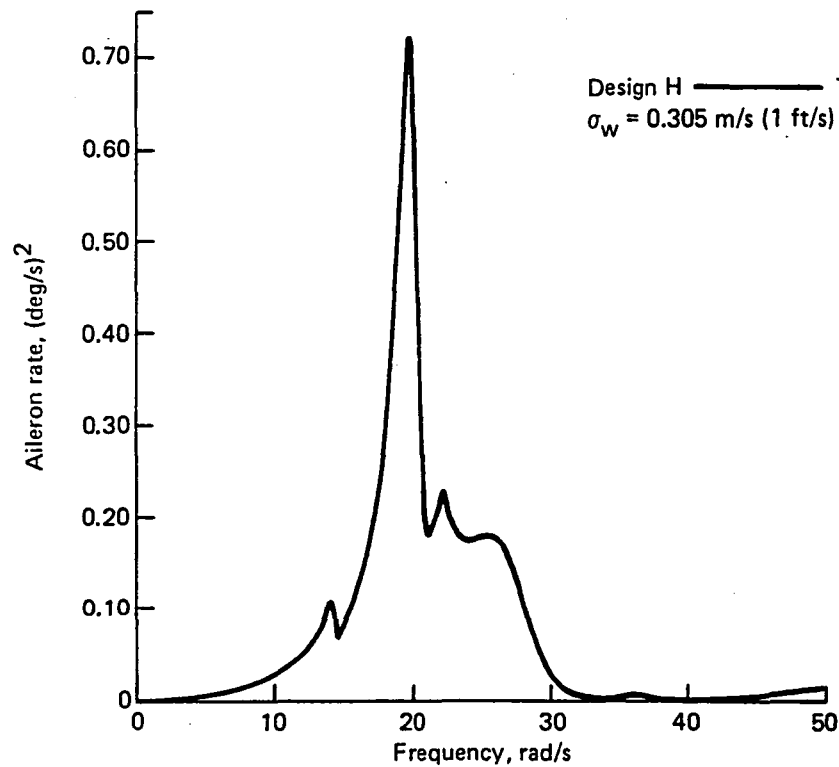
*Figure F-123. Power-Spectral-Density Plot, Flight Condition 6
(Aileron Rate)*
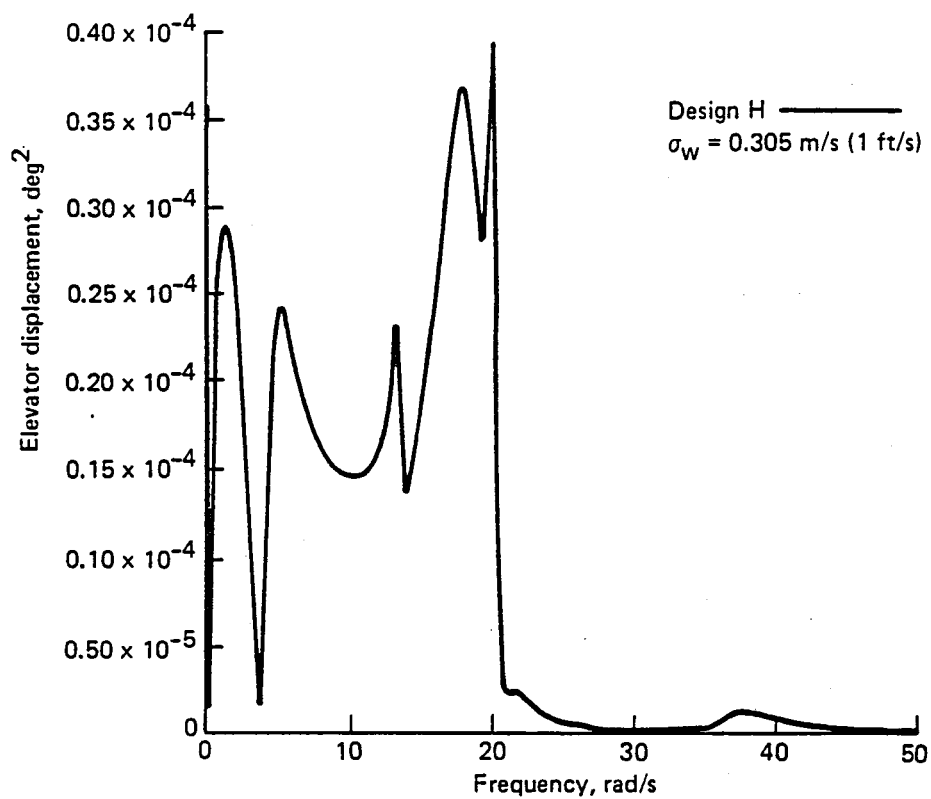
Figure F-124. Power-Spectral-Density Plot, Flight Condition 7
(Elevator Displacement)
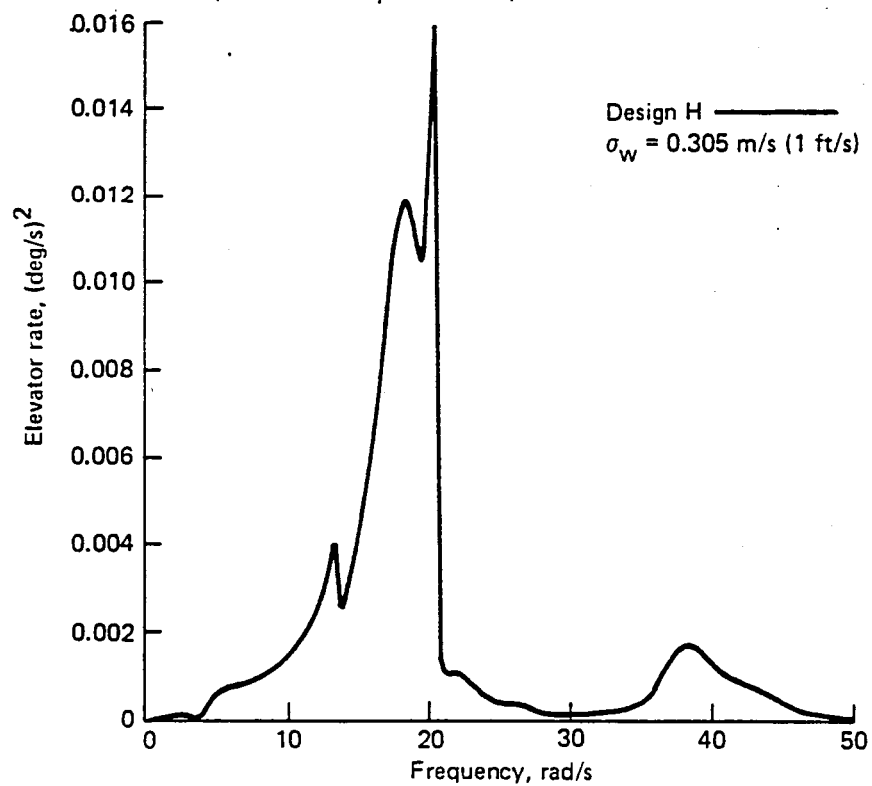
Figure F-125. Power-Spectral-Density Plot, Flight Condition 7
(Elevator Rate)
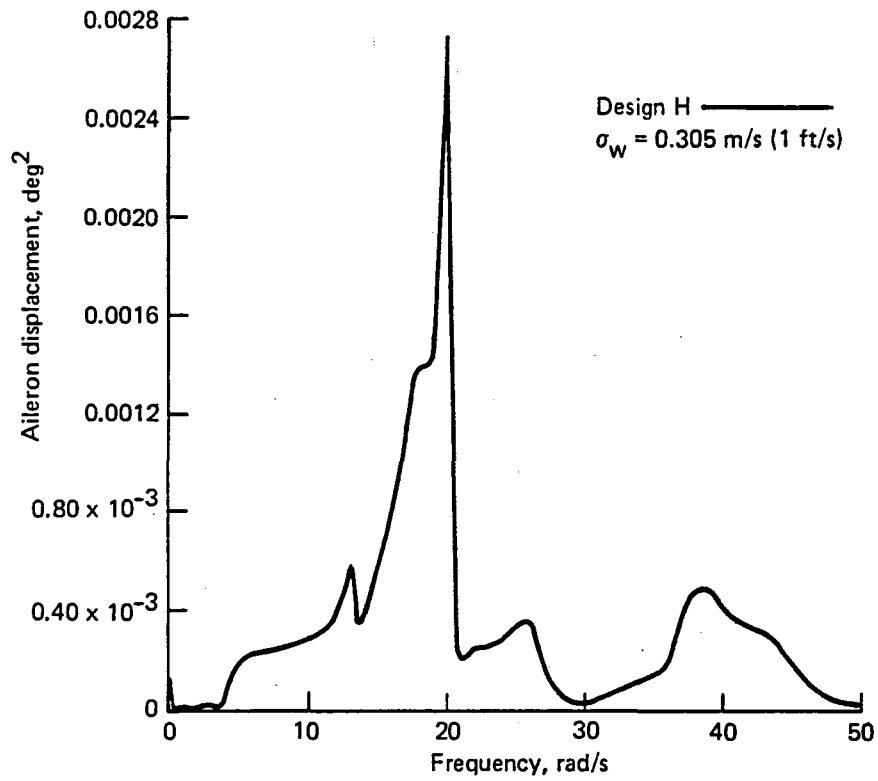
Figure F-126. Power-Spectral-Density Plot, Flight Condition 7
(Aileron Displacement)
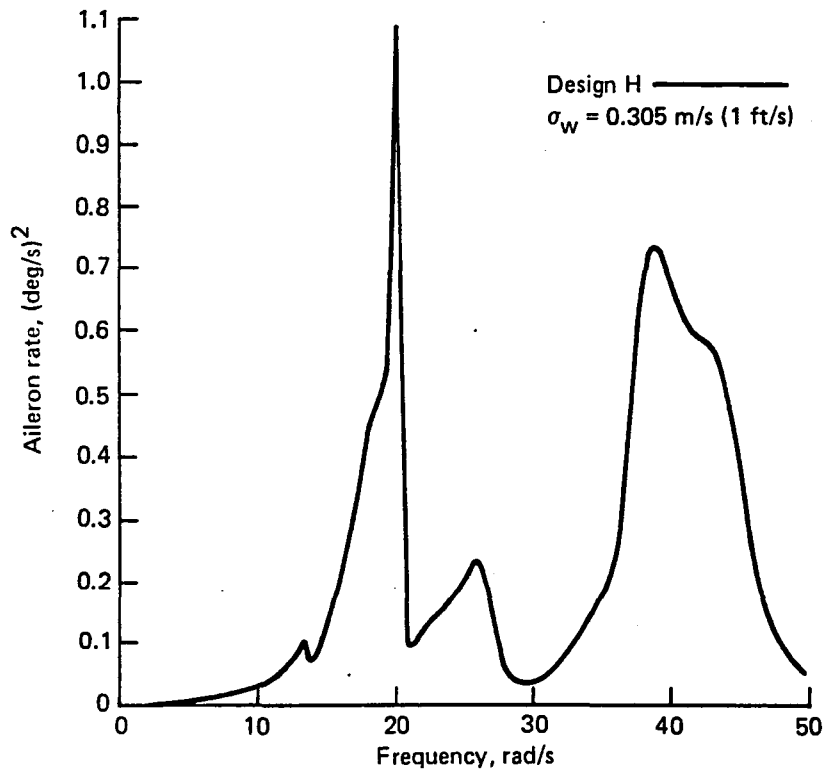
Figure F-127. Power-Spectral-Density Plot, Flight Condition 7
(Aileron Rate)
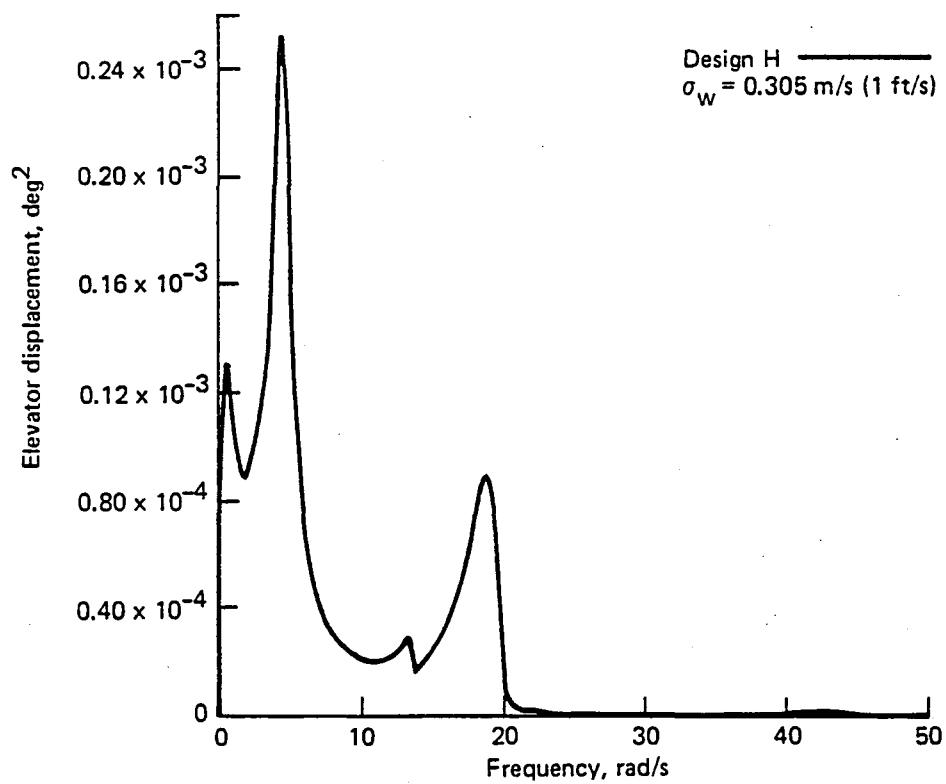
Figure F-128. Power-Spectral-Density Plot, Flight Condition 8
(Elevator Displacement)
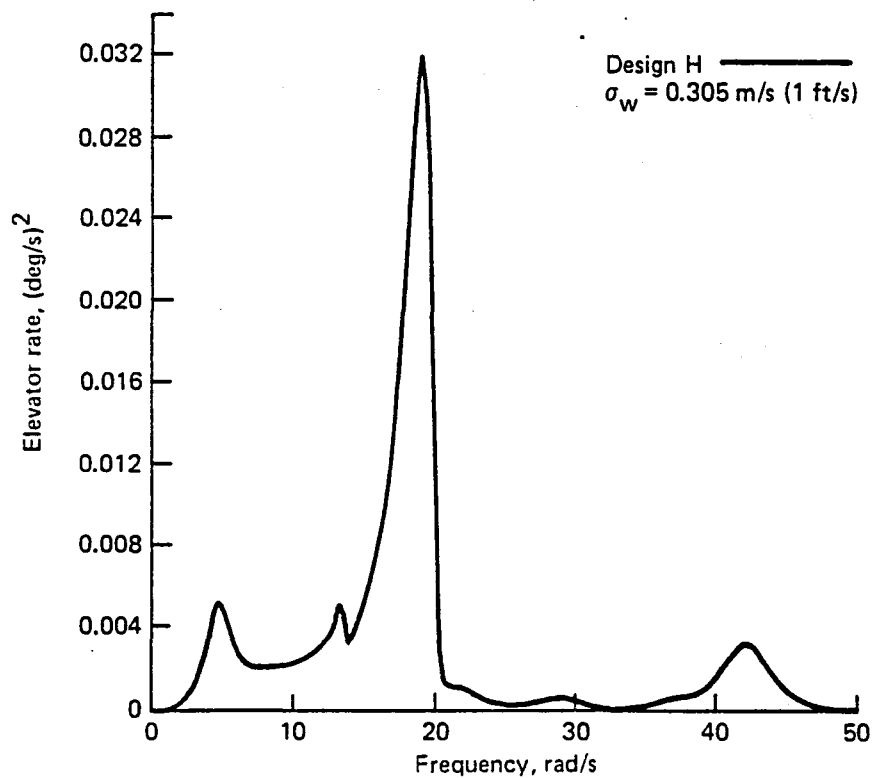
Figure F-129. Power-Spectral-Density Plot, Flight Condition 8
(Elevator Rate)
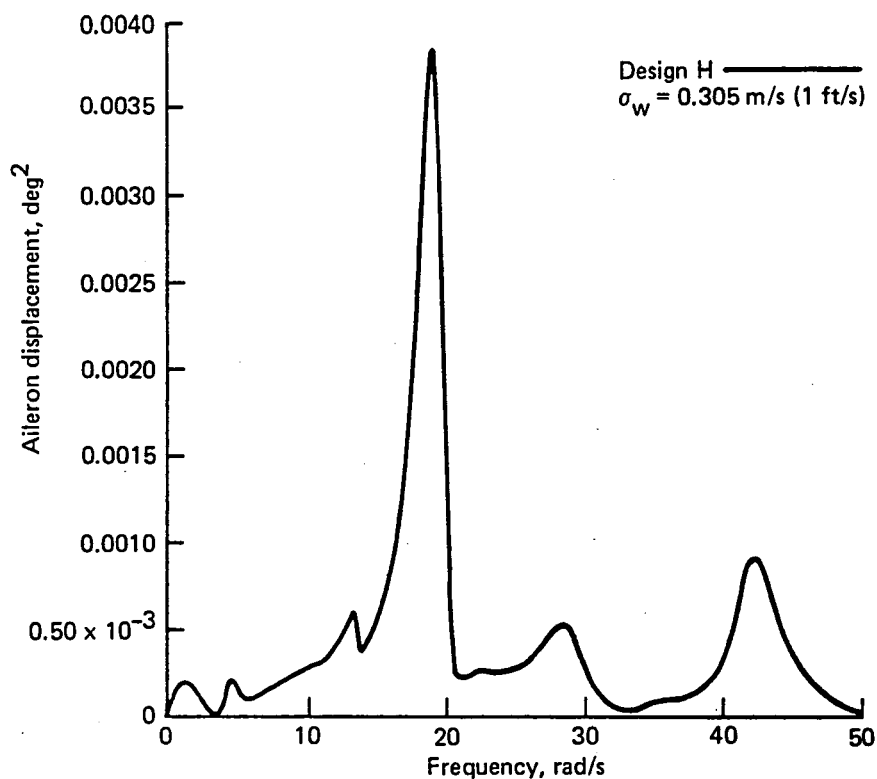
Figure F-130. Power-Spectral-Density Plot, Flight Condition 8
(Aileron Displacement)
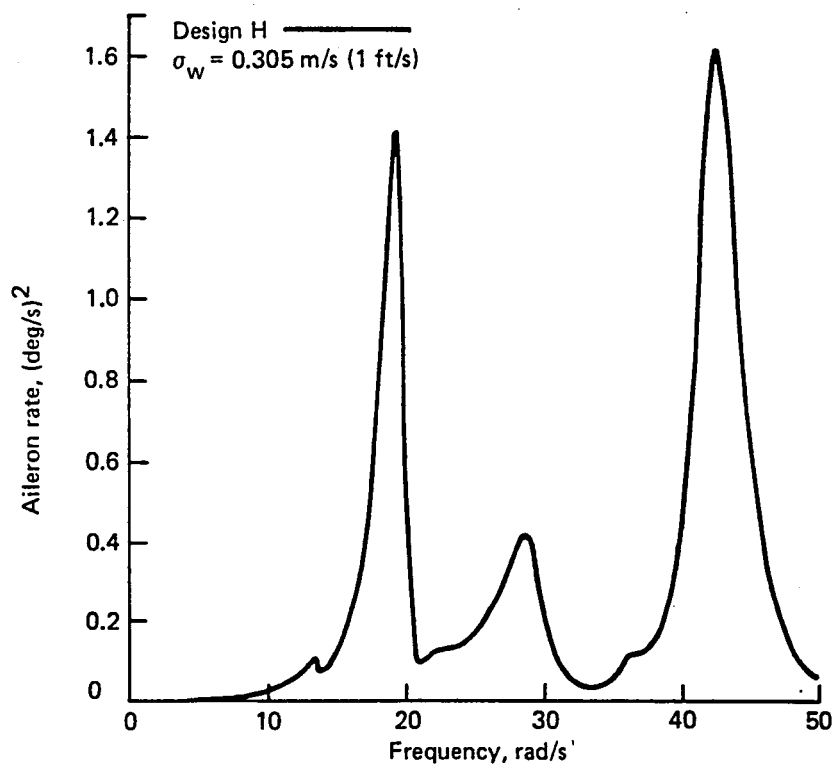
Figure F-131. Power-Spectral-Density Plot, Flight Condition 8
(Aileron Rate)

F.4.3 EFFECTS OF ACTUATOR NONLINEARITIES

F.4.3.1 GUST RESPONSE TIME HISTORIES

Figures F-132 through F-179 show the open- and closed-loop discrete gust responses of the following parameters for various flight conditions and with linear and nonlinear actuators: shear, torsion, and bending at various wing stations and the corresponding elevator and aileron deflections and rates.
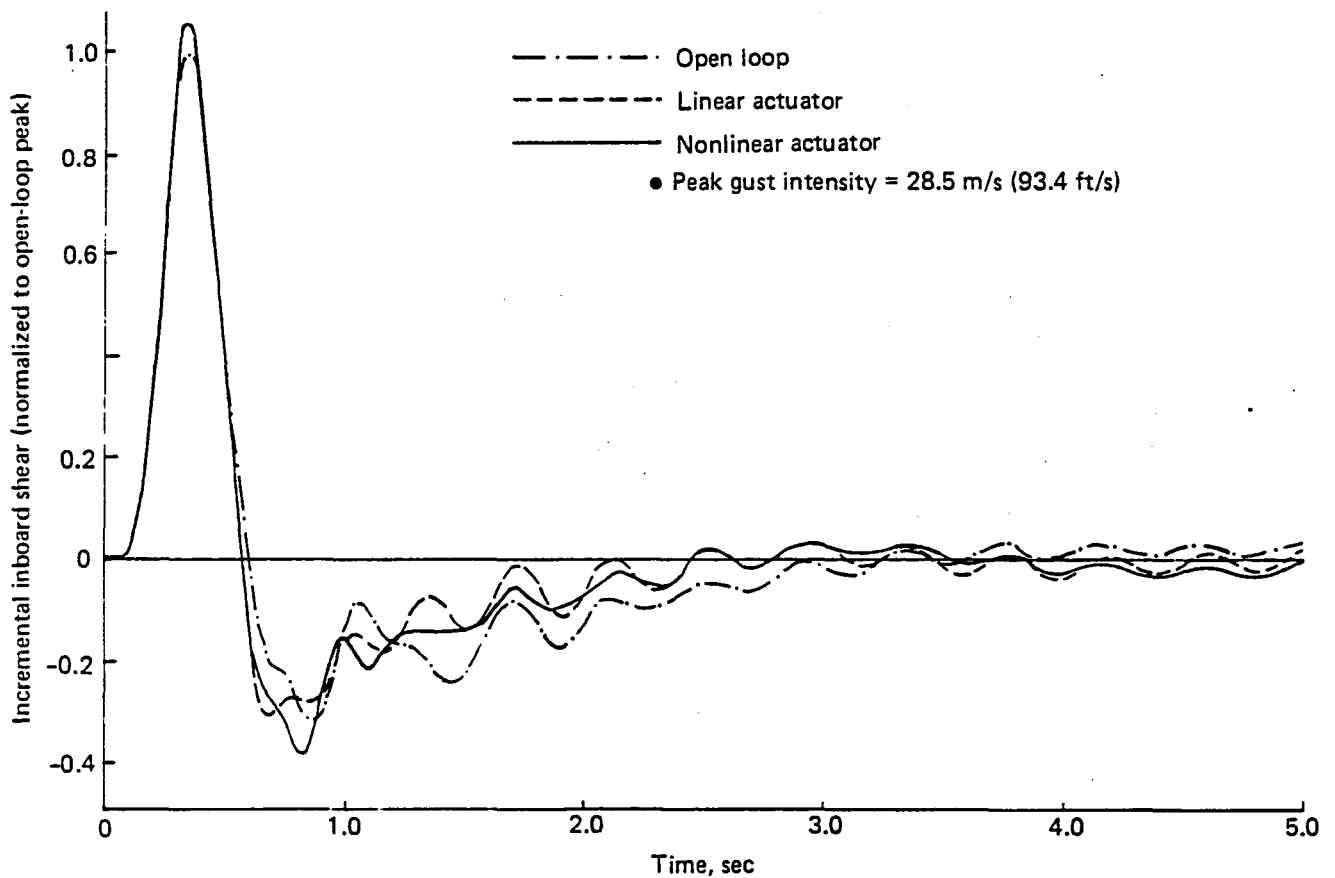
Figure F-132. *Response of Inboard Shear ($\eta = 0.25$) to a Discrete (1-cos) Gust, Flight Condition 1, Time History Simulation*
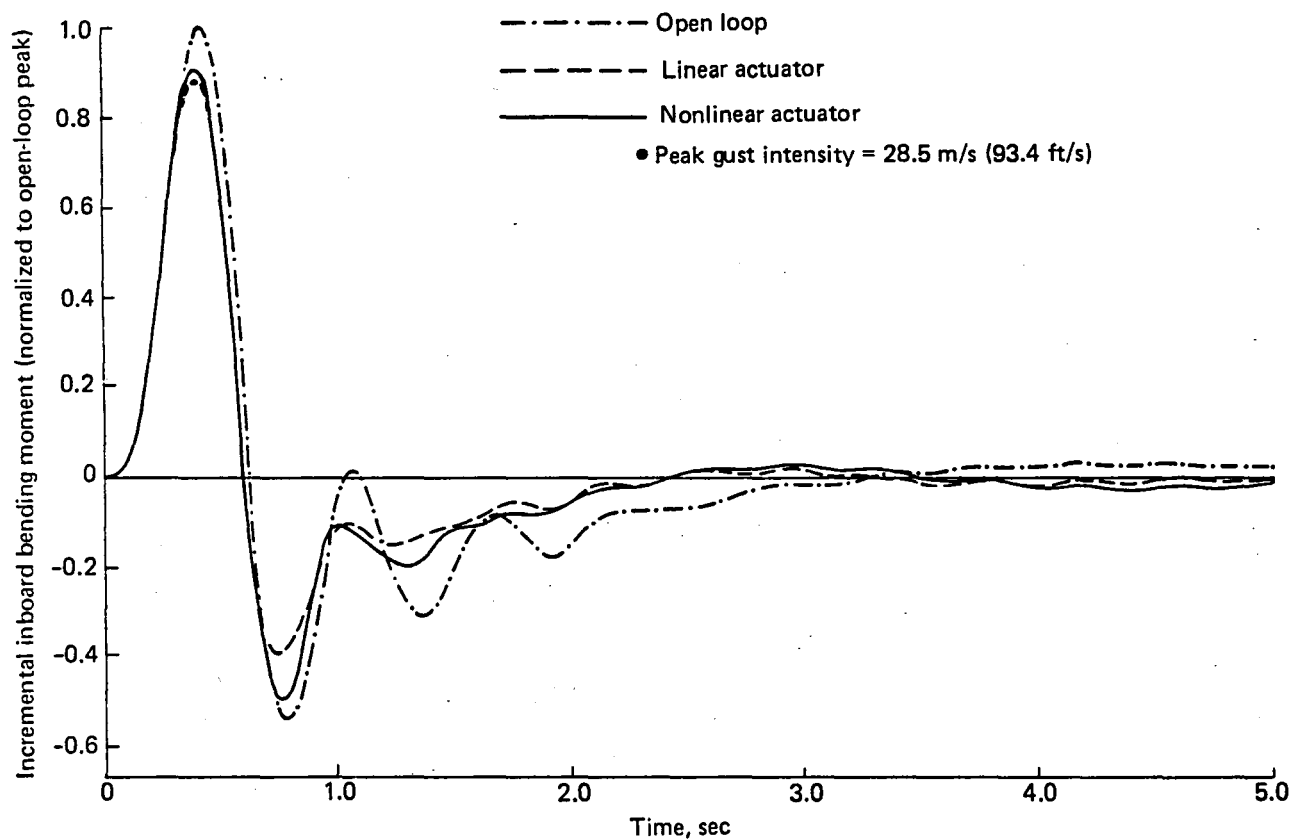
Figure F-133. Response of Inboard Bending Moment ($\eta = 0.25$) to a Discrete
(1-cos) Gust, Flight Condition 1, Time History Simulation
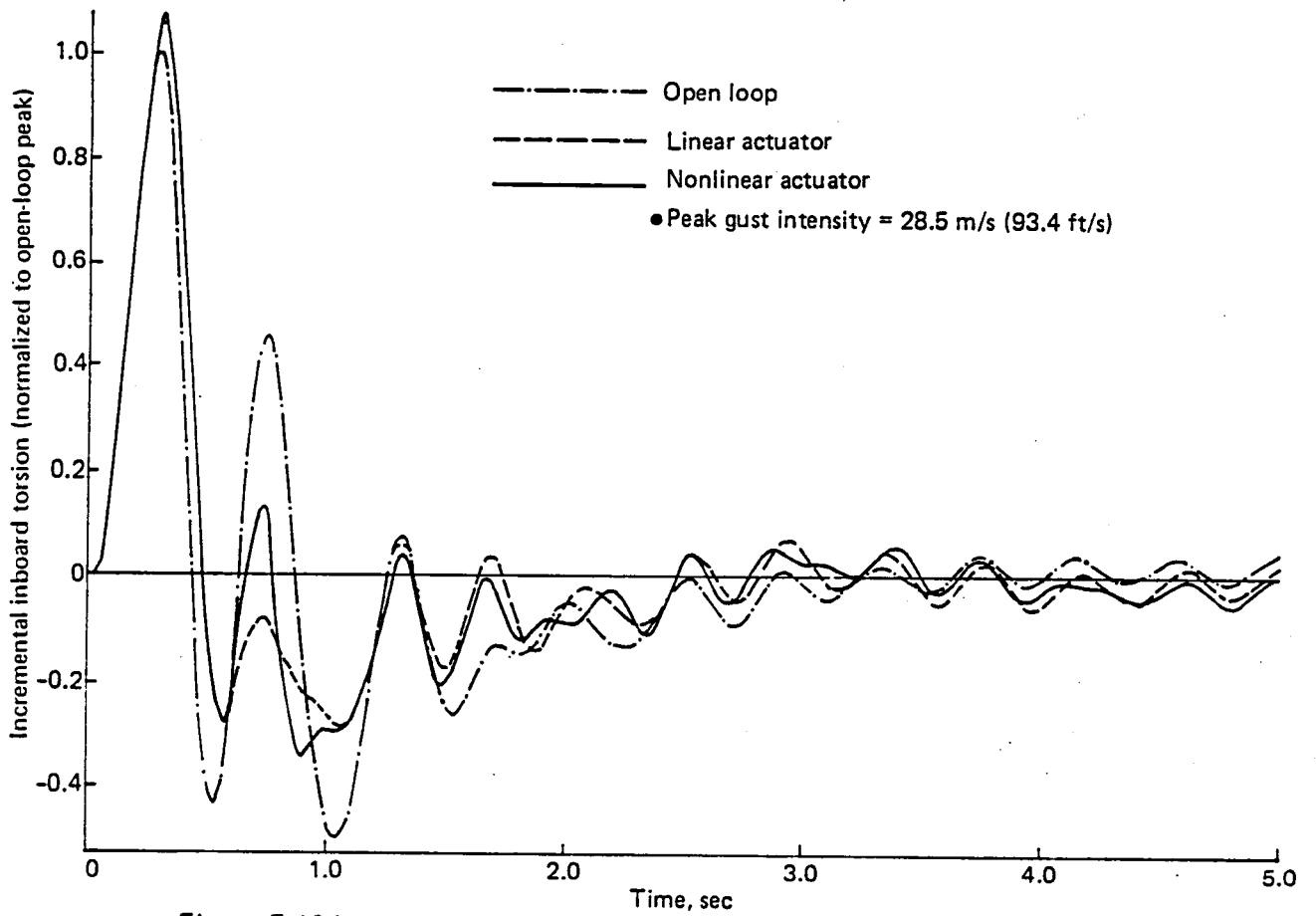
*Figure F-134. Response of Inboard Torsion ($\eta = 0.25$) to a Discrete (1-cos) Gust,
Flight Condition 1, Time History Simulation*
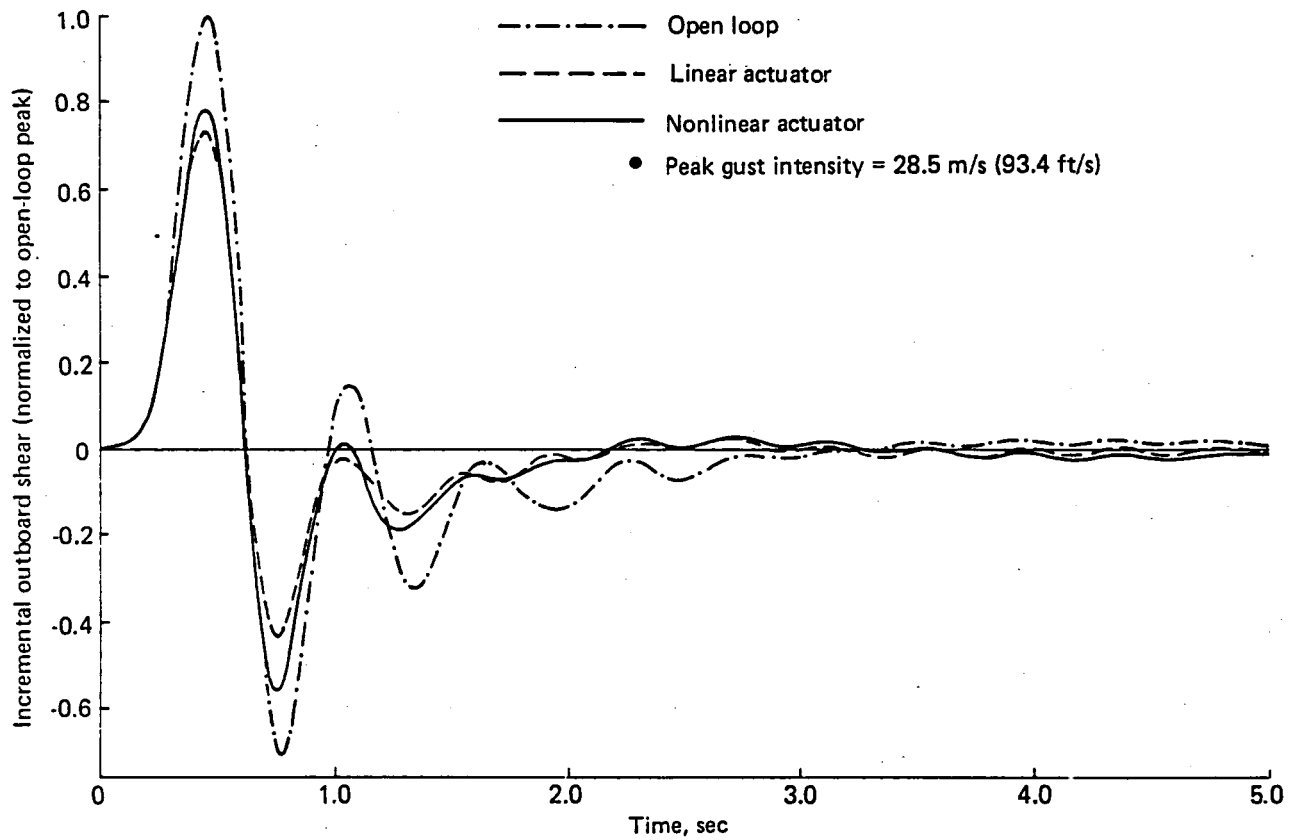
Figure F-135. Response of Outboard Shear (η = 0.75) to a Discrete (1-cos) Gust, Flight Condition 1, Time History Simulation
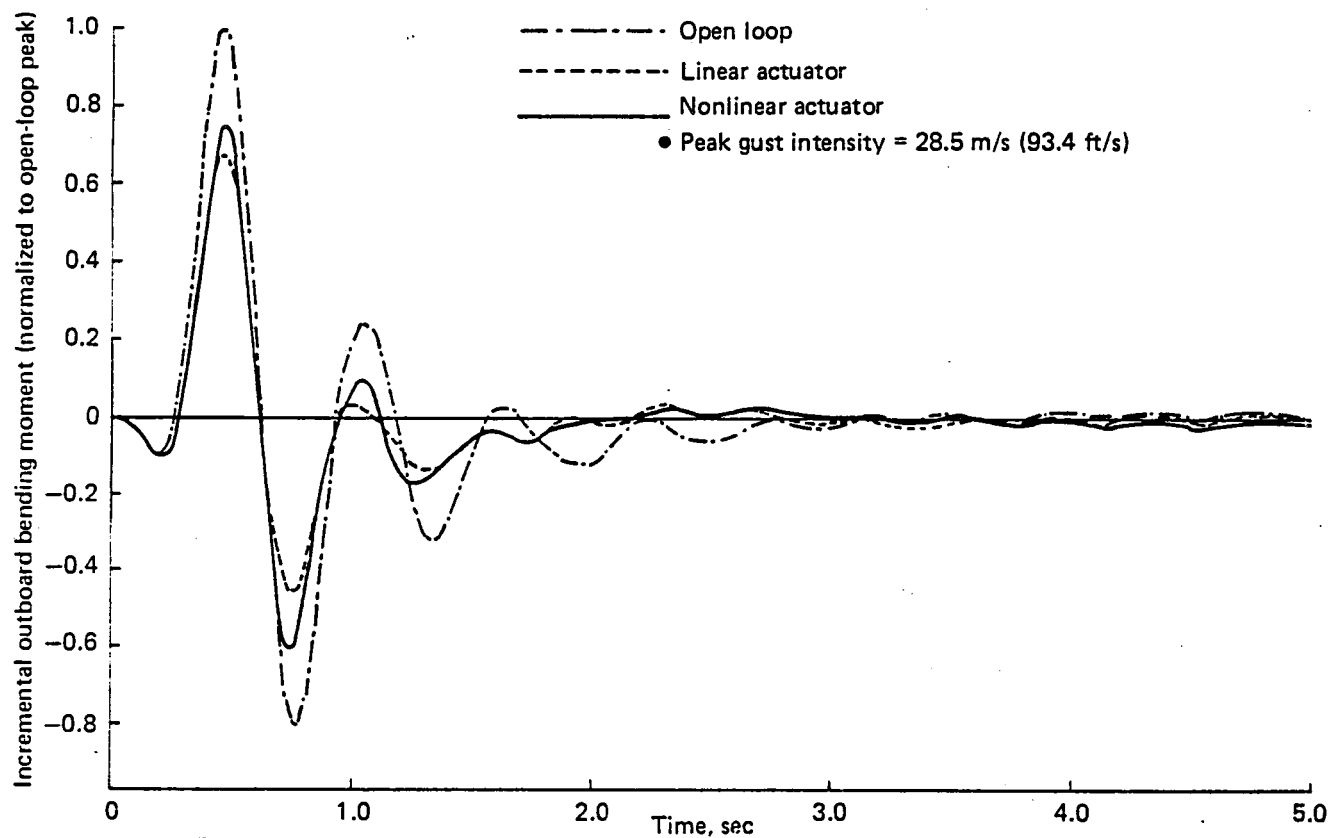
Figure F-136. Response of Outboard Bending Moment (η = 0.75) to a Discrete
(1-cos) Gust, Flight Condition 1, Time History Simulation

Figure F-137. Response of Outboard Torsion ($\eta = 0.75$) to a Discrete (1-cos) Gust, Flight Condition 1, Time History Simulation
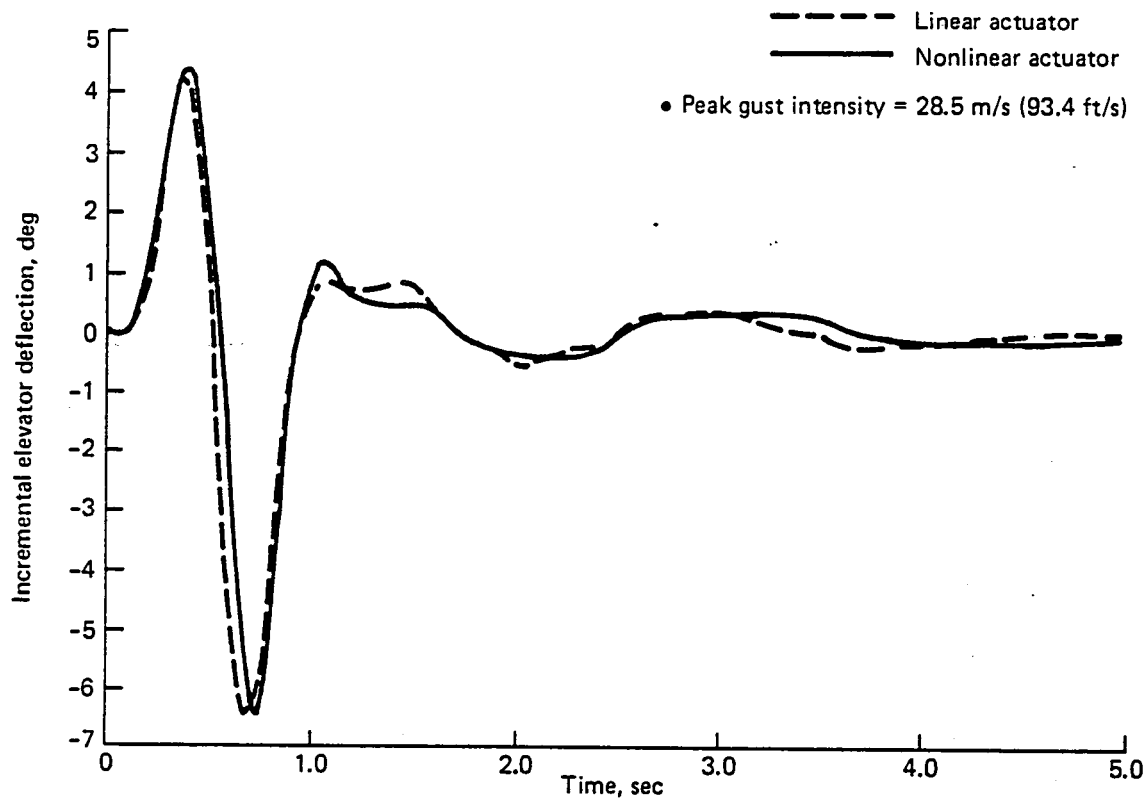
Figure F-138. *Response of Elevator Deflection to a Discrete (1-cos) Gust,*
Flight Condition 1, Time History Simulation
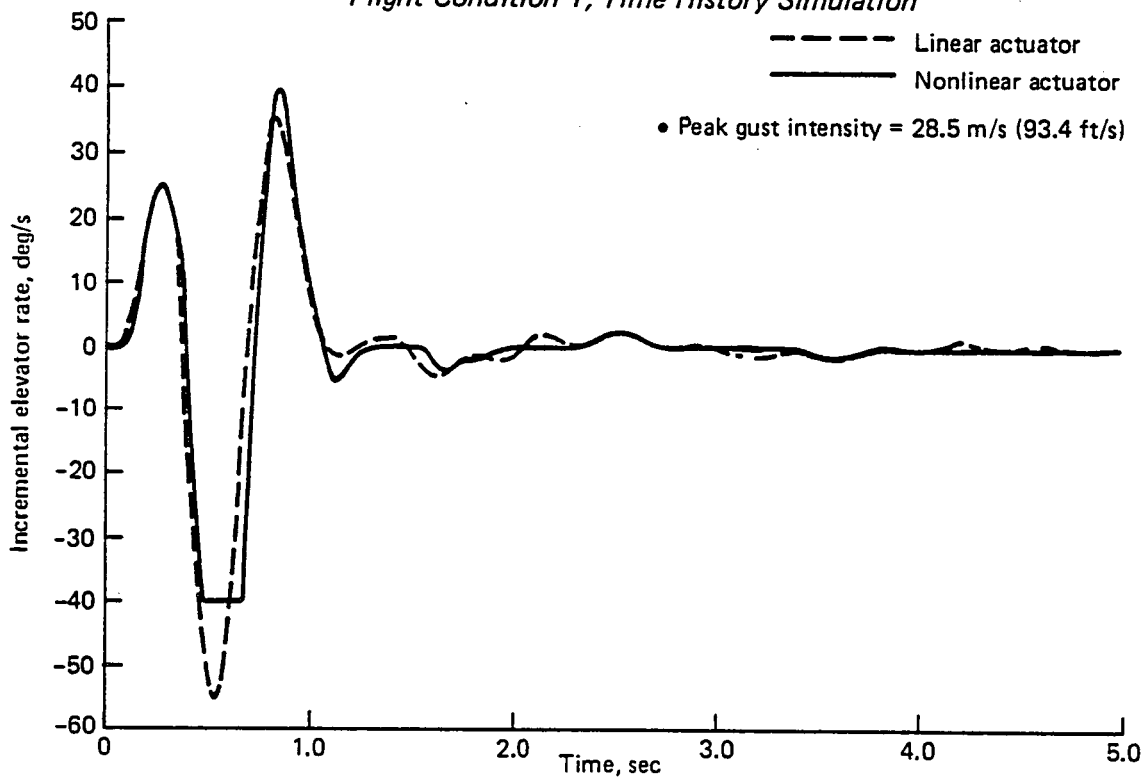
Figure F-139. *Response of Elevator Rate to a Discrete (1-cos) Gust,*
Flight Condition 1, Time History Simulation
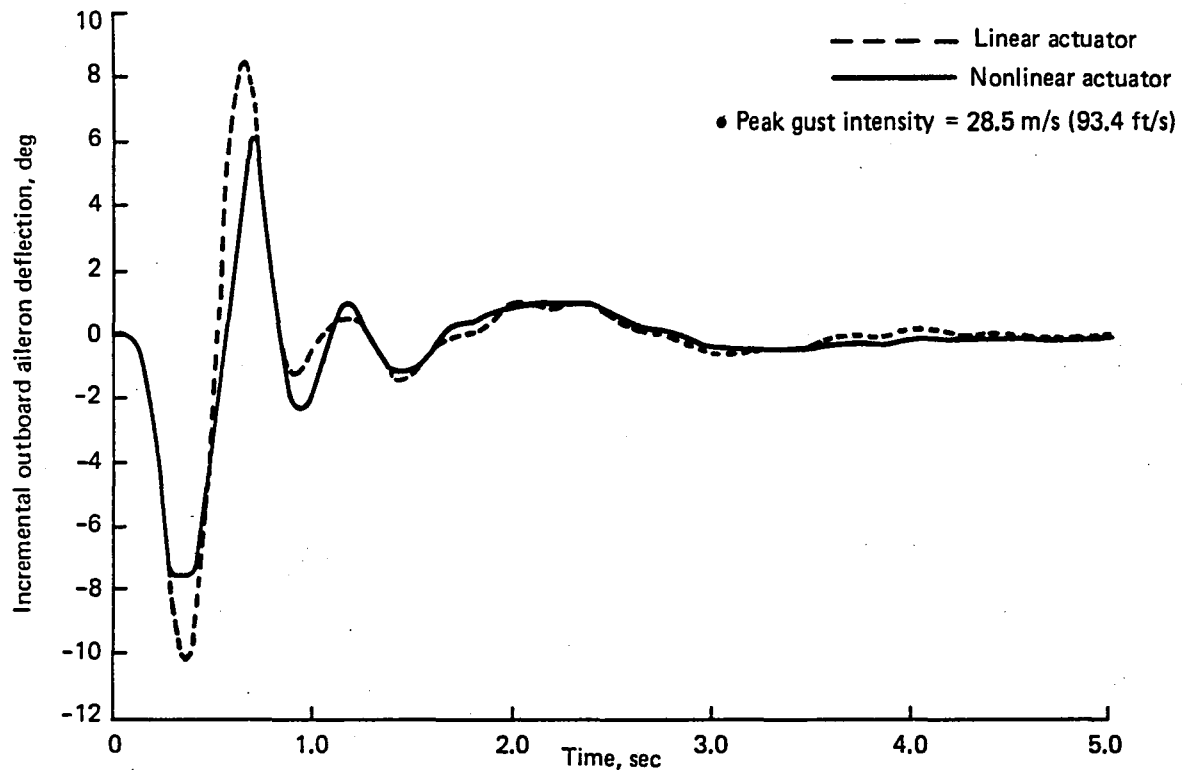
Figure F-140. Response of Outboard Aileron Deflection to a Discrete (1-cos) Gust, Flight Condition 1, Time History Simulation
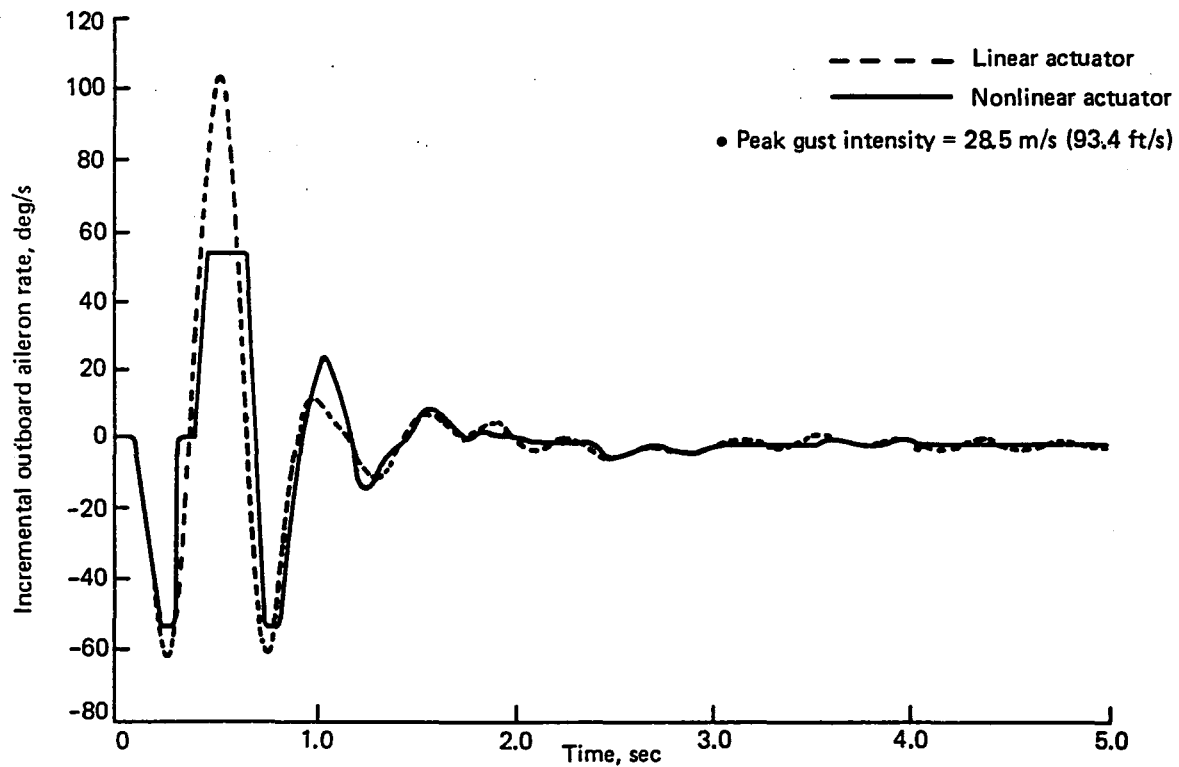
Figure F-141. Response of Outboard Aileron Rate to a Discrete (1-cos) Gust, Flight Condition 1, Time History Simulation
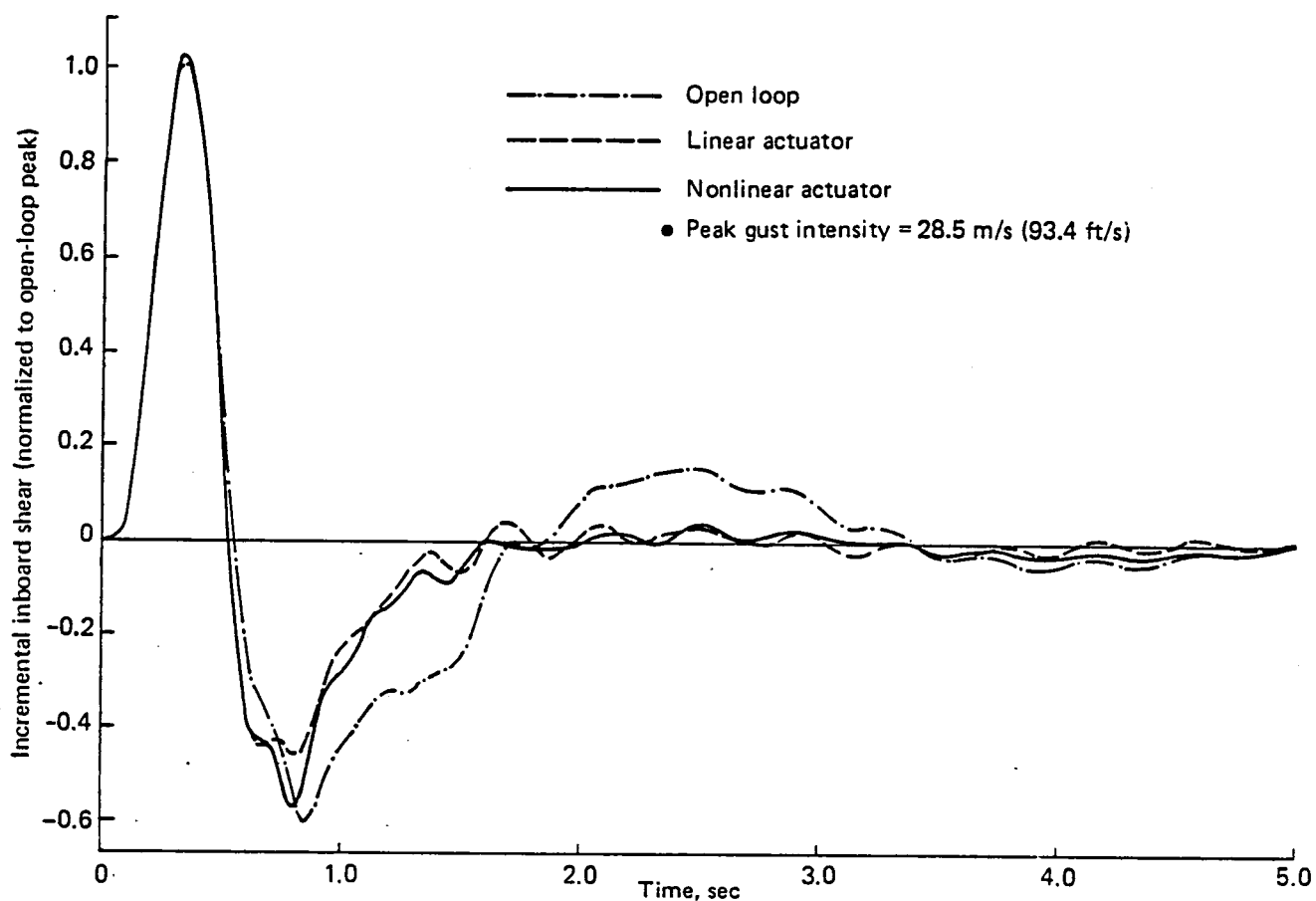
Figure F-142. Response of Inboard Shear (η = 0.25) to a Discrete (1-cos) Gust, Flight Condition 2, Time History Simulation

Figure F-143. *Response of Inboard Bending Moment (η = 0.25) to a Discrete (1-cos) Gust, Flight Condition 2, Time History Simulation*
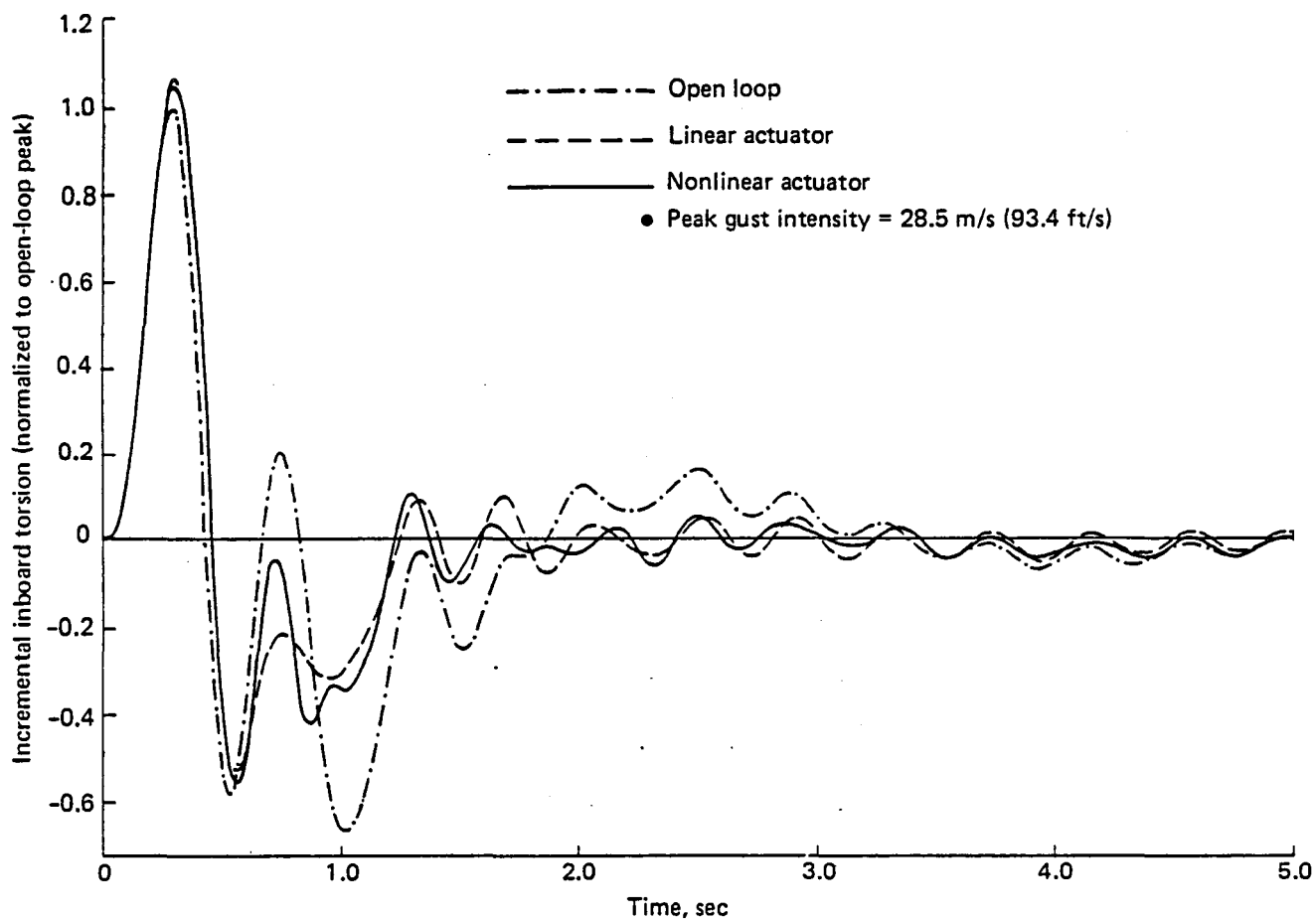
Figure F-144. Response of Inboard Torsion ($\eta = 0.25$) to a Discrete (1-cos) Gust,
Flight Condition 2, Time History Simulation
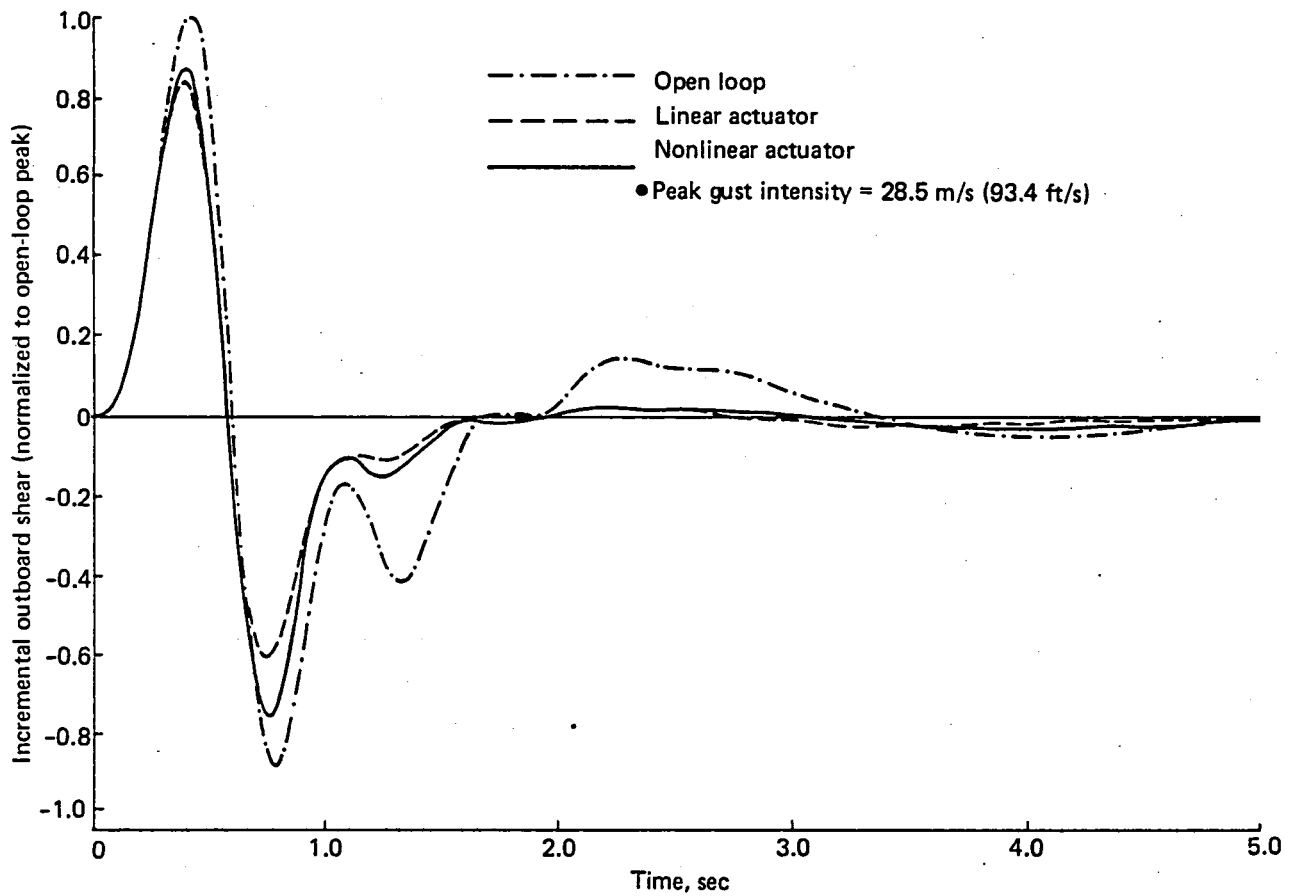
Figure F-145. Response of Outboard Shear (η = 0.75) to a Discrete (1-cos) Gust,
Flight Condition 2, Time History Simulation

Figure F-146. Response of Outboard Bending Moment ($\eta = 0.75$) to a Discrete
(1-cos) Gust, Flight Condition 2, Time History Simulation
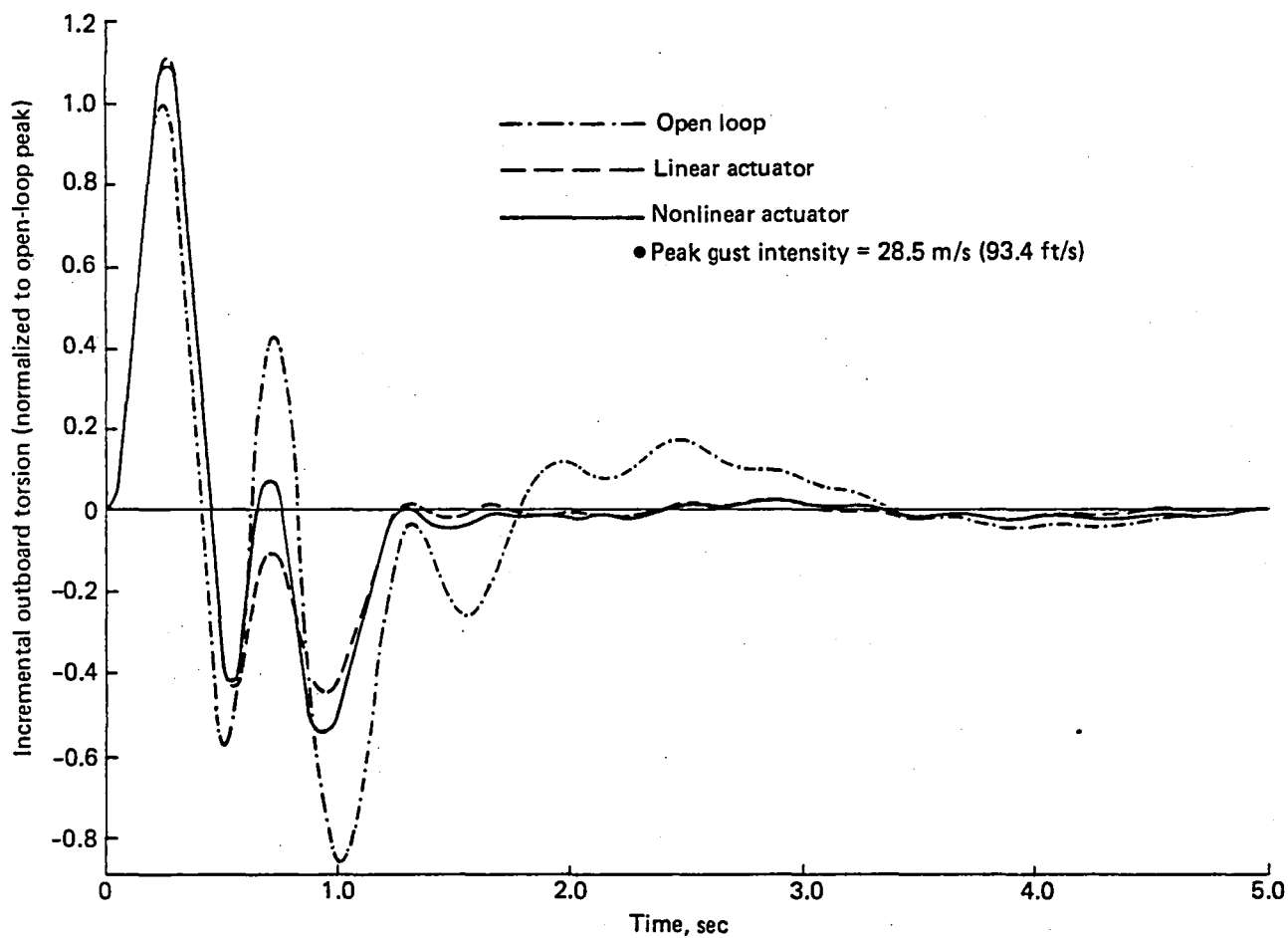
Figure F-147. *Response of Outboard Torsion (η = 0.75) to a Discrete (1-cos) Gust, Flight Condition 2, Time History Simulation*

Figure F-148. Response of Elevator Deflection to a Discrete (1-cos) Gust,
Flight Condition 2, Time History Simulation
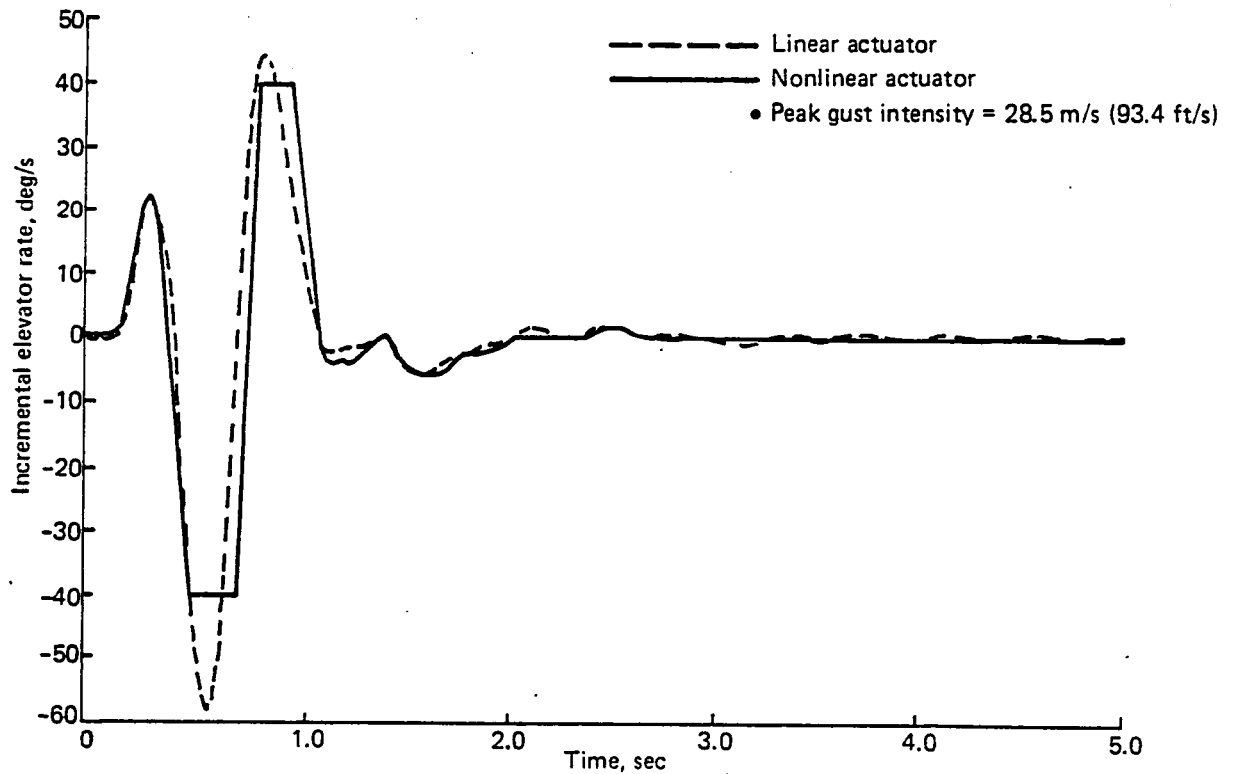
Figure F-149.   Response of Elevator Rate to a Discrete (1-cos) Gust,
Flight Condition 2, Time History Simulation

F-110
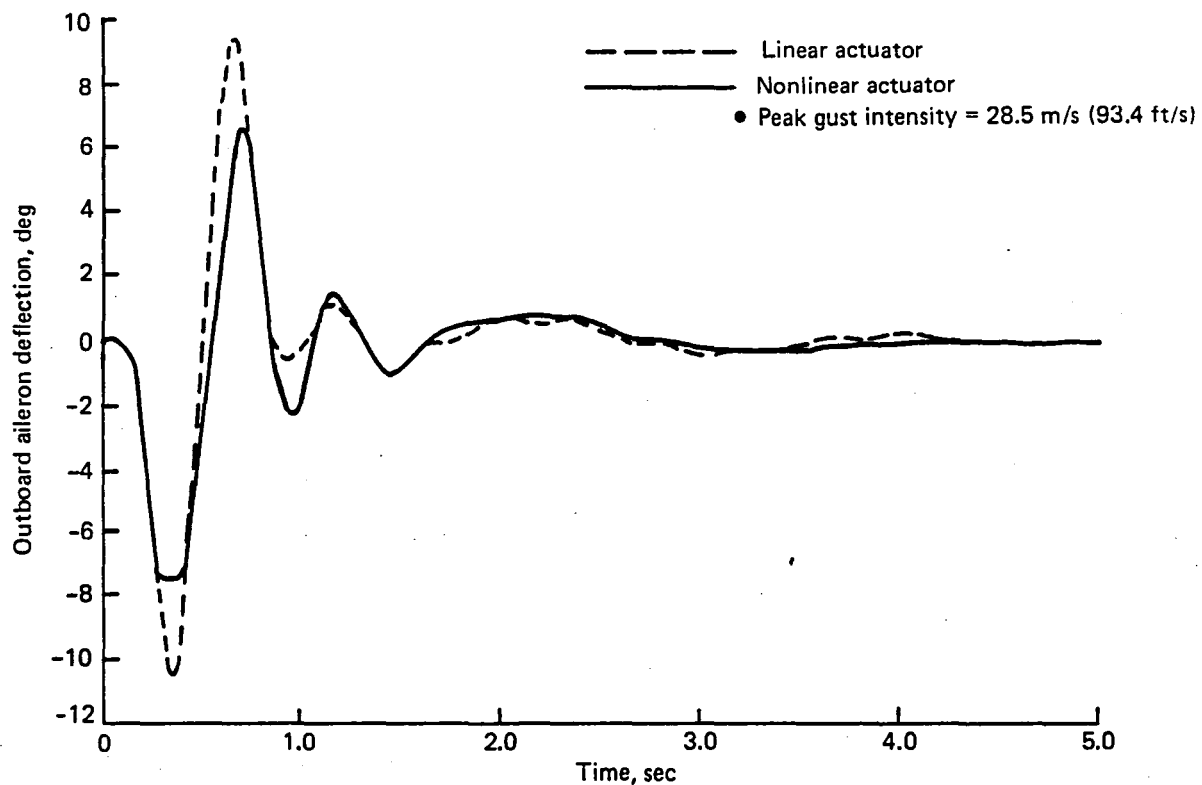
Figure F-150. Response of Outboard Aileron Deflection to a Discrete (1-cos)Gust, Flight Condition 2, Time History Simulation
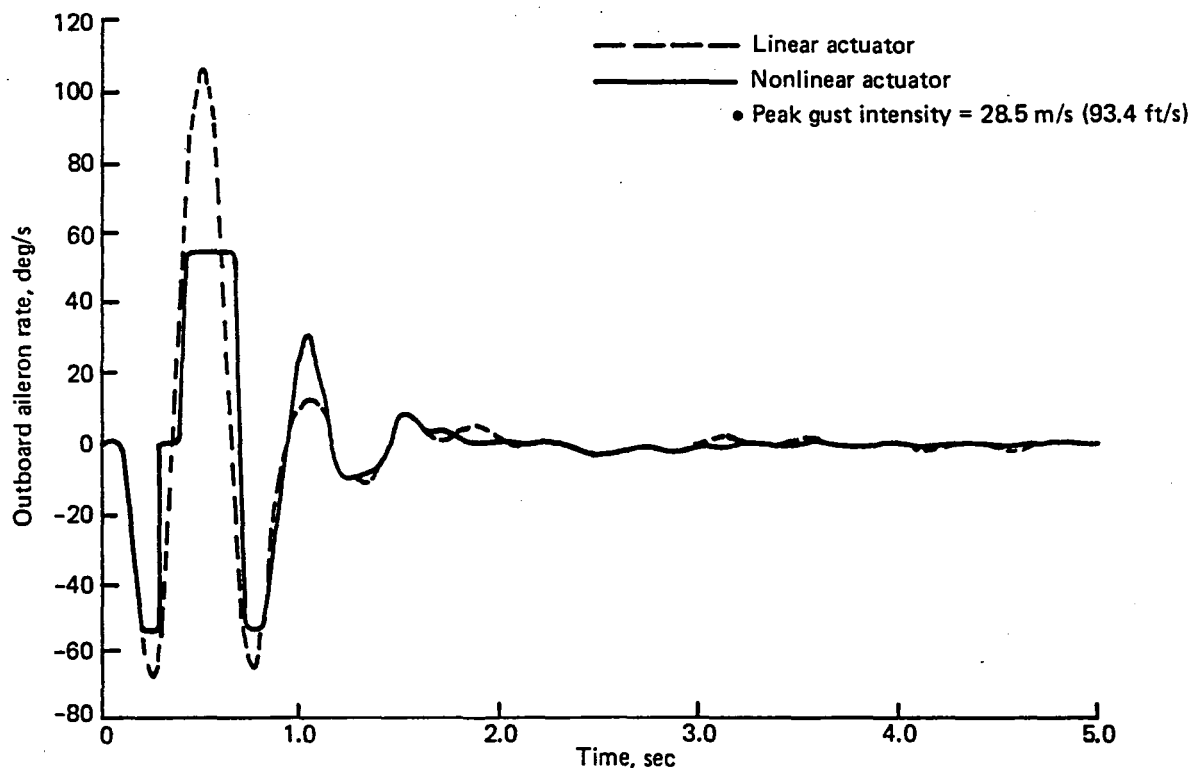
Figure F-151. Response of Outboard Aileron Rate to a Discrete (1-cos) Gust, Flight Condition 2, Time History Simulation
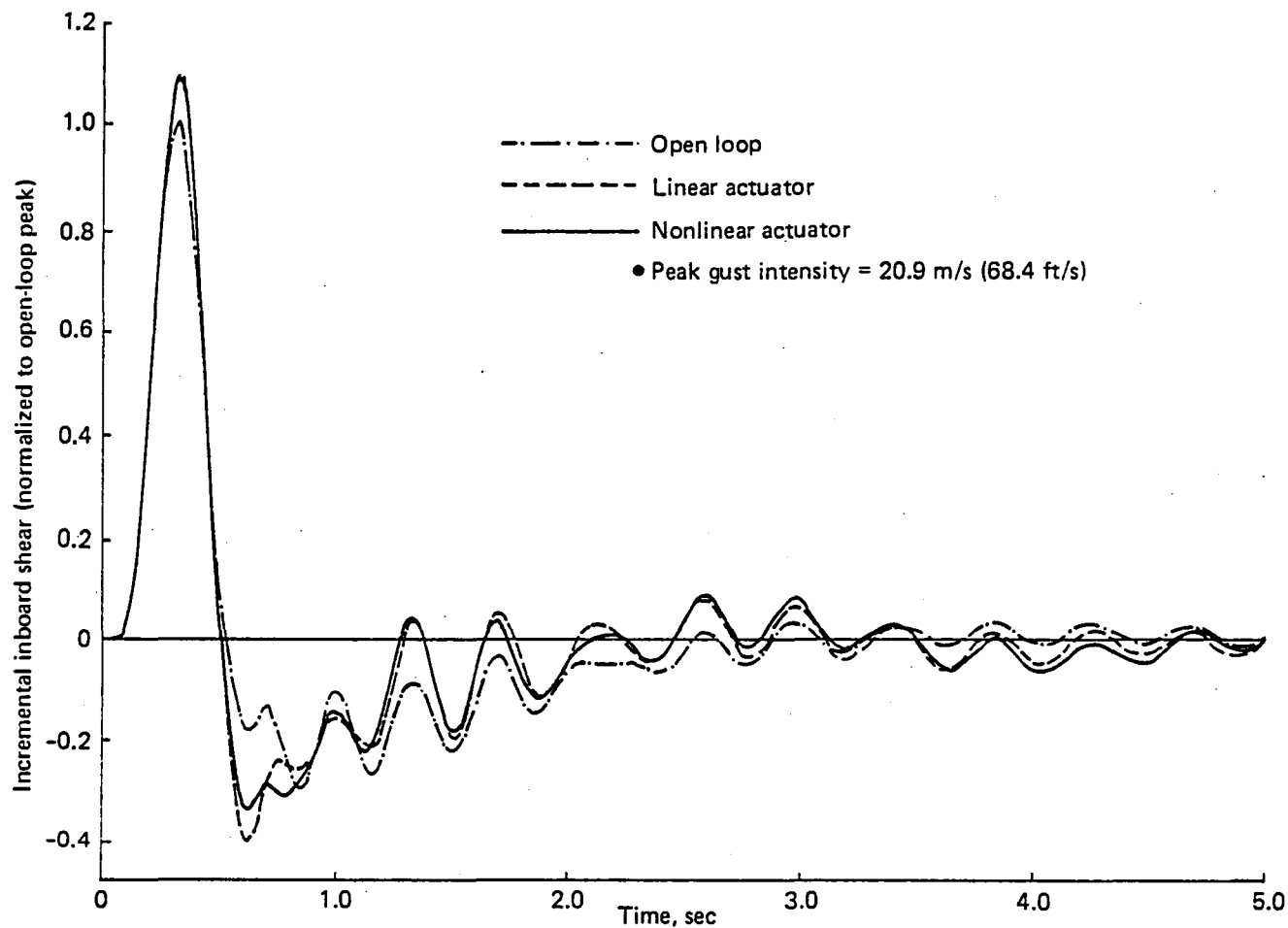
Figure F-152. Response of Inboard Shear (η = 0.25) to a Discrete (1-cos) Gust, Flight Condition 3, Time History Simulation
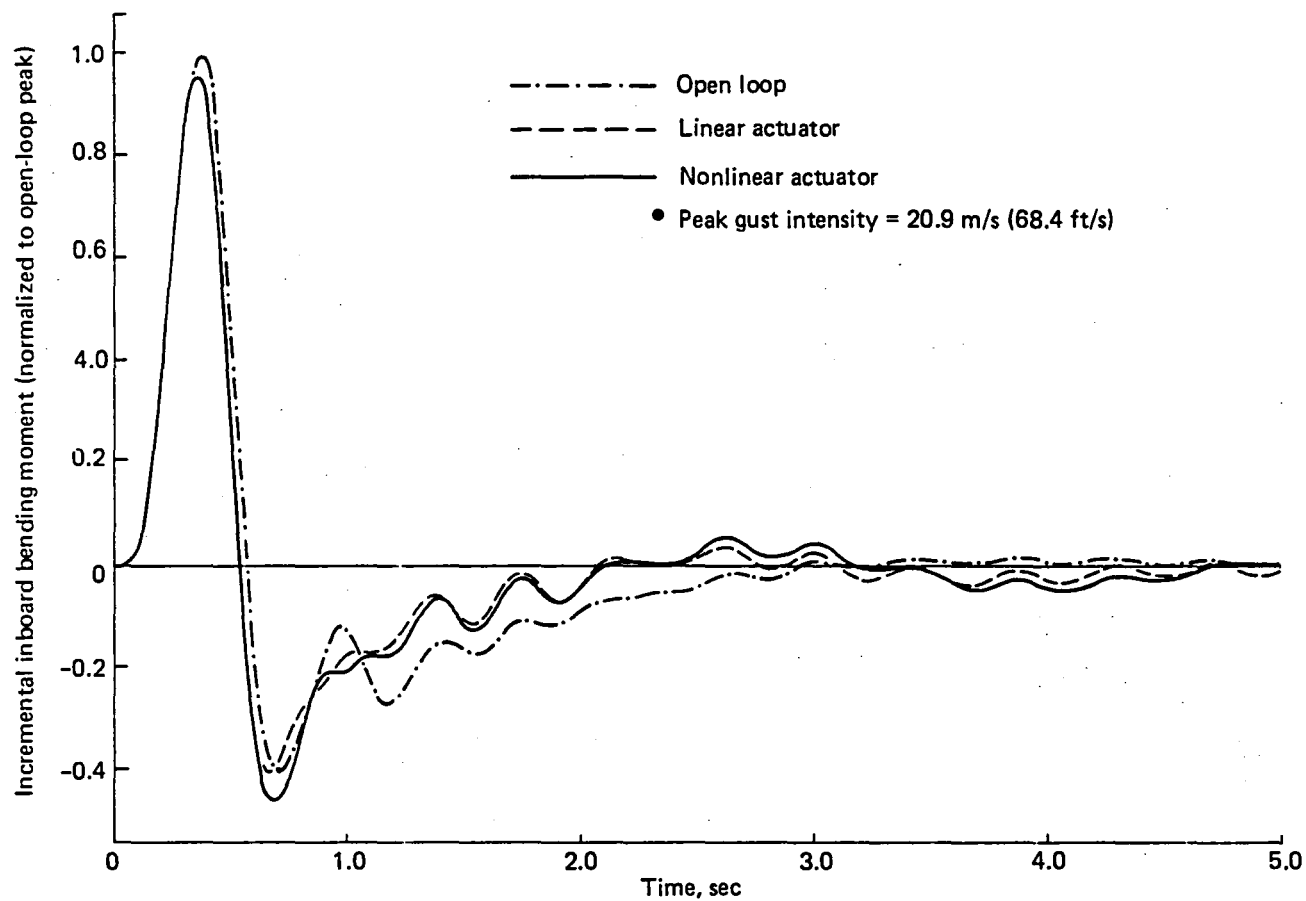
Figure F-153. *Response of Inboard Bending Moment (η = 0.25) to a Discrete (1-cos) Gust, Flight Condition 3, Time History Simulation*
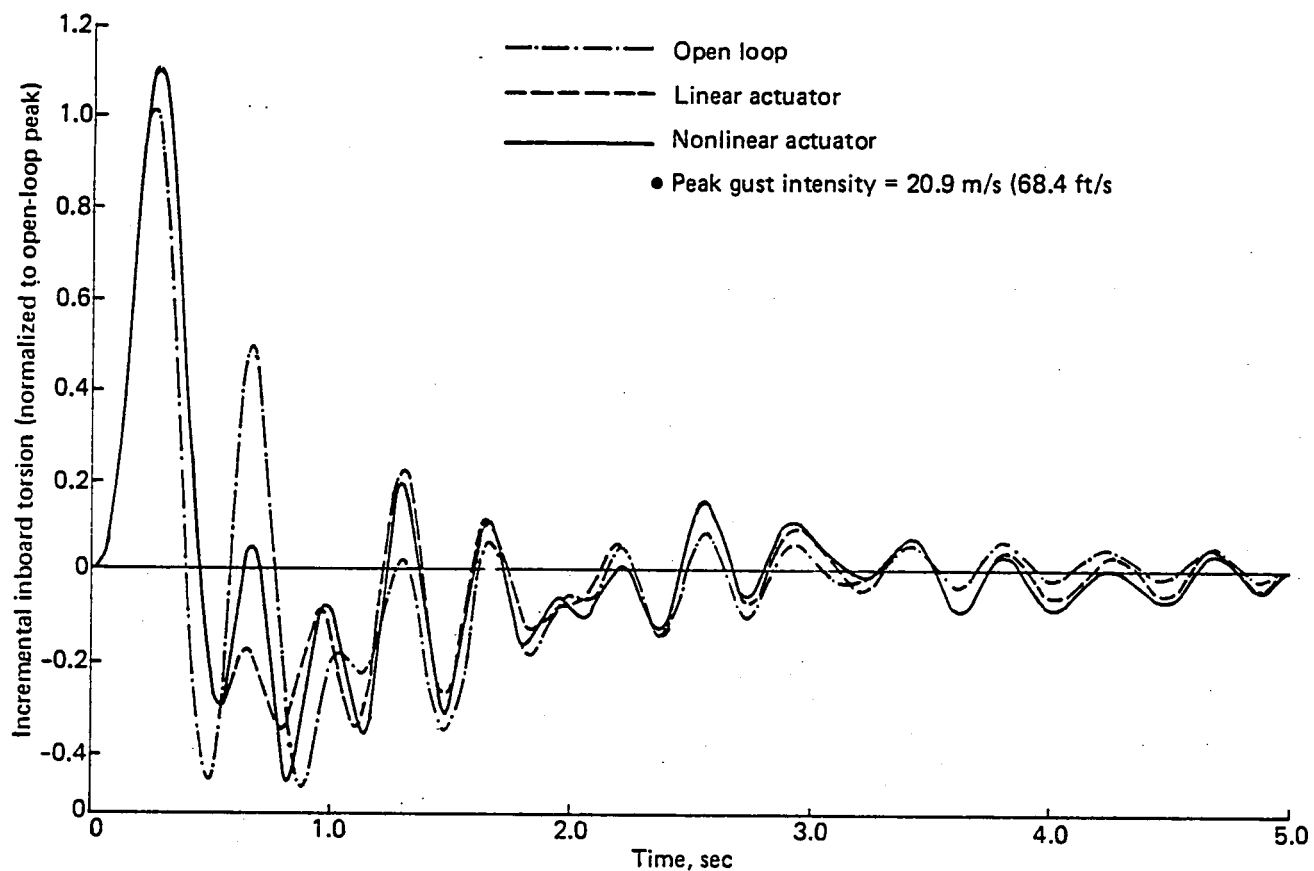
Figure F-154. Response of Inboard Torsion (η = 0.25) to a Discrete (1-cos) Gust, Flight Condition 3, Time History Simulation
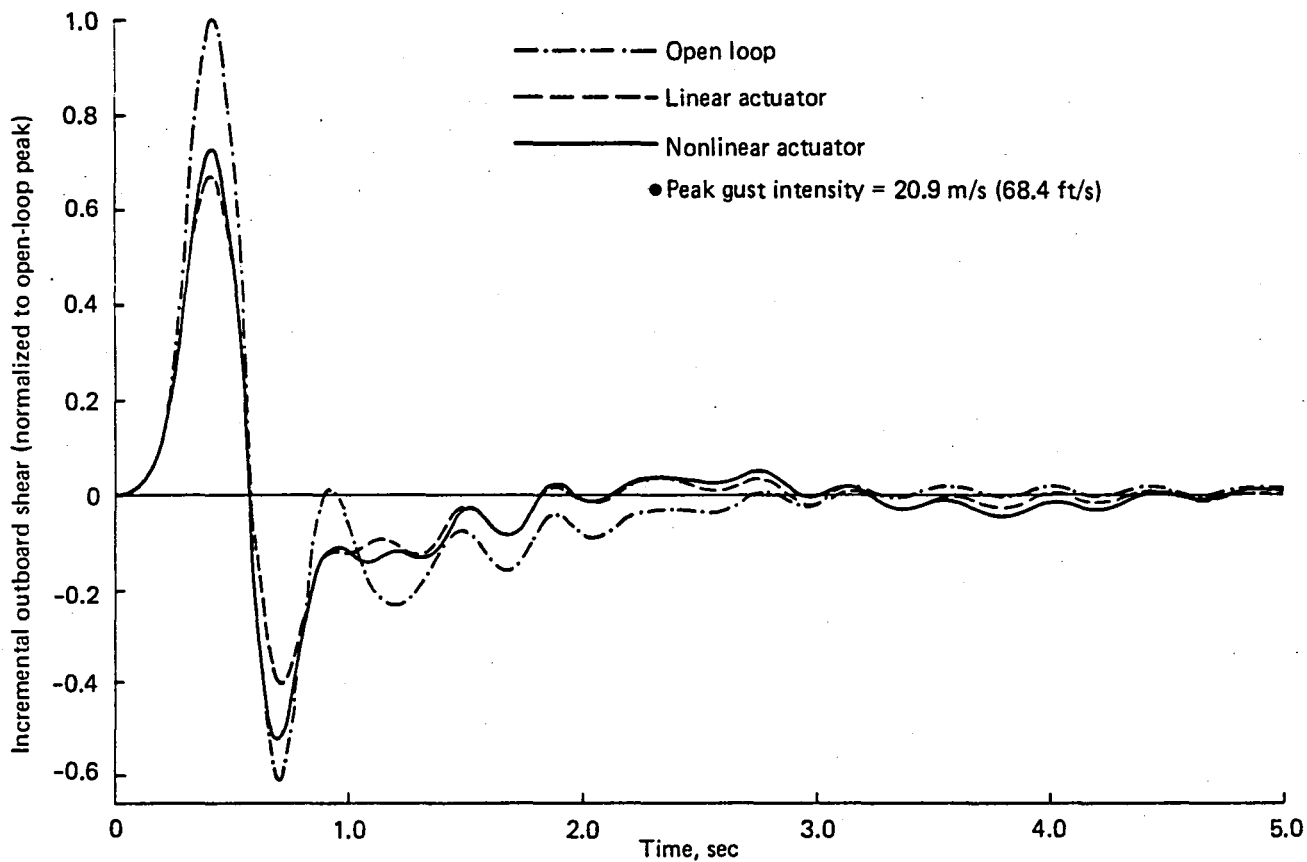
Figure F-155. Response of Outboard Shear ($\eta = 0.75$) to a Discrete (1-cos) Gust, Flight Condition 3, Time History Simulation

F-115
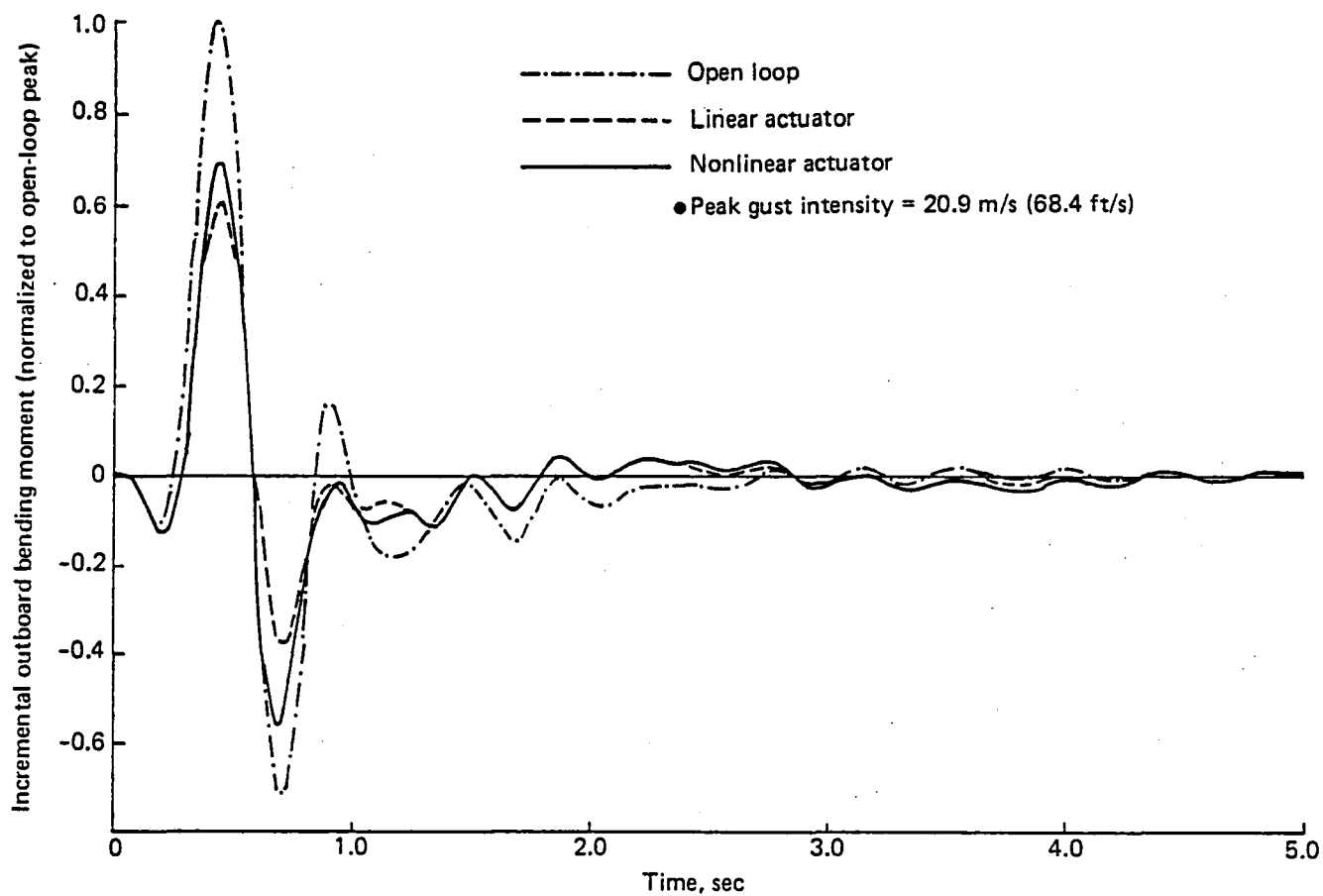
Figure F-156. Response of Outboard Bending Moment (η = 0.75) to a Discrete (1-cos) Gust, Flight Condition 3, Time History Simulation

*Figure F-157. Response of Outboard Torsion (η = 0.75) to a Discrete (1-cos) Gust,
Flight Condition 3, Time History Simulation*
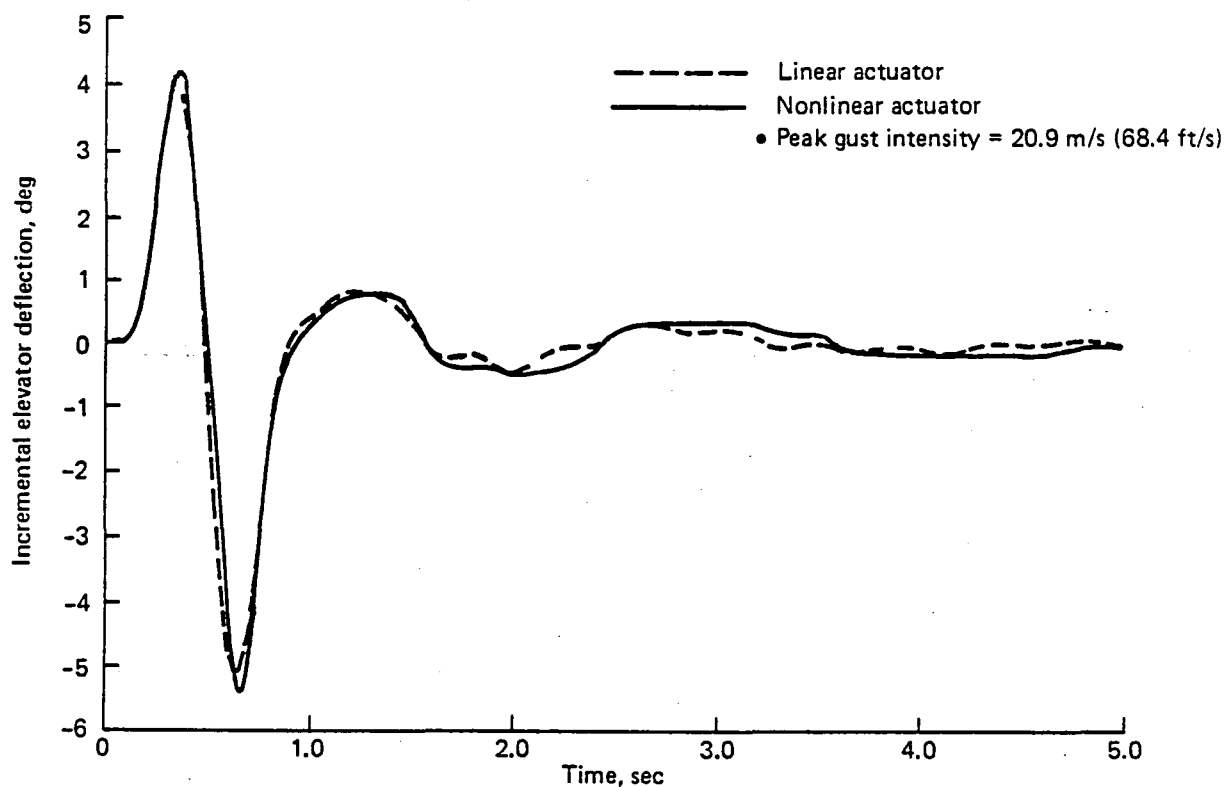
Figure F-158. Response of Elevator Deflection to a Discrete (1-cos) Gust,
Flight Condition 3, Time History Simulation
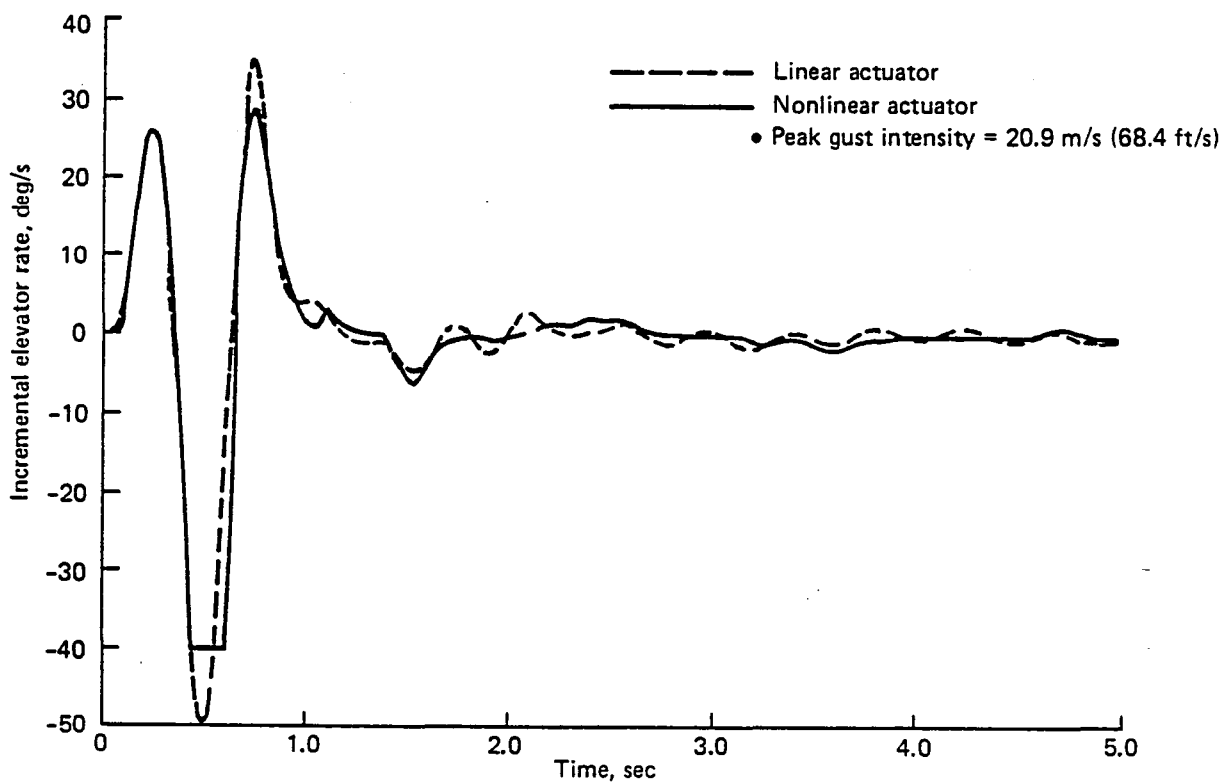
Figure F-159. Response of Elevator Rate to a Discrete (1-cos) Gust,
Flight Condition 3, Time History Simulation
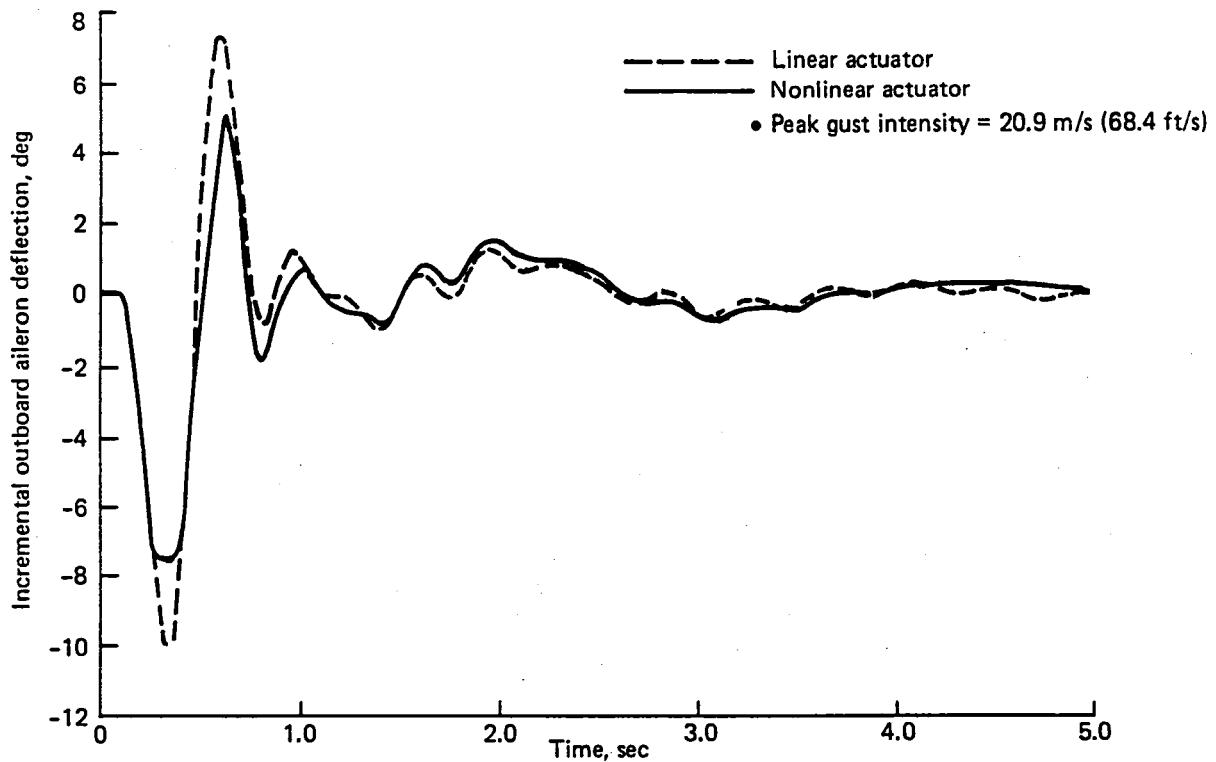
Figure F-160. Response of Outboard Aileron Deflection to a Discrete (1-cos) Gust, Flight Condition 3, Time History Simulation
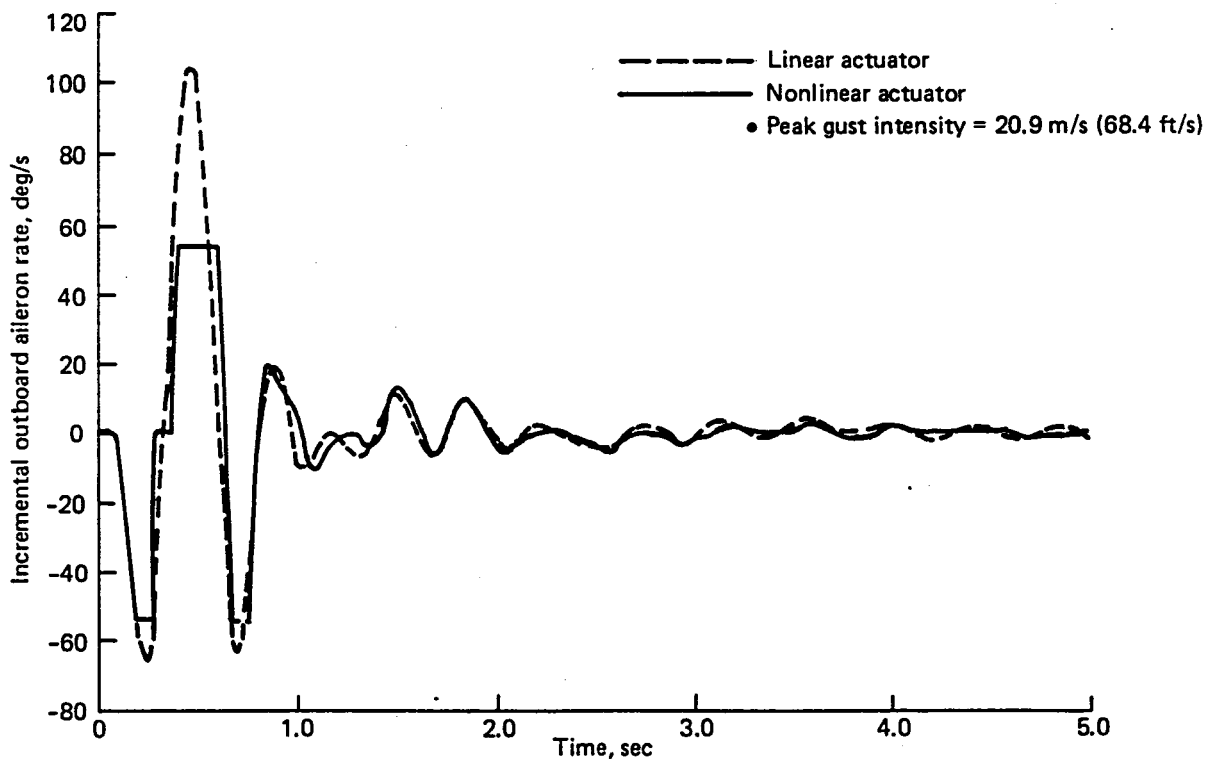
Figure F-161. Response of Outboard Aileron Rate to a Discrete (1-cos) Gust, Flight Condition 3, Time History Simulation
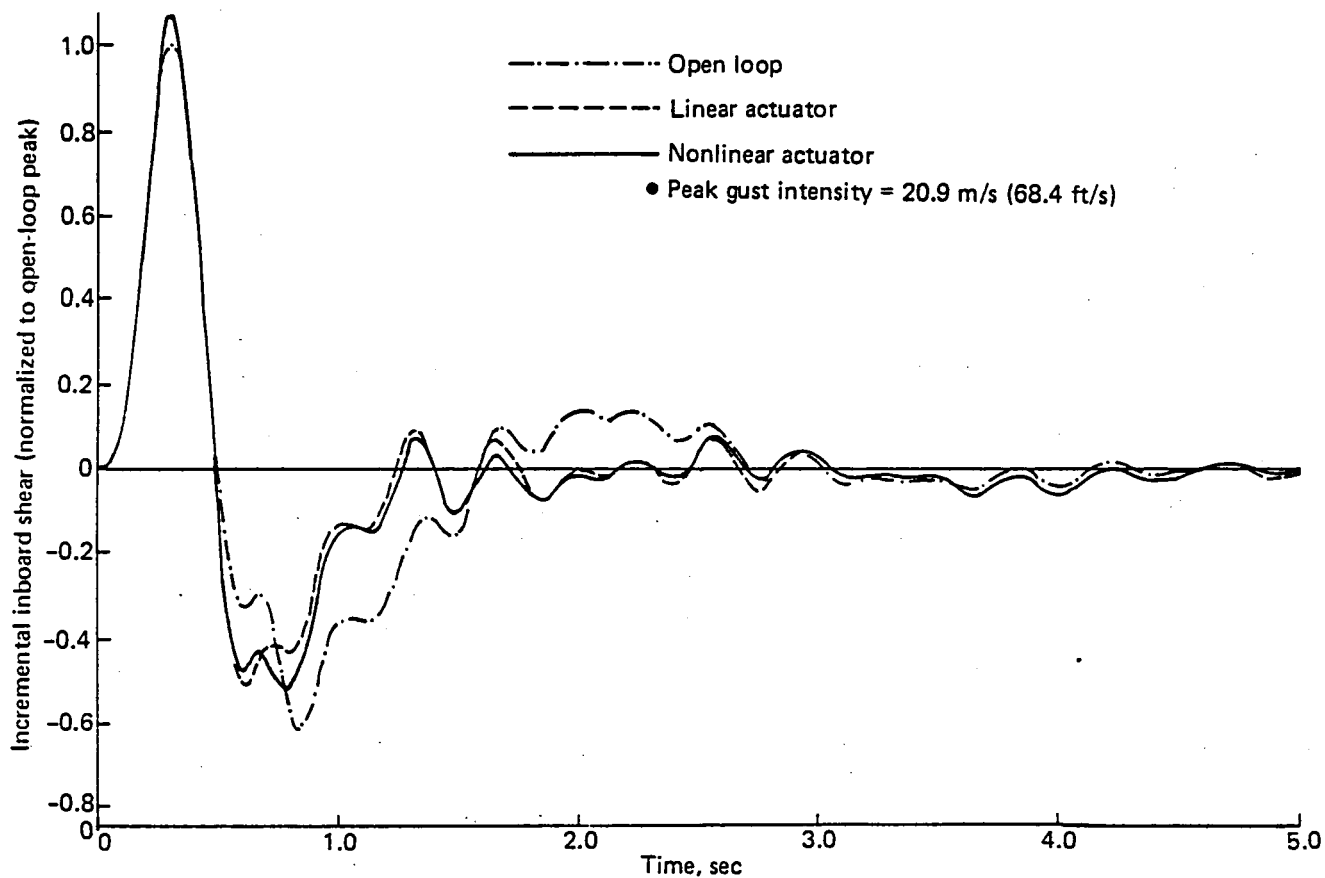
Figure F-162. Response of Inboard Shear (η = 0.25) to a Discrete (1-cos) Gust, Flight Condition 4, Time History Simulation
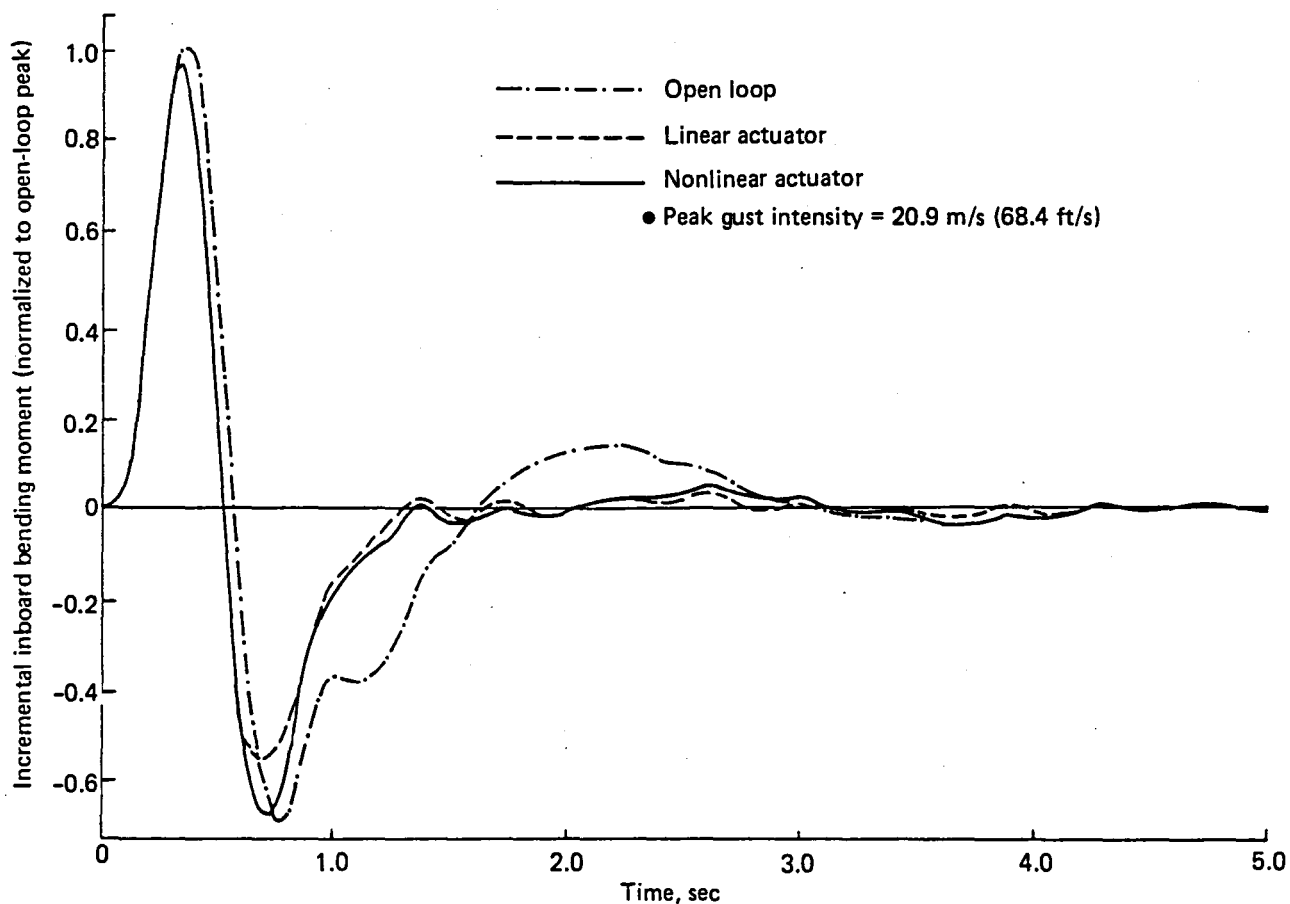
Figure F-163. Response of Inboard Bending Moment ($\eta = 0.25$) to a Discrete (1-cos) Gust, Flight Condition 4, Time History Simulation
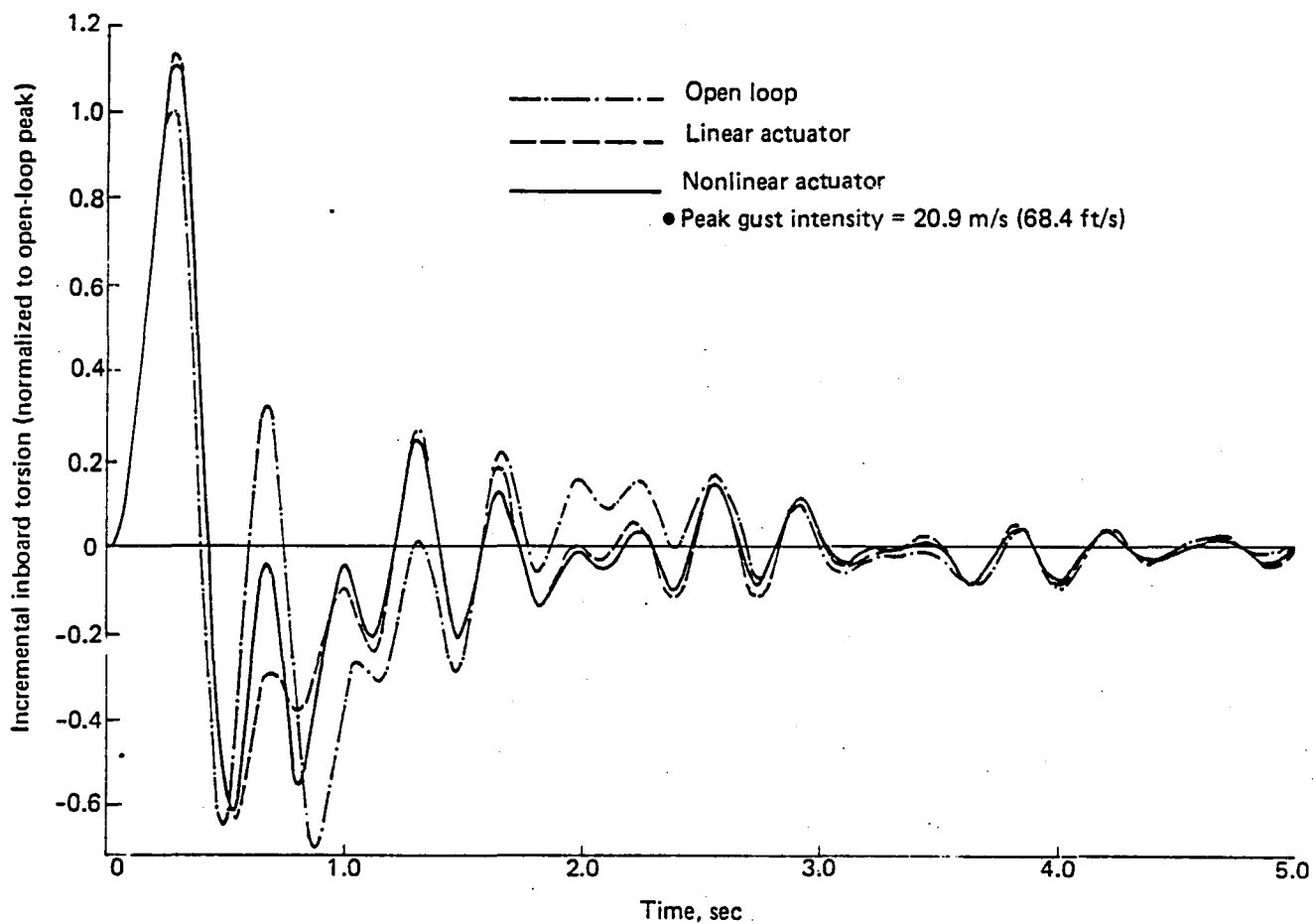
Figure F-164. *Response of Inboard Torsion (η = 0.25) to a Discrete (1-cos) Gust, Flight Condition 4, Time History Simulation*
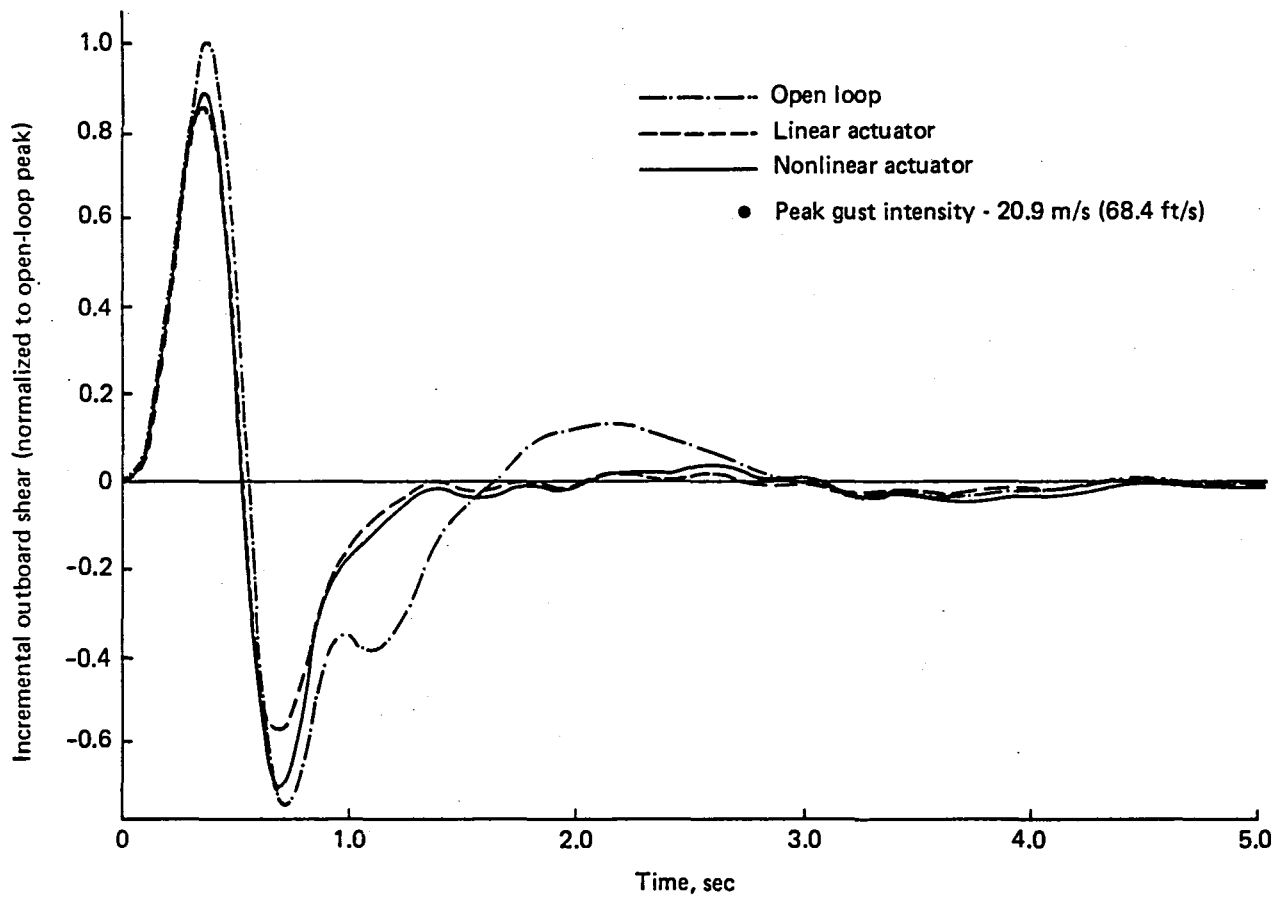
Figure F-165. Response of Outboard Shear (η = 0.75) to a Discrete (1-cos) Gust, Flight Condition 4, Time History Simulation

Figure F-166. Response of Outboard Bending Moment (η = 0.75) to a Discrete
(1-cos) Gust, Flight Condition 4, Time History Simulation
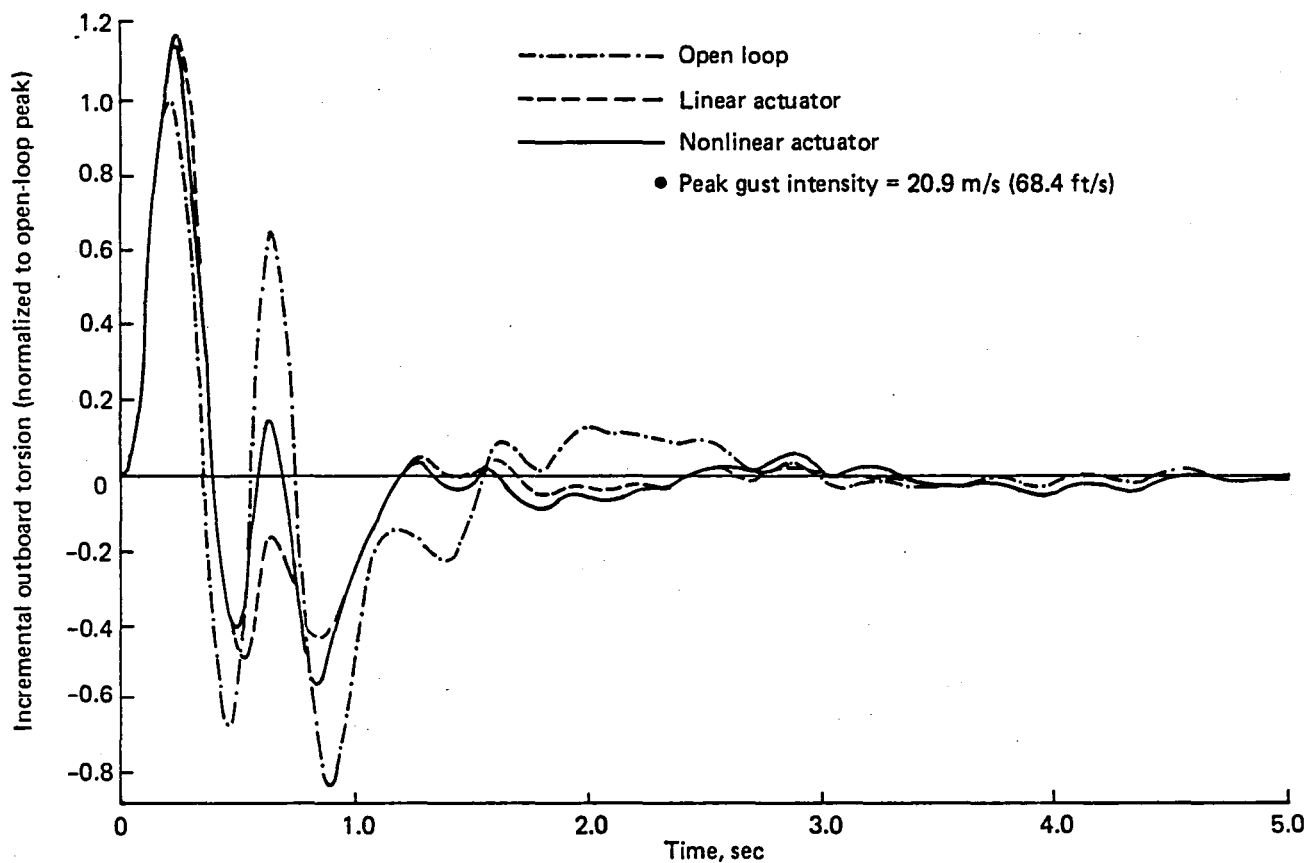
Figure F-167. Response of Outboard Torsion (η = 0.75) to a Discrete (1-cos) Gust, Flight Condition 4, Time History Simulation
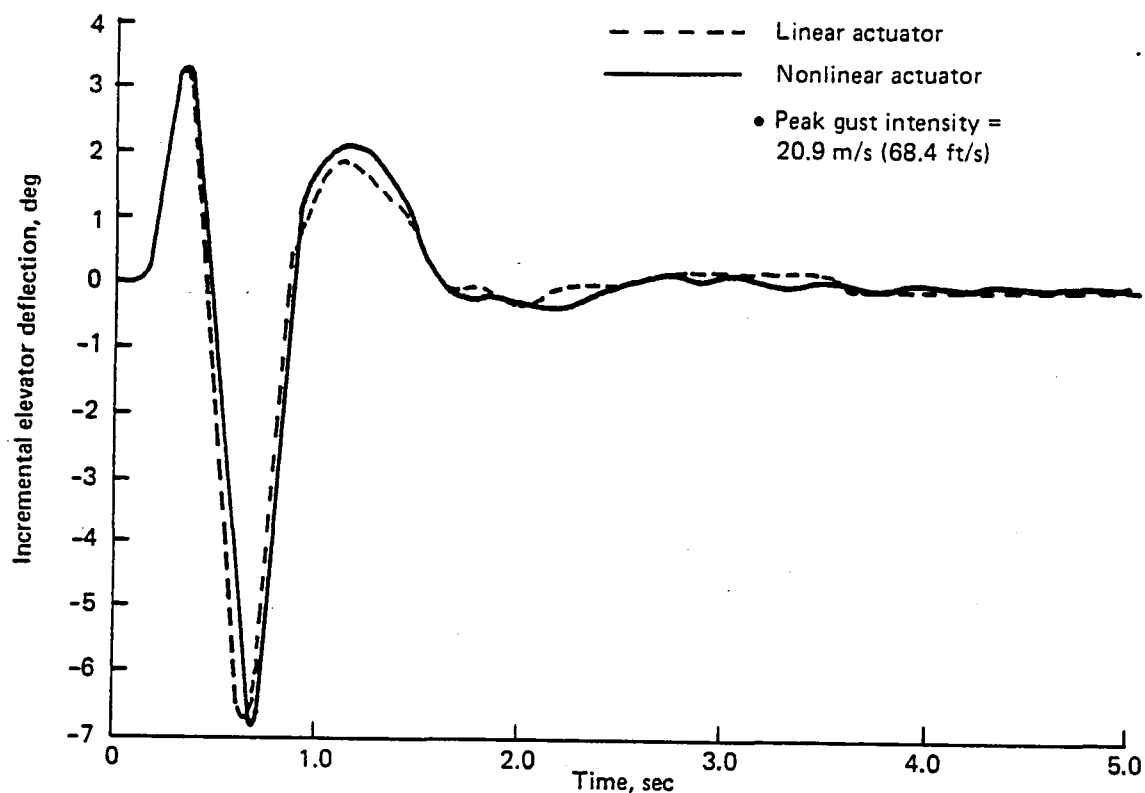
Figure F-168. Response of Elevator Deflection to a Discrete (1-cos) Gust, Flight Condition 4, Time History Simulation
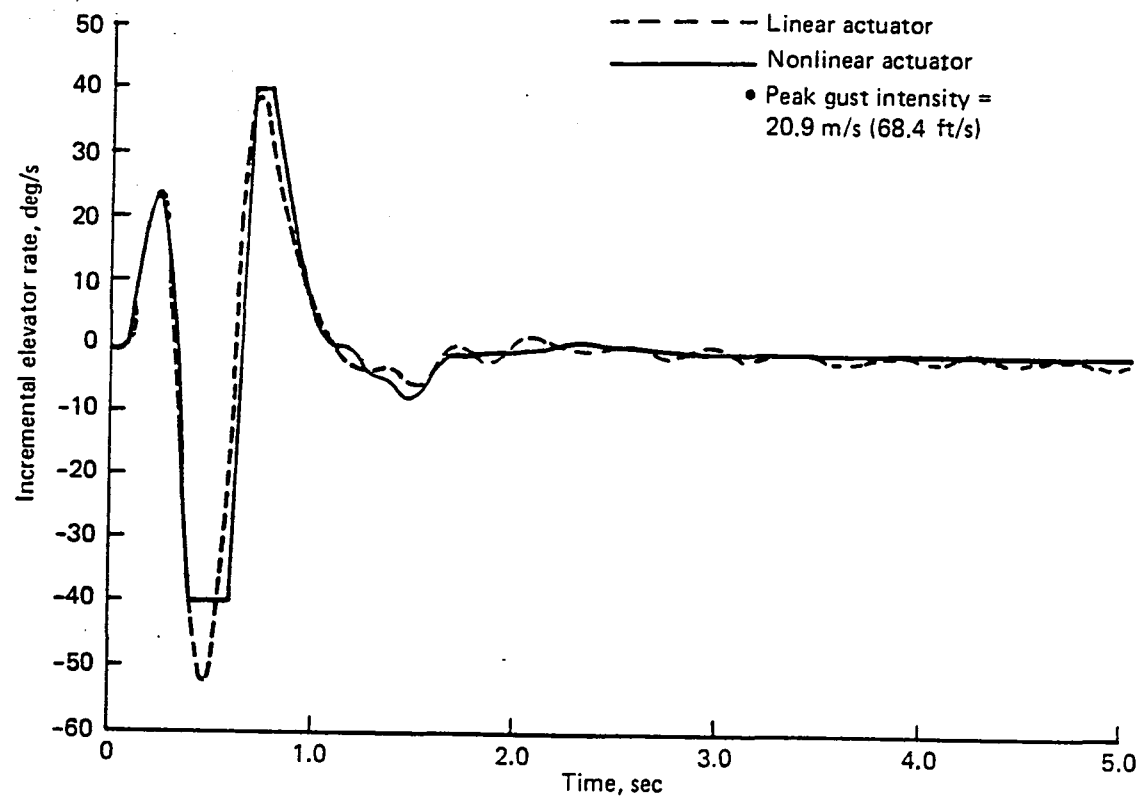
Figure F-169. Response of Elevator Rate to a Discrete (1-cos) Gust, Flight Condition 4, Time History Simulation
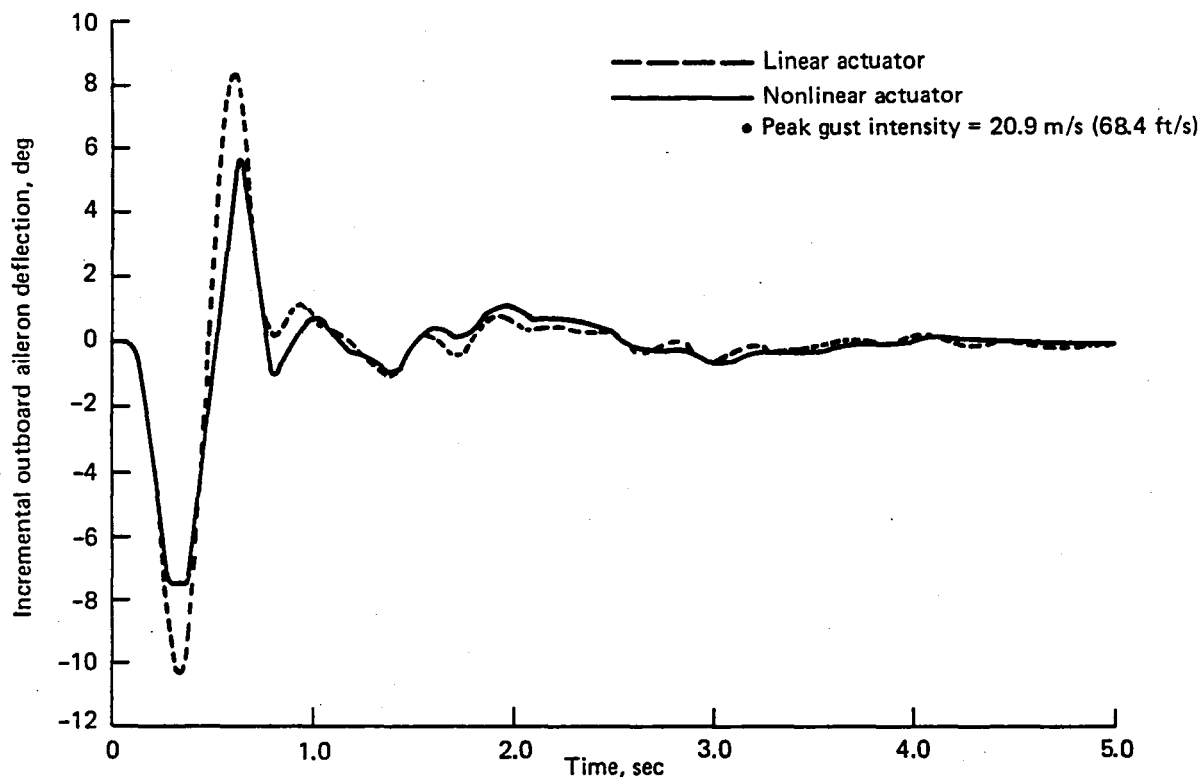
Figure F-170. Response of Outboard Aileron Deflection to a Discrete (1-cos) Gust, Flight Condition 4, Time History Simulation
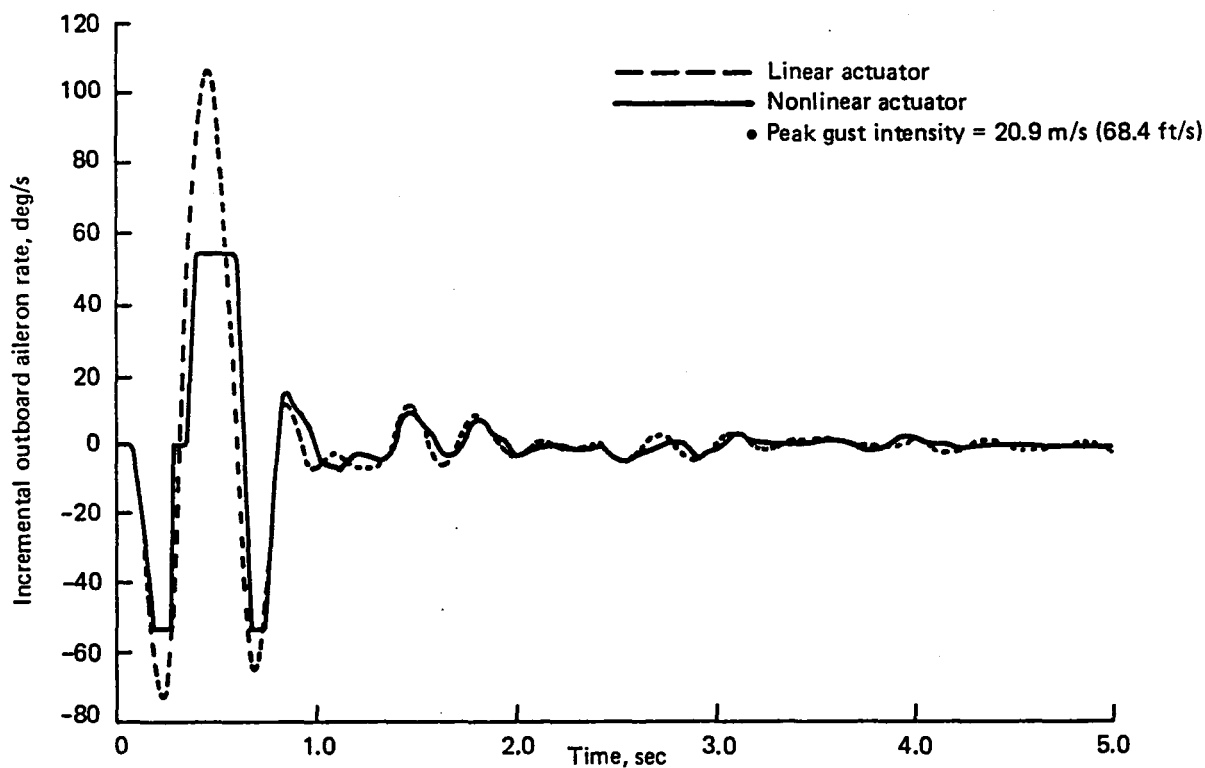
Figure F-171. Response of Outboard Aileron Rate to a Discrete (1-cos) Gust, Flight Condition 4, Time History Simulation

F-127
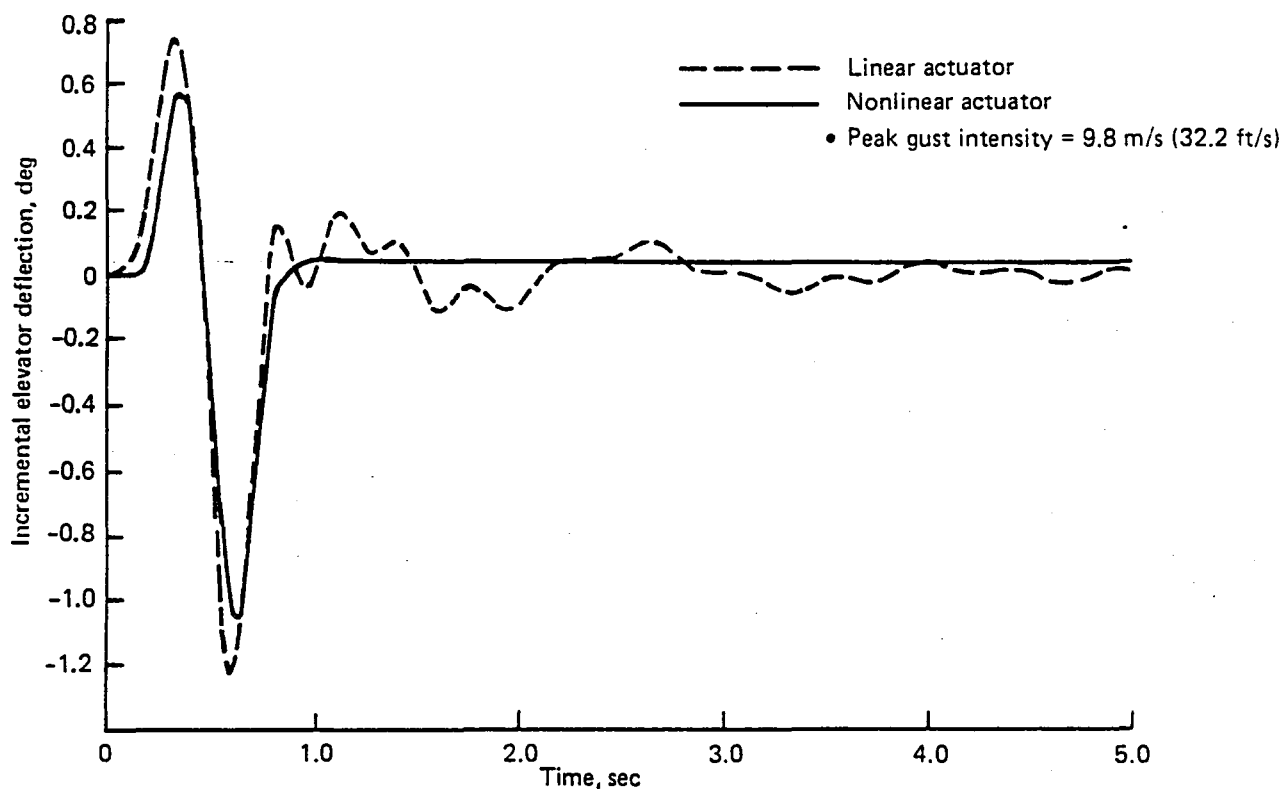
Figure F-172. Response of Elevator Deflection to a Discrete (1-cos) Gust, Flight Condition 5, Time History Simulation
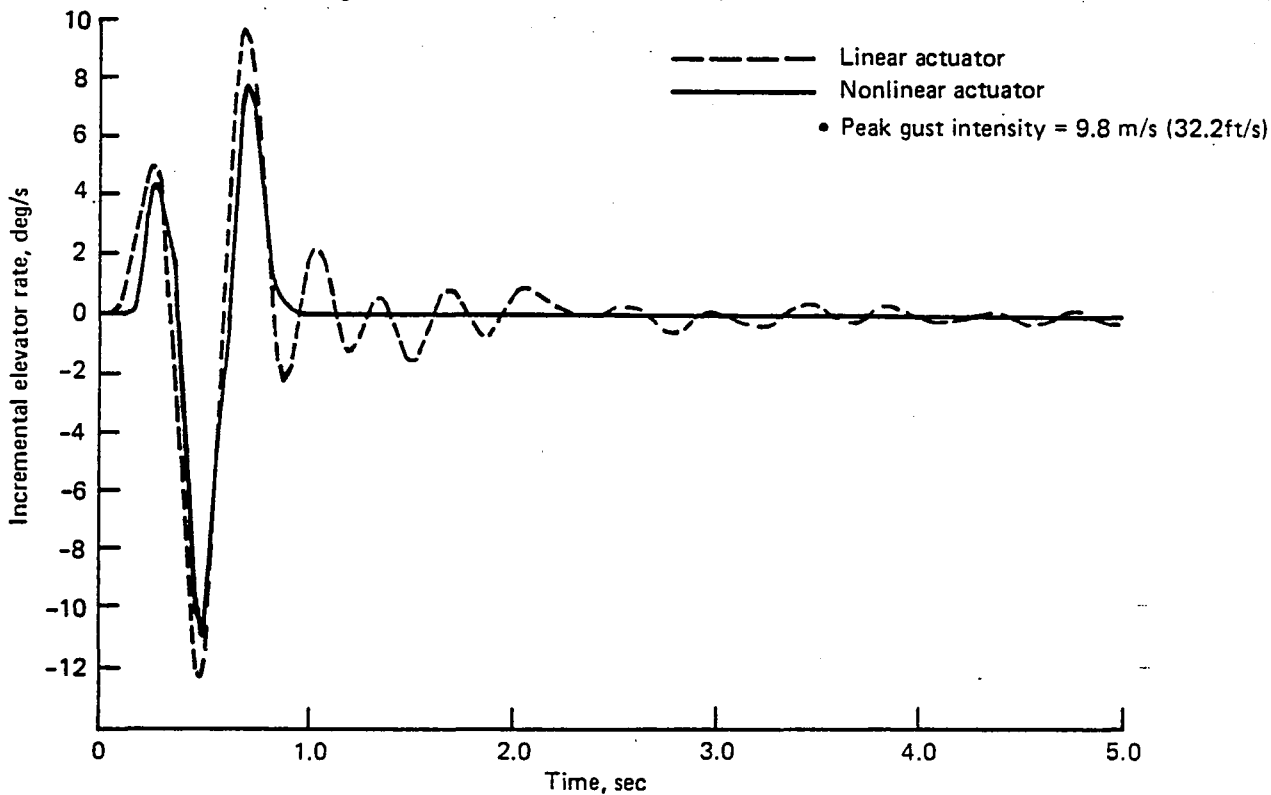
Figure F-173. Response of Elevator Rate to a Discrete (1-cos) Gust, Flight Condition 5, Time History Simulation
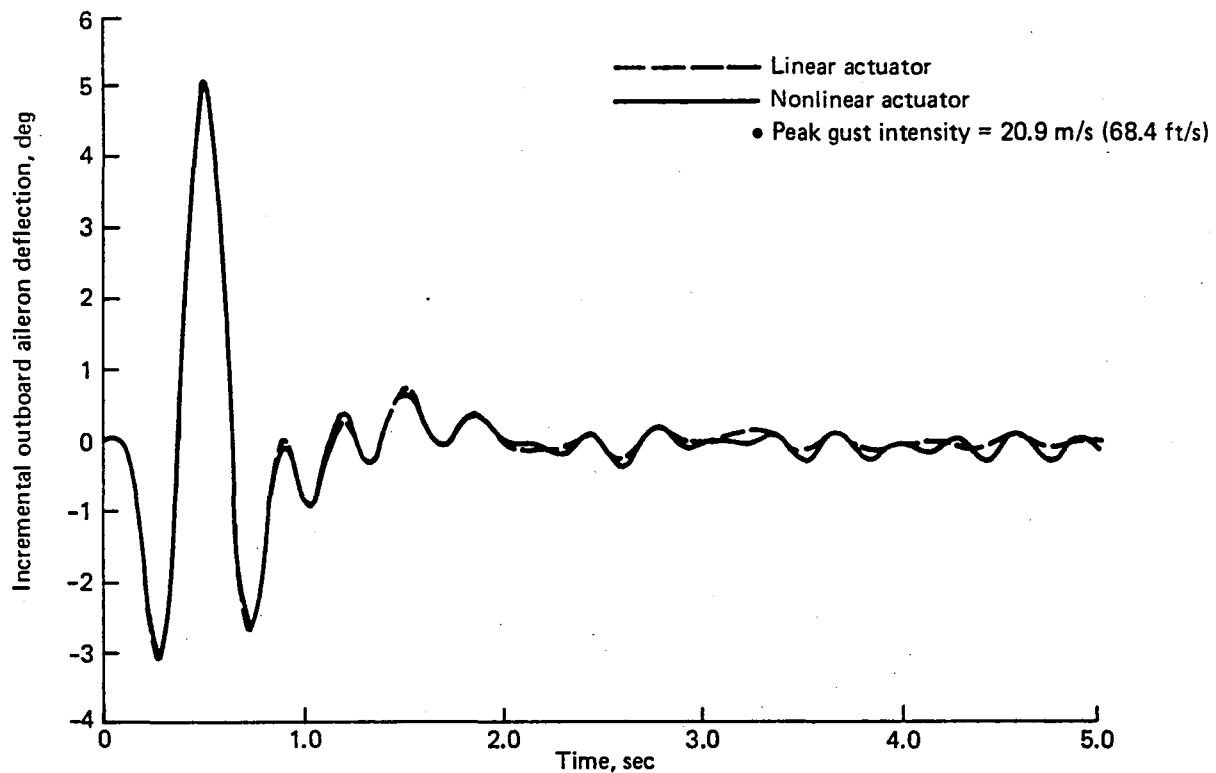
Figure F-174. *Response of Outboard Aileron Deflection to a Discrete (1-cos) Gust, Flight Condition 5, Time History Simulation*
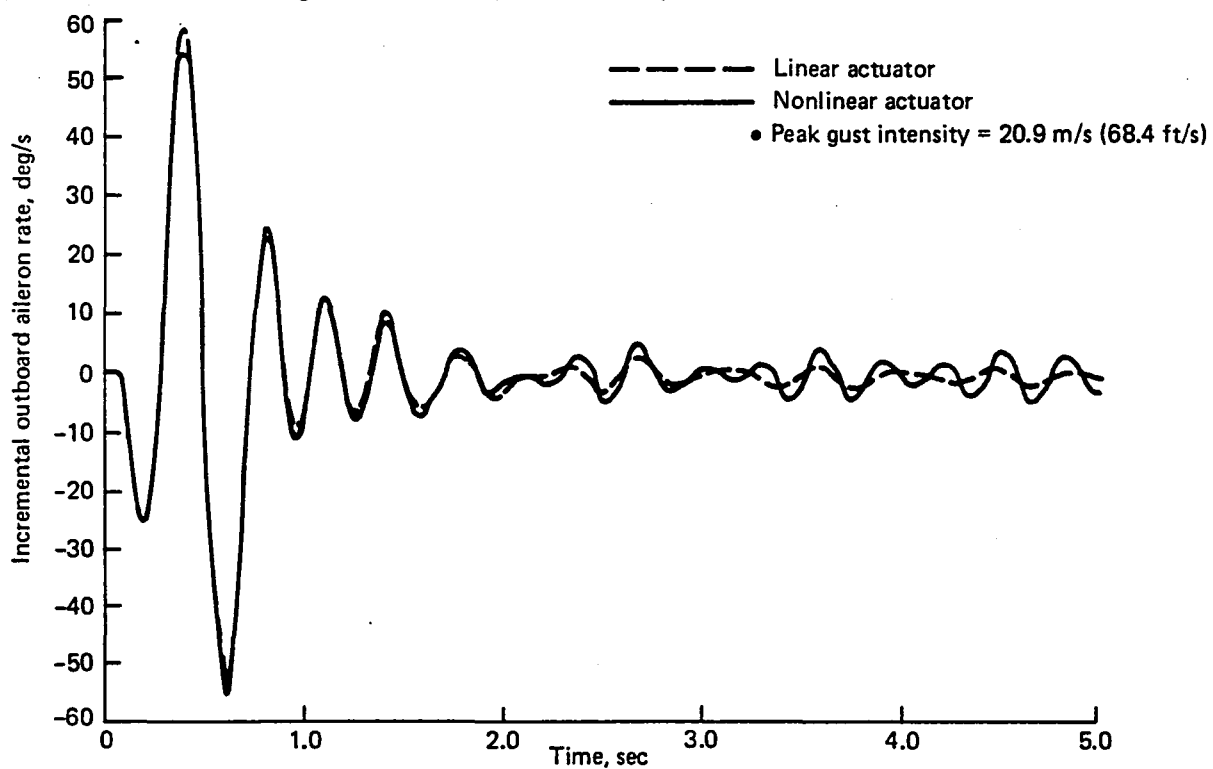
Figure F-175. *Response of Outboard Aileron Rate to a Discrete (1-cos) Gust, Flight Condition 5, Time History Simulation*
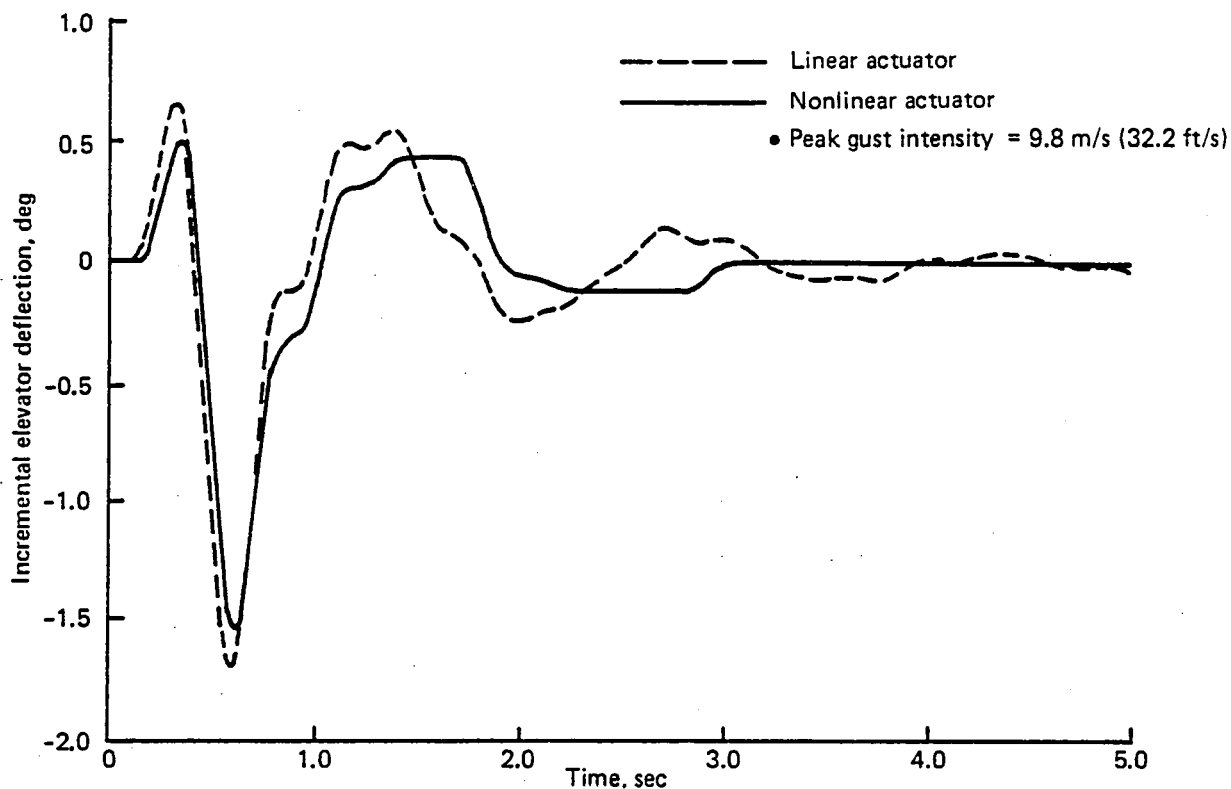
Figure F-176. *Response of Elevator Deflection to a Discrete (1-cos) Gust, Flight Condition 6, Time History Simulation*
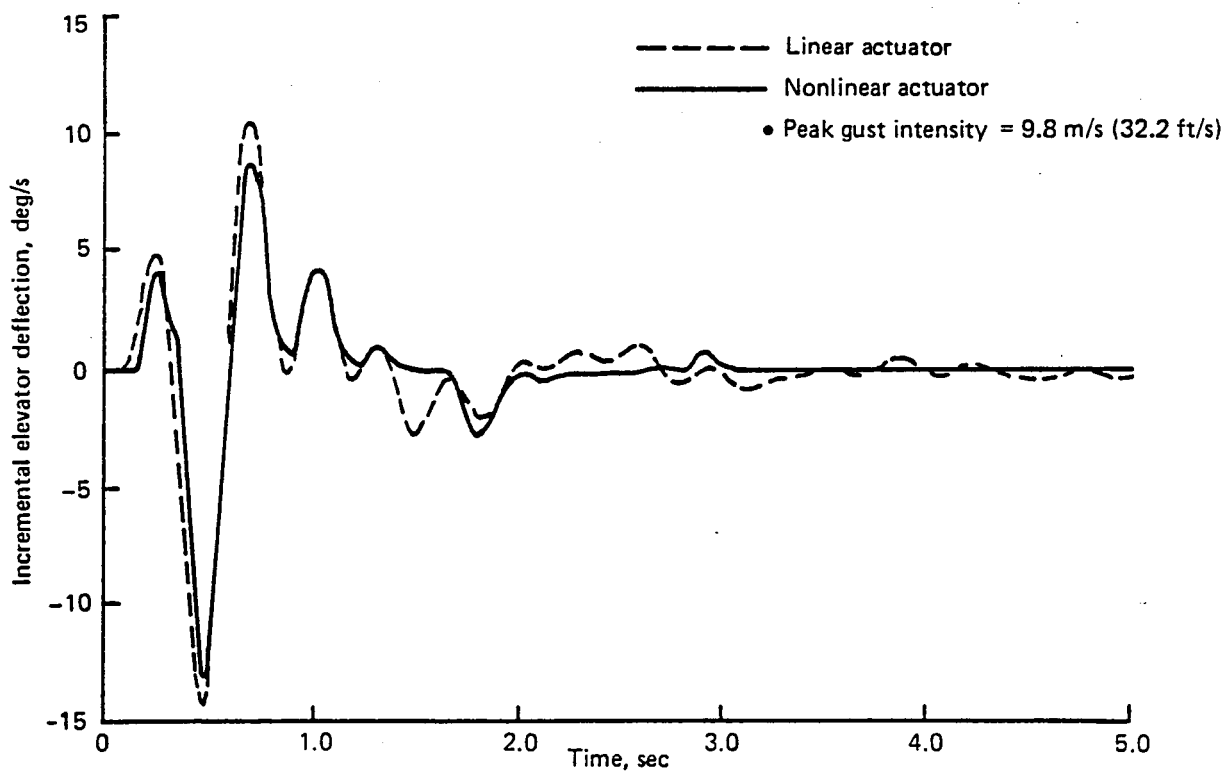
Figure F-177. *Response of Elevator Rate to a Discrete (1-cos) Gust, Flight Condition 6, Time History Simulation*
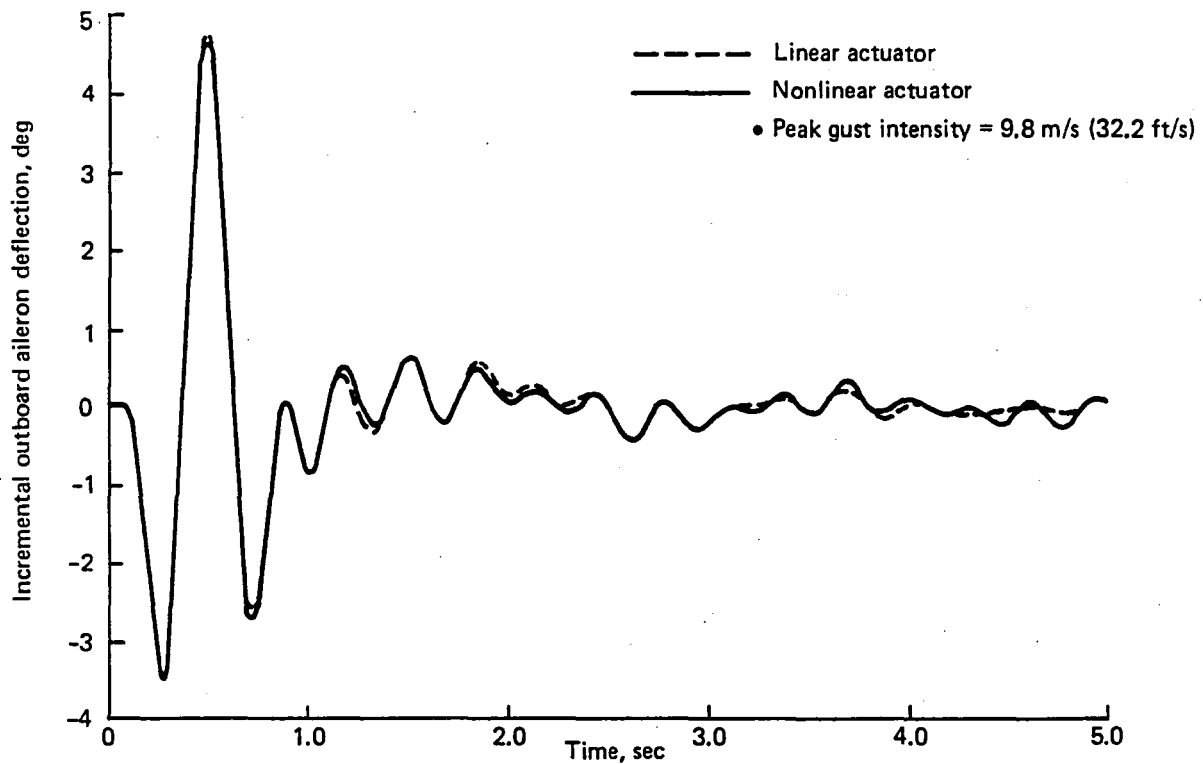
Figure F-178. *Response of Outboard Aileron Deflection to a Discrete (1-cos) Gust, Flight Condition 6, Time History Simulation*
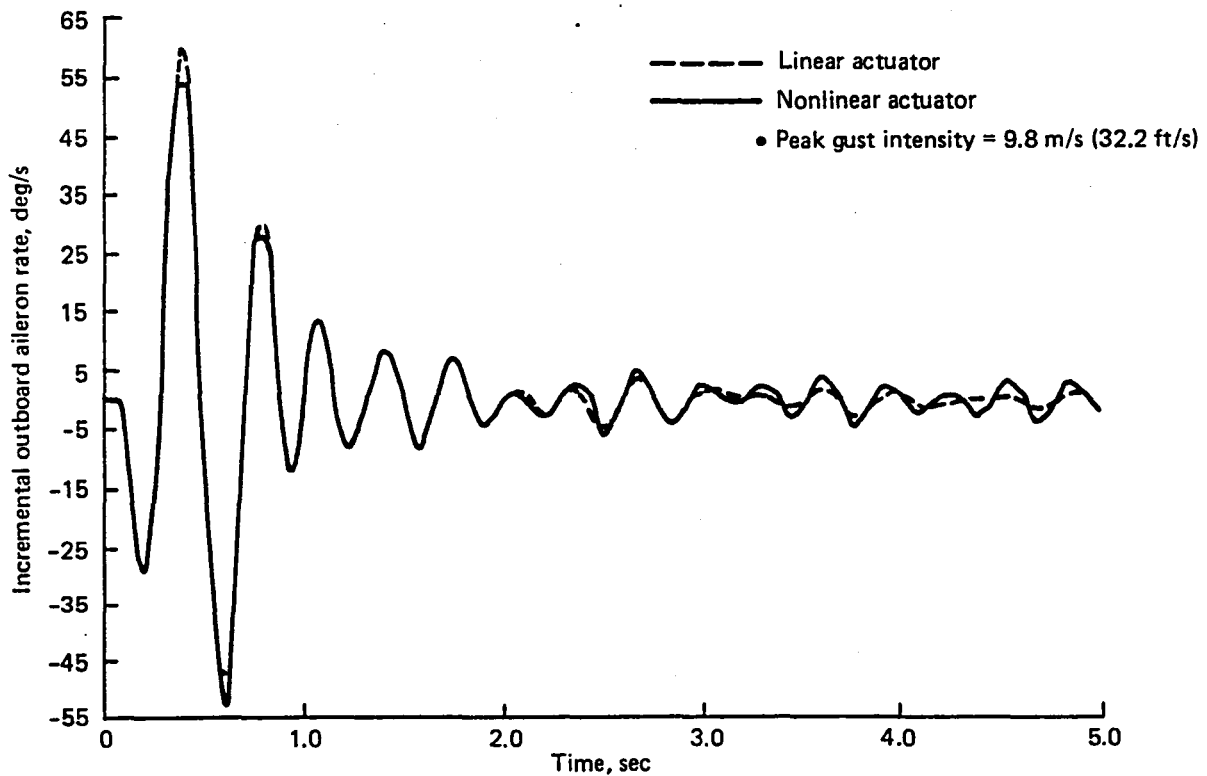
Figure F-179. *Response of Outboard Aileron Rate to a Discrete (1-cos) Gust, Flight Condition 6, Time History Simulation*

F.4.3.2 EFFECT OF GUST MAGNITUDE

Figures F-180 through F-195 show for various flight conditions the effects of increasing gust magnitude on the wing-load relief provided by a GLA system incorporating nonlinear actuators.
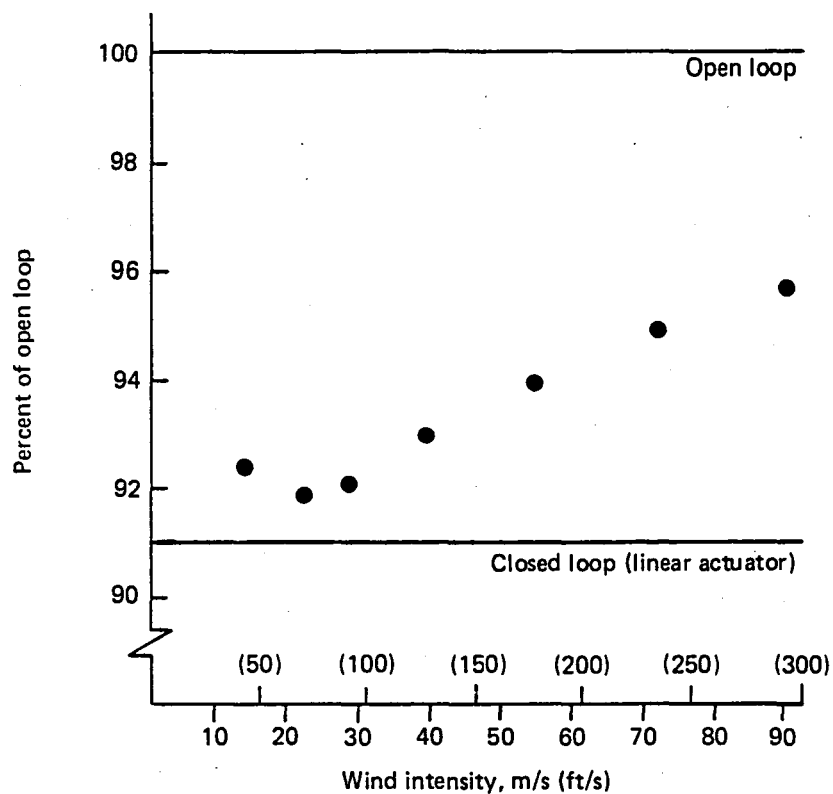
Figure F-180. *Effect of Actuator Nonlinearities on Incremental Inboard Bending Moment (η = 0.25), Flight Condition 1*

Figure F-181. *Effect of Actuator Nonlinearities on Incremental Inboard Torsion (η = 0.25), Flight Condition 1*

F-133

Figure F-182. Effect of Actuator Nonlinearities on Incremental
Outboard Bending Moment (η = 0.75), Flight Condition 1
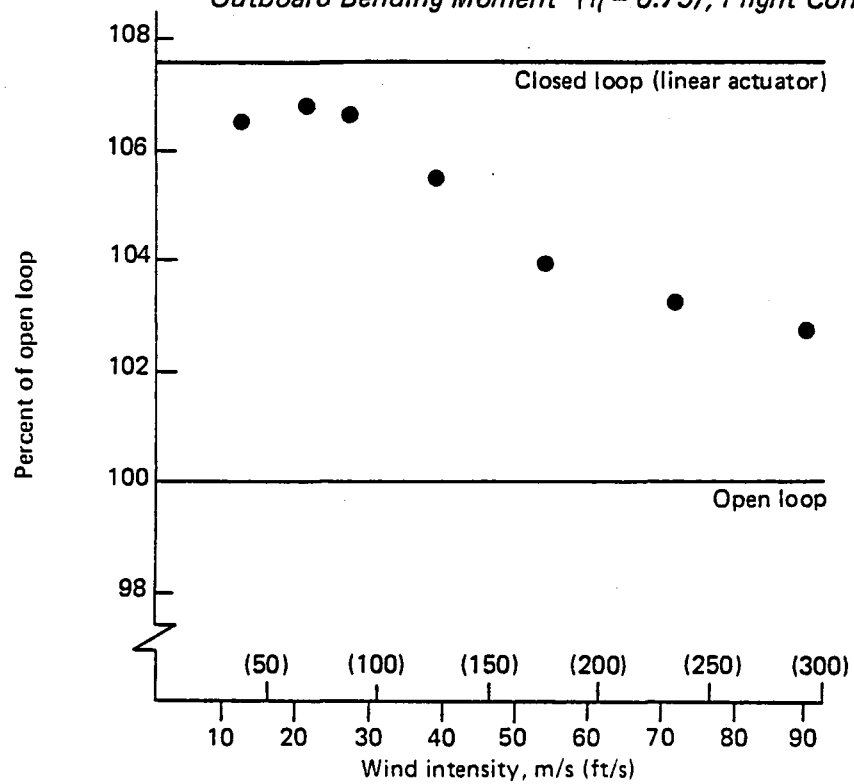
Figure F-183. Effect of Actuator Nonlinearities on Incremental
Outboard Torsion (η = 0.75), Flight Condition 1
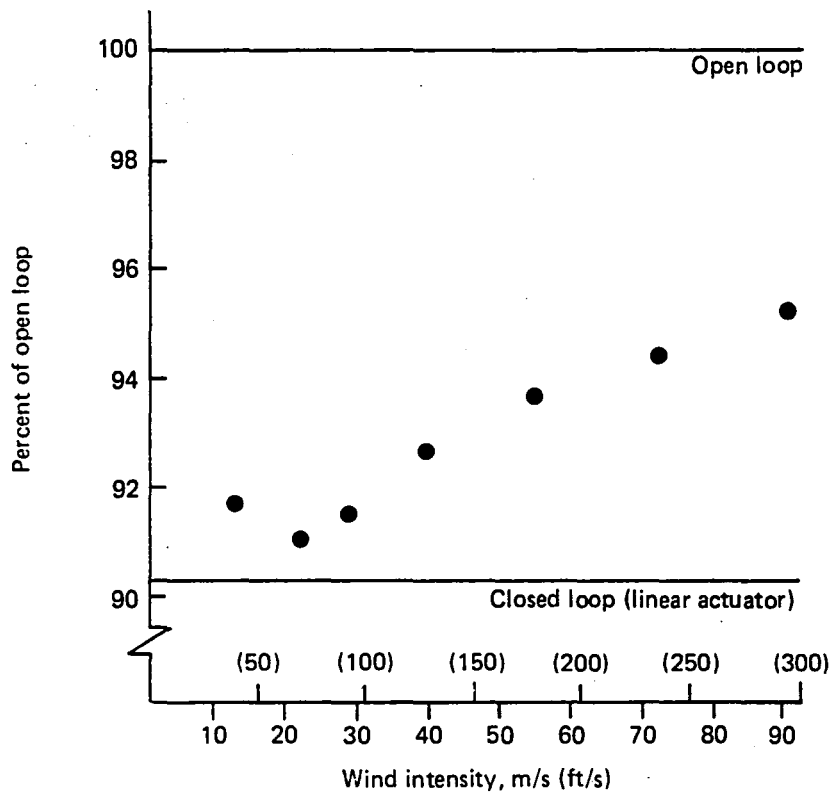
Figure F-184. Effect of Actuator Nonlinearities on Incremental Inboard Bending Moment (η = 0.25), Flight Condition 2

Figure F-185. Effect of Actuator Nonlinearities on Incremental Inboard Torsion (η = 0.25), Flight Condition 2

Figure F-186. Effect of Actuator Nonlinearities on Incremental Outboard
Bending Moment (η = 0.75), Flight Condition 2
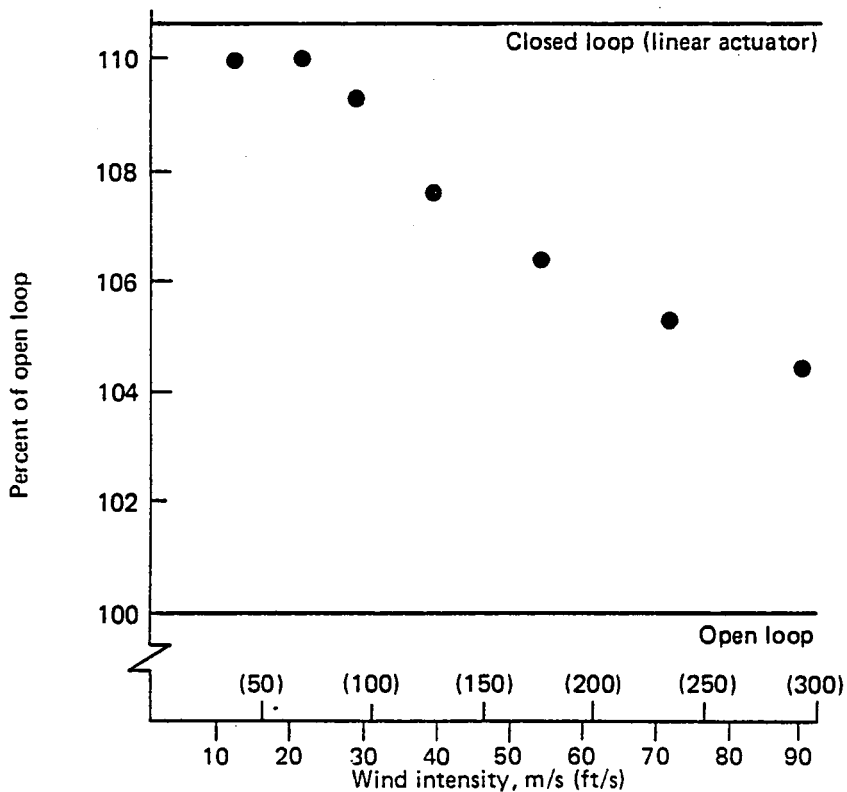
Figure F-187. Effect of Actuator Nonlinearities on Incremental Outboard
Torsion (η = 0.75), Flight Condition 2
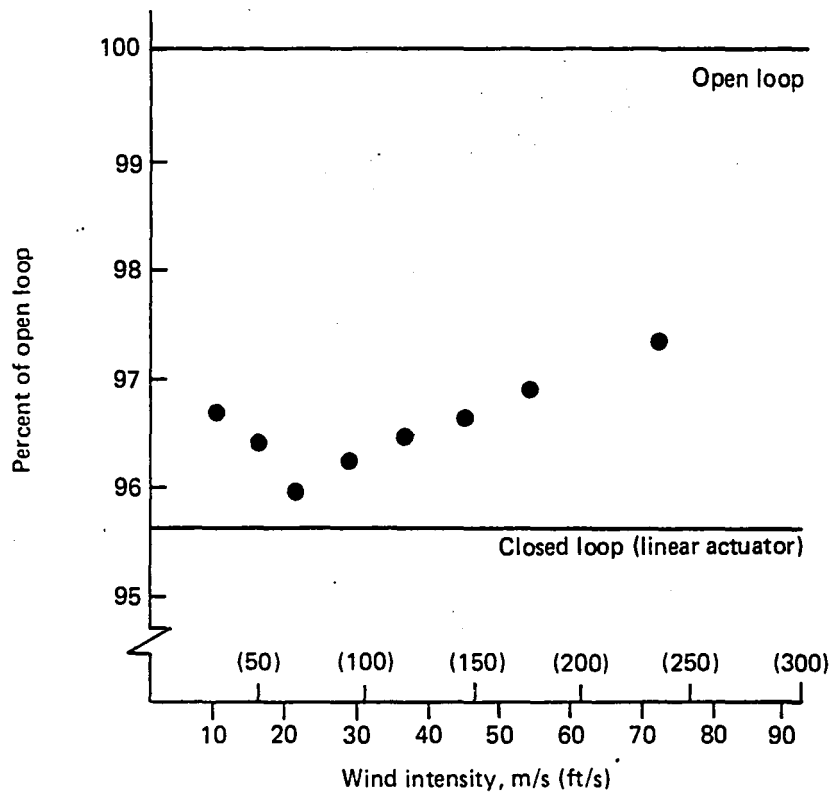
Figure F-188. Effect of Actuator Nonlinearities on Incremental Inboard Bending Moment ($\eta = 0.25$), Flight Condition 3
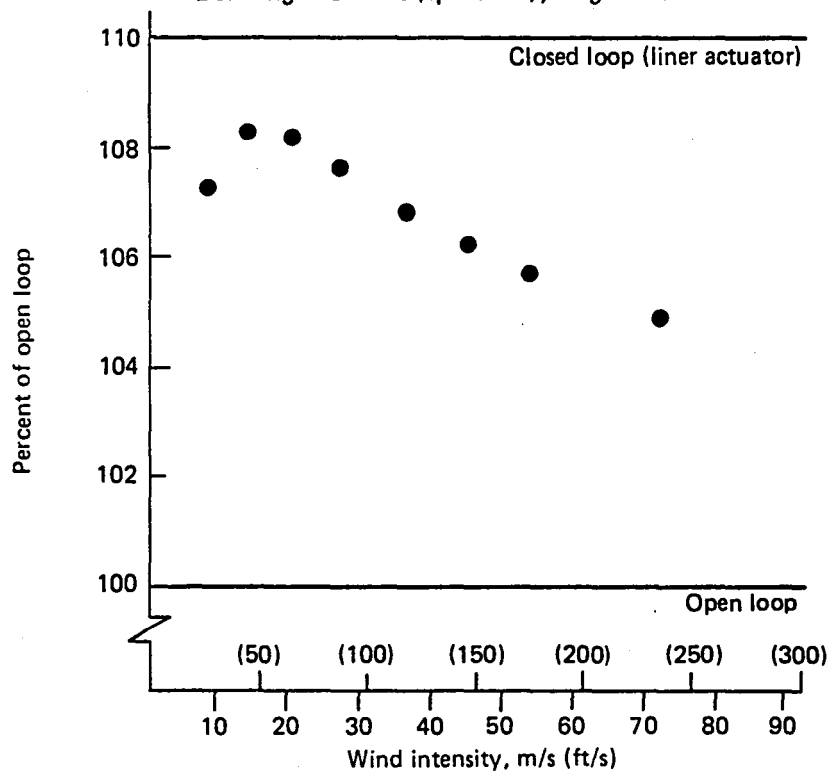
Figure F-189. Effect of Actuator Nonlinearities on Incremental Inboard Torsion ($\eta = 0.25$), Flight Condition 3

F-137
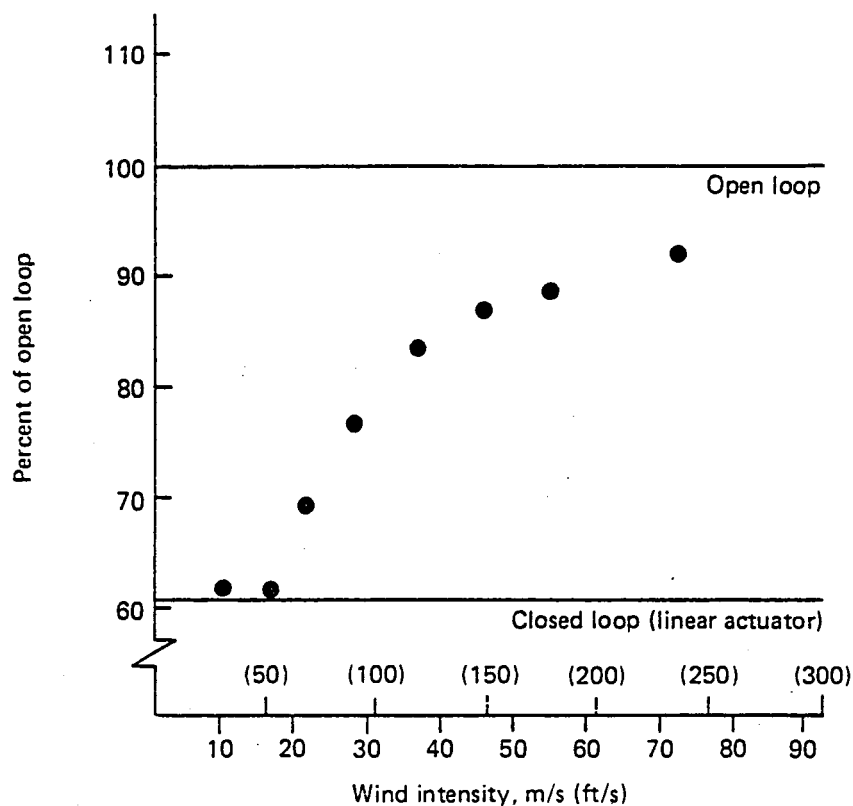
Figure F-190. Effect of Actuator Nonlinearities on Incremental Outboard
Bending Moment (η = 0.75), Flight Condition 3
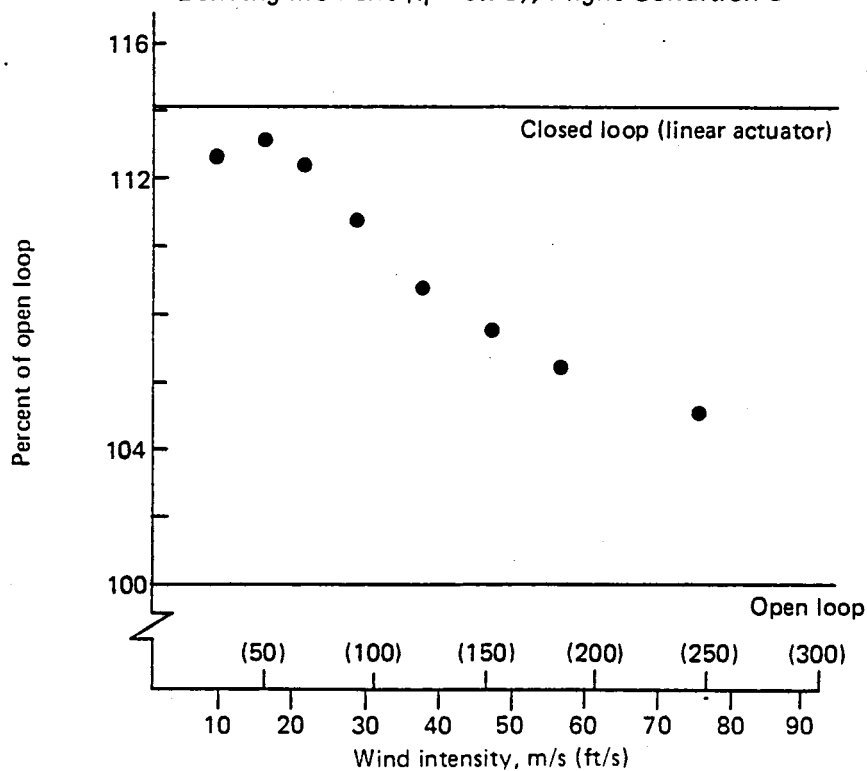
Figure F-191. Effect of Actuator Nonlinearities on Incremental Outboard
Torsion (η = 0.75), Flight Condition 3
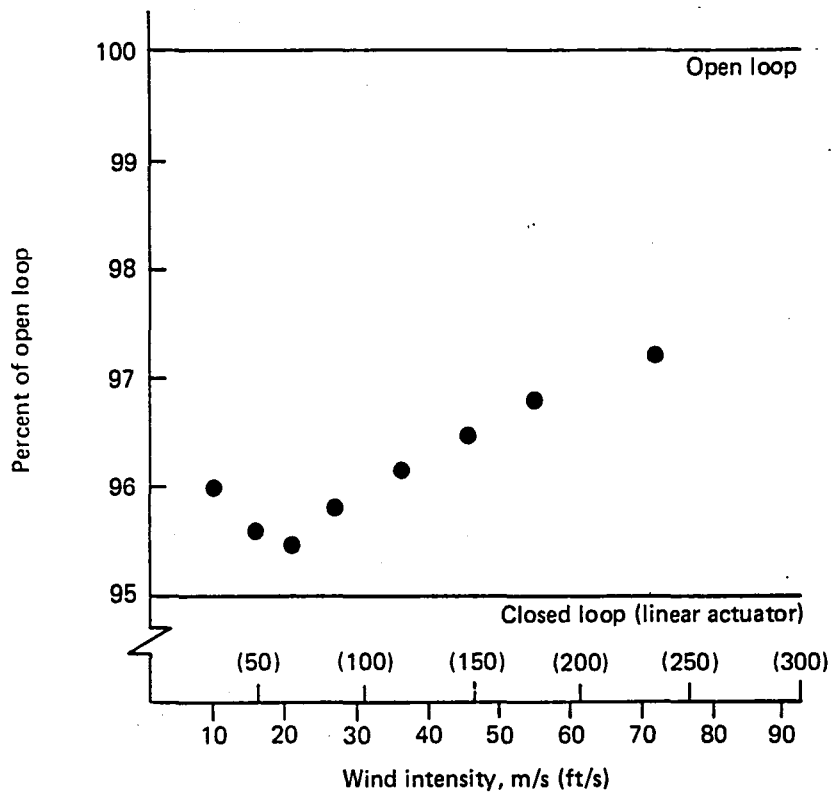
Figure F-192. Effect of Actuator Nonlinearities on Incremental Inboard
Bending Moment (η = 0.25), Flight Condition 4

Figure F-193. Effect of Actuator Nonlinearities on Incremental Inboard
Torsion (η = 0.25), Flight Condition 4

Figure F-194. Effect of Actuator Nonlinearities on Incremental Outboard Bending Moment (η = 0.75), Flight Condition 4
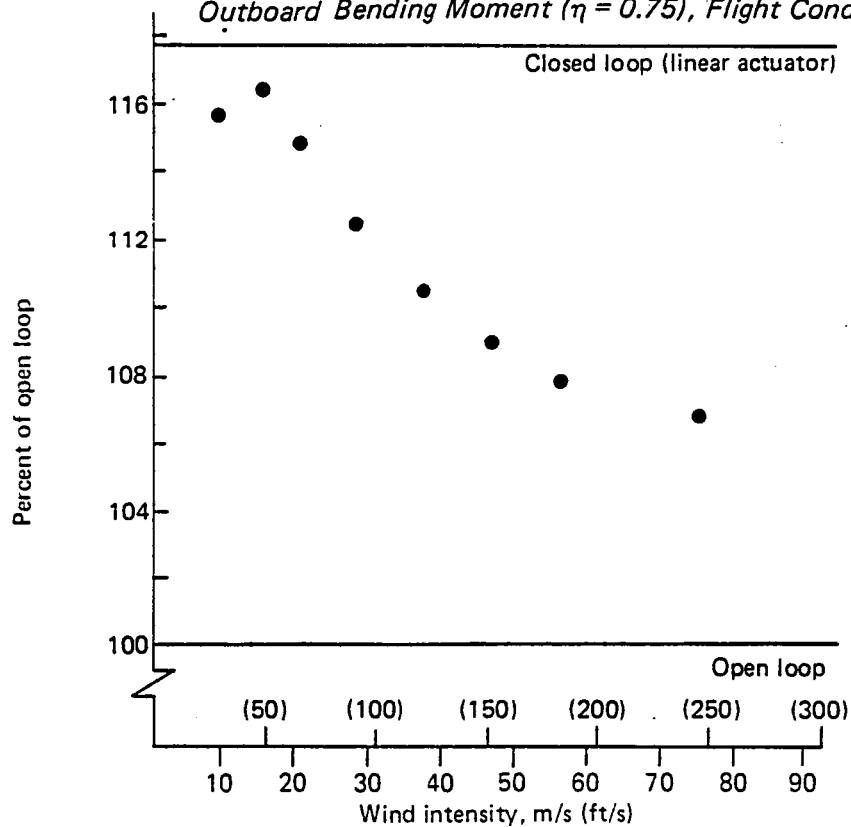
Figure F-195. Effect of Actuator Nonlinearities on Incremental Outboard Torsion (η = 0.75), Flight Condition 4

APPENDIX G: ALTERNATIVE
IMPLEMENTATION OF ACT

APPENDIX G: ALTERNATIVE IMPLEMENTATION OF ACT

G.1.0 INTRODUCTION

One of the objectives of the Integrated Application of Active Controls (IAAC) Technology to an Advanced Subsonic Transport Project is the evaluation of the cost-of-ownership advantage of Active Controls Technology (ACT) when applied to an advanced subsonic transport. The purpose of the work, which was conducted by Honeywell Incorporated, was to assess the effect of advancing technology in the electronics and automatic control areas on these cost-of-ownership advantages. More specifically, the effects of the technology advances associated with the implementation of an ACT system that embodies properties and characteristics expected to be available for a circa-1990 commercial airplane were evaluated. Results of this work are reported in this appendix.

Figure G-1 shows the study tasks comprising the Advanced Technology ACT System definition. A familiarization phase required for Honeywell engineers involved in the project was followed by surveys of applicable technology developments and forecasts to better identify elements appropriate to a 1990 operational system. The control element surveys are described in Section G.2.0.

Three alternative systems were defined: low risk, medium risk, and high risk. Conceptually, the low-risk system is similar to a 1980 implementation of a crucial control function embodying conservative estimates of electronic technology advances. The medium-risk system represents a significant step beyond current capability. The high-risk system includes projections of standard computing elements that best accommodate the existing failure state. These three systems are detailed in Section G.3.0.

Alternative actuation systems also were studied, but the high-, medium-, and low-risk perspective was not followed. These actuation systems could be applied to any one of the computing and sensing alternatives. Electromechanical actuators were selected for flaperon control. Integrated hydraulic actuators, including self-contained servo-loop and bus interface electronics, were selected for the other surfaces. Actuator studies are described in Section G.4.0.

A 1990 ACT system was defined based on the preceding work. Its qualities were evaluated with emphasis on those affecting cost of ownership to the airlines. Results of this evaluation are defined in Section G.5.0. Section G.7.0 contains conclusions and recommendations.
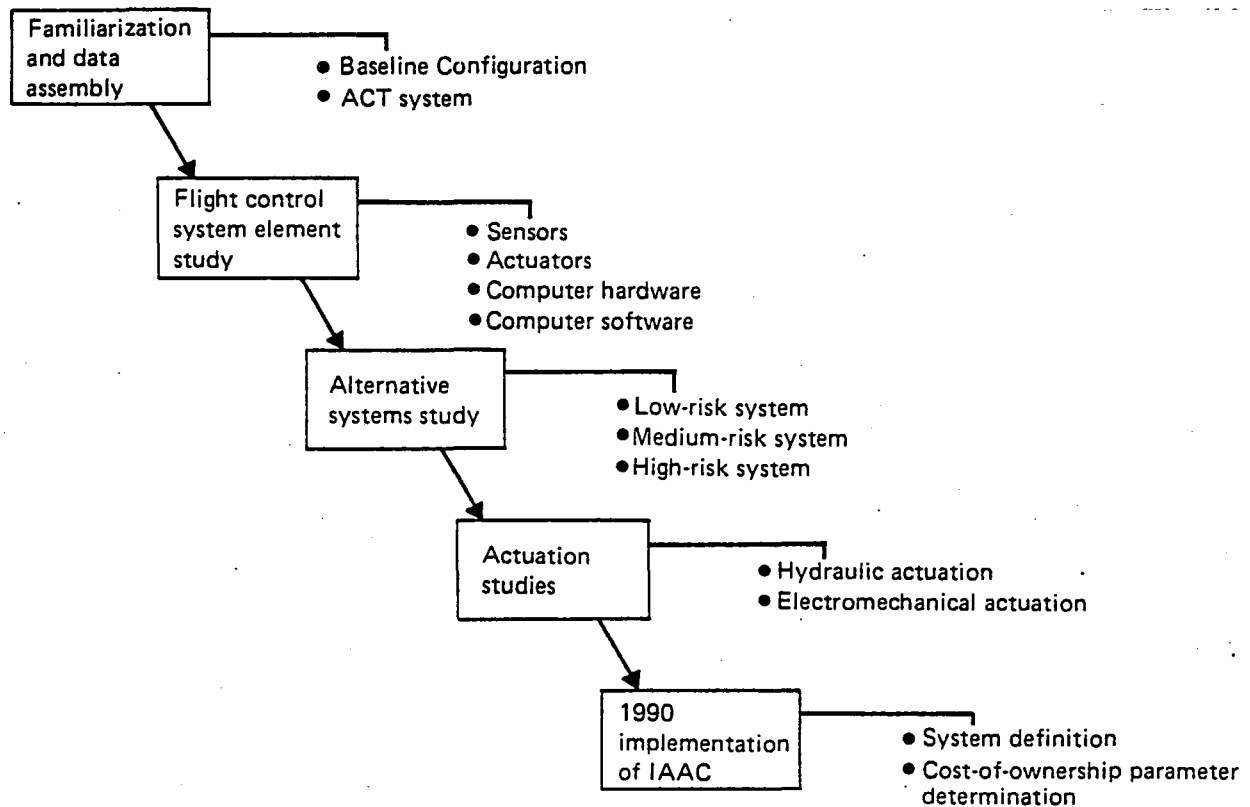
Figure G-1. Advanced Technology ACT System Study Elements

G.2.0 1990 CONTROL TECHNOLOGIES

G.2.0 1990 CONTROL TECHNOLOGIES

Flight control element surveys were conducted to identify and assess advanced sensors, computing elements, and actuators appropriate for Active Controls Technology (ACT) flight control implementations that will be operational in 1990. Elements that are expected to be available for the advanced ACT system implementation are identified in this section.

Subsection G.2.1 describes the sensor survey. Although improvements are expected in air data sensors, the basic concept of air data computers, which is to service all avionic subsystems requiring air data, will not change. Ring laser gyros will continue replacing mechanical rate sensors to a greater extent because they cost less and are not subject to mechanical wear. Use of laser gyro rate signals implemented as separate outputs from the inertial reference system (IRS) is recommended for the advanced ACT system. Piezo-resistive accelerometers are recommended for flutter-mode control (FMC) and wing-load alleviation (WLA) wing-mounted accelerometers.

Subsection G.2.2 discusses computer hardware advances. Significant microcomputer advances are expected. Large-scale integrated circuit developments will decrease the circuit card area required and increase the reliability of each function. Standardization of computer instruction sets will encourage use of a higher order language.

Actuators are discussed in Subsection G.2.3. It is concluded that conventional, cylinder-type hydraulic actuators should be applied in all instances except the flaperon control surfaces, where electromechanical actuators (EMA) are recommended.

Subsection G.2.4 discusses software design and validation. Methodologies will be available so that the software can be designed and validated for flight control applications and so it can be certified to be error free.

G.2.1 SENSORS

Implementation of active control functions requires a number of diverse sensor types:

- Air data signals are required for:

  - Control parameter gain scheduling
  - Airspeed feedback for pitch-augmented stability (PAS)
  - Angle-of-attack feedback for angle-of-attack limiter (AAL)

- Angular rate signals for PAS and lateral/directional-augmented stability (LAS)

- Roll attitude signal for LAS

- Accelerometers for WLA and FMC

- Position transducers for pilot control column, slat, and flap position measurement as required for fly by wire (FBW), PAS, LAS, and AAL

The element introduced by IAAC that has the greatest impact on the choice of sensors is the extreme reliability required for both the crucial and critical functions. Sensors must be selected that are highly reliable, accurate, and dynamically responsive while low cost.

Table G-1 shows a preliminary assessment of the sensor characteristics required for IAAC. In the following subsections, technology trends for each of the required sensor types are examined and selections made for the 1990 IAAC system.

G.2.1.1 AIR DATA PARAMETERS

The traditional method of providing pressure-related air data information is to transmit static and dynamic pressures by tubing from the pitot and static pressure probes to the air data computer. The accuracy of the outputs is dependent on the quality of the pressure transducers and computers used to develop the desired altitude, airspeed, and Mach signals. Digital computers have become the preferred way to compute air data signals

Table G-1. IAAC Preliminary Sensor Requirements

Sensor type	Sensed quantity	Range	Resolution	Null offset	Bandwidth
Accelerometer	Normal acceleration at center of gravity				
	WLA	±4g	±0.005g	±0.01g	30 Hz
	Vertical acceleration, wing				
	WLA, FMC	±20g	±0.05g	±0.01g	250 Hz
Angular rate sensors	Pitch-rate (body) short-period PAS	±20 deg/s	±0.01 deg/s	±0.05 deg/s	30 Hz
	Yaw rate (body) LAS	±20 deg/s	±0.01 deg/s	±0.05 deg/s	30 Hz
Attitude sensors	Roll attitude LAS	±45 deg	0.1 deg	0.5 deg	5 Hz
Air data	Indicated airspeed				
	PAS critical gain schedule	50 to 800 kn	0.5%	1%	0.25 Hz
	PAS critical airspeed	200 to 700 kn	0.05%	1%	1.0 Hz
	WLA gain schedule	100 to 700 kn	0.5%	1%	0.25 Hz
	FMC gain schedule	100 to 700 kn	0.5%	1%	0.25 Hz
	AAL gain schedule	100 to 400 kn	0.5%	1%	1.0 Hz
	Mach number				
	FMC, AAL gain schedule	0 to 1	0.5%	1%	0.25 Hz
	Angle of attack				
	AAL	±60 deg	1%	—	1.0 Hz
Position transducers	Column sensor Pitch, FBW, PAS, roll, LAS	As required	0.1%	0.5%	10 Hz
	Rudder pedal sensor FBW, LAS		0.5%	1%	1 Hz
	Slat position AAL		1%	1%	1 Hz
	Flap position AAL, LAS		1%	1%	1 Hz

because the computations are simple, and the capability to compensate the pressure transducers for anomalies is readily provided.

Air data systems that use remote pressure transducers located adjacent to the pitot static parts are under development. Their outputs are transmitted electrically to computers that develop the desired air data signals. This is expected to reduce the lag associated with the sometimes very long lengths to tubing. In addition, maintenance and cost advantages are also expected. Air data parameters wanted could be processed in the ACT computers if desired.

Angle-of-attack transducers currently in use perform satisfactorily for the AAL function. These transducer outputs are normally corrected for position errors within the air data computers.

As shown in Table G-1, it is apparent that the air data signals required for IAAC have requirements that do not exceed the capabilities of digital air data computers (DADC). Also, triplex DADCs provide redundancy consistent with the reliability requirements for the air data signals. It is therefore recommended that the air data signals required for IAAC be obtained from the aircraft complement of DADCs and that this complement be required to be triplex.

G.2.1.2 ANGULAR RATE SENSORS

The main stabilization control loops in the IAAC pitch and yaw axes require highly reliable sources for angular pitch rate (q) and yaw rate (r). The pitch-rate signal is part of crucial PAS because without this control loop the aircraft is unstable beyond the pilot's ability to control.

Fundamental sources of angular rates have been gyroscope-based measurements. These sensors require precisely spinning rotors with an angular displacement being observed proportional to a rate input on an orthogonal axis. Accuracy has been increased by reverse torquing the rotor back into place and by measuring the torque-driving current. This method, which has tightly confined spinning masses, has been prone to failure due to mechanical wear. Many years of development by numerous companies, however, have produced highly reliable devices accurate enough for flight control use.

Inertial grade devices have also evolved from the spinning rotor gyroscope. These devices have achieved high accuracy at relatively high costs.

The advent of increased computer capabilities and the dynamic range, accuracy, and high reliability of the laser gyro have resulted in very desirable packages for strapdown navigation and attitude reference determination. Sharing this information with the flight control system is a natural outgrowth. Body rate sensors, therefore, fell into two categories: (1) strapdown IRS, inertial navigation system (INS) sensors that are shared with the flight control system and (2) dedicated flight control system sensors.

Table G-2 summarizes existing and emerging sensor concepts for angular rate sensing. The concepts range from the inertial grade strapdown sensors likely to be shared with the flight control system (e.g., laser gyro) to low-cost gyros that are competitive for standalone flight control.

Some conclusions that can be drawn from Table G-2 are:

- The laser-gyro-based IRS system offers a very accurate source of rate data if the reliability and redundancy levels are sufficient for the crucial functions.

- The nuclear magnetic resonance gyro offers great potential accuracy at low cost. The probability of realizing this potential will be studied later.

- The fiber gyro is not a reasonable alternative at the current cost of single-mode fibers.

Sharing IRS strapdown body rate sensors and accelerometers with the flight control system was pioneered with the Boeing 767 aircraft. This trend is likely to continue because:

- Accuracy requirements for flight control are easily met by inertial grade components.

- Current IRS components (i.e., ring laser gyros) have sufficiently high bandwidth for flight control applications.

- Reliability requirements of attitude reference dictate a triple IRS, which is roughly equivalent to flight control system reliability needs. If extra redundant sensors are needed for a given flight control system axis reliability requirement, low-grade—but highly reliable—flight control system sensors are available at moderate costs.

The global positioning system (GPS) may impact the number of IRSs provided per aircraft. This very accurate position-finding system would allow a user to locate himself to within 3m to 6m (10 to 20 ft) anywhere in the world. This capability will have a profound effect on navigation and could reduce the need for INSs. However, it is still expected that triple

Table G-2. Angular Rate Sensors
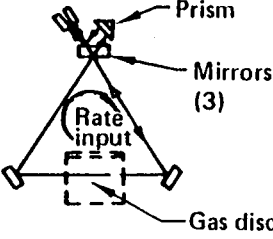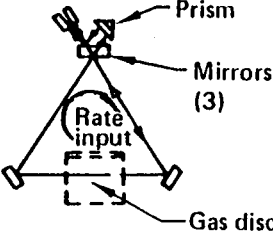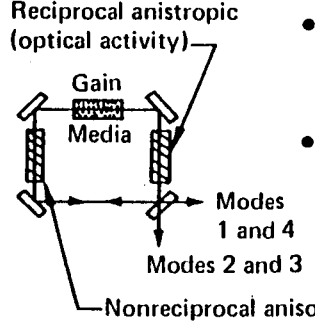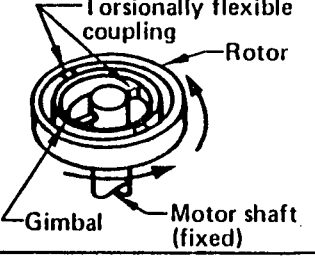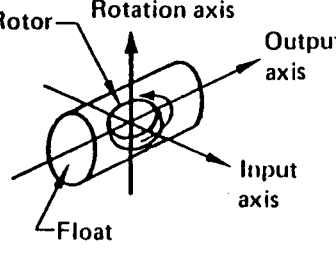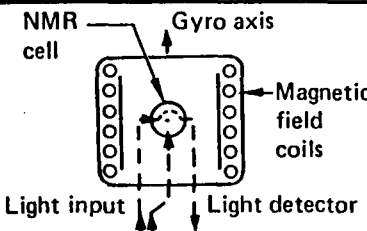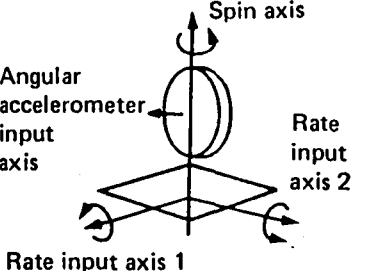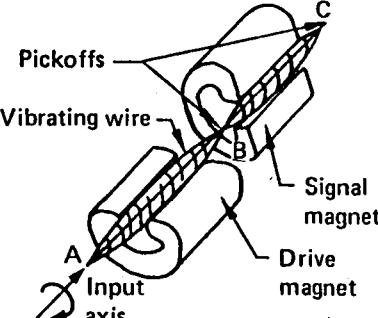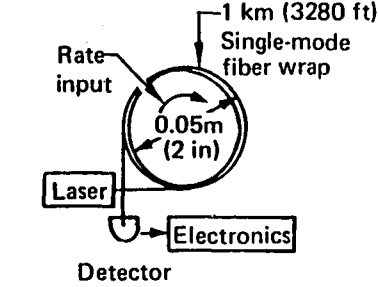
Sensor/vendor	Principle		Range	Accuracy	Reliability (MTBF)	Size, weight, power	Comments
• Ring laser gyro Honeywell (GG 1342)	Photodiodes — Prism — Mirrors (3) Rate input — Gas discharge	• Relatavistic properties of light result in a detectable frequency shift of laser beam due to motion • Mechanical dither used to prevent low-rate frequency lock-in	±400 deg/s	0.01 deg/h	20.8K hr	• 17.8 x 15.2 x 5.1 cm (7 x 6 x 2 in) • 1600g (3.5 lb) • 4.0W	• Strapdown navigation • Boeing IRS
• Honeywell (GG 1328)			±400 deg/s	0.1 deg/h	20.8K hr	• 11.4 x 10.2 x 5.1 cm (4.5 x 4 x 2 in) • 1135g (2.5 lb)	• Usable for blended navigation
Multioscillator gyro ring laser • Litton • Raytheon	Reciprocal anistropic (optical activity) Gain Media Modes 1 and 4 Modes 2 and 3 Nonreciprocal anisotropic (Faraday)	• Avoidance of lock-in by beam bias using a magnetic field on active gain media • Elimination of mechanical dither	Assumed acceptable for strapdown	0.33 deg/h	Good	• 820 cm³ (50 in³)	• Experimental results only • More electronics and less accurate than dithered ring laser gyro
Dry-tuned rotor • Litton	Torsionally flexible coupling — Rotor Gimbal — Motor shaft (fixed)	• Motion normal to spin axis causes cyclic gimbal oscillation • Resulting gimbal reaction canceled by setting the torsion spring constant	±400 deg/s (instantaneous) ±200 deg/s (continuous)	0.05 to 10 deg/h	13.2K hr	• 2.5 cm (1 in) diameter • 70g (0.15 lb) • Low power	• 2 degrees of freedom • Predictable warmup characteristics
Floated gyro	Rotor — Rotation axis Output axis Input axis — Float	• Fluid floated spinning momentum wheel • Procession caused by input rate nulled by servo feedback • Torque generator current is used for measurement	±400 deg/s	1 to 10 deg/h	17.2K hr (failure types are unpredictable during warmup)		• State of the art • Warmup delays

Table G-2. Angular Rate Sensors (Continued)

Sensor/vendor	Principle	Range	Accuracy	Reliability (MTBF)	Size, weight, power	Comments
Nuclear magnetic resonance (NMR) gyro • Litton • Singer	NMR cell — Gyro axis — Magnetic field coils — Light input — Light detector • Processional magnetic frequency of aligned nuclei is altered about the input axis • Shift small, but measurable	Strapdown capability	Strapdown capability	Very good	• 6.4 x 6.4 cm (2.5 x 2.5 in) diameter • 635g (1.4 lb)	• Rapid warmup • High g environment • Handles high spectrum of requirements • Available by 1985 • Could be accelerometer also
Magnetohydrodynamic gyro (MHD) • Honeywell (GG 2500)	Spin axis — Angular accelerometer input axis — Rate input axis 2 — Rate input axis 1 • Spinning angular accelerometer (torus of liquid metal) creates a sine wave whose magnitude is a rate measurement • Two-phase reference input yields two-rate output	±360 deg/s	0.01 deg/s	Good (moving parts not demanding)	• 4.5 x 1.8 cm (1.8 x 0.7 in) diameter • 70g (0.15 lb) • 4W	• Rapid startup
Vibrating wire rate sensor (VWRS)	Pickoffs — Vibrating wire — Signal magnet — Drive magnet — Input axis — A B C • Input rate causes point deflection on B-C path detectable by signal magnet	±300 deg/s	0.1 deg/s	50K hr	• 5.1 x 3.0 x 2.8 cm (2.0 x 1.2 x 1.1 in) • 100g (0.22 lb) • Low power	
Fiber optic laser gyro	1 km (3280 ft) Single-mode fiber wrap — Rate input — 0.05m (2 in) — Laser — Electronics — Detector • Interferemetrically sensed laser phase shift • Detector technology requires 1-km (3280-ft) single-mode fiber for output resolution	±400 deg/s	0.01 deg/s	Very good (greater than ring laser gyro)	• Size as per figure • 2.5 cm (1 in) thick	• Price depends upon cost of single-mode fibers

IRSs will be provided for transport aircraft in 1990 because of the need for highly reliable attitude and heading reference signals.

To achieve high performance at low cost, it is concluded that the available IRS angular rate signals should be used for IAAC to the greatest extent possible.

G.2.1.3 ACCELEROMETERS

As shown in Table G-1, acceleration data are required for WLA modes; i.e., gust load, maneuver-load control (MLC), and FMC systems. Accelerations also can be used when analytical redundancy and state reconstruction for reversion modes are considered.

Because MLC requires an acceleration signal measured at the center of gravity (cg), acceleration sharing with the IRS system is used. Table G-3 contains accelerometer concepts ranging from inertial grade sensors, suitable for the IRS and MLC, to structural mode control sensors suitable for FMC and gust-load alleviation (GLA) applications.

The order (table G-3) is determined by an accuracy parameter that is the ratio of the given device's maximum range to its resolution. Inertial grade requirements are typically range and resolution of 10^4 to 10^6, while flight control system requirements are 10^2 to 10^4.

Further trends in accelerometers are summarized as follows:

● Inertial grade accelerometer costs are going down, providing IRS-INS and shared flight control system functions with low-cost derivations. Extra redundancy for higher reliability of functions is very desirable with such devices.

● Piezo-resistive concepts show promise, particularly for low-cost, highly reliable structural control systems, and are recommended for the WLA and FMC wing-mounted acceleration packages for IAAC.

● New concepts appear to be either too undeveloped for useful evaluation (e.g., passive magnetic suspension) or have no identified benefit for shared INS and flight control system functions (e.g., laser accelerometer).

Table G-3. Accelerometer Concepts
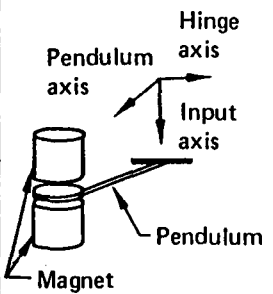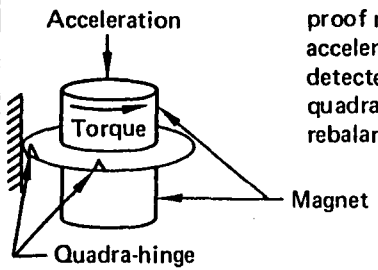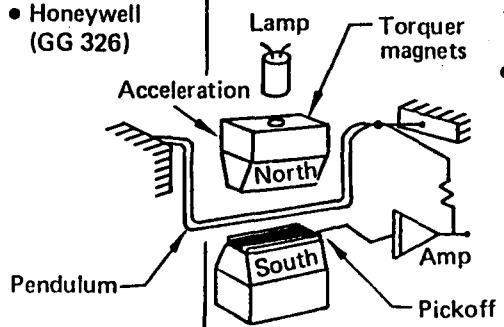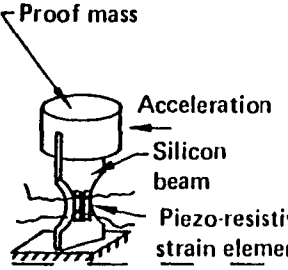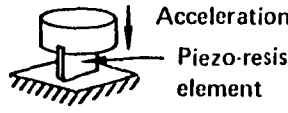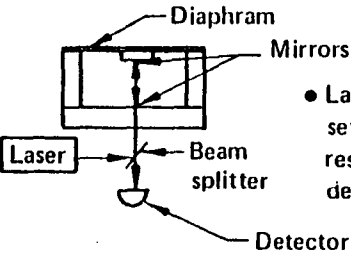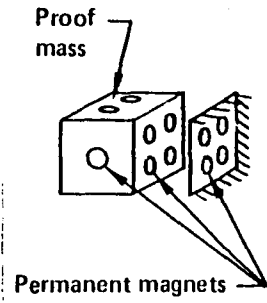
Sensor/vendor	Principle	Accuracy parameter (range/ resolution)	Reliability (MTBF)	Size, weight, power	Comments
Floated pendulum • Sundstrand (QA 2000)	Hinge axis, Pendulum axis, Input axis, Pendulum, Magnet • Magnetic force rebalance used to restore pendulum position	10^4	30K hr		
• Donner (4852)	• Restoring current command used for measurement	10^4	30K hr		Boeing IRS
• Honeywell (GG 177)		10^6	20K hr		
Quadra-hinge • Honeywell (GG 2550)	Acceleration, Torque, Magnet, Quadra-hinge • Torsional input to proof mass from acceleration input detected through quadra-hinge and rebalanced magnetically	10^6	50K hr (goal)	• 2.5 x 2.0 cm (1 x 0.8 in) • Small weight and power	• IRS capability • Available before 1985 • Instant on
Quartz fiber • Honeywell (GG 326)	Lamp, Torquer magnets, Acceleration, North, South, Pendulum, Amp, Pickoff • Quartz-fiber pendulum suspended in a permanent magnetic field. • Optical pickoff provides dc measurement and torquer-magnet rebalance signal	10^5	30K hr	3.8 x 3.0 x 3.3 cm (1.5 x 1.2 x 1.3 in)	IRS-INS capability at low cost

Table G-3. Accelerometer Concepts (Continued)

Sensor/vendor	Principle	Accuracy parameter (range/ resolution)	Reliability (MTBF)	Size, weight, power	Comments
Piezo-resistive • Honeywell (GG 322)	Proof mass — Acceleration — Silicon beam — Piezo-resistive strain elements • Piezo-resistive strain elements diffused into silicon cantilever beam • Bridge network provides measurement	10^4	>50K hr	• 3.0 x 2.2 cm (1.2 x 0.85 in) diameter • 34.0g (1.2 oz) • 0.3W	• Solid state (no moving parts) • ac or dc operation
• Kulite	Acceleration — Piezo-resistive element	>10^3	Very high	• 1.9 x 1.6 cm (0.75 x 0.62 in) diameter • 28g (0.06 lb)	• Accurate for 1 Hz up
Laser inter-ferometer	Diaphram — Mirrors — Laser — Beam splitter — Detector • Laser interferometer setup provides high-resolution acceleration detection	Assumed very good	High		• Proposal stage only • Available 1990 if developed
Passive magnetic suspension	Proof mass — Permanent magnets • Passive precision magnetic suspension possible • Capacitance pickoffs provide low-power, high-accuracy measurement	Variable	High	Size and weight not factors; power is low	• Three-axis measurement • Concept only • Available 1990 if developed

G.2.2 AIRBORNE COMPUTER TECHNOLOGY

The adoption of standards will have a positive impact on avionic systems because of the enormous support standardization will bring to software development. The trend to standard instruction sets is discussed in Subsection G.2.2.1. In Subsection G.2.2.2, current avionic computers are reviewed—especially the HDP-5301. The input/output (I/O) structures of microcomputer systems are included to show the need for chips supporting the microprocessor; the 8086 family is used as an example. The design of a general-purpose computer expected by the mid-1980s using very-large-scale integrated, very-high-speed integrated circuits (VLSI/VHSIC) is examined in detail. Speed and flexibility are found to be greater than that needed for flight control calculations. The complicated software now used for self-monitoring and cross-channel voting will be replaced by hardware functions to make the software computational load light. Figure G-2 shows the projection of avionic computing needs; the curve extrapolates to 1.5M operations per second (ops) in 1990. This is light when compared to the 5M to 6M ops expected to be available for mid-1980 microcomputer systems. Bus issues will be the limiting factors in avionic systems as the central computing structures become routine. Fiber optics will become important communication components. Although current costs and coupling techniques are not acceptable, they will change.

G.2.2.1 STANDARD INSTRUCTION SET TREND

The U.S. Department of Defense and NASA have developed programs for standardizing certain characteristics of embedded computers. The objective is to establish a standard instruction set so that a compiler can operate independent of the particular machine being used. Software engineers, for example, can work with any of the standardized digital processors without learning the peculiarities of the different machines.

A standard higher order language that is a step toward reducing software costs and improving software understanding is another objective.

One program directed toward standardization is the U.S. Air Force's MIL-STD-1750 instruction set. There have been several evaluations of the 1750, and, as a result, the program was revised to the current 1750A instruction set, which is described in the following paragraph. (Reference G-1 is one evaluation of the set.)
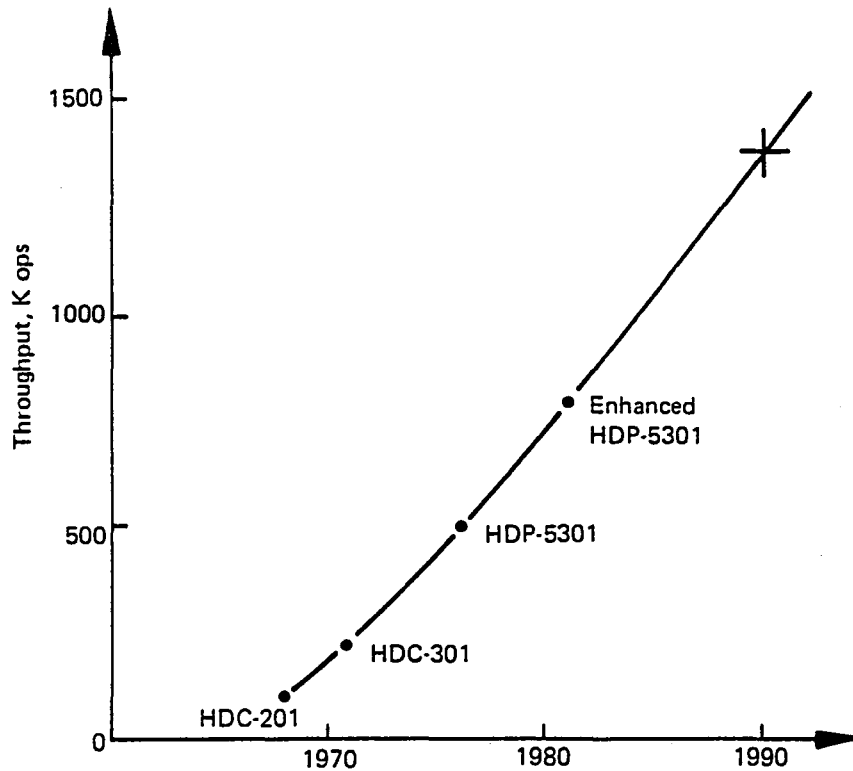
Figure G-2. Throughput of Honeywell Computers Used in Avionic Division Products

The standard defines a general-purpose computer architecture as seen by a programmer writing in machine language. It prescribes data and instruction formats and computer organization and operation enabling establishment of standard software development resources. In addition to its benefit to support software, such as compilers and instruction-level simulators, the 1750A is expected to make software development mainly independent of hardware development. The features of the 1750A instruction set are summarized in the following list:

● 16-bit structure (registers, memory addressing, instruction size)
● 16 general registers (16 bits)
● Three registers usable as base registers
● Good range of address modes:
    ● Immediate
    ● Register
    ● Memory direct
    ● Memory indirect
    ● Base relative

- Wide range of operand types:
    - Bit
    - Byte
    - Fixed (16)
- Double fixed (32)
- Floating (32)
- Extended floating (48)
- Expanded memory addressing (optional):
    - Virtual to physical mapping, to 1M words
    - Block protect
- Interrupts, 16 levels, priority, vectored
- I/O, control of I/O interrupts, times (via two commands)

Four implementations have been built, and at least 13 computer manufacturers are developing 1750-based computers. Most of the implementations are bipolar bit-sliced designs, but other approaches are possible. Low-power integrated injection logic (I^2L) technology using gate arrays or radiation-hard complementary metal-oxide semiconductor/silicone on sapphire (CMOS/SOS) has been considered. It may be possible to change the microprogram of a current 16-bit, single-chip microprocessor to incorporate most of the 1750A features. An example of a VLSI/VHSIC chip set is discussed later in this section. In the example, a very general capability is sought to make the architecture fit other standards in addition to 1750A. These ask for a 32-bit structure that causes some inefficiencies when restricted to the 16 bits of 1750A.

G.2.2.2 CURRENT AVIONIC COMPUTERS

Most of the computers used in the flight control systems are constructed with the 2900 family of bipolar components to form a microprogrammed bit-sliced architecture. This approach provides a very flexible method for the design of high-performance microcomputers.

In the following subsections, the bit-slice designs and chips are reviewed, and the architecture of the HDP-5301, which is typical of current avionic computer designs, is outlined.

G.2.2.2.1 Bit-Slice Architecture

Bit-slicing is the construction of a processor with several building blocks, each having data paths of a few bits. A usual construction is to use four 4-bit microprocessors to produce a 16-bit architecture. Bipolar circuits are fast but draw substantial power. One reason for bit-slicing was that too much heat would be generated in a single 16-bit processor package. However, with the newer technologies, this is no longer an important factor.

The 2900 series is a family of low-power Schottky transistor-transistor logic (TTL) building blocks for high-performance applications. A wide variety of instruction sets or logical designs may be implemented; the user is not limited to a single, fixed instruction set as in the whole-chip, 8- and 16-bit microprocessors. The building blocks are relatively low level to provide for flexible designs. This results in a high chip count compared to metal-oxide semiconductor (MOS) microprocessor systems. The HDP-5301 requires 42 chips.

A generalized computer architecture is shown in Figure G-3. Each of the blocks can be constructed from members of the 2900 family. Reference G-2 shows how the design can be made to meet throughput requirements and to execute special algorithms.

G.2.2.2.2 Example of a Current Avionic Computer

The HDP-5301 is a bit-slice design using the 2900 family. This processor comes on a single printed circuit board 15.9 by 16.5 cm (6.25 by 6.50 in). It is lightweight, 0.34 kg (12 oz), consumes 12.5W, and needs one +5V power source. Instructions are rapidly executed by interleaving the fetch and execution cycles. In summary, the HDP-5301 features are:

- Bipolar microprocessor using Schottky circuitry
- Expandable instruction and data memory up to 64K words
- 16-bit instruction word length
- Data word length of:
    - 16 bit, single precision, fixed point
    - 32 bit, double precision, fixed point

- Floating point, with 32-bit mantissa, and 16-bit exponent in extended capability option
- Minimum execution times of:
- 0.6-μs clear
- 1.0-μs add/subtract
- 6.2-μs multiply
- 18.8-μs divide
- Priority interrupt with vectoring to 16 locations
- Power recovery interrupt
- 16-bit parallel direct input and direct output channels
- Direct memory access (DMA) capability

Figure G-4 shows the organization of the processor. The register/arithmetic logic unit is constructed of four slices, each 4 bits wide, cascaded to provide 16-bit arithmetic and logic operations. It contains a 16-word, two-port register file and a single register for
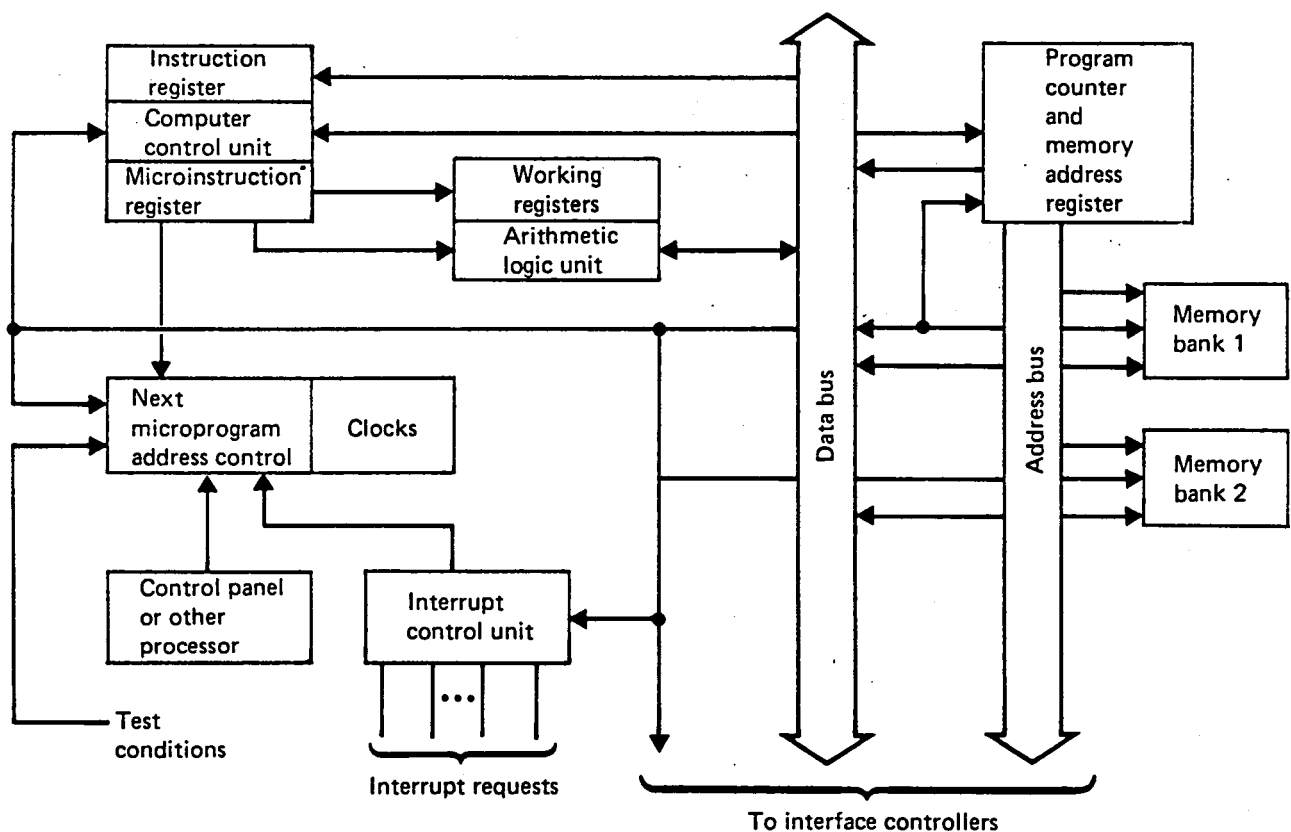
Figure G-3. Generalized Computer Architecture

extended arithmetic and logic operations. For double precision operation, data words are held in the concatenated A and B registers. The file and special registers perform the following conventional functions:

- Six temporary registers for microprograms
- Program counter
- Base save register
- A register
- B register
- E (exponent) register
- X (index) register
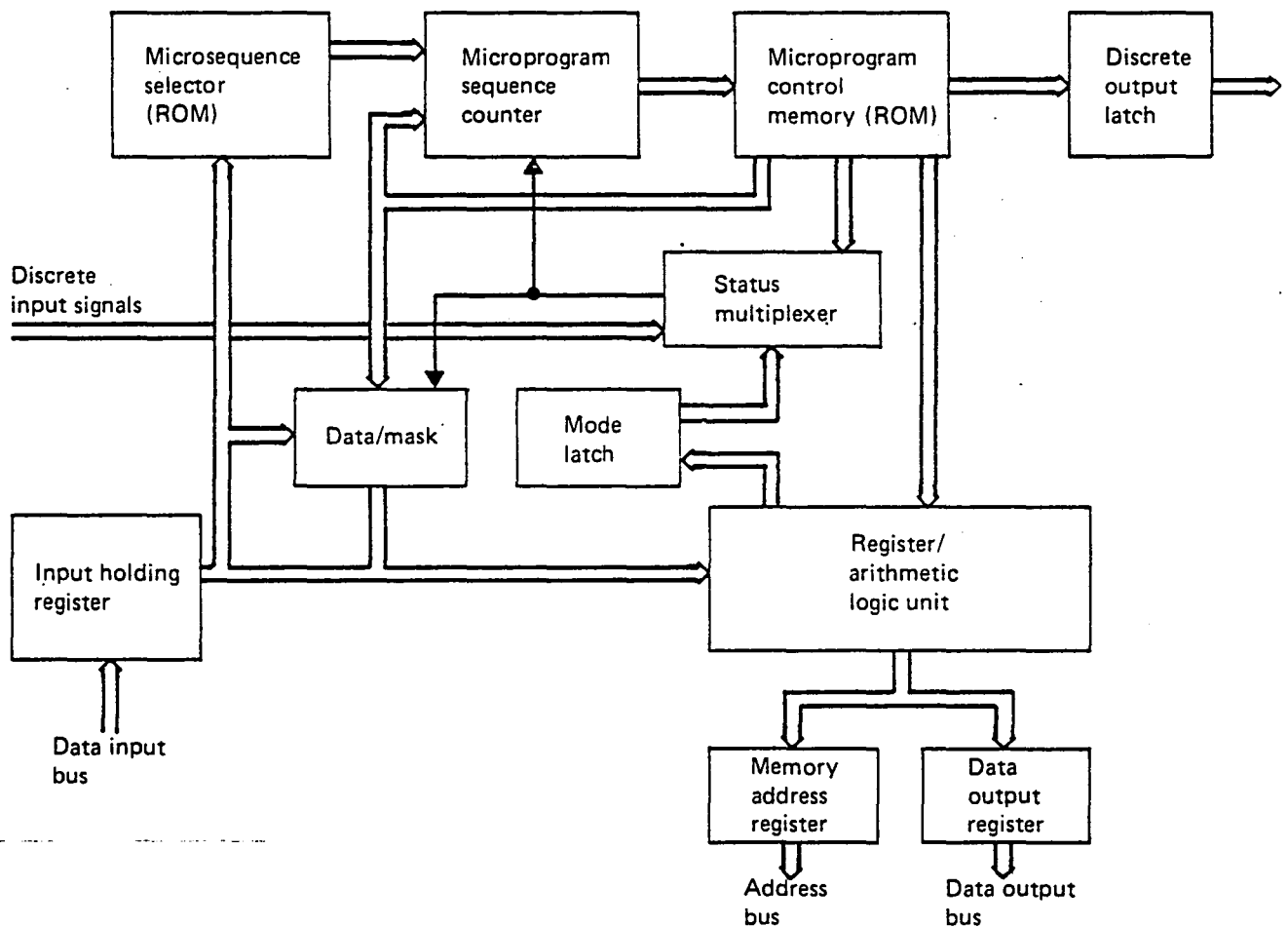
Figure G-4. Organization of the HDP-5301 Processor Unit

- Base register
- Alternate base register
- Stack point
- Mode register

The programmer has access to all but the first three of these registers. Definitions of items in Figure G-4 are:

- Memory address register—a 16-bit register that provides the address of either instructions or data to the memory.

- Input holding register—a 16-bit latch register that holds the fetched instruction or data.

- Microsequence selector—a read-only memory (ROM) addressed by the instruction operation code bits to determine the starting location of the microprogram to be executed; ROM output is fed into the microprogram sequence counter as an initial condition.

- Microprogram sequence counter—addresses the microprogram control memory to derive the control signals and other functional elements of the central processing unit (CPU).

- Microprogram control memory—an ROM addressed by the microprogram sequence counter to determine the control signals and other functional elements of the CPU.

- Mode latch—a register that determines the mode of operation of the processor (i.e., single or double precision, fixed or floating point, etc.).

- Status multiplexer (MUX)—selects the individual discretes and modes of the CPU.

- Data mask—a latch used to introduce constants into the microprocessor from the microprogram control memory.

- Data input bus—contains 16 lines that transmit data from the memory and the I/O to the CPU.

- Data input bus—contains 16 lines that transmit data from the CPU to the memory and the I/O.

- Address bus—contains 16 lines that specify the memory location to be accessed for instruction fetch or data transfer or the I/O device to be accessed for data transfer.

- Discrete output latch—has eight outputs that are controlled by the microprogram control memory.

The processor may be used with a variety of memories; however, the selection may influence the processor cycle time. The minimum cycle time of the processor is 200 ns. The basic memory reference instruction requires five processor cycles for a minimum instruction time of 1 μs. For the CPU to operate at maximum speed, memory access time must be less than 250 ns, and the memory cycle time must be less than 400 ns for both instructions and data. The clock must be slowed down when it is used with memories with longer cycle times.

Words are classified according to the following scheme:

- Instruction words:
  - Memory references or control transfers
  - I/O instructions
  - Generic instructions

- Data words:
  - Single precision, fixed point
  - Double precision, fixed point
  - Double precision, floating point

The formats of these words are conventional.

The addressing structure allows relative, indexed, and indirect modes to be used for memory reference and control transfer instructions. There are no memory banks or pages for either instruction or data memory. One of the registers of the register file is used as a base register. The displacement field of the memory reference instruction is a signed

integer offset of the desired memory location relative to the base address held in the base register. The inactive base register is provided to facilitate operations with two or more base address values. The two base values may be interchanged to ease handling when more than 1K of data words are required. The base register is cleared at power "on"; the inactive base register is not cleared at power "on." Indirect addressing is also provided, permitting access of addresses beyond the active base register range. Pseudo-indexing is available in addition to true indexing. Control transfer addressing is similar to memory reference addressing, except that the displacement field refers to an address relative to the current contents of the program counter rather than the base register. The base register is used in the indirect jump mode to fetch the address that is the location of the next instruction.

The instruction set is microprogrammed. It may be altered and new instructions may be added for special purposes. The instructions are grouped as:

- Load and store
- Arithmetic
- Control
- Logical
- Shift
- Transfer control
- Input/output

One clock cycle is required for the execution of a single microinstruction step. The minimum cycle is 200 ns, corresponding to a primary clock frequency of 5 MHz. Indexing requires one additional machine cycle; indirect addressing requires two additional machine cycles.

A comparison of the HDP-5301 with similar computers is made in Table G-4. All computers have a 16-bit word length, provide double precision arithmetic operations, access 64K of memory, have 16 interrupts, and claim a reliability of more than 1500 hr. These computers were designed in the early 1970s. Although they appear to be similar machines, there are many differences.

Table G-4. Comparison of Avionic Computers

Instruction mix	Instruction mix, percent	Instruction time, µs						
		Rolm 1664	Delco 362F	SKC 3100	IBM ML-1	TD 43S	SKC 2516	HDP-5301
Fixed point								
Load	10.0	2.0	2.5	1.92	2.7	2.25	0.95	1.0
Store	10.9	2.0	2.5	1.92	3.4	2.25	0.95	1.2
Add/subtract	4.0	1.0	2.5	1.92	1.9	2.25	0.95	1.0
Multiply	0.5	5.6	4.75	8.16	4.3	6.75	1.95	5.0
Divide	—	12.6	9.0	13.76	6.3	—	7.75	18.0
Floating point								
Load	11.7	4.6	3.75	2.88	2.7	3.25	1.45	1.6
Store	12.8	5.3	3.75	2.88	3.6	3.25	1.45	2.0
Add/subtract	4.7	1.9	9.8	14.0	4.7	4.0	4.0	7.6
Multiply	4.5	2.2	7.0	26.0	11.4	4.0	9.4	12.0
Divide	0.2	2.6	12.0	100.0	19.4	10.0	50.0	25.0
Shift	4.6	3.5	3.0	4.5	3.2	3.0	2.7	4.2
Logical	4.6	1.2	3.0	1.92	3.0	2.25	0.95	1.0
Test/branch	30.5	2.3	2.5	2.1	1.4	1.75	1.15	0.8
I/O control	1.0	1.8	2.5	4.16	2.0	1.0	1.7	2.0
Throughput (K ops)		353	293	236	331	390	541	456

G.2.2.2.3 Computer Design Based on a Single-Chip Microprocessor

The new 16-bit, single-chip microprocessors, in particular the 8086, the 68000, the Z8000, and the 9900, bring enough capacity to be the basis of the design of avionic computers. General Dynamics has developed a 350K ops airborne computer using the Z8002 microprocessor. Honeywell is using the 8086 for several avionic advanced development projects, including the NASA Demonstration Advanced Avionics System and the AFFDL Multimicroprocessor Flight Control System. The former is a multicomputer package for general aviation aircraft; the latter is a highly redundant experimental configuration. Environmental requirements of temperature and radiation are a major concern in development of the machines. The new microprocessors are targeted for the commercial market. It may be some time before versions with full environmental capability for aircraft are available.

G.2.2.2.4 Current Chip Families

The introduction of new microprocessor chips into the market has reached a plateau (ref G-3). Although there have been no major new families to add to the Electronic Design News (EDN) chip directory, there have been additions and refinements to the established families. The position of the EDN editor is that these families will remain the choices of designers in the 1980s because of the advantages of dealing with one instruction set, one hardware architecture, one bus structure, and one development system. Further, the software support accumulates to produce a momentum that is hard to abandon. Development of chips to augment the families has been predictable (ref G-4). These views are heavily influenced by the commercial market that is finding the present families suitable for their products. The development of ruggedized versions lags behind the commercial introductions by 2 or 3 years. One of the objectives of the VHSIC program is to redress this situation. As the VLSI and VHSIC technologies mature, there will be a new surge of innovations.

G.2.2.2.5 Input/Output Methods

In some computer architectures, the memory has two interfaces: the first to the processor, the second to the I/O peripherals. The processor has separate instructions for memory reference and for I/O operations. This arrangement is called a data channel I/O. In other architectures, the data transfer registers of all devices are considered as locations in memory with assigned addresses. No separate output channel is designated, nor are any special I/O instructions necessary. This is called a memory-mapped I/O. Often in the data channel architecture, instead of a separate I/O bus and a device selection bus, part of the address bus is used as the device selecting lines; the data are delivered on the data bus. There is an I/O request line controlled by the microprocessor that determines that the data and address buses are either acting as a data channel or that they are acting as a memory reference. The processor has a set of instructions to read or write to the I/O ports.

Peripheral devices can send and receive data at limited rates. A method is needed to determine when to make data transfers. In the approach called polling, the microprocessor periodically examines status registers of the input devices to determine if new data are ready on any of them. Another approach, called interrupt-driven I/O, uses

an interrupt to tell the processor that new data are ready. If there are multiple interrupt lines, the processor knows which device is ready. If there is only one interrupt line, the processor must have a polling routine to determine the source of the data. Polled I/O initialization uses simple hardware, but it requires more processing time than the interrupt-driven methods.

Some systems allow a peripheral device to take control of the computer bus to transfer data into and out of the memory directly without the intervention of the processor; this is called direct memory access. The approach provides high transfer rates and reduces processing time. There are several methods for removing the processor from the bus during the DMA cycle. The simplest way—and the usual method in microcomputer systems—is to stop the processor and float its address, data, and control lines. A request line is available to the DMA devices that causes the microprocessor to go into an idle state as soon as it completes its current instruction. When this is done, a bus acknowledge signal is sent back to the peripheral to show that the bus is ready for the DMA transfer. This process is referred to as cycle stealing, because the clock cycles used for the DMA transfer are stolen from the processor that otherwise would do useful manipulations. To avoid losing processing time, an interleaved method is sometimes used. The DMA takes control of the bus when the processor is not using it. If the processor has a queue of instructions, it can continue its operation during the DMA transfer without significant interruption.

Microprocessors are sometimes classified as register oriented or memory oriented, or whether they are designed for simple controlling tasks or have more complicated instruction sets for arithmetic computations. The 8086 is an example of a microprocessor. It is a 16-bit, two-address machine using the high-performance metal-oxide semiconductor (HMOS) technology. The processor chip contains 29 000 transistors and runs on a single 5V power supply at a clock rate of 5 or 8 MHz. The 8086 can perform arithmetic operations on signed and unsigned 8- and 16-bit binary integers as well as provide correction operators for arithmetic on packed and unpacked decimal integers. The usual logic operations and intramodule and intermodule transfers of control are provided. Six primitive string operations and specialized control operators for building arbitrarily complex functions are included.

A large family of processors and supporting chips are offered. The 8086 is the general data processor, the 8089 is the I/O processor, and the 8087 is the numerical data processor (NDP). An 8289 bus arbiter chip manages bus contention in a multiprocessing system. Other support elements are:

- 8282/83 octal latches
- 8286/87 octal transceivers
- 8284 clock generator
- 8288 bus controller
- 8259A interrupt controller
- 8291 general-purpose interface bus (GPIB) talker/listener
- 8292 GPIB controller
- 8237-2 programmable DMA controller
- UPI-41A universal peripheral interface
- 8202 dynamic random-access memory (RAM) controller
- 8231 arithmetic processing unit
- 8232 floating point processor
- 8251A universal synchronous/asynchronous receiver/transmitter (USART)
- 8253-3 programmable interval timer
- 8255A-5 programmable perhipheral interface
- Other peripheral device chips

The 8089 I/O processor improves the computational efficiency of the system processor by removing the I/O tasks from the CPU and provides the capabilities for DMA. The CPU performs an I/O operation by building a message in memory that describes the function. The I/O reads the message, performs the function, and then informs the CPU that the task has been completed. All I/O devices appear to the CPU as transmitting and receiving whole blocks of data. The I/O processor assumes all device controller overhead, performs both programmed and DMA transfers, and covers "soft" I/O error without CPU intervention. The CPU is left to do the computation.

The 8087 NDP implements the Institute of Electrical and Electronics Engineers (IEEE) floating-point standard and handles single- and double-precision formats, double-extended format, rounding control, infinity control, and the associated required instructions. An escape instruction in a sequence of 8086 operations activates the 8087 NDP coprocessor

and makes the 8086 perform a read-to memory. The CPU ignores the returned data. Concurrently, a 6-bit operation code in the escape command tells the coprocessor what operation to perform. The coprocessor accepts the data brought by the 8086 and uses it as either data or as a pointer to the start of the data. The coprocessor has temporary control of the data and address buses for retrieving and storing data and results. To the programmer, the combined 8086 and 8087 appear as a single machine. The 8087 adds seven data types and eight registers to the basic machine.

The GPIB family performs all the bus functions required by the IEEE 488 Standard. This allows transfers between microprocessors, peripherals, and instruments from various manufacturers. The 8291 is a microprocessor-controlled chip that interfaces a variety of microprocessors, including the 8086 family. In addition to its ability to interface both 8- and 16-bit microcomputers to the GPIB, the talker/listener provides a complete source and acceptor handshake and complete talker/listener functions with extended addressing. It can operate in a clock range from 1 to 8 MHz. The 8292 controls the bus using three bus lockup timers to detect any major problems on the GPIB bus. The 8293 is a bidirectional transceiver that can be hardwired to one of four modes of operation to support a talker/listener environment.

The device also can be used as a general-purpose push-pull or open-collector bus transceiver with nine receiver/drivers. The three components form a complete IEEE-488 talker/listener/controller bus interface for a microprocessor. The electric interface is performed by transceivers, data transfers by the 8291, and control of the bus by the 8292.

The 8237-2 DMA controller provides microcomputer peripherals for 8086-based systems with a direct link to system memory. The 5-MHz DMA controller operates at 1.6 megabytes per second. This transfer rate allows an 8086-based system to interface to hard disks, serial communcation links, and high-speed parallel links. Less CPU time is spent in the idle state while data are being transferred to the bus, which improves the overall system throughput. This is an advantage in systems performing cathode-ray-tube (CRT) refresh and dynamic RAM refresh. Applications for the DMA controller include disk control telecommunications, GPIB interfaces, and high-speed scanning or "frame-grabbing" types of operations.

The UPI-41A 8-bit microcomputer is a general-purpose, programmable interface device that functions as a peripheral controller. It contains a microcomputer with program memory; data memory; and 8-bit CPU, I/O ports, time/counter, and clock. As a complete microcomputer, the device provides more flexibility for the designer than conventional large-scale integrated interface devices. The UPI-41A is an efficient controller as well as an arithmetic processor. Basic applications include keyboard scanning, printer control, display multiplexing, and similar functions that involve interfacing peripheral devices to microprocessor systems.

The 8202 dynamic RAM controller can directly address, refresh, and drive up to 64K bytes of RAM memory without buffering. Also, the single-chip controller provides on-chip, all-multiplexed addresses and address strobes, automatic asynchronous refresh/address arbitration, and system-acknowledge and transfer-acknowledge signals. A refresh timer and refresh counter are provided. The refresh requests are generated either internally or externally. The external refresh request offers users a transparent capability.

Other standard peripherals compatible with the 8086 family of processors include an arithmetic processing unit, a programmable interval timer, and a variety of controllers and interface devices. The 8231 arithmetic processing unit provides high-performance fixed- and floating-point arithmetic and floating-point trigonometric operations and may be used in lieu of the 8087 coprocessor. Chebyshev polynominals are used in the implementation of arithmetic algorithms. This unit may be used to compute square roots, logarithms, and exponentials. It allows float-to-fixed and fixed-to-float conversions and offers both trigonometric and inverse trigonometric functions. The 8232 floating-point processor handles 32- and 64-bit precision addition, subtraction, multiplication, and division operations.

The 8251A programmable communication interface is an enhanced USART designed for data communications. The 8251A is used as a peripheral device and is programmed by the CPU to operate using virtually any serial data stream for serial transmission. It can simultaneously receive serial data streams and convert them into parallel data characters for the CPU. The 8253-5 is a programmable interval/timer chip for use as a microcomputer peripheral. It is organized as three independent 16-bit counters; all modes of operation are software programmable. The 8255-5 programmable peripheral interface

is a general programmable I/O device that contains 24 programmable I/O pins that can be individually programmed in two groups of 12 and be used in three modes of operation for flexible I/O design.

Note that there is a very extensive set of chips from which the system designer may construct a computer suited to specific needs. The advantages of this set are mainly due to the need of I/O interfaces to a large variety of peripheral equipment. Implementation in larger scale integration is discussed in the following paragraphs.

G.2.2.2.6 Future Microcomputer Chips

There are two distinct trends in microcomputer chips: (1) the maturing of the established chip families to provide the main choices of original equipment manufacture (OEM) designers in the 1980s and (2) developments in VLSI and VHSIC technologies that are leading bolder projects toward 32-bit microprocessor chips and 16-bit microcomputer chips. To explore the possibilities offered by the second trend, the preliminary design of a general-purpose computer is reviewed. Analysis shows that a full order-of-magnitude improvement in performance over current avionic computers can be expected. Power and weight will be reduced, and a greater degree of flexibility will be offered. The VLSI will reduce the chip count, which should lead to substantial improvement in reliability because the connections between chips are a large source of failures.

The complexity brought on by the large-scale integration increases the problems of testing, fault isolation, and fault tolerance. Much more attention must be paid to testing and design verification than with the small-scale circuits that presented many accessible points for testing. While testing will be more expensive in design and development, these requirements will eventually lead to reliable circuits with well-defined failure modes and failure coverage.

G.2.2.2.7 VLSI Avionic Computer Architecture

The preliminary design of a general-purpose VLSI avionic computer is an example of a direction for architectures that uses the capacity of the VLSI and VHSIC technologies. To cover the development costs of the architecture and the chips, this design has a very wide scope of avionic applications; it is tailored for only flight control applications. The design

provides much more performance than is needed for flight controls. The surplus capability may be used to extend the self-tests and fault diagnosis or to perform additional avionic tasks.

The computer configuration is shown in Figure G-5. The CPU is 16-bit architecture that is implemented using a set of "macrocells" or chip building blocks that also can be used for other architectures, including 32-bit ones. If the full 32-bit capability is provided, the power requirements will be higher than those estimated and reported here. The memory management unit (MMU) maps logical addresses of the CPU into the physical addresses of the external memory. The programmable protocol for the memory bus accommodates memories of any speed. The MMU has a cache memory to improve the memory access time. The I/O controller provides the interface between the I/O adapter chips and the processor bus. It can manipulate complex data structures in memory, which may be required for communication between processors in a distributed computing system.

A comparison of the Honeywell HDP-5301 computer board and this hypothetical VLSI design is listed in Table G-5. The new design shows a tenfold improvement in performance with more flexibility; the chip count is less by a factor of seven. This will greatly improve the reliability of the computer by reducing the troublesome connections between chips. Details of the design follow.
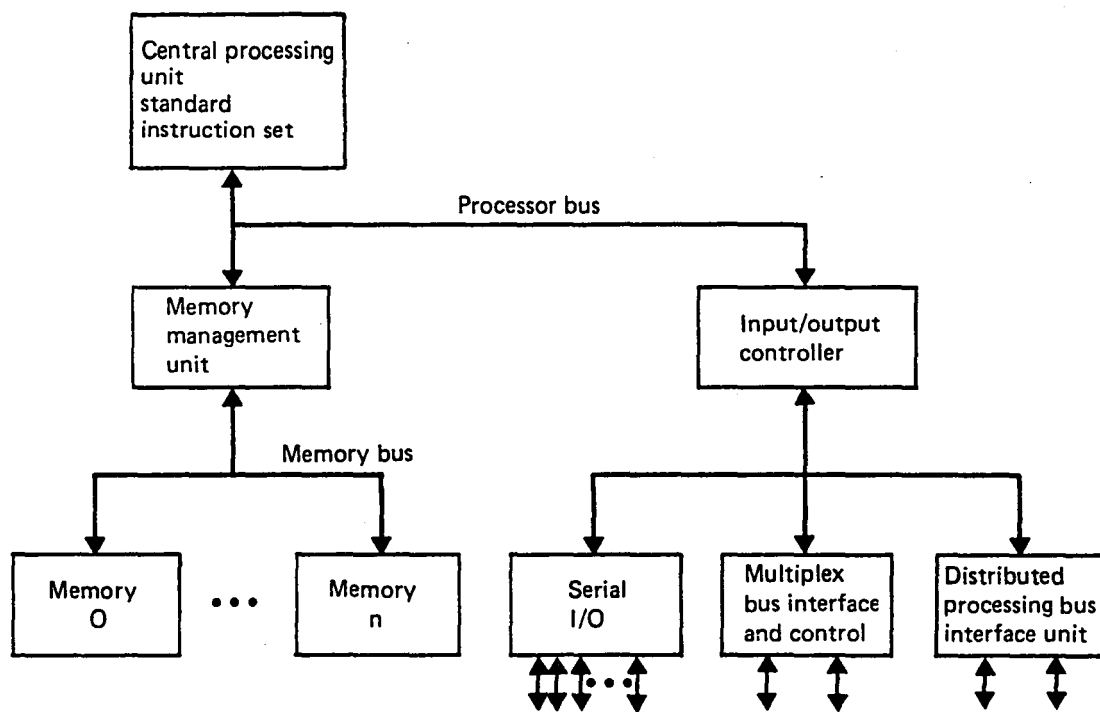
Figure G-5. Very-Large-Scale Integrated Circuit Avionic Computer Architecture

Table G-5. Comparison of Current and Projected Avionic Computers

Characteristics	HDP-5301	1990 VLSI
Throughput	500K ops	6000K ops
Memory address capability	64K words	16M words
Power	12.5W	8.5W
Number of integrated circuits	42	6
Memory access time	250 ns	25 ns (cache memory) 85 ns (main memory)

The key features of the CPU architecture are:

● A prefetch instruction buffer is used to overlap instruction fetching with other operations.

● The microcode ROM is slow to minimize power consumption. A double pipeline register is needed to assemble microinstructions.

● The register file and arithmetic logic unit (ALU) are conventional and would be similar for other instruction-set architecture.

● Miscellaneous functions include bus control logic, the bus arbiter, and test-and-fault tolerance logic.

A block diagram of the CPU is shown in Figure G-6.

The processor bus is synchronous; transfer over the bus is timed by a two-phase clock. It takes 20 ns to make one transfer. The bus is allocated by a centralized arbiter, located in the CPU, using bus-request and bus-grant signals. The arbitration process is overlapped with the transfer over the bus; hence, no additional time is required for bus allocation.
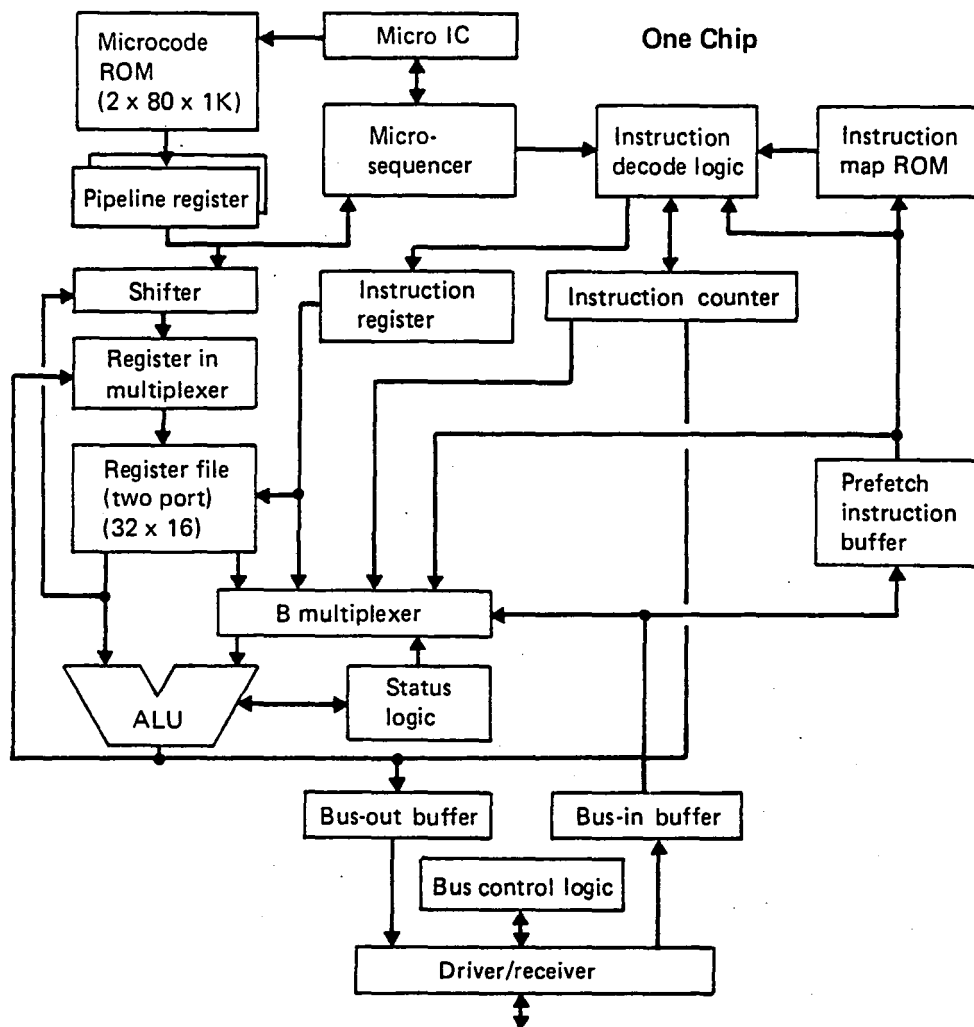
Figure G-6. Central Processing Unit Block Diagram

The bus is split cycle. When the current bus master is performing a read operation, the master sends the address over the bus with the proper control signals, and control of the bus is then released. Once the data are available and the responding device receives control of the bus, the data are returned via a completely separate bus-write transfer. This split-cycle operation allows bus transfers to be overlapped with the accessing of data within the responding devices. For instructions with register and short, immediate operands, only the instruction word must be fetched from memory. With the split-cycle bus, MMU and CPU prefetch overlap. The steady-state instruction execution for a sequence of these instructions is eventually determined by the memory access time. One instruction takes 75 ns under the assumption of a 60-ns memory.

The power dissipation of the 16-bit CPU chip is estimated to be 1.3W. The microcycle time of the CPU is 25 ns; i.e., the propagation time through the ALU and shifter is, at most, 25 ns. Also, the propagation time through the sequencer and control ROM is, at most, 25 ns. The CPU uses a pipelined organization so that instruction fetch, instruction decode, and instruction operation can be overlapped. The instruction prefetch unit has a four-word, first-in/first-out buffer that it attempts to keep filled. It operates in parallel with the rest of the CPU and makes independent accesses of memory over the processor bus. Under the assumptions of a 75-ns access time of main memory (from the MMU) and an instruction mix of 30% register-to-register and 70% memory-to-register instructions, the CPU achieves an instruction execution rate of 4.6M ops. With a 20-ns cache memory in the MMU and a 65% hit ratio, the execution rate becomes 6M ops.

A block diagram of the MMU is shown in Figure G-7. All accesses to memory are routed through the MMU. The receiving side of the MMU is a three-level pipeline processor. The three activities that can occur in parallel are (1) input from the processor bus, (2) mapping RAM access and/or cache memory access, and (3) main memory access over the memory bus. The mapping RAM and control translate virtual addresses into physical addresses and perform access-error checks. In the case of a read, if the virtual address is contained in
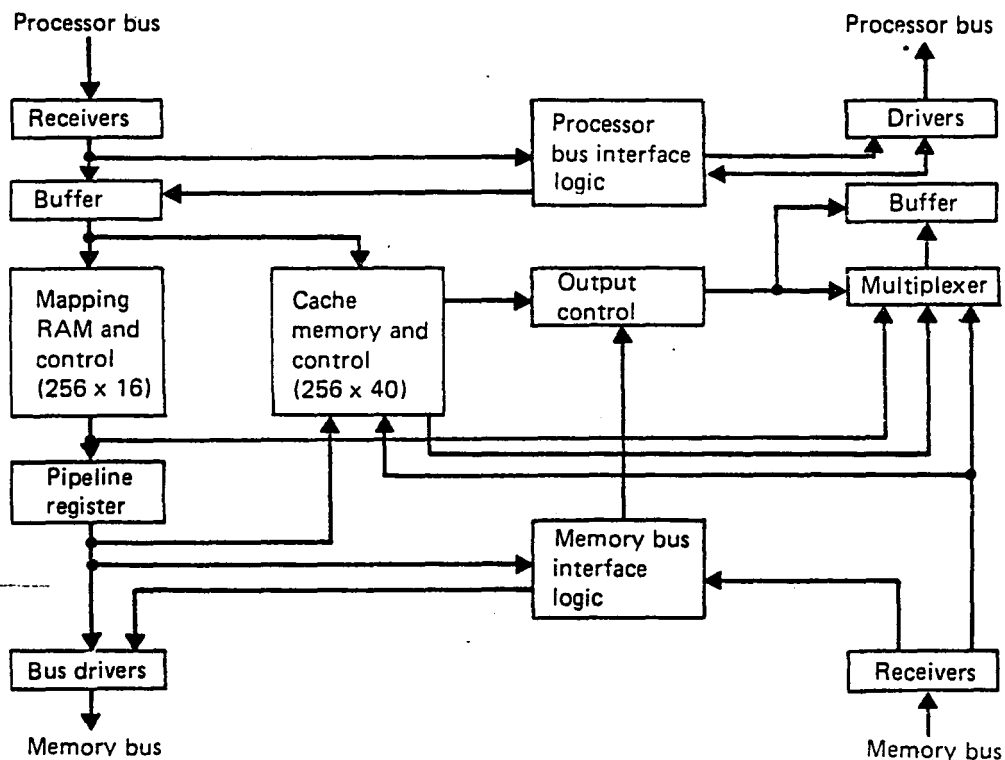
Figure G-7. Block Diagram of the Memory Management Unit

the cache memory, the word is routed from the cache memory to the output buffer; no memory access is required. If the word is not present in the cache memory, it is read from memory, placed in the output buffer, and then placed in the cache memory if the read request was from the CPU. A write-to memory causes a write into the cache memory if the word is present in the cache memory.

The MMU requires 25 ns to map a virtual address into a physical address; in parallel with this mapping, the cache memory is accessed to determine if the word is present. For read accesses, if the word is not present in the cache memory, an additional memory access time (up to 75 ns) is required to retrieve the word. The cache memory is 256 pairs of memory words. Based on studies of similar cache systems, the hit ratio for the cache memory should be at least 65%. A 1K cache memory would increase the hit ratio to well over 90%.

The instruction set allows 16 address states. For each state there are 16 mapping registers for instructions and data and 16 mapping registers for DMA transfers. Thus, there can be 512 mapping registers; 256 mapping registers have been specified for the present MMU. The mapping can be bypassed for those applications that do not use the mapping features. The MMU requires approximately $2.58 \times 10^{-5} m^2$ (40 000 mil^2) of chip area and 1.6W of power. Power is the major limit on chip size, and most of the power is used by the RAMs (cache and mapping) and the bus drivers. (The processor bus requires 6-mW drivers, and the memory bus requires 10-mW drivers.) The I/O controller (fig. G-8) is the interface between the processor bus and an asynchronous I/O bus. Any programmed I/O transfers executed by the CPU are recognized and processed by the I/O controller, which processes interrupts from the I/O interfaces and directs them to the CPU as appropriate. DMA transfers are buffered and processed by the I/O controller, which can function as an I/O channel and execute the I/O instructions. The I/O controller interfaces to the processor bus. It also can act as a processor bus master to execute memory transfers and recognizes I/O transfers with the I/O bus over which it makes asynchronous self-timed transfers to and from the I/O interfaces. Interrupts from the I/O interfaces also are received over the I/O bus. It has a buffer RAM for buffering messages and DMA transfers and an ALU for performing address calculations. Total power for the I/O contoller chip is less than 1.5W.
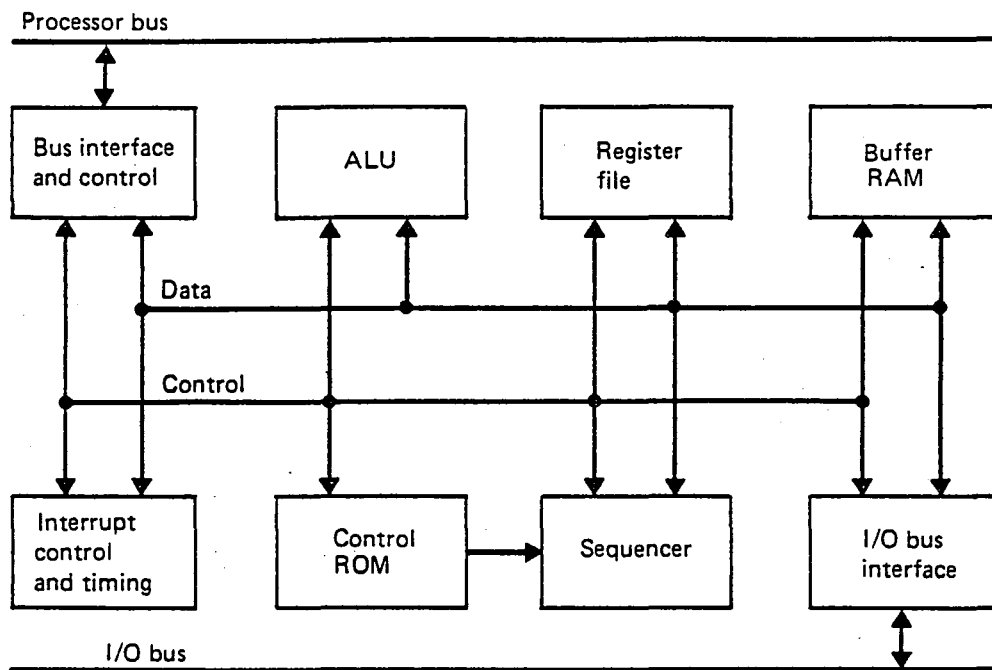
Figure G-8. Input/Output Controller

Three I/O interface chips have been proposed. The first of these, shown in Figure G-5, is a multiple universal asynchronous receiver/transmitter (UART)-like device with 10 UART units. These may transmit and receive at different baud rates; the maximum rate is approximately 10 MHz. The multiplex bus interface and controller of Figure G-8 provide redundant multiplexed bus paths. The distributed processing bus interface unit connects multiple processing units.

The multiplex bus interface chip is diagrammed in Figure G-9. It contains the necessary components to connect to two buses, but communication can occur on only one bus at a time. The bus adapter chip will monitor the inactive bus for mode commands. The I/O controller fetches the bus adapter instructions from main memory and stores them in the bus adapter control registers. The bus adapter is microcontrolled and has the capabilities for error-recovery retries and low-level management functions. It is designed to only need attention from the I/O controller on a message basis. The buffer RAM is sized to accommodate the maximum message of 32 words. Two modes of operation are allowed: (1) the master mode in which the bus interface chip is the controller of bus traffic and (2) the remote mode. In the latter case, the master is somewhere else on the bus. The bus interface chip in remote mode transmits and receives only on command from the
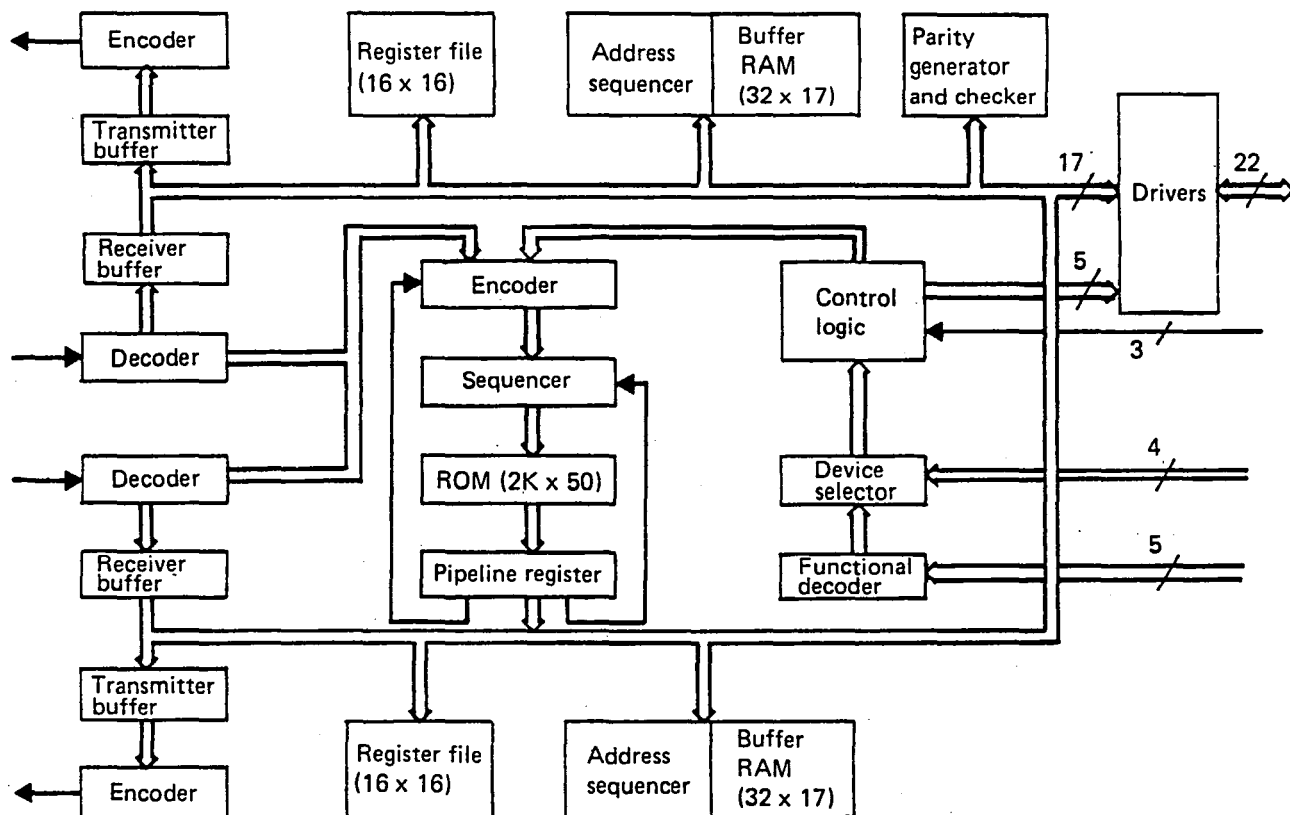
Figure G-9. Multiplex Bus Interface Chip

multiplex bus. The bus interface chip will use just under 1W of power and approximately $2.58 \times 10^{-5} m^2$ (40 000 mil^2) of chip area. The Schottky TTL drivers and the control ROM are the macrocells that consume the most power; together they use nearly half of the total power.

G.2.2.2.8 Testing

The complexity of testing grows exponentially with the size of the circuit. Facilities for controlling and observing the inner states of large chips must be provided to partition the circuit into testable segments. While this need is universally recognized, there is no general agreement on how it should be achieved.

There are many demands on testing and they often require complicated tradeoffs. The requirements change during the life cycle from design verification to manufacture, assembly, field use, and maintenance; they change with level of detail from circuit to

macrocell, chip, board, and system; and they change with the critical situation of the application. All these factors must be reconciled with a minimum overhead of chip area and circuit delays. The testing provisions should not distract from the chip designer's primary task of producing clear, regular circuits to perform the functions of the application.

Critical systems, such as flight controls, must have adequate test facilities. To establish a background for adding tests to the VLSI avionic computer example, some current techniques will be reviewed. A technique in the functional category seeks to demonstrate that the item under test performs its required functions. The techniques must consider the specific processes that the unit accomplishes. A nonfunctional technique tests the structure at the gate level disregarding the overall functions that the network is to perform. Testing for stuck-at-one and stuck-at-zero faults is nonfunctional because each gate is checked independently of the purpose of the circuit. In general, tests must cause observable operation of all internal devices. Internal storage items, particularly "flip-flops" and latches, must be set and observed directly with nonfunctional techniques. The controllability and observability of the storage items, other than arrays of memory, are of primary concern to the test designer. Specific methods are summarized in the following paragraphs.

Serial-Shift Registers—Provisions to set and read internal flip-flops or latches may be added without much overhead in gate or pin counts. This is done by grouping convenient sets of these storage items to form serial-shift registers. These may be read out when the testing mode of operation is called. The contents of the register may be set by shifting in a test sequence, or the contents may be read out as a bit string by similar sequential shifting of the register.

Nonserial-Shift Registers—The serial approach requires a larger number of clock cycles to shift the testing data in and out and to restore the register to its original condition when the testing is during normal operations. An alternative is to construct the internal latches of flip-flops to be directly addressable. This approach has the following advantages:

● Tests for random logic and memory arrays can be handled in one unified method.

● Combinational output points can be scanned with very little overhead; two extra gates are required.

- The scan-out operation does not disturb logic circuit states as does the serial-shift register technique.

- The scan-in and scan-out operations will need considerably shorter time compared with the serial-shift register techniques.

Nonserial-shift registers have the following disadvantages:

- Three to four extra gates per storage element are required.
- Extra I/O pins (10 to 20) may be needed for a VLSI chip.
- Long internal connections are needed for busing the address lines and scan clock.

Signature Analysis—The shift-register techniques require overhead that can be reduced by a built-in test technique. The areas of overhead are a large data base, the long computing times for test generation, and the long time for test application. Instead of using software test generators for producing the test list, hardware test generators are used. Further, instead of shifting the contents of the registers to compare results every time a test is applied, a signature register can collect this information. After applying a certain number of tests, the final result is shifted to compare it with the expected signature.

A shift register with appropriate feedback can be used as a hardware test generator. By adding a few gates, a built-in test generation/signature module can be constructed. This module combines the advantages of built-in test and serial-shift register techniques. This technique requires that all registers in a given design be constructed in this form. The design is partitioned into modules consisting of two registers—input and output—with combinational logic between. The registers may easily be multiplexed to also be used in a serial-shift mode. Thus, there is the possibility of using the same combination for factory testing and for self-testing in the field.

Behavioral-Level Testing—The design of a digital network usually requires several different descriptions. A description is used for modeling, simulating, and testing of the network. The model depends on many factors, such as the types of faults, the comprehensiveness of the test, the data base size, and the testing cost. With the increasing use of very dense logic, geometrical modeling is needed to check for design rules and to ensure the accurate physical placement of the devices inside the chip.

At the behavioral level, abstract specification of the network is described in a language similar to ALGOL. Program operators such as ADD, SUB, MULT, and DIV can be used. No fault model is used for testing; the tests are for functional accuracy.

Tests are generated and applied to check whether the network behaves according to specifications.

The behavioral-level test generation process is:

a. A thorough analysis is done to provide adequate exercise of all possible components of the network under test.

b. Selected components or macrounits are to be exercised to ensure adequate test coverage.

c. A path from inputs to the target component is sensitized.

d. A path from the target to the output is sensitized.

e. Conflicts are resolved. If this is not possible, a different path or test is selected.

f. Items b to e are repeated until tests are generated for all selected components or macrounits. As a result of applying such tests to the network, a response for a given target will be obtained.

The capabilities of the behavioral-level tests, in summary, are:

- They are available early in the design cycle.
- Test analysis can be done early.
- Each step in the design cycle may be independently verified.
- There is a large reduction in test data.
- Application time for tests is short.
- The diagnosis may be made to functional subunits.

The limitations of the method are:

- It is neither traditional nor systematic.
- It is not useful with bottom-up designs.
- The timing and implementation details are not evident.
- Fault models may not exist.
- The techniques for general path sensitizations have not been universally developed.
- Diagnosis to gate level is not possible.

Self-Testing Circuits—If enough logic is added to the normal functional logic of a chip, a very high percentage of faults can be detected. Then the test problem is reduced to the determination of the proper test stimulus; all faults are detected by the logic itself. Three types of self-test circuits will be reviewed: (1) residue coding, (2) invariant checking, and (3) duplicated logic.

The theory of residue codes is well established. Data are encoded and the code is checked periodically along the data path to ensure that no faults have occurred. It is possible for the VLSI components to carry such a pattern and provide a self-test capability.

In many circuits, it is possible to define an invariant that monitors the relations between the input and the output. If the circuit is working properly, this invariant is a constant. The ultimate in self-checking circuitry is to duplicate the logic and carry all data in error-detecting codes. This approach requires considerable overhead.

Test Engine on a Chip—The VLSI technology may make it practical to include more automation and support of testing on the chip than is possible with current integrated circuit (IC) methods. This opens the complicated architectural choice of which testing facilities to put on the chip and which to include in external support equipment. For example, on the chip, provisions may be included for:

- Storage of test vectors and test signatures
- Generation of test vectors
- Control of the configuration for normal functions or for testing
- Test sequences for simultaneous or independent checks of section of logic

If the chip has several components, it may be advantageous to collect some of the common testing facilities into a separate component called the test engine. At a minimum, the test engine would read the test and error information from each of the components, format these results, and communicate this information to points external to the chip. In a maximum configuration, the test engine would control the testing phase for each application component, send out test vectors, check the results of the test, and communicate the status of each macrocell to outside the chip. It is clear that the distribution of testing facilities between the test engine and the individual application components will strongly depend on the functions required of the whole family of components on the chip.

Testing Facilities for the VLSI Avionic Computer—Some possibilities for the computer architecture of test engine on a chip are outlined in these paragraphs. The approach is diagrammed in Figure G-10. The chip interfaces are checked by shifting registers at the boundaries. Nonfunctional tests are used for all combinational logic segments, but functional tests are used in memory-intensive areas. A microcontrol sequencer in the CPU controls the test vector generation and comparison for all the components. External control, through an automatic test equipment (ATE) system, may be used for more extensive fault isolation and extended fault coverage.

The chip interconnects and associated circuitry will be much more susceptible to field error than the circuitry on the chip. To increase fault tolerance, a redundant line can be added to data paths to allow a single interconnect failure in the data path without bringing the subsystem down. This involves using nonfunctional testing at the chip boundaries and requires control support to allow the CPU chip to dynamically reconfigure the lines to lock out the faulty line.

The problems of testing at chip manufacture and in the later stages of fabrication and utilization will have an impact on flight control architecture. These facilities will be integrated and complemented with other tests in software and hardware, which is a very complicated realm for analysis. Only basic approaches are available now.

External control to
shift in test vectors
and to shift out results

Central processing
unit

Microcontroller generates
test vector sequences,
compares results

Testing, serial shifting
controlled from CPU

Memory
management
unit

I/O
controller

Each chip in system
has registers connected
as serial-shift path with
feedback points to support
signature analysis and
external test vector control

Memory

Memory

Serial
I/O

Multiplex
bus interface
and control

Distributed
processing
bus interface

Figure G-10. Testing Approach

G.2.2.2.9 Buses

The structure of the internal transfers of data, addresses, and control signals in the computer is a major component of the computer architecture, as is the transfer of data between sensors, computers, and actuators. Internally, the concern is the speed of transfer; control of simultaneous processes; and economy of registers, lines, and other local hardware. External transfers, particularly if serial multiplexing is used, call for a host of decisions on control, protocol, redundancy, fault tolerance, and testing. The hardware design is at a much larger scale than registers; it involves interface chips, some of which may be as complex as microprocessors.

Reference G-5 gives a useful approach to outlining the choices for multiplexed bus architecture. A summary of the outline is:

- General system characteristics:
  - Description of application
  - System configuration
  - Description of subsystems

- Bus control:
  - Control site
  - Bus allocation:
    - Mode
    - Inputs to algorithms
    - Allocation algorithms
    - Synchronization of transmitting/receiving elements
    - Allocation scenario

- Multiplex data paths:
  - Physical and electric characteristics:
    - Medium
    - Modulation scheme
    - Speed
    - Maximum distances

- Transfer scheme:
  - Synchronization of messages

- Bus protocol:
  - Transactions:
    - Types
    - Scenarios

  - Addressing:
    - Name binding
    - Naming conventions
    - Levels of addressing

- Message acknowledgments:
  - Types of acknowledgments
  - Information returned with acknowledgments
  - Action to positive/negative acknowledgments

- Message size:
  - Fixed or variable
  - Minimum/maximum lengths
  - Determination of length

- Fault tolerance:
  - Bus control:
    - Error types detected
    - Error types not detected
    - Error handling

  - Transmission content errors:
    - Error types detected
    - Error types not detected
    - Error handling

  - Hard versus transient errors

  - Physical redundancy:
    - Bus
    - Processors
    - Interfaces
    - Reconfigurations

  - Self-tests:
    - Features
    - Coverage
    - Active or passive monitoring

- Bus interfaces and processors:
  - Types of interfaces
  - Distribution of communication functions:
    - Bus interface
    - Processor/subsystem

- Application processors:
  - Types
  - Process assignments
  - Processor/bus interface
  - Software interface
  - Type of executive

- Implementation:
  - Subsystem terminals
  - Physical modularity
  - Complexity

This outline was used in Reference G-5 to describe and compare a number of bus architectures, in particular the standards:

- MIL-STD-1553A
- General-Purpose Multiplex System (GMPS)
- Atomic Energy Commission Computer Automated Measurement and Control
- IEEE 488-1975

In the following paragraphs, MIL-STD-1553B, ARINC 429, and fiber optic buses are reviewed to examine problems and make predictions on the direction of bus architectures.

MIL-STD-1553B bus architecture provides more flexibility and capability than is needed for flight control systems. Its increasing use for avionic systems and industrial applications (ref G-6) led to the production of component chips for implementations. This also allows the flight control system to communicate with other subsystems, including the pilot display. Reference G-6 was used in describing the bus. MIL-STD-1553B establishes the requirements for serial, digital, command/response, and time-division

multiplexing techniques on aircraft. The bus allows for the transmission of information among several signal sources interconnected by a single, twisted-shielded pair of wires. The bus is a transformer-coupled, fault-isolated transmission line; data appear differentially on the signal-carrying wires. The serial-data bus operates asynchronously in a command/response mode. In this serial system, remote terminals (RT) receive and transmit data on the bus under the command of a bus controller. Military systems require at least one redundant data bus. The bus is a half-duplex system; i.e., transmission of information is bidirectional but in only one direction at a time. Information control resides solely with the bus controller. In addition to issuing commands to the RTs, the bus controller continously monitors traffic on the bus. For aircraft applications, a general-purpose airborne computer serves as the bus controller, but in less complex configurations, a dedicated microcomputer fills that role.

Information flow on the transmission line is in the form of messages composed of command, data, and status words. Each word is 20 bits long and is transmitted in a serial, digital, pulse-code-modulated format. Information flows along the bus at a 1-MHz bit rate. Bits are transmitted in biphase mode as a bipolar, trapezoidal signal with a positive pulse followed by a negative pulse and vice versa. Regardless of the word type—command, data, or status—the first 3-bit time period is called the sync field. The sync field distinguishes between a command or status word and a data word. It is an invalid waveform because the pulse period lasts for 3-bit times instead of the usual 2-bit times. After the sync field, the 16 bits that contain the information to be transmitted or received follow the sync field. The last, or 20th bit, is parity. It checks the validity of the 16 data bits. Odd parity is used in 1553 systems.

The bus controller directs signal traffic by issuing command words containing the address of the RT that must either listen to or transmit data on the bus. The words that constitute data can be transferred from a controller to an RT, or vice versa, or between RTs. In a controller-to-RT transfer, the RT can receive up to 32 data words and responds to the controller with a status word. For the reverse transmission, an RT-to-controller transfer, the RT sends a status word and up to 32 data words. In an RT-to-RT transfer, messages pass from one RT to another. The controller first designates a receiver and then issues a second command word to identify the transmitter. The transmitter responds with a status word and up to 32 data words. The receiver answers with its own status word. In a fourth type of transfer—a broadcast message—the controller issues a receive

command to a specific address and follows with up to 32 data words. Only RTs equipped to recognize broadcast commands can recognize the address and receive the data. No status words are issued.

G.2.2.2.10 ARINC 429

This specification defines the current standards for the transfer of digital data between elements of avionic systems used in the air transport industry (ref G-7). The transmission is in a single direction from the output port of the sending element over pairs of twisted and shielded wires to all other elements requiring the data.

Numerical data may be coded either in two's that complement fractional binary notation or in binary-coded decimal. A parity bit is used. The receiver is not required to acknowledge receipt of the data. Alphanumeric data may be encoded in International Standards Organization (ISO) alphabet No. 5. Provisions for transmitting graphic data will be included when a need is established.

The specification carefully defines the format of each data word. These consist of 32 bits that are partitioned to identify the type of information (8 bits), data source and destination (2 bits), sign and status (2 bits), and parity (1 bit). Files containing 1 to 127 records may be transferred; each record contains 1 to 126 data words. A command/response protocol is defined for these transmissions.

The error detection is based on the single parity bit that is the last bit of each word. It is encoded as odd parity on all of the preceding 31 bits in the word. There are no provisions for retransmission of messages or for the inclusion of redundant bits or other means of error correction in the words.

Return-to-zero bipolar modulation is used. Voltage levels, transmitter output impedance, receiver input impedance, and fault tolerance to overvoltages and short circuits are specified. The high-speed operation is at 100K bits per second (bps); low-speed operation is between 12.0K and 14.5K bps. These are not intermixed on the same bus. A digital word is synchronized by reference to a gap of a minimum of 4-bit times between the periods of word transmission. The beginning of the first transmitted bit following this gap signifies the beginning of a new word.

There is a trend toward military applications of avionic equipment originally designed for the airlines. This will produce the need for some interfacing equipment to allow Mark 33 digital information transfer system (DITS) to couple to a 1553 data bus.

G.2.2.2.11 Fiber Optics

Transmitting digital information by pulses of light in glass waveguides offers advantages beyond its technical merits. For flight controls, the use of fiber optic buses is advantageous because of high data rates with few errors, their immunity to electromagnetic interference (EMI) and electromagnetic pulse (EMP) disturbances, and low-weight installations. Transmission rates are expected to go up to 100M bps with a bit error less than one in 10^9 bits. When they do occur, failures are almost always in the receiver. The life and reliability of the current light-emitting diode (LED) light sources are low. Bus configurations are much more difficult to design than using wires because of the loss in signal strength in branches and connections. The connectors are difficult to align, there is little standardization of equipment, and the associated electronics are still expensive. These costs will come down as more integration is designed into the circuitry; however, better techniques of bus control must be developed. Unless the transmission is point to point in a single direction, couplers must be used to gain access to the bus. These are T-couplers and transmissive and reflective star couplers. Bifurcation devices are necessary if a station transmits and receives on the same fiber. The cable may consist of a single fiber or a bundle of fibers; the trend is to a single fiber. Connectors are a problem for single-fiber systems because the optical cores must be carefully aligned to avoid excessive losses of signal strength.

The transmitters are LED or injection laser diodes (ILD). The ILD has an output of 5 to 10 MW compared to 0.01 and 0.02 MW for LEDs. However, the ILDs are more temperature sensitive, are not as long lasting, and cost more than the LEDs. The receivers are p-layer intrinsic n-layer (PIN) photodiodes or avalanche photodiodes (APD). The APDs are more sensitive, but their high bias voltage, high temperature sensitivity, and high price make the PIN photodiode the usual choice for the receiving element.

The structure of the bus system must be carefully designed to maintain sufficient signal strengths. Reference G-8 analyzes a number of configurations for a command and control system. Projecting from this analysis, a similar structure probably would be best for

flight controls. This architecture uses a single transmissive star coupler to form a remote terminal to service many local users (fig. G-11). Based on 1977 data, a 55m (180-ft) bus, using LED sources and APD detectors, would result in a 30-dB loss, which is state of the art.

G.2.2.3 CONCLUSIONS

A safe prediction is that ultrareliable central processing components will be available in the late 1980s to meet the needs of digital calculations for flight controls. The reliability will come from increased integration with reduction of chip counts and connections between chips and also by fault-tolerant and self-testing mechanisms added to the chips. The size, weight, and power requirements of the systems will no longer be significant considerations. Costs will also be reduced to relatively unimportant levels.
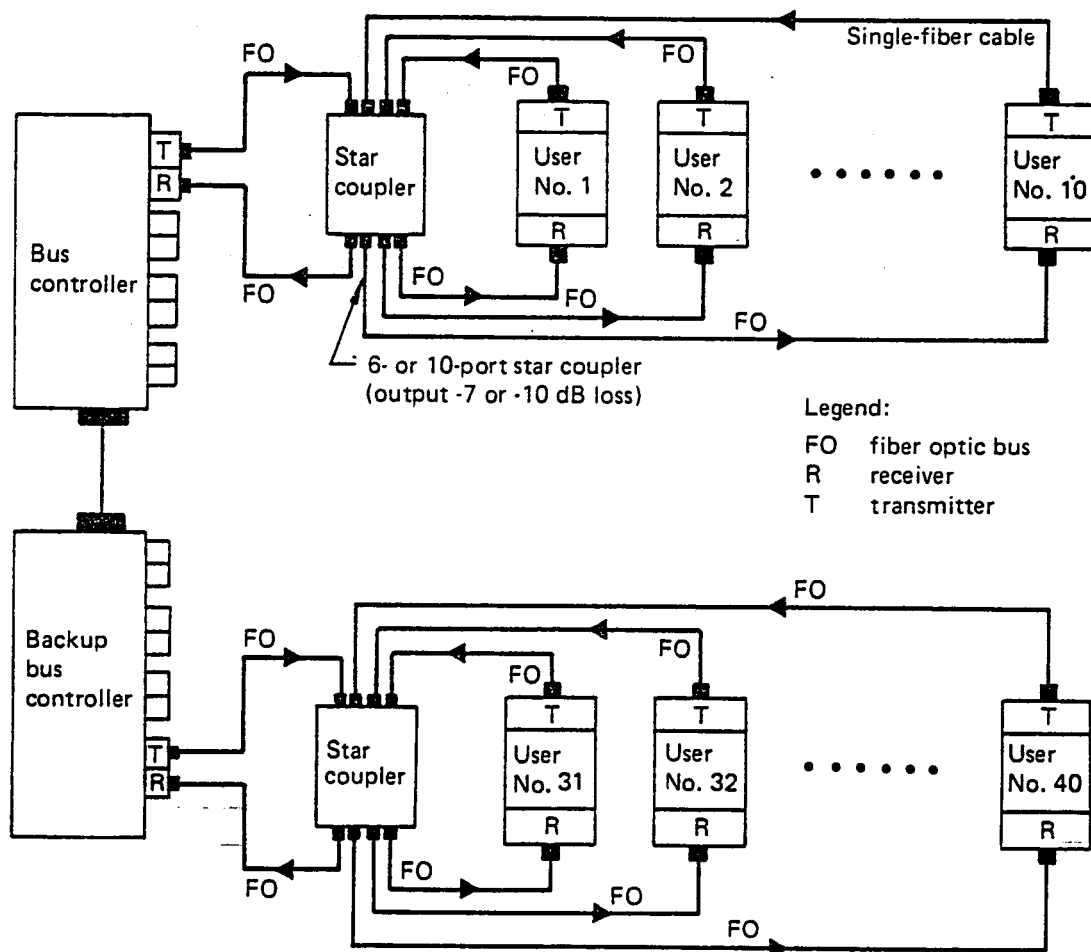
Figure G-11. Fiber Optic Bus Architecture

Standardization of instruction sets will permit accumulation of software support systems and development tools so that software development for flight control calculations will be low cost and certifiably reliable. This will be enhanced by the trend to do fault tolerance and self-testing in hardware rather than with complicated software.

The I/O functions, already the largest part of the system design problem, will become even more dominant as the central computing structures become routine. Multiplexed busing of sensor data and actuator commands will provide the critical technical problems. Fault-tolerant components that will provide much more capability than is necessary for flight controls will be used in these systems because of large production runs and experience in similar systems. Fiber optic busing will be developed because its resistance to electric interference will justify the costs over wire buses.

There have been many reviews and projections of avionic computer technology; e.g., References G-9, G-10, and G-11. Reference G-11 contains some especially relevant information, including speed, power, weight, and size estimates of avionic computers projected for the next 20 years.

G.2.3 SERVOACTUATORS

G.2.3.1 INTRODUCTION

The purpose of the servoactuator task was to review the state of the art in actuation systems and select candidates from configurations now in development. While a number of systems showed promise for the 1990 time frame, many had deficiencies that precluded their selection at this time. The study included investigations of power characteristics as well as control system capabilities and involved a wide variety of devices.

G.2.3.2 CANDIDATE SYSTEMS

Systems to be considered were divided into two power source categories (hydraulic and electric) and then classified in accordance with their energy efficiency. A graphic representation of the overall field is shown in Figure G-12. Note that all actuation system types are included, from conventional with independent functional control augmentation system (CAS) elements to integrated FBW.

Hydraulic Power Source

Low-Power Efficiency

Conventional, cylinder-type actuator, fixed-pressure servovalve control	Hinge moment For fixed response from aircraft	

Manual and CAS:	Fly by wire

Conventional surface, cylinders and redundant CAS actuators 	With secondary actuators 	Integrated actuators

Valid configurations for surface and secondary actuators

I Surface actuators
• Integrated cylinder and servovalve
  • Single cylinder and single valve—individually or a combination
  • Dual cylinder and dual valve
  • Triple cylinder and triple valve
• Separate cylinder(s) and servovalve(s)
  • Single cylinder and single servovalve
  • Two cylinders and dual valve
  • Three cylinders and triple valve
• Combinations of any of the above
	II CAS and secondary actuators
	• Control and hydraulic channels dedicated
	  • Force summed
	  • Active, online
	  • Active, standby
	• Control and hydraulic channels cross fed
	  • Position summed and monitored
	  • Velocity summed and monitored
	• Independent electro-mechanical actuators
	  • Force summed with hydraulic channels
	  • Position summed with hydraulic channels
	  • Force summed
	  • Velocity summed
	  • Position summed
		III Integrated actuators
		• Control and hydraulic channels dedicated; all summing on main servo-valve
		  • Force-summed
		  • Active, online
		  • Active, standby
		• All control channels to each hydraulic channel
		  • Single actuators used singly or in combination *
		  • Redundant actuators synchronized and sum-med at main servovalve *
		
		* May be summed and monitored by force, velocity, or position

Control surface actuator	No. per airplane	Maximum hinge moment, in-lb	Maximum rate, deg/s	Average rate, deg/s	Deflection maximum, deg	Power, peak, kW	Power, average, kW
Outboard aileron, outboard portion	4	9 000	70	54	+15, -30	1.243	0.959
Outboard aileron, inboard portion	2	4 700	130	100	±15	1.205	0.927
Inboard aileron	4	42 000	42	30	±20	3.480	2.486
Outboard flaperon	2	24 000	65	45	+10, -20	3.077	2.131
Inboard flaperon	2	24 000	65	45	+10, -20	3.077	2.131
Elevator	6	65 000	55	40	+20, -30	7.052	5.125
Rudder	4	185 000	55	40	±25	20.07	14.60
					Total per airplane	156.2	113.3

Figure G-12. Candidate Power Source Systems

Hydraulic Power Source		
High-Power Efficiency		
Geared, variable-displacement hydraulic motors; fixed-pressure secondary or pilot actuator required to drive motor displacement control	Hinge moment, Surface load — Actuator capability — Surface rate	
Manual and CAS	Fly by wire	
Surface driven by geared variable-displacement motor controlled by redundant ACT	With secondary actuators	Integrated servomotor
CAS / Manual input / CV / CYL / M / V / Motor / Surface	EHV / CYL / M / V	EHV / M / V
Valid configurations for surface and secondary actuators		
IV Surface actuators • Linear output (ballscrew drive) • Independent motor/ gearbox units used singly or in combination • Redundant motors geared to common gearbox • Rotary output (direct gearing to surface hinge) • Independent motor/ gearbox units used singly or in combination • Redundant motors geared to common gearbox	V CAS actuators and secondary actuators (see column II)	VI Integrated actuators All configurations require internal stroking servo; characteristics similar to those in column III

Figure G-12. Candidate Power Source Systems (Continued)

Electric Power Source
High-Power Efficiency

Electric motor-driven variable-displacement servopumps powering conventional cylinder-type actuators (variable pressure)	Hinge moment / Surface rate / Actuator / Surface	Hinge moment Geared servomotor (EMA) Surface rate / Actuator / Surface
Manual and CAS	Fly by wire	Fly by wire

Surface driven by cylinders powered by servopump controlled by separate ACT	With secondary actuator	Integrated servopump	Geared servomotor
CAS, PF, EM, CV, CYL, P/V, Manual input, CYL — Control surface	PF, EM, EHV, CYL, P/V, CYL — Control surface	EHV, PF, EM, CYL — Control surface	Motor controller, EM, Surface

			• Electromechanical surface actuation; only practical mechanization is with completely integrated surface actuator

Valid configurations for surface and secondary actuators

VII Surface actuators	VIII CAS actuators and secondary actuators (see column II)	IX Integrated actuators	Geared servomotor
• Nonregenerative; no recovery of control surface energy		All configurations require internal stroking servo; characteristics similar to those in column III	• Linear output (ballscrew drive)
• Regenerative; control surface energy recovered			• Single motor/gearbox used singly or in combination
• Mechanical; flywheel on drive motor			• Multiple-wound motors used singly with one gearbox
• Ac induction motor			• Multiple motors on common gearbox
• Dc motor/generator			• Rotary output (direct gearing to control surface hinge)
			• Single motor/gearbox used singly or in combination
			• Multiple-wound motors used singly with one gearbox
			• Multiple motors on common gearbox

Figure G-12. Candidate Power Source Systems (Concluded)

G.2.3.2.1 Actuation Systems Using Hydraulic Power

Present aircraft use a complex hydraulic power generation and distribution system that has evolved after many design cycles. It is reliable and relatively easy to maintain. Careful design has provided adequate protection from probable failure patterns, but the simple cylinder-type actuators used in most systems operate with low energy efficiency. There are alternatives, but their performance appears questionable.

Conventional Cylinder-Type Actuators—Most of these devices operate from a fixed-pressure hydraulic supply. They use a simple, reliable, flow-control servovalve (mechanically or electrically operated) to vary the amount of fluid entering and leaving the cylinder. A thorough knowledge of servomechanisms and structural dynamics enables systems to be built with complete control of acceleration, velocity, and position.

Hydromechanical surface actuators may be built in a variety of forms, any of which may use separate electrohydraulic or electromechanical servoactuators for the insertion of the automatic control signal. Redundant signal and power supply paths are included for reliability.

Hydromechanical surface actuators are servomechanisms that use hydraulic energy to position the control surface against variable aerodynamic loads. The mechanical input energy required can be very low. The basic elements needed are cylinder and mechanically operated servovalve. Redundancy requirements dictate the use of multiple separated hydraulic supplies, so dual or triple valves and cylinders are commonly used. These may be arranged in tandem or parallel (sometimes joined) construction, or they may be mounted as individual assemblies. Valves may or may not be integrated into the cylinder construction.

Electric command signals from the automatic control system(s) are used to position the output of these servoactuators. Reliability requirements dictate the use of redundancy, and it is the methods by which the redundancy is mechanized that distinguish the various types of actuation systems. Electrohydraulic systems may use methods that dedicate a hydraulic channel to a control channel, or the control channels may be crossfed to all hydraulic channels. Electromechanical actuation channels are normally dedicated to a control-channel-related electric supply.

When the aerodynamic efficiency of an airplane is improved by reducing the stability margin, the reliable operation of a stability augmentation system (SAS) becomes a matter of flight safety. To comply with flight safety requirements, redundant electric servoposition commands are used to control a suitably redundant actuator. The resulting control system is so reliable that electric pilot commands can be used to replace the mechanical control system, and FBW system advantages are realized.

An effective mechanical crossfeed may be achieved by using a full-authority redundant electrohydraulic or electromechanical servoactuator to position a conventional hydromechanical surface actuation system. The former, termed a secondary actuator, may be mounted in any manner that provides a convenient, reliable, mechanical interconnect.

The secondary actuator may be packaged with the surface actuator to eliminate any exposed mechanical linkage, or the secondary actuator may be sized to handle the control surface loads directly. In either case, they are called integrated actuators. Contemporary examples of integrated actuator systems are on the F-16 and F-18 aircraft.

High-Efficiency Hydraulic Power Actuators—The heavy losses associated with servovalve-controlled cylinders may be reduced by using alternative actuation methods; i.e., methods that do not use loss-generating devices such as closed-center servovalves.

One scheme uses a variable-displacement hydraulic motor that is geared to the control surface. Increasing the displacement of the motor has an effect similar to the opening of the servovalve in a conventional valve and cylinder arrangement. Unfortunately, motor displacement control usually requires input forces and velocities greater than those available in a manual system, so some type of boost actuator is required.

The motor may be geared directly to the surface hinge line, to an operating lever, or to the surface horn via a ballscrew. In any design, the failure modes and probabilities must be carefully assessed for each redundant system being considered.

The variable-displacement hydraulic motor can be used either in a manual plus CAS configuration or in an FBW configuration, as shown in Figure G-12. For FBW applications. an integrated actuator can be achieved by incorporating an electrohydraulic servoactuator into the motor for displacement control.

G.2.3.2.2 Actuation Systems Using Electric Power

Using multiple electric power distribution systems and electrically powered actuators offers several advantages over a hydraulic system. How that power is used at the control surface depends on space requirements and on how redundancy must be achieved.

Servoamps—A constant-speed electric motor, driving a variable-displacement hydraulic pump directly connected to a cylinder, can be controlled in a way similar to the variable-displacement hydraulic motor described previously. However, because there is no supply of constant-pressure hydraulic fluid for the "stroking servo," a small hydraulic system also must be driven by the motor. Because there is no large servovalve and because some of the surface positioning energy can be recovered, a minimal amount of heat is generated, and electric motor power can be quite low.

The stroking servo can be commanded by mechanical signals from the pilot and a CAS actuator. If only electric commands must be followed, an FBW actuator results.

An electrically powered FBW actuation package is easy to maintain; only the rod ends and the electric connectors need to be removed for service.

A multichannel secondary actuator, powered by the single local supply, can be used to control the servopump, or several servopumps may be controlled by one secondary actuator. The latter involves an added set of mechanical connections or some hydraulic interconnects or both.

Integral stroking pistons, controlled by a pump-mounted electrohydraulic servovalve (EHV), can provide control for a completely integrated package.

Electromechanical Actuator—Development of high-efficiency brushless dc servomotors resulted in a beneficial way to power control surfaces. Compact, hinge-line actuator designs and ballscrew drives both appear as candidate systems. The gearing method must be carefully selected, as the reliability and failure-mode considerations of those elements are most important.

While it is possible to build an EMA with mechanical inputs that could replace hydromechanical surface actuators in a conventional manual control system plus CAS or FBW with a secondary actuator system, the real potential for the EMA is in integrated actuator designs for FBW.

G.2.3.3 QUALITATIVE TRADES

Four basic actuation systems were examined from the point of view of performance, weight, cost, maintainability, and developmental risk. Of particular interest were their applicability to FBW and their potential for simplification.

G.2.3.3.1 Conventional Hydraulic Cylinder-Type Actuators

These have been the most popular actuators for flight control surfaces because they have excellent design flexibility (bore/stroke ratios, tandem and side-by-side combinations, etc.) and have progressed through years of development, resulting in a thorough understanding of the principles involved. Excellent dynamic performance can be achieved in both single and multichannel systems, and failure modes can be well defined. These are the lightest weight actuators now available (advanced, higher pressure actuation systems are even lighter) and costs, which include the control electronics, are low. Although maintenance of conventional, individual-component systems is more difficult, advanced integrated actuator FBW designs, using "plug-in" line replaceable units (LRU), show substantial improvements in this area. Reliability and service life are excellent.

G.2.3.3.2 Geared Variable-Displacement Hydraulic Motors

Theoretically, this arrangement is energy efficient; however, the performance is inadequate. No known motor designs (there are improved configurations under development) can meet the small-signal deadband requirements for a high-performance flight control system.

G.2.3.3.3 Electrically Powered Servopumps

The concept of electrically powered servopumps was developed by the Germans during World War II. It was made flightworthy by the English and used commercially in the

VC-10. The element geometry is similar to the variable-displacement motor, and it also has deadband and small-signal performance deficiencies. However, it shows the potential for greatest overall efficiency if performance weakness can be overcome. Maintainability is excellent, reliability is high, and adaptability to FBW is encouraging.

G.2.3.3.4 Electromechanical Actuation

Although EMAs have been used for autopilot and SAS actuators for years, recent developments in high-efficiency, brushless, permanent-magnet motors have prompted the design of higher powered devices. It now appears that actuators for all surfaces of the subject vehicle are feasible. However, the design of high-ratio, high-efficiency gearing that can allow the actuator to meet both performance and failure-mode requirements remains risky, particularly for the larger sizes. Weight, including the associated electronics, is low enough to be competitive, and maintainability is an outstanding feature.

G.2.3.4 CONCLUSIONS

The ACT configuration has relaxed static stability in the pitch axis for energy efficiency. An operable pitch-augmentation system is essential to safe flight. A minor extension of the pitch-augmentation system allows incorporation of FBW control. FBW control in all three axes is recommended so that performance, weight, cost, and maintainability benefits attributable to FBW will be at a maximum.

A close examination of all control surfaces showed that the loads, dynamic performance, and redundancy necessary for FBW could best be met by conventional, cylinder-type hydraulic actuators. The lightest weight, lowest cost, most reliable, and most acceptable maintainability will be possible if conventional hydraulic actuators of the integrated type are used.

The flaperon installations required that power to the actuator be supplied across the wing-flap interface. In this instance, the use of an EMA to operate the flaperon simplifies the problem and is therefore recommended. The use of EMAs throughout the aircraft was also considered, but the relatively large number of unknowns and the added study effort required to properly define a design were sufficient causes for rejection.

G.2.4 SOFTWARE DESIGN AND VALIDATION

This subsection discusses the possibility of designing, verifying, and validating flight control software so that it can be certified to be free of technical and global errors and so that it will respond to all normal circumstances and all hypothetical failures as specified.

Flight control software must be error free. In a multichannel system that is critical to flight safety, a software error that is copied into each channel may result in a serious single-point failure. Software errors usually are thought of as technical errors such as typing mistakes, spelling errors, misplaced decimal points, or mistakes in signs or operation symbols. Segment-by-segment simplicity of flight control software and attention to inspection, testing, and the use of software development tools will eliminate software technical errors.

Design errors of a global nature are harder to prevent. These appear as inconsistencies or conflicts between two separate functions, or as errors of omission in which some combination of events has been overlooked in the analysis. However, the special nature of flight controls allows a systematic description and analysis so a design and validation methodology can be constructed to eliminate such situations. This methodology has not yet been completely demonstrated, but progress is being made by a number of investigators. Thus, flight control software can be specified, designed, analyzed, and tested so it can be certified to be free of design and technical errors for all normal operations and for a specified class of hardware failures.

Because it is important to be precise about what is being covered and what is not, attention should be directed to definitions. A distinction is made between verification and validation. Verification applies to software; it is the process of demonstrating that software is technically correct by showing that each software function performs as specified and the technical aspects of inputs, outputs, and the passage of data between functions are correct. It must be shown that the data that define the state of the function are not corrupted by any side effect so that the data survive to the subsequent cycles of the calculations. Validation applies to the system; it is the process of showing that the system performs according to its requirements and reacts favorably to all situations.

The importance of verification and validation grows proportionately with the trend to delegate larger percentages of the system functions to software. As the software becomes more complex or more critical, verification and validation must become more systematic and formal, and they must establish complete confidence in the performance of the software. This implies that "black-box" testing is no longer adequate. To handle the complexity, the system structure must be clear, precise, and complete. This inevitably leads to a more mathematical approach; we have found that hierarchies of finite-state machines are very suitable for the description and design of flight control systems.

The functional and performance requirements of the system must be made sufficiently precise to provide a basis for design and subsequent verification and validation. In this case, "requirements" refers to the informal descriptions from the customer and "specifications" refers to the precise written description compiled from the requirements. The preparation of an adequate specification is difficult and tedious but crucial to the success of design and validation of the system. Specifications will be discussed in more detail in a subsequent section.

Although the verification and validation methodology proves many functions, there are several that it cannot prove. It is not possible to predict the response of a computer to all possible failures of its hardware. The most elaborate failure-and-effects analysis can only enumerate the most probable failure modes. Because there is a vast number of states in which the computer may be when a failure occurs, the outcome can be only a guess. The system must be configured so that there are no failures that can put the airplane in jeopardy. Although our proofs can only show that the system is safe against classes of hypothetical mathematical failures, experience has shown that all physical failures have been covered.

Software development begins with writing the specifications that describe what the system will do. Specifications do not describe how the system performs. The next step is to design the software and verify that the specifications have been captured correctly. When this is done, the design is coded and the code is verified to implement the design. After the software has been integrated with the hardware, the validation that the system performs as specified begins.

In detail, the conclusions (ref G-12) to be supported in this section are:

1. Software for flight controls is not intricate. The observation that the functions of flight control systems are elementary is important to the discussion. The assembly programs for current triply redundant systems are about 10 000 lines, but the code may be structured into a large number of simple functions. The data structures are also elementary. There are fixed sets of inputs, outputs, and state variables. The control structure is direct with no complicated "while-do" loops. The flight control laws require only straight-line computations that have no peculiar singularities that need delicate numerical analysis. The logic functions may be structured as finite-state machines to allow precise design and verification. A construction that causes problems on special circumstances will probably not survive a careful inspection on the code. This includes obscure assembly programming manipulations that are easily detected by an independent inspection.

    Testing is primarily used to show that there are no typographical errors in the code. It is generally very effective.

    The software for high-performance aircraft may be more complicated in the future. Examples of new control techniques that require more complicated calculations are:

    ● Adaptive gain mechanizations
    ● Flutter-mode suppression
    ● Analytical redundancy for sensor failures
    ● Wing-load alleviation

    Verification of these functions will not require special techniques.

2. Each function may be verified by one or more techniques. For most of the functions, input and output predicates may be written, and the computation may be verified by symbolically evaluating all the path conditions. Boolean symbolic evaluation of the logic functions is certain because of the cross-checks afforded by multiple paths. The control laws may be verified with confidence by frequency-response analysis on a simulation. Petri nets may be drawn to check the synchronization of the redundant computers.

3. Integration of functions into the total program may be verified completely. Data flows, initialization and integrity of state variables, consistency and lack of circularity of function references, and all the technical details required in combining the individual functions may be demonstrated by hand or with the assistance of tools.

4. The approach to design and verification can be made systematic and formal to any desired level. The word "formal" implies that precise definitions, rigorous analysis, and systematic procedures are written. Tools may be added until a completely machine-supported approach to verification is achieved. Thus, technical verification that the software conforms to its design specifications may be done with complete certainty. However, the reliance that must be placed upon the programmer or verifier is directly related to the lack of automation of the methodology. Automation enforces discipline on the design and verification process.

5. Most tools or techniques prove only a particular aspect of the design or code; some are clearly directed at particular properties. The set/use checker and the circular reference checker are examples. Even the more general tools and techniques require explicit and sometimes implicit assumptions to hold during their use. An automatic theorem prover assumes that the input and output assertions are complete and represent the functional requirements of the segment. Thus, combinations of tools are required and judgment in their use must be exercised. There is always the fundamental assumption that the requirements are complete and have been captured correctly by the top-level mathematical model of the system.

The tools of static analysis can be very useful in the software development process. Not only may they be used at the coding level, but, at the cost of introducing formal languages with syntax, they may be used at the design and specification levels. Dynamic tools greatly facilitate and systematize the testing procedures. It has been customary to leave the testing at the function level to the control analyst/programmer. Instrumentation and drivers to monitor and execute tests are generally customized by the flight control analyst to check out his particular program.

6. Validation of the normal system operation is possible. The work becomes more difficult as it moves out of the realm of verification of software into the total system. Performance measures may be checked, and computation of control laws may be verified and validated by checking the frequency response of the system. The normal operation of a flight control system is not so complicated that it cannot be thoroughly checked in simulation. Inductive arguments in this regard are seldom explicitly considered or stated.

7. Validation of the system response to hardware failures is difficult. It will be possible to demonstrate the consistency of failure management provisions and global performance of the system. This is a subject for current research. The effects of hypothetical sets of failures may be validated. It is not possible, however, to be certain that the responses to all hardware failures are covered by the mathematical description of the system.

In the following paragraphs, a methodology for flight control software, from specifications to validation, will be outlined. Although many approaches and variations are possible, only one will be demonstrated.

G.2.4.1 FLIGHT CONTROL FUNCTIONS

The software for a flight control system usually:

- Initializes the computers
- Performs preflight built-in tests
- Synchronizes the computers
- Initializes filter variables and status variables
- Monitors the dynamic sensors
- Manages system redundancy
- Performs the mode logic
- Calculates the control laws
- Runs the in-flight self-tests
- Selects signals for outputs
- Provides status and warning signals

A study of typical systems suggests that:

● The functions separate well to allow a carefully structured design for each.

● The interfaces between the functions can be clearly defined. Circular references may be avoided.

● The state variables of each function are easily identified. These are quantities that must be preserved for the next iteration of the computations.

● The functions may be packaged into any executive structure that is appropriate.

● There are only a few "while-do" loops. These loops wait for an external signal to cause synchronization, trap the computation until the watchdog times out to shut down the system, or wait until the real-time counter times up to a particular value. There are no doubts about termination of the loops in any of these. All other loops are indexed for a fixed number of iterations. Thus, the theoretical structure of the software is not complicated.

● Most of the functions are easy to design and may be exhaustively tested for all events.

● There is usually only a very simple interrupt structure for responding to the watchdog timer or fluctuations in the power supply.

● The data structure is elementary. There are no problems with overflow of the data base because the numbers of variables, parameters, and constants are fixed. The state of each module is determined by a fixed number of variables. There are no problems with dynamic indexing of arrays.

● The functions that control the flow of the calculations (synchronization, monitoring sensors, redundancy management, mode logic, and signal selection) may be represented as finite-state machines.

These points are listed to emphasize that the software for flight controls is not complicated. The huge error counts that occur in large, general software systems are not relevant here. In addition, the criticality of the system requires careful attention to the quality of the software; a system cannot be put into the field to let the customer find the errors as has been done with large operating systems. Because the software is elementary, a precise verification methodology is possible and can be used effectively.

G.2.4.2 SPECIFICATIONS

A mode of description is needed that will make the specifications public and easily accessible for review and changes. It should be complete so that omissions and inconsistencies are readily detected. Fortunately, there is such a mode for flight controls.

A flight control system provides stability augmentation, control augmentation, outer loop modes for relieving the pilot, and warning and status signals. The state of the system is described by the servo engagements, the mode being computed, and the status of its redundant facilities. The system can be in one of a small fixed number of possible states. Abstractly, it is a finite-state machine, which is a device that has a fixed set of internal storage elements that determines the state. When an input is received, the machine switches to a new state depending upon the input and the current state. While any practical computing device has a finite number of states, the concept has utility only if the number of states is small. Describing the flight control system as a finite-state machine, which, in turn, is represented as a group of smaller machines, defines a structure that can be used for the basis of the specification. At each subsequent stage of development, verification begins by showing that this structure has been correctly implemented.

Two levels of specifications are needed: the first describes the functions of the system regardless of whether they are implemented by hardware or software and the second describes the software functions, taking into account the hardware facilities. The software is designed and coded to the second specification, but it must be verified that the software functions plus the hardware facilities perform the system functions as specified. Those functions that are done completely by the software are the same at each

level and need not be specified twice. This approach has been used for a simple flight control system (ref G-13). That application provides a convenient example, which is discussed in the following paragraphs.

At the system level, the state may be defined in terms of the services being provided. In the example, these are commands to the flight director, the yaw damper, and the autopilot. Interpretation of the requirements leads to defining the system by six states, as listed in Table G-6. After the system is defined, the next task is to list all the events that may cause the system to change to a new state. Only the 17 events in Table G-6 control this aspect of the flight control functions. The events are assumed to occur independently. If combinations can occur, they should be listed as defining a new event. The list, which was arrived at by much discussion, shows one of the advantages of the approach: the specifications are highly visible. The entries in the body of the table show the new state to which the system transitions when the event occurs. The dashes indicate that for the given state, the event cannot occur. For example, if the system is in state 1 with the flight director switch ON, the flight director switch must already be on, so event 1 is not possible. The table describes an abstract machine; it makes no distinctions on how the hardware and software interface. That comes in the next step.

Table G-7 lists the transitions that must be implemented by the software. Some of the events of Table G-6 have been combined with events in this table, and the features of the interfacing hardware have been used. The following terms are used in both tables:

- Flight director flag   Vertical gyro valid AND BIT reports OK

- Yaw damper flag   Flight director flag AND NOT autopilot dump switch AND yaw rate power ON

- Autopilot flag   Yaw damper flag (NOT manual electric trim on OR control wheel steering switch ON) AND trim monitor OK

The software provides the transitions and outputs shown in Table G-7. A verification task is to show that the system correctly performs the events listed in Table G-6.

Table G-6. Abstract System Machine

State	Event:	1 Flight director switch ON	2 Flight director switch OFF	3 Yaw damper switch ON	4 Yaw damper switch OFF	5 Autopilot switch ON	6 Autopilot switch OFF	7 Control wheel steering switch ON	8 Control wheel steering switch OFF	9 Go-around switch ON	10 Manual electric trim ON	11 Autopilot dump ON	12 Not vertical gyro valid	13 Not yaw rate power ON	14 Not trim monitor OK	15 G-dump signal TRUE	16 Not BIT reports OK	17 A mode switch ON when flight director is OFF
0	Flight director OFF / Yaw damper OFF / Autopilot OFF	1	–	2	–	0	–	1	–	1	0	0	0	0	0	0	0	1
1	Flight director ON / Yaw damper OFF / Autopilot OFF	–	0	3	–	1	–	1	–	1	1	1	0	1	1	1	0	–
2	Flight director OFF / Yaw damper ON / Autopilot OFF	3	–	–	0	2	–	3	–	3	2	0	0	0	2	2	0	3
3	Flight director ON / Yaw damper ON / Autopilot OFF	–	2	–	1	(a▷) 1	–	3	–	3	3	1	0	1	3	3	0	–
4	Flight director ON / Yaw damper ON / Autopilot ON	–	4	–	(b▷) 1	–	(b▷) 3	5	–	(b▷) 3	(b▷) 3	(b▷) 1	(b▷) 0	(b▷) 1	(b▷) 3	3	(b▷) 0	–
5	Flight director ON / Yaw damper ON / Control wheel steering ON	–	5	–	(b▷) 1	–	(b▷) 3	–	(a▷) 4	(b▷) 3	5	(b▷) 1	(b▷) 0	(b▷) 1	(b▷) 3	3	(b▷) 0	–

(a▷) Initiates a 2.5-sec fade-on ramp.

(b▷) All transitions shutting off the autopilot flash light and sound horn; the g-dump is directly wired.

Note: Starting: state 0. The control wheel steering switch alters the flight director output in 1, 3, 4, 5.

Table G-7. Software System Machine

	State	Flight director flag FALSE	Flight director button ON AND flight director flag TRUE	Go-around switch ON AND flight director flag TRUE	Control wheel steering switch ON AND flight director flag TRUE	Control wheel steering OFF	A mode switch ON AND flight director flag TRUE (AND NOT FD)	Yaw damper engaged TRUE AND yaw damper flag TRUE	Yaw damper engaged FALSE OR yaw damper flag FALSE	Autopilot engaged TRUE AND autopilot flag TRUE	Autopilot engaged FALSE OR autopilot flag FALSE	Output
												Event
0	Flight director OFF Yaw damper OFF Autopilot OFF	0	1	1	1	0	1	2	–	0	–	Bias flight command indicator bars out of view
1	Flight director ON Yaw damper OFF Autopilot OFF	0	0	1	[d]▷ 1	[d]▷ 1	–	3	–	1	–	Flight director lighted
2	Flight director OFF Yaw damper ON Autopilot OFF	0	3	3	3	2	3	–	0	2	–	Bias flight command indicator bars out of view, yaw damper lighted, yaw damper enabled
3	Flight director ON Yaw damper ON Autopilot OFF	0	2	3	[d]▷ 3	[d]▷ 3	–	–	1	[a]▷ 4	–	Flight director lighted, yaw damper lighted, yaw damper enabled
4	Flight director ON Yaw damper ON Autopilot ON	[c]▷ 0	4	[c]▷ 3	5	–	–	–	[b]▷ 1	–	[c]▷ 3	Flight director, yaw damper, and autopilot lighted; yaw damper, autopilot enabled, engage autopilot (control wheel steering)
5	Flight director ON Yaw damper ON Autopilot ON Control wheel steering ON	[c]▷ 0	5	[c]▷ 3	–	[a]▷ 4	–	–	[b]▷ 1	–	[c]▷ 3	Flight director, yaw damper, and autopilot lighted; yaw damper, autopilot engaged, disengage autopilot (control wheel steering)

[a]▷ Initiates 2.5-sec fade-on ramp

[b]▷ Transition mechanically enforced, flash autopilot four times and sound warning horn

[c]▷ Flash autopilot four times and sound warning horn

[d]▷ Control wheel steering alters flight director output

Because the mode logic for this basic flight control system is done entirely by the software, no corresponding abstract-level machine is necessary. State transition tables are well suited to specifying these functions, which are detailed in Reference G-14. Figure G-13 shows the structure of the control of flow functions. The switch enables control the yaw damper and autopilot switches through holding solenoids. The control laws were specified by traditional control engineers' block diagrams.

The description of specifications by the state transition tables of finite-state machines may be extended to more complicated flight control systems. Those functions in which the flow of control of the software is closely connected with the hardware will require two levels of description.

Specifications may be written in a completely formal language with automatic analysis of syntax, consistency, and completeness. A notable example is the methodology developed by SRI-International (ref G-15). However, it is felt that the ease of review, change, and communication with flight control engineers afforded by the state transition tables more than compensates for the lack of automatic aids.
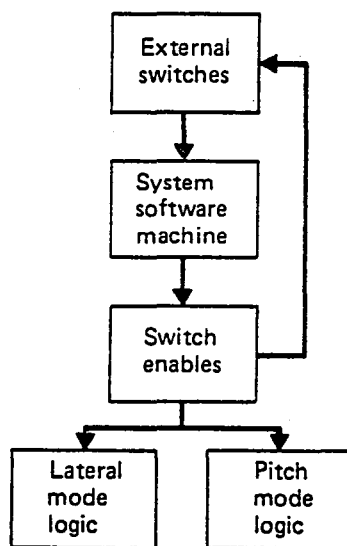
Figure G-13. Software Flow Control

G.2.4.3 SOFTWARE DESIGN AND CODE

Hierarchy-plus-I/O charts adequately express the software design. A partial chart is shown in Table G-8. The consistency of the I/O relations between software modules may be demonstrated by hand or machine analysis. The software is designed in pseudocode without concern to implementation, whether it is in assembly language or a high-order language. The transition tables for the finite-state machines are easily translated into pseudocode.

The coding from the hierarchy-plus-I/O charts is straightforward. If the specifications have been done completely and precisely, the design and coding flow quickly. The specifications, design, and code constitute a package of documentation that is relatively easy to understand and modify because there is close correspondence in structure between the three items.

G.2.4.4 VERIFICATION AND VALIDATION

The approach to verification and validation is to prove that the control of flow is correct and to demonstrate that the calculations called up by the program flow are correct. For verification of the software design or code, this translates into establishing groups of relations:

● The transitions and outputs of the finite-state machines for system control, mode control, signal selection, signal monitoring, redundancy management, and synchronization are correct.

● The computations of the control laws, built-in tests, and in-flight self-tests are correct.

● The data and filter states are correctly initialized, and all state variables are preserved to the next computational cycle.

● The rate executive structure of calling the software modules for computation is correct.

● The data transfers between software modules are correct.

Table G-8. Partial Hierarchy-Plus-Input/Output Chart

	Process system machine	
Input	Process	Output
BIT reports OK, vertical gyro valid	Flight director flag ←vertical gyro valid AND BIT reports OK	Flight director flag

Autopilot state	IF flight director flag = FALSE
	    THEN flight director state ←OFF
	        yaw damper state ← OFF
	        IF autopilot state = ON
	            THEN autopilot state ←OFF
	            autopilot warning ←ON
		Flight director state
		
		Yaw damper state
		
		Autopilot state
		Autopilot warning

Flight director button	IF flight director button = OFF
	    THEN flight director latch ←OFF
	IF flight director latch = OFF AND flight director button = ON AND flight director flag = TRUE
	THEN flight director latch ←ON
	    IF flight director state = OFF THEN flight director state ←ON
	    ELSE
	        IF autopilot state = OFF THEN flight director state ←OFF
		Flight director latch

Go-around switch	IF go-around switch = ON AND flight director flag = TRUE
	    THEN
	        IF flight director state = OFF THEN flight director state ←ON
	        ELSE
	            IF autopilot state = ON THEN autopilot state ← OFF
	            Autopilot warning ←ON	

Control wheel steering switch	IF control wheel steering = ON AND flight director flag = TRUE
	    THEN control wheel steering state ←ON flight director state ←ON
	IF control wheel steering state = ON AND control wheel steering switch = OFF
	    THEN control wheel steering state ←OFF
	        IF autopilot state = ON
	            THEN autopilot fader = ON
		Control wheel steering state
		
		Autopilot fader

For the simple flight control system used as the example, a systematic test procedure is feasible for exhaustively testing each of these five groups. However, the finite-state machine structure may be demonstrated with confidence by analytical means; data initialization and transfers may be shown to be correct by careful tabulations, and the control laws may be demonstrated by frequency response on a simulation. An automated procedure may be set up to check the transitions of all the machines.

The validation of the total system performance may follow much of this outline. The global consistency of the self-testing and redundancy management facilities is more

difficult to demonstrate. It should be possible to model these functions as finite-state machines and perform a systematic analysis for normal operation and for classes of hypothetical hardware failures.

G.2.4.5 CONCLUSIONS

In the preceding paragraphs, it has been stated that flight controls have a regular structure that can be used as the basis for specification, design, coding, verification, and validation. Many variants of a systematic methodology can be shaped about this structure. It will be possible to develop flight control software that is certifiably free of technical software errors and performs according to precisely defined specifications. Determining the system response to all possible hardware failures depends on how well the models of faults determined from failure effects and modes analysis actually represent all the possible failures. However, experience with digital flight control systems is accumulating, and by 1990 we shall have complete confidence in our analysis.

Elaborate software tools and development benches are useful in speeding the development process; they are not essential in providing certifiable flight control software.

This Page Intentionally Left Blank

G.3.0 THREE SYSTEM CONFIGURATIONS FOR 1990

G.3.0 THREE SYSTEM CONFIGURATIONS FOR 1990

G.3.1 INTRODUCTION

Three different system configurations that were developed are characterized as being of low, medium, and high risk. These three alternatives were formulated so that a single alternative could be identified with an awareness of the likelihood of the implementation being advanced in concept and realizable by 1990.

The low-risk system, described in Subsection G.3.2, follows the path of the developments of the 1970s in that redundant computers are run in a macrosynchronized manner. Data are exchanged between the redundant computers via a dedicated serial bus. Bit for bit, all computations are identical between computers as a result of the redundancy management used and the data exchange qualities. Sensor and servo interfaces are predominantly analog. Only minor integrated circuit advances are required for this implementation.

The medium-risk system, covered in Subsection G.3.3, is characterized by the use of multiple microcomputers in each computing channel, the extensive use of busing for both sensor and actuator interfaces, and asynchronous operation between computing channels. An increased number of success paths for greater flight safety and dispatch reliability and a reduction in software preparation costs are expected in this system.

Section G.3.4 reviews the fault-tolerant multiple processor (FTMP) and software-implemented fault-tolerance (SIFT) architectures. The high-risk system has certain similarities to these architectures. Busing is well advanced when compared to the medium-risk system.

G.3.2 LOW-RISK SYSTEM FOR 1990

G.3.2.1 SYSTEM ARCHITECTURE

The low-risk system is based on principles of digital fly-by-wire (FBW) control developed over the last 10 years. The extrapolation to the 1990 time frame includes a projection of only moderate technology growth in large-scale integrated circuits.

The system is an integrated one in the sense that the crucial FBW and short-period pitch-augmentation functions are accomplished by the same computer set as the critical augmentation functions. Sensors and servos are used for various functions, as required by the control laws.

Pitch axis FBW control is implemented because the aircraft could not be flown with mechanical primary flight controls alone. Short-period pitch-augmented stability (PAS) is required for safe flight. Minor additions to the crucial PAS are required to achieve the FBW-PAS combination. In this instance, improvements in cost, weight, reliability, and maintainability are a result of FBW control.

The hydromechanical primary flight control system is the same as it was in the Baseline Configuration for the roll and yaw axes. Although FBW control also may be advantageous in these axes, safe flight does not require stability augmentation as is the case in pitch augmentation.

Figure G-14 shows the low-risk Active Controls Technology (ACT) system architecture. Quadruple ACT computers develop servocommands based on quadruple or triple sensor inputs. The computers also interface with the ACT display and control panel, the caution and warning system, and the caution and warning discrete display.

The interfaces between the ACT and the digital air data computer (DADC) and the inertial reference system (IRS) are Aeronautical Radio Incorporated (ARINC) 429 type serial buses. ARINC 429 buses also are used to interface with each of the ACT display and control panels, the caution and warning system, and the caution and warning discrete display.

The ACT interfaces with the other sensors are analog. These sensors are powered by the ACT computer. Signals from the sensors are returned to the computer for signal conditioning via dedicated aircraft wiring.

The servo-loop electronics are contained within the ACT computer in each case. The servoamplifier output is fed to each servovalve, and feedback sensor signals are returned to the computer. The servoengage solenoids are powered from the computer.
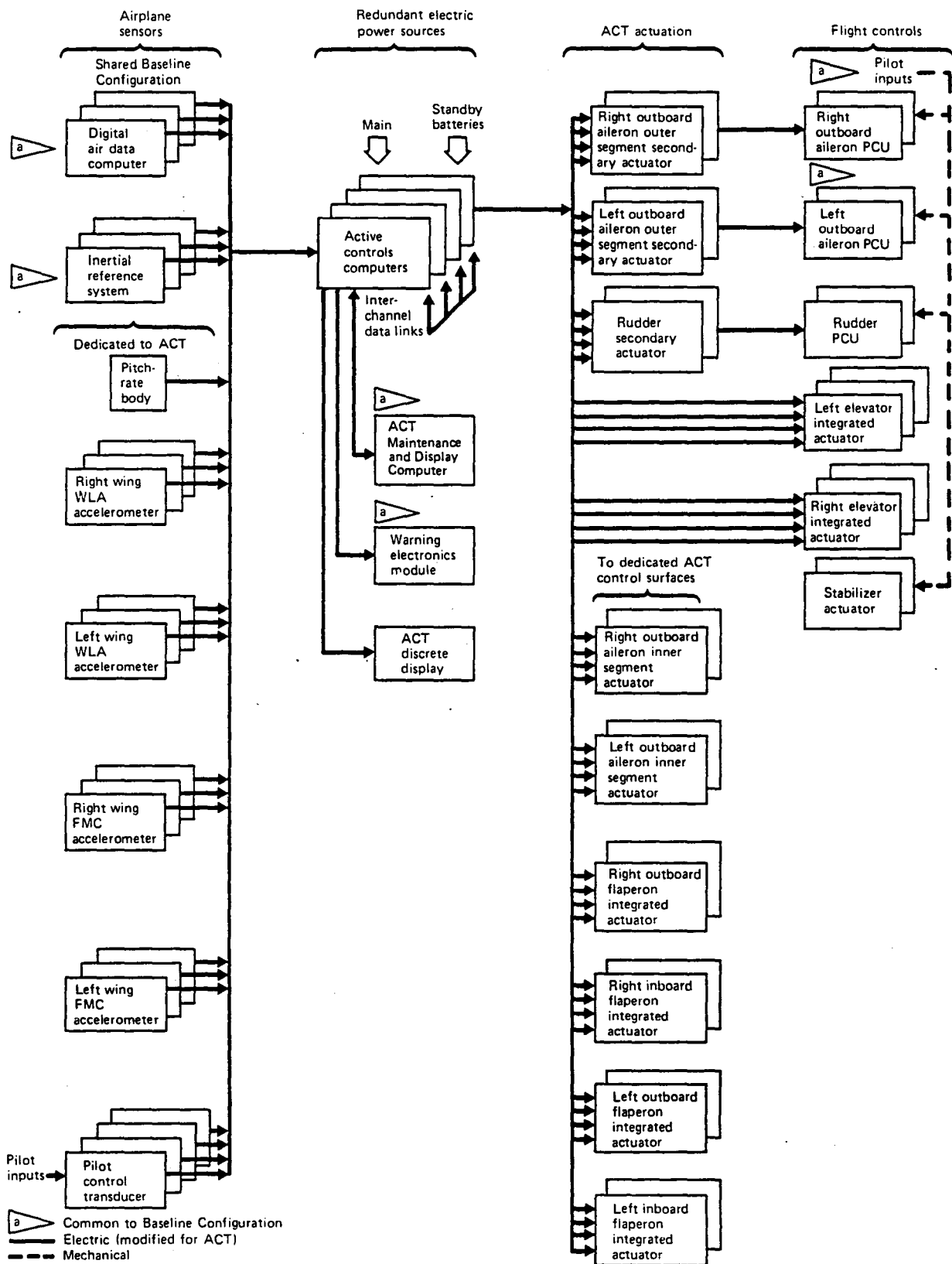
Figure G-14. Low-Risk ACT Architecture

The computers are frame synchronized (i.e., each minor cycle of computation is initiated at the same time by all operable computers as a result of the halt-release implementation used), thus eliminating time skew in the sensor input and servo output data. Sensor data are exchanged and monitored, and signals are selected for each parameter so that control law computations are identical in each control channel. Fault detection is enhanced, and the requirement for channel equalization is avoided.

G.3.2.2 REDUNDANCY MANAGEMENT

As shown in Figure G-15, four channels of computing interface with four channels of crucial sensors to provide two fail-operational controls for the crucial FBW and short-period PAS systems. A combination of comparison monitoring and built-in testing is used for fault detection and correction.
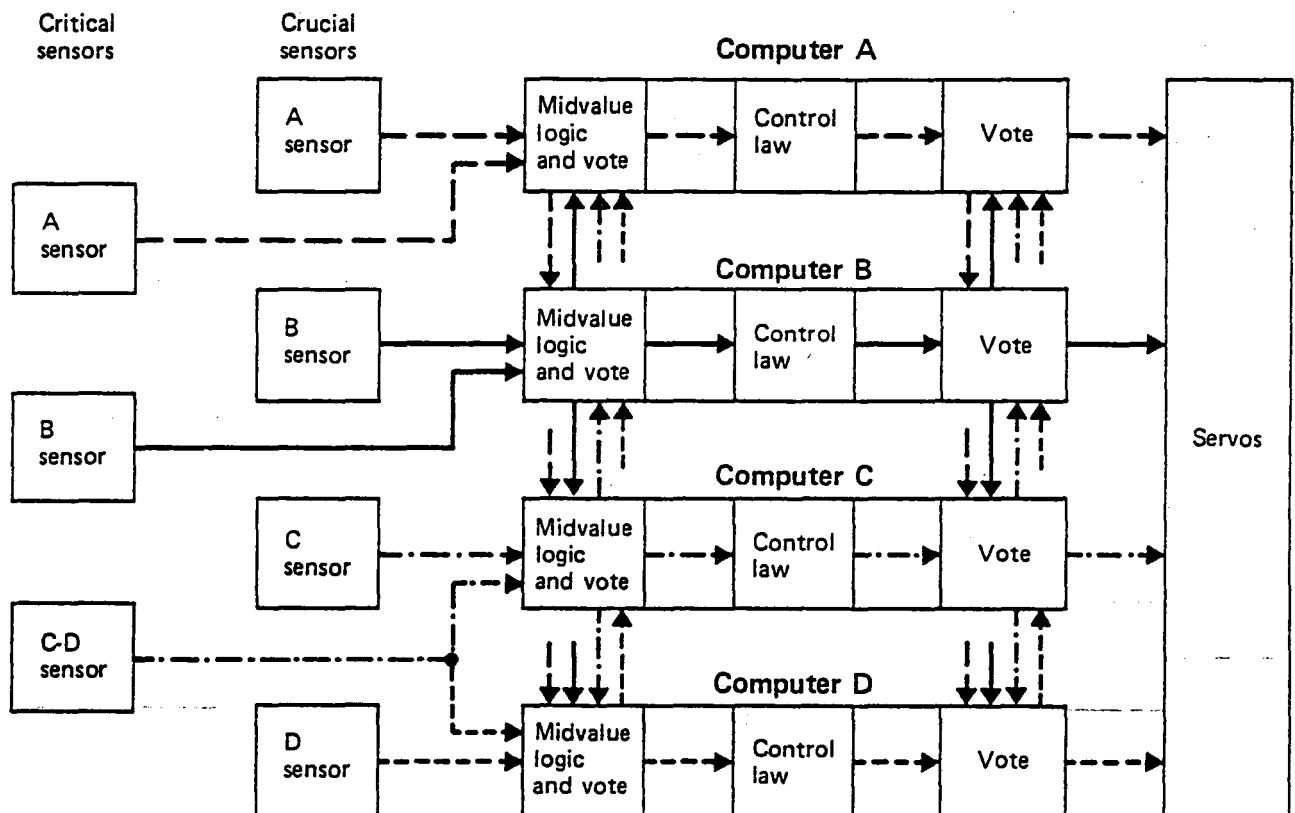
Figure G-15. Sensor, Computer, and Servo Interfaces

Each computer includes both analog and digital electronics as required for power supplies, input/output (I/O), sensor processing, digital computing, and sufficient analog electronics for reversion to an analog mode under certain failure states. Data exchange between channels is via a serial link, which greatly simplifies aircraft wiring and related redundancy management.

Sensors associated with critical functions are triplicated and fed to the four computer channels in the manner shown in Figure G-15.

G.3.2.2.1 Computers

With no failures, each computer comparison monitors all sensor inputs, using the median of the A, B, C, and D sensors for subsequent control computations. Each computer, therefore, uses identical input data. Because the computers are synchronized, the output command servo signals are identical, permitting bit-by-bit comparison monitoring of the outputs. This output monitoring is the primary failure detection and isolation means for first computer failures. Because normal servocommand signals are identical, redundant servo tracking errors are only due to tolerances or failures in the servo loops themselves. With the precise monitoring implicit in comparing identical outputs, failure detection for the computers is thorough. Furthermore, any divergence tendencies of redundant control law integrations are avoided with the macrosynchronized computers.

A second computer fault can be isolated by comparison monitoring techniques. Three computers were operating prior to the failure.

A third computer failure results in a miscompare that can be isolated only by inline self-test routines. The critical flight control functions are disengaged, and this failure state is indicated on the fault annunciator panels. To isolate third computer failures so that crucial control functions are maintained, inline self-test routines are continually run by each computer. The tests verify power-supply voltages, processor memory function, and I/O execution. If a self-test is not successful, a watchdog timer for the faulty unit will not be reset to initiate the next computation cycle because this disables the computer and disrupts a validity signal to the other computer.

G.3.2.2.2 Sensors

If a first quadruple sensor fails in A, B, C, or D, the failed unit will be detected by majority vote and disabled by its associated computer. Following the first failure of a triplex sensor set, or the second quadruple sensor failure, further control computations will use an average of the two remaining sensors.

A subsequent sensor failure of a given type is detected by comparison monitoring. Upon detection of a failure of one of two sensors by comparison monitoring, the action taken will vary with sensor type.

The control position transducers are linear variable differential transformers (LVDT) that have center-tapped secondary signals available as outputs; the center tap is grounded. The desired displacement signal is the difference between voltages appearing at the other two output leads. The sum of these voltages is roughly a constant, independent of transducer input position for a properly operating device. Upon loss of excitation or any transducer failure, the summation voltage will significantly change, usually falling to zero. By monitoring this voltage, second control position transducer faults can be readily isolated to the failed transducer.

Four pitch-rate signals are provided. Three are taken from the triple IRS; the fourth is from a separate sensor. The pitch-rate signals, whether from the IRS or from the fourth separate rate gyro, can be monitored by certain techniques, but only 70% of the failures can be isolated. Certain analytical redundancy techniques are available from either of two sources to improve the capability to select a good pitch-rate signal. The two techniques, however, do not compare. Other sensors are not crucial, so no attempt is made to isolate a failure between two that miscompare. The function associated with those sensors is disabled.

G.3.2.2.3 Servoactuators

Each computer provides servo-loop closure electronics for specific servoactuators. The servos are also monitored by the computers that drive them.

The nature of the servo interface depends on the servoactuator selected. Alternative actuation concepts are discussed in Subsection G.4.2, independent of the system architecture.

G.3.2.2.4 Analog Reversion Mode Description

The analog reversion (AR) mode is block diagrammed in Figure G-16. With AR, aircraft can still be landed safely after a series of digital computing failures.

The AR mode is engaged in one of two ways. If the FBW system reaches a failure state where no digital success paths remain, the logic will automatically engage the AR mode. In addition, an AR engage switch enables the pilot to command engagement of the AR mode any time.

With the AR mode, the simplest relationship exists between sensors and surface motions that will allow safe flight. Level 3 handling qualities of MIL-F-8785 are deemed adequate. The sensors are those required for the pitch axis FBW and crucial PAS control systems. The same elevator servoactuators are driven.

If the pitch axis requires forward-loop integration for satisfactory control, these integrators must be equalized to prevent a divergence of the computing channels. The midvalue logic circuit, as well as the limited error feedback signal, equalizes the integrators. Prior to engagement of the AR mode, the integrators synchronize the computing circuit outputs, resulting in transient-free engagement of the pitch axis of the AR mode.

All four channels of the AR mode are engaged at once. The only monitoring and fault correction logic provided is that inherent in the servoactuators. This imposes an added constraint on the servoactuator concept to be chosen.

G.3.2.3 ACT COMPUTER

Figure G-17 is a functional block diagram of the ACT computer, including preliminary functional partitioning to the card level.
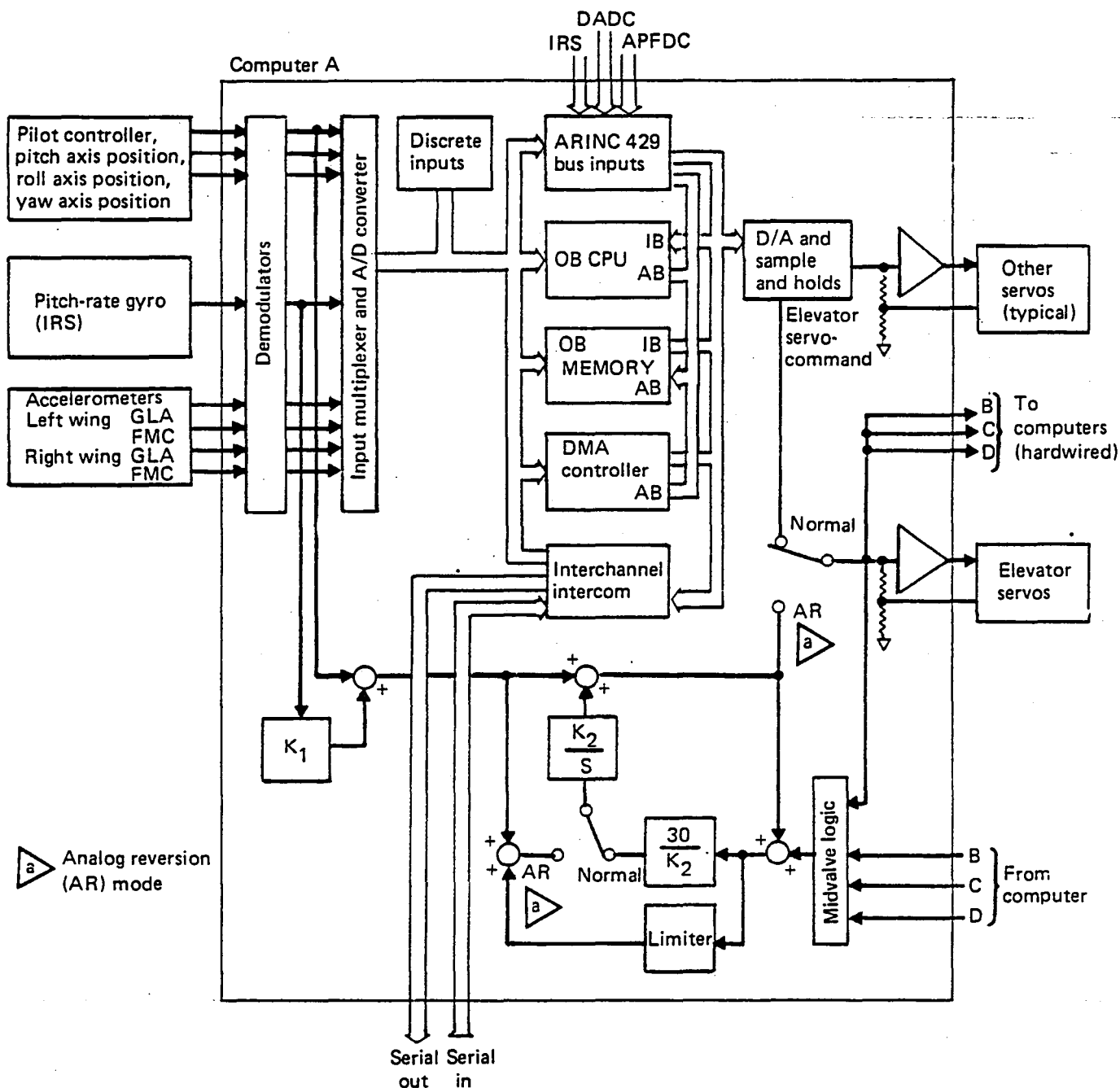
Figure G-16. Low-Risk Approach Functional Block Diagram (Showing Analog Reversion Mode)
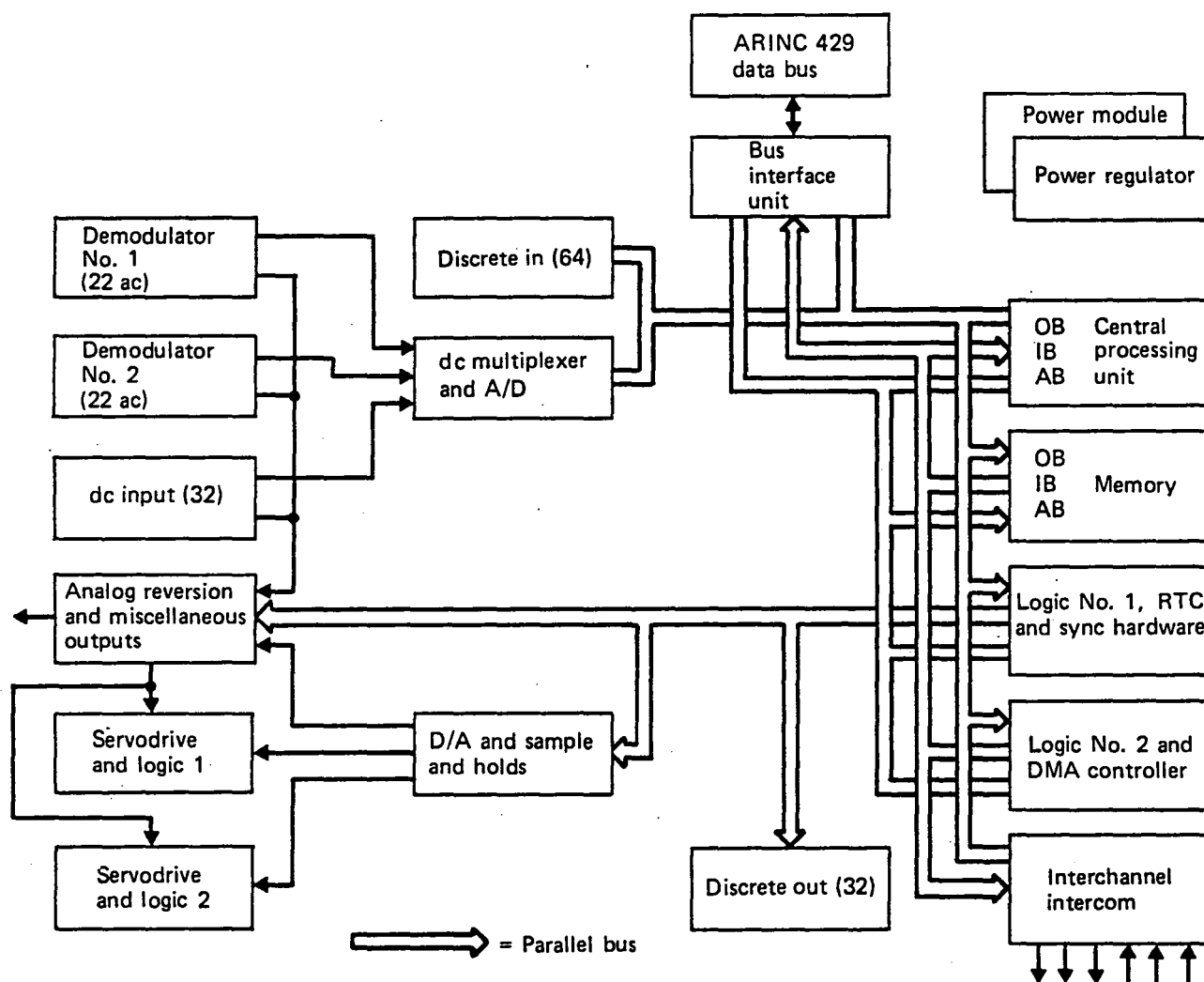
Figure G-17. ACT Computer Block Diagram

G.3.2.3.1 Digital Processing Function

The digital processing function of the ACT computer is accomplished by the central processing unit (CPU), memory, and logic 1 and logic 2 subassemblies. The memory subassembly provides 32K words of 16 bits-per-word (bpw) fast-access memory. There are 28K words that are erasable, programmable, read-only memory (ROM), and 4K words that are random-access memory (RAM). The memory address logic is designed so that a second memory subassembly could be added to expand the memory to 64K words.

The logic 1 and 2 subassemblies provide the logic and timing circuitry for:

- Memory parity generation and checking
- Priority interrupts with automatic vectoring
- Real-time counter
- Synchronization hardware
- Direct memory access (DMA) priority logic
- DMA controller

G.3.2.3.2 Input/Output

The entire I/O function of the ACT computer is under DMA control. All I/O addressing and logic control functions are accomplished via a programmable DMA controller.

The DMA controller determines what information is desired by decoding a command from the CPU and generates all timing and control signals needed to manipulate data to or from memory to outside the system. All the system analog inputs and outputs, discrete inputs and outputs, intercom inputs and outputs, and other data of a packed-word format are taken from or stored into the channel memory under DMA by the processor-controlled DMA controller.

The DMA controller is semi-free-running. The CPU software determines when it needs data brought into memory for the computations that follow. The processor command to the I/O controller points to the memory location where the first datum is to be stored, and the processor indicates how many consecutive words of information should be acted upon. The processor can request that from 1 to 128 consecutive locations be accessed. Whether they are inputs or outputs is defined within the controller. Upon receiving the command, the DMA controller starts and continues on to completion of the block of I/O operations desired. When this is complete, it waits for a new command.

G.3.2.3.3 Intercom

Digital data among the four ACT computers are exchanged via DMA control by the interchannel intercom subassembly. This is a serial interface whereby each transmitter provides a data line and a clock line to each of the other three computers. The data shift

rate is 1 MHz, and all lines are differentially driven, twisted pairs. The data words are time-slot identified and consist of 16 bits plus parity. In addition to using cooperative, fixed data exchange between computers for self-test, the intercom interface permits an internal wraparound test for fault isolation.

G.3.2.3.4 Discrete Outputs

The discrete output subassembly provides the capability for up to thirty-two 28V outputs. The outputs are addressed as four 8-bit words. Critical discrete outputs will be monitored by wraparound to the discrete input subassembly.

G.3.2.3.5 Discrete Inputs

The discrete input subassembly accepts 64 discretes. They are accessed as 8-bit words and are used for three different functions: wraparound, internal, and external discretes. The wraparounds enable testing of discrete outputs, and the internal discretes provide status and test results required for various self-test functions. All accept inputs. Self-test stimulation of all the discrete inputs to either logical one or logical zero is possible regardless of the state of the actual input discretes.

G.3.2.3.6 Analog Outputs

The digital-to-analog (D/A) and sample-and-hold (S/H) subassembly contains a 12-bit (11 bits plus sign) D/A converter that provides a $\pm 10V$ dc range output signal for multiplexing to the S/H outputs. Up to 24 outputs can be accommodated.

The current mode drivers for the servoactuator electrohydraulic valves and the required failure and analog reversion mode switching for the servoactuators are contained on the two servodrive and logic subassemblies.

The AR and miscellaneous output subassembly contains the dedicated analog signal circuitry necessary to generate the servo position commands for the AR mode.

G.3.2.3.7 Analog Inputs

The analog input conversion is implemented by the demodulator, dc input and dc multiplexer, and analog-to-digital (A/D) converter subassemblies.

Each demodulator subassembly has 22 synchronous demodulators that are multiplexed to the dc multiplexer and A/D subassembly.

The dc input subassembly provides for buffering, scaling, and analog switching of 32 differential dc input signals to the dc multiplexer and A/D subassembly.

The dc multiplexer and A/D subassembly enables switching of 96 dc inputs to the A/D converter.

G.3.2.4 RELIABILITY ASSESSMENT

The preliminary failure probability assessment for the low-risk system considered only the aircraft flight safety as affected by the crucial sensors and computers. Servo failure probabilities were neglected.

Table G-9 shows the failure probabilities used in the assessment. Results of the assessment showed that the probability of failure in a 1-hr flight for crucial ACT functions was:

- With four channels operative, 3.8×10^{-12}
- Dispatch with three channels operative, 1.29×10^{-8}

Table G-9. Failure Probabilities—1990

Element	Failure rate (per million hr)	Symbol	Self-test confidence
Laser gyro	30	λ LG	0.68
Flight control gyro	30	λ FCG	0.68
Column sensor	3	λ P	1.00
Computer	150	λ C	0.95

Servo failure rates were not included.

These results indicate that the low-risk ACT is a viable system; however, airplane dispatch with only three channels operative would not be permitted.

G.3.3 MEDIUM-RISK SYSTEM

An IAAC medium-risk flight control system can be constructed using projections for component and software technologies that have a reasonable probability of being available by 1990. A diagram of the medium-risk system is shown in Figure G-18. The features of this system are summarized in the following subsections.

G.3.3.1 SENSORS

The medium-risk sensor concepts are based on a combination of existing hardware and advanced software techniques used to minimize cost of ownership.

Triple outputs from the IRS laser gyros will be used for the primary source of pitch rate (q) and the entire source of yaw rate (r). Roll attitude (ϕ) is also taken from the IRS output in triplicate. Taking the outputs directly from the sensor instead of from the IRS output terminals increases the reliability of the q and r sources; i.e., 20 000-hr mean time between failures (MTBF) as opposed to 2400 hr. The crucial flight control system specification requires either more sources for pitch rate or some alternate way of achieving stable pitch control. Both solutions are achieved in effect with a software Luenberger observer, which uses normal acceleration to derive pitch rate when the IRS laser gyros have failed.

Three-axis FBW implementation is used with quadruply redundant pitch and roll command LVDT transducers on the pilot yoke and pedal quadruple LVDTs for yaw inputs.

G.3.3.2 COMPUTER AND SYSTEM ARCHITECTURE

The medium-risk system architecture is based on emerging technologies in microprocessors, data bus and bus control logic capabilities, and advanced failure management techniques.
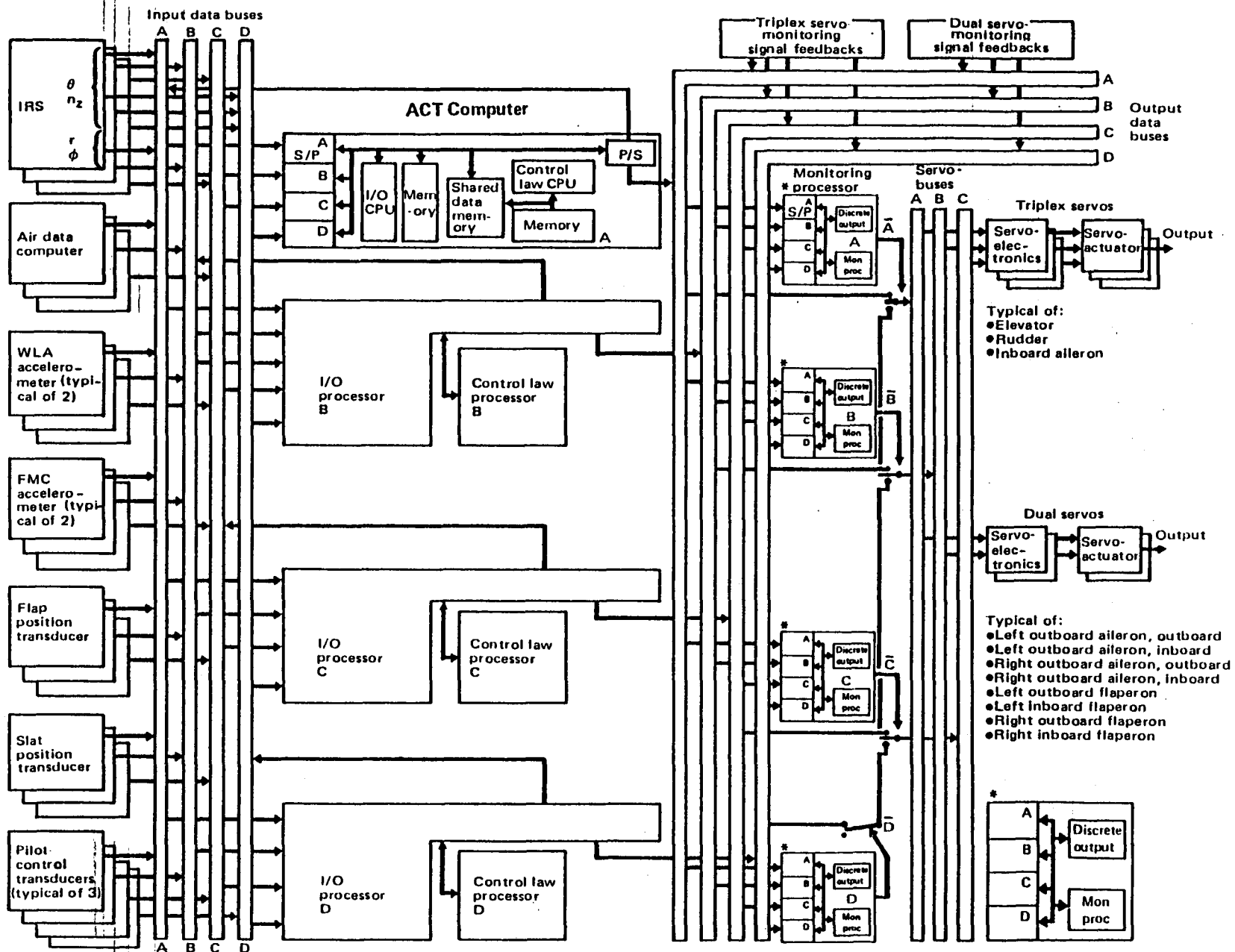
Figure G-18. IAAC 1990 Medium-Risk System

G.3.3.2.1 Input Data Bus

Input data buses route the sensor inputs to the four I/O processors. Three of the four are identical in that they carry one channel of the triple sensor data and one channel of the quadruple sensor data. The fourth data bus contains the fourth channel sensor data plus an extra copy of all crucial IRS sensor data; i.e., all three pitch-rate and normal acceleration outputs. The key issue for this type of busing is throughput versus available bandwidth. A rough calculation for each of the A, B, or C buses is:

- The 15 sensors, plus 6 discretes, plus 4 spares = 25 signals
- Each slot contains 12 bits of data plus 13 bits of address and protocol = 25 bits
- Data rate = 512 Hz

Therefore

throughput = 25 x 25 x 512 = 320K bits per second (bps)

This is very conservative for projected bandwidths of 1M bps for standard bus hardware and 10M bps for fiber optics. The 512-Hz rate purposely is set high to allow asynchronous operations for all channels.

G.3.3.2.2 I/O Processors

Quadruple I/O processors perform basic failure management on the four-channel sensor data coming in. Assuming that all channels are identically loaded (the D channel has a lower load), the sensor processor must accept 25 signals at 512 Hz from each of four channels or 51 200 words per second (wps). Using a 4-sec time to buffer into the processor to memory, the loading operation takes about 20.4% of the available time.

The I/O processor performs midvalue selection followed by comparison monitoring on all triple and quadruple sensors. The loading for this is approximately 200K operations per second (ops), which is considered quite feasible by 1990. This estimate allows for the pitch-rate observer discussed in Section G.6.0.

G.3.3.2.3 Sensor Electronics

An A/D conversion is performed on each sensor's output by sensor electronics circuitry packaged with the sensor output to be transmitted in serial digital form. The sensor data are output to the input data buses upon command from the bus controller.

The I/O processor also transmits all the control commands to the output data buses and performs control command equalization. These commands are received from the control law processors via a DMA. For extra failure tolerance, the crucial control functions; i.e., PAS and stick commands, are processed in the I/O processors.

G.3.3.2.4 Control Law Processor

All control commands are calculated in the control law processors (CLP). The sensor information is transmitted to the CLP via the shared memory. Using the Initial ACT Configuration loading figures, the CLP operates at approximately 260K ops.

G.3.3.2.5 Output Data Buses

Quadruple output buses transmit all the control commands to the servo inputs, and all servo information used in servo failure management is transmitted to the output monitor processor by way of these buses. The throughput for this (assuming 256-Hz data transmission) is estimated at 440K bps.

G.3.3.2.6 Output Monitor Processors

The output monitor processor performs downstream checks on control command validity coming from the I/O processors and failure management for the servos. The unique feature of this processor is that it is not in the control loop; therefore, a time delay is eliminated. Its function is failure management exclusively. The output monitor processor:

● Switches bus routes to the servos
● Monitors servos
● Shuts down servos
● Shuts down upstream computers

The loading is estimated at 160K ops.

G.3.3.3 FAILURE MANAGEMENT FOR THE MEDIUM-RISK SYSTEM

Figure G-19 shows a simplified failure management diagram. Because the diagram emphasizes the crucial functions, quadruply redundant sensors (as exemplified by the pilot control position transducers) are shown. Triplex servos, as used for elevator control, also are shown.

Each sensor output is assigned to one of the four "input data buses." Data from all four input data buses are fed to each ACT computer. Periodically, the corresponding sensor signals are compared to one another and the midvalue of the signals is determined. The comparison monitoring detects a sensor failure. Once a sensor has been determined to have failed, the signal selection and monitoring proceeds, using the remaining operative sensors.
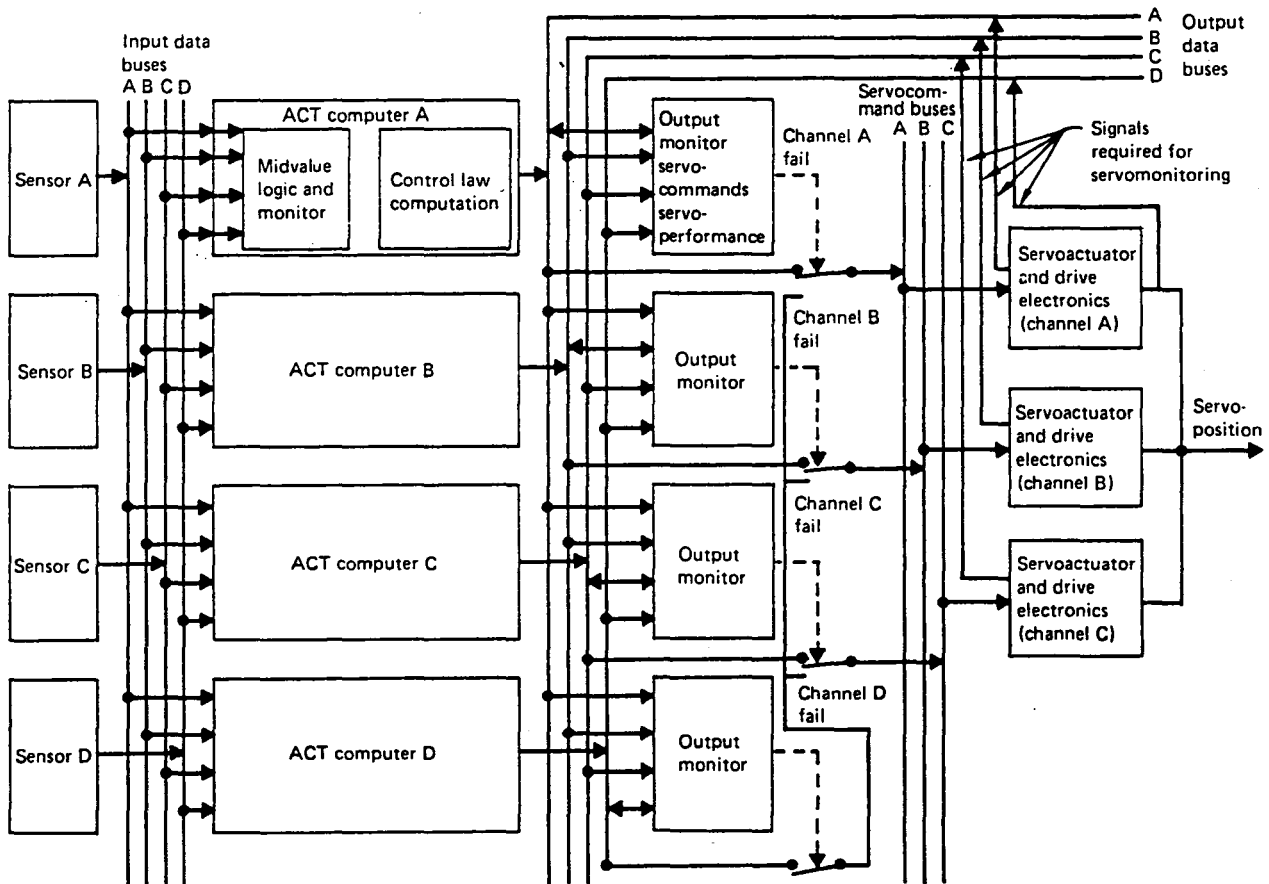
Figure G-19. Simplified Failure Management Diagram

The midvalue of each set of sensor signals is then used in the control law computation. The servoactuator position commands so determined are output on the output data buses. Each of the four ACT computers outputs its servocommands on one of the four output data buses.

The output monitor processor has access to the servocommands transmitted by all four of the ACT computers on the output data buses. The output monitor processor compares the corresponding commands and determines any failure that may have occurred in the ACT computer or output buses. It will correct for first failures of the servocommands by bus switching between the output data buses and servocommand buses, as indicated in Figure G-19. Subsequent failures are corrected by disabling servoactuator channels.

The monitor processor also monitors each servoactuator channel. Signals necessary to allow such monitoring are fed back from the servos via the output data buses. A servoactuator channel is disabled by a monitor processor by means of a communication via the output data and servocommand buses.

Triplex sensor signals for the critical functions are handled in the same manner as the quadruple signals except that no signal appears on the D input data bus. All action is the same as the quadruple sensor case after the D sensor has failed.

The exception to this is the treatment of the IRS pitch-rate and normal acceleration signals. Here, each of these signals is applied to the D input data bus as well as to one of the A, B, or C buses. Upon experiencing a second pitch-rate signal failure, an estimated pitch-rate signal derived primarily from the normal acceleration feedback is used for continued control. The manner of accomplishing this advanced form of failure tolerance is described in Section G.6.0.

G.3.3.4 RELIABILITY ASSESSMENT

Table G-10 shows the failure rates used in the preliminary reliability assessment for the medium-risk system. Table G-11 shows the results of the assessment.

It is concluded that the reliability is comfortably in excess of that required for the crucial functions. Dispatch with certain failed elements could be safely allowed.

Table G-10. Component Failure Rates

Element	Failure probability for 1 flight hour (x 10^{-6})		Comments	Self-test coverage percent (1990)
	1980	1990		
Pitch-rate gyro	30	20	Laser gyro	68 (95)
Accelerometers, N_z	25	20		–
Position transducer	7	5	LVDT type	100
Servocurrent sensors	1	1	Resistor network	–
Sensor output chip	–	5	Including output processing protocol	–
One bus and serial/parallel	20	7		–
Sensor processor	150	50	I/O CPU memory	95 (99)
C-L processor	150	50	I/O CPU memory	95 (99)
Monitor process and logic	170	55	I/O CPU memory	95
Critical sensors	35	25		(100)*

* Assuming paired accelerometers

Table G-11. Medium-Risk System Reliability Analysis
(Crucial Functions Only)

Equipment	Failure probability for 1 flight hour	
	Fault free	1 faulty element (dispatch)
Sensors • Column LVDT (including bus interface)	< 10^{-13}	4.3 x 10^{-10} (95% LVDT self-test)
• g (including bus interface)	< 10^{-14}	4.3 x 10^{-10}
Computer • I/O processors (processor and bus)	< 10^{-12}	4.0 x 10^{-10} (95% self-test)

G.3.4 HIGH-RISK SYSTEM

Central to the problem of suggesting an advanced architecture for an ultrareliable flight control system in 1990 is the prediction of what microelectronic circuitry will be available at that time. The prototypes of two current research systems for flight controls, FTMP (refs G-16 and G-17) and SIFT (ref G-18), are implemented in state-of-the-art hardware. While advances in electronic technology will help reduce cost and improve characteristics, these systems are not directed at incorporating trends in circuits in any fundamental way. FTMP uses massive hardware redundancy. The design isolates functions to facilitate fault containment and functional replacement; it will be difficult to use the trend to integration. The SIFT design is relatively independent of the hardware. It relies on software to manage redundant facilities and is a general-purpose computing system. The approach taken by Jet Propulsion Laboratory (JPL) (ref G-19) is to outline an architecture that anticipates advances in electronics. They plan to be in a position to use the new circuits in a fundamental manner as they become available, without making a completely new departure in system architecture for each innovation. While a difficult task, this is more in line with the purpose of studying a high-risk architecture. We will modify the JPL approach, which is directed at very-long-life space probes, to fit ultrareliable flight controls.

G.3.4.1 FAULT-TOLERANT MULTIPLE PROCESSOR AND SOFTWARE-IMPLEMENTED FAULT TOLERANCE

The FTMP configuration is shown in Figure G-20. Two internal buses are diagrammed, but the clock bus for producing and distributing the totally synchronized clock signal is not shown. All elements are synchronized by a massively redundant clock structure. Thus, there are six separate buses: memory access, clock, interprocessor-1, interprocessor-2, input, and output.

The last four buses are grouped in the diagram as the interface access bus. The buses are protected from faulty elements by the bus guardians. These dual-redundant units also enforce the configuration of memory and processor triads and select which of the multiple bus wires are to be used to constitute the respective buses. The intelligence for these allocations is by software. The processors and memory modules are dynamically assigned to triads so that all calculations and transactions are in groups of three. This allows each
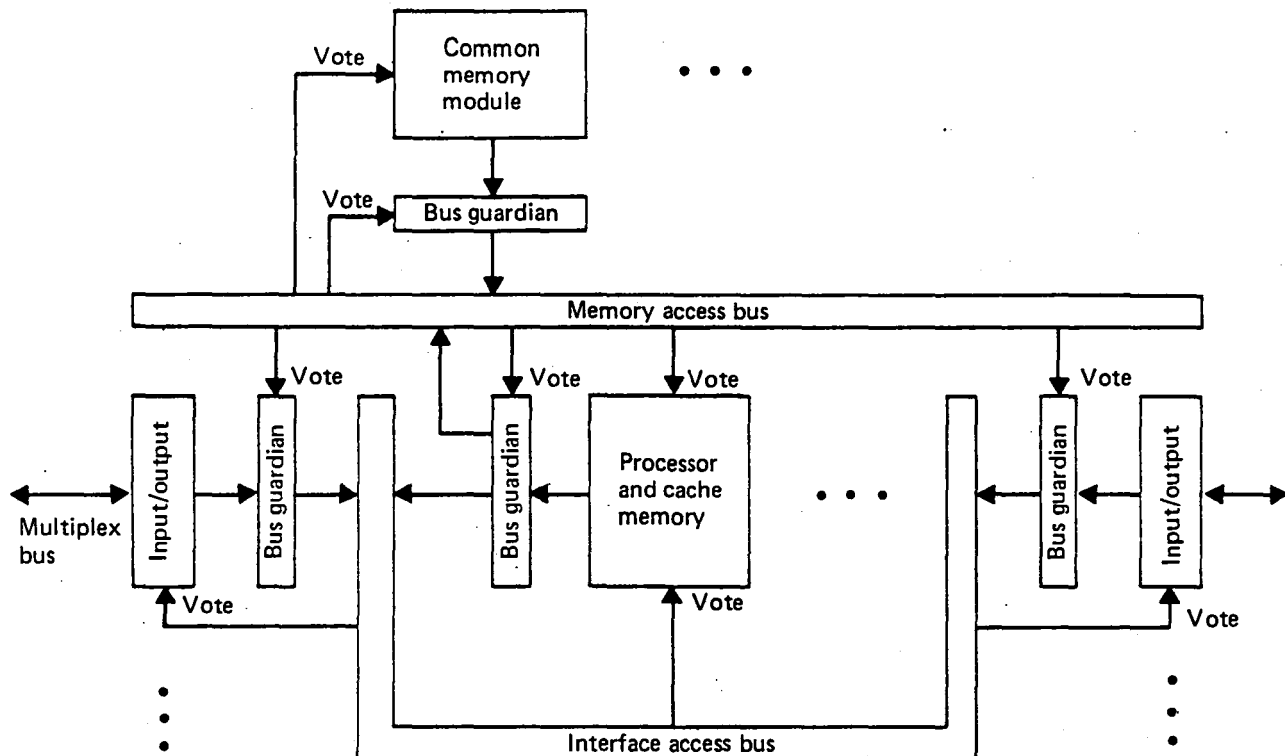
Figure G-20. Fault-Tolerant Multiple Processor Configuration

bus transmission to be voted upon at the receiving element. The triads are reconfigured upon detecting a failed element. This is the major level of redundancy management; there are sublevels of bus error correction, clock element replacement, and bus wire assignment. Inline tests are used to detect latent failures in standby elements.

The SIFT configuration (fig. G-21) determines bus or processor failures. Redundancy is managed by the software executives. No hardware mechanisms are used other than those embedded in the standard hardware. A few inline tests are used to differentiate between causes of failure in several ambiguous cases not handled by the primary diagnostic algorithm.

G.3.4.2 MICROELECTRONICS TRENDS

The following paragraphs review the points that help justify the choice of a high-risk architecture. As in any prediction, these points are subjective. Reference G-11 is an example of one of many trend surveys.
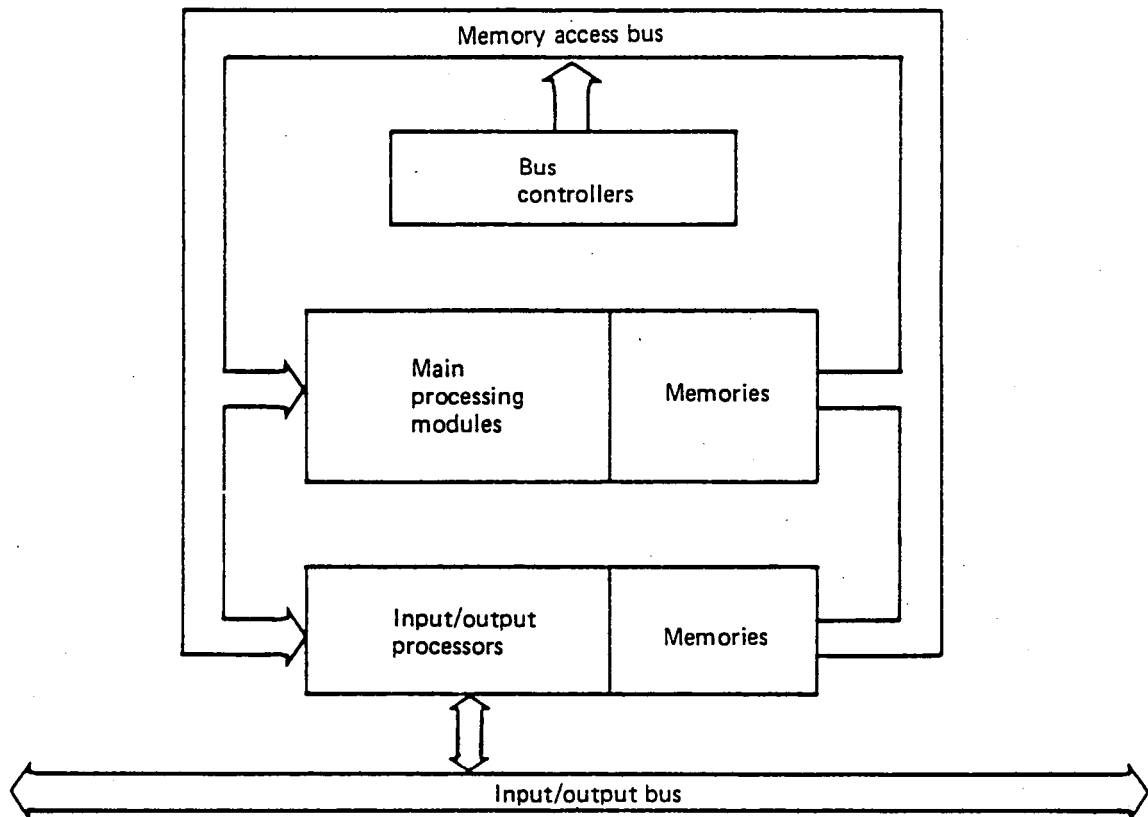
Figure G-21. Software-Implemented Fault Tolerance Configuration

a. Most faults are in off-chip connections—the reliability of on-chip circuits is excellent. With wide application of the chip, very-large-scale integration (VLSI) results in reliable and economical circuits. A flight control architecture must use a small number of universal VLSI circuits to reduce the number of interconnections.

b. Testing problems grow exponentially with the number of gates in a circuit. In addition to circuit complexity, other aspects must be considered to establish the importance of testing on circuit design and applications. There are two major dimensions to testing: (1) the level of component assembly (circuit, macrocell, chip, board, and system) and (2) the place of the tests in the life cycle (design verification, chip manufacture, board assembly, system assembly, and field use).

The field-use period has several divisions:

- Preoperational checkout
- Normal operations
- Fault isolation to the line replaceable unit (LRU)
- Maintenance testing to locate faults for repair of the LRU

During normal operation, there are self-tests to find current and latent faults, comparisons of redundant facilities, and error-correcting mechanisms in circuits and codes. Rather than adding ad hoc provisions for each of these items, a more structured approach will be necessary to control the cost of testing for large chips and complicated systems. For some chips, the cost of testing is already more than the cost of manufacturing.

More attention will be placed on designing circuits so that they can be economically and easily tested. Because circuitry is inexpensive, overhead costs for testing are now lower. The ultimate level of self-test is shown in Figure G-22. Actual functions are duplicated but are in complementary logic to avoid material or pattern-sensitive faults. Inputs and outputs are carried by redundant error-detecting and correcting code. Smaller, totally self-checking circuits are possible. Even at more than 100% overhead in circuitry, number-of-gates growth is linear, while testing is exponential.

In addition to making VLSI circuits fault tolerant, testing and self-checking provisions will be included in the circuits in 1990. Our architecture should take advantage of this; the FTMP and SIFT designs do not directly look to these techniques for their fault handling.

c. In the past, computer processing throughput was limited, which required computers to be synchronized if any comparison of outputs, even by analog, was to be made. With higher speeds, synchronization is needed only for precise cross-channel comparison. Hence, unsynchronized channels with final comparisons performed as in the medium-risk system may be considered, or an attempt may be made to uncouple
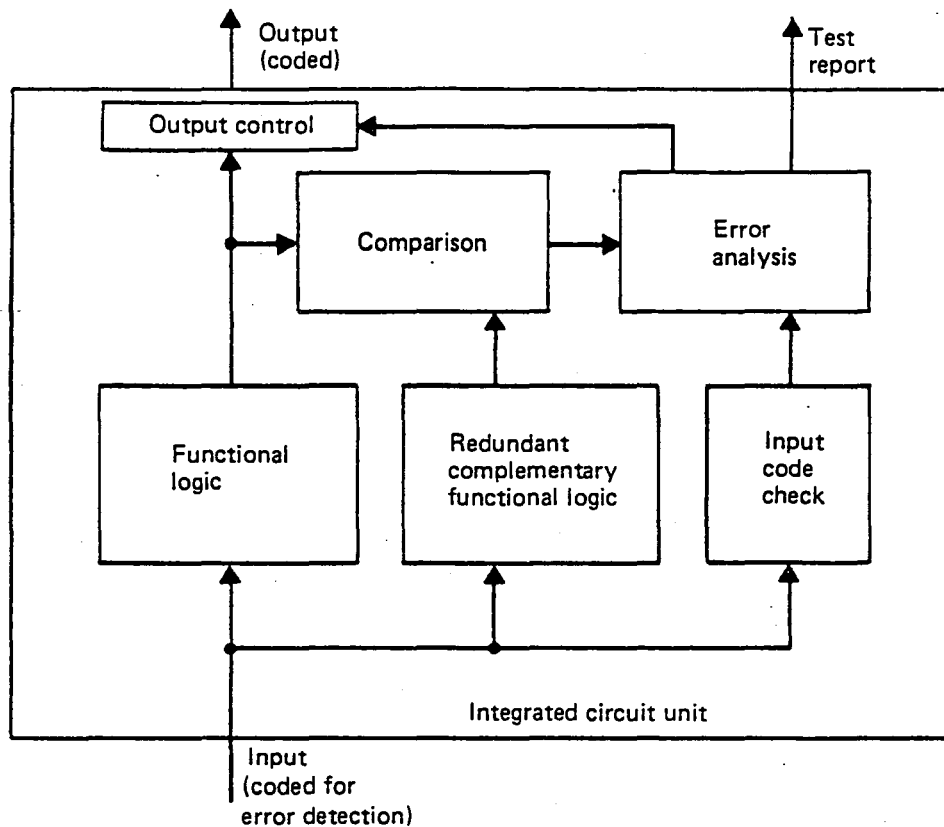
Figure G-22. Self-Testing Configuration

each channel with force-summing actuators receiving the final outputs. This would require that the computing hardware be capable of 100% detection of critical faults. Such hardware may be available by 1990.

d. SIFT reconfigures buses and processors, and FTMP goes further in its redundancy management. By 1990, the more reliable hardware should provide at least the level of confidence of SIFT by fault isolation to the channel. This will avoid complicated monitoring and difficulty in validating the system. Fault isolation could be done by cross-channel voting but would not be needed if the hardware is 100% self-checking.

G.3.4.3 HIGH-RISK ARCHITECTURE

If the foregoing premises apply, the self-checking computer module shown in Figure G-23 can be considered. This is modeled after the JPL approach (ref G-20). All circuits except the processors and the memory are assumed to be totally self-checking. The processors

are tightly synchronized and run the same programs in step to check each other. Processors are inexpensive, and any standard processor may be used. Without the complicated redundancy management and software self-tests, there is adequate throughput for the ACT control functions and signal select and sensor monitoring. The processors will include the memories by 1990. The memory shown in Figure G-23 is coded for error detection and correction. A tristate internal bus carries internal communications. (Tristate refers to the three levels of impedance that each device presents to the bus depending on whether the signal is a 1, a 0, or whether the device is inactive.) There are no provisions for the processors of one module to exchange data with any other module.
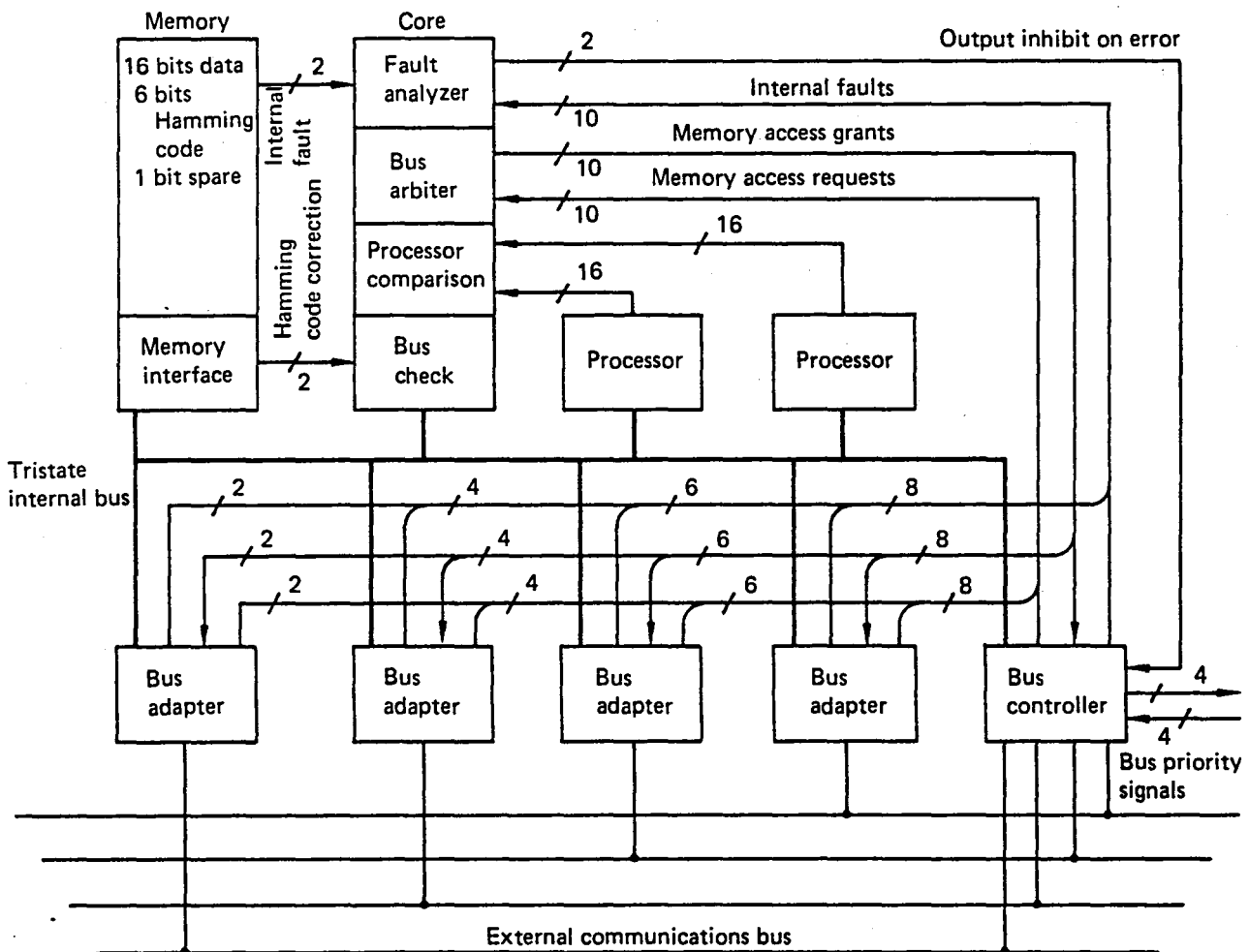
Figure G-23. Self-Checking Computer Module

The memory interface allows access to the storage array. It provides code correction to damaged memory data, replacement of a faulty bit plane with a spare, parity encoding and decoding to the internal bus, and detection of faults within its own circuitry. This element requires about 2000 gates.

The chip for the bus adapter may be microprogrammed to work as the bus controller or as a remote terminal. The controller and adapters on a particular bus operate together autonomously. The bus controller reads a control table from the memory that specifies the source and destination of the information along with the transmission length. It then broadcasts appropriate commands over the bus system to bring up the transmitting and receiving adapter circuits and monitors the transfer of information, records status messages, and notifies the host computer upon transfer completion. This is an unnecessarily complicated sequence for the input from sensors and the output to actuators for flight control; however, these are mass produced, which results in features directed to a wider audience.

The bus adapter chip consists of five elements (ref G-20): a bus interface element, a microprogram control unit, a control ROM, a data path element, and a DMA controller. The bus interface element translates incoming bus signals supplying a bus-synchronized clock and data signals. It also accepts data, clocks, and signals and encodes them for bus transmission. The microprogram control unit provides control sequences. A microprogram location counter is started at one of several fixed addresses by command or data synchronization or a host processor command. The location counter proceeds through sequential addresses or branches on the basis of incoming data, internal flags, or other internal circuit conditions. A unique set of address sequences is produced for each type of incoming bus command, data sequence, or computer command. This output sequence is then mapped through a control ROM to generate the detailed control signals required to drive the data path, microprogram control unit, and DMA control elements. The control ROM maps the microprogram address sequence into control signals for the various circuits. The data path section contains registers to buffer addresses and data; a ROM to store memory protection bounds, data keys, and table addresses; and an arithmetic logic unit for addressing computations. This circuit is similar to existing bit-slice processors, with the exception that serial-parallel conversion registers, ROM, and several holding registers are required for the unique bus interface and DMA functions. The DMA control circuit is responsible for obtaining control of the internal bus and

transferring data between the bus adapter and the memory. The fault detection techniques used are based on parity coding to protect memory information and duplication with morphic comparison for most of the logic circuitry.

The core compares the outputs of the two processors for disagreement, encodes the outputs of the processors for transmission, checks parity on the internal bus, allocates the internal bus to the bus adapters and controller, detects its own faults, collects fault indications from other elements, disables the module output under error conditions, and halts computation on recurring faults.

The flight control system comprises four of these self-checking computing modules plus the complements of sensors, actuators, and power supplies. If a module detects a failure, it inhibits its output. Presumably, the bus controller, if not at fault, would continue to call for the appropriate signals from the sensors so they would be available to other channels. Massive failures that overwhelm the error-detecting codes would be handled by the force-summed actuators and their related circuitry. Provisions would be needed so that the actuator would inhibit an offending computer module.

G.3.4.4 SUMMARY

The high-risk architecture seeks to accommodate the following premises:

- High reliability will be obtained by integrating circuitry on chip and by minimizing connections between chips.

- The trend toward integration makes the testing problem severe.

- Future designs will incorporate much more substantial provisions for testing, self-checking, error correction, and fault tolerance.

- The reliability of microelectronics in 1990 will allow asynchronous, independent channel operation.

- The software of autonomous channels is simpler than systems that reconfigure at lower levels.

- Bus technology is the key issue, and whether self-checking, ultrareliable bus adapters and controllers will be available in 1990 is a major consideration. Because the bus is the central issue in many systems, the probability that they will be available is high.

G.4.0 SERVOACTUATOR CONCEPTS OF IAAC

G.4.0 SERVOACTUATOR CONCEPTS OF IAAC

The actuators that would interface with any of the three systems (low, medium, and high risk) described in Section G.3.0 and the selected alternative, described in Section G.5.0, are addressed in this section. Electromechanical actuators (EMA) should be used to drive the flaperons. The relative ease of electric power transmission across the flaperon hinge line was the motivating factor for this decision. Subsection G.4.1 describes the resulting EMA design.

Conventional hydraulic actuators were selected for control of other surfaces. Subsection G.4.2 describes the hydraulic actuators to be used in the 1990 Active Controls Technology (ACT) system.

G.4.1 FLAPERON CONTROL WITH ELECTROMECHANICAL ACTUATOR

EMAs drive the flaperons for the 1990 ACT control system. EMAs are used in this application because of the ease with which electric power can be transmitted across the wing-flap interface as compared with the hydraulic power alternative.

G.4.1.1 ELECTROMECHANICAL ACTUATOR SYSTEM

Flaperon EMAs are shown in Figure G-24. The performance capability conforms to the performance requirements in all respects. The EMA is composed of two dual-wound, brushless, permanent-magnet (PM) motors whose outputs are mechanically summed to the output through a differential gearing. The EMA may be described as dual channel mechanical and quadruple channel electric.

The EMA system for each flaperon is composed of an actuator and two servodrive electronics units (SDEU), as shown in Figure G-25.

Two dual-wound, torque-summed, PM, brushless, 270V dc motors are velocity summed in differential compound planetary gearing in a hinge-line rotary actuator mechanism. Each motor shaft passes through a brake assembly that is spring-loaded "on" and electrically powered "off" by either of two dual-solenoid windings.
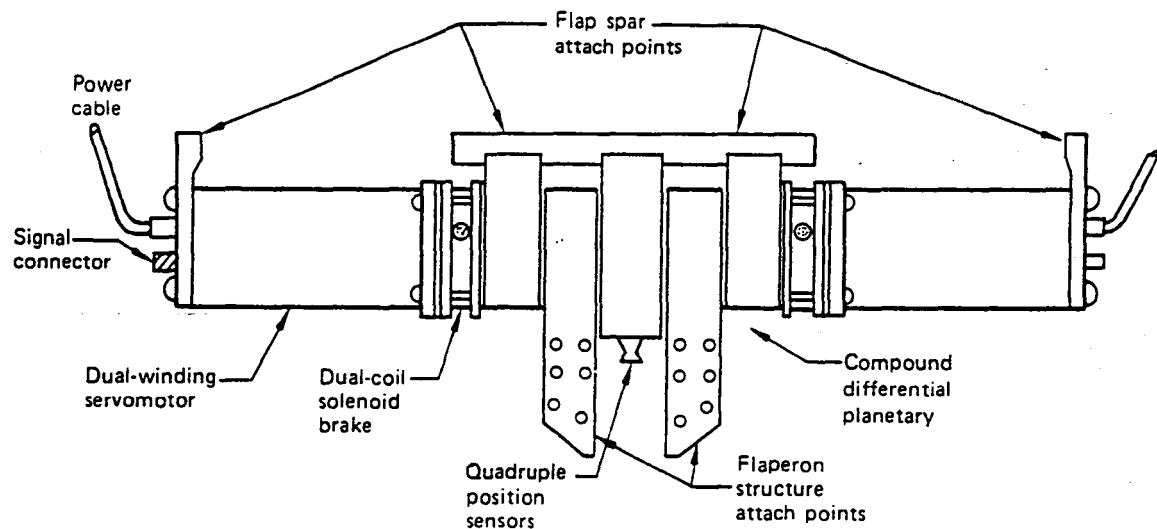
Design characteristics

- 0.76m (30 in) long, 0.1m (4 in) diameter
- 22-kg (48-lb) actuator assembly
- Dual-dual motors, velocity summed
- Dual, power off, brake
- Passive thermal mass temperature control
- 270V dc power
  - 12A (6 each) at stall
  - 1A (0.5 each) at no-load maximum rate

Performance capability

- 4240-N·m (37 500-in-lb) minimum stall torque with two of four channels
- 80-deg/s no load with two motors
- Capability to hold stall continuously
- 40-rad/s minimum bandwidth
- Two-channel fault tolerance
- +120° to -68°C (+250° to -90°F) operational environment

Figure G-24. Electromechanical Flaperon Hinge-Line Actuator
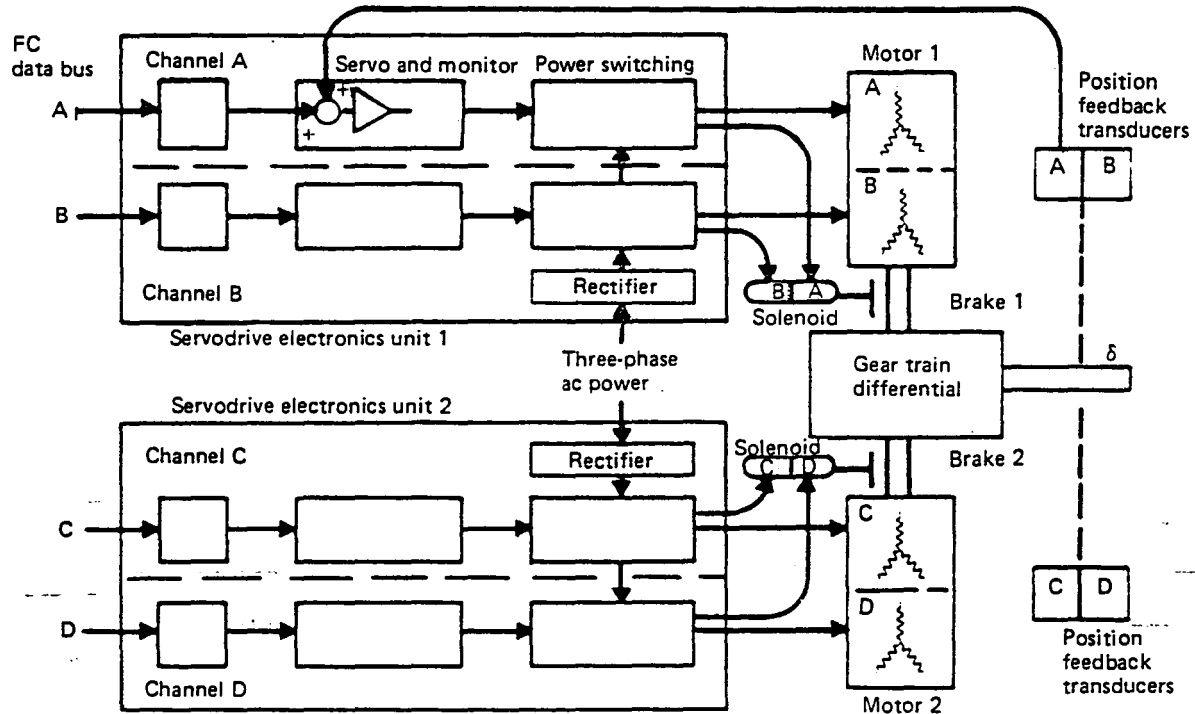
Figure G-25. Electromechanical Actuator Block Diagram

G-102

Quadruple surface position encoder assemblies are embedded in the actuator housing assembly to reflect compliance and to avoid the need of reference position cycling.

Four identical channels of servo control and monitoring electronics are contained in two identical SDEUs. Both are mounted within the movable flap structure with only redundant 28V dc and 115V ac power and data buses bridging the flap-to-wing structural interface. Each SDEU weighs 6.4 kg (14 lb) and has a volume of 9.4×10^{-3} m^3 (576 in). Data bus inputs and outputs are shown in Table G-12.

SDEUs provide resident redundancy management. Fault detection is based on proven comparison monitoring techniques augmented by inline monitoring checks. For periodic ground or preflight test, built-in-test (BIT) routines are provided to be initiated by the ACT computer command. Thermal-limit shutdown is provided to avoid inadvertent stress during ground operations.

Table G-12. Servodrive Electronics Unit Data Bus Words

Inputs from FC computer	Outputs to FC computer

Status commands
 	
• On/off command channel A (or C)
• On/off command channel B (or D)
• Failure reset command channel A (or C)
• Failure reset command channel B (or D)
• Self-test initiate command
 	
Control commands
 	
• Surface position command channel A (or C)
• Surface position command channel B (or D)
	Status commands
	
	• On/off status channel A (or C)
	• On/off status channel B (or D)
	• Surface position feedback
	• RM fail status
	  • Fail/not fail channel A (or C)
	  • Fail/not fail channel B (or D)
	• Continuous BIT status
	  • SDEU channel A fail (or C)
	  • SDEU channel B fail (or D)
	  • Actuator channel A fail (or C)
	  • Actuator channel B fail (or D)
	  • 270V dc fail
	  • 28V dc fail

Development of the flaperon actuator (its physical, electric, thermal, and dynamic characteristics) is based on a systematic method of structured modeling and on hardware and software correlation iteration cycles. Properly applied, this methodology optimizes many performance and programmatic variables for a particular actuation application prior to commitment of a design to hardware production.

Figure G-26 is an analytical block diagram of the flaperon actuation system. Table G-13 identifies system parameters that have been or need to be identified.

G.4.1.2 REDUNDANCY MANAGEMENT

The flaperon actuation system is basically quadruple redundant. Fault detection and reconfiguration are primarily by comparison monitoring of the servo error signals. Comparison monitoring is augmented by inline monitoring of the control electronics and certain motor-feedback sensor characteristics to improve fault detection capabilities.

Although the EMA system configuration conceivably would allow continued operation after the failure of three electric channels, this is not planned for ACT application. At least two channels of drive electronics always will be operative or the EMA will be shut down and braked.

The flaperon actuation combination of magnetic torque summing with velocity gear-train summing results in varied tolerance to primary string faults. Stall torque is sized for any two of four motor windings inoperative; therefore, with no faulted windings, twice the stall torque would be available if not intentionally limited. The maximum surface no-load rate is produced when both velocity-summed motors are functional, although each motor may have one torque-summed winding inoperative. If one velocity-summed motor is inoperative and its brake locked, the maximum surface rate will be half of the two-motor value, but the full-stall torque capability still will be present. These fault-down characteristics are inherent in each of the summing types used. The following table summarizes these fault effects.

Fail state	Effect
One motor winding open	None; full torque and rate
Two windings open; one each motor	Half torque, full rate
Two windings open; one motor braked	Half rate, full torque

Figure G-26. Flaperon Actuation Analytical Diagram

Table G-13. Electromechanical Actuator Parameters and Variables, Flaperon Application

SYMBOL	VALUE	UNITS	DESCRIPTION
KT	*	FT-LB/AMP.	MOTOR TORQUE GAIN
TI	.001	SEC	CURRENT SOURCE TIME CONSTANT
KE	*	V/(R/S)	BACK EMF CONSTANT
NO1,NO2	2,2	NUMBER OF MOTORS TORQUE SUMMED (MAX)	
ILIM	*	AMP	CURRENT LIMIT
TMAX	*	FT-LB	MAX TORQUE PER WINDING
JM	*	FT-LB-S**2	MOTOR AND GEAR MOMENT OF I
ODM	10000	RPM	MAX MOTOR SPEED
N	*	DEG/DEG	DIFF OUTPUT-TO-SURFACE GEAR R
KO	*	IN-LBS/RAD	STRUCTURAL SPRING RATE
JP	*	IN-LB-S**2	LOAD MOMENT OF INERTIA
BP	*	IN-LB/(R/S)	LOAD DAMPING
TC	*	IN-LB	LOAD FRICTION
TS	*	IN-LB	LOAD STICTION
KFB	.625	V/RAD	POSITION SENSOR GAIN
KR	*	V/(R/S)	RATE GAIN
KA	*	AMP/V	SERVO POSITION GAIN
TAU	*	SEC	POS FBK TIME CONSTANT
VBATT	270	VOLTS	BATTERY VOLTAGE
L	0.0	HENRY	MOTOR INDUCTANCE
RM	.2	OHMS	MOTOR RESISTANCE
KW	0.0	FT#/(R/S)**2	MOTOR WINDAGE
1/T	100	HZ	SAMPLING FREQUENCY
RPSQ	15	DEG	RPS QUANTIZATION
TM	--	FT-LB	MOTOR TORQUE (TOTAL)
OM1,OM2	--	RAD	MOTOR #1,#2 POSITIONS
OD	--	RAD	DIFF OUTPUT SHAFT POSITION
	--	OHMS	POWER SOURCE RESISTANCE
	--	HENRY	POWER SOURCE INDUCTANCE
TPA	--	DEG-F	ACTUATOR CP TEMP
TPE	--	DEG-F	ELECTRONICS CP TEMP
OG	--	RAD	POWER HINGE POSITION
DELTA	--	RAD	PANEL POSITION
DELTA-SEN	--	RAD	SENSED PANEL POSITION
TP	--	IN-LB	DEVELOPED TORQUE AT HINGE
TAERO	--	IN-LB	AERO LOAD TORQUE

* TO-BE-SUPPLIED

The flaperon control and redundancy management (RM) architecture have been established to accept realistic skew and transport delays from redundant flight control computers.

G.4.1.3 DESIGN CHARACTERISTICS

G.4.1.3.1 Servo-Loop Features

The flaperon position servo design provides the following functions and features:

- Surface position control

- Maximum surface response characteristics

- Stabilization compensation in the presence of structural compliance

- Stabilized motor control in the presence of velocity- and torque-summing perturbations

- Realistic tolerances and variations of interfacing and parallel elements

Position control is accomplished by comparing flight control digital data bus position command to encoded surface-position feedback with compensation applied to the position error signal. Redundancy-related elements alter gain as a function of redundant motor-channel status.

Servo-loop response time is optimized by:

- Closed-loop motor-current feedback control
- Maximum motor and electronics torque-to-inertia ratio
- Minimum associated gear ratio

Servo-loop stability is maximized by motor-rate feedback and blending of motor shaft position with surface position for compliance compensation. Motor shaft rate is derived from the rotor position sensor (RPS) used for commutation logic.

G.4.1.3.2 Thermal Considerations

Flaperon actuation elements meet the in-flight hinge moment rate profiles, including stall for an indefinite period, with no active auxiliary cooling. Thermal mass heat sinking will accommodate the power-loss heat rates without exceeding reasonable temperature ratings of EMA materials. Avoidance of active cooling while avoiding unnecessary weight requires the use of carefully structured and hardware-correlated thermal models and flight simulations.

The flaperon indefinite-period in-flight stall provides the primary thermal sizing requirements. Two other special conditions, however, required a design handshake with redundancy management functions to avoid component thermal degradation or failure propagation: (1) high ground-soakback temperature plus inadvertent actuator stall during ground operations and (2) motor-shorted turn(s) fault. Because ground soakback may result in EMA temperatures of 70° to $120^{\circ}C$ (160° to $250^{\circ}F$), any significant power dissipated in the EMA elements could raise the respective temperatures to intolerable levels.

A motor-winding shorted turn causes a dynamic damping effect that requires overcoming a higher power level of summed motors. Power dissipated in the shorted turn(s) and the increased compensating power result in an increased temperature rate versus command profile. Both special cases are accommodated by adapting a high-temperature-sensor circuit to interrupt the power drive when the motor or electronics approaches the over-temperature state. Provision is made for flight control override on a need-decision basis.

Note that although the EMA elements may survive an application of high temperature, the ultimate life of the element will decrease. Lengthy testing of motor-winding insulation indicated that ultimate electric breakdown is a function of accumulated temperature and time. That is, the insulation life may be used by several high-temperature, short time cycles or an infinite number of low-temperature, long time cycles. Design and operation of the EMA must reflect both normal and abnormal thermal considerations to provide reliable long-life operation.

G.4.1.3.3 Preflight Checkout, Built-In Test

Flaperon SDEUs contain BIT routines in an erasable, programmable read-only memory (ROM) state that may be initiated by flight control and/or crew command to thoroughly test the actuator, its control and monitoring functions, and system elements before or after a flight. The BIT requires no rollup support hardware and is intended to provide nearly 100% confidence in the flaperon functional status.

G.4.1.3.4 Electromagnetic Interference

Electromechanical actuation poses two concerns for development consideration. Use of high voltage (270V dc) in conjunction with high currents, modulated by variable frequency or pulse width, inherently produces broad-spectrum conducted and radiated electromagnetic interference (EMI). Use of digital-processor-based electronics in close proximity to these noisy circuits predicates use of enclosures, shielding, filtering and optical isolation, and/or fiber optics to avoid interaction.

Conducted EMI on the high-voltage power buses will require several techniques to minimize interaction among flaperon controllers or other avionics. Current industry techniques involve (1) flat laminated cables, (2) coaxial cables, and (3) ac/dc converters with filters for each EMA. Power-spectral-density profiles, as a function of flaperon mission timeline profiles, will allow selection of the best cable and source EMI technique for this application.

G.4.2 ADVANCED HYDRAULIC CONCEPTS

The objective of the advanced hydraulic concepts task was to define the hydraulic actuators to be used on the 1990 ACT system. This objective was arrived at following the actuation survey studies described in Subsection G.2.3. According to these studies, it was decided that:

- Fly-by-wire (FBW) control will be applied in all three axes.

- Conventional cylinder-type hydraulic actuators will be used in all hydraulic control actuator applications.

- All ACT control surfaces will be driven by hydraulic actuators except for the flaperons, which will be driven by EMAs.

G.4.2.1 ACTUATION CONCEPTS

Two classes of actuators were examined: the first uses magnetic summing of torque motor current; the second uses active, online principles. These two classes of actuators were judged to represent concepts that will be probable industry leaders in the 1990s.

The magnetic summing of torque motor currents is embodied in a class of actuators that includes position-summed modulating pistons, as shown in Figure G-27, or a unique form of flow summing, as shown in Figure G-28. In both cases, all control loops are electrically closed. The alternative of closing the loop mechanically from the modulating piston to the single-stage valve is apparent in both actuators.

The two actuators operate similarly. The servo loops for each electric channel are closed from sensors on the modulating pistons (or main control valves) and the output cylinders. It is not necessary to have the same number of electric channels and hydraulic channels because all servo torque motor signals are sent to all electrohydraulic valves (EHV) where they are magnetically summed.

Each hydraulic channel has two EHVs. The actuator in Figure G-27 has each of the two EHVs driving modulating pistons with an output that drives the main control valve through a summing lever arrangement. In Figure G-28, the two EHVs are connected in series, and the output (a low-pressure gain signal) positions the main control valve.

Output from the main control valve positions the output cylinder. Output cylinder feedback transducers are provided, and their signals are used to close the position loop of the actuator.

The electronic channels are monitored by comparison of the torque motor currents between electric channels. The hydraulic channels are monitored by noting outputs from the position-difference sensors, as is shown in Figure G-27, and from the pressure sensor shown in Figure G-28. The pressure sensor detects failures in either EHV by ensuring that

the pressure in the center connecting leg of the series-summed valves is equal to half the sum of the supply and return pressures.

This type of actuator can be built as a large integrated surface actuator or as a small secondary actuator. The cylinder may be integral with the main control valve, as it is in the F-18 stabilizer actuator, or remote, as it is in the F-18 leading-edge flaps.

Parker-Bertea has built actuators of the type illustrated in Figure G-27. National Waterlift is producing actuators of the type shown in Figure G-28 for the F-18 stabilizer application.

- Electronic channels magnetic summed
- Hydraulic channels force summed (low-pressure gain equalized)
- Dual load-path hydraulic position monitoring
- All loop closures electronic (modified Parker-Bertea)
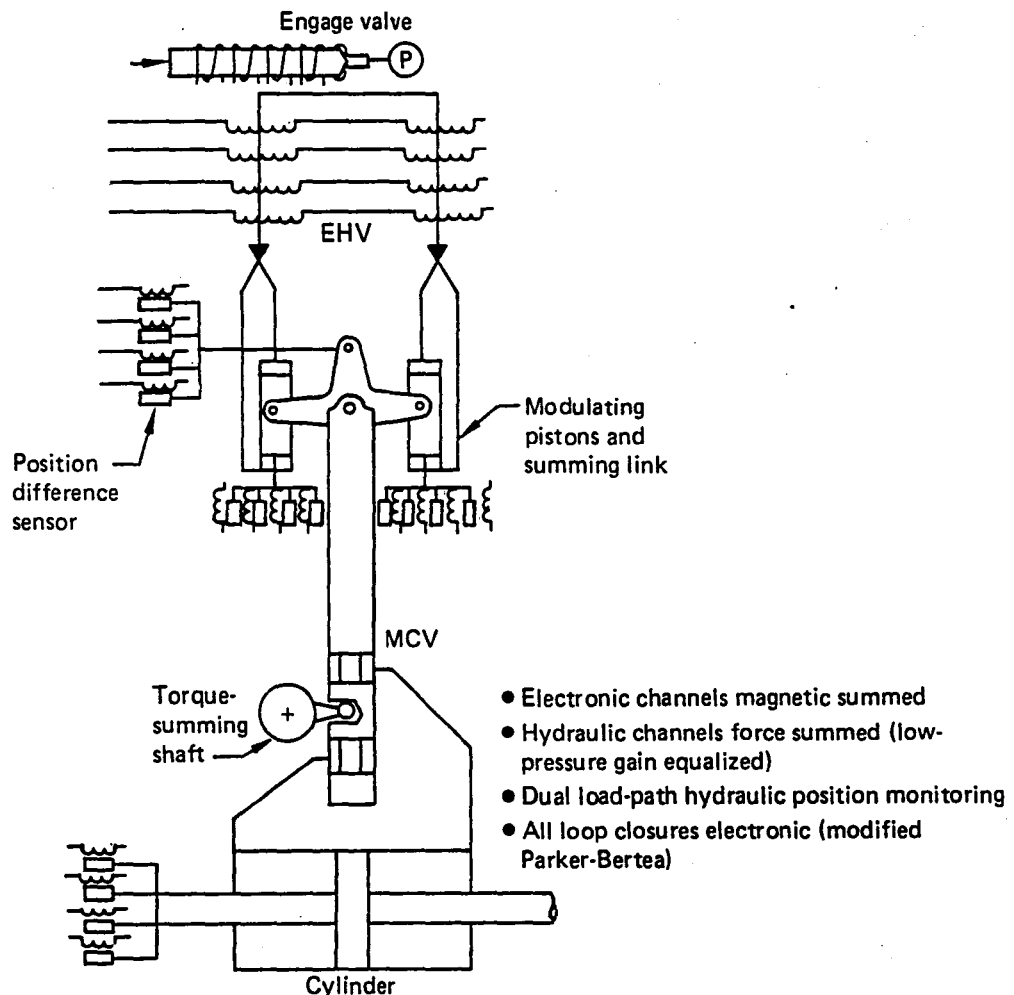
Figure G-27. Position-Summed Modulating Pistons

- Electronic channels magnetic summed
- Hydraulic channels force summed (low-pressure-gain equalized)
- Dual load-path hydraulic pressure monitoring
- All loop closures electronic
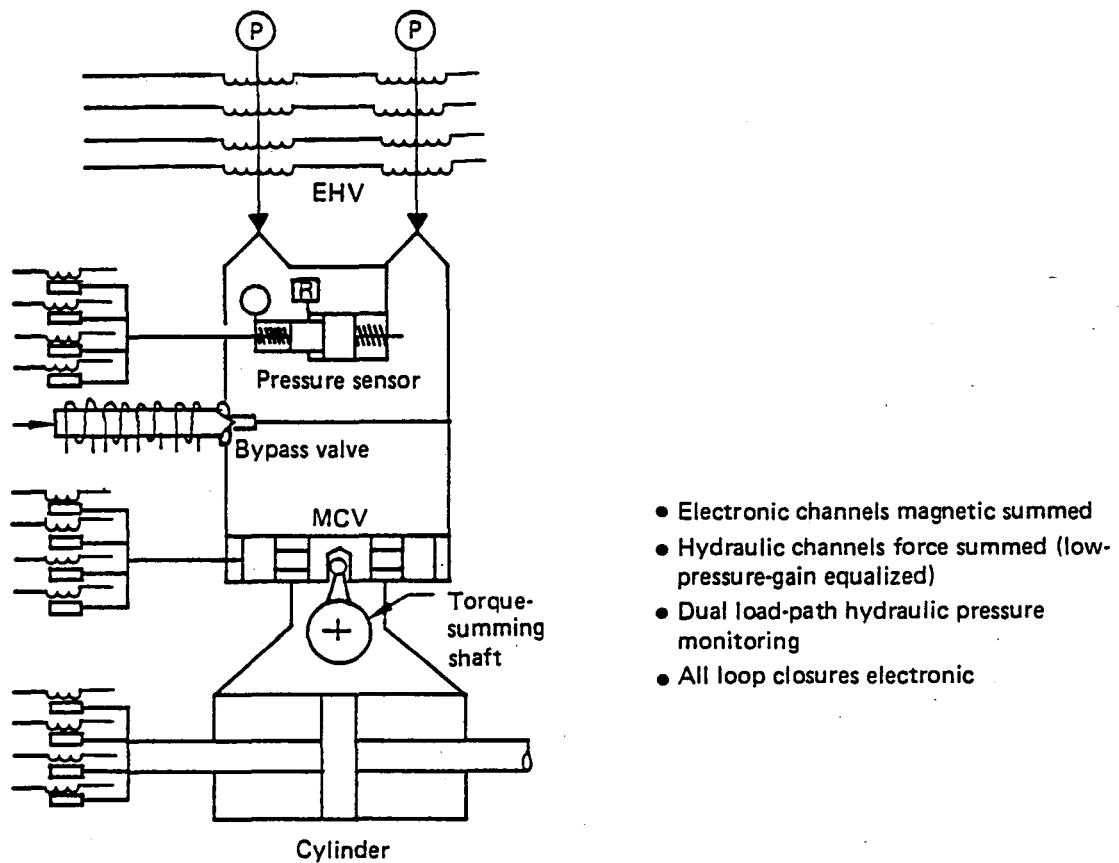
Figure G-28. Flow Summing

Figure G-29 shows an active, online actuator. A single hydraulic channel is shown. The single channel shown may be one of several similar units force summed on the control surface or may be one of a number of tandem units. Each channel has transducers for cylinder position and force feedback (pressure sensor) and for velocity feedback (EHV second-stage spool position).

Error signals are supplied to a conventional two-stage EHV with a flow that positions the output cylinder and closes the position loop.

As shown in Figure G-30, the active channel used the pressure sensor feedback signal only for commanding the force output of the online channels. Online channels use the pressure feedback signal to compare with that of the active channel and compensate for any static load differences.
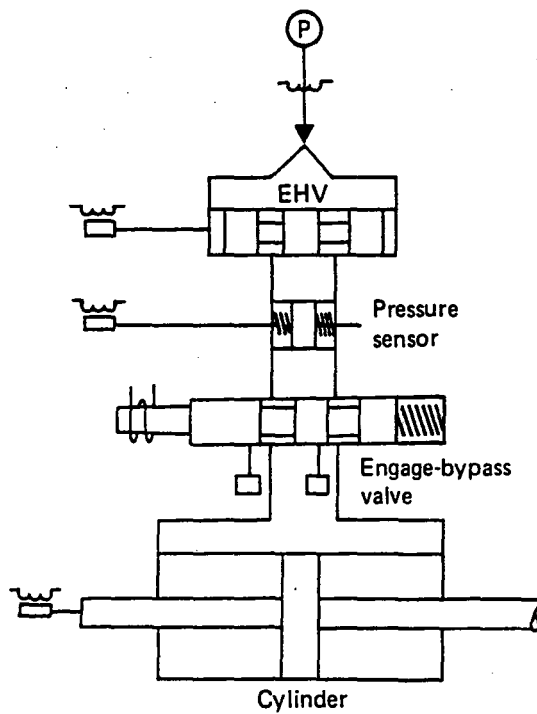
- Active, online, force summed (one channel shown)
- Electronic position, velocity and force feedback
- Electronic model monitoring and engage-bypass operation

Figure G-29.   Active, Online Actuator
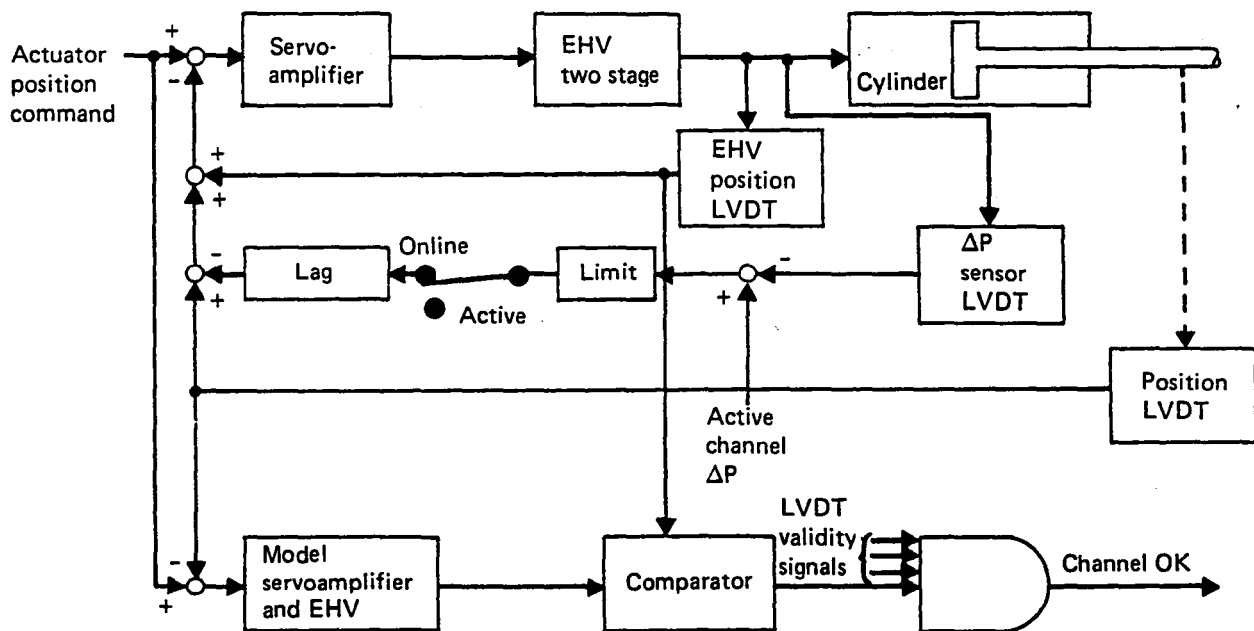
Figure G-30.   Active, Online Actuator Channel Block Diagram

Each channel of actuation is monitored electrically by a modeling technique. The position of the second-stage spool of the EHV is easily modeled as a function of the actuator position, position command, and pressure feedback signals.

Ideally, the several actuation channels could operate in concert with one another in an each-channel-active configuration. However, because of the high-pressure gain characteristic of actuator valves, small tolerances in the actuator control loops would lead to significant force opposition between channels. The pressure feedback path in the online channels must overcome this force-fight tendency by offsetting the tolerances between channels.

A limiter is provided in the pressure feedback path, as shown in Figure G-30. This limiter is set at a value so that the pressure feedback signal can slightly exceed the maximum tolerance between channels. Previous tolerance studies of a similar servoactuator control loop indicated a maximum tolerance between any two channels in terms of torque motor currents to be 2.8 mA. In these studies, full displacement command to a centered actuator corresponded to 800 mA of torque motor current. An 8-mA EHV was used, and a pressure feedback limit of ± 4 mA was chosen.

Thus, the pressure feedback is effective in allowing the actuators to share the output load. However, the online actuator (or actuators) will oppose any active channel malfunction as soon as a displacement corresponding to 4 mA (4/800 of full travel) is exceeded.

Upon detection of any failure in the active channel by the monitor computer, one of the online channels will be switched to the active status by removing the pressure feedback.

The active, online actuator concept was successfully test flown by Boeing-Vertol on the 347 helicopter as a part of the Heavy Lift Helicopter Advanced Technology Components Program.

G.4.2.2 ACTUATOR COMPARISONS

The two candidate actuator concepts were used to determine the type of surface actuation system that would be the least expensive. Three elevator actuation systems were hypothesized for the subject aircraft (fig. G-31).

A three-channel (hydraulic) secondary actuator was used to drive six conventional hydromechanical surface actuators. The secondary actuator used magnetic summing of four control channels and operated like a small F-18 stabilizer actuator.

Three (hydraulic) channels of an F-18 type manifold (similar to those used on the leading-edge flaps) were used to drive six surface-mounted cylinders. Four-channel magnetic summing was used.

Six identical active, online actuators (three per surface) were used to drive the surfaces direct. The remote terminal would be used to provide the proper signal selection.

This study showed that the active, online concept was by far the lowest cost arrangement (approximately half the cost of the other concepts) and that reliability, determined on the basis of parts count, was significantly better. These results are shown in Table G-14.

Performance was judged to be adequate for any of the three alternatives.

The integrated active, online actuator was therefore selected for the 1990 ACT system.

G.4.2.3 ACTUATOR COMPLEMENT FOR ACT AIRCRAFT

ACT has 14 control surfaces (7 pairs).of which 10 are hydraulically actuated and 4 are electromechanically actuated. All the hydraulic actuation systems use simple, single-cylinder active, online actuators except those for the outboard aileron, inboard segment—for this installation, a dual-tandem design is used. Control paths and hydraulic power distribution patterns are shown in Figure G-29.

G-115
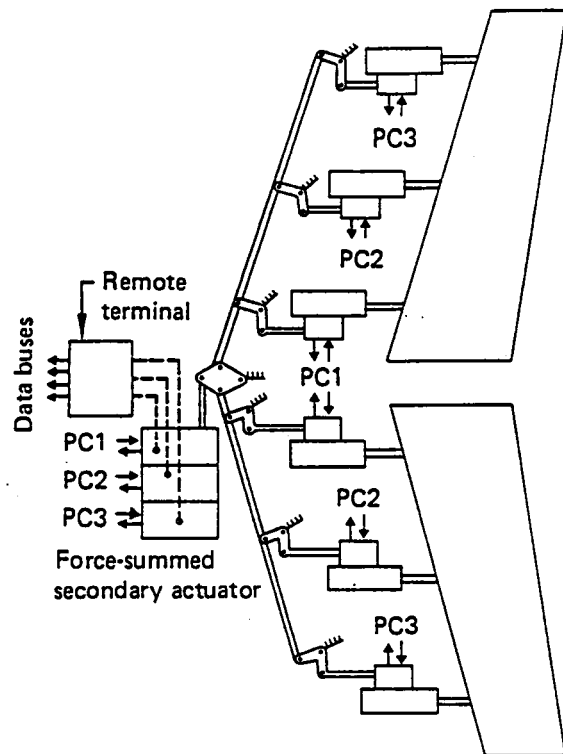
I   **Secondary Actuator Hydromechanical Surface Actuator**
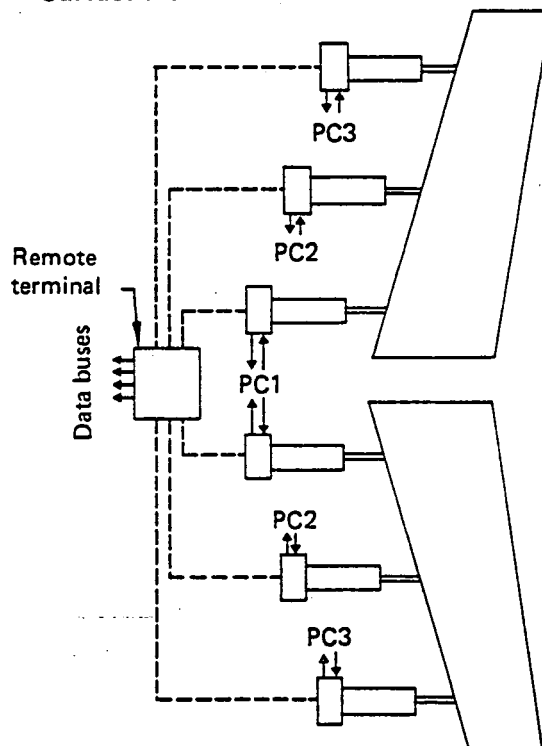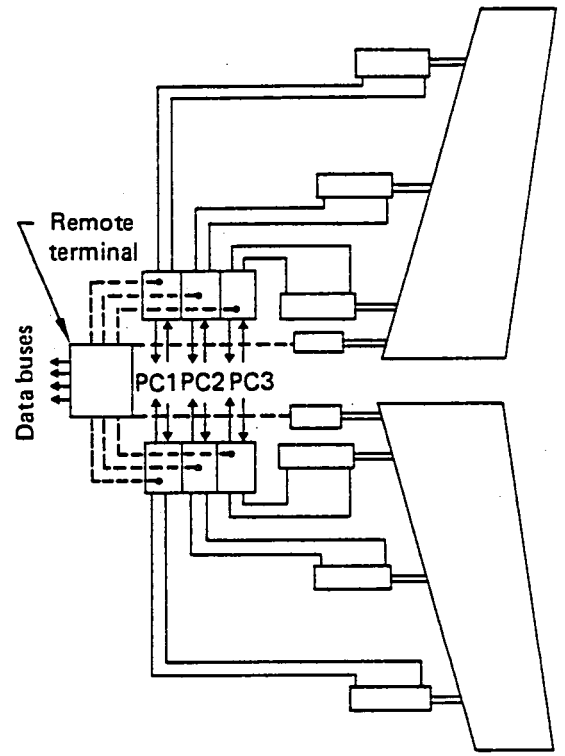
II   **Integrated With Remote Cylinders**

III   **Integrated Active Online**

════════	Mechanical
────────	Hydraulic
────────	Electronic

Figure G-31. IAAC Elevator Actuation Concepts

Table G-14. Servo-Concept Comparisons

Servo-concept	Relative cost	Failure rate (per hour)
I Secondary actuator	1.0	800×10^{-6}
II Integrated actuator with remote cylinders	1.25	840×10^{-6}
III Integrated active, online actuators	0.62	670×10^{-6}

The actuator characteristics are shown in Table G-15—the geometry of the hydraulic actuators is representative only; bore-stroke and surface-horn dimensions may be adjusted for the individual installation.

The requirements show that most of the actuators are relatively low powered and that design details such as cylinder wall thickness (all designed with steel barrels) and piston rods are sized for handling and side loads, as opposed to being optimized for tension or compression loading.

Bypass valves are of minimum size because the actuator provides flutter damping in the "off" condition.

Two actuators were sized for high-pressure hydraulic systems: the outboard aileron, outboard segment, and the rudder. Note that the effect on the weight of the larger unit is much more pronounced.

Figure G-32 shows how the signal paths are distributed to the control surface actuators and their terminals. While EMAs for the trailing-edge flaperons have servodrive electronics units (SDEU), remote from the actuator, integral remote terminals are a part of the hydraulic actuators.

The integral actuator terminal and its interconnects are shown in Figure G-33. Note that the command signals (position pressure and mode select) drive the actuator, while the sensor validity signals are used for monitoring by the ACT computer. Structural compensation also can be included in the remote terminal.

Table G-15. IAAC Hydraulic Actuator Characteristics

Control surface	Outboard aileron outboard segment	Outboard aileron inboard segment	Inboard aileron	Elevator	Rudder
Hinge moment, N·m (in-lb)	1017 (9000)	553.6 (4900)	4 745 (42 000)	7 344 (65 000)	20 902 (185 000)
Deflection, deg	+15, -30	±15	±20	+20, -30	±25
Average rate, deg/s	54	100	30	40	40
Cylinder diameter, cm (in)	3.81 (1.500)	2.54 (1.000)	8.573 (3.375)	7.381 (2.906)	10.475 (4.125)
Rod diameter, cm (in)	1.587 (0.625)	1.587 (0.625)	1.587 (0.625)	1.905 (0.750)	2.857 (1.125)
Stroke, cm (in)	3.957 (1.558)	2.522 (0.993)	5.898 (2.322)	7.473 (2.942)	10.693 (4.210)
Horn radius, in	2.053	1.920	3.395	3.499	4.985
Net piston area, cm^2 (in^2)	9.4245 (1.4608)	3.0877 (0.4786)	28.406 (4.403)	39.9406 (6.1908)	79.806 (12.370)
Maximum flow, cm^3/s (in^3/s)	60.025 (3.663)	34.167 (2.085)	180.67 (11.025)	340.75 (20.794)	950.48 (58.002)
Average flow, cm^3/s (in^3/s)	45.04 (2.748)	25.61 (1.563)	135.5 (8.267)	255.6 (15.59)	712.8 (43.49)
Orifice diameter for 6 894 700 Pa (1000 lb/in^2),cm (in)	0.05 (0.020)	0.038 (0.015)	0.089 (0.035)	0.122 (0.048)	0.206 (0.081)
Actuator weight for 20 684 100 Pa (3000 lb/in^2), kg (lb)	2.78 (6.14)	5.08 (11.2)	3.43 (7.56)	4.73 (10.43)	8.0 (17.64)
Actuator weight for 55 157 600 Pa (8000 lb/in^2), kg (lb)					7.085 (15.62)
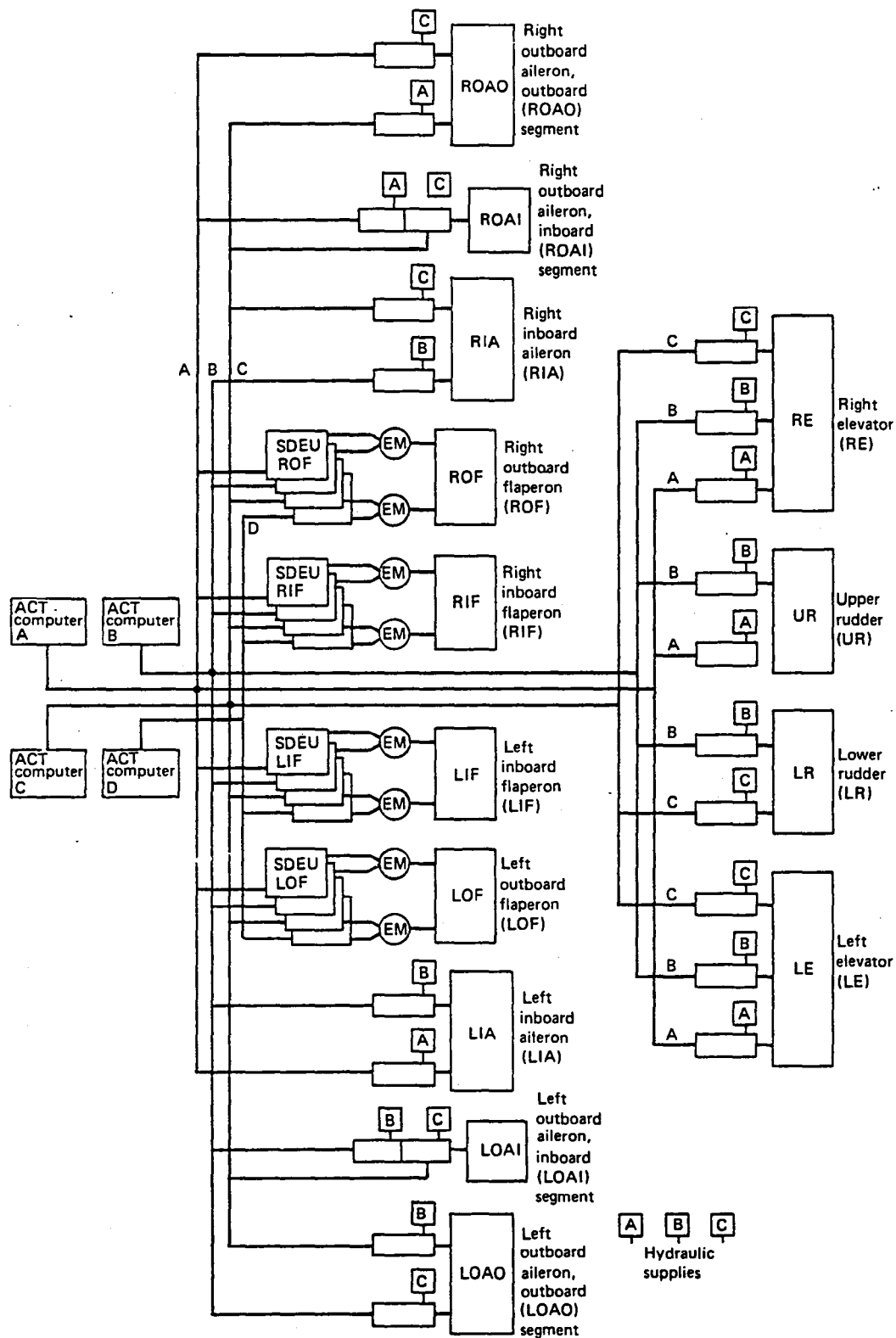
Figure G-32. Surface Actuator Control System

Figure G-33. Remote Terminal Hydraulic Servo

The hydraulic actuation system uses 22 electrohydraulic servovalves (6 in supply system A, 8 in B, and 8 in C), one for each actuation cylinder. Each is a line replaceable unit (LRU) and may be replaced without removing the actuator from the aircraft. Integral connectors and lack of mechanical interfaces (e.g., feedback wires) are contributing design details.

The differential pressure sensor, with its integral transducer, is also an LRU. Some consideration should be given to the use of two-gage pressure sensors, one in each cylinder line. This would allow continuous monitoring of EHV erosion and provide the load pressure sensing. The former would be a distinct advantage over present servovalve maintenance methods.

Solenoid-operated engage bypass valves would also be of LRU design. Valve area is sized to provide flutter damping in the "off" position. The size of the solenoid required is minimized.

This Page Intentionally Left Blank

G.5.0 1990 SYSTEM IMPLEMENTATION FOR IAAC

G.5.0 1990 SYSTEM IMPLEMENTATION FOR IAAC

The 1990 ACT system is described in this section. Selection of the 1990 ACT system was based on the three system definitions (low, medium, and high risk) described in Section G.3.0. It most closely resembles the medium-risk system described in Subsection G.3.2.

Features of the 1990 ACT system are:

- Extensive busing techniques are used for sensor-computer and computer-actuator interfaces:

    - Aircraft wiring is reduced in weight and cost.
    - All sensor data are available to all channels of computing.

- Sensors and actuators have self-contained electric power supplies and bus interface circuitry.

- Software costs are reduced, and software validation and verification is simplified:

    - Separate microcomputers perform input/output (I/O), control law computations, and redundancy management.

    - Computing channels are asynchronous.

- Crucial function reliability is enhanced by a microcomputer reconfiguration strategy:

    - I/O computer does crucial control law computation if control law computing fails.

Subsections G.5.1 and G.5.2 describe the 1990 ACT system. Subsection G.5.3 presents the reliability projections for the system. Subsection G.5.4 presents the cost-of-ownership parameters.

G.5.1 SYSTEM CONFIGURATION

G.5.1.1 SYSTEM ARCHITECTURE

The 1990 ACT system is an integrated one; i.e., all functions are performed by each of a set of four ACT computers. Sensors and control surface actuators are shared between functions to the extent allowed by the control laws.

The 1990 ACT system is fly by wire (FBW). All control surface actuators are driven only by the electric signals; there is no mechanical control system.

The system architecture is shown in Figure G-34. A set of four buses interfaces the sensors with the computers. Similarly, a set of four buses interfaces the computers with the surface actuators. The ACT Maintenance and Display Computer, warning electronics module, and dedicated ACT panel also interface with the four ACT computers by means of the same set of four buses associated with the power actuators.

The digital air data computer (DADC) and inertial reference system (IRS) are airplane sensors that interface with the ACT computers via buses. For the aircraft, they are defined as intersystem buses. The IRS is capable of interfacing with the ACT system via the quadruple intrasystem buses as well as the intersystem buses. This is necessary because the pitch-rate and acceleration signals, used for crucial functions, need to be obtained more reliably and faster than is possible with an intersystem bus presumed to be of the Aeronautical Radio Incorporated (ARINC) 429 type.

Figure G-35 shows the aircraft interconnect wiring. In addition to the sensor and actuator buses, Figure G-35 shows the airplane electric power distribution to each of the ACT flight control system line replaceable units (LRU). Only +28V dc power is used to power the system except for the flaperon electromechanical actuators (EMA). Four +28V dc power buses are provided. These are designated:

- Transformer-rectifier (T-R) bus 1 (T-R1)
- T-R bus 2 (T-R2)
- Battery bus 1 (B1)
- Battery bus 2 (B2)
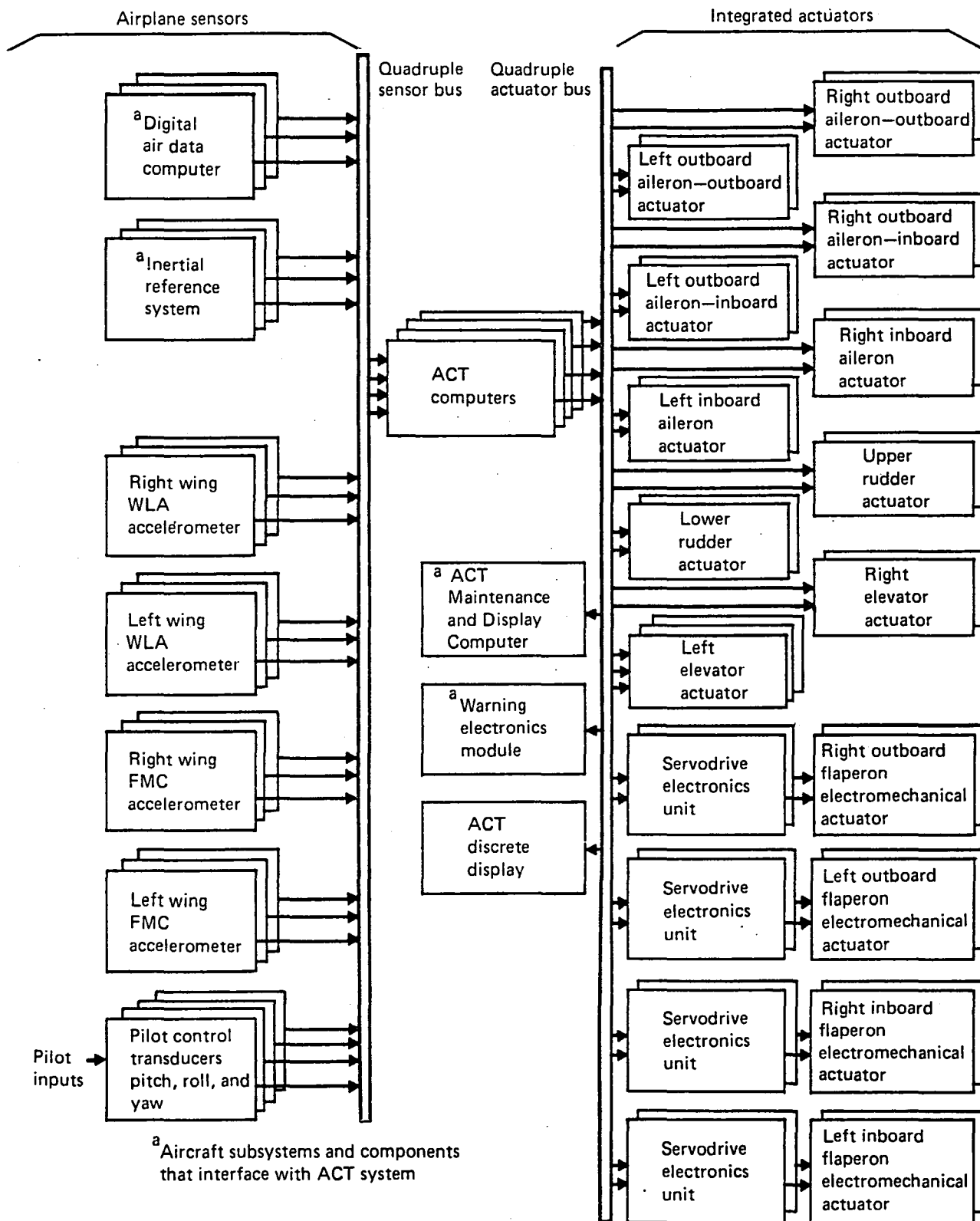
Figure G-34. 1990 ACT System Architecture

Surface	Power bus		Actuator data bus	
	Actuator No. 1	Actuator No. 2	Actuator No. 1	Actuator No. 2
ROAI	T-R1, B1	T-R1, B2	A_A	C_A
RIA	T-R2, B1	T-R1, B2	B_A	C_A
LIA	T-R1, B1	T-R2, B1	A_A	B_A
LOAI	T-R2, B1	T-R1, B2	B_A	C_A
LOAO	T-R2, B1	T-R1, B2	B_A	C_A
UR	T-R1, B1	T-R2, B1	A_A	B_A
LR	T-R2, B1	T-R1, B2	B_A	C_A

	ACT No. 1	ACT No. 2	ACT No. 3	ACT No. 1	ACT No. 2	ACT No. 3
RE	T-R1, B1	T-R2, B1	T-R1, B2	A_A	B_A	C_A
LE	T-R1, B1	T-R2, B1	T-R1, B2	A_A	B_A	C_A
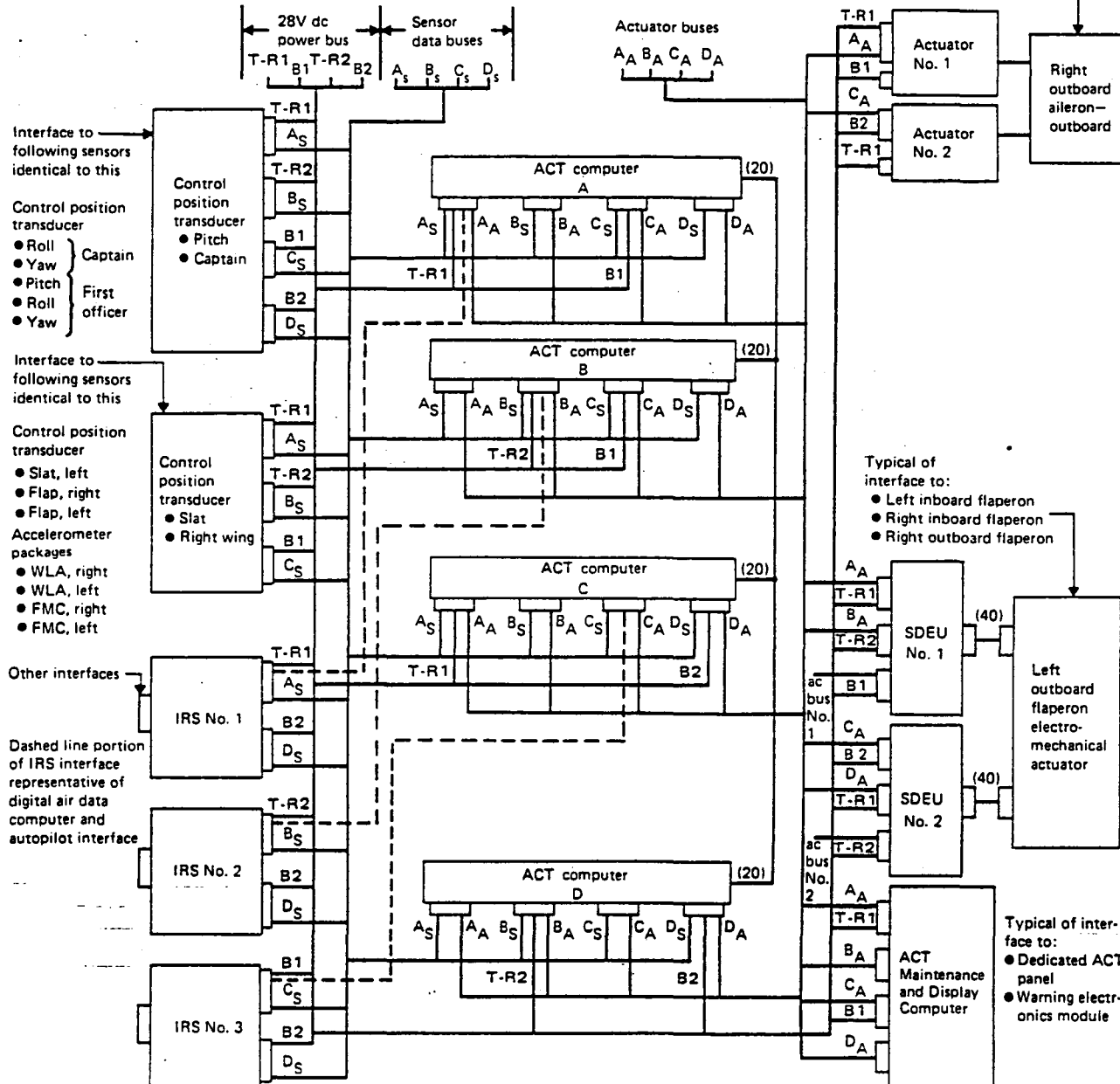
Figure G-35. IAAC 1990 ACT Aircraft Interconnect Wiring Diagram

As shown in Figure G-35, each LRU is provided with two sources of +28V dc power. One source of power is a T-R bus; the other is a battery bus. These two sources of power are diode "ORed" within each LRU. With this arrangement, and with the basic reliability of the airplane dc buses, the loss of power to any flight control system LRU is virtually impossible.

Each sensor contains bus interface electronics, which include an analog-to-digital (A/D) converter, an asynchronous serial I/O communications circuit, and logic required to recognize a data request and format the data response for transmission to the computers on the sensor bus. Each response will include data, label, and a parity bit.

Each sensor bus is controlled from one of the ACT computers. Each computer receives the data from all four sensor buses and stores it in memory locations corresponding to the label.

The actuator buses provide a communications path from the ACT computers to the actuators. Four actuator buses are provided that are normally assigned to each of the four ACT computers. The servoactuators are controlled from the computers. The specific assignment of each hydraulic actuator to a bus is indicated in Figure G-35. This assignment is consistent with the Baseline Configuration assignment of hydraulic systems to surface actuators. An address, a position command signal, a servo state signal, and a parity bit are transmitted to each actuator.

Each hydraulic servoactuator contains electronics to receive and decode the serial data, convert the command to an analog signal, demodulate the feedback signals required for servo control, and close the servo loop. The servoelectronics also transmit signals on the bus in response to ACT computer requests, which include the feedback signals required for monitoring of the servo.

The EMAs associated with the flaperons similarly interface with the ACT computers. However, each EMA has two servodrive electronics units (SDEU) because the control electronics required for the EMAs are considerably more elaborate than those required for the hydraulic servos. Much of the EMA monitoring and redundancy management is done in the SDEUs.

The ACT Maintenance and Display Computer interfaces with the servo buses. It receives data from the ACT computers indicating the failure state of the active controls system and provides fault annunciation messages and signals to the caution and warning system.

The ACT discrete display also interfaces with the actuator buses and provides an independent source of system failure status information to the crew.

The caution and warning system discrete displays also interface with the actuator buses.

G.5.1.2 ACT SYSTEM FUNCTIONAL CONFIGURATION

The 1990 ACT system has the same functional capabilities as the Baseline Configuration ACT system. In addition, FBW control is incorporated in all three control axes. Improved reliability, maintainability, control quality, and cost result from the change from a conventional control system with control augmentation to FBW control, including the same augmentation functions.

The 1990 ACT control functions are:

- FBW, crucial pitch-augmented stability (PAS)
- Critical PAS
- Lateral/directional-augmented stability (LAS)
- Angle-of-attack limiter (AAL)
- Wing-load alleviation (WLA)
- Flutter-mode control (FMC)

Figure G-36 shows the FBW, crucial PAS functional block diagram for the pitch axis. The elevator is commanded according to the pilot's control column position and the aircraft pitch rate. Both the pilot control position and pitch-rate signals are gain scheduled with dynamic pressure (q) as measured by the DADC. The gain is reduced at high dynamic pressures so that a lesser elevator deflection is commanded for a given applied stick force. As a result of this gain schedule, a simple constant spring-gradient feel system may be used.
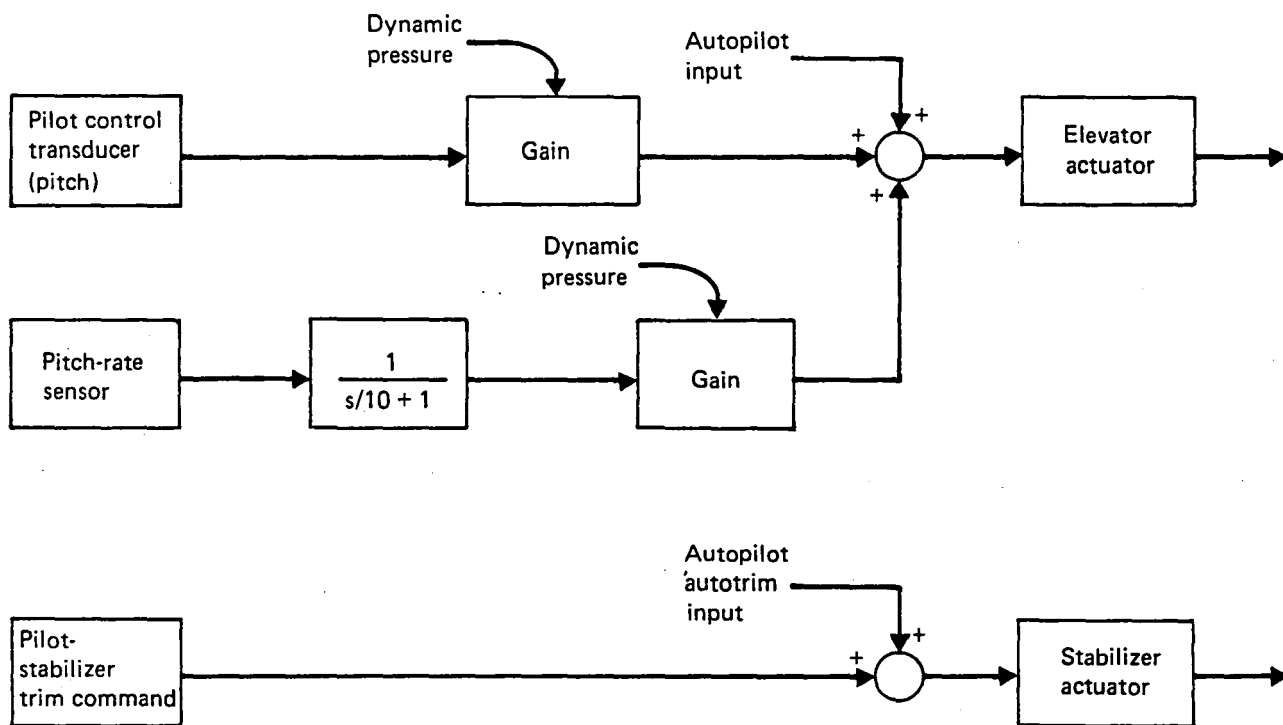
Figure G-36. Fly-by-Wire, Crucial Pitch-Augmented Stability Elevator Control Functional Block Diagram

However, neither the gain schedule of the control column command nor the gain schedule of pitch rate is essential to the realization of a control system that allows safe flight. Loss of the dynamic pressure signal due to a combination of DADC failures is not catastrophic.

The pilot stabilizer trim command is channeled directly to the stabilizer actuator controls, as in the Baseline Configuration control system. Automatic trim, as required for autopilot control, is supplied directly from the autopilot-flight director system.

FBW control in the roll and yaw axes consists of pilot control column and rudder pedal commands to the roll and yaw control surface actuators, respectively. Trim in these axes is provided by an integration of the trim signal commands within the ACT computers.

The 1990 ACT control functions—other than the FBW, crucial PAS—are functionally the same as in the Baseline Configuration ACT system.

Table G-16 shows the ACT sensors and the way they relate to the ACT functions. For example, the air data parameters required for gain scheduling are required for all functions except FBW. The angle-of-attack signal is required for the AAL function only.

Pitch-rate and normal acceleration signals are obtained from the IRS. The IRS is triplex, and dispatch should be possible with one IRS failed. FBW, crucial PAS reliability will be adequate if pitch rate is estimated from normal acceleration. This technique also allows airplane dispatch with one IRS failed. The manner in which the pitch-rate estimation is achieved is described in Section G.6.0.

Table G-17 shows the ACT system matrix relating control surface actuators to control functions. Note that safe flight can be achieved with either the upper or lower rudder actuation system failed and deployed in a damped trail position. Similarly, safe roll control is possible with either the inboard aileron or both outboard aileron surfaces properly controlled. Both right and left elevator surfaces must be controlled properly for safe flight.

Table G-16. ACT Sensor Control Function Matrix

Control mode function	Digital air data computer q,V,M	α	Normal acceleration WLA Left	Right	Normal acceleration FMC Left	Right	Inertial reference system $\dot\theta$	n_z	ϕ	r	Control position transducer Pitch	Roll	Yaw	Slats	Flaps
Fly by wire, crucial PAS							X*	X*			X	X	X		
Critical PAS	X						X				X				
Lateral/directional-augmented stability	X								X	X		X			X
Wing-load alleviation	X		X	X				X							
Flutter-mode control	X				X	X									
Angle-of-attack limiter	X	X					X							X	X

* Either pitch rate or
normal acceleration signal
required for safe flight.

Table G-17. ACT Actuator Control Function Matrix

Control surface	Number of actuators	Function					
		FBW	Critical PAS	AAL	LAS	WLA	FMC
Elevator	6	X	X			X	
Upper rudder	2	X ᵃ			X		
Lower rudder	2	X ᵃ			X		
Outboard aileron outboard	4	X ᵇ				X	
Outboard aileron inboard	4	X ᵇ				X	X
Inboard aileron	4	X ᵇ					
Outboard flaperon	4					X	
Inboard flaperon	4					X	

ᵃEither upper or lower rudder required for safe flight.

ᵇEither inboard aileron or both outboard aileron surfaces are required for safe flight (both left and right wings).

G.5.1.3 1990 ACT SYSTEM COMPONENTS

The 1990 ACT system components are characterized by the use of advanced large-scale integrated circuit (LSIC) technology. As noted in Subsection G.2.2, developments in very-large-scale integrated circuit (VLSIC) and very-high-speed integrated circuit (VHSIC) technologies are expected to allow a full order-of-magnitude improvement in performance for a computing function. Power and weight will be reduced, and the very-large-scale integration will significantly reduce the chip count.

The integrated circuit developments listed below are planned if they are not available as standard circuits. The quantity utilization estimated for the ACT system alone would justify their developments as custom LSIC:

- Switching regulator
- Serial terminal interface
- Bus transceiver
- Demodulator and A/D converter
- A/D, digital-to-analog (D/A) converter and multiplexer
- Analog servoelectronics
- Microcomputer
- Servoamps

The switching regulator input controller (IC) would be used as part of a power supply module, as illustrated in Figure G-37. The switching regulator provides the drive to a switching pass transistor to regulate the output voltage as required. The switching occurs at approximately 120 kHz. Additional discrete parts are added to produce a power supply module with a negative voltage. Similarly, a 2-kHz power supply module is produced by adding a discrete-part oscillator driven by a regulated dc input voltage. Short-circuit protection is provided within the switching regulator IC.

The function of the other LSICs will be described in conjunction with the LRUs in which they are used.
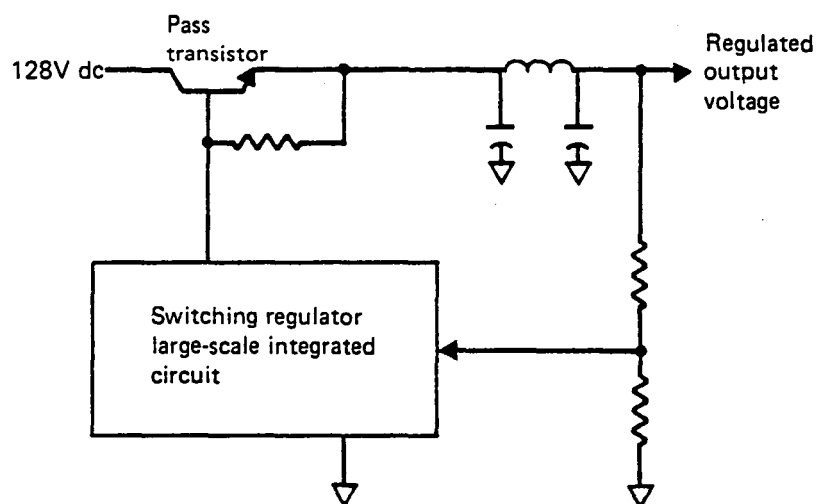
Figure G-37. Power Conditioning Module

Control position transducers sense motions of the pilot control columns and rudder pedals and provide voltages proportional to slat and flap deflection. These transducers are either triple or quadruple redundant depending on the criticality of the function.

The quadruple control position transducers contain four sets of sensor electronics, one for each linear variable differential transformer (LVDT) type of transducer. Four connectors on pigtails are supplied to mate with aircraft connectors. In this way, the four channels of the transducer are electrically isolated and, to a large extent, mechanically isolated from one another.

One-channel sensor electronics is shown in Figure G-38. Four power conditioning modules are supplied so that the required local power supply voltages are realized. Excitation is provided to the LVDT. The LVDT center tapped output is demodulated so that two signals are provided. The difference of these two signals is proportional to the mechanical input to the position transducer. The sum is a signal that remains approximately constant for a properly functioning transducer. These two signals are converted to digital words by the A/D converter and transmitted on the serial data bus by the serial terminal interface and bus transceiver in response to bus controller requests. The triplex control position transducers used to sense flap and slat position operate this way. The only difference is in the number of sensor electronics sets and LVDTs.
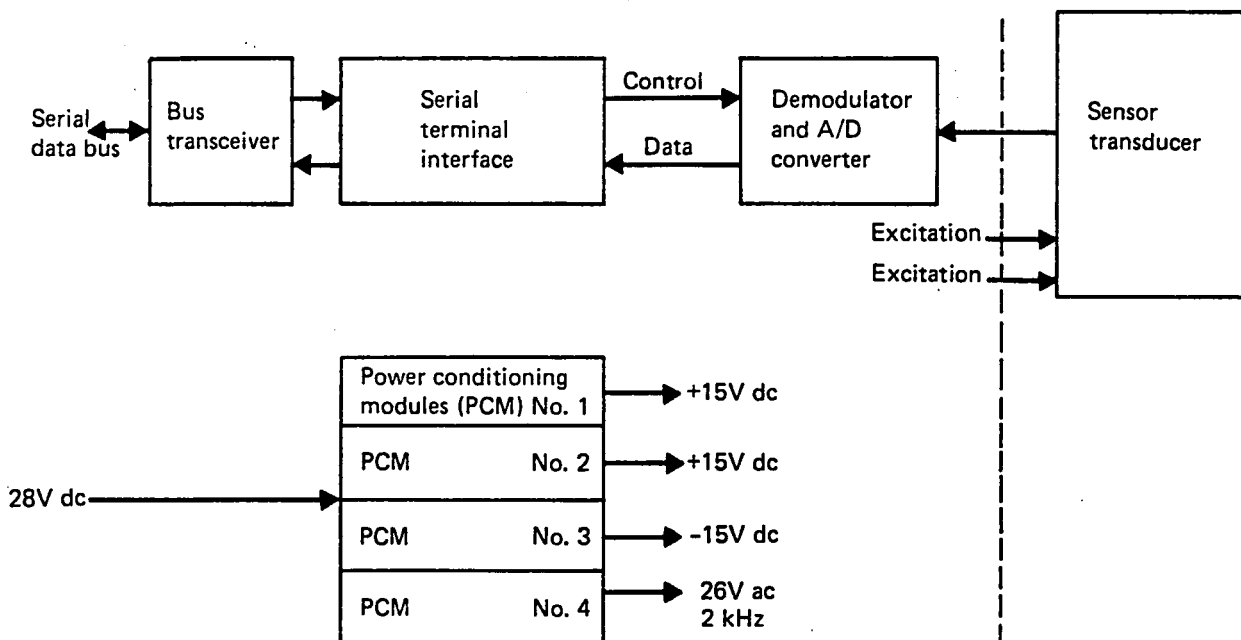
Figure G-38. Sensor Electronics

G-133

Each hydraulic servoactuator, described in Subsection G.4.2, includes a hydraulic servo remote terminal, as shown in Figure G-39. Four power conditioning modules are required, and 26V ac is provided to the three LVDTs required in the actuator. Servo-loop closure is effected by the analog IC as shown. The A/D, D/A, and multiplexer circuit decodes the servo position command and servo state signals, which are passed to the analog IC. The circuit also converts the three LVDTs outputs to digital words for transmittal to the ACT computers for monitoring of the servoactuator.

SDEU interfaces the ACT computers with the EMAs used to drive the flaperons. The SDEU function is shown in Figure G-40. Use of a 16-bit, fixed-point microcomputer integrated circuit, including 1K words of read-only memory (ROM) and 512 words of random-access memory (RAM), is unique in SDEU implementation. The microcomputer is used for actuator monitoring and also for commutating the power to the field of the dc permanent magnet. The field is commutated in accordance with the position error signal, the rotor position signal, and a motor rate signal derived from the rotor position sensor.
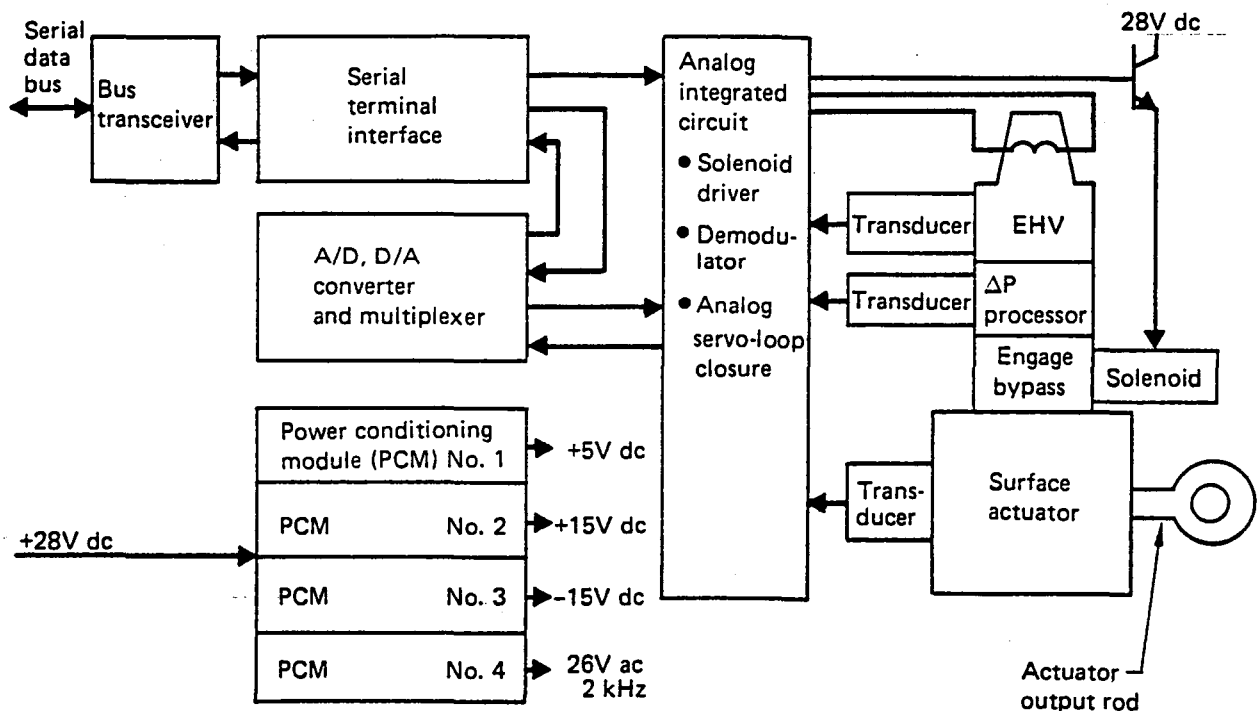
Figure G-39. Hydraulic Servo Remote Terminal
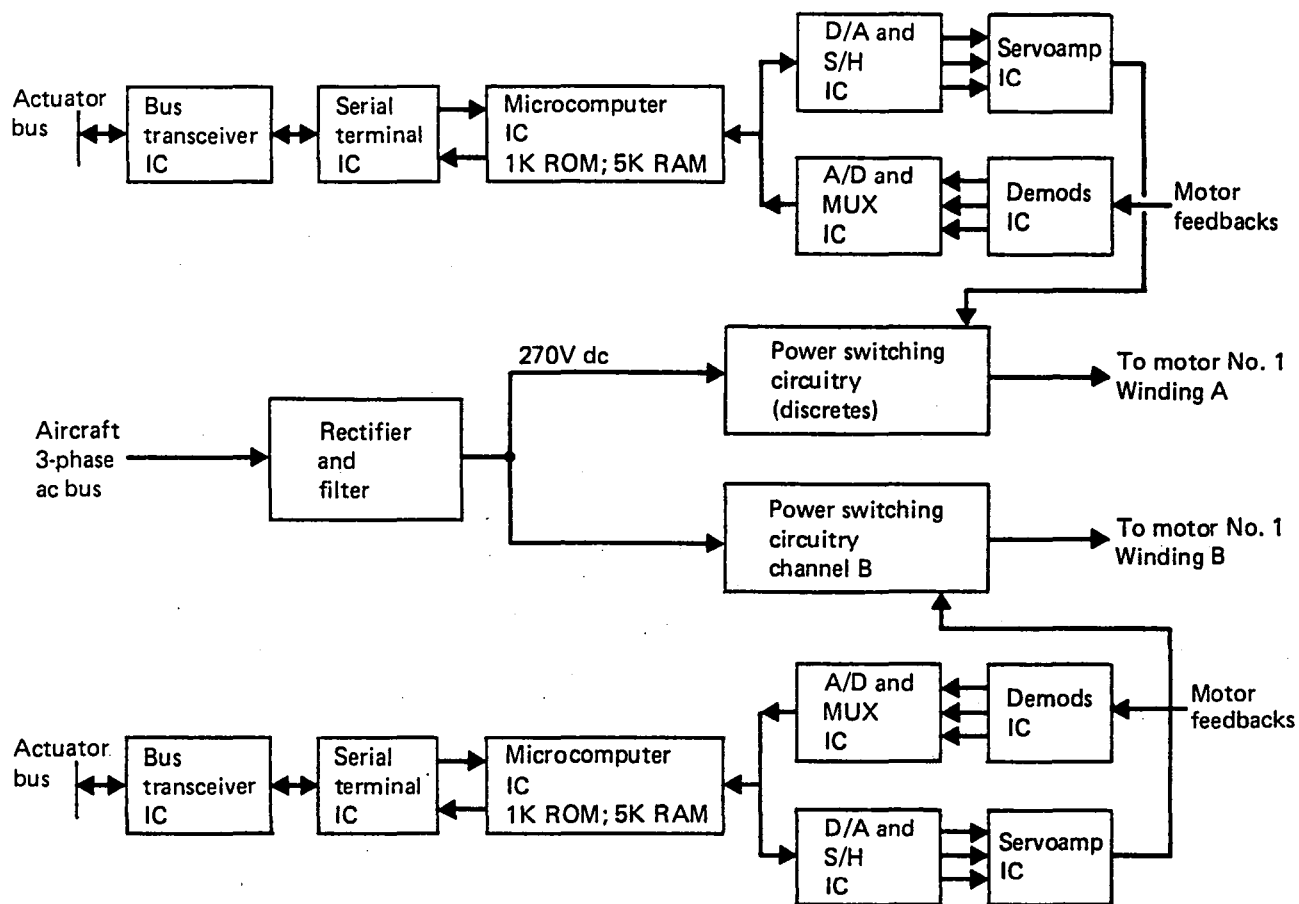
Figure G-40. Servodrive Electronics Unit

In addition to the LSIC shown in Figure G-40, the SDEU contains power supply circuitry associated with the 270V dc power and the high-power circuits necessary to switch this power to the motor.

The ACT computer is shown in Figure G-41. Major functional sections include I/O, control law computing, and redundancy management. A common power supply and clock are provided for all three sections of the ACT computer.

The I/O section includes the input and actuator bus interface circuitry. Input data are received in serial digital data form and converted to parallel data. When data have been received, the DMA controller stores it in memory according to its label and predefined memory location. Data output is accomplished similarly. The DMA controller initiates a
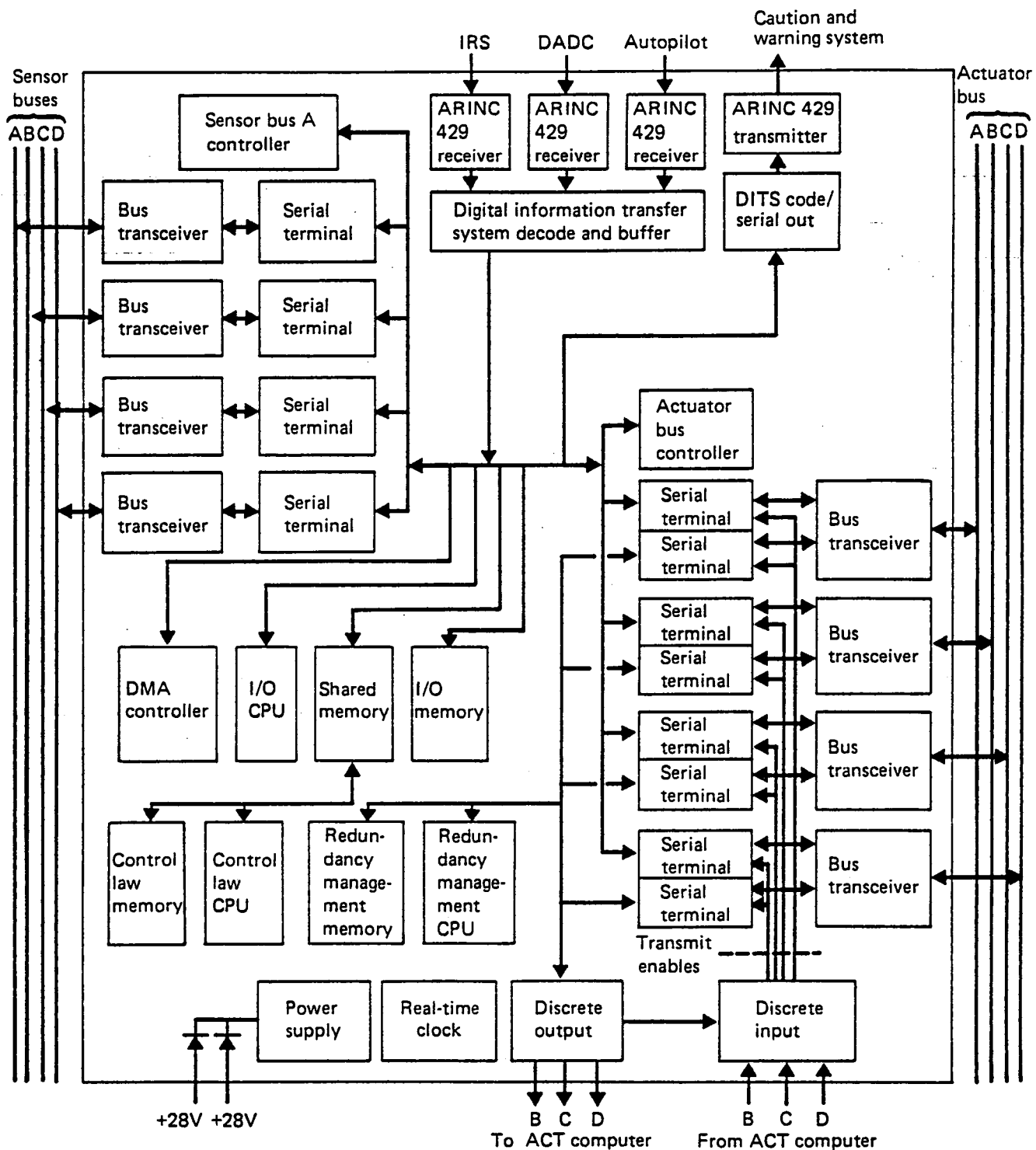
Figure G-41. ACT Computer Block Diagram

fetch from the memory location where the desired output has been stored. The output is passed to the actuator bus or sensor bus serial terminal and bus transceiver ICs to complete the output operation.

Data inputs are of two forms: most inputs are from sensors or actuators associated with the intrasystem buses of the ACT control system. IRS, autopilot, and air data computer signals are input through intersystem buses. ARINC 429 buses, as used today, are assumed for the 1990 ACT intersystem buses.

The I/O central processing unit (CPU) periodically performs comparison monitoring of the input sensor data and sets failure flags as appropriate. The midvalue of the sensor data is defined for each case and stored in the shared memory.

The shared memory interfaces the I/O processor and the control law processor. It is available to one of these processors during the in-phase half-cycle of the computer clock and available to the other during the out-of-phase half-cycle. Memory access time is less than one-half clock period, so the shared nature of the memory is transparent to both processors. A relatively small amount of memory is required here as it is used only for scratchpad to accommodate parameters that must be passed between the two processors.

The control law computer implements the control laws using the midvalue sensor data that have been stored in the shared memory by the I/O processor. The servocommands that result from the control law computations are also stored in the shared memory so the I/O processor has access to the command. The I/O processor periodically outputs the servoactuator command and the sensor failure flag status on the actuator bus.

The redundancy management computer receives the actuator commands from each of the four ACT computers via the actuator buses. It monitors the four commands and ensures that all are correct. The servoactuators are also monitored by the redundancy management computer. Signals necessary for actuator monitoring are received via the actuator buses. The failure status of each actuator is defined. The sensor failure flag output by each I/O processor is also received and analyzed as a part of the overall ACT system failure state assessment.

The redundancy management computer outputs discrete commands to each servo via the servo buses. These discretes command each actuator to be active, online, or bypassed in accordance with the system failure state. It also outputs a system failure status word or words for use by the ACT Maintenance and Display Computer, the ACT discrete display, and the caution and warning system discrete display.

G.5.2 FAILURE MANAGEMENT

Figure G-42 illustrates the redundancy management used in the 1990 ACT system. Quadruple (or triple) sensors are interfaced with quadruple ACT computers by a set of sensor data buses so that each ACT computer has access to all the redundant sensor data. The sensors are monitored, and the actuator commands are computed in the ACT computers operating asynchronously with one another. The actuator commands are output on quadruple actuator buses to hydraulic actuators and EMAs assigned to specific control surfaces. Monitor processors contained within the ACT computers monitor the actuator commands and the actuator performance and effect fault correction, as appropriate.

The sensor bus structures multiplex sensor data to the four ACT computers. There are approximately 20 data inputs to these buses. The transfer rate will approximate 500 samples per second per sensor.

Each bus is similar to a MIL-STD-1553 bus and is controlled by a bus controller located in one of the ACT computers. The bus controller is dependent only on the computer power supply and clock for its proper operation. Highest reliability for each bus and bus controller is of paramount importance.

The fault of a dead controller or a dead terminal (located with each sensor) will be detected by sensor comparison monitoring within the ACT computer and, secondarily, by watchdog-timer-type checks associated with the bus controller.

Parity bit errors will reject specific data transmissions.

Certain sensor data, typified by air data signals, are transmitted to the ACT computers by ARINC 429 type buses. Each of the A, B, and C ACT computers receives data from one
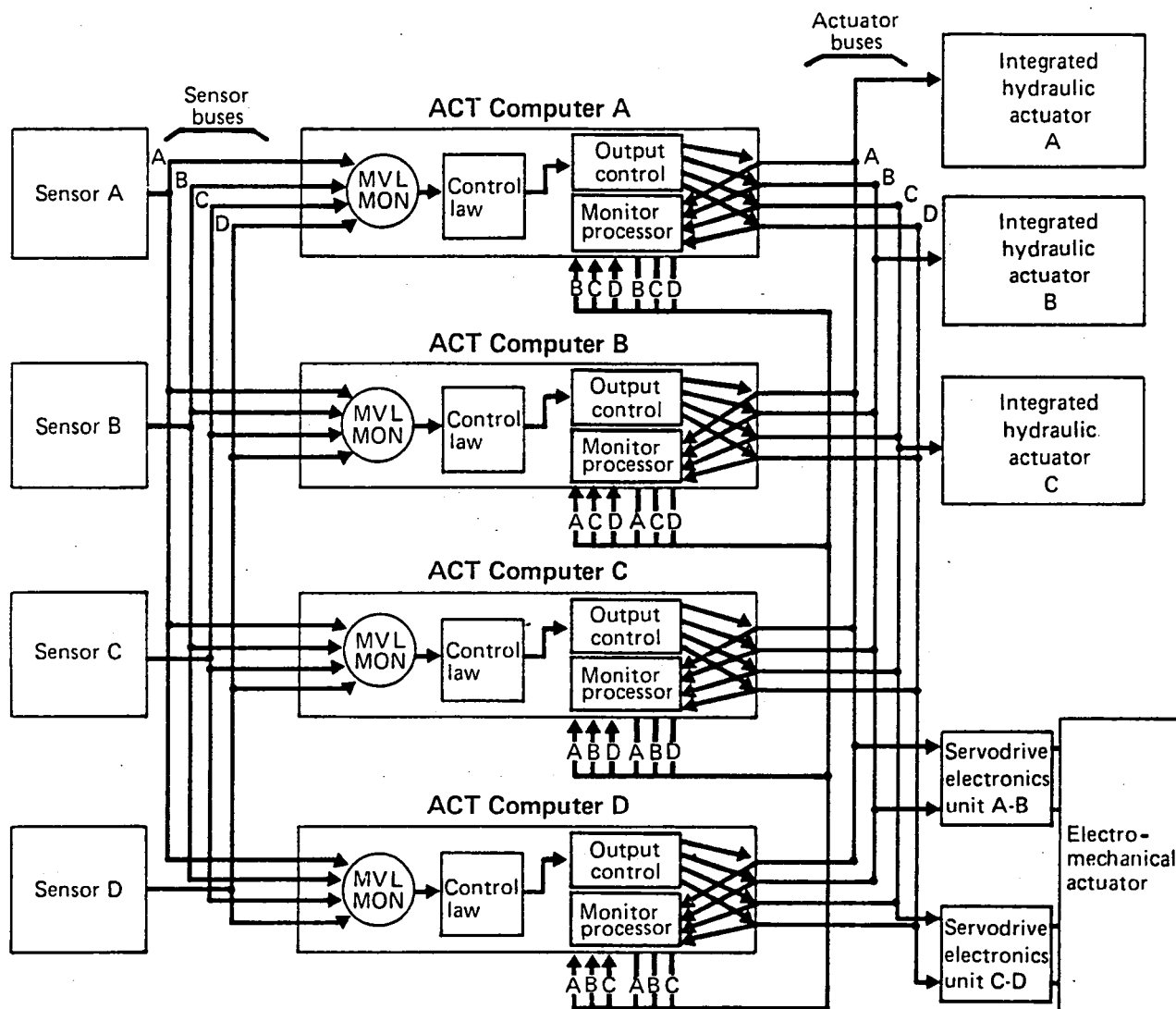
Figure G-42. 1990 ACT System Simplified Redundancy Management Block Diagram

of the three DADCs in this manner at a relatively low sample rate. These data output on the sensor buses by the ACT computers at a rate of 500 samples per second so that each computer has access to all three sets of air data.

The midvalue of the redundant sensor data is determined in each of the four ACT computers. The midvalue of four signals is defined as the average of the two middle signals. When only two sensors are valid, their average is determined in lieu of a midvalue.

The sensor data are compared across channels. Miscompares detect sensor failures and isolate the fault whenever possible. When a miscompare of two valid sensors occurs, fault isolation is not attempted in the case of most sensors. Both sensors are presumed failed and the ACT system continues to function in a degraded state, normally discontinuing the function associated with the failed sensor type. The pilot command transducer and pitch-rate signals, which are essential to safe flight, are treated differently.

If faults occur in the quadruply redundant pilot command transducers so that a miscompare of only two remaining signals occurs, a sensor validity signal identifies the good sensor. Safe flight is continued using this single good sensor. The sensor validity signal is obtained by means of circuitry, which takes the sum and difference signals formed when the LVDT secondary center tap is grounded. The difference signal is proportional to the transducer signal; the sum remains nearly constant for a properly functioning transducer.

The pitch-rate signal is compared not only with the other pitch-rate signals but, following a sequence of failures, is also compared with an estimated pitch-rate signal based on normal acceleration and other signals. Failure management is described in Section G.6.0.

The control laws compute the servoactuator commands in each ACT computer. Because asynchronous computation is involved, the servocommands computed by the four ACT computers will not agree precisely. Channels are equalized by noting the difference between a particular ACT computer servocommand and that associated with the active channel.

Each ACT computer is assigned a particular bus on which it outputs the servocommands. The monitor processor compares the servocommands as issued on each bus. Faulty servocommands are detected and isolated by the monitor processor using comparison monitoring techniques. If three computer failures ever occur, the third computer failure is isolated by the computer self-test. The computer self-test confidence is greater than 95%. Single-channel operation is permitted following a third computer failure because there is not an apparent better alternative.

Following the detection and isolation of a computer fault, failure correction must be effected by a reassignment of the actuator buses. Table G-18 shows the computer failure

states. Computer serial-terminal-transmit-enable discretes are used to effect this logic. The logic discretes are a function of the system status as determined by all the operable monitor processors collectively.

Failure of a computer may be caused by a failure of the I/O computing section, the control law computer, or the power supply or ACT computer clock. I/O computing can still output a satisfactory set of commands to the actuator bus if the monitor processor fails.

Failures are isolated to the I/O section, the control law section, or the power supply or clock through self-test features described in Subsection G.2.2. If the control law section fails, that ACT computer will reconfigure so that the I/O section monitors and midvalue selects only the crucial sensor inputs. Thus, adequate time is made available for the I/O processor to perform the FBW, crucial PAS control calculations. The ACT computer will stay in a hot-spare state until the system reaches such a failure state that only the FBW, crucial PAS is functional. At that time, it is automatically returned to an active control status. The result of this reconfiguration strategy is that the control law computing section is not required for safe flight; the system flight safety reliability is improved.

Table G-18. ACT Computer Assignment to Actuator Buses

Computers failed	Actuator bus			
	A	B	C	D
None	A	B	C	D
A	B	B	C	D
B	A	A	C	D
C	A	B	D	D
D	A	B	C	C
A, B	C	D	C	D
A, C	B	B	D	D
A, D	B	B	C	C
B, C	A	A	D	D
B, D	A	A	C	C
C, D	A	B	A	B
A, B, C	D	D	D	D
A, B, D	C	C	C	C
A, C, D	B	B	B	B
B, C, D	A	A	A	A

Computer assigned to actuator bus

The servoactuator position commands are transmitted to the individual actuators by the actuator buses with bus-actuator assignments, as shown in Figure G-35. Actuator feedback signals are returned to the monitor processors over the actuator buses. Each actuator is modeled by the monitor processors, as described in Subsection G.4.2. As failures of the actuators occur, they are detected by the monitor processors, and the failed actuators are disengaged (bypassed). If an active actuator is disengaged, an online actuator is made active. The active, online, disengaged status discretes are transmitted to each actuator by one of the monitor processors.

G.5.3 SYSTEM RELIABILITY

In this subsection, the system failure probability is computed as it relates to flight safety and to the loss of any of the ACT functions. Dispatch reliability is also considered.

The probability of any failure that might require a maintenance action is covered in Subsection G.5.4, "Cost-of-Ownership Data."

G.5.3.1 PRELIMINARIES

Failure rates taken down to the level necessary for the desired reliability calculations are shown in Table G-19. These failure rates were estimated as the average rate over a 30 000-hr life for the sensors, actuators, and computing electronics. The aircraft electric and hydraulic system failure rate was derived from Reference G-21.

The structure of the 1990 ACT system is such that the calculation of failure probability can be conveniently separated into three parts:

- Sensors and sensor bus
- ACT computers
- Actuators and actuator bus

Tables G-20, G-21, and G-22 show simplified failure effects matrices that aid in writing the system failure probability equations. They show the effect of a number of similar faults on the operability of the various functions. Where no entries are found in the table, failures of the particular element have no effect on the availability of that function; i.e., that function does not require that element.

G-142

Table G-19. Failure Rates for 1990 ACT System Elements

Element	Symbol	Per-channel failure rate $\times 10^{-6}$ (per hour)
Sensor bus and controller	λ_{SB}	1
Pilot command, slat, flap, transducers	λ_X	5
Pitch rate (IRS source)	λ_q	30
Normal acceleration (IRS source)	λ_{nz}	22
Yaw rate (IRS source)	λ_r	30
Bank angle (or IRS fail)	λ_{IRS}	250
Accelerometer (WLA or FMC)	λ_A	22
Air data computer	λ_{ADC}	80
Computer power supply and clock	λ_{PS}	3
Input/output section	$\lambda_{I/O}$	40
Control law computation	λ_{CL}	30
Monitor computation and redundancy management	λ_M	55
Actuator bus	λ_{AB}	1
Hydraulic servoactuator	λ_H	50
Servodrive electronics unit (per channel)	λ_{SDEU}	13.5
Electromechanical actuator, electrical (four per actuator)	λ_{EMAE}	44
Electromechanical actuator, mechanical (two per actuator)	λ_{EMAM}	44
Hydraulic power source	λ_{HPS}	28.6
Electric power source	λ_{EPS}	0

Table G-20. Simplified Failure Effects Matrix, Sensors

Failed ACT element	Number of similar faults	FBW, crucial PAS	Critical PAS	LAS	WLA	FMC	AAL
Sensor buses	1	I	I	I	I	I	I
	2	I	O	O	O	O	O
	3	I	O	O	O	O	O
	4	O	O	O	O	O	O
Pilot command transducers	1	I	I	I			
	2	I	I	I			
	3	I	I	I			
	4	O	O	O			
Pitch rate, normal acceleration (IRS)	1	I	I				I
	2	I	O				O
	3	I	O				O
	4	O	O				O
Normal acceleration — Left and right WLA	1				I		
	2				O		
	3				O		
Normal acceleration — Left and right FMC	1					I	
	2					O	
	3					O	
Normal acceleration — Center of gravity (IRS)	1				I		
	2				O		
	3				O		
IRS, r, ϕ	1			I			
	2			O			
	3			O			
Air data — q, Ve, h, M	1		I	I	I	I	I
	2		O	O	O	O	O
	3		O	O	O	O	O
Air data — α	1						I
	2						O
	3						O
Slat, flap transducers	1			I			I
	2			O			O
	3			O			O

Legend:
I   function operative
O   function inoperative

Table G-21. Simplified Failure Effects Matrix, ACT Computers

Failed section	Number of similar faults	Function					
		FBW, crucial PAS	Critical PAS	LAS	WLA	FMC	AAL
Power supply—clock	1	I	I	I	I	I	I
	2	I	I	I	I	I	I
	3	I	O	I	O	O	O
	4	O	O	O	O	O	O
I/O section	1	I	I	I	I	I	I
	2	I	I	I	I	I	I
	3	I	O	I	O	O	O
	4	O	O	O	O	O	O
Control law computing	1	I	I	I	I	I	I
	2	I	I	I	I	I	I
	3	I	O	I	O	O	O
	4	I	O	O	O	O	O
Monitor computing	1	I	I	I	I	I	I
	2	I	I	I	I	I	I
	3	I	I	I	I	I	I
	4	O	O	O	O	O	O

Legend:

I   function operative
O   function inoperative

Table G-22. Simplified Failure Effects Matrix, Actuators

Control surface	Number of similar failures	Function					
		FBW, crucial PAS[a]	Critical PAS	LAS[b]	WLA	FMC	AAL
Actuator bus	1	I	I	I	I	I	
	2	I	I	I	I	O	
	3	O	O	O	O	O	
	4	O	O	O	O	O	
Elevator actuator, left or right	1	I	I		I		
	2	I	I		I		
	3	O	O		O		
Rudder actuator upper or lower	1	I		I			
	2	O		O			
Aileron — Inboard	1	I					
	2	O					
Aileron — Inboard Outboard	1	I			I	I	
	2	O			O	O	
Aileron — Outboard Outboard	1	I			I		
	2	O			O		
Flaperon	1				I		
	2				I		
	3				O		
	4				O		
Hydraulic system	1	I	I	I	I	I	
	2	I	I	I	I	O	
	3	O	O	O	O	O	

● Failures presumed to occur in order of A, B, C, D for actuator bus and hydraulic system.

I   function operative
O   function inoperative

[a] Both left and right elevator control required, either inboard aileron or both outboard aileron segments control required, either upper or lower rudder control required.

[b] Both rudder segments control required.

The tables were prepared assuming the failures occur in the order A, B, C, and then D. For example, in Table G-20, the first sensor bus failure is of the A bus. The fourth is of the D bus. The D bus is the one that carries only the crucial sensor signals. If it were to fail first, it would have no effect on the operability of the critical ACT functions. A second servo bus failure would then result in all the critical ACT functions being operable.

Combinations of failures of different elements in a given channel are not considered, but these effects must be included in the failure equations.

Table G-23 shows the relationship between the ACT functions and the dispatchability of the aircraft and the manner in which flight restrictions are applied as functional capabilities are lost. Information in Table G-23 was obtained from Table 16 (vol. I).

G.5.3.2   FUNCTIONAL RELIABILITY

G.5.3.2.1   Loss of FBW, Crucial PAS

The equations for computing the probability of failure of the FBW and crucial PAS functions of the ACT system are shown in Table G-24. Results of the calculations using the failure rates of Table G-19 are shown as follows.

Table G-23. Dispatch and Flight Restriction Requirements

Function	Flight restriction associated with function loss	Dispatch with function loss	Additional dispatch requirements
FBW			Failure probability $< 10^{-9}$/hr
Critical PAS	A	Yes	Flight restriction A will apply when one more failure could result in loss of PAS function
LAS	B	No	Flight restriction B will apply when one more failure could result in loss of LAS function
WLA	None	No	—
FMC	C	Yes	—
AAL	None	No	—

Flight diversion required for combined loss of critical PAS, LAS, and WLA.

Element	Failure situation	Equation
Sensors	Failure occurs if four pilot-control transducers fail or two pitch-rate signals and two normal acceleration signals fail	$Q_{SENSORS} = 6Q_X^4 + 9Q_q^2 \, Q_{n_z}^2 + (Q_{SB} + Q_{PS})^4$
Computers	Failure occurs if three I/O computers fail and self-test does not indicate failed computer (95%) or if four monitor computers fail	$Q_{COMPUTING} =$ $4Q_{I/O}^3 \, (1 - 0.95) + Q_M^4 + Q_{PS}^4$ $+ 4Q_{PS}^3 \left(Q_{I/O} + Q_M \right)$ $+ 6Q_{PS}^2 \left[Q_{I/O} \, (1 - 0.95) + Q_M^2 \right]$ $+ 4Q_{PS} \left[Q_{I/O}^2 \, (1 - 0.95) + Q_M^3 \right]$
Actuators	Failure occurs if four of four rudder actuators fail, or three of three right elevator actuators fail, or three of three left elevator actuators fail, or two of two inboard aileron and two of two outboard aileron inboard section fail, or two of two outboard aileron outboard sections fail	$Q_{ACTUATORS} =$ $Q_H^4 \ (\text{rudder}) + 2Q_H^3 \ (\text{elevator}) +$ $2Q_H^2 \left(Q_H^2 + Q_H^2 \right) (\text{aileron}) +$ $\left(Q_{AB} + Q_{HPS} \right)^3 + \left(Q_{AB} + Q_{HPS} \right)^2$ $\left(12Q_H + 7Q_H^2 \right)$ $+ \left(Q_{AB} + Q_{HPS} \right) \left(12Q_H^2 + 10Q_H^3 \right)$

$Q = \lambda t$, where Q = failure probability
λ = failure rate
t = mission time

Probability of FBW, Crucial PAS Failure Function

	1-hr flight	4-hr flight
Sensor	4.04×10^{-18}	1.03×10^{-15}
Computing	1.39×10^{-14}	890.4×10^{-15}
Actuation	1.69×10^{-12}	108.16×10^{-12}
System	1.70×10^{-12}	109.0×10^{-12}

G.5.3.2.2 Loss of Normal Mode

The equations for computing the probability of loss of any of the ACT functions are shown in Table G-25. The results of the calculations are shown as follows.

Probability of Loss of Any ACT Function

	1-hr flight	4-hr flight
Sensors	2.15×10^{-7}	3.45×10^{-6}
Computing	1.56×10^{-12}	99.6×10^{-12}
Actuation	5.4×10^{-8}	865.0×10^{-9}
System	2.70×10^{-7}	4.312×10^{-6}

Table G-25. Failure Probability Equations, 1990 ACT—All Control Functions

Element	Failure situation	Equation
Sensors	Failure occurs if four command transducers fail, or two: • Slat or flap transducers fail • Pitch-rate signals fail • WLA accelerometers fail • FMC accelerometers fail • IRS fails • ADC fails • Two of sensor buses A, B, or C fail	$Q_{SENSORS} =$ $6Q_X^4 + 120Q_X^2 + 120Q_A^2 + 3Q_{IRS}^2$ $+ 3Q_{ADC}^2 + 3(Q_{SB} + Q_{PS})^2$ $+ 6(Q_{SB} + Q_{RS})(4Q_X + 4Q_A + Q_{IRS} + Q_{ADC})$
Computing	Failure occurs if three power supply/clocks fail or three control law computing sections fail, or four monitor computers fail	$Q_{COMPUTING} =$ $4Q_{PS}^3 + 4(Q_{I/O} + Q_{CL})^3 + Q_M^4$ $+ 12Q_{PS}^2 \left[Q_{I/O} + Q_{CL} + Q_M^2\right]$ $+ 12Q_{PS}\left[(Q_{I/O} + Q_{CL})^2 + Q_M^3\right]$
Actuators	Failure occurs if two of two upper or lower rudder actuators fail, or two of three right or left elevator actuators fail, or two of two right or left outboard ailerons outboard fail, or two of two right or left outboard ailerons inboard fail, or two of two right or left inboard ailerons fail, or two of three actuator bus or hydraulic power sources fail, or three of four EMA electric channels fail for either right or left inboard or outboard flaperons	$Q_{ACTUATORS} =$ $2Q_H^2 + 8Q_H^2 + 3(Q_{AB} + Q_{HPS})^2$ $+ (Q_{AB} + Q_{HPS}) \times 16Q_H$ $+ 4\left[4(Q_{SDEU} + Q_{EMAE})^3 + Q_{EMAM}^2\right]$ $+ 6Q_{AB}^2\left[4(Q_{SDEU} + Q_{EMAE})\right]$ $+ 4Q_{AB}\left[4(Q_{SDEU} + Q_{EMAE})^2\right]$

$Q = \lambda t$, where Q = failure probability
λ = failure rate
t = mission time

G.5.3.3 DISPATCH RELIABILITY

Dispatch was examined for the following cases:

- One ACT computer failed
- One IRS failed
- One air data computer failed
- One aileron actuator failed
- Flaperon EMA, SDEU, or FMC accelerometers

G.5.3.3.1 ACT Computer

The airplane can be dispatched with one ACT computer failed. The probability of functional failure of the remaining ACT computers during a 2-hr flight is:

- 2.6×10^{-10} for crucial functions
- 1.6×10^{-8} for critical functions

It is assumed that a sensor bus controller function is not lost as a result of the ACT computer failure.

G.5.3.3.2 Inertial Reference System

Loss of either a pitch-rate signal or an accelerometer signal would result in the crucial function sensor failure rate being dominated by the term associated with pitch rate and normal acceleration. This sensor failure rate term would be:

$$Q_{SENSOR} \text{ (due to } q + n_z) \leqslant 3 \, Q_q^2 \, Q_{nz} \text{ or } 3 \, Q_q q_{n_z}^2$$

$$Q_{SENSOR} \leqslant 8.1 \times 10^{-14} \text{ (1-hr flight)}$$

(This is explained in more detail in Section G.6.0.)

A failure of one IRS does not cause the loss of any critical ACT functions, but the probability of loss of function of LAS becomes approximately 5×10^{-4} during a 1-hr flight. This is the probability of either of the two remaining IRSs failing.

G.5.3.3.3 Air Data Computer

A failure of one of three air data computers does not result in any functional loss. However, the probability of loss of the ACT functions requiring air data signals becomes 1.6×10^{-4} during a 1-hr flight.

The loss of any one sensor of types other than the IRS or air data computer would not preclude airplane dispatch.

G.5.4 COST-OF-OWNERSHIP DATA

Cost of model input data is provided in this subsection. These data were prepared to allow Boeing to compute the cost of ownership for the 1990 ACT system. Cost-of-ownership data are presented in Tables G-26 and G-27.

Table G-26. Line Replaceable Unit Cost and Reliability Data

	A	B	C	D	E
Component	Quantity per shipset	MTBF (LRU)	MTBUR	Spares per airplane	LRU weight, kg (lb)
Flight control computer	4	7 674	2 257	5	5.4 (12.0)
Servodrive electronics unit	8	37 000	10 882	4	6.35 (14.0)
Sensors Control position transducer					
● Pitch	2	50 000	14 706	3	0.9 (2.0)
● Roll	2	50 000	14 706	3	0.9 (2.0)
● Yaw	2	50 000	14 706	3	0.9 (2.0)
● Stabilizer	1	50 000	14 706	3	0.9 (2.0)
● Slat position	2	66 666	19 608	3	0.7 (1.5)
● Flap position	2	66 666	19 608	3	0.7 (1.5)
Accelerometer, wing FMC	2	15 150	4 456	3	0.9 (2.0)
Accelerometer, wing WLA	2	15 150	4 456	3	0.9 (2.0)
Servos Electromechanical, flaperon	4	3 773	1 110	7	21.8 (48.0)
Electrohydraulic					
● Outboard aileron inboard	2	10 000	2 941	4	5.08 (11.2)
● Elevator	6	20 000	5 882	4	4.72 (10.4)
● Rudder	4	20 000	5 882	4	7.98 (17.6)
● Outboard aileron outboard	4	20 000	5 882	4	2.77 (6.1)
● Inboard aileron	4	20 000	5 882	4	3.45 (7.6)

Table G-27. Maintenance Labor and Materials

Component	A Removals per flight hour	B Maintenance hour per flight hour Line	C Maintenance hour per flight hour Shop	D Dollars per flight hour Line	E Dollars per flight hour Shop	F Dollars per flight hour Material
ACT computer	0.000443	0.15	1.25	0.002	0.017	0.0155
Servodrive electronics unit	0.000092	0.15	1.25	0.0004	0.0034	0.0032
Sensors						
Control position transducer				0.0005	0.0026	0.0024
• Pitch	0.000068	0.25	1.25	0.0005	0.0026	0.0024
• Roll	0.000068	0.25	1.25	0.0005	0.0026	0.0024
• Yaw	0.000068	0.25	1.25	0.0005	0.0026	0.0024
• Stabilizer	0.000068	0.25	1.25	0.0005	0.0026	0.0024
• Slat position	0.000051	0.25	1.25	0.0004	0.0019	0.0018
• Flap position	0.000051	0.25	1.25	0.0004	0.0019	0.0018
Accelerometer, wing FMC	0.000224	0.25	1.25	0.0017	0.0084	0.0078
Accelerometer, wing WLA	0.000224	0.25	1.25	0.0017	0.0084	0.0078
Servos						
Electromechanical, flaperon	0.0009	0.5	1.25	0.0135	0.0338	0.0315
Electrohydraulic						
• Outboard aileron inboard	0.00034	0.5	1.25	0.0051	0.0128	0.0119
• Elevator	0.00017	0.5	1.25	0.0026	0.0064	0.006
• Rudder	0.00017	0.5	1.25	0.0026	0.0064	0.006
• Outboard aileron outboard	0.00017	0.5	1.25	0.0026	0.0064	0.006
• Inboard aileron	0.00017	0.5	1.25	0.0026	0.0064	0.006

The spoiler actuators, flap actuators, air data computer, IRS and caution and warning system, ACT Maintenance and Display Computer, and dedicated ACT panel are considered either associated equipment or unchanged from the Baseline Configuration. Table G-27 shows the maintenance cost estimate.

Maintenance manual preparation cost is estimated at $547 000. These costs are prorated across 10 airlines assumed to buy fleets of 30 aircraft each ($55 000 per airline). "Line Operational Check and Maintenance" handbooks, "Intermediate and Depot Fault Isolation Repair and Overhaul" manuals, and "Illustrated Parts Breakdown" manuals are included.

The cost for developing and conducting a training course consisting of 16 hr of flight-line operation training and 40 hr of shop training is $17 000. This number is applicable to training as an investment cost.

The cost per airline for additional 56-hr training classes is $2900. Assuming a requirement of 2.5 classes per year for the first 5 years results in a yearly cost of $7500. Only one class per year would be anticipated after 5 years ($2900 per year).

All LRUs of the ACT system can be tested on general-purpose automatic test equipment (ATE) procured separately by the airlines. Software costs for the ATE are estimated at $10 000 per airline assuming that the ATE program requires only minor diagnostic sequence additions to the factory-test ATE software.

This Page Intentionally Left Blank

G.6.0 IAAC PITCH-RATE OBSERVER

G.6.0 IAAC PITCH-RATE OBSERVER

The reliability specifications for the IAAC 1990 contract require that the probability of a catastrophic failure be less than 1×10^{-9}. This specification, the crucial failure requirement, dictates a sensor failure probability budget of 1×10^{-10}. (This is a conservative number; the estimated order of magnitude is the key design parameter.)

The open-loop aircraft is statically unstable; therefore, the pitch-rate signal in the Boeing control law (fig. G-43) is the crucial sensed output. To reduce costs, sensors should be shared with the inertial reference system (IRS), which is manufactured by Honeywell.

Although the IRS provides three accurate pitch-rate signals from ring laser gyros (RLG), three sources are not enough to meet the crucial specification. Triplex voting provides a catastrophic failure probability of

$$P_F = 3\lambda^2_Q - 2\lambda^3_Q \text{ (estimate for 1 hr)}$$

$$\lambda_Q = 30 \times 10^{-6} \text{ RLG failures/hr}$$

Therefore

$$P_F \cong 3\lambda^2_Q = 8.1 \times 10^{-9}$$

Eight gyro status signals provide about 95% coverage on self-test. The failure probability then becomes

$$P_F \cong \lambda^3_Q + 3\lambda^2_Q (1-C) - 3\lambda^3_Q(1-C)$$

where

$$C \overset{\Delta}{=} \text{coverage, } 0 < C < 1$$

for $C = 0.95$

$$P_F \cong 3\lambda^2_Q(0.05) = 4.05 \times 10^{-10}$$

$$\delta_E = \delta_{EO} + \delta_{EI}$$

$\bar{q} > 9576\ Pa\ (200\ lb/ft^2),\ KQ = 2.0$

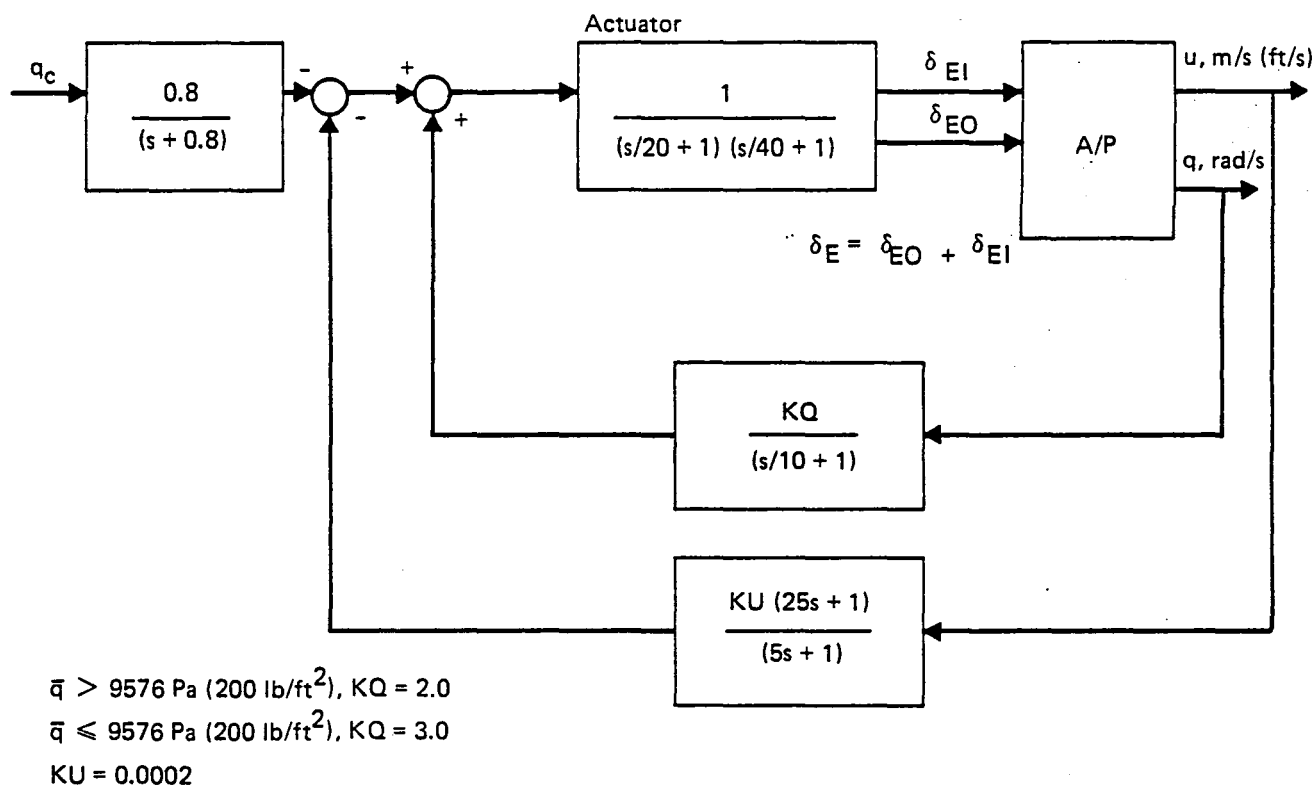$\bar{q} \leqslant 9576\ Pa\ (200\ lb/ft^2),\ KQ = 3.0$

$KU = 0.0002$

Figure G-43. IAAC Pitch-Augmented Stability

This is close to the budget of 1×10^{-10} and probably would be acceptable. However, the airlines would like to dispatch an airplane from a remote location (a route stopover without maintenance facilities) with one failed component. This desire dictates dispatching with only two IRS pitch-rate signals. The failure probabilities for meeting the crucial specification with only dual sensors do not come close to compliance.

One software technique makes optimum use of the IRS to provide the extra missing signals. Because the IRS contains triplex accelerometers, the possibility can be explored of using normal acceleration (n_z) in the crucial flight control system in lieu of failed pitch-rate gyros.

The design constraints of a pitch-rate observer from normal acceleration, assumed at the outset, are:

●   A simple design is desired for maximum reliability; i.e., minimum order with minimum sensor inputs.

- IRS sensors have superior noise characteristics; therefore, a minimum variance design is a secondary consideration.

- The closed-loop design must meet a root locus specification, as shown in Figure G-44. Gain and phase margin specifications are:

  - Low frequency (phugoid), $\omega < 0.05$ rad/s
    - Gain margin = ± 4 dB
    - Phase margin = 20 deg

  - High frequency (short period), 0.05 rad/s $< \omega <$ bending frequencies
    - Gain margin = ± 6 dB
    - Phase margin = ± 45 deg

G.6.1 REDUCED ORDER LUENBERGER OBSERVER

To demonstrate the feasibility of the observer concept, a design at one flight condition was modeled. The objective was to duplicate the closed-loop performance of the Boeing design (fig. G-43) with an n_z feedback (estimating q) in lieu of actual pitch rate. The chosen flight condition and aircraft model are displayed in Figure G-45.

Although the model includes the phugoid dynamics, the design was modeled only on the short-period representation plus a first-order actuator ($w_c = 20$ rad/s). Using Honeywell's eigenspace placement software, a second-order observer was designed. Observer poles were placed at 7 and 15 rad/s. Implementation of the resulting design is shown in Figures G-46 and G-47.

G.6.2 DESIGN RESULTS

Closed-loop roots for both the Boeing and the observer designs are shown in Table G-28. Figure G-48 shows the stability margins for the Boeing control law; Figure G-49 shows a transient response to a step command. Figure G-50 shows the stability margins for the observer in the loop, and the observer design step response is shown in Figure G-51. Pitch-rate observer performance is shown in Figure G-52. Design results, in summary, are:
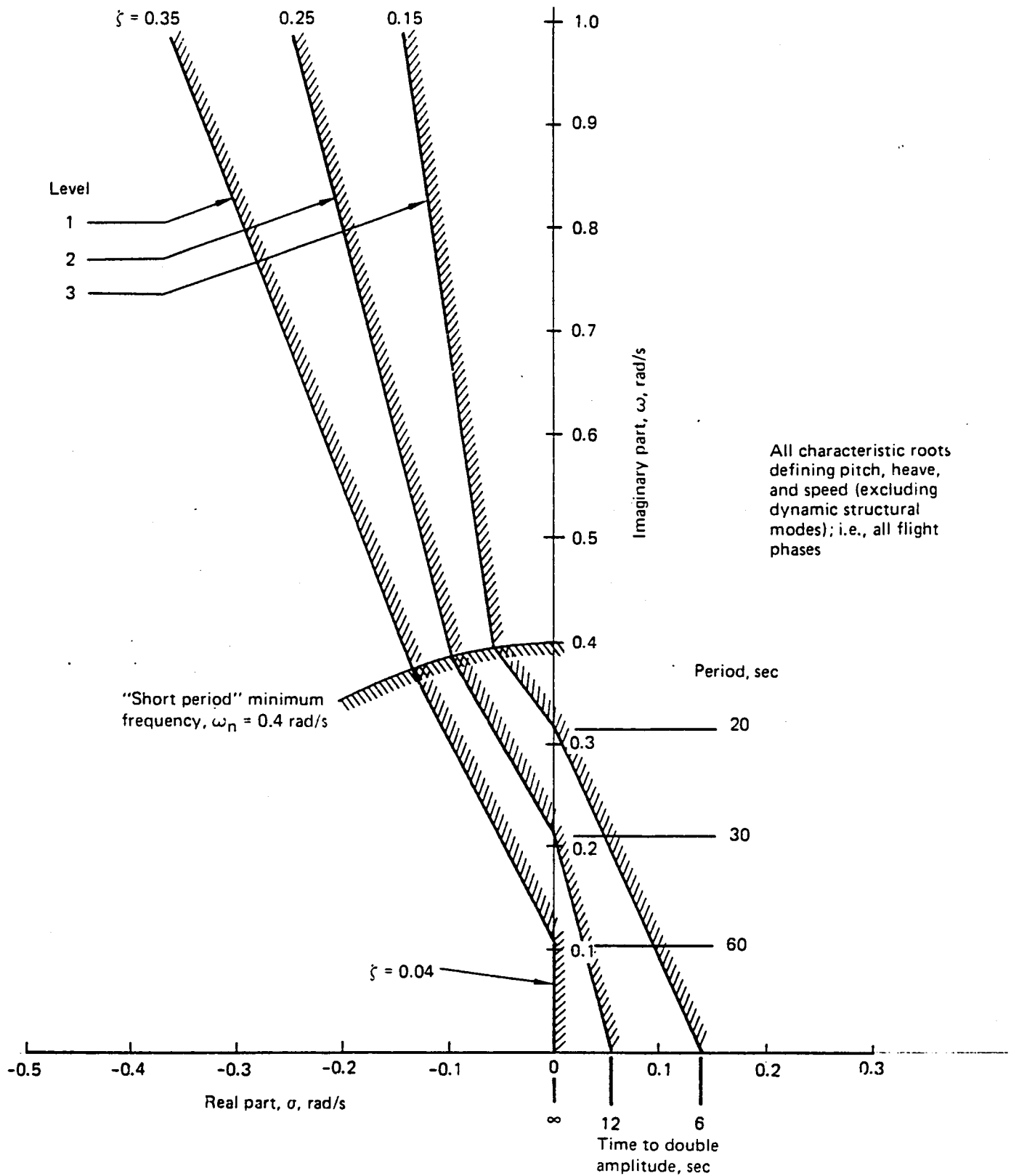
Figure G-44. Minimum Damping Requirements—Longitudinal Roots

- Some high-frequency gain margin is sacrificed using the n_z feedback, but the result (8 dB) is still within specification.

- The roots for both designs are well within specifications.

- The transient responses are very close (to 10 sec), which indicates that for this condition, at least, the flight can continue unrestricted.

- A plot of actual pitch rate versus estimated q (fig. G-52) indicates a good high-frequency match, but less than perfect low-frequency comparison. This agrees with the high-frequency (short-period) design philosophy.

Flight Condition 8, Altitude = Sea Level, V_T = 128.7 m/s (422.1 ft/s)

Using state-space differential equations
$$\dot{x} = Ax + Bu$$
where
- x is the state vector
- u is the control vector
- A is the state coupler matrix
- B is the control coupler matrix

a. Short-period and phugoid modes (for use with control laws)

$$A = \begin{bmatrix} -5.89 \times 10^{-3} & 3.37 \times 10^{-1} & -2.71 \times 10^1 & -3.21 \times 10^1 \\ -2.08 \times 10^{-4} & -8.65 \times 10^{-1} & 9.80 \times 10^{-1} & -4.99 \times 10^{-3} \\ -3.75 \times 10^{-5} & 8.32 \times 10^{-2} & -6.61 \times 10^{-1} & 0 \\ 0 & 0 & 1.00 & 0 \end{bmatrix} \quad ; B = \begin{bmatrix} 1.34 \\ -4.83 \times 10^{-2} \\ -1.74 \\ 0 \end{bmatrix}$$

$$x^T = (u, a, q, \theta); u = \delta_E$$

b. Observer design model (includes 20-rad/s actuator)

$$A = \begin{bmatrix} -8.65 \times 10^{-1} & 9.79 \times 10^{-1} & -4.83 \times 10^{-2} \\ 8.32 \times 10^{-2} & -6.61 \times 10^{-1} & -1.74 \\ 0 & 0 & -2.00 \times 10^1 \end{bmatrix} \quad ; B = \begin{bmatrix} 0 \\ 0 \\ 2.00 \times 10^1 \end{bmatrix}$$

$$x^T = (a, q, \delta e); u = \delta_{E_c}$$

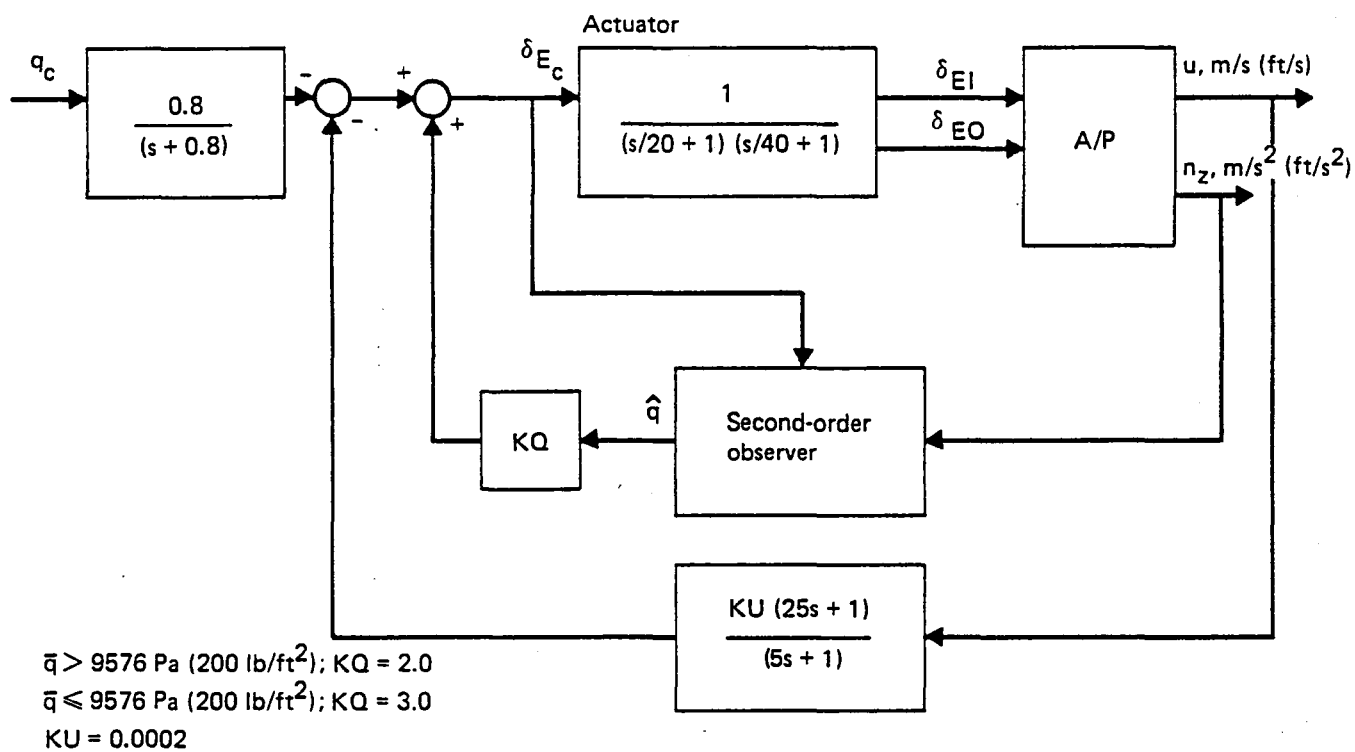*Figure G-45. IAAC Longitudinal Axis Models*

Figure G-46. IAAC Pitch-Augmented Stability With Observer
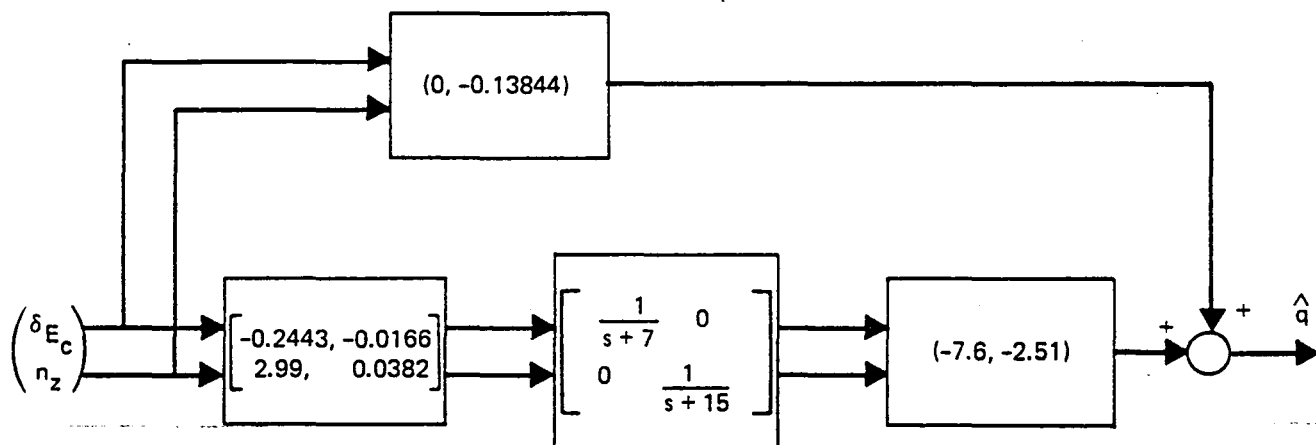
$\bar{q} > 9576$ Pa (200 lb/ft^2); KQ = 2.0
$\bar{q} \leqslant 9576$ Pa (200 lb/ft^2); KQ = 3.0
KU = 0.0002

Figure G-47. Pitch-Rate Observer

Table G-28. Pitch-Augmented Stability Design Roots

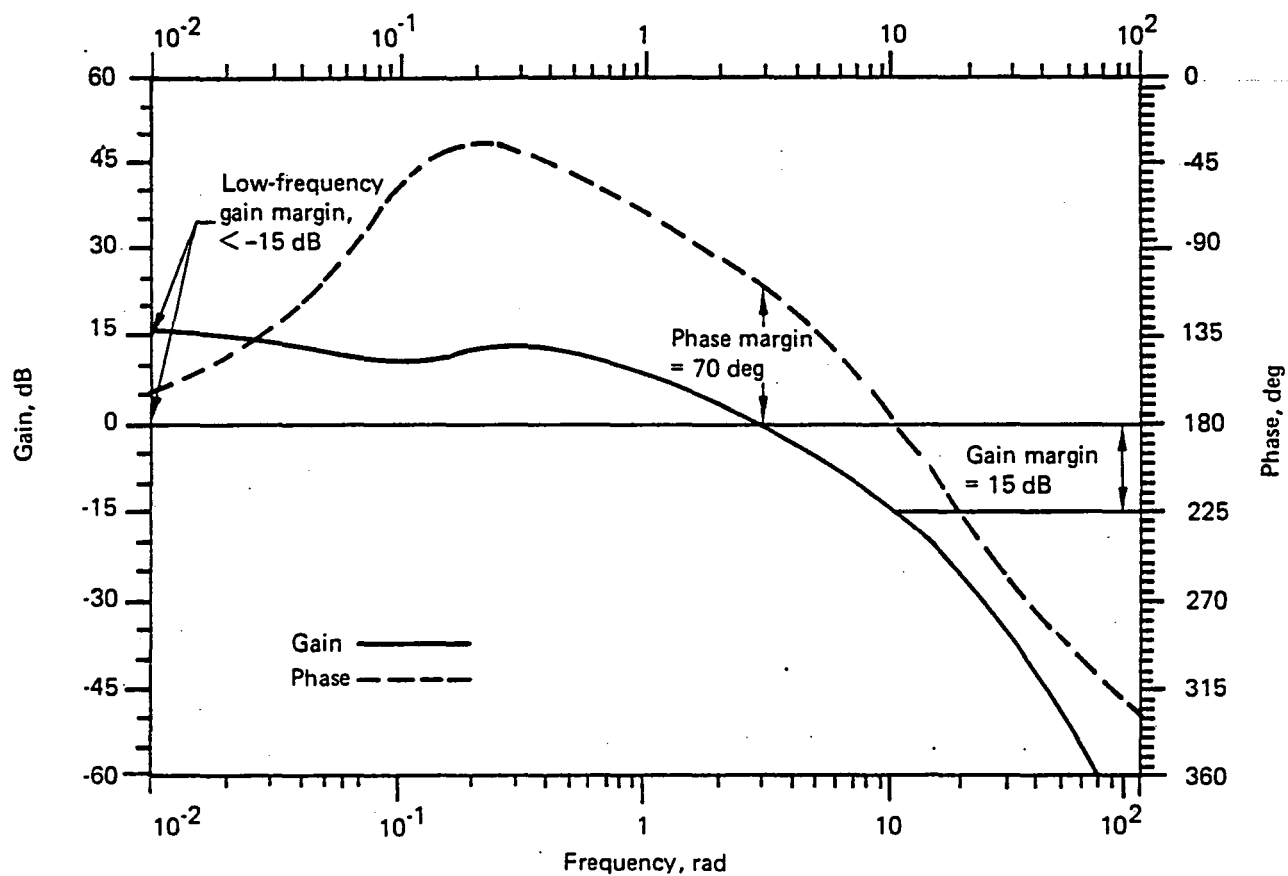|	Eigenvalues		Frequency	Damping ratio
	real	Imaginary		
Open loop	-1.06469178			
	-10.00000048			
	-0.44270060			
	-0.20004747			
	0.04717238			
	-0.07205359			
	-20.00000000			
	-40.00000000			
Closed loop, observer design	-25.07090735			
	-38.62446833			
	-3.48650715	4.69497484	5.84795010	0.59619304
	-3.48650718	-4.69497484	5.84795016	0.59619304
	-0.86118771			
	-0.06577497	0.04580707	0.08015382	0.82060931
	-0.06577497	-0.04580707	0.08015382	0.82060931
	-0.07119391			
Closed loop, Boeing design	-18.38132358			
	-57.38672113			
	-6.35998458	4.43677247	7.75463432	0.82015274
	-6.35998464	-4.43677240	7.75463438	0.82015274
	-5.45896631			
	-0.88066266			
	-0.06735528	0.08903743	0.11164407	0.60330373
	-0.06735528	-0.08903743	0.11164407	0.60330373
	-0.05206975			

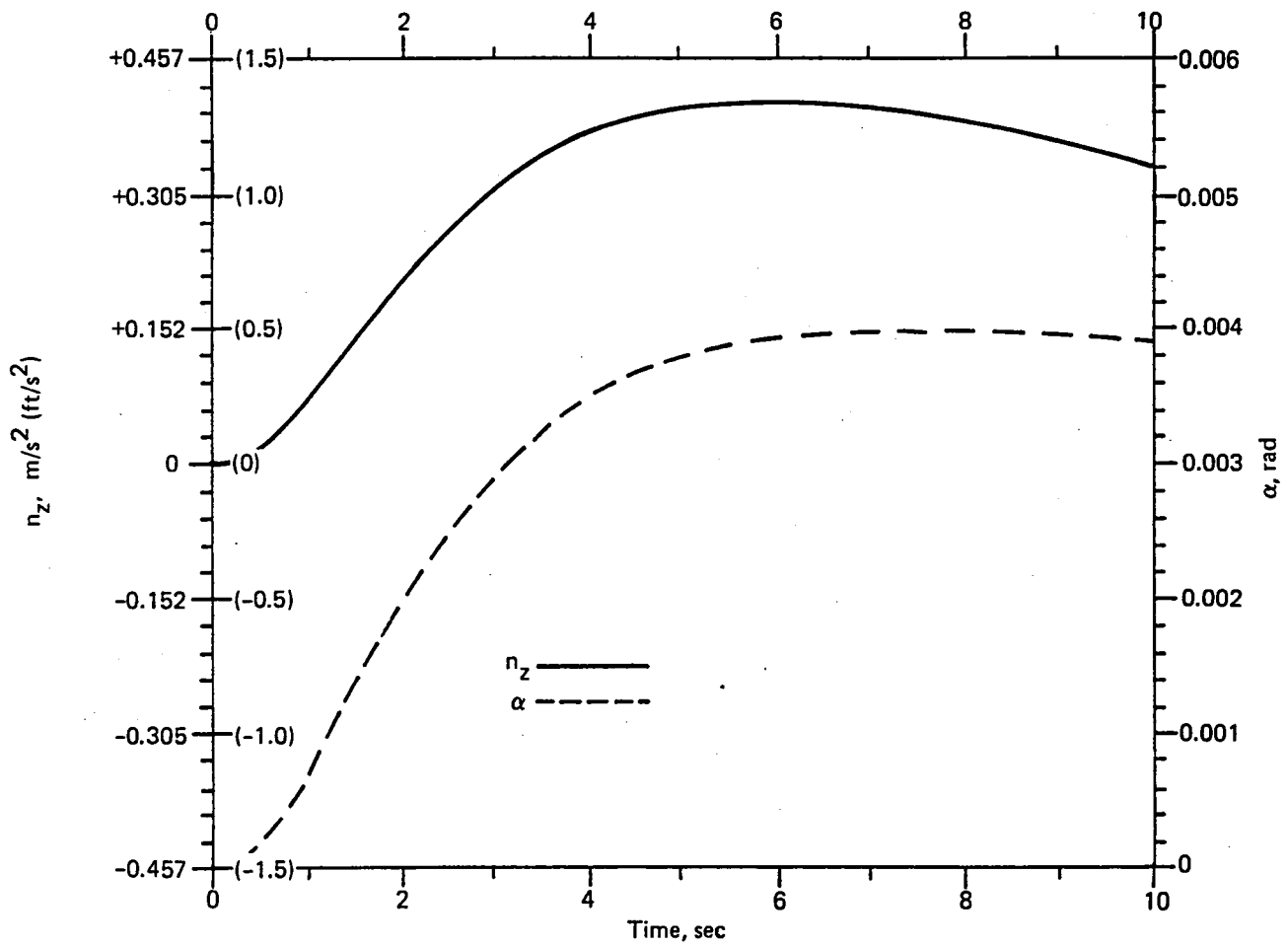Figure G-48. Boeing Design Stability Margins

Figure G-49. Pitch Axis Step Response, Boeing Design

Figure G-49. Pitch Axis Step Response, Boeing Design (Continued)

Figure G-49. Pitch Axis Step Response, Boeing Design (Concluded)

Figure G-50. Stability Margins, Observer Design

Figure G-51. Pitch Axis Step Response, Observer Design
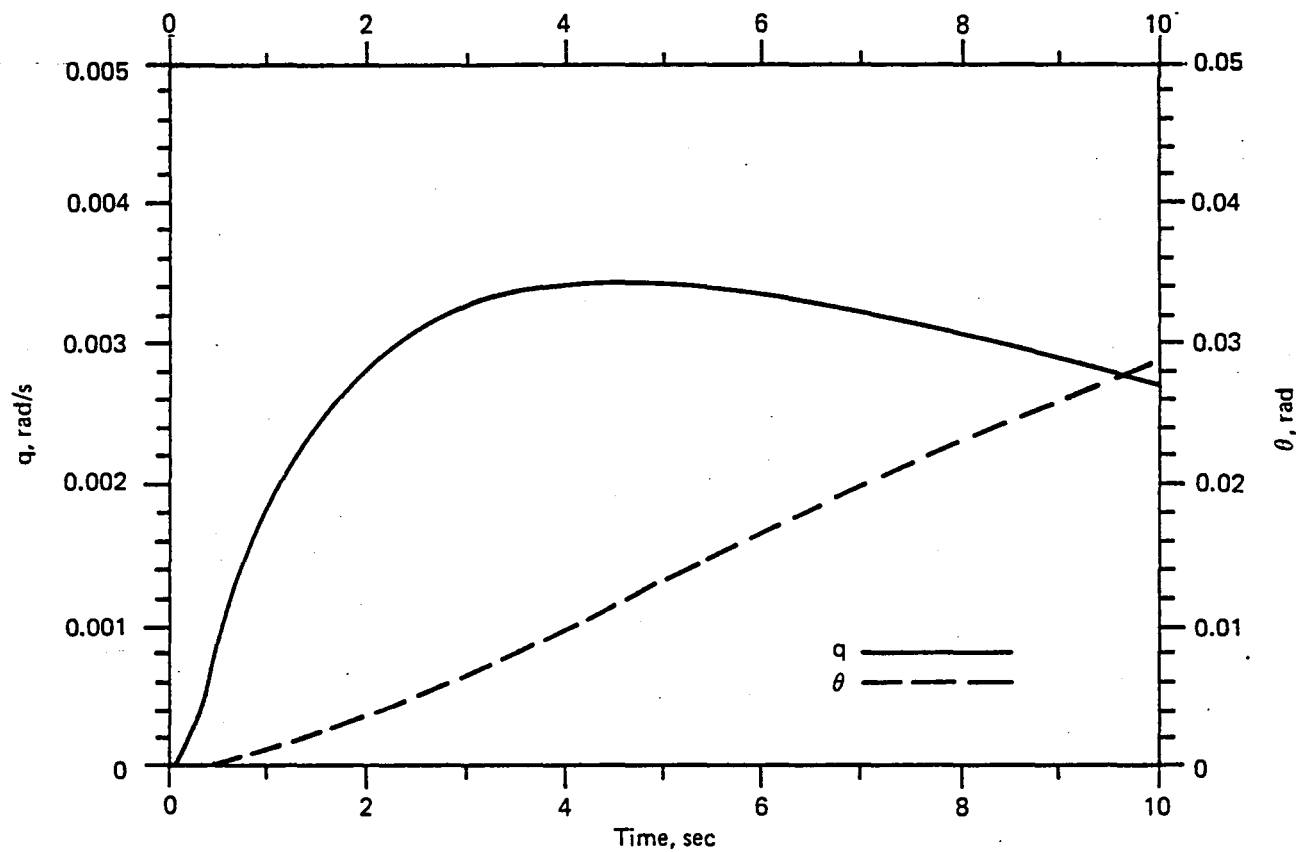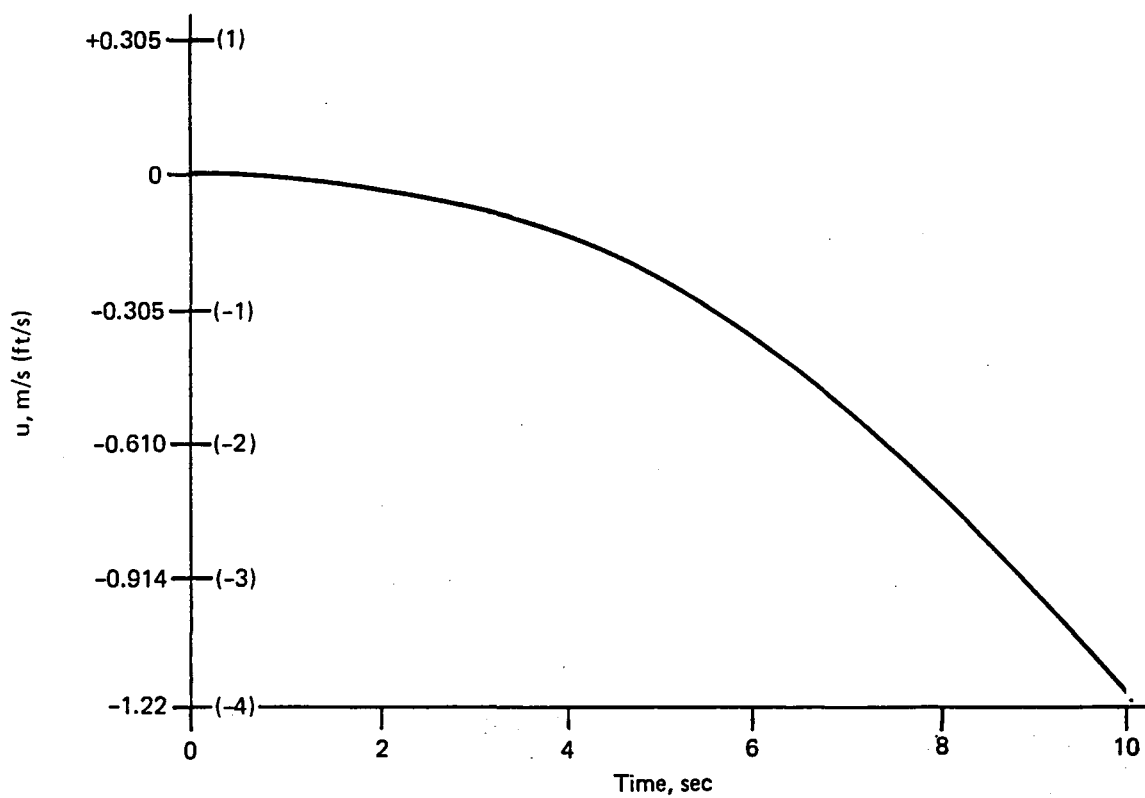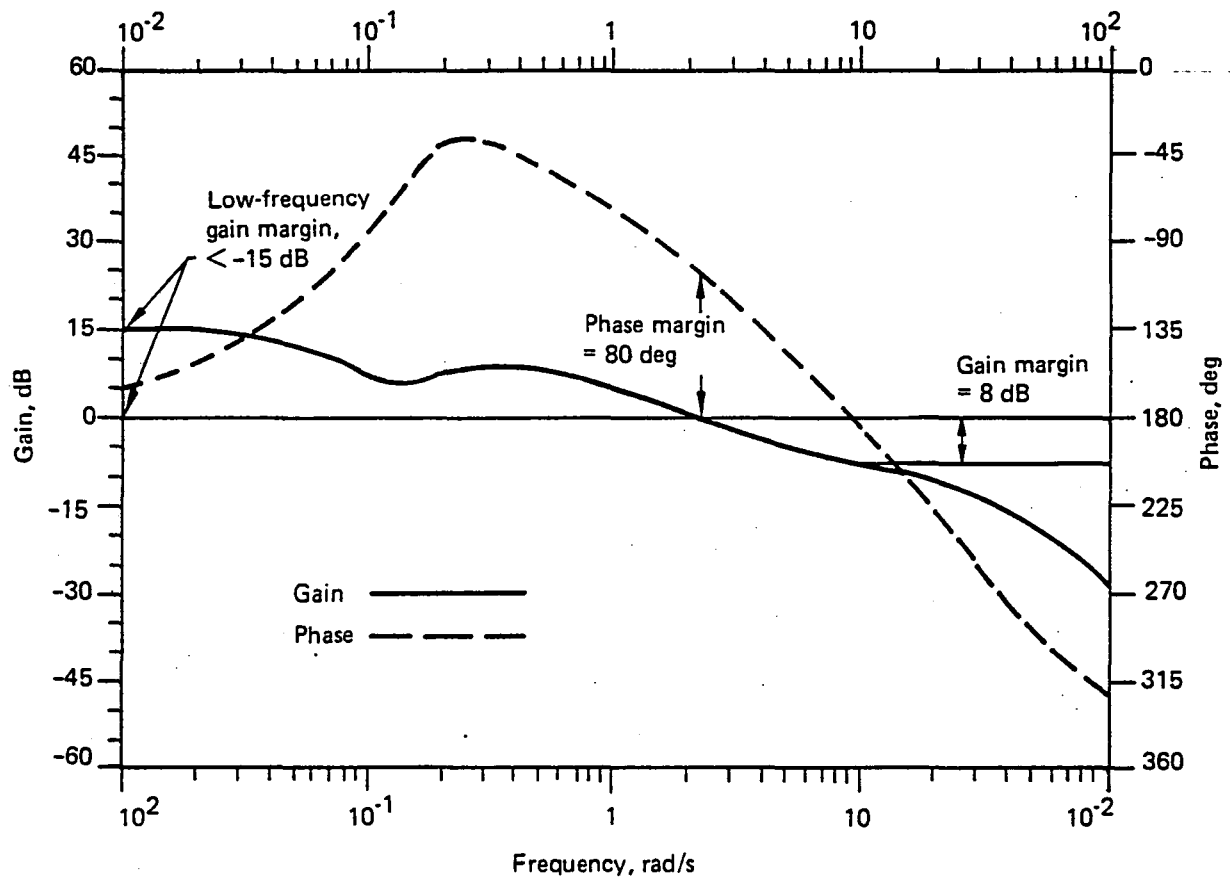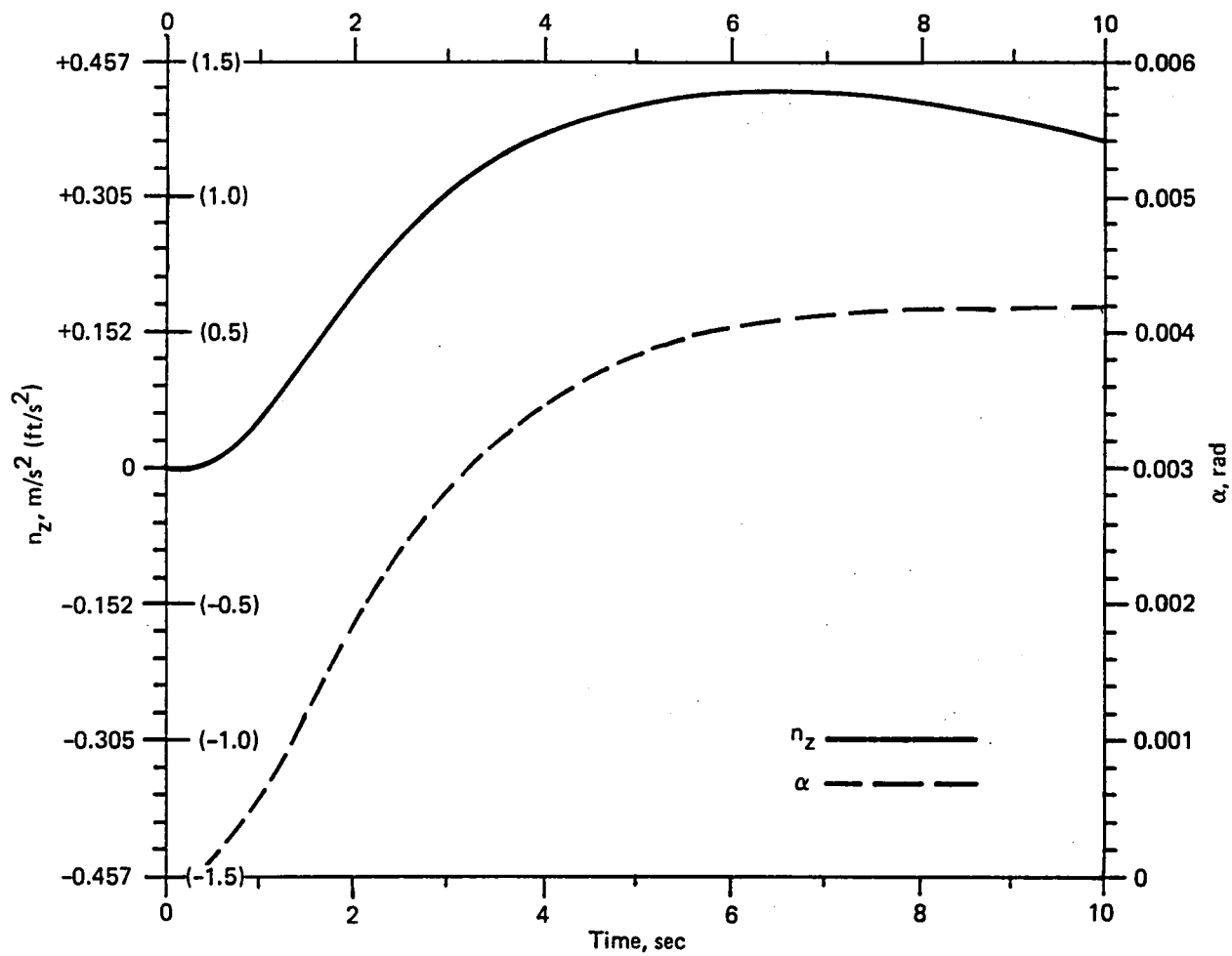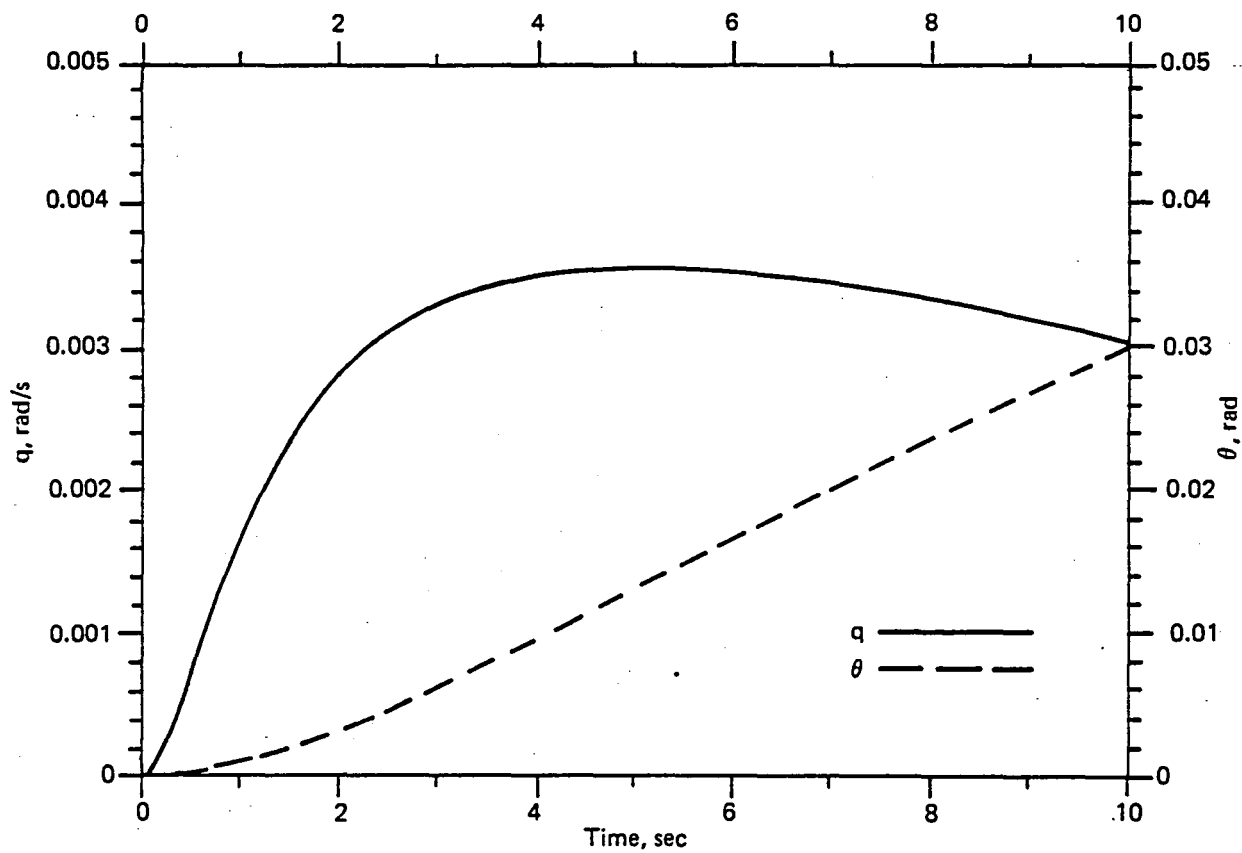
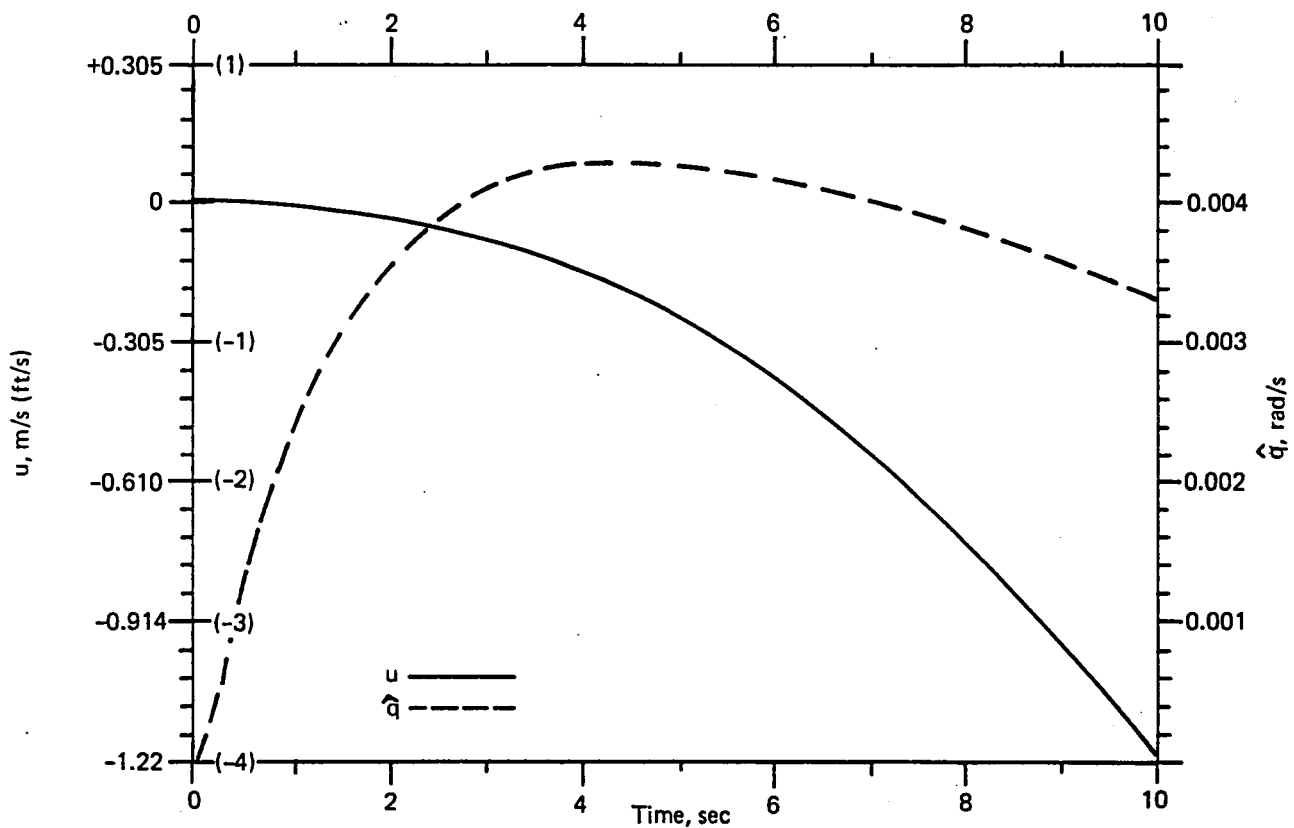Figure G-51. Pitch Axis Step Response, Observer Design (Continued)

Figure G-51. Pitch Axis Step Response, Observer Design (Concluded)
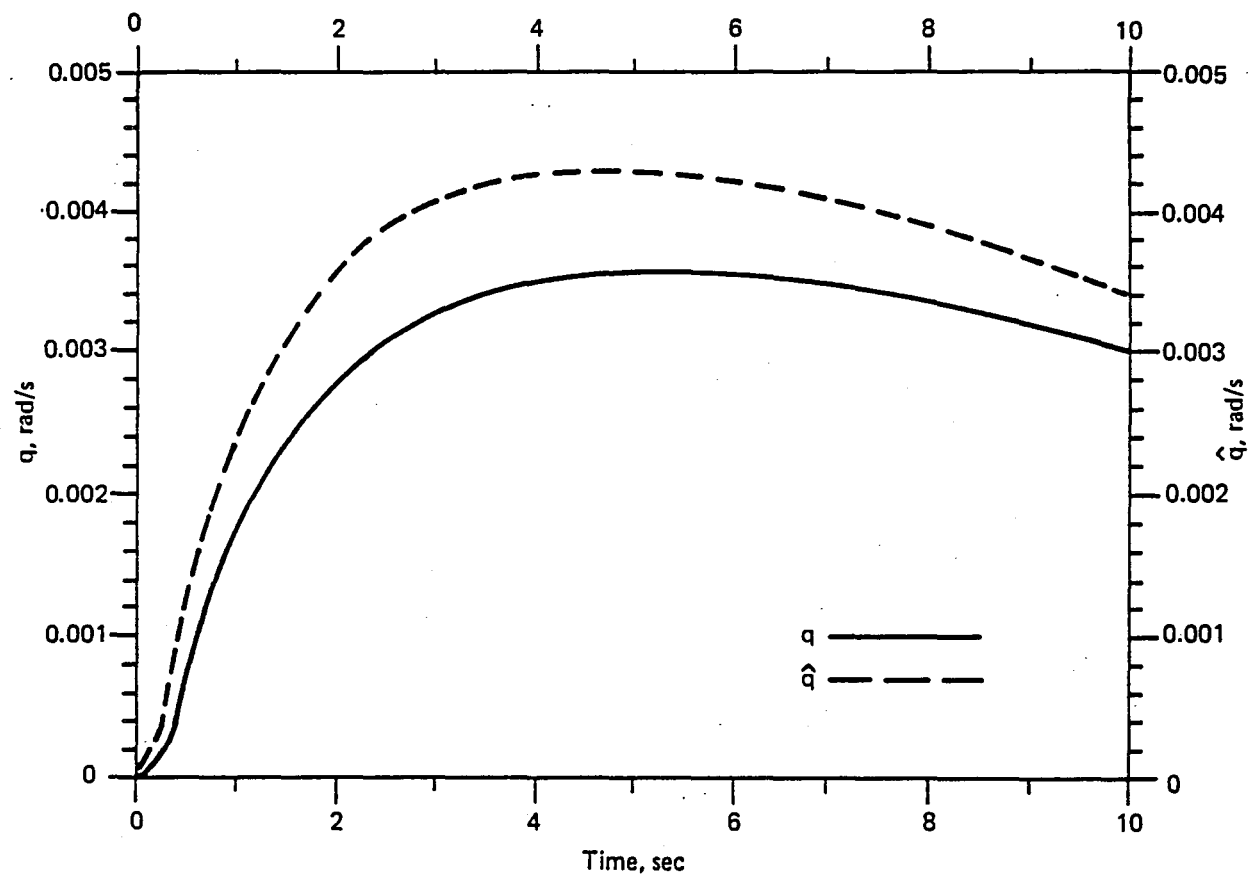
Figure G-52. Pitch-Rate Observer Performance

G.6.3 CONCLUSIONS

The feasibility of using an observer in lieu of a pitch-rate sensor was demonstrated in the IAAC control law for one flight condition. The end result is a net increase in system reliability at no extra hardware cost and at low software costs.

Using a failure management scenario, as shown in Table G-29, the catastrophic failure probability is

$$P_F < 3\lambda_Q^2 \cdot 3\lambda_{nz}^2 \quad \text{(for 1 hr)}$$

Assuming

$$\lambda = \lambda_Q = \lambda_{nz} = 3.0 \times 10^{-5} \text{ failures/hr}$$

$$P_F < 9\lambda^4 = 7.3 \times 10^{-18}$$

(λ_{nz} is a conservatively high failure rate for accelerometers)

Furthermore, if a sensor (either gyro or accelerometer) fails, the dispatch catastrophic failure probability is

$$P_F < 3\lambda^3 = 8.1 \times 10^{-14}$$

Both numbers are well below the budget of 10^{-10} for sensors.

Other features are:

● Failure detection and isolation is performed with high-coverage comparisons.

● Analytical redundancy can add capability to the system; however, the simplified reliability analysis used here indicates that it is not necessary.

Table G-29. Fail-Operational Scenario for Crucial Pitch-Augmented Stability

Failure mode	Status prior to failure	Failure detection scheme	Reversion mode
First gyro fails	Three gyros, plus three accelerometers up	Midvalue select and cross-channel monitor	Run control law on average of remaining gyros
Second gyro fails	Two gyros, plus three accelerometers	Cross-channel monitor to reject both gyros	Switch to q observer using n_z sensors *
First accelerometer fails	No usable gyros, plus three accelerometers	Midvalue select and cross-channel monitor	Run observer on average of remaining accelerometers
Second accelerometer fails	An AR determined "good" gyro and two accelerometers	Cross-channel monitor to reject both accelerometers	Run PAS with remaining gyro

Note: This scenario is not the only fault sequence; it is used to illustrate the management system.

* Use analytical redundancy to determine healthy gyro or accelerometer for later use.

G.7.0 CONCLUSIONS AND RECOMMENDATIONS

G.8.0 REFERENCES

G.7.0 CONCLUSIONS AND RECOMMENDATIONS

An ACT system has been defined that demonstrates that the cost-of-ownership parameters will be favorably affected by the anticipated technological advances. Most important of the developments are:

● Integrated circuit developments
● Extensive busing
● Software improvements

Integrated circuit developments will decrease the volume and increase the reliability of a given computer function by a factor of 4 to 10. Comparable speed increases will be realized. The effect of the military stimulus to the development of very-large-scale, very-high-speed integrated circuits will result in full-temperature-range standard circuits being available to respond to many requirements. Custom large-scale integrated circuits will be favorable financially in many other cases.

Partially as a result of these developments, more extensive busing will be used. Remote terminals will be included with each sensor and servoactuator. Essentially, all signal transmission will be via serial data buses with attendant reduced weight and cost. The ease with which signals from all sensors may be made available to all controllers will allow data crossflow, which will enhance reliability.

Software will be easier to prepare and validate. Most of the software will be prepared using a higher order language. The timing difficulties associated with synchronous computer operations are avoided in the 1990 ACT system. The software is naturally partitioned by the separation of functions brought about by the inclusion of input/output, control law, and monitor computers. The speed of the computers is high, so the time loading is of little consequence to the software designer.

Fly-by-wire control, included in all three axes, will improve performance and allow added flexibility in cockpit design.

It is recommended that additional work be performed on advanced architectures for flight control. The digital fly-by-wire system architecture of today is exemplified by the low-

risk architecture described in Subsection G.3.2. Its features have evolved over a decade of industry development. Several shortcomings were uncovered in the studies of the 1990 ACT architecture. In each case, these were corrected so they are not present in the system described in Section G.5.0. However, it is likely that additional examination and definition will point to still other areas for change. .

G.8.0 REFERENCES

G-1   Denton, D. D., H. R. Samuelson, and W. T. Pryor. An Independent Review of Military Standard Airborne Computer Instruction Set Architecture MIL-STD-1750 USAF. Northrup Corporation Report NOR 79-353, Hawthorne, California, June 1979.

G-2   Mick, J., and J. Brick. Bit-Slice Microprocessor Design. McGraw-Hill, New York, 1980.

G-3   Cushman, R. H. "μP/μP Chip Directory." EDN, pp. 133-240, October 20, 1979.

G-4   Cushman, R. H. "Support Chips Gain in Depth But No Surprises Appear." EDN, pp. 243-254, October 20, 1979.

G-5   Jensen, E. D., et al. Characterization of Data Multiplexing and Distributed Processing Systems for Future Shipboard Applications. Honeywell Systems and Research Center Report 77SRC74, Minneapolis, Minnesota, September 30, 1977.

G-6   Bloom, S. "Serial Digital Bus Heads for Industrial Systems." Electronic Design, pp. 137-141, September 13, 1980.

G-7   Airlines Electronic Engineering Committee. Mark 33 Digital Information Transfer System (DITS). ARINC Specification 429-4, Aeronautical Radio, Incorporated, Annapolis, Maryland, August 1, 1980.

G-8   Schaefer, A. Marine Corps Command and Control Fiber Optic Data Bus Feasibility Study. Naval Ocean Systems Center Report TR342, San Diego, California, November 1978.

G-9   Seacord, C. L., and D. Vaughn. Computer Technology Forecast Study for General Aviation. NASA CR-137880, Honeywell, St. Louis Park, Minnesota, June 30, 1976.

G-10   Smythe, R. K., ed. _State of the Art Survey of Technologies Applicable to NASA's Aeronautics, Avionics and Controls Program._ NASA CR-159050, Washington, D.C., May 1979.

G-11   Wise, K. D., K. Chen, and R. E. Yokely. _Microcomputers: A Technology Forecast and Assessment to the Year 2000._ John Wiley and Sons, New York, 1980.

G-12   Rang, E. R., et al. _Digital Flight Control Software Validation Study._ AFFDL-TR-79-3076, Wright-Patterson Air Force Base, Ohio, June 1979.

G-13   Rang, E. R. "The Use of Finite-State Machines for Describing and Validating Flight Control Systems." Proceedings of NAECON '80, Vol. 1, pp. 347-353, Dayton, Ohio, May 1980.

G-14   Rang, E. R., and M. J. Gutman. _Design and Validation Techniques for Flight Control Systems._ Honeywell Systems and Research Center Report 79SR92, Minneapolis, Minnesota, December 1979.

G-15   Robinson, L. · _The HDM Handbook, Vol 1: The Foundations of HDM._ SRI-International Report on SRI Project 4828, Menlo Park, California, June 1979.

G-16   Smith, T. B., et al. _A Fault-Tolerant Multiprocessor Architecture for Aircraft—Volume I._ Charles Stark Draper Laboratory, Inc., Report 4-1140, Cambridge, Massachusetts, July 1976.

G-17   Hopkins, A. L., Jr., T. B. Smith, and J. H. Lala. "FTMP—A Highly Reliable Fault-Tolerant Multiprocessor for Aircraft." _IEEE Proceedings_, Vol. 66, No. 10, pp. 1221-1239, October 1978.

G-18   Wensley, J. H., et al. "SIFT: Design and Analysis of a Fault-Tolerant Computer for Aircraft Control." _IEEE Proceedings_, Vol. 66, No. 10, pp. 1240-1255, October 1978.

G-19   Rennels, D. A. "Architecture for Fault-Tolerant Spacecraft Computers."
        IEEE Proceedings, Vol. 66, No. 10, pp. 1255-1268, October 1978.

G-20   Wakerly, J. Error-Correcting Codes, Self-Checking Circuits and Applications.
        Elsevier North-Holland, Inc., New York, 1978.

G-21   Integrated Application of Active Controls (IAAC) Technology to an Advanced
        Subsonic Transport Project—Initial ACT Configuration Design Study. NASA
        CR-159249, Boeing Commercial Airplane Company, July 1980.

1. Report No. NASA CR-165631	2. Government Accession No.	3. Recipient's Catalog No.
4. Title and Subtitle Integrated Application of Active Controls (IAAC) Technology to an Advanced Subsonic Transport Project—Current and Advanced ACT Control System Definition Study, Volume II, Appendices		5. Report Date October 1981
		6. Performing Organization Code
7. Author(s) Boeing Commercial Airplane Company Preliminary Design Department		8. Performing Organization Report No. D6-48673
		10. Work Unit No.
9. Performing Organization Name and Address Boeing Commercial Airplane Company P. O. Box 3707 Seattle, Washington 98124		11. Contract or Grant No. NAS1-14742 and NAS1-15325
		13. Type of Report and Period Covered Contractor Report July 1978 to October 1980
12. Sponsoring Agency Name and Address National Aeronautics and Space Administration Washington, D. C. 20546		14. Sponsoring Agency Code

15. Supplementary Notes

Technical Monitors: D. B. Middleton and R. V. Hood
                        NASA Langley Research Center

16. Abstract

This report documents the Current and Advanced ACT Control System Definition Study Tasks of the Integrated Application of Active Controls (IAAC) Technology Project within the Energy Efficient Transport Program. These system definitions support the Initial ACT Configuration, Wing Planform Study, and Final ACT Airplane Configuration with data to validate the assessment of their energy efficiency. Study ground rules required the current technology system to use only elements fully demonstrated and available in 1980; the advanced technology system represents technology of the 1990s era. The systems mechanize six active control functions: pitch-augmented stability, angle-of-attack limiting, lateral/directional-augmented stability, gust-load alleviation, maneuver-load control, and flutter-mode control. The redundant digital control systems defined meet all function requirements with required reliability and declining weight and cost as advanced technology is introduced. They indicate the advisability of demonstrating key system elements in laboratory and flight test.

17. Key Words (Suggested by Author(s)) Energy Efficient Transport, Active Controls Technology, Redundant Digital Control System, Augmented Stability, Wing-Load Alleviation, Flutter-Mode Control, Angle-of-Attack Limiting, Control Configured Vehicle	18. Distribution Statement FEDD Distribution

19. Security Classif. (of this report) Unclassified	20. Security Classif. (of this page) Unclassified	21. No. of Pages 510	22. Price

Available: NASA's Industrial Applications Centers

N-305

End of Document